Understanding the role of long non-coding RNA (LncRNA) in vascular pathology

Margaret Ballantyne

Bsc (Hons), MRes

Submitted in the fulfilment of the requirements of the degree of Doctor of Philosophy in the College of Medical Veterinary and Life Sciences, University of Glasgow.

Institute of Cardiovascular and Medical Sciences, College of Medical, Veterinary and Life Sciences, University of Glasgow.

April 2017

Author's Declaration

I declare that this thesis has been entirely written by myself and is a record of work performed by myself with the exception of the RNA extractions from the atherosclerotic samples which was performed by Dr Louise Diver and Dr Ruth Mackenzie, the RNA extraction and qRT-PCR for plasma and media samples which was performed by Dr Karine Pinel and the ^{18F}-FDG and ^{18F}-NaF imaging that was performed by Dr Alex Vessey. Triple transfection preparation of lenti-SMILR was performed by Nicola Britton. The optimisation of the *SMILR* biotin pulldown was a collaborative effort between myself and Dr Amira Mahmoud. This thesis has not previously been submitted for a higher degree. This research was carried out at the Institute of Cardiovascular and Medical Sciences, University of Glasgow and the BHF Centre for Cardiovascular Science, University of Edinburgh under the supervision of Professor Andrew H. Baker and Dr Robert McDonald.

Margaret Ballantyne

November 2016

Acknowledgement

First and foremost, I would like to thank my supervisors Professor Andrew H Baker and Dr Robert McDonald for all of the support, guidance and advice they have provided throughout my studies. Knowledge does pass in both directions and I don't think I will ever forget our conversations on 'pieces' (sandwiches) and why certain roundabouts get formal names like 'The Raith'. A massive thank you also goes to Dr Angela Bradshaw for taking the time to read the 1st and 2nd draft of my thesis.

An important acknowledgement must go to the British Heart Foundation who awarded me a studentship that funded this work.

I would also like to say a massive thank you to all members of the Baker group, past and present. A special mention goes to Dr Rachel Dakin for all the bioinformatic help and attempts to understand R, to Karine Pinel for all her help extracting RNA from media and plasma especially our attempts to trawl through the 3 -80°C freezers to find samples that were in no logical order, to Dr Raquel Garcia for teaching me my cloning knowledge, and to, most recently, Dr Amira Mahmoud for the support when optimising the SMILR pulldown experiments. Additionally I would like to thank Nicola Britton and Gregor Aitchison for teaching me the basics and for all their help throughout the last 3 years.

A thanks also goes to Prof. Naveed Sattar, Dr Alex Vessey and Prof. Dave Newby for the access to key clinical samples that were crucial to my project.

To the girls: Emma, Lisa, Nina, Small, Tall and Laura – thank you for your continued hilarity and distractions from all things science and special thank you for making sure that I was present at every birthday (through photoshop) even when I was working through in Edinburgh. I have had so much fun with all of you during our nights out, dinners and board games (even when Laura and I always lose) and I look forward to the many more experiences to come! Thanks for all the memories.

Lastly, I would like to thank my family for all their love and encouragement. For my parents who raised me with a love of science and supported me in all my

pursuits and for my brothers and sister, well what can I say? Thanks for ensuring me that it’s not just me that is mental! And finally to my supportive and encouraging husband Lorenzo, I thank you for listening to all my science and non-science ramblings and making sure I stuck to my deadlines.

Table of Contents

List of Tables

List of Figures

List of Publications and presentations

Publications:

"A role for the long non-coding RNA SENCR in commitment and function of endothelial cells" Mounia Boulberdaa, Elizabeth Scott, Margaret. D. Ballantyne, Raquel Garcia, Betty Descamps, Gianni D Angelini, Mairi Brittan, Martin McBride, John McClure, Joseph M Miano, Costanza Emanueli, Nicholas L Mills, Joanne C Mountford, Andrew H Baker. Molecular Therapy, April 2016, 24(5):978-90.

"Smooth muscle enriched long non-coding RNA (SMILR) regulates cell proliferation" Margaret. D. Ballantyne, Karine Pinel, Rachel Dakin, Alex. T, Vesey, Louise Diver, Ruth Mackenzie, Raquel Garcia, Paul. Welsh, Naveed Sattar, Graham Hamilton, Nikhil Joshi, Marc, R, Dweck, Joseph, M, Miano, David, E, Newby, Robert. A. McDonald, Andrew. H. Baker. Circulation, May 2016, 133(21):2050-65.

"LncRNA/MicroRNA Interactions in the Vasculature" Margaret. D. Ballantyne, Robert. A. McDonald, and Andrew. H. Baker. Clinical Pharmacology & Therapeutics, May 2016, 99(5):494-501.

Abstracts Presented:

Cytokine and Growth Factor Induction of lncRNA in Vascular Smooth Muscle Cells. Margaret. D. Ballantyne, Rachel. Dakin, Robert. A. McDonald, Andrew. H. Baker. **Oral presentation.** Long Non-coding RNAs: From Evolution to Function (C7), March 15—20, 2015. Keystone Resort, Keystone, Colorado USA

Transcriptional profiling of IL1α and PDGF inducible lncRNA in vascular smooth muscle cells. Margaret. D. Ballantyne, Louise. Diver, Robert. A. McDonald, Andrew. H. Baker. **Poster presentation**. 83rd European Atherosclerosis Society (Pedersen et al.) meeting, March 22-25 2015, Glasgow, UK

Summary

Coronary heart disease is a major cause of morbidity and mortality in the Western society. In the case of severe atherosclerosis, percutaneous intervention and coronary bypass grafting remain the preferred form of surgical treatment. However, the patency of both these treatments is limited and several bypass grafts and stents fail due to neointimal formation and in stent restenosis attributable to the proliferation of VSMCs. The resultant luminal renarrowing may manifest clinically with the return of symptoms such as chest pain or shortness of breath and ultimately requires further surgical intervention. Unfortunately, current antiproliferative therapies to inhibit VSMC proliferation have off target effects and can inhibit vessel re-endothelialisation resulting in thrombus formation. As such, novel therapies that specifically target VSMC proliferation but do not affect endothelial growth are urgently required.

Long non-coding RNA (lncRNA) are transcripts >200 nucleotides that have been shown to bind DNA, RNA and proteins in order to exert their function. To date a few lncRNAs have been identified that control key aspects of VSMC phenotype, including contraction, proliferation, migration and apoptosis, however, very little is known as to the role of lncRNA in the proliferative and inflammatory phenotype associated with this phenotypic switching. It was therefore hypothesised that lncRNA may be dysregulated in the setting of inflammatory and proliferative vascular pathology and may provide novel therapies to counteract VSMC proliferation and hence vascular disease.

The project sought to identify lncRNA expression in quiescent, non-proliferating human saphenous vein (HSV) SMCs, and HSVSMCs that had been treated with the IL1α cytokine and PDGF growth factor. This cytokine and growth factor pair have been implicated in the synergistic activation of the NF-κB transcription factor and in the control of vascular diseases including in stent restenosis, neo intimal formation and atherosclerosis. Using RNA-sequencing, >300 lncRNAs were identified whose expression was altered in HSVSMCs following stimulation with IL1α and PDGF. These lncRNA exhibited distinct expression patterns in a tissue cohort and all showed enrichment in vascular SMCs from either an arterial or venous lineages. Experiments focused on a novel lncRNA (Ensembl: RP11-94A24.1) which showed specific expression in HSVSMCs following treatment but

no expression in endothelial cells. This lncRNA was termed smooth muscle induced lncRNA enhances replication (*SMILR*). Following stimulation, *SMILR* expression was increased in both the nucleus and cytoplasm, and was detected in conditioned media from dual stimulated HSVSMCs.

Furthermore, knockdown of *SMILR* markedly reduced cell proliferation. Mechanistically, it was noted that expression of genes proximal to *SMILR* were also altered by IL1α/PDGF treatment possibly indicating that these two genes are under the same promoter control, and HAS2 expression was reduced by *SMILR* knockdown. Additionally the proliferation of HSVSMCs was increased in a dose dependent manner following administration of a lentivirus containing the full *SMILR* transcript, confirming the knockdown data.

In human samples, increased expression of *SMILR* was detected in plaque compared to adjacent non-plaque sections by qRT-PCR and following on from the detection of *SMILR* in conditioned media, *SMILR* was also detected in plasma samples from patients with inflammatory CVD. Interestingly, the levels of *SMILR* correlated with plasma C-reactive protein, a current biomarker capable of detecting atherosclerosis progression in patients.

These results identify *SMILR* as a driver of VSMC proliferation and suggest that modulation of *SMILR* may be a novel therapeutic strategy to reduce vascular pathologies. Additionally the detection of *SMILR* in plasma highlights the possibility that this lncRNA may have the potential as a biomarker of vascular disease. However, further large cohort studies are required to identify this potential clinical role.

Definitions/Abbreviations

Act D	Actinomycin D
AngII	Angiotensin II
APP	Amyloid protein precursor
BACE	ß site amyloid precursor protein
BM	Buffer Mix
BMS	Bare metal stent
BMT	Bone marrow transplant
BrdU	DNA bromodeoxyuride
c. elegans	Caenorhabditis elegans
CABG	Coronary artery bypass graft
CAD	Coronary Artery Disease
CDK	Cyclin dependent kinase
COSHH	Control of substances hazardous to health
CRP	C Reactive Protein
CT	Computed Tomography
CURVES	Carotid Ultrasound and Risk of Vascular disease in Europeans and South Asians
CVD	Cardiovascular disease
DBE	DNA Binding Element
DEPC	Diethylpyrocarbonate
DES	Drug eluting stent
DMEM	Dulbecco's Modified Eagle's Medium
ds	Double stranded
E	Embryonic day

E coli	*Escherichia coli*
ECM	Extracellular matrix
EDC	N-Ethyl-N′-(3-dimethylaminopropyl)carbodiimide hydrochloride
EdU	5-ethynyl-2′-deoxyuridine
EGTA	Ethylene glycol tetra-acetic acid
ENCODE	The Encyclopaedia of DNA Elements
eNOS	Endothelial nitric oxide synthase
FBS	Fetal bovine serum
FC	Fold change
FDG	Fluorodeoxy glucose
FDR	False discovery rate
FISH	Fluorescent in situ hybridisation
FKBP12	FK-506 binding protein
FLI1	Friend leukemia integration 1
FPKM	Fragments Per Kilobase of transcript per Million mapped reads
FRET	Fluorescence resonance energy transfer
GAPDH	Glyceraldehyde 3-phosphate dehydrogenase
GFP	Green Fluorescent Protein
GSP	Gene Specific Primers
HA	Hyaluron
HAS2	Hyaluronic Acid Synthase 2
HCASMC	Human coronary artery smooth muscle cell
HCT-116	Colorectal cancer cell
HGP	Human genome project
HOTAIR	Hox antisense intergenic RNA
HOTTIP	HOXA transcript at the distal tip

HSF1	Heat shock factor 1
HSVEC	Human saphenous vein endothelial cell
ICAM-1	Intercellular Adhesion Molecule 1
IL1α	Interleukin 1 alpha
IL6	Interleukin 6
ILR1	Interleukin receptor 1
IPA	Ingenuity pathway analysis
IRF7	Interferon regulatory factor 7
KLF4	Kruppel-like factor 4
LB	Luria Broth
LDL	Low density lipoprotein
lncRNA	long non-coding RNA
LV	Left ventricular
M	Mitosis
MHC	Myosin heavy chain
MI	Myocardial infarction
miR	MicroRNA
mTOR	Mammalian target of rapamycin
MV	Micro Vesicles
NF-κB	Nuclear Factor Kappa Beta
NLS	Nuclear localisation signal
NO	Nitric oxide
OAS1	2'-5'-Oligoadenylate Synthetase 1
OxLDL	Oxidised low density lipoprotein
PCR	Polymerase chain reaction
PDGF	Platelet derived growth factor

PFA	Paraformaldehyde
PGI1	Prostacyclin
PI3K	Phosphatidylinositol-4,5-bisphosphate 3-kinase
PolII	Polymerase II
pRb	Retinoblastoma protein
PRC2	Polycomb Repressive Complex 2
PSA	Prostate-Sepcific Antigen
QC	Quality Control
qRT-PCR	Quantitative reverse transcription polymerase chain reaction
RACE	Rapid amplification of cDNA ends
RIN	RNA integrity number
RNA-seq	RNA sequencing
ROS	Reactive oxygen species
RQ	Relative Quantity
RT	Reverse Transcriptase
S	Synthesis
SEM	Standard Error Mean
SENCR	Smooth muscle and Endothelial cell-enriched migration/differentiation-associated long Non-coding RNA
siRNA	Small interfering RNA
SMC	Smooth muscle cell
SMILR	Smooth Muscle Induced LncRNA enhances Replication
SRF	Serum response factor
STAU1	Staufen 1
SUV	Standard uptake values
SVGF	Saphenous vein graft failure

t1/2	half life
TALEN	Transcription activator-like effector nucleases
TBE	Tris/Borate/EDTA
TBR	Tissue Backround Ratio
TNF-α	Tumour necrosis factor alpha
TSP-1	Thrombospondin 1
U-2OS	Osteocarcinoma cell line
UBC	Ubiquitin C
UCSC	University of California, Santa Cruz
UTR	Untranslated region
VCAM-1	Vascular cell adhesion protein 1
VSMC	Vascular smooth muscle cells
Wnt	Wingless-type MMTV integration site family member
ZFN	Zinc fingered nuclease
αSMA	alpha smooth muscle actin

Chapter 1 Introduction

1.1 Cardiovascular Disease

Cardiovascular disease (CVD) refers to any disorder of the heart or circulatory system and represents a leading cause of health care burden, morbidity and mortality. According to the World Health Organisation (WHO), 17.5 million or almost 46.2 % of global deaths resulted from CVD in 2012 and the annual cardiovascular disease mortality is expected to rise from 17.5 million in 2012 to 22.3 million in 2030 (WHO, 2012).

1.1.1 Epidemiology of cardiovascular disease in the UK

In 2012, for the first time since 1961, CVD dropped from being the first main cause to the second main cause of death in the United Kingdom, accounting for 28 % of the national deaths compared to 29 % for cancer (BHF cardiovascular Statistics 2014). However, if broken down by gender, CVD still remains the main cause of death for women within the UK. In men, cancer accounted for 32 % of deaths and CVD 29 %, whilst in women these Figures were 27 % and 28 % respectively (Figure 1.1A and B respectively) Furthermore, in 2009, the direct healthcare cost of all CVD in the UK was £8.7 billion (BHF cardiovascular Statistics 2014). This highlights the need for improved CVD treatment in order to reduce patient mortality.

Coronary heart disease (Mitra et al.) is the most prominent manifestation of CVD and accounts for just under half (46 %) of the CVD deaths (BHF cardiovascular Statistics 2014). The primary consequences of CHD are lack of oxygen to the heart muscle and myocardial infarction, both of which are the result of the presence of atherosclerotic plaques within the vessel wall and can be worsened by rupture of unstable plaques producing thrombosis (Danesh et al., 2004).

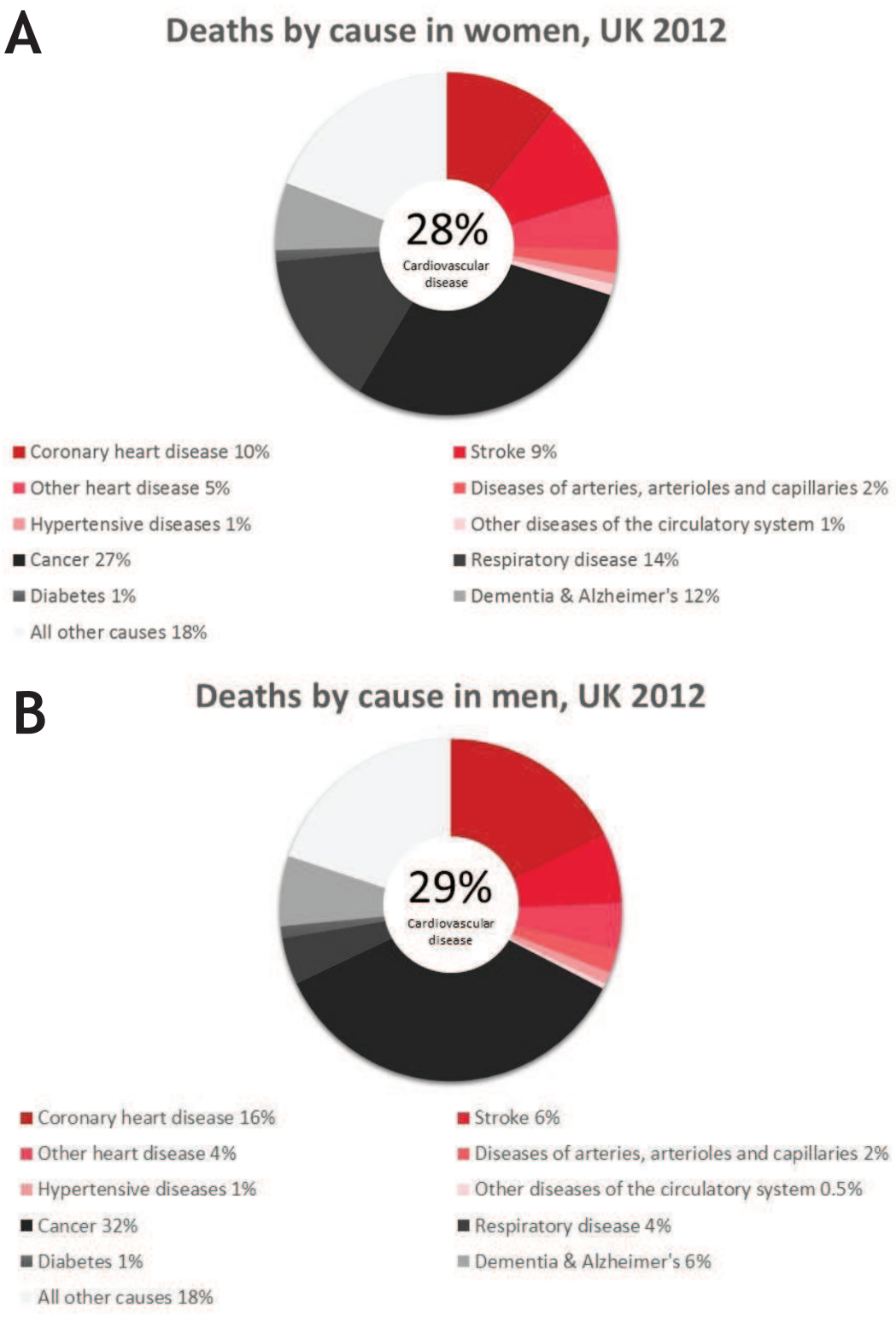

Figure 1-1: Deaths by cause in women and men, UK 2012.
A: In the UK cardiovascular disease is the greatest cause of death to women, accounting for 28 % of all deaths. **B:** For men cardiovascular disease accounts for 29 % of deaths and is the second largest killer. Adapted from BHF cardiovascular Statistics 2014.

1.2 The vasculature

Structural differences between arteries and veins have long been recognised by anatomists. Generally, veins are larger in diameter than arteries but have much thinner walls. Regardless, both consist of three well defined layers: the tunica intima, the tunica media and the tunic adventitia (Figure 1-2).

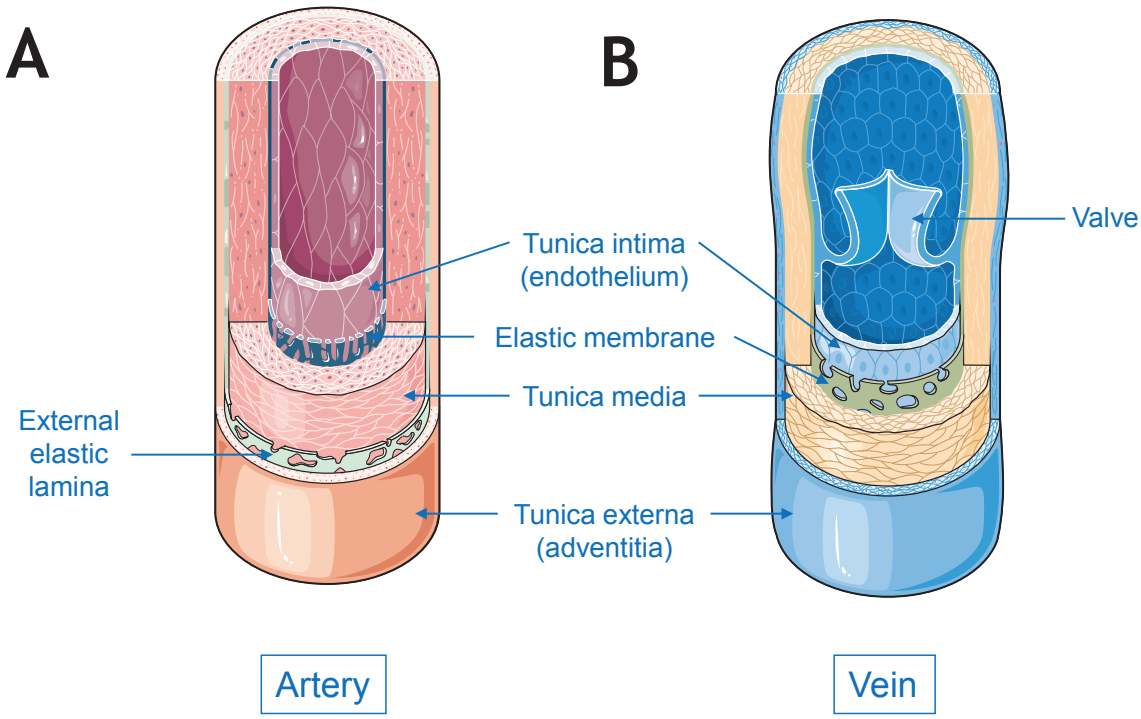

Figure 1-2: Anatomy of human arteries and veins.
A: Human aretery. **B**: Human vein. Both arteries and veins are composed of a tunica intima that is lined with endothelial cells (ECs), a tunica media that contains SMCs and elastic fibre and a tunica adventitia made up of fibrous connective tissue. Arterial blood vessels are characterised by long narrow ECs that are aligned in the direction of blood flow, multiple layers of smooth muscle cells and in the case of muscular arteries elastic fibres that are arranged in two distinct bands (inner and outer elastic laminae). In contrast, venous blood vessels are lined with rounder non-aligned ECs, lack elastic laminae and most possess valves that project into their lumen. Adapted from Servier medical art.

The different layers of arteries and veins have thus evolved to meet the needs of supplying oxygen and nutrients to distal organs and tissues and for returning the waste products (Monahan-Earley et al., 2013). The intima is the innermost vessel layer and is in direct contact with the blood. The most defining feature of the tunica intima is the endothelial cells which are attached to this layer, line the vessel and play a profound role in vascular homeostasis (Rubanyi, 1993) (reviewed in detail in Section 1.2.1). As such, this thin layer of cells allows the

diffusion of important factors to and from the blood. The *tunica intima* also includes a supportive matrix of connective tissue composed of collagen and elastic fibres, the latter forming a distinct band called the internal elastic lamina in most arteries. One major difference between arteries and veins is the absence of the elastic lamina in veins. However, one of the most striking differences is the presence of valve structures in veins preventing the backflow of blood as it is returned back to the heart (dela Paz and D'Amore, 2009). Additionally, distinct differences exist between endothelial cell (EC) shape between arteries and veins. Arterial ECs are generally thicker than those in veins, are long and narrow and align in the direction of blood flow (dela Paz and D'Amore, 2009). Venous EC, in contrast, are short and wide. This is due to the lower blood flow rates in the venous circulation when compared to the arterial circulation (dela Paz and D'Amore, 2009).

The middle layer is the medial layer. This is composed of elastin fibres, circumferentially oriented smooth muscle cells (SMCs) and collagen (Stary, 1992). Medial SMC express a repertoire of contractile proteins that allow the contraction and relaxation of the artery (Gomez and Owens, 2012), while the elastin fibres allow the vessel to stretch and recoil (Sherratt, 2009). In arteries of all sizes, the tunica media is typically the thickest layer and is composed of multiple layers of SMCs and a large amount of elastic material. Both veins and arteries contain SMCs and elastic fibres, however, the tunica media of the venous circulation is not as clearly defined and organised as in the arterial counterparts. As such, the walls of veins are typically thinner and less rigid than that of an artery (dela Paz and D'Amore, 2009).

The outermost layer is the adventitia, which is comprised of loosely woven collagen fibres surrounded by connective tissue that protect the blood vessel and anchor it to surrounding structures (Stenmark et al., 2013). Fibroblasts are dispersed within the adventitia but are generally absent from the intima and medial layers. The vascular adventitia has recently been identified as a major biological processing centre for the storage and release of key regulators for vessel wall function and comprises a variety of cells. Recent evidence indicates that stem/progenitor cells are present in the adventitia and participate in vascular repair and the formation of neointimal lesions in severely damaged

vessels (Hu and Xu, 2011). Data suggests that these stem cells have the capability to differentiate into SMCs and participate in neointimal formation (Hu and Xu, 2011).

The formation of blood vessels occurs via two processes: vasculogenesis, the formation of nascent blood vessels, and angiogenesis, the sprouting of new blood vessels from existing blood vessels. Vasculogenesis initially promotes the vascular endothelial progenitors (angio-blasts) to form new vessels *in situ*. It is the primary means of generating the first major vascular system during embryogenesis (Weinstein, 1999). The process of vasculogenesis first occurs in the embryonic yolk sac of mammalian embryos (Goldie et al., 2008). During gastrulation, embryonic ectodermal (epiblast) cells are recruited to the primitive streak where they undergo an epithelial to mesenchymal transition (Goldie et al., 2008). These cells then migrate between the visceral endoderm and epiblast to form either mesoderm or endoderm. In the yolk sac, the visceral endoderm is thought to produce soluble signals which target the underlying mesoderm to induce the formation of primitive endothelial and hematopoietic cells, the first differentiated cell types to be produced in the mammalian embryo (Goldie et al., 2008). Primitive endothelial and hematopoietic cells merge to form blood islands that then fuse to form a primitive network of tubules known as a capillary or vascular plexus (Ribatti et al., 2015). Remodelling and maturation of the capillary plexus into a circulatory network requires the subsequent recruitment of mural cells (smooth muscle cells and pericytes) to form the outer blood vessel wall (Goldie et al., 2008). Following generation of the initial circulation, additional vessels are then formed via angiogenesis resulting from environmental cues.

1.2.1 Endothelial cells

The vascular endothelium is no longer thought of as an inert barrier, but a critical regulator of vascular homeostasis. This first became apparent through electron microscopic studies of the vessel wall by Palade in 1953 (Palade, 1953) and was further confirmed by physiological studies by Gowan in 1959 (Gowans, 1959). Detailed study of endothelial function first became feasible with the development, in the 1970s, of techniques to culture ECs *in vitro* and as such

subsequent studies led to the current view of the endothelium as a dynamic organ that possesses vital secretory, synthetic, metabolic and immunologic functions (Aird, 2004).

Endothelial cells line every blood vessel in the body, forming a continuous monolayer of cells linked to each other by different types of adhesive structures or cell-to-cell junctions. These are complex structures formed by transmembrane adhesive molecules and 3 types of junctions have been identified in EC: tight junctions, adherens junctions and gap junctions (Bazzoni and Dejana, 2004). Gap junctions are communication structures which allow the passage of small molecular weight solutes between neighbouring cells (Figueroa and Duling, 2009). Tight junctions serve the major functional purpose of providing a barrier function between vessels and circulating blood and adherens junctions play an important role in regulating endothelial permeability to circulating leukocytes and solutes (Wallez and Huber, 2008).

Endothelial cells play a wide variety of critical roles in the control of vascular function. This includes control of coagulation and thrombosis, regulation of vascular tone and participation in inflammatory reactions. The surface of healthy endothelium is both anticoagulant and antithrombotic (Pearson, 1999). This occurs, in part, through the production of anti-thrombotic mediators, such as prostaglandins and nitric oxide (NO)(West et al., 2001, Buttery et al., 1996), facilitating an anti-thrombotic surface in which blood and cellular constituents can pass with ease. Haemostasis is a defence mechanism against vessel wall injury and bleeding and is triggered by a response to damage of the vessel wall by the exposure of blood to subendothelial tissue. Von Willebrand Factor, a blood glycoprotein, acts as a bridge between platelets and tissue, binding to collagen exposed at sites of vascular injury and to the platelet membrane glycoprotein Ib-V-IX. This leads to the formation of a platelet plug allowing the initial sealing of the vascular lesion. Prostacyclin (PGI_2), a prostaglandin member of the eicosanoid family of lipid molecules, inhibits platelet activation, thus promoting anti-thrombotic effects (Smith et al., 1980). PGI_2 performs its function through a paracrine signalling cascade that involves G protein-coupled receptors on nearby platelets and endothelial cells. Activation of the PGI_2 receptor leads to production of cAMP and inhibition of platelet activation and

hence aggregation (Majed and Khalil, 2012). The effect of PGI_2 is enhanced by nitric oxide (NO) (Davidge et al., 1995). NO is a heterodiatomic free radical product generated through the oxidation of L-arginine to L-citrulline by NO synthases. NO inhibits platelet adhesion and activation, in part, through a cyclic-GMP dependent mechanism within platelets (Loscalzo, 1998). In addition, it has been shown that NO can inhibit phosphoinositide 3-kinase (PI3K) activity induced by thrombin activation, an effect that reduces platelet thrombin stability by promoting dissociation of fibrinogen from its platelet surface receptor (Loscalzo, 1998).

In the quiescent state endothelial cells maintain blood fluidity by promoting the activity of numerous anticoagulant pathways. One of the main pathways is the C/protein S pathway, which involves two vitamin K-dependent plasma proteins that work in concert as a natural anticoagulant system. This pathway is initiated when thrombin interacts with the endothelial cell receptor thrombomodulin leading to binding of protein C to protein S and subsequent activation of protein C. Activated protein C inactivates two essential blood coagulation factors: factors VIIIa and Va (Michiels, 2003). Additionally, the endothelial cell surface also contains rich heparin-like glycosaminoglycans which bind antithrombin and can thus inactivate active thrombin, further decreasing the anticoagulant pathways and allowing the smooth flow of blood within the vessels (Michiels, 2003).

Finally, endothelial cells can also regulate vascular tone. Furchgott and Zawadzki (Furchgott and Zawadzki, 1980) demonstrated that the relaxation of vascular smooth muscle cells in response to acetylcholine is dependent on the integrity of the endothelium. It was later discovered that both PGI_2 and NO, in addition to their anti-thrombotic effects, can also mediate relaxation of blood vessels via the endothelium. PGI_2 was shown to relax the underlying smooth muscle cells through activation of adenylate cyclase and subsequent generation of cAMP while NO, produced from EC, diffuses to vascular smooth muscle cells where it stimulates soluble guanylate cyclase, resulting in an increased formation of cyclic GMP and subsequent relaxation (Sandoo et al., 2010).

1.2.2 Smooth Muscle Cells

Vascular smooth muscle cells (VSMC) are integral components of the blood vessel wall. These highly specialised cells provide structural integrity and regulate blood vessel diameter by contracting and relaxing dynamically in response to vasoactive stimuli, which enables blood vessels to maintain an appropriate blood pressure. (Marchand et al., 2012). However, vascular SMCs also perform other functions which become progressively more important during vessel remodelling following vascular injury. This requires the SMC to switch from a contractile SMC to a synthetic SMC phenotype, allowing SMC proliferation and migration (Figure 1-3). This is promoted by the SMC microenvironment reviewed in Section 1.5. At the contractile extreme are SMCs with fully functional contractile machinery. These SMCs are typically composed of tightly bundled myofilaments and minimal rough endoplasmic reticulum, golgi or free ribosomes (Beamish et al., 2010). In culture these SMCs possess a strict uniform morphology. At the synthetic extreme are fibroblast-like SMCs with minimal contractile proteins which secrete extracellular matrix (ECM). The contractile and synthetic phenotypes represent the two ends of the SMC phenotypic spectrum and intermediate phenotypes can also be observed which have different morphologies. Phenotypic switching of SMCs and the role of this process in vascular pathology will be reviewed in detail in Section 1.5.

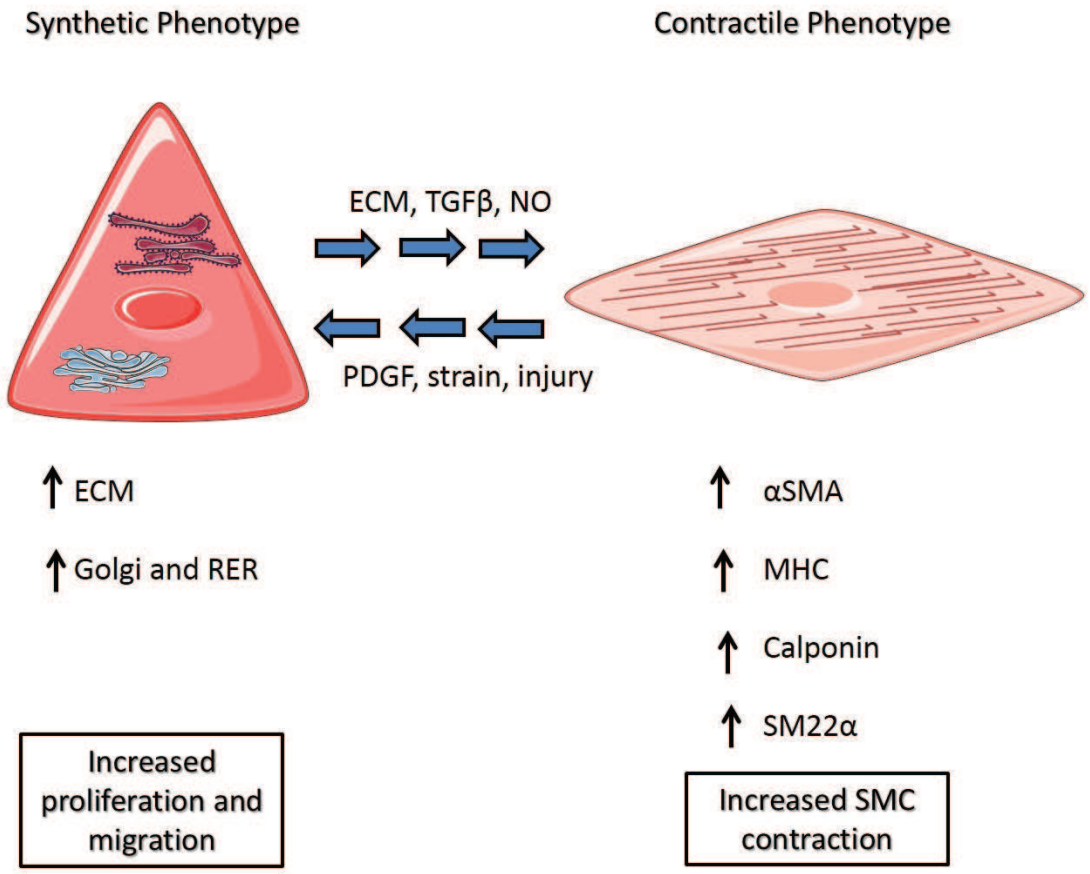

Figure 1-3: Schematic of SMC phenotypic switching.
SMC are not terminally differentiated and can switch between a contractile and synthetic phenotype. Synthetic SMC exhibit greater production of ECM and enhanced proliferation and migration while contractile SMC exhibit a full repertoire of contractile machinery such as MHC and SM22α. Typically contractile SMC exhibit a more uniform morphology with synthetic SMC looking 'fibroblast' like. Factors such as PDGF and mechanical strain promote a synthetic phenotype while factors such as ECM and NO promote a more contractile SMC.

VSMCs lack the striated band pattern observed in cardiac and skeletal muscle and the contractile state of these SMCs is controlled by the microenvironment orchestrated by hormones, autocrine/paracrine agents and local chemical signals (Tabas et al., 2015). SMCs contract in order to regulate blood pressure and tone by utilising cross-bridge cycling between actin and myosin filaments in response to changes in Ca^{2+} (Rhee and Brozovich, 2000). Smooth muscles are typically defined by their expression of key contractile proteins such as Alpha smooth muscle actin (αSMA), myosin heavy chain (MHC) and SM22α.

αSMA is a 42 kDa protein, encoded by ACTA2 gene, and is the actin form that predominates within vascular smooth muscle cells and contributes to vascular motility and contraction. αSMA is located primarily in the microfilament bundles of vascular SMCs, is a major constituent of the SMC contractile machinery and is the single most abundant protein (40 %) within smooth muscle cells (Skalli et al., 1986). αSMA is the first SMC differentiation marker to appear during development, although it is also transiently expressed in the myocardium and skeletal muscle during the development of the embryo and is expressed in myofibroblasts during wound healing (Rensen et al., 2007). As such, a single marker is not sufficient to provide definitive evidence of a SMC lineage. Mature SMCs express a number of myosin isoforms, each representing an essential component of the contractile mechanism. Out of all the isoforms, MHC SM-1 (204 kDa) and -2 (200 kDa) are the most rigorous markers for differentiated SMCs. The expression of MHC-SM is completely restricted to SM tissue and is developmentally regulated (Nagai et al., 1989). SM-1 is found in vascular SMCs from the late fetal stage through adulthood (Kuro-o et al., 1989) while SM-2 appears only in fully differentiated SMCs after birth (Kuro-o et al., 1989). SM-1 and SM-2 are splice variants and specific knockdown of these variants results in smooth muscle cells that adopt a proliferative state (Kim et al., 1993). Interestingly neointimal cells in balloon-injured rabbit aortas express SM1 but not SM2, indicating that these cells resort to expression of fetal gene networks (Aikawa et al., 1997). SM22α, also known as transgelin, is a smooth muscle cell cytoskeletal protein. SM22α directly interacts and co-localises with F-actin, thus participating in the organisation of the actin cytoskeleton in differentiated VSMCs (Kobayashi et al., 1994). SM22α transcripts can be detected in vascular smooth muscle cells in mouse embryos from around embryonic day (E) 9.5 and

thereafter show continued expression in all smooth muscle cells into adulthood (Li et al., 1996). These SMC contractile markers are decreased in SMC of a synthetic phenotype. SMCs with different phenotypes typically express varying levels of these protein markers rather than the complete disappearance of these proteins (Rensen et al., 2007). As such multiple protein markers along with complementary data on morphology and proliferation characteristics is required to distinguish between a contractile and synthetic SMC (Rensen et al., 2007).

1.3 Atherosclerosis

Atherosclerosis, a multifactorial disease involving both genetic and environmental factors, is one of the greatest causes of mortality within the western world (Faxon et al., 2004).

Evidence of atherosclerosis has been reported as far back as the pharaohs of Egypt (David et al., 2010), however for the past 160 years scientists have puzzled over the mechanism by which atherosclerotic lesions form. Rudolf Virchow proposed in 1856 that atherosclerosis was caused when plasma components, including lipids, initiated an inflammatory response in the arterial wall (Zarifis, 2005). Despite this proposition, many believed that atherosclerosis was a cholesterol storage disease, characterised by the collection of cholesterol and thrombotic debris in the artery wall. The term ‘atherosclerosis’, derived from the Greek words ‘athere’, meaning gruel (accumulation of lipid) and ‘sclerosis’ meaning hardening (Singh et al., 2002) was first introduced by Felix in 1904 and it was suggested that atherosclerosis was responsible for almost all obstructive processes in the arteries (Mehta and Khan, 2002). This was quickly followed by the first key piece of evidence that atherosclerosis could be induced in laboratory animals. Ignatowski, in 1908, demonstrated that rabbits fed a diet enriched in animal proteins (mainly meat, milk and egg yolk) formed lesions in their aortic walls (Konstantinov and Jankovic, 2013). Later, a Russian experimental pathologist, Anitschkow, used a cholesterol diet dissolved in vegetable oil to produce aortic atherosclerosis in rabbits similar to those seen in humans (1983) and suggested that atherosclerosis is characterised by the accumulation of lipids within sub-endothelial regions and subsequently leads to narrowing of the vessel and reduction in blood flow (Singh et al., 2002, Konstantinov et al., 2006). Anichkov’s elucidation of the role of cholesterol in

the pathogenesis of atherosclerosis is often referred to as one of the greatest discoveries of the 20th century. These pioneering studies provided the first experimental evidence and basis for the establishment of the 'lipid hypothesis' of atherosclerosis. Since then various animal species, such as rabbits, mice, rats, guinea pigs, hamsters, birds, dogs and non-human primates have been used for experimentation. These have provided crucial information about the pathologicall mechanisms underlying the initiation and subsequent development of atherosclerotic plaques. With time, improvements have occurred in modern immunology and molecular techniques and, as such, the process of atherosclerosis and the underlying risk factors have now been well studied (reviewed below in section 1.3.1).

1.3.1 Clinical presentation, epidemiology, atherosclerosis progression, risk factors and gender differences

In most cases atherosclerosis will remain symptomless until the artery is severely narrowed or totally blocked. In either case, the symptoms are dependent on which arteries are affected. Blockage of the coronary artery will result in chest pain and, if the artery is sufficiently blocked, will result in myocardial infarction, the main cause of atherosclerosis associated mortality. Additionally, atherosclerosis can occur in other arteries such as the carotid artery. The carotid artery supplies blood to the brain and blockage of this artery will result in stroke and, if severe, will result in mortality.

Epidemiological research relating to atherosclerosis has been studied and reviewed by the British Heart Foundation. In 2012, atherosclerosis and subsequent myocardial infarction or stroke, accounted for 80,000 deaths in the UK. The death rates vary substantially, with highest levels reported in Scotland and the North of England and lower levels in the South of England. It was also reported that 1 in 5 men and 1 in 7 women die as a cause of atherosclerosis; these gender differences are attributed to the difference in how risk factors affect men and women and are reviewed below. Additionally, higher mortality rates are associated with lower socio-economic groups (BHF cardiovascular statistics 2012).

Evidence of atherosclerosis has been found in autopsies of teenagers and young adults (Berenson et al., 1992), suggesting that the process of atherosclerosis development can start early in life. Several risk factors are known to predispose to atherosclerosis and have been elucidated from large scale epidemiological studies over the past 50 years. These risk factors were initially identified in the Framingham Study, the 1st study to ever identify cardiovascular risks (Kannel et al., 1961). The study was initiated in the middle of the 20th century by Dr Thomas R Dawber. Arterial endothelium changes rapidly in response to stimuli and on the basis of animal experiments and observations in human specimens, most data suggests that atherosclerosis is caused by an initial change in the monolayer of endothelial cells that lines the inner arterial surface (Cines et al., 1998). The endothelium, under normal homeostatic conditions, exhibits little or no expression of pro-inflammatory factors (See section 1.2.1). However, damage or excessive activation of endothelial cells can lead to endothelial dysfunction. Endothelial injury/dysfunction is the first stage in the atherosclerotic process. This results in chronic inflammation, loss of antithrombotic factors and an increase in vasoconstrictor and pro-thrombotic gene products followed by uptake of lipids into the vessel wall, vessel remodelling and eventually plaque calcification (Rajendran et al., 2013). Figure 1-4 highlights the process of atherosclerosis development and each stage will be discussed below. The initiating factor of atherosclerosis, endothelial dysfunction, can result from several factors including generic cardiovascular risk factors such as smoking, hypertension and high cholesterol and shear stress.

Smoking represents one of the most important preventable risk factors for the development of atherosclerosis. Studies have shown an increased risk of developing myocardial infarctions, due to atherosclerosis, at all levels of cigarette smoking, and increased risks have been demonstrated even in persons who smoked fewer than five cigarettes per day (Rosengren et al., 1992), (Bjartveit and Tverdal, 2005). Additionally, mortality studies conducted in 1960 and 1970 showed an increase in myocardial infarction mortality significantly correlated with an increase in the number of cigarettes smoked per day, regardless of the actual number (Doll and Peto, 1976). In 2004, a longitudinal study was published that utilised serum levels of cotinine, a nicotine metabolite, as a biomarker of cigarette exposure. The patients enrolled in this study were

non-smokers but were involuntarily exposed to cigarette smoke. Nicotine exposure was examined by quartiles of blood cotinine as follows: less than or equal to 0.7 nanograms per milliliter (ng/mL), 0 to 1.4, 1.5 to 2.7, and 2.8 to 14.0. The number of cardiovascular events, which included deaths and non-fatal myocardial infarctions, were significantly increased at all upper quartiles compared with the lowest exposure quartile, after adjustment for other established cardiovascular risk factors (Whincup et al., 2004). This suggests that not only smoking, but also passive smoking can alter the risk of cardiovascular events. Interestingly, cigarette smoking has been associated with higher levels of myocardial infarction, associated with atherosclerosis, in women than in men (Mons et al., 2015). Cigarette smoke contains approximately 4000 different chemicals; the effects of many on the human body still remain unknown. It is highly likely that it is not one single chemical but a combination of chemicals that is responsible for atherosclerotic disease initiation and progression. Evidence of vascular damage and endothelial dysfunction due to cigarette smoke has been shown in an array of clinical studies analysing endothelial function using various techniques. Zeiher et al, demonstrated that continuous smoking impairs flow mediated dilation of coronary arteries in a dose-dependent manner (Zeiher et al., 1995). Additionally, inflammation is known to constitute an essential element in atherogenesis. Smoking activates the immune system both systemically and locally. Smokers have been shown to have significantly elevated white blood cell counts, which was tightly correlated to the formation of carotid atherosclerotic plaques (Ishizaka et al., 2004). Furthermore, reports document that smokers have significantly increased serum levels of proinflammatory cytokines, such as tumor necrosis factor α and interleukin-1ß which have been shown to activate key inflammatory pathways known to potentiate atherosclerosis progression (Barbieri et al., 2011). Serum C-reactive protein, a widely accepted marker for the occurrence of inflammation, has also been found to be increased in smokers when compared to non-smokers (Wannamethee et al., 2005). Finally, leukocyte recruitment following endothelial dysfunction is an essential part in the initiation of atherosclerotic plaque development. Cavusoglu et al (Cavusoglu et al., 2004) showed that smoking increased plasma concentrations of vascular cell adhesion molecule-1 (VCAM-1). This data, therefore, suggests that cigarette smoke can have profound effects on multiple key pathways involved in atherosclerosis progression.

Emerging data implicate increases in systemic oxidative stress and vascular inflammation in the pathogenesis of hypertension and reductions in both have been shown to reduce endothelial dysfunction (Widlansky et al., 2003). Mechanistic studies utilising mouse carotid arteries exposed to increasing intraluminal pressure, showed reductions in endothelium-dependent vasodilation to acetylcholine and increase in NADPH oxidase activity (Vecchione et al., 2009). This imbalance of NAPDH expression has been linked with increased production of O_2^-, a key reactive oxidant species (ROS). Additionally it has been shown that production of this superoxide leads to endothelial eNOS uncoupling and amplification of ROS production (Landmesser et al., 2003). O_2^- has been shown to induce the oxidation of LDL, reviewed below, thus potentiating the process of atherosclerosis (Rueckschloss et al., 2001). These results have been confirmed in experimental animal models. Mice deficient in key aspects of the NADPH oxidase pathway crossed on to an ApoE (apolipoprotein E) $^{-/-}$ background have shown that NADPH oxidase deficiency retards the development of atherosclerotic lesions in the mouse aorta (Barry-Lane et al., 2001). Taken together this shows that hypertension associated ROS potentiates atherosclerosis development. Interestingly, systolic blood pressure rises more steeply in ageing women compared with men, and this may be related to the decline in oestrogen levels in menopause transition (Barton and Meyer, 2009). After menopause there is an upregulation of the renin-angiotensin system, with an increase in plasma-renin activity. Salt sensitivity and sympathetic activity are also increased in postmenopausal compared with premenopausal women. This suggests that post menopause, women may be of greater atherosclerotic risk due to increased blood pressure.

Cholesterol exists in everyone's diet. It can slowly be absorbed into intestine lymphatic vessels through gastrointestinal (GI) tract and enters the blood through the mucosa of the digestive system. Cholesterol is then transported to and from cells via low-density lipoprotein, LDL, and high-density lipoprotein, HDL. Data has shown that there is a direct relationship between (Xin et al.) LDL and atherogenesis. The Lipid Research Clinics Coronary Primary Prevention Trial, which was published in 1984, was one of the first studies to highlight that therapeutic interventions to lower cholesterol levels resulted in reduced risk of cardiovascular morbidity or mortality (Probstfield and Rifkind, 1991). Increased

LDL promotes accelerated atherosclerosis as greater levels are taken up into the plaque. Interestingly, at younger age, the relative risk of hypercholesterolaemia is lower in women compared with men. During menopause, total cholesterol and low-density lipoprotein (LDL) levels rise by 10 and 14 % respectively. This is in agreement with reports that men, at an earlier age, are more susceptible to atherosclerosis than women and that women, on average, develop atherosclerosis 7-10 years later than men (Maas and Appelman, 2010).

Shear stress, the frictional effect of blood force, can affect endothelial integrity, especially when blood flow is disturbed. Altered arterial haemodynamics around vessel curvatures and at bifurcations, in addition to systemic risk factors (Wang et al., 2016b), leads to the formation of complicated plaques. For example, atherogenesis is promoted by decreased shear stress (<5 dynes/cm^2) because it is associated with reduction in several vascular wall functions including endothelial nitric oxide synthase production (Cheng et al., 2005), vasodilatation and endothelial cell repair (Chiu and Chien, 2011). Additionally, reactive oxygen species (ROS), produced from sites of injury and inflammation, are highly damaging to endothelial cells (Panth et al., 2016).

A number of studies have demonstrated that endothelial injury induces activation of several inflammatory pathways, the second key stage of atherosclerosis. One example is the increase in nuclear transcription factor κB (NFκB) resulting in increased expression of inflammatory cytokines such as IL1α, TNF-α and MCP-1 (Lawrence, 2009). This promotes the expression of adhesion molecules that allow the capture of leukocytes to the endothelial surface and increases vessel permeability, allowing circulating inflammatory cells such as monocytes and lymphocytes to penetrate into the intima (Figure 1-4B). In addition to the recruitment of inflammatory cells, parallel changes in endothelial permeability and the composition of the extracellular matrix beneath the endothelium promote the entry and retention of cholesterol-rich low-density lipoprotein (LDL) particles in the artery wall. (Figure 1-4B). Once within the vessel wall LDL can become oxidised through the action of free radicals, such as O_2^- generated via sheer stress and increased by cigarette smoke, or direct activity of leukocytes, to become oxidised LDL (ox-LDL).

Oxidized LDL is particularly atherogenic and is chemotactic for macrophages. This early atherosclerotic plaque is termed a ‘fatty streak’ (Mitra et al., 2011).

Once resident within the artery wall, monocytes can differentiate into tissue macrophages. In the atheroma, these mononuclear phagocytes engulf LDL particles and become foam cells, a term that reflects the microscopic appearance of these lipid-laden macrophages (Figure 1-4B) (Yu et al., 2013). Uptake of LDL renders the macrophages less mobile, thereby promoting the accumulation of these lipid-laden cells in the intima (Yu et al., 2013). Foam cells maintain their metabolic activity, releasing inflammatory cytokines such as interleukin 1 (IL1α) and tumour necrosis factor (TNF)(McLaren et al., 2011) that further promote the recruitment of inflammatory cells but also stimulate the migration of smooth muscle cells from the media into the intima (Figure 1-4C) where these SMC proliferate in response to mediators such as platelet-derived growth factor (PDGF) (Rudijanto, 2007). The accumulation of foam cells, monocytes, macrophages and smooth muscle cells leads to the rapid growth of the atherosclerotic plaque and protrusion into the lumen of the vessel (Figure 1-4C).

In the intima, the SMCs produce extracellular matrix molecules and form a fibrous cap that covers the plaque (Sukhovershin et al., 2016). This cap typically covers a collection of foam cells, some of which die and release lipids that accumulate extracellularly. The inefficient clearance of dead cells can promote the accumulation of cellular debris and extracellular lipids, forming a lipid-rich pool called the necrotic core of the plaque (Figure 1-4D) (Seimon and Tabas, 2009). Not all atherosclerotic plaques are identical, and it appears that there are substantial differences in the stability of plaques. One such mechanism of stability is through plaque calcification. The process can begin early and accelerates as the disease progresses and more complex lesions develop. Coronary artery or carotid artery calcification can be detected independently by computed tomography and calcification of plaques can predict an increased likelihood of adverse coronary events. The characteristics of atherosclerotic plaques have been extensively studied and as such plaques can now be classified into vulnerable or stable depending on their composition (see Table 1.1).

Interestingly, it has been shown that vessels with developing atherosclerotic plaques can undergo outward ‘positive’ remodelling, where the external elastic lamina expands, or inward ‘negative’ remodelling where the external elastic lamina shrinks at the site of the plaque (Hermiller et al., 1993, Nishioka et al., 1996). Reduction in lumen area is higher in negatively remodelled vessels than positively remodelled vessels (Nishioka et al., 1996, Pasterkamp et al., 1995). Conversely, atherosclerotic plaques with positive remodelling have been shown to contain larger lipid and macrophage content (Varnava et al., 2002).

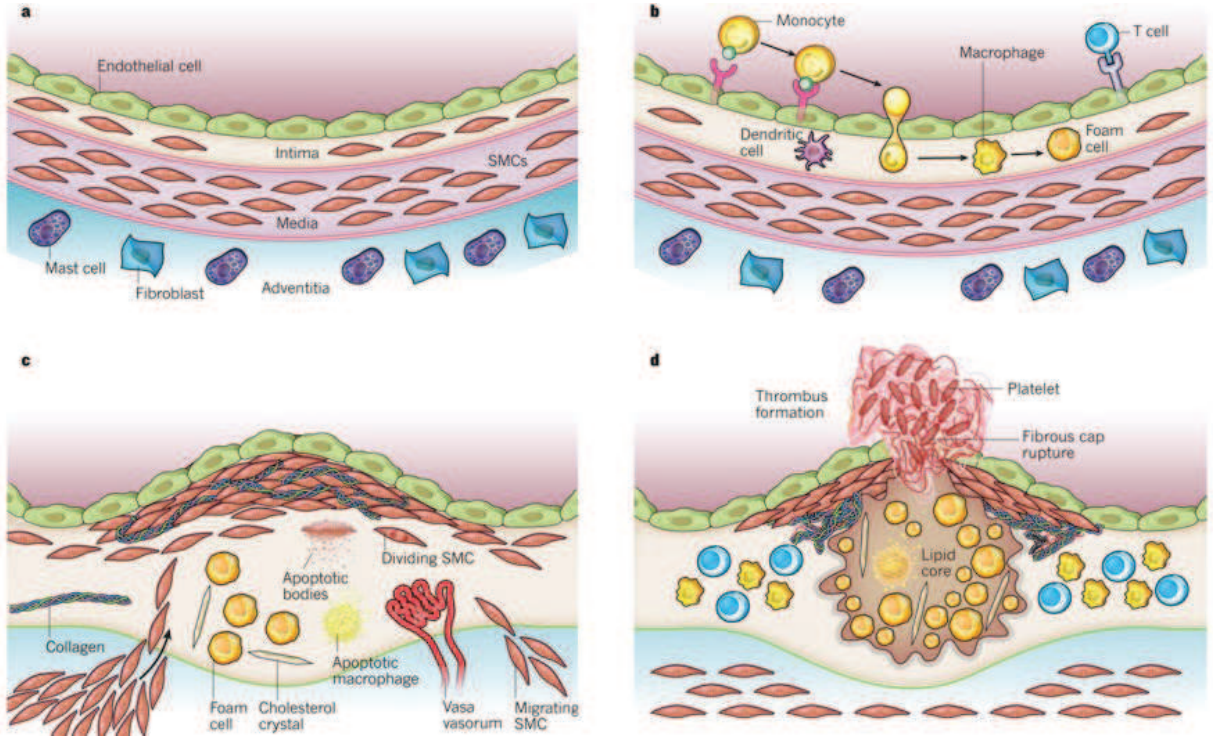

Figure 1-4: Progression of an atherosclerotic lesion.
(A): Normal healthy artery. (B): The initial steps of atherosclerosis include adhesion of blood leukocytes to the activated endothelial monolayer, directed migration of the bound leukocytes into the intima, maturation of monocytes (the most numerous of the leukocytes recruited) into macrophages, and their uptake of lipid, yielding foam cells. (C): Lesion progression involves the migration of SMCs from the media to the intima, the proliferation of resident intimal SMCs and media-derived SMCs, and the heightened synthesis of extracellular matrix macromolecules such as collagen, elastin and proteoglycans. Plaque macrophages and SMCs can die in advancing lesions, some by apoptosis. Extracellular lipid derived from dead and dying cells can accumulate in the central region of a plaque, often denoted the lipid or necrotic core. Advancing plaques also contain cholesterol crystals and microvessels. (D): Thrombosis, the ultimate complication of atherosclerosis, often complicates a physical disruption of the atherosclerotic plaque. Shown is a fracture of the plaque's fibrous cap, which has enabled blood coagulation components to come into

contact with tissue factors in the plaque's interior, triggering the thrombus that extends into the vessel lumen, where it can impede blood flow. Taken from (Libby et al., 2011).

Table 1-1: Characteristics of Vulnerable Atherosclerotic Plaque.
Adapted from (Halvorsen et al., 2008).

Features	Vulnerable Plaque	Stable Plaque
Fibrous Cap	-	+
Lipid-rich core	+	-
Inflammation	+	-
Haemorrhage	+	-
Calcification	-	+
Matrix remodelling	+	-
Necrosis	+	-
Apoptosis	±	±

Plaques are prone to rupture and vulnerable plaque consists of a large necrotic core surrounded by a thin (<65 μm) fibrous cap which is heavily infiltrated by macrophages and absent of SMCs. This well-characterized lesion is considered to be of greater susceptibility of plaque rupture (Bentzon et al., 2014). Physical disruption of the plaque is most commonly caused by a rupture of the fibrous cap. This leads to the exposure of pro-coagulant material in the plaque's core to coagulation proteins in the blood, triggering thrombus formation and ultimately impeding blood flow (Bentzon et al., 2014).

Recently it has been documented that more vulnerable plaques are associated wuth a reduced number of SMC relative to inflammatory lipid-loaded macrophages, particularly in the area of the fibrous plaque (Tabas et al., 2015). However, it is difficult to definitively determine which cells are SMC derived and which are macrophage derived. As such, lineage tracing experiments are beginning to arise. SMC lineage tracing in atheroprone Apoe−/− mice revealed that in advanced lesions, intimal SMCs lacked detectable expression of smooth muscle α-actin and smooth muscle myosin heavy chain (Gomez et al., 2013). Additionally, cholesterol loading of cultured SMCs was reported to down-regulate SMC marker genes and induce macrophage markers, including CD68 and Mac2 (Rong et al., 2003).

Depending on the stage of progression, atherosclerotic lesions can be classified into 6 groups. The initial (type I) lesion contains a small proportion of LDL which promotes an increase in macrophages and formation of scattered foam cells. As in subsequent lesion types, the changes are more marked in locations of arteries with adaptive intimal thickening. Type I lesions do not protrude into the lumen and therefore do not alter blood flow (Stary et al., 1995). Type II lesions consist primarily of layers of foam cells, lipid-laden smooth muscle cells and include lesions designated as fatty streaks (Stary et al., 1995). Type III is the intermediate stage between type II and type IV (symptom-producing lesions) (Stary et al., 1995). In addition to the lipid-laden cells of type II, type III lesions contain scattered collections of extracellular lipid droplets. This extracellular lipid is the immediate precursor of the larger and more disruptive core of extracellular lipid that characterises type IV lesions. Beginning around the fourth decade of life, lesions that usually have a lipid core may also contain thick layers of fibrous connective tissue (type V lesion) and thrombus (type VI lesion) (Stary et al., 1995). Some type V lesions are largely calcified (type Vb), and some consist mainly of fibrous connective tissue and little or no accumulated lipid or calcium (type Vc) (Halvorsen et al., 2008).

1.3.2 Treatment of atherosclerosis

Treatments for atherosclerosis depend on the severity and size of the atherosclerotic plaque. Small plaques can typically be stabilised with lifestyle changes such as healthy heart approach or through the use of medicinal therapies such as statins, anti-thrombotics of ACE inhibitors. The healthy heart approach aims to improve patient lifestyle through the cessation of smoking, increased exercise and reduction in cholesterol levels via improved eating habbits.

The 4S trial, published in 1994 (Pedersen et al., 1994), was the first trial to demonstrate improved survival in coronary heart disease patients through the utilisation of statins. Since then, several studies have documented a clear reduction in cardiovascular events with statin treatment in different settings. Statins reduce LDL levels and the benefits are clear, however the effect of statins on atherosclerotic plaques composition have not yet been fully elucidated. Nevertheless, a few imaging studies have highlighted that statin use

might result in atherosclerotic plaque regression as early as 6 months after initiation of therapy (Lima et al., 2004), (Nissen et al., 2006). This observation may be due to a reduction in LDL cholesterol levels within the plaque core.

Experimental evidence suggests that in animal models of atherosclerosis it is possible to blunt the development of atherosclerotic via utilisation of ACE inhibitors. For example it was shown that 9 months of captopril treatment, a key ACE inhibitor, in hyperlipidaemic rabbits reduced the total aortic intimal area affected by atherosclerosis, as well as the cholesterol content of the lesion (Curzen and Fox, 1997). In humans, long term ACE inhibition significantly reduces mortality, myocardial infarction and stroke as well as reduces the intima to media ratio of carotid arteries in patients at high risk for cardiovascular events (Germing, 2005). ACE inhibitors have been shown to improve NO availability and reduce ROS, resulting in improved vascular function.

Despite improved lifestyle and drug therapies, if the atherosclerosis is severe and the plaque causes narrowing of the lumen to a degree in which blood flow through the coronary artery is significantly impaired, then intervention procedures and surgery are required.

1.3.2.1 Balloon angioplasty and stenting

Coronary angioplasty, conceptually described by Dotter and Judkins in 1964, was first performed by Andreas Gruntzig in 1977 (Hor et al., 1980). Since then percutaneous management of obstructive coronary artery disease (CAD) has expanded greatly. The technique involves insertion of a balloon catheter into the artery to disrupt the atherosclerotic plaque through displacement. This action results in stretching of the adventitia thereby increasing the lumen diameter in the treated vessel. There is no doubt that balloon angioplasty was a revolutionary technique, however it did have its own drawbacks, especially arterial recoil. As such, the procedure has since evolved to include the deployment of metallic support, known as a bare metal stent (BMS), to prevent the vessel closing and recoil from occurring. Although stent deployment was shown to reduce arterial recoil following balloon angioplasty, they were also limited by drawbacks. These stents had high metallic properties and were therefore treated as foreign objects by the body. This resulted in increased sub-

acute stent thrombosis. In 1993, two landmark trials, the Belgium Netherlands Stent Arterial Revascularisation Therapies Study (BENESTENT) and the North American Stent Restenosis Study (STRESS), both highlighted the superiority of bare metal stents over balloon angioplasty and establishing stent implantation as an accepted standard for revascularisation.

However, follow up studies investigating 115 lesions in 103 patients at implantation of stents and following 5.4 ± 3.8 months eventually found that between 20-30 % of patients receiving balloon-expandable bare metal stents had angiographic evidence of restenosis, caused by smooth muscle cell proliferation and migration, 6 months after surgery (Fischman et al., 1994).

As such, stents have now undergone incessant refinement, leading to the development of drug eluting stents (DES) introduced in 2001 and designed to release anti-proliferative agents at the site of arterial injury to attenuate neointimal formation. DES were composed of a stainless steel stent platform coated with durable polymer-releasing anti-proliferative drugs. Despite improvements in restenosis these DES led to an increase in very late stent thrombosis due to delayed re-endothelialisation or a hypersensitivity reaction to the stent polymer (Daemen et al., 2007). As such new polymers and the utilisation of thinner stent struts have been employed, however, delayed re-endothelialisation and stent thrombosis still remain a problem.

1.3.2.2 Coronary artery bypass grafting

Coronary artery bypass grafting (CABG) is defined as open heart surgery where a section of blood vessel, typically the saphenous vein, is grafted from the aorta onto the coronary artery in order to “bypass” a blocked section of artery. This fundamentally restores perfusion to the myocardium. The first ever bypass graft was performed in 1950 at McGill University in Montreal, QC, Canada, where Vineburg and Buller implanted the internal mammary artery into the myocardium to treat cardiac ischemia and angina (Shrager, 1994). Shortly after this Sidney Smith in 1955 harvested the first ever saphenous vein and was capable of grafting this from the aorta to the myocardium (Diodato and Chedrawy, 2014).

In April 2012, the results of the ASCERT trial were published in the New England Journal of Medicine. This study examined nearly 190,000 patients of 65 years or older with two or three vessel disease. 86,244 underwent CABG and 103,549 underwent PCI. At 1 year post surgery, no difference in the mortality rate was evident amongst the 2 treatment groups, however, at 4 years post-surgery a significantly lower mortality rate was observed for the CABG group (16.4 % versus 20.8 %).

Multiple conduits can be used to perform CABG and establish cardiac revascularisation. The internal mammary artery is the conduit of choice due to their long term patency and reduced rate of developing atherosclerosis (de Vries et al., 2016). However, due to the increasing number of patients requiring multiple bypass grafts, saphenous vein is typically the vessel of choice owing to its length and ease of access. In 2012 17,000 CABG operations were performed in the UK (Bhatnagar et al., 2015). Despite a slight drop in the number of CABG surgeries from the early 2000's, CABG, typically with saphenous vein, remains the standard revascularisation care for patients with multi-vessel disease (Diodato and Chedrawy, 2014). However, the disadvantage of using saphenous vein is their declining patency: between 10-25 % will occlude within 1 year of CABG. An additional 1 % to 2 % occlude each year within years 1-5 post-surgery and 4 % to 5 % occlude each year between 6 and 10 years post-surgery(Fitzgibbon et al., 1996). Saphenous vein graft failure (SVGF) can be divided into 3 temporal categories. 1: early (0-30 days), midterm (30 days-1 year) or long term (after 1 year). Early SVGF is typically due to thrombosis of the vein graft or surgical problems while midterm SVGF is typically due to intimal hyperplasia.

1.3.3 Carotid Endarterectomy

The endarterectomy procedure was developed and performed by surgeon Joao Cid dos Santos at the University of Lisbon in 1946. Later, surgical intervention to relieve atherosclerotic obstruction of the carotid arteries was successfully performed by Michael DeBakey in 1953. Carotid endarterectomy is a surgical procedure to remove plaque from the carotid artery in an attempt to reduce the risk of stroke. Most often this is done through a longitudinal incision in the artery and removal of all plaque debris. The artery is then closed using sutures and a

patch to increase the size of the lumen. This procedure has since been shown to reduce the incidence of stroke in vulnerable patients.

1.3.4 Formation of in stent restenosis and neointimal formation

Research on the development of intimal hyperplasia is divided into two main regions: arterial restenosis caused by PCI or stenting and neointimal formation following implantation of a vascular graft. After vein engraftment, the grafted vein is subjected to different haemodynamic pressures than in the venous circulation. Additionally, implantation of a stent or the expanding of the carotid artery due to balloon angioplasty induces vessel damage. These altered vessel conditions ultimately lead to intimal formation (Figure 1-5). Despite the differences in venous and arterial vessels, it is generally accepted that the sequence of events leading to intimal formation is similar in both cases. Animal models and human post-mortem studies have demonstrated that the mechanisms underlying intimal hyperplasia are similar to those associated with wound healing (Bentzon et al., 2014).

As with atherosclerosis, intimal hyperplasia associated with vein grafting and stenting is initiated via endothelial injury. In the setting of vein grafting, engraft of the saphenous vein into an arterial pressure system results in shear stress and subsequent endothelial damage. On the other hand, stent deployment destroys the endothelial layer. As mentioned in section 1.2.1, healthy endothelial cells produce prostacyclin and NO, which inhibits SMC proliferation. Removal of these anti-proliferative agents promotes SMC proliferation. In addition to the loss of prostacyclin and NO, damaged EC also produce basic fibroblast growth factor (bFGF), which further potentiates SMC proliferation within the medial layer. The activation of these SMCs also leads to an increased production of ECM with proliferating SMC producing 4 to 5 times more ECM than that of a contractile SMC (Moore, 1981). The ECM layer is continually altering via matrix synthesis and by the actions of matrix metalloproteinases (MMPs). An intact ECM prevents SMC proliferation, however injury promotes the production of tissue-type plasminogen activator (tPA) which degrades the ECM and activates MMPs (Murphy and Docherty, 1992). The production of PDGF then promotes SMC proliferation from the medial layer into the intima (Reviewed in Section 1.7). This migration typically begins 4 days post injury and can continue up to 1 month post injury

(Moore, 1981). The next stage of the process involves intimal expansion. This is mainly due to continued SMC proliferation, SMC migration and ECM deposition (Lemson et al., 2000).

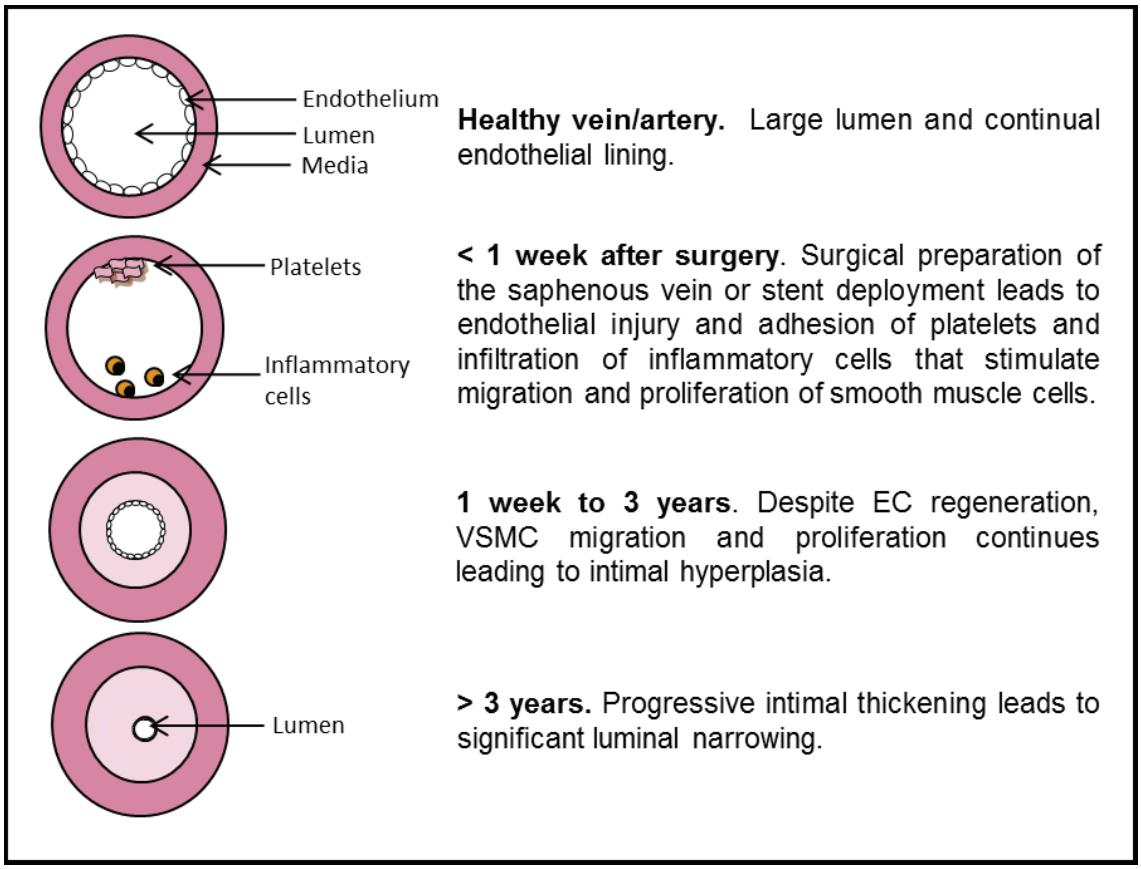

Figure 1-5: Progression of intimal hyperplasia.
Healthy veins of arteries consist of an intact endothelial layer and large luminal diameter. Stent deployment of surgical preparation of the saphenous vein promotes endothelial dysfunction and aggregation of platelets. This promotes the infiltration of inflammatory cells and the production of certain mitogenic factors that stimulate VSMCs to proliferate and migrate from the media into the lumen creating intimal hyperplasia. Despite reendothelialisation VSMC proliferation occurs resulting in significant luminal narrowing and the requirement for repeat surgery.

1.4 SMC cell cycle

The cell cycle is a complex process involved in the growth and proliferation of SMC. Cell division involves 2 processes: Mitosis (M), the division of a mother cell into 2 daughter cells and synthesis (S) in which the DNA is replicated in anticipation of mitosis (Bertoli et al., 2013). These phases are interrupted by gap phases (G_0, G_1 and G_2) which act as check point controls to ensure appropriate cell cycle occurs (Sechler and Schwarzbauer, 1998). An overview of cell cycle is shown in Figure 1.6. G_0 represents cells that are quiescent and non-proliferative. G_1 represents cells which are assembling the necessary factors required for DNA replication and represents a key check point in which cells reach a threshold, defined as a key point in which the cell is committed to DNA replication (Sechler and Schwarzbauer, 1998). During the gap between DNA synthesis and mitosis, the cell will continue to grow and produce new proteins. At the end of this gap is another control checkpoint (G_2 Checkpoint) to determine if the cell can now proceed to enter M phase and divide (Kastan and Bartek, 2004). During mitosis, cell growth and protein production stops. All of the cell's energy is focused on the complex and orderly division into two similar daughter cells (Schafer, 1998).

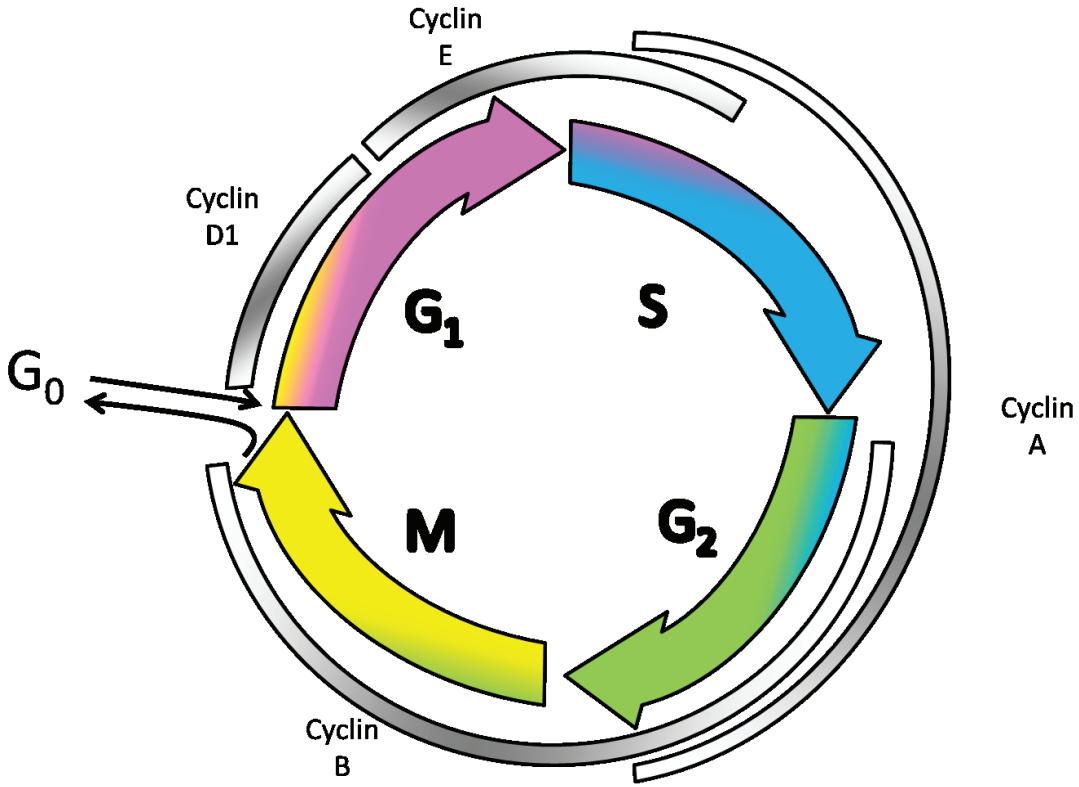

Figure 1-6: Cell cycle of SMC.

Schematic showing cell cycle phase-specific phases. S: synthesis phase. M: Mitosis phase. G1: Gap 1 phase and G2: Gap 2 phase. G0 are quiescent and non-proliferative cells. The progression of cell cycle is tightly regulated through specific cyclin proteins that are transcribed and translated at specific points during the cell cycle.

The progression of cell cycle is tightly regulated by the sequential expression, activation and inactivation of key cell cycle molecules. One group of molecules that is important for controlling cell cycle progression is the cyclins and cyclin-dependent kinase (CDK) complexes (Figure 1-7). CDKs are serine/threonine proteins kinases that are activated at key points during cell cycle and comprise a regulatory cyclin sub-unit and a catalytic CDK sub-unit (Suryadinata et al., 2010). CDKs are essential for cell cycle progression, as specific inactivation can prevent mitosis (Foley et al., 1999). Different cyclins bind to different CDKS during cell cycle inducing their activation. Thus, the expression pattern of cyclins determines CDK activation. Cyclins have no enzymatic activity and thus require CDK to exert their function. At present, 8 cyclin families have been identified (Dynlacht, 1997). They share homology in a 150 bp pair region known as the cyclin box that contains the binding site for specific CDKs (Ferreira et al., 1994). Cyclins also contain PEST sequences, protein motifs rich in proline (P), glutamate (E), serine (S) and threonine (T) which target them for ubiquitination and degradation (Rogers et al., 1986). It is therefore said that a cycling cell enters and exits cell phases in association with the synthesis and degradation of specific cyclins (Figure 1-7). Each of the cyclin-CDK complexes in a cell modifies a specific group of down-stream protein substrates required for the different cell cycle stages. In the G_2 and M phase this leads to the production of nuclear lamin (Ottaviano and Gerace, 1985) and microtubules (Okada et al., 2014) required for nuclear cytoskeleton assembly, while, in the G_1 phase retinoblastoma protein (pRb) is phosphorylated on multiple residues by as specific CKDs. Hyperphosphorylated pRb binds E2F, a known cell cycle transcription factor, rendering it unable for transcription (Dyson, 1998). When the specific cyclin is degraded E2F is freed and participates in cell cycle. 8 E2F family members are known, 3 of which act as activators: E2F1, 2 and 3a while the other 6 act as suppressors: E2F3b, E2F4-8 of cell cycle (Chong et al., 2009). All are involved in the regulation of cell cycle in mammalian cells and function by binding to TTTCCCGC consensus binding site in the target promoter sequence. The E2F family play a role in the control of transition from the G_1 to S phase of cell cycle via altered transcription of key cell cycle molecules.

Additionally, key inhibitors of cell cycle have also been studied. In G_1 and S phases the most well-known inhibitors are the p16 and p21 families. Both inhibit

specific CKDs by binding to the CKD before the attachment of cyclin, inhibiting the phosphorylation of downstream targets by the CDK-cyclin pair (Aprelikova et al., 1995).

Growth factors primarily act on cells in the G_1 and G_0 phase of cell cycle. Growth factors stimulate cells in G_0 to enter cell cycle, however, if the growth factor is removed early in the G_1 cycle then the cells will return to G_0. This is due to a restriction point mid-way between the G_1 phase. The restriction point is therefore the time at which the cell is committed to entering cell cycle and this is believed to be under the control of pRb, however, the exact mechanism is unknown (Weinberg, 1995).

1.5 SMC phenotypic switching

The fully differentiated SMCs of human vessels are typically quiescent and are characterised by a low proliferative index. However, unlike many mature cells in the adult body, they do not terminally differentiate and retain remarkable plasticity (Rzucidlo et al., 2007). In order to perform their diverse functions, VSMC may adopt a contractile or synthetic phenotype (Reviewed in section 1.2.2). Striking examples of SMC phenotypic switching are exhibited during vascular development when SMC display remarkable rates of proliferation and migration in order to form the circulatory system and during vascular disease where vascular injury promotes SMC proliferation and migration resulting in intimal hyperplasia. Although the term, phenotypic switching was originally based on morphological criteria, over the past several decades the term has been expanded to encompass the full range of possible alterations in functional and structural properties.

Smooth muscle cells, identified from within a vessel wall are not homogeneous. This was originally illustrated by immunohistochemical staining patterns of contractile SMC phenotypic markers. These revealed highly heterogeneous staining patterns and intensities between adjacent SMCs and these patterns became more distinct following vascular injury (Christen et al., 1999). Although it is known that contractile protein markers are reduced following vascular injury, the response is remarkably heterogeneous between the different SMCs in the vessel wall. Remarkably, a similar phenomenon is also observed with the re-

introduction of contractile genes at later time points, where these genes are not re-introduced uniformly (Regan et al., 2000). These observations have been further confirmed via *in vitro* culture of primary SMCs. Enzymatic digestion followed by protein analysis revealed that SMCs not only contain different amounts of these protein markers but some do not contain markers at all (Christen et al., 1999), (Rensen et al., 2007). Despite these SMCs existing within the same microenvironment, genetic programming may also influence the phenotypic state of individual SMCs.

The vast majority of research suggests that phenotypic modulation of the SMC is controlled actively and not simply by the loss of positive differentiation signals (Owens et al., 2004). This ultimately requires the activation of certain gene networks and has been proposed to be under the control of key environmental cues such as mechanical force, ECM components, ROS, EC and SMC interactions and growth factors.

Mechanical transduction, the transduction of physical forces into chemical signals can affect cellular behaviour. At the surface of the cell, numerous receptors have been shown to exhibit mechanosensitivity. Mechanical strain leads to activation of stretch-activated ion channels and changes in ion flux. Additionally, mechanical forces appear to enhance the expression of both ECM and contractile proteins by SMCs in the vessel wall (Reusch et al., 1996).

Although the effects of several biochemical factors have been implicated in SMC phenotype, it appears that the ECM in which the SMCs are embedded is of equal importance. The extracellular matrix that surrounds vascular cells is a highly organised structure composed of several macromolecules. ECM is made up of mainly type I and type III collagen isoforms, proteoglycans and elastins. Among these, heparin, mainly known for its anti-coagulant effects, has been shown to inhibit SMC proliferation and hence promote a contractile SMC both *in vivo* and *in vitro* cultures (Lindner et al., 1992). Heparin's antiproliferative activity may be related to disruption of exogenous or autocrine bFGF signalling (Lindner et al., 1992). However, heparin may also directly stimulate extracellular receptors and can be internalised allowing it to modulate cytoplasmic signalling pathways (Castellot et al., 1985). While most ECM components promote a contractile SMC state, fibronectin, another major ECM component stimulates cells towards a

more pro-migratory and pro-proliferative phenotype (Hedin et al., 1988). The authors found that the use of a recombinant peptide to inhibit fibronectin polymerisation reduced carotid intima by 63 %, media by 27 % and adventitial thickening by 40 % compared to the control peptide (Chiang et al., 2009). Additionally, hyaluronan (HA) a glycosaminoglycan which is present in the medial ECM, has also been shown to enhance proliferation and migration of SMCs. Moreover, the expression of HA is also implicated with the accelerated formation of atherosclerosis (Lorentzen et al., 2016).

Shear stress, caused by increased blood pressure, alters endothelial parameters such as NO and this is then sensed by smooth muscle cells. Endothelial cells co-ordinate the response of SMC to this mechanical stress. This not only occurs through NO production, but also via direct cell to cell interactions. Additionally, EC can produce and secrete certain microRNA known to regulate SMC phenotype (discussed in more detail in section 1.9).

Vascular insult promotes activation of the inflammatory cascade via increased expression of adhesion molecules such as selectins, vascular cell adhesion molecule-1 (VCAM-1), and intercellular adhesion molecule-1 (ICAM-1) in EC, thus promoting the adherence of inflammatory cell monocytes, leukocytes, neutrophils and macrophages (Manka et al., 1999). Following inflammatory cell infiltration and activation, these cells begin to produce cytokines. Most cytokines initiate a complex and varied repertoire of responses on SMCs and can initiate, advance, and resolve inflammation and as such are classified into pro- and anti-inflammatory cytokines. Two of the most important cytokines known to play prominent roles in vascular pathology include interleukin IL6 (Ikeda et al., 1991) and IL1α (Libby et al., 1988), produced from activated macrophages. Both of these cytokines not only promote immune cell proliferation and differentiation, but also promote the migration of VSMC and the reduction of SMC specific markers (Wang and Newman, 2003). In addition to cytokines, certain growth factors, such as platelet derived growth factor (PDGF)(Li et al., 2011a) , also induce a proliferative SMC phenotype (the PDGF and IL1α pathways will be discussed in greater detail below in Section 1.7). Moreover, Angiotensin II and TGFß can both regulate SMC genes and thus phenotypic switching. AngII is part of the renin-angiotensin system that functions to regulate SMC tone and

thus blood pressure. AngII is a peptide hormone derived from the precursor molecule angiotensinogen, a serum globulin produced in the liver. Effects of AngII are mediated via the AT1 and AT2 receptors and regulate SMC contraction through tight control of downstream signalling pathways. Activation of the AT1 receptor mediates changes in intracellular calcium levels that are a major determinant of SMC contraction while activation of the AT2 receptor is essential for αSMA expression through increased expression of the transcription factor myocardin, described in detail below (Yoshida et al., 2004).

TGFβ is a multifunctional cytokine belonging to the transforming growth factor superfamily that includes three different isoforms, TGFβ1-3, and is essential for the induction of a contractile SMC phenotype, both during development and in disease (ten Dijke and Arthur, 2007). Genetic KO of many TGFβ signalling components including both receptors and isoforms, leads to embryonic lethality due to defects both in angiogenesis and vasculogenesis. Additionally, cell-specific KOs of both EC and SMCs also exhibit embryonic lethality albeit at different days post conception. The level at which these defects are manifested therefore varies between strain and as such EC KO of receptors die at E10 due to defects in vascular development while SMC KOs die at E12.5, due to defective pericyte recruitment, SMC differentiation and SMC function. Additionally, it has been shown that TGF-β1 increases α-SMA, SM-MHC and SM-calponin levels in cultured rat SMCs (Hautmann et al., 1997) and TGF-β2 increases α-SMA and desmin levels in cultured porcine SMCs (Hao et al., 2002). In line with this observation, TGFβ induces the cell cycle protein p21 (Yoo et al., 1999), which has an inhibitory role on SMC cell cycle thus inhibiting SMC proliferation and tipping the SMC into a more contractile phenotype.

Enormous progress has now been made to identify mechanisms that regulate the transcription of specific SMC marker genes, indicating that the transcription of these genes is dependent on complex combinatorial actions of multiple elements and their binding factors.

Site directed mutagenesis studies in transgenic mice have identified that that the expression of many SMC-specific genes are dependent on one or more CArG elements (CC(AT)6GG motif) found within their promoter and intronic

sequences. For example, mutations in any of the three conserved CArG regions of the αSMA promoter completely abolished αSMA expression in transgenic mice (Mack and Owens, 1999). Similar effects were also observed with SM22α and MHC (Manabe and Owens, 2001). Interestingly, mutations in specific CArG regions of MHC resulted in differential effects on MHC expression. Mutations in the third CArG region resulted in complete loss of MHC expression in transgenic mice, while mutations in the middle MHC CArG resulted in loss of MHC from large-conduit arteries and the coronary circulation but had no effect in muscular arteries, pulmonary airway SMC or gastrointestinal SMC (Manabe and Owens, 2001).

CArG regions bind the transcription factor SRF (serum response factor), a major signalling molecules that governs SMC phenotype. SRF is a member of the MADS (MCM1, Agamous, Deficiens, and SRF) box superfamily of transcription factors. SRF binds the CArG box as a dimer and has been shown to regulate key genes such as c-fos, involved in cell cycle. Myocardin, a smooth and cardiac muscle-specific transcriptional coactivator, directly interacts with SRF and functions in the control of SMC expression of contractile genes. Homodimerisation of myocardin-SRF complexes results in maximal transcriptional activity, imparting SMC specificity to the ubiquitously-expressed SRF (Wang et al., 2003). The pivotal role of myocardin in SMC gene expression is underlined by the phenotype of mice homozygous for a myocardin loss-of-function mutation. This mutation removed exons 8 and 9 of myocardin, abolished all myogenic activity and rendered myocardin non-functional (Li et al., 2003). Mice heterozygous for this mutation were viable and fertile however, breeding determined that homozygous mice died at E10.5 (Li et al., 2003). Further analysis revealed no abnormalities before E8.0 and most embryos appeared to develop normally up to E8.5. However, after this point homozygous mutant embryos could be readily identified at E9.5 by their pale yolk sacs, which lacked blood vessels. Additionally, these embryos displayed growth retardation and delayed development, despite complete morphology of the heart (Li et al., 2003). Staining of both mutant and wild type embryos revealed that these embryos at E9.5 showed similar endothelial cells staining compared to their WT counterparts, indicating normal endothelial cell differentiation and organisation. However, staining of E9.5 embryos with antibodies to SM α-actin showed the

presence of SM α-actin positive cells in the WT embryos but no such positive cells were detected in the vasculature of myocardin-/- embryos. Comparison of transverse sections of SM α-actin-stained embryos revealed that SMCs were missing from the dorsal aortae of myocardin-/- embryos despite no decrease in the expression of SM α-actin in myocardin-/- hearts, indicating that defects were present in vascular SMC Differentiation in myocardin-/-embryos (Li et al., 2003). Additionally, it has been shown that myocardin is downregulated following vascular injury in both humans and mice and may play a role, in part, in regulating the pro-proliferative and pro-migratory phenotype of diseased SMCs (Hendrix et al., 2005). The interaction between SRF and CArG domains is illustrated in Figure 1-7. It is believed that key environmental cues such as ANG II and TGF-β can alter expression of SMC differentiation marker genes. For example, there is evidence that ANG II stimulates SMC promoter activity at least in part through increased expression of Mhox, a homeodomain protein that enhances formation of the CArG-SRF-myocardin complex (Yoshida et al., 2004). A vast array of studies have shown that TGF-β strongly stimulates SMC markers in a number of cell types including mesenchymal and embryonic stem cells, lung fibroblasts, and aortic SMC (Mack, 2011). This effect relies on the activation of Smad2 and/or Smad3, studies have demonstrated that these Smads interact with the SMC-specific promoters via Smad binding elements (SBE). This is not the only TGF-β mechanism and the effects of TGF-β are also CArG/SRF-dependent (Hautmann et al., 1997). Interestingly, studies by Qui et al have shown that Smad3 physically interacts with SRF to facilitate SMC-specific gene expression (Qiu et al., 2003). This study identified that smad3 can recruit myocardin to the promoter of the SM22α gene via direct interaction (Qiu et al., 2005). An additional group have also highlighted the requirement for δEF1 in mediating TGF-β induced gene expression. Nishimura, et. al. have shown that Smad3 also interacts with δEF1, a zinc finger- and homeodomain-containing protein expressed in SMC (Nishimura et al., 2006). TGF-β upregulated δEF1 and δEF1 formed a complex with SRF and Smad3 on the SM α-actin promoter. This formation was found to be required for the full effects of TGF-β on SMC-specific gene expression (Nishimura et al., 2006).

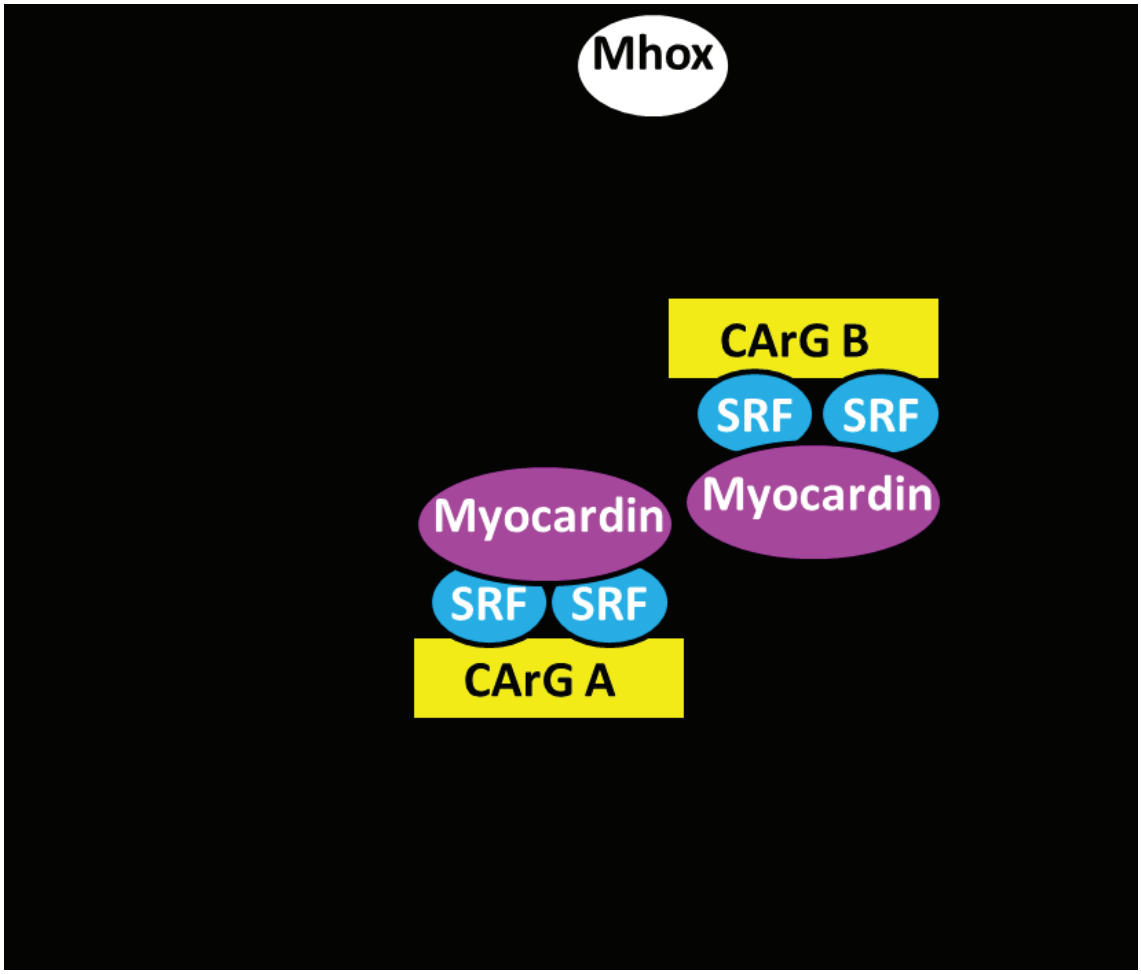

Figure 1-7: TGFβ, Ang II and PDGF control of SMC specific markers.
SMC-specific gene expression is dependent on complex combinatorial interaction of multiple elements and binding factors. This Figure presents a schematic model illustrating some of the complex protein:protein and DNA:protein interactions that are hypothesised to be important in determining cell-selective expression of multiple SMC differentiation marker genes with a focus on the importance of cooperative interactions of multiple CArG elements [CC(AT)6GG] located within both 5′ and intronic promoter regions, serum response factor (SRF), and SRF accessory proteins (SAPs) such as myocardin. (Adapted from (Owens et al., 2004)).

Kruppel-like factor 4 (KLF4) is a member of the KLF family of transcription factors and regulates proliferation, differentiation, apoptosis and somatic cell reprogramming. KLF4 is not normally expressed in terminally differentiated cells of mesenchymal origin, including VSMCs; however, several studies have now shown that this KLF4 expression is induced under disease conditions and functions to regulate VSMC phenotype (Liu et al., 2005). KLF4 is expressed within lesions of ApoE$^{-/-}$ mice on a Western diet (Sharma et al., 2012),(Garvey et al., 2010) and has been shown to repress both the expression of myocardin itself and myocardin-SRF activation of the α-SMA gene by binding to SRF at the same domain utilised by myocardin. Interaction of KLF4 with SRF prevented SRF from binding to the CarG box in the α-SMA promoter and thus prevented activation of α-SMA transcription (Liu et al., 2005). KLF4 is recruited to a TCE, located adjacent to the SRF CarG binding site in the promoter region of contractile genes (e.g. α-SMA, SM-MHC and SM22α) following vascular injury, which allows the interaction between SRF and KLF4 (Adam et al., 2000, Liu et al., 2005, Yoshida et al., 2008). KLF4 has also been shown to mediate the effects of PDGF-BB on VSMC phenotype and knockdown of KLF4 partially blunted PDGF-induced phenotypic switching (Deaton et al., 2009). Additionally, KLF4 can bind to smad proteins, preventing smad-mediated tansactivation of SMC promoters via TGFß control elements (Liu et al., 2005).

Phenotypic switching is a requirement of vascular repair however insufficient termination of SMC proliferation is a hallmark of several vascular pathologies including atherosclerosis, neointimal formation caused by coronary artery bypass grafting and in-stent restenosis caused by stent deployment.

1.6 Evidence of VSMC switching and proliferation in atherosclerosis, in-stent restenosis and neointimal formation

Despite decades of research into atherosclerosis, there are still some fundamental gaps in the understanding of the mechanisms governing plaque formation and progression. What is known is that in the setting of atherosclerosis, VSMC proliferation and migration into the plaque is crucial for plaque stability. It has been shown that these SMCs are derived from resident medial SMCs that undergo phenotypic modulation and migration into the intima

where they proliferate, produce extracellular matrix and participate in fibrous cap formation and as such, a vast array of data has been generated to confirm the observation of phenotypic switching in the setting of atherosclerosis. First, studies of human atherosclerotic lesions have routinely described cells with morphological characteristics of SMCs which appear to be in the process of migrating through the internal elastic lamina into the intima (Thomas et al., 1976), (Schwartz et al., 2000). One controversial hypothesis is that the SMC located within the plaque are derived from haematopoietic cell origin, however, several adoptive transfer experiments and lineage-tracing studies showed that a large fraction of cells within atherosclerotic lesions of Western diet fed ApoE−/− mice were not derived from haematopoietic cells, however discrepancies over the validity of atherosclerotic mouse models still remain (Psaltis and Simari, 2015). Additionally, as described above, myocardin is an SRF co-activator involved in the expression of contractile SMC genes. Myocardin$^{+/-}$ mice on an apoE$^{-/-}$ background exhibit increased atherosclerosis and increased accumulation of macrophages when compared to their myocardin$^{+/+}$ littermates (Psaltis and Simari, 2015). Although this was not a VSMC specific knockout, the only cells in the vasculature that express myocardin are VSMC. Loss of myocardin also initiated the activation of a variety of inflammatory pathways resulting in increased macrophage recruitment. Conversely, gain of myocardin experiments resulted in reduced inflammation and reduced neointimal formation (Bennett et al., 2016).

In 2002 a direct role of PDGF-induced phenotypic modulation was identified. Kozaki ef al. administered PDGFR blocking antibodies to ApoE$^{-/-}$ mice on a Western diet and found that there was up to 67 % reduction in atherosclerotic lesion size with reduced SMC investment in the neointima (Kozaki et al., 2002).

It has been shown that several well-known SMC markers which are required for the contractile phenotype of SMCs are down regulated in vascular injury and atherosclerosis. Interestingly, it has been previously demonstrated that mutation of a highly conserved G/C repressor element found within the 5′ end of the CARG element in the SM22α promoter nearly abolished down-regulation of this gene *in vivo* in response to vascular injury (Regan et al., 2000) or in atherosclerotic lesions in ApoE−/− mice (Wamhoff et al., 2004). Additionally, KLF4 (Reviewed in

section 1.3), has been shown to be expressed in both atherosclerotic lesions of ApoE−/− mice on a Western diet (Cherepanova et al., 2009) as well as following vascular injury (Yoshida et al., 2008). This is a fetal gene that is known to play a role in SMC phenotype. Additionally, conditional knockout of KLF4 was associated with a transient delay in repression of SM α-actin and SM22α following vascular injury in vivo, but with subsequent hyperproliferation of SMC and increased neointima formation, likely as the result of reduced KLF4-dependent activation of the cell cycle inhibitory gene p21 (Yoshida et al., 2008). Of note, this KLF4 knockout was a global knockout and additional studies utilising a SMC specific KLF4 are still required to investigate how this impacts SMC phenotypic switching, overall lesion development and plaque composition.

From a human perspective, Aikawa and colleagues identified altered expression of MHC isoforms (SM-1 and SM-2) and αSMA in tissue samples obtained from autopsied patients and atherectomy specimens from patients undergoing coronary angioplasty. Medial SMC exhibited expression of all three markers, however, 16–20 days after treatment, neointimal cells contained αSMA but little or no SM-1 or SM-2 indicating at the most basic level that SMC had undergone phenotypic switching. Interestingly, 6 months post-surgery, SMCs sequentially recovered SM-1 and then SM-2 expression thus adopting a more mature phenotype. These results were further confirmed in a rabbit hypercholesterolemic angioplasty model of atherosclerosis (Aikawa et al., 1998). Phenotypic switching of SMC has been shown to be induced by cytokine and growth factor treatment, the most prominent examples being activation by the IL1α cytokine and PDGF growth factor.

1.7 IL1α and PDGF signalling pathways

The highly conserved IL1α and PDGF pathways play prominent roles in VSMC-associated pathologies(Marx et al., 2011, Schermuly et al., 2005). IL1α belongs to the IL1 family which encompasses 11 proteins, encoded by 11 different genes in humans and mice. IL1α is the predominant isoform associated with vascular pathology and is synthesised as a precursor protein. It is constitutively expressed and stored in the cytoplasm of cells with a mesenchymal origin. Alternatively, monocytes and macrophages do not contain pre-formed IL1α precursors, but instead synthesise IL1α, de novo, when required. Following synthesis IL1α

precursors undergo processing by Calpain, a calcium-activated cysteine protease. This processing liberates the N-terminal propiece cleavage product, resulting in the 'mature' form. Both the 31kDa precursor form of IL1α and its 18kDa mature form are biologically active. Interestingly, IL1α has been documented to not only act as a classical cytokine but can also translocate to the nucleus to act as a transcription factor, however, the intranuclear actions of IL1α family members remains a poorly understood, potentially important area of IL1α biology (Luheshi et al., 2009).

The mRNA coding for IL1α, and by extension the IL1α protein, is not expressed in healthy cell types, tissues or blood. However, following vascular injury, several vascular and blood borne cells, such as endothelial cells, macrophages and monocytes can be induced to transcribe the IL1α gene. Following transcription and subsequent maturation, IL1α can bind to the IL receptor 1 (ILR1). The initial step of IL1α signal transduction is a ligand induced conformational change that allows the recruitment of the IL-1RAcP co-receptor. Through conserved cytosolic regions called Toll and IL1αR like (TIR) domains, the trimeric complex rapidly assembles two intracellular signalling proteins, myeloid differentiation primary response gene 88 (MYD88) and interleukin-1 receptor–activated protein kinase (IRAK) 4 (Weber et al., 2010). Thus IL1α, IL-1R, IL-RAcP, MYD88 and IRAK4 form a stable IL-1–induced signalling module (Brikos et al., 2007). Additionally, IRAK4 is auto phosphorylated leading to the phosphorylation or IRAK1 and IRAK2 and the recruitment of tumor necrosis factor–associated factor (TRAF) 6. Both IRAK1 and IRAK2 can function as adaptors and protein kinases leading to downstream signalling and activation of important signalling proteins. This includes mitogen-activated kinases (JNK, p38, ERK1/2), as well as transcription factors, including NFκB (p65 and p50 subunits) and c-Jun (a subunit of AP-1), which control the expression of a number of inflammatory and catabolic genes (as shown in Figure 1-8). Animal intervention studies have implicated IL1α in a number of vascular pathologies. For example, studies have demonstrated that unilateral common carotid artery (CCA) ligation leads to low shear stress in the ligated artery and results in remodelling and intimal hyperplasia. CCA ligation in IL1α receptor knockout mice resulted in a 7 fold reduction in neointimal formation when compared to wild type counterparts (Rectenwald et al., 2000). In an additional model, specific inhibition of the key IL1α signalling molecule IRAK abrogated

balloon injury–induced neointimal formation in the rat. A time dependent increase in IRAK was observed 15 min, 30 min, 1 h, 6 h, 12 h and 24 h after carotid balloon injury in rats. Perivascular application of IRAK1 inhibitor or administration of IRAK1 siRNA in pluronic gel abrogated balloon injury induced proliferative signalling pathways, such as ERK. Hematoxylin and eosin staining and immunohistochemistry of proliferating cell nuclear antigen and smooth muscle actin demonstrated that balloon injury–induced intimal thickening and neointimal vascular smooth muscle cell proliferation were significantly abrogated in the presence of IRAK1 inhibitor and IRAK1 siRNA (Jain et al., 2015).

In the mid 1970's, several groups demonstrated the existence of a major growth factor for fibroblasts and smooth muscle cells that was derived from platelets. This factor was named platelet derived growth factor (PDGF) and purified a few years later by Heldin et al. PDGF is a 30kda dimer composed of an A and/or B chain, which are encoded by separate genes. Two additional genes, PDGF-C and PDGF-D, have since been identified. At present, 5 dimeric compositions are known to exist: PDGF-AA, PDGF-BB, PDGF-AB, PDGF-CC and PDGF-DD. These PDGF isoforms bind 2 distinct classes of type III receptor tyrosine kinases, PDGFRα and PDGFRß. Binding of the ligand leads to auto phosphorylation of the receptors at the tyrosine residues leading to the activation of key downstream signalling molecules such as NFκB (as shown in Figure 1-8). Individual PDGF chains have varying affinities for the 2 receptors. PDGFRα has high affinity for A, B and C chains while PDGFRß has high affinity for B and D chains only. PDGF is a major mitogen for many cell types of mesenchymal origin and is known to play a role in aberrant wound healing associated with several vascular pathologies. Interestingly, blockade of PDGF-BB in a baboon model of vascular grafting, resulted in a significant overall decrease in smooth muscle cell nuclear density of the neointima (Davies et al., 2000). Conversely, an increase in PDGF-BB expression promotes vascular smooth muscle cell proliteration, thus leading to a greater intimal thickening and cellular content of the neointima (Desfaits et al., 2000).

Activation of both IL1α and PDGF signalling pathways simultaneously results in activate of common downstream targets leading to an additive or synergistic effects. It was demonstrated that NFκB was vital for the synergistic effects of

this cytokine and growth factor. Zymography experiments assessing MMP-9 secretion from rabbit dermal fibroblasts found that both IL1α and PDGF alone did not increase MMP-9 secretion, however, MMP-9 was significantly increased following dual stimulation. These results were also confirmed in human foreskin fibroblasts (Bond et al., 1998). Northern blot analysis revealed that the synergistic up-regulation of MMP-9 was observed as early as 4 h post stimulation. It was proposed that IL1α and PDGF synergistic effects were due to dual activation of NFκB. As such, a recombinant adenovirus overexpressing IκBα, the NF-κB inhibitory subunit was employed. Infection of rabbit dermal fibroblasts with the virus completely blocked the synergistic up-regulation of MMP-9 to IL1α and PDGF stimulation when compared to the control virus, highlight the essential need for NF-κB, highlighted red in Figure 1-8, in mediating synergistic IL1α and PDGF regulation (Smith et al., 1991).

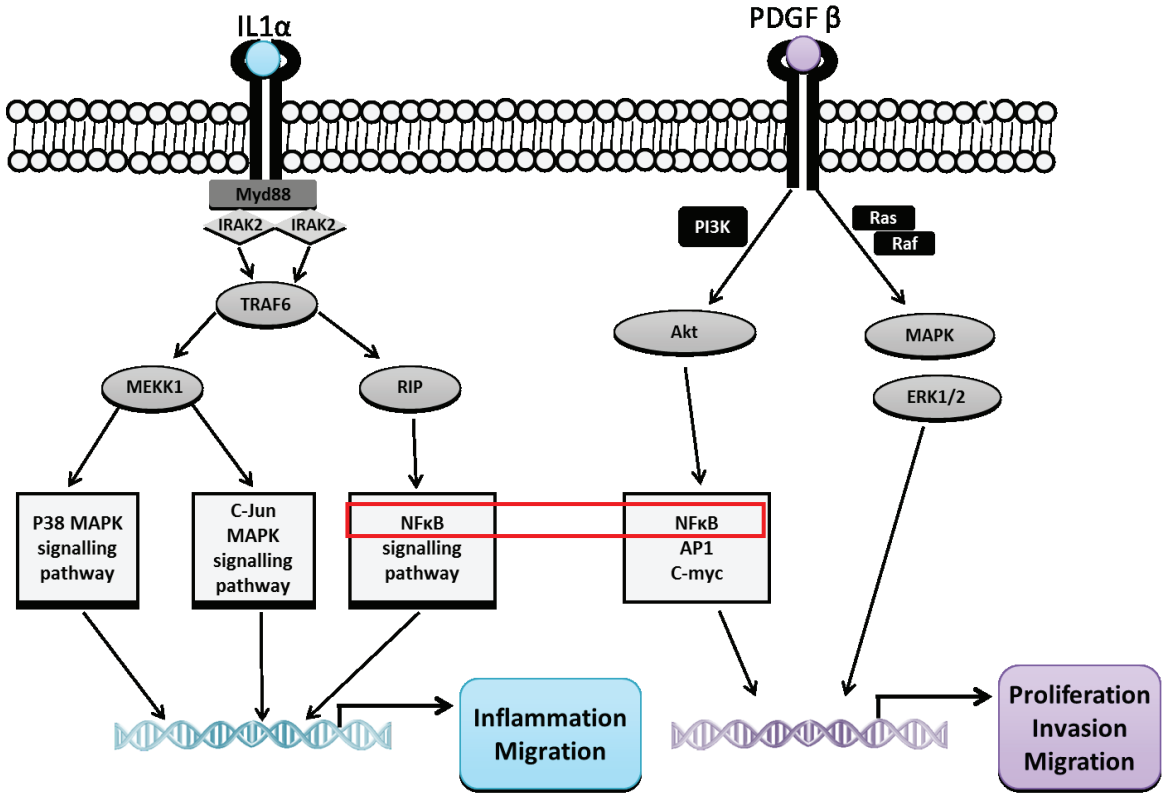

Figure 1-8: Overview of the IL1α and PDGF signalling pathways.
The major role of IL-1 type cytokines is to control pro-inflammatory reactions in response to tissue injury. Upon receptor engagement a complex is formed between the type 1 receptor and the receptor accessory proteins Myd88 and IRAK2. Binding of IL-1 to the receptor complex leads to the activation of the transcription factors NF-κB and AP1 via either the MAPK or NFKB signalling pathway. This leads to migration of cells and activation of inflammatory mediators. PDGF plays a central role in

cellular proliferation and development. Upon binding the PDGF receptor is tyrosine phosphorylated and leading to the docking of accessory proteins and the phosphorylation of several downstream mediators leading to proliferation, migration and invasion by cells. Dual activation of NF-κB is highlighted by the red box.

1.8 Targeting of cell cycle regulation as therapeutic strategy for treatment of proliferative vascular diseases

The aetiology of restenosis, neointimal hyperplasia and atherosclerosis involves aberrant proliferation of VSMCs, rendering compounds with anti-mitogenic properties promising candidates for combating cardiovascular disease. Therapeutic targets upstream of the cell cycle pathway have had limited clinical effectiveness. As the molecules that directly regulate the cell cycle have been identified, the focus in antiproliferative therapeutics has now shifted to targeting the cell cycle using specific anti–cell cycle drugs and genetic tools. Several considerations remain when designing anti-proliferative agents. Inhibition of SMC proliferation requires adequate delivery of the drug to the site of interest and several therapeutics have failed due to requiring systemic delivery. Additionally, in the setting of in-stent restenosis, drug-eluting stents (DES) are associated with reduced restenosis rates when compared with bare-metal stents (BMS) – see section 1.3.2.1 for further detail. Stent thrombosis following BMS implantation typically occurs within the first 30 days after, although rarely can occur later. In contrast, tent thrombosis after DES can occur years afterward, with an annual incidence of 0.4-0.6 % (Wenaweser et al., 2008). Thus, stent thrombosis rates arising from within the original stent are higher with DES than BMS, with the differences emerging predominantly beyond the first year after implantation (Stone et al., 2007). A variety of potential causes of late stent thrombosis occurring with DES have been implicated and include delayed or absent endothelialisation of the stent struts. This is due to off target effects of the drugs and the ability to inhibit both SMC and EC proliferation. As mentioned in Section 1.2.1, intact endothelial cells act as an anti-thrombotic barrier and disruption of this cellular monolayer leads to the production of pro-thrombotic agents and occlusion of the deployed stent. New drugs will require to be SMC selective to inhibit off target effects. Many different approaches have been undertaken as a means of altering SMC cell cycle. An overview of classical and novel methods is provided below and illustrated in Figure 1-9A and B.

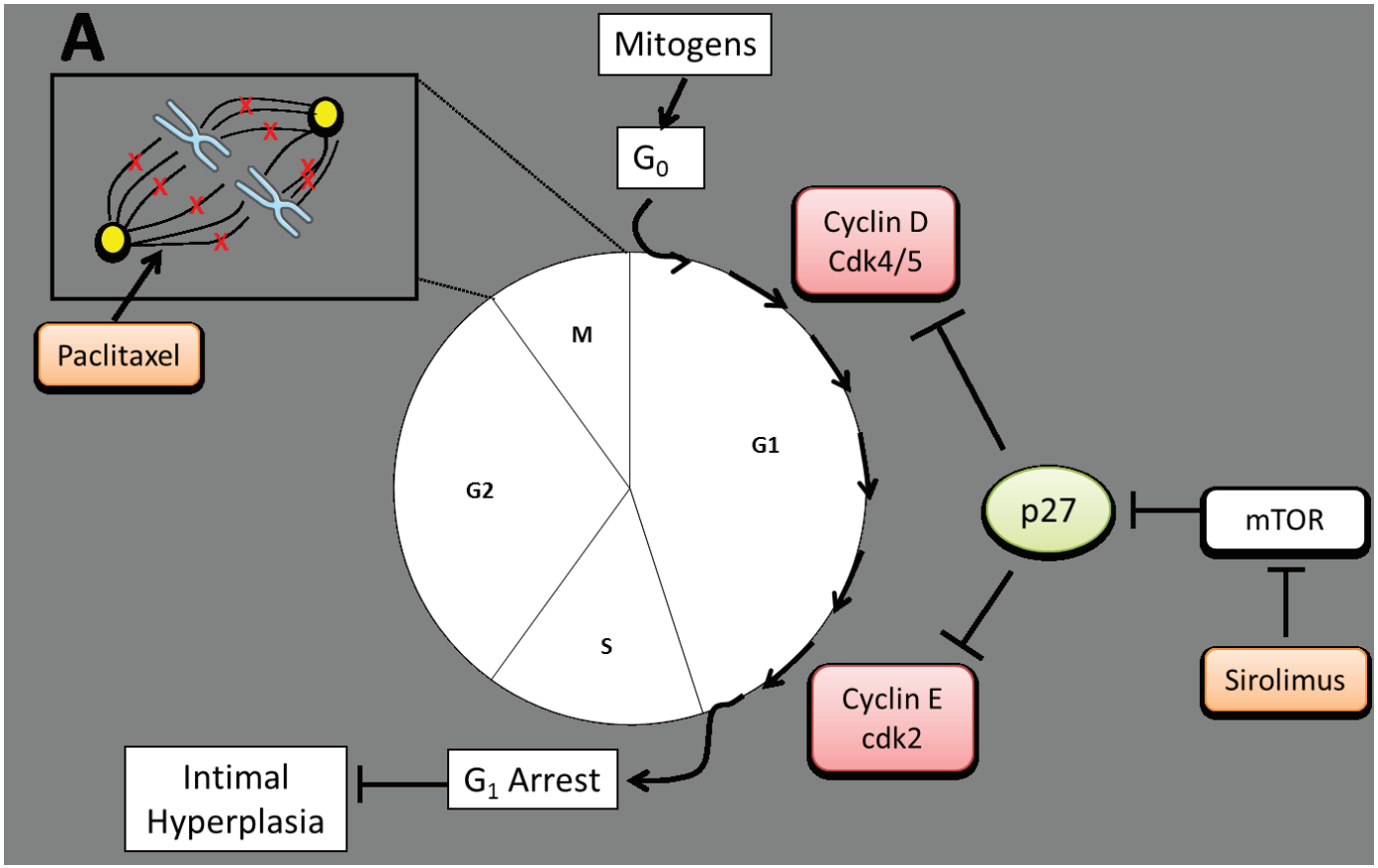
A
Mitogens
G_0
Cyclin D
Cdk4/5
Paclitaxel
M
G1
G2
S
p27
mTOR
Sirolimus
Cyclin E
cdk2
Intimal
Hyperplasia
G_1 Arrest

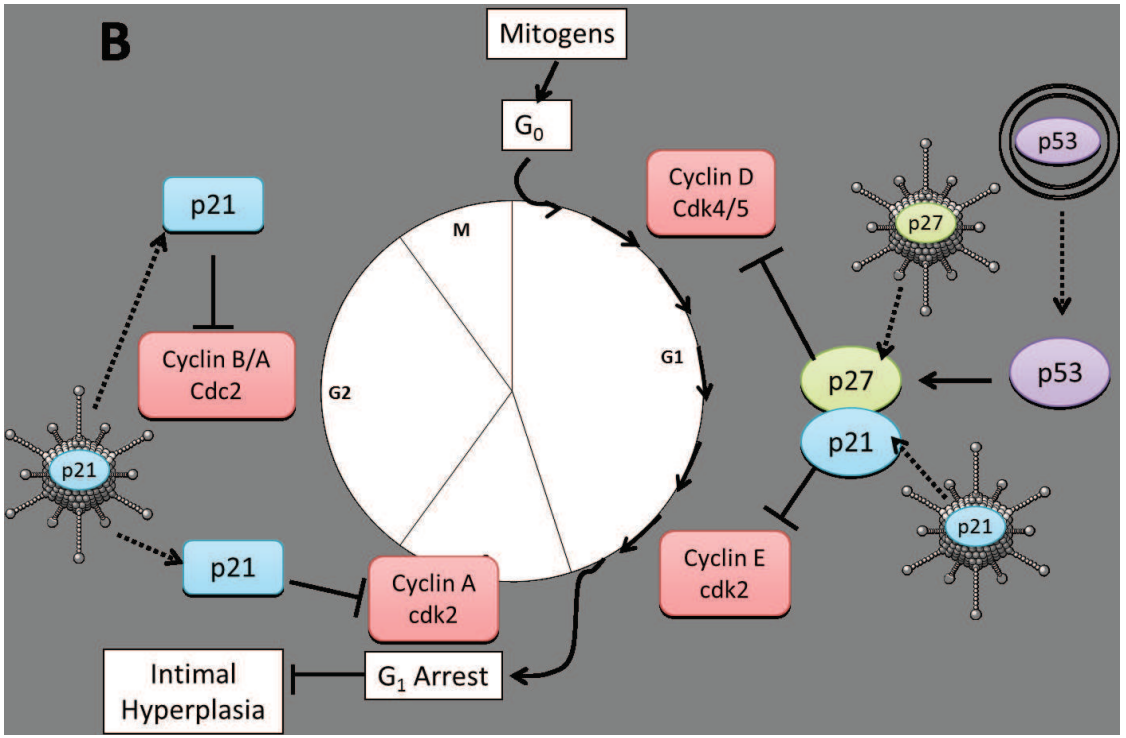

Figure 1-9: Overview of methods to inhibit SMC cell cycle.
Schematic illustration of the cell cycle and its regulatory mechanisms that are relevant for the inhibitory effect of classical and novel cell cycle inhibitors. Cell cycle is regulated by the specific activities of cyclin/cyclin-dependent kinase (CDK) complexes. Cyclin-dependent kinase inhibitors (CKIs) negatively control the activity of distinct cyclin/CDK complexes. The CKIs are major regulators of the cell cycle. CKI include p21, p27 and p53 among others. All of which are critical cell cycle regulators in smooth muscle cells. **(A):** Sirolimus inhibits the activity of mammalian target of rapamycin (mTOR). mTOR is a pivotal protein kinase that mediates mitogen-induced cell proliferation. The inhibition of mTOR by sirolimus attenuates p27 degradation, thus increasing p27 protein stability. Increased p27 has the ability to inhibit key cyclin proteins resulting in cell cycle arrest. Paclitaxel impacts predominantly during cell division in the mitosis (M) phase of the cell cycle through

centrosomal impairment, induction of abnormal spindles and suppression of spindle microtubule dynamics**. (B):** Specific adenoviral production of key CKI p21 and p27 have been utilised to inhibit cell cycle as to has the plasmid deliver of p53. Delivery of p21 inhibits cyclin B/A, cyclin D and cyclin E. p27 inhibits CyclinD and p53 inhibit cyclin D and E.

Classical drug therapy as a means of targeting the cell cycle machinery

Sirolimus, also known as rapamycin, is a macrolide drug produced by the bacterium Streptomyces hygroscopicus. The intracellular receptor for sirolimus is the immunophilin FK506 binding protein, 12 kDa (FKBP12), which has been shown to be upregulated in patients with in-stent restenosis (Sabatini et al., 1994). The sirolimus-FKBP12 complex binds to and inhibits the activation of mammalial target of rapamycin (mTOR). mTOR is an atypical serine/threonine kinase located in the cytoplasm of SMC. Stent- or balloon-induced vascular injury activates mTOR, which in turn leads to downregulation of p27. P27 prevents the activation of cyclin E-CDK2 or cyclin D-CDK4 complexes, and thus this downregulation of p27 allows the activation of cyclin-E and cyclin-D promoting progression at G_1 (Nadal et al., 2016). Systemic administration of Sirolimus in a porcine model showed inhibition of restenosis following balloon angioplasty (Tepe et al., 2006). The encouraging results from animal experiments led to clinical trials for rapamycin to prevent in-stent stenosis in humans. As there is a high risk of short- and long-term complications with systemic use of immunosuppressive drugs such as sirolimus, novel methods for drug delivery were explored. This led to the development of a rapamycin-eluting stent, which delivers the drug locally to the vessel wall. Despite successful inhibition of in-stent restenosis in porcine models, human results proved variable and led to significant side effects. Major improvements have led to the production of sirolimus analogue (everolimus) eluting stents. Excellent safety and efficacy results of everolimus-eluting stents in preclinical studies led to the First Use To Underscore restenosis Reduction with Everolimus (FUTURE) clinical trial program (Grube et al., 2004). The FUTURE I study was a prospective, randomised, single-centre, single-blind feasibility study designed to compare the safety and performance of the everolimus-eluting stent (n = 27) to that of the bare metal stent (n =15), no adverse effects were reported at 6 or 12 months post implantation. FUTURE II was a prospective, randomised, multicentre study designed to assess the safety and efficacy of the everolimus-eluting stent (n = 21) compared with a bare-metal stent (n = 43). FUTURE II also included diabetic patients and showed no adverse effects.

Paclitaxel, similar to sirolimus, is used as a coating for drug eluting stents under the name Taxus by Boston Scientific in the United States. Paclitaxel is a

cytoskeletal drug that works via targeting of tubulin. Paclitaxel binds specifically to the ß-tubulin subunit and antagonises the disassembly of this complex. This results in the accumulation of tubule bundles in the mitotic phase of cell cycle and arrest in mitosis (G_2/M phase) follows (Waugh and Wagstaff, 2004). *In vivo* investigation of this compound identified that administration of paclitaxel after balloon angioplasty in a rat model caused inhibition of VSMC proliferation and restenosis (Sollott et al., 1995). *In vivo* studies using stents to locally administer paclitaxel have also resulted in reduced neointimal growth in rabbit (Drachman et al., 2000), (Herdeg et al., 2000) and in pig models (Heldman et al., 2001). A number of successful clinical trials were also initiated using this drug to treat restenosis. The ELUTES and TAXUS trials used paclitaxel-coated stents to produce a significant reduction in restenosis after 6 months.

Despite, initial trials of these drugs suggesting that they were extremely useful in the treatment of neointimal formation and in-stent stenosis (Bicknell et al., 2003), both these compounds have now been identified to inhibit re-endothelialisation of the deployed stent leading to late stage thrombosis. In 2010, work by Liu et al., utilised 3 animal models, involving both dogs and rats, to identify that clinically relevant levels of rapamycin impede re-endothelialisation after drug-eluting stent implantation by inhibiting the proliferation and migration of coronary endothelial cells, inducing endothelial progenitor-cell apoptosis and decreasing vascular endothelial growth factor expression in the circulation (Liu et al., 2010b). Additionally the PASSION (Paclitaxel Eluting Stent Versus Conventional Stent in ST-segment Elevation Myocardial Infarction) trial found higher rates of stent thrombosis with paclitaxel eluting stents when compared to BMS at 5 years (Brodie et al., 2011). These results have since been confirmed via several independent researchers (Camici et al., 2010), (Hayashi et al., 2009) .

Novel drug therapy as a means of targeting the cell cycle machinery

Gene therapy provides an additional means to modulate the cell cycle in vasculoproliferative diseases. This method is amenable to both overexpression of cell cycle inhibitors and knockdown via antisense technique of cell cycle activators. It has been shown that overexpression of p27 and p21 utilising adenoviral technology can effectively reduce neointimal formation (Goukassian

et al., 2001), (Chang et al., 1995). Additionally overexpression of the cell cycle-inhibitory transcription factor p53, via plasmid vectors was also shown to reduce neointimal formation (Matsushita et al., 2000). It is worth emphasizing that plasmid-based gene delivery is transient and adenoviruses stimulate an immune response that can prevent repeated administration, thereby limiting the usefulness of these technologies.

To date most treatments for the control of SMC proliferation associated with neointimal formation and in-stent restenosis have proved ineffective or exhibit off target effects. Recently, non-coding RNA have emerged as a new layer of regulatory control and as such may possess the ability to specifically target smooth muscle cell proliferation without affecting endothelial cell function.

1.9 Non-coding RNA

Nucleic acids were first discovered in 1868 by Friedrich Miescher and by 1939 RNA had been implicated in protein synthesis(Dahm, 2005). Two decades later, Francis Crick predicted a functional RNA component which mediated translation and later it was discovered that non-coding RNA was in fact functional (Eddy, 2001).

The first non-coding RNA to be characterised was an alanine transfer RNA (tRNA) found in baker's yeast and its structure was published in 1965 (Gorbulev et al., 1977). To produce a purified alanine tRNA sample, Robert W. Holley et al. used 140kg of commercial baker's yeast to give just 1g of purified tRNA Ala for analysis. Finally in 1974 X-ray crystallography analysis performed by two independent research groups identified the secondary structure of this RNA. This was closely followed by the discovery of ribosomal RNA, followed by URNA in the early 1980’s. Since then the discovery of new non-coding RNAs has continued with microRNA, snoRNAs, piwiRNA, lncRNA, CRISPR and many more.

Most of these RNA molecules have been identified through sequencing of the human genome as part of the Human Genome Project (HGP), initiated independently and simultaneously by Robert Sinsheimer, then Chancellor of the University of California–Santa Cruz (UCSC) and Charles DeLisi of the United States Department of Energy (Lander, 2011). The Human genome project was

initiated in 1990 and completed in 2003. Although this project provided an advanced understanding of the human genome and its complexity, many questions such as how does DNA work, which elements regulate it and how does this regulation occur? remained unanswered. As such, follow up investigations such as the ENCyclopedia of DNA Elements (ENCODE) were launched in an attempt to unravel the remaining mysteries (Qu and Fang, 2013). Specifically, the ENCODE project aimed at preparing a complete catalogue which contained all functional elements codified in the human genome, for example, protein coding and non-coding genes, elements that regulate transcription, elements responsible for the structure of the chromosome and any other functional sequence considered relevant (Qu and Fang, 2013).

A major discovery from these studies was the identification that greater than 90 % of the human genome is transcribed, yet only 2 % is subsequently translated into proteins (Baird, 2001). For example, these projects identified that humans possess 20,000 protein-coding genes, similar to that encoded in the nematode genome (Hattori, 2005). However, nematodes are composed of ~1,000 cells compared to the 10^{14} cells belonging to humans (Mattick, 2001). In contrast, the proportion of non-coding RNA increases in concert with developmental complexity as shown in Figure 1-10. As such, it is proposed that this non-coding RNA provides the extra layers of developmental complexity required for the evolution from eukaryotes to the human brain.

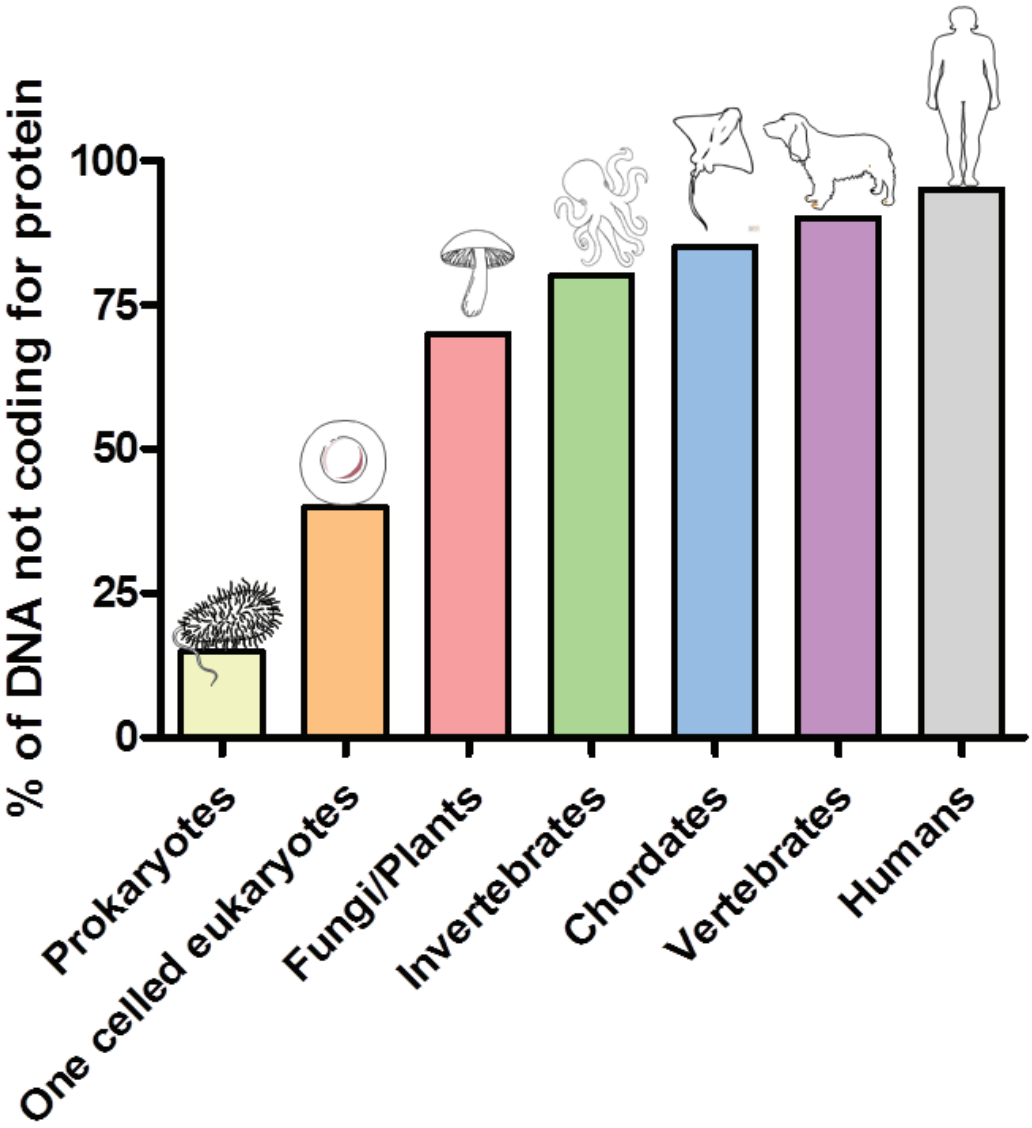

Figure 1-10: Genetic complexity of organisms compared to lncRNA content.
Protein coding genes make up approximately 2 % of the human genome. Among eukaryotes, as organism complexity increases, as to does the proportion of DNA encoding non-coding transcripts.

The field of DNA and RNA sequencing has rapidly improved due to the exponential reduction in the cost of obtaining genome sequence data. In the past the traditional scope of comparative genomics was to compare the differences and similarities between species. However, the recent explosion in sequencing has made it possible to sequence specific tissues and the genomes of normal and diseased cells within an individual (van den Bos et al., 2016). This has highlighted that the non-coding 'transcriptional noise' is in fact transcribed to varying degrees under different experimental conditions and has now highlighted the role of ncRNA in regulating gene expression (Ceman and Saugstad, 2011). The varying functions of ncRNA are performed by individual subtypes of ncRNA molecules. Classically, ncRNAs were either ribosomal RNA (rRNA), which associates with a set of proteins to form ribosomes, or transfer RNA (tRNA), an adaptor molecule known to carry amino acids to their respective polypeptide chain. However, newer ncRNA variants include microRNA (miRNA), long ncRNA (lncRNA), PIWI interacting RNAs, Y RNAs and small nuclear RNA. In order to exert some order, non-coding RNA are generally classified according to their length. To date, lncRNA and microRNA have received the greatest interest and as such both microRNA and lncRNA have now been implicated in the control of key SMC phenotypes and associated with vascular disease processes.

1.9.1 MicroRNA

MiRNAs belong to a class of small (18-22 nucleotide), endogenous non-coding RNA molecules that have been described in almost all plants and animals, and even some unicellular eukaryotes. MiRNA negatively regulate gene expression by targeting specific messenger RNAs, thereby inducing their degradation or translational repression. MicroRNA supress gene expression by binding to complementary sequences found within the 3' untranslated region (UTR) of the mRNA.

MicroRNA were discovered in 1993 by the joint efforts of Ambros's and Ruvkun's laboratories(Bartel, 2004, Lee et al., 1993). The discovered microRNA, lin-4, was found to be essential for *Caenorhabditis elegans* (c. elegans) development and required for the transition from the L1 to L2 stage of larval life cycle. Both labs reported that lin-4 transcripts were complementary to a repeated sequence in

the 3′UTR of the lin-14 transcript, leading to mRNA degradation and reduction in functional lin-14 protein levels.

According to the latest edition of the miRNA database (miRbase), there are 2585 mature microRNA catalogued, however the functional importance of many of these miRNAs remains to be elucidated. In many species, there are multiple microRNA loci with similar sequences. MiRNA genes in a family can exhibit full conservation of the mature miRNA or partial conservation of only the seed sequences at positions 2–8 of the functional mature miRNA (Mathelier and Carbone, 2013). Typically miRNA families have been found to work to within similar gene network pathways, however this is not always the case.

MiRNA sequences are located within various genomic contexts. In humans, microRNA have been identified in the introns of coding and non-coding genes as well as exonic regions. Often several miRNA loci are in close proximity allowing the transcription of a microRNA clusters. However, individual regulation of a single microRNA can still occur at the post transcriptional level.

1.9.1.1 MicroRNA biogenesis

MiRNA genes are transcribed by RNA polymerase II (Pol II), and the long primary (pri-miRNA) transcript has a local hairpin structure where miRNA sequences are embedded. The long pri-miRNA is typically greater than 1kb in length. For miRNA clusters, a single pri-miRNA may be produced that houses several miRNA. Following transcription, the pri-miRNA undergoes several steps to maturation (see Figure 1-11). Firstly pri-microRNAs are processed in the nucleus through activity of DROSHA into precursor miRNAs (pre-miRNA) that are then transported into the cytoplasm, via exportin 5. This double stranded 60-90 nt miRNA precursor forms the classical stem and loop structure in the cytoplasm. In the cytoplasm pre-miRNA-s are cleaved by DICER into a mature RNA duplex that associates with argonaute proteins which load specific miRNA strands into the RNA-induced silencing complex to form a RISC-miRNA duplex that subsequently represses mRNA transcription or enhances mRNA degradation.

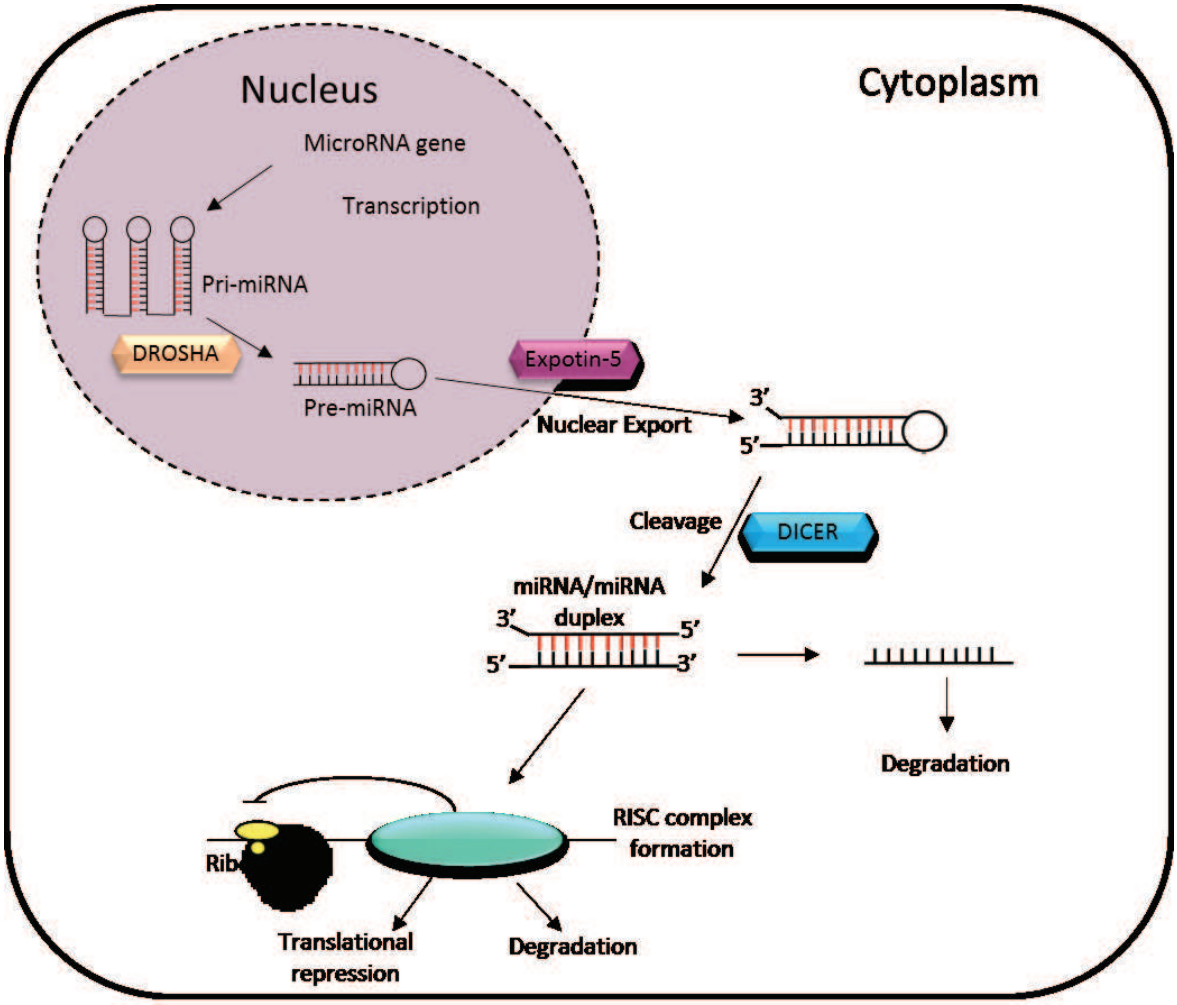

Figure 1-11: MicroRNA synthesis pathway.
Production and maturation of miRNA relies upon the production of pri-miR-NA and the action of DROSHA, exportin-5 and dicer to create the mature RNA capable of binding the RISC complex and inducing either translational repression or mRNA degradation.

1.9.1.2 Role of microRNA in VSMCs and cardiovascular disease

MicroRNAs such as miR-26a, miR-143/145 and miR-21 have been implicated in the control of multiple aspects of SMC physiology and function. MicroRNA-26a has been shown to promote VSMC proliferation and migration and to inhibit apoptosis (Leeper et al., 2011). MiR-26a was identified in human coronary artery smooth muscle cells (HCASMCs) where its expression was shown to be elevated in synthetic, proliferating SMCs (Leeper et al., 2011). Previous studies had predicted miR-26a to target SMAD-1 and SMAD-4, key components of the TGF-ß and BMP signalling pathways. As such, loss of function experiments highlighted that SMCs deficient in miR-26a exhibited increased appearance of differentiation markers including myosin heavy chain (MYH11) and smooth muscle α actin. These experiments were confirmed through subsequent overexpression of miR-26a. Consistent with an anti-differentiation effect, SMCs also exhibited reduced proliferation and migration when miR-26a levels were decreased (Leeper et al., 2011). Further experiments confirmed the direct effect of miR-26a on SMAD-1 andSMAD-4 (Leeper et al., 2011). It therefore appears that miR-26a may act as a 'biological brake' that dampens cellular differentiation in cell culture. By inhibiting SMAD proteins, miR-26a helps maintain the balance of SMCs in the synthetic and contractile states and thus governs phenotypic switching (Leeper et al., 2011).

MiR-143 and miR-145 encoding genes are highly conserved across human and mouse genomes and are clustered on murine chromosome 18 and human chromosome 5 (Boettger et al., 2009). Both these microRNA are transcribed as a cluster via a stem loop structure. Analysis of the miR-143/145 promoter revealed a key binding site for serum response factor (SRF). As such, Cordes et al. showed that SRF could independently activate the expression of miR-143/145 in human smooth muscle cells (Cordes et al., 2009). As mentioned in Section 1.5 myocardin is an important co-activator of SRF and is considered as the molecular switch that controls smooth muscle differentiation. It was therefore shown that myocardin and SRF synergistically activate miR-143/145 expression and miR-143/145 are therefore implicated in the control of SMC fate (Cordes et al., 2009). Cheng et al. identified that specific overexpression of miR-145 alone was sufficient to increase the expression of VSMC differentiation marker genes, such as smooth muscle α-actin, calponin and MHC. Accordingly, levels were decreased

with miR-145 knockdown (Cheng et al., 2009). These in vitro findings suggested a crucial role of miR-143/145 in VSMC phenotype determination and the effects were further validated in in vivo models. Three independent groups all generated knock out mouse models of the miR-143/145 cluster and showed that the expression of miR-143/145 is essential for VSMCs to acquire a contractile phenotype (Boettger et al., 2009), (Ella et al., 2009), (Xin et al., 2009). One interesting discovery was that smooth muscle layers of the aorta and other arteries from miR-145 and miR-143/145 KO mice were noticeably thinner than those of wild-type or miR-143 KO mice, indicating a more prominent and distinct role of miR-145 compared with miR-143 (Xin et al., 2009). These microRNA, may have therapeutic potential in the setting of proliferative vascular disease and in line with this, Cheng et al demonstrated that miR-145 is downregulated in neointimal lesions in rat carotid arteries following balloon angioplasty and that restoration of the downregulated miR-145 is sufficient to inhibit the neointimal formation (Cheng et al., 2009).

One final example is the miR-221/222 cluster whose gene resides on the X chromosome. Both are significantly upregulated *in vivo* in VSMCs following balloon injury of the carotid artery (Liu et al., 2009) and miR-221 has also been shown to be increased in SMCs stimulated with PDGF (Davis et al., 2007). As with other microRNA, this cluster does not have one single effect on SMCs and has been implicated in the reduced expression of contractile genes and increased proliferation and migration of SMCs. MiR-221/222 regulate these functions through multiple targets, including p27, p57 and c-kit. p27 and p57 are cyclin-dependent kinase inhibitors that negatively regulate cell proliferation (Yu and Li, 2014). One interesting feature of the miR-221/222 cluster is the opposing function in vascular SMC and ECs. In SMCs, knockdown of the cluster inhibits proliferation but in EC knockdown promotes proliferation and migration. As such this microRNA cluster would prove beneficial in the treatment of in-stent restenosis where lack of re-endothelialisation but prominent SMC proliferation is problematic.

Due to the profound effect of microRNA on several cardiovascular disease, focus has now shifted to additional non-coding RNA molecules.

1.9.2 Long non-coding RNA

Long non-coding-RNA (lncRNA) have gained widespread attention in recent years as key regulators of cellular function and disease. LncRNA are a large family of transcribed RNA molecules with a length of greater than 200 nt. LncRNAs are transcribed throughout the genome and display remarkable similarity to classical mRNA. They are highly versatile and function to regulate gene expression by diverse mechanisms.

1.9.2.1 Identification and classification of lncRNA

While widespread attention on lncRNAs is a rather recent phenomenon, it fits into the broader historical interest in studying the size, evolution, and function of genomes. The concept of functional lncRNA was first introduced over 20 years ago, with the discovery of the imprinted H19 lncRNA. The imprinted H19 locus belongs to a conserved gene cluster on chromosome 7 in the mouse and 11p15.5 in human. The H19 gene is expressed exclusively on one parental allele in a phenomenon known as imprinting. H19 is only transcribed from the maternally inherited allele; the paternal H19 allele is not expressed (Monnier et al., 2013).

The H19 gene encodes a 2.3 kb spliced, capped, and polyadenylated long non-coding RNA that has an important role in embryonic development and growth control. The targeted deletion of the H19 gene induces an overgrowth phenotype, which can be rescued by transgenic re-expression of H19 (Ripoche et al., 1997).

In the past decade, however, large-scale analyses have focused on identifying ncRNA species in a comprehensive fashion. This is primarily due to the improvement of large scale sequencing technologies, including DNA tiling arrays and next generation RNA-sequencing (RNA-seq). As a consequence lncipedia v4.0 now contains 118,777 human annotated lncRNAs. One way to exert order to the plethora of discovered lncRNA is to classify them according to their orientation to protein coding genes. Utilising this technique lncRNA can be grouped into 5 classes: Intronic, intergenic, antisense, overlapping and bidirectional (Figure 1-12).

Intronic

Intronic lncRNAs are RNA molecules that overlap with the intron of annotated coding genes in either the sense or antisense orientation. Most of the intronic lncRNAs exhibit similar tissue and cell expression as the overlapping transcript. Generally this indicates that they are regulated by the same transcriptional machinery. Intronic lncRNA may stabilize protein-coding transcripts or regulate alternative splicing of the host transcript (Nakaya et al., 2007).

Intergenic

Intergenic lncRNAs (lincRNA) are long non-coding RNAs which are located between annotated protein-coding genes and are at least 1 kb away from the nearest protein-coding genes. Gene expression patterns have implicated these lincRNAs in diverse biological processes, including cell-cycle regulation, immune surveillance and embryonic stem cell pluripotency. LincRNAs are well known to modulate the expression of nearby genes by regulating chromatin modifying proteins (Khalil et al., 2009).

Antisense

Antisense lncRNAs are RNA molecules that are transcribed from the antisense strand and partially overlap with the exon of the sense RNA. Antisense-overlapping lncRNAs are typically less likely to be spliced and show lower expression levels than the sense counterpart. The basal expression levels of antisense-overlapping lncRNAs and sense mRNAs in different tissues and cell lines can be either positively or negatively regulated (Katayama et al., 2005).

Overlapping

These lncRNAs can be considered transcript variants of protein-coding mRNAs, as they overlap with a known annotated gene on the same genomic strand. The majority of these lncRNAs lack substantial open reading frames (ORFs) for protein translation, while others contain an open reading frame but do not produce functional proteins.

Bidirectional

A bidirectional lncRNA is located in the head to head orientation with an additional protein coding gene, with a maximum of 1kb distance between the 2 start sites. Bidirectional lncRNA exhibit similar expression patterns as their

protein coding counterpart suggesting that they share transcriptional pressures. However, inverse expression patterns of expression have been identified between protein coding genes and bidirectional lncRNA (Hu et al., 2014).

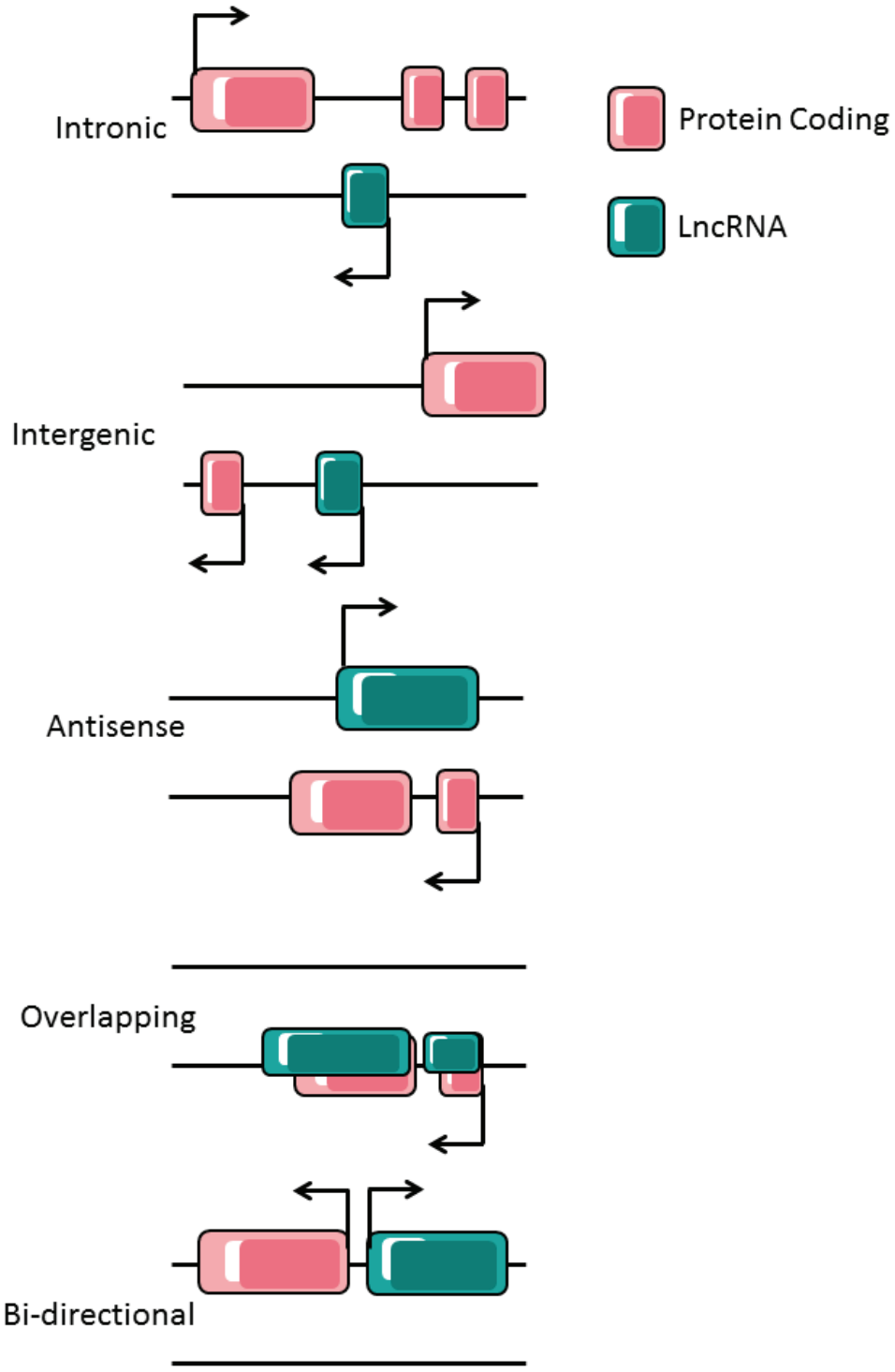

Figure 1-12: Classification of lncRNA based upon proximal protein coding genes. Classification of lncRNAs on the basis of their location with respect to the protein-coding genes: A) Intronic lncRNAs are originated from the intronic regions of the protein-coding genes and are produced by alternative splicing of the pre-mRNA and do not overlap with exons of the protein-coding gene. B) Intergenic lncRNAs are also called as lincRNAs. LincRNAs are separate transcriptional units from protein-coding genes. LincRNAs are transcribed from intergenic regions.C) Bidirectional lncRNAs are transcripts whose transcription initiate in a divergent fashion from the promoter of a protein-coding genes. D) Sense-overlapping lncRNAs are lncRNAs that are present within the boundaries of the protein-coding gene. Such lncRNAs are transcript variants of protein-coding mRNAs. Some sense-overlapping lncRNAs do not possess a functional open reading frame for translation into proteins. E) Antisense lncRNA are coded in antisense strand of the genome and transcribed as antisense transcripts.

1.9.2.2 LncRNA biogenesis

As mentioned above, more than 90 % of the human genome is transcribed as non-coding RNA as revealed by a number of deep sequencing methods. These studies suggest that the majority of lncRNA are synthesised by the RNA polymerase II (Pol II) complex, similar to protein-coding RNAs. However, experimental analysis utilising amanitin, an inhibitor of RNAP II, still lead to the production of lncRNA molecules suggesting that some lncRNAs are also transcribed by RNAP III and single-polypeptide nuclear RNA polymerase IV (spPol IV). LncRNA transcription shares many features with mRNA biogenesis in that lncRNA are typically polyadenylated, 5' capped, contain a multi-exonic structure, are subject to normal and alternative splicing mechanisms, RNA editing processes, and display unique patterns of transcriptional activation (Khandelwal et al., 2015).

1.9.2.3 Conservation of lncRNA

Several non-coding RNA, such as microRNA, exhibit strong conservation across species genomes. In contrast, lncRNA exhibit little species conservation suggesting that these non-coding RNA may be under differential selection pressures. Unlike mRNAs, which have to conserve the codon usage and prevent frameshift mutations in a single long ORF, selection may only conserve short regions of long ncRNAs that are constrained by structure or sequence-specific interactions.

The function of RNA is indeed widespread: mRNAs encode proteins, tRNA are in involved in translation, and microRNAs act by RNA:RNA interactions to modulate mRNA function. In contrast to microRNAs which act as post transcriptional repressors: lncRNAs functions include both positive and negative regulation of protein-coding genes, and range from lncRNA:RNA and lncRNA:protein to lncRNA:chromatin interactions (Johnsson et al., 2014). Due to this functional diversity, it seems reasonable to presume that different evolutionary constraints might be operating. However, the lack of species conservation does prove difficult in switching between human samples and animal models of disease.

The functional importance of lncRNAs are now becoming apparent. Although only a handful have been functionally characterised, this number has been increasing, with more lncRNA being found involved in disease states.

1.9.2.4 LncRNA function

LncRNA exhibit the ability to pair to other DNA, RNA and protein molecules. Recent attempts have been made to catergorise the various types of molecular mechanisms involved in lncRNA function. As such, lncRNA may be defined by 4 different archetypes (Figure 1-13).

Archetype 1: signal archetype meaning that the lncRNA functions as a molecular signal or indicators of transcriptional activity. Some lncRNAs in this archetype possess regulatory functions, while others are merely by-products of transcription, it is the act of initiation, elongation, or termination that is regulatory. An example of modulation of gene activity in response to external stimuli is found in the mammalian CDKN1A promoter, whereupon DNA damage the lncRNA PANDA is transcribed from the genome (Hung et al., 2011). Several signal archetypes may become beneficial in the hunt for new biomarkers of disease.

Archetype 2: Decoy archetype - lncRNA can bind to and titrate away other regulatory RNA or proteins. Examples of this include H19 and MALAT1. H19 is a lncRNA conserved across humans and rodents. Abundantly expressed in human muscle, H19, has been implicated in several genetic conditions (Brown et al., 1996). The functional role of H19 remained unknown until Kallen et al., discovered that H19 harbours both canonical and non-canonical binding sites for the let-7 family of microRNAs (Kallen et al., 2013). Utilising both knock down and overexpression approaches to modulate H19 expression, the authors discovered that H19 modulates let-7 availability by acting as a “molecular sponge”, reducing the level of free let-7 able to bind its target mRNA. Physiologically, this has implications in the control of SMC phenotype where knockdown of H19 caused precocious muscle differentiation, a phenotype recapitulated by let-7 overexpression.

MALAT1 is an abundant nuclear lncRNA that is localised to nuclear paraspeckles. MALAT1 binds and sequesters arginine/serine splicing factors to these paraspeckles. Knock-down of MALAT1 leads to differential localisation of splicing factors and aberrant splicing for a set of mRNA (Wang and Chang, 2011). Thus

lncRNA decoys are not only apparent in the cytoplasm of cells but also possess regulatory functions in the nucleus.

Achetype 3: Guide archetype – lncRNA direct the localisation of specific ribonucleotide proteins to their specific targets. For example,lncRNA fetal-lethal non-coding developmental regulatory RNA (Fendrr), which is specifically transcribed in nascent lateral plate mesoderm of the developing mouse embryo, guides polycomb repressor complex 2 (PRC2) to target genes to increase PRC2 occupancy and trimethylates H3K27me3, subsequently leading to attenuation of target gene expression (Grote et al., 2013).

Archetype 4: Scaffold archetype – lncRNA can act as a structural platform upon which relevant components may act to stabilise nuclear structures or signalling complexes. LncRNAs act as protein scaffolds to control gene expression. An example of this is the subnuclear structure-specific lncRNAs taurine (TUG1) and nuclear-enriched autosomal transcript 2 (NEAT2) which bind to methylated and unmethylated polycomb 2 protein (Pc2) respectively to mediate assembly of multiple corepressor or coactivator protein complexes (Yang et al., 2013).

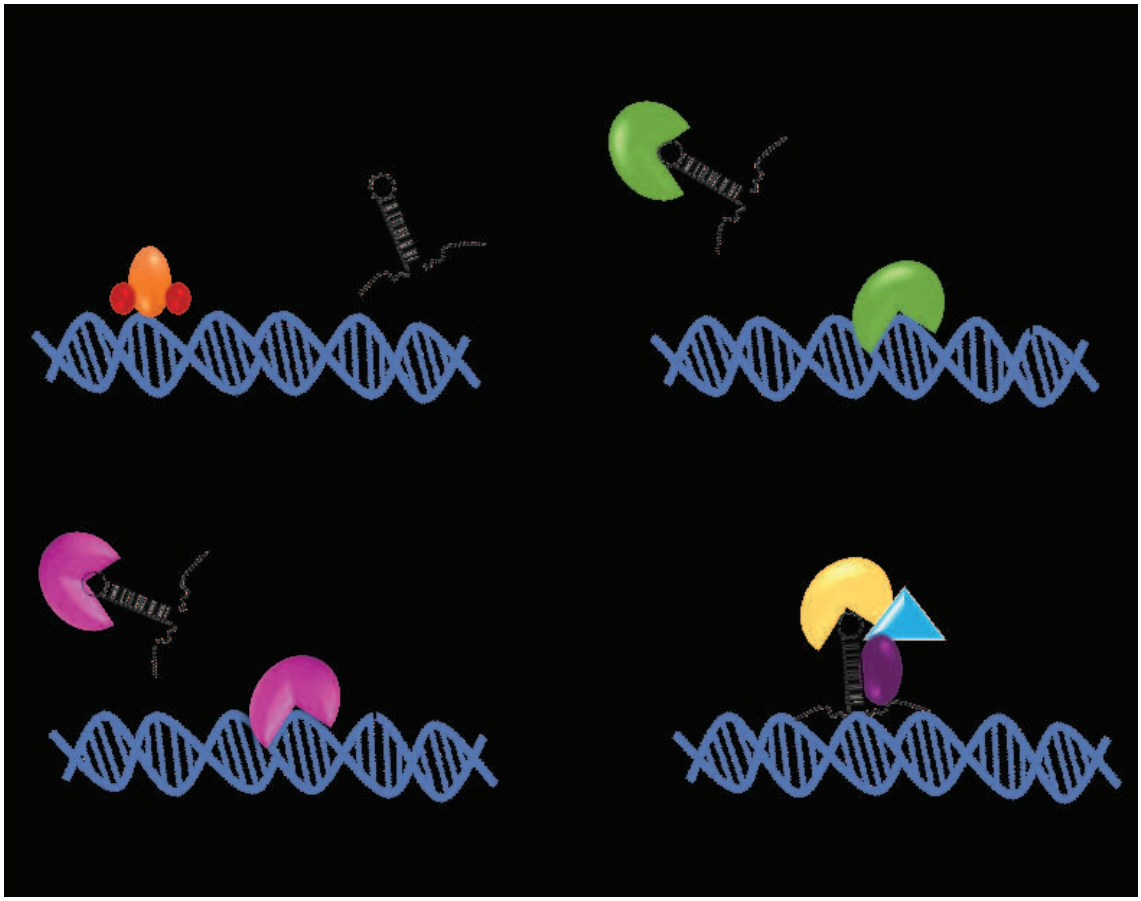

Figure 1-13: LncRNA classification based on function.
Signals: function as molecular signals to indicate gene regulation in space and time. Decoys: binding to proteins and titrating them away from chromatin, acting as a 'molecular sponge'. Guides: binding to protein and then directing the localization of the ribonucleoprotein complex to specific target genes to regulate their expression. Scaffolds: providing a platform to assemble different effector molecules to function together.

1.9.2.5 *Cis* and *trans* activating lncRNA

Mechanistically, most well-characterised lncRNAs to date show a functional role in regulating gene expression, typically transcriptionally rather than post transcriptionally. Two terms are utilised to identify the location at which lncRNA act. LncRNA action can either occur by targeting genomically local genes known as cis-regulation or by acting away from the site of transcription known as trans-regulation.

Cis-regulation by lncRNAs contributes to local control of gene expression by recruiting histone modification complexes to specific areas of the genome. This effect can either be highly specific to a particular gene, such as the regulation of IGF2 by lncRNAs (Matouk et al., 2015) or it can encompass a wide chromosomal region, such as X chromosome inactivation in women through XIST lncRNA (Sarkar et al., 2015).

Trans-acting lncRNAs may operate at geographically distant locations of the genome or within the cytoplasm of the cell. Thus, it is generally thought that the mature lncRNA transcript is the primary actor in these cases, as opposed to cis-regulating lncRNAs which may function through the act of transcription itself. One such example of this is BACE1-AS, a natural antisense lncRNA, that plays a role in regulating BACE1's expression. In the cytoplasm BACE1-AS1 forms a duplex with BACE1 mRNA. The formation of this duplex protects BACE1 from microRNA induced repression by masking the binding site for miR-485-5p (Faghihi et al., 2010).

1.9.2.6 Cell type and cell state specificity of lncRNA expression.

One key trait of lncRNA is their specific expression patterns in tissues, cell types and subcellular compartments. Transcriptome-wide studies have shown that lncRNAs, in general, exhibit more specific expression profiles than mRNAs (Quinn and Chang, 2016), indicating that they are expressed in a cell type, tissue, developmental stage or disease state specific manner. This restricted lncRNA expression may prove beneficial in the targeting of lncRNA for therapeutic effects, bypassing the normal off target effects seen with several drugs. Due to lncRNA research being a relatively new area, critical gaps in our knowledge as to

why lncRNA show cell and tissue restricted expression and what mechanisms control the expression patterns still remain.

1.9.2.7 LncRNA in vascular SMC and disease

To date, currently only a few lncRNA have been shown to regulate key aspects of SMC function/phenotype. As shown in Figure 1-14, lncRNA can modulate key SMC processes such as proliferation, migration and contraction. The 5 key lncRNAs are SENCR, HIF1-AS1, Linc-p21, Lnc-Ang362 and HAS2-AS1.

SENCR

SENCR, a smooth muscle and endothelial enriched lncRNA, is situated in the antisense orientation to a protein coding gene called Friend Leukaemia virus Integration 1 (FLI1). Further characterisation revealed that SENCR and FLI1 expression correlate with each other in various tissues, implying that these transcripts share common transcriptional machinery. Additionally, spatial distribution of a lncRNA is likely to imply its function, thus SENCR was identified as being a solely cytoplasmic lncRNA in both endothelial and smooth muscle cells, indicating that SENCR may act in *trans* to exert it cellular function. Consistent with this, siRNA mediated knockdown of SENCR dysregulates several SMC contractile genes such as MYOCD but does not affect the expression of FLI1. Concomitant with suppression of SMC contractile genes, SENCR knock-down also promoted the migration of vascular cells (Bell et al., 2014). As with several lncRNA, the mechanism by which SENCR promotes contraction of SMC is still unknown, however, it has been proposed that SENCR sponges a low abundant microRNA that otherwise would function to regulate the SMC contractile gene program. Other potential underlying mechanisms still have to be elucidated.

HIF1A-AS1

HIF1α is a transcription factor that responds to hypoxia. HIF1α-AS1 is a lncRNA that overlaps HIF1α in the antisense orientation. Previously it has been shown that HIF1α regulates Angiotensin II mediated vascular remodelling. This was determined through the generation of a SMC specific HIF1α knockout mouse. Ang II infusion induced medial thickening and vascular fibrosis, accompanied by Hif-

1α up-regulation, in the aortae of control mice, but not in the KO mice (Imanishi et al., 2014). With the identification of an antisense lncRNA, the role of HIF1α-AS1 was evaluated in SMC. Interestingly, in cells incubated with palmitic acid, an inducer of apoptosis, HIF1α-AS1 expression was found to be greater than in control cells. Furthermore, knock-out of endogenous HIF1α-AS1 with small-interfering RNA (siRNA) resulted in the protection of VSMC from palmitic acid induced apoptosis (Zhao et al., 2014). Further work by an additional lab identified that knockdown of HIF1α-AS1 not only protected VSMC from apoptosis but also stimulated proliferation. Additionally, the authors identified HIF1α-AS1 in the serum of patients with thoracic aortic aneurysms. Additionally VSMC apoptosis is a key feature of aortic aneurysms and as such the authors speculated that HIF1α-AS1 may be implicated as a causal factor in several vascular pathologies including aortic aneurysms. It was also documented that HIF1α -AS1 expression is positively regulated by Brahma-related gene 1 (BRG1), a central catalytic subunit of numerous chromatin-modifying enzymatic complexes. Although it has been shown that BRG1 modulates HIF1α-AS1, the mechanism of action of HIF1α-AS1 remains to be elucidated (Bai et al., 2012).

Linc-p21

Linc-p21, a conserved lncRNA, is located ~15kb upstream of the cell cycle regulator gene p21. Linc-p21 is ~3kbp in length and has been shown to promote cell proliferation, apoptosis and DNA damage response in a variety of disease states (Wu et al., 2014). Linc-p21 is a transcriptional target of p53, a tumour suppressor that regulates cell cycle. The expression of Linc-p21 is dramatically downregulated in atherosclerotic lesion from mice maintained on an atherogenic background. Subsequent gain and loss of function studies revealed that loss of Linc-p21 expression is associated with an increase in SMC proliferation and reduction in apoptosis in vascular smooth muscle cells. Furthermore, lentiviral mediated knockdown of Linc-p21 expression enhanced neo-intimal formation in murine arteries subjected to wire injury, events associated with increased SMC proliferation and survival. Genome-wide analysis revealed that lincRNA-p21 inhibition dysregulated many p53 targets. This study was one of the first to demonstrate that modulation of lncRNA has therapeutic potential in the setting of acute vascular injury. Linc-p21 has been shown to exert its function by acting

as an endogenous sponge to miRNA-130b in smooth muscle cells to modulate SMC phenotypes (Bertero et al., 2014).

LncAng-362

Aberrant regulation of angiotensin II (Ang II), has been linked to hypertension and atherosclerosis (Weiss et al., 2001). Following RNA-sequencing in Ang II treated cells Leung et al. identified a collection of Ang II responsive lncRNA. Among these lncAng 362 was identified (Leung et al., 2013). LncAng362 is located proximal to 2 microRNA, miR-221 and miR-222, which have been linked with regulation of SMC proliferation via suppression of c-kit and p27kip (Liu et al., 2009, Davis et al., 2009) . Knockdown of lncAng-362 is associated with a reduction in SMC proliferation and expression levels of these microRNAs, indicating that these miRNAs are co-regulated with lncAng-362. Furthermore, specific manipulation of either miRNA has been shown to reduce neo-intimal formation associated with smooth muscle cell proliferation (Liu et al., 2009). These studies raise the intriguing possibility that modulation of lncRNA could provide a novel mechanism to attenuate the hyper proliferative effects of Ang II within multiple vascular pathologies including coronary artery disease, PAH and atherosclerosis since both these miR-221 and miR-222 are implicated in proliferative vascular remodelling .

HAS2-AS1

The hyaluronan (HA) is a ubiquitous component of the extracellular matrix (ECM) with a wealth of cellular functions in both the physiological and pathophysiological context. HA is synthesised, in SMC, by the HA synthase enzyme, encoded in humans by the corresponding HAS2 leading to ECM production and SMC proliferation. HAS2 is located on the minus strand of human chromosome across from the natural antisense lncRNA HAS2-AS1. Studies performed in human aortic SMCs revealed that HAS2-AS1 was necessary for the transcription of the HAS2 gene by working in cis to open the chromatin structure around the HAS2 gene, allowing HAS2 transcription (Vigetti et al., 2014). It is therefore proposed that due to its effect on HAS2, HAS2-AS1 should induce SMC proliferation via ECM remodelling.

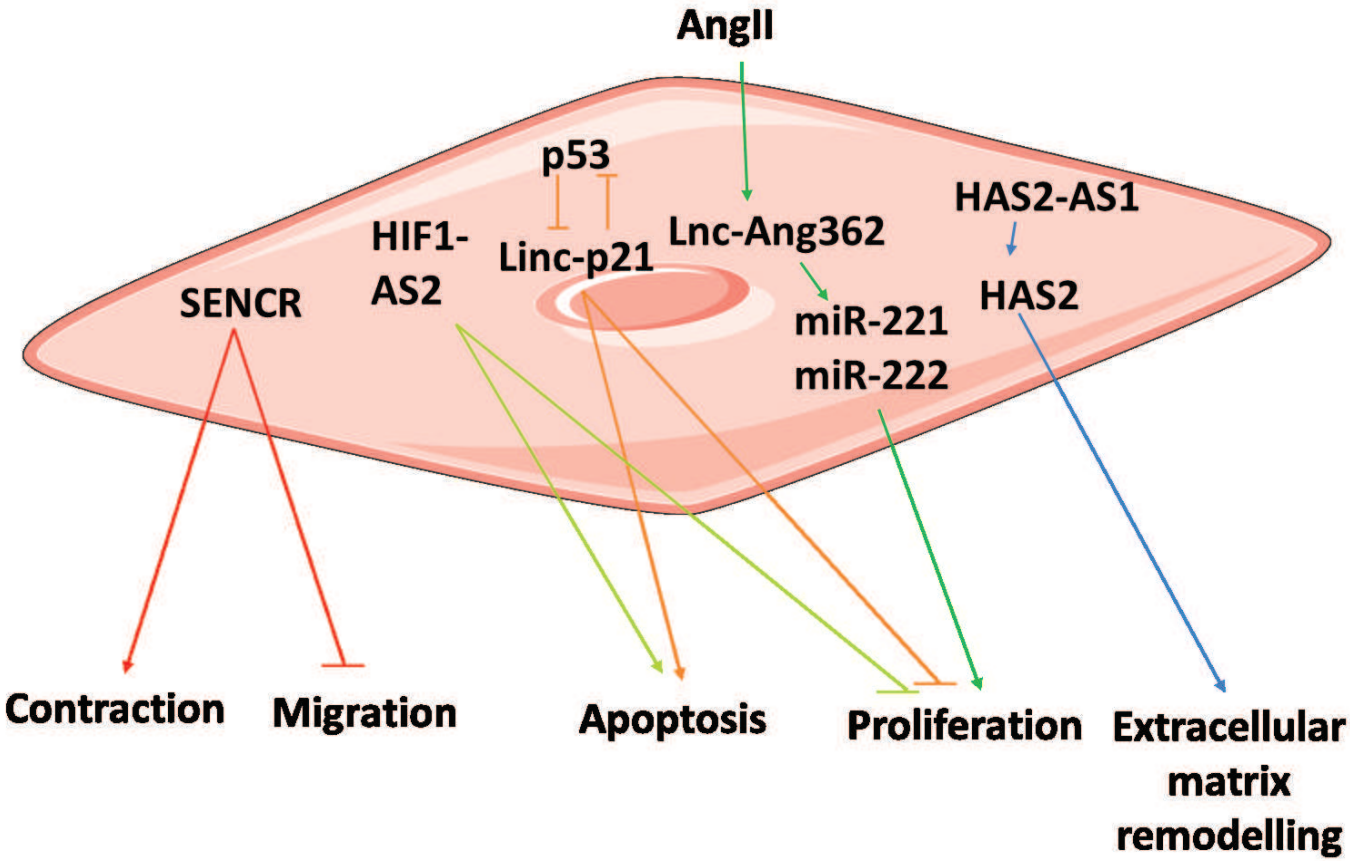

Figure 1-14: Overview of lncRNA function in VSMC.
Vascular SMC processes regulated by lncRNA. LncRNA expression can be altered through extracellular stimulation by components such as AngII and IL1α or PDGF. These lncRNA can then control processes such as contraction, migration, apoptosis, proliferation and extracellular matrix remodelling. Adapted from (2016) utilising Servier Medical Art.

1.10 Clinical applications of lncRNAs

1.10.1 LncRNA as diagnostic biomarkers

For clinical medicine, lncRNA offer many benefits. LncRNA typically show tissue restricted and vascular disease restricted patterns of expression (Clark et al., 2015, Jiang and Ning, 2015). Given this specificity, lncRNA may be superior biomarkers than current protein coding genes for cardiovascular disease.

A study of plasma levels of the lncRNA LIPCAR was the first proof of principle experiment highlighting the possible role of plasma lncRNA as biomarkers of prognosis in cardiovascular diseases. The initial lncRNA screening was performed according to the level of left ventricular (LV) remodelling in a echocardiographic study of patients after myocardial infarction (MI). One-year echocardiographic follow-up was completed on the patients and LV remodelling was assessed. From this population, 15 male patients with high LV remodelling and 15 male patients without LV remodelling were used in the initial cohort. Utilising these 30 patients, lncRNA microarray was performed on RNA isolated from plasma samples. Hierarchical clustering analysis clearly distinguished the 2 groups of patients based on a specific signature of detectable and significantly regulated circulating lncRNAs. One lncRNA called long intergenic non-coding RNA predicting cardiac remodelling (LIPCAR) showed greatest correlation and greatest change in expression between the two patient populations (Kumarswamy et al., 2014). Longitudinal studies in larger cohorts and at 1, 3 and 12 months post myocardial infarction, LIPCAR showed a time dependent increase and significantly higher levels in patients developing LV remodelling. Additional experiments in a cohort of 344 heart failure (HF) patients identified that LIPCAR levels were even higher in chronic HF than in patients with ongoing LV remodelling 1 year after myocardial infarction(Kumarswamy et al., 2014). This study was the first to examine the potential role of lncRNA biomarkers in the setting of cardiovascular disease and demonstrated that lncRNA serve as potential biomarkers due to their stability.

Another example is CoroMarker (AC100865.1), a lncRNA that is markedly overexpressed in coronary artery disease (CAD). The study screened lncRNAs by microarray analysis in plasma from CAD patients and control individuals and

found that 265 lncRNAs were differentially expressed. To identify candidates, the results were filtered according to the strict criteria of signal intensity ≥8, fold change >2.5 and P<0.005. This identified 5 lncRNA that were validated by qRT-PCR. Further analysis on an additional set of 40 patients highlighted CoroMarker as the most appropriate marker for CAD. The predictive value of CoroMarker was the further assessed in a large cohort with 221 CAD patients and 187 control individuals. CoroMarker was able to successfully identify 78.05 % of CAD patients (Yang et al., 2015a). CoroMarker is stably expressed within the plasma and further test to evaluate its ability to detect CAD are currently underway.

1.10.2 LncRNA as therapeutics

The transition from lncRNA biomarkers to lncRNA therapeutics is also showing promising advances. Companies and organisations such as Miragen Therapeutics and Regulus are developing ncRNA-based strategies against cancer, cardiovascular and neurological diseases. Although lncRNA clinical trials are still several years away, it is generally accepted that targeting of lncRNA therapeutically may lead to less off target effects, due to their enhanced tissue specificity. Additionally, the advantage of using RNA as a therapeutic medium would allow quick regulatory functions to be altered without the need for protein translation. There are several therapeutic approaches for targeting lncRNA in man:

Therapeutic silencing of long non-coding RNA. LncRNA expression can be altered through the use of RNAi technology. Therapeutic RNAi technology has now been tested in several mammals including man (Zimmermann et al., 2006), (Tabernero et al., 2013). Current clinical trials are investigating the safety and efficacy of RNAi mediated therapeutics, one example of this is the therapeutic RNAi mediate inhibition of PCSK9 as a LDL cholesterol lowering therapy for hypercholesterolemia. RNAi could therefore be relatively easily adapted to allow RNAi therapies targeting lncRNA.

1. Functional block of lncRNA. This could be achieved through the utilisation of small molecules that block binding sites on protein interacting partners or oligonucleotides that bind to the lncRNA blocking

the interaction with partners such as miRNA, whilst allowing the lncRNA to bind additional partners at other sites not associated with disease. Current research has already assessed the use of high throughput screening to identify small molecule disruptors for the lncRNA HOTAIR (Pedram Fatemi et al., 2015). The authors sought to determine whether the HOTAIR-EZH2 interaction could be assayed, quantified and adapted for high-throughput screening to identify modulators of this interaction. Utilisation of a small library of 320 compounds only identified one hit, camptothecin, a cytotoxic quinoline alkaloid which inhibits the DNA enzyme topoisomerase, however during validation this compound was shown to affect control conditions (Fatemi et al., 2015). Further large scale high-throughput analyses are thus required to identify disrupter small molecules that can interrupt lncRNA-protein interactions.

2. Structure disruption. Small molecules can be utilised to bind to the lncRNA of interest and disrupt its secondary structure thus disrupting the binding site on the lncRNA or small molecules can be utilised to mimic the structure of the lncRNA thus competing with the lncRNA for target sites. As such no work has been performed on lncRNA, however, work on other RNA molecules has proved promising (Stelzer et al., 2011), (Sanchez and Huarte, 2013). One such example was performed by Stelzer et al., where small molecules that target the entire structure of the transactivation response element (TAR) from HIV type 1 (HIV-1) were assessed. Analysis of binding affinities identified 6 compounds that bind different RNA conformations with high affinity and inhibit its interaction with a Tat peptide in vitro. Of particular interest was one compound that bound HIV-1 TAR with marked selectivity and inhibited Tat-mediated activation of the HIV-1 long terminal repeat by 81 % in T-cell lines and HIV replication in an HIV-1 indicator cell line. This therefore highlights the applicability of this technique to be utilised on RNA molecules.

3. Finally, gene therapy could be utilised to deliver beneficial lncRNA. Gene therapy describes the transfer of genes to a target cell or organ to treat or prevent disease. Successful delivery of a gene to the target is paramount to therapeutic efficacy and a number of viral and non-viral

based vectors have been developed. In 2012, over 1800 gene therapy clinical trials had been completed, were ongoing or had been approved worldwide (Ginn et al., 2013). Gene therapy provides advantages and allows the delivery to specific cell types. One example of this is the plasmid BC-819 (DTA-H19) that has been developed to make use of the tumour-specific expression of the H19 lncRNA. This plasmid carries the gene for the A subunit of diphtheria toxin under the regulation of H19 promoter. The intra-tumour injection of this plasmid induces the expression of high levels of diphtheria toxin in the tumour, resulting in a reduction of tumour size in human trials in a broad range of carcinomas, whilst leaving non tumour cells untouched (Mizrahi et al., 2009). Viral gene therapy has yet to be utilised clinically for lncRNA. However, the vast majority of gene transfer studies, not just those pertaining to cardiovascular diseases, have focussed on the use of adenoviruses (Wolfram and Donahue, 2013). One such example of an ongoing clinical trial is the administration of adeno associated viruse containing Human Factor IX Gene for the treatment of patients with Haemophilia B. The success of these clinical trials will undoubtedly pave the way for lncRNA gene therapy.

Due to their multiple functional roles, the therapeutic potential of lncRNA is extremely vast.

1.11 Hypothesis and aims

The work described in this thesis addressed the hypotheses that:

1. LncRNA are dysregulated in vascular pathologies involving IL1α and PDGF signalling pathways.

2. LncRNA play a significant role in altering vascular smooth muscle proliferation associated with vascular pathologies.

In order to address these hypotheses, the aim of the specific studies performed was to answer the following questions:

1. Are lncRNA dysregulated in VSMC treated with IL1α, PDGF and a combination of IL1α and PDGF?

2. What role do these lncRNA have on VSMC behaviour?

3. How do these lncRNA function and what are they binding?

4. Are these lncRNA dysregulated in human cardiovascular disease states?

Chapter 2 Materials and Methods

2.1 General laboratory practice

Laboratory reagents and equipment were of the highest commercially available standard. All chemicals, unless otherwise stated, were purchased from SigmaAldrich, Dorset, UK. Hazardous chemicals were handled and disposed of in compliance with Control of Substances Hazardous to Health (COSHH) guidelines. Laboratory coats, nitrile powder-free gloves and fume hoods were used where appropriate.

2.2 Isolation and culture of human primary cells

2.2.1 Human tissue samples

Surplus human saphenous vein tissue was obtained from patients undergoing CABG surgery. Carotid plaques were obtained from patients undergoing endarterectomy following an acute and symptomatic neurovascular event. Human plasma samples were utilised from a previously published study: Carotid Ultrasound and Risk of Vascular disease in Europeans and South Asians (CURVES). All patients gave their written, informed consent. All procedures had local ethical approval (06/S0703/110, 12/WS/0227, 09/S0703/118 and 12/NW/0036). All studies were approved by East and West Scotland Research Ethics Committees and all experiments were conducted according to the principles expressed in the Declaration of Helsinki.

2.3 General cell culture techniques

All cell culture was performed in standard biological safety class II vertical laminar flow cabinet under sterile conditions. Cabinets were cleaned before and after use with 1 % virkon and 70 % ethanol.

2.3.1 2.4.1 Isolation of primary vascular endothelial cells from the human saphenous vein

Primary human saphenous vein endothelial cells (HSVECs) were isolated on the day of surgery by collagenase digestion, based on the method previously described by Jaffe and colleagues (Jaffe et al., 1973). Briefly, the lumen was flushed with wash media (Dulbecco's Modified Eagle's Medium (DMEM), supplemented with 100 IU/ml penicillin, 100 µg/ml streptomycin and 2 mM L glutamine; all Gibco, Paisley, UK). The lumen was filled with 2 µg/ml collagenase solution diluted in wash medium and incubated at 37ºC in 5 % CO_2 for 15 min. The lumen was then flushed with wash medium to obtain HSVECs in suspension. This process was repeated with collagenase digestion time reduced to 10 min. The wash medium/HSVEC suspension was centrifuged at 2000 x g for 15 min and the pelleted HSVECs were resuspended in EC growth medium (Large Vessel Endothelial Basal Cell Medium) (TCS Cellworks Ltd, Bucks, UK), supplemented with 20 % (v/v) FCS, 100 IU/ml penicillin, 100 µg/ml streptomycin and 2 mM L-glutamine. Cells were plated in 25 cm^2 vented cap cell culture flasks and maintained in a 37ºC, 5 % CO_2 incubator for 24 h to ensure cell adhesion before media was refreshed.

2.3.2 Isolation of primary vascular smooth muscle cells from the human saphenous vein

Primary human saphenous vein smooth muscle cells (HSVSMCs) were isolated within 48 h of surgery by an explant technique originally described by Southgate and Newby (Southgate and Newby, 1990). Briefly, the lumen was flushed with wash medium before the vein was cut longitudinally and the 4 corners pinned out with the lumen face up. HSVECs were removed by gently running a rubber policeman over the lumen surface. Vessels were scored with a scalpel blade and the medial SMC layer peeled back with forceps. The SMC tissue was cut into small pieces (~1 mm^2) using the McIlwain tissue chopper. SMC tissue was washed twice with wash medium and once in SMC growth medium (Smooth Muscle Cell Growth Medium 2 containing: 0.5 ng/ml epidermal growth factor, 2 ng/ml basic fibroblast growth factor and 5 µg/ml insulin) (PromoCell, Heidelberg, Germany) supplemented with 15 % FCS, 100 IU/ml penicillin and 100 µg/ml streptomycin. SMC tissue was plated in 25 cm^2 vented cap cell culture flasks and maintained in

a 37ºC 5 % CO_2 incubator. All excess SMC growth medium was removed to allow HSVSMCs to adhere to the flask before SMC growth medium was replaced 24 h later.

2.3.3 Culture of HSVEC and HSVSMC

Following growth in 25 cm^2 flasks, both HSVSMC and HSVEC were bulked into 75 cm^2 vented-cap cell culture flasks (Corning, Poole, UK) and media was replenished every 2-3 days or as required. Cells were passaged at 70 %-80 % confluency to avoid overgrowth. All cells were utilised between passages 3-5. To passage, culture medium was removed and cells were washed once with PBS. 3 mL 1x trypsin was then added to each flask and cells were incubated at 37˚C, 5 % CO_2 for 2-3 min. When the majority of cells had detached from the flask, 6 mls of media containing FBS was added to neutralise the trypsin. Cells were then collected and pelleted by centrifugation at 1,500 rpm for 5 min. The supernatant was then discarded and cells were re-suspended in an appropriate volume of fresh culture medium before being distributed amongst flasks.

2.3.4 Culture of HEK-293Ts for lentivirus production

For lentivirus preparation (section 2.15) HEK-293Ts (ATCC, Teddington, UK) were passaged at a ratio of 1:2 24 h prior to triple transfection of lentivirus producing plasmids. When cells were needed at specific densities, e.g. titration of lentivirus particles, cells were counted using a haemocytometer prior to seeding in appropriate cell culture vessel.

2.3.5 IL1α and PDGF treatment of HSVSMC

Human recombinant IL1α and PDGF-BB (R&D systems, Abingdon, UK) were re-constituted at 10 µg/ml and 20 µg/ml in PBS containing 0.5 % FBS and 4 mM HCl respectively. All reagents were aliquoted and stored at -80ºC. Freeze thaw was performed a maximum of twice before reagents were discarded. For stimulation of cells, HSVSMC were plated at the appropriate density ($1x10^5$ cells/ well or $5x10^4$ cells/well for 6 or 12 well plates respectively) and left to attach for a minimum of 6 h. Complete media was removed and cells washed with 1x PBS. Media was replaced with 2 ml/well or 1 ml/well of DMEM supplemented with 0.2

% FBS, 50 µg/ml penicillin and 50 µg/mL streptomycin ('serum-free media') for 48 h for 6 and 12 well plates respectively. Following incubation a master mix of media +/- cytokines or growth factors was produced, as required. 1 µl of IL1α and/or 1 µl of PDGF-BB was added per ml of media to a final concentration of 10 ng/ml and 20 ng/ml respectively. 0.2 % media was removed, cells washed 1x with PBS and stimulation media applied. Cells were stimulated for various time points from 4-72 h depending on experiments, as detailed below.

2.4 RNA extraction

Total RNA was extracted utilising a miRNeasy kit, as per manufacturer's instructions (Qiagen, Hilden, Germany). An on-column DNase treatment was also performed during the extraction via the use of the accompanying RNase-free DNase Set (Qiagen).

Culture media was removed and washed 1x PBS. 700 µl QIAzol lysis reagent was added per well. Sampled were homogenised by pipetting up and down and samples placed into a 1.5 ml Eppendorf. All sampled were stored at -80°C until required.

When required, cell lysates were thawed on ice before the addition of 140 µL chloroform. Samples were mixed and incubated at RT for a further 3 min to allow the contents to settle. Sampled were then centrifuged at 12,000 x g at 4°C for 15 min. Centrifugation allowed sampled to separate into 3 distinct phases; an upper, aqueous phase, containing total RNA, a middle interphase, containing DNA and a lower, organic phase, containing proteins. The upper aqueous phase was transferred into a new 1.5 ml tube. 550 µL of 100 % ethanol was added and the nucleic acids precipitated by pipetting up and down. Samples were then transferred to RNeasy spin columns, and centrifuged at 16,000 x g for 30 s and the flow through discarded. This allowed total RNA to bind to the column, whilst phenol and other contaminants were efficiently washed away. 350 µL RWT buffer was then added and columns were centrifuged again at 16,000 x g for 30 s at RT. At this point an optional DNase treatment was carried out in order to remove any contaminating DNA. DNase was prepared according to manufacturer's instructions and 10 µL of enzyme was mixed with 70 µL RDD buffer per sample. 80 µL of the DNase/RDD buffer mix was then added directly

onto each column and left to incubate for 15 min at RT. After 15 min, a further 350 µL of RWT buffer was added and columns were centrifuged for 30 s at 16,000 x g at RT. The eluate was discarded and 500 µL RPE wash buffer was added. Columns were centrifuged for 30 s at 16,000 x g at RT and a further 500 µL RPE wash buffer was added. Columns were spun, as before, for 2 min. miRNeasy spin columns were then transferred to clean 2 mL collect tubes and centrifuged at full speed for 1 min. This spin ensured removal of residual ethanol and avoided carryover of buffers which may have interfered with downstream reactions. Total RNA was then eluted by passing 36 µL of nuclease-free water through the spin column for 1 min at 16,000 x g. The eluate was then collected and passed through the column again to obtain an optimal RNA yield.

RNA concentration was determined via NanoDrop 1000 spectrophotometer (Thermo Scientific, Paisley, UK) and samples stored at -80°C until required.

2.4.1 Evaluation of RNA quality

Quality control of RNA was performed using the Agilent® 2100 Bioanalyser. The Aligent® 2100 Bioanalyser is used to measure the quality of RNA, via the calculation of a RNA integrity number (RIN). RIN is calculated based on the presence or absence of degradation productions within the sample. This technique was used to assess RNA-seq samples before submission, with RIN values greater than 8 being deemed as high quality.

2.5 RNA-sequencing

RNA-seq was performed on ribosomal RNA-depleted samples using an Illumina Hiseq platform by Beckman Coulter Genomics. Paired-end sequencing was carried out with a read depth of 70 million reads per sample (n=4/group). RNA-seq reads were processed and trimmed to ensure quality, adapter sequences removed using Flexbar (Dodt et al., 2012) and mapped to the Ensembl annotation of GRCh37.75 using TopHat2 version 2.0.9 (Kim et al., 2013). The transcriptome was assembled from the aligned reads and quantified using Cufflinks version 2.2.1 (Trapnell et al., 2010). The differential expression levels between the groups was assessed using Cuffdiff version 2.2.1 (Trapnell et al., 2013). The data sets are deposited in the GEO repository, study number

GSE69637. The biotype of each transcript was annotated according to the Ensembl database. Normalisation and statistical analysis of differentially expressed transcripts was carried out using edgeR and data filtered to find transcripts that were differentially expressed ($p<0.01$) between 0.2 % media controls and each treatment group. Multiple comparison analysis was performed according to Table 2-1. Differentially expressed lncRNAs, between control and both IL1α/PDGF treatment, were explored using more stringent criteria ($p<0.01$, FDR<0.01, LogFC>2) and filtered according to transcript abundance (FPKM>1 in at least one group). Data outputs such as pie charts and heatmaps were generated using R. IPA analysis was carried out using protein coding genes differentially expressed (FDR<0.01) from Edge R analysis.

Table 2-1: EdgeR Groupings for differential analysis.

Control x Group 1	Control x Group 2	Control x Group 3
	Group 1 x Group 2	Group 1 x Group 3
		Group 2 x Group 3

Group 1 = PDGF
Group 2 = IL1α
Group 3 = IL1α + PDGF

2.6 Quantitative real time PCR (qPCR) for gene and microRNA expression analysis

2.6.1 Reverse transcription polymerase chain reaction (RT-PCR) – Analysis of gene expression

For gene expression analysis, cDNA was generated from total RNA using the Multiscribe Reverse Transcriptase kit (Thermo Fisher, Paisley, UK).

Each reaction contained 100-300 ng RNA. RNA was combined with 1x reverse transcription buffer, 5.5 mM MgCl2, 0.5 mM of each dNTP, 2.5 µM random hexamers, 0.4 U/µL RNase inhibitor enzyme and 1.25 U/µL Multiscribe™ Reverse Transcriptase. A final volume of 20 µl was achieved through the addition of nuclease-free H_2O. Samples were subjected to the following temperature cycle in a thermal cycler: 10 min at 25°C to allow for annealing of random primers, 30 min at 48°C for reverse transcription and 5 min at 95°C to inactivate the reverse transcriptase. Samples were then removed from the thermal cycler and placed at -20°C until required.

2.6.2 SYBR Green quantitative RT-PCR (qRT-PCR) – Analysis of gene expression

The abundance of mRNA was quantified using SYBR qRT-PCR utilising Power SYBR green (Thermo Fisher) with custom PCR primers (Eurofins MWG, Ebersberg, Germany) (detailed in Table 2-2). All primers were designed spanning intron-exon boundaries and were reconstituted in nuclease-free H_2O at 100 µM, aliquoted and stored at -20^{o}C. During SYBR green qPCR, direct detection of the PCR product is monitored by measuring the increase in fluorescence caused by the binding of SYBR® Green dye to double-stranded (ds) DNA thus, the more abundant the transcript the greater the incorporation of the dye during each PCR cycle.

2.5 µl of cDNA produced in section 2.6.1 was added to 5 µl Power SYBR Green master mix, 4.9 µl nuclease-free H_2O and 0.05 µl each of 100 µM forward and reverse SYBR green primers. All plates contained appropriate housekeeping genes, a gene which should maintain relatively stable expression levels throughout a sample set. This allowed for comparison of expression levels between samples. For gene expression analysis, Ubiquitin protein C (UBC) was selected as a stable housekeeping gene and was used as a reference gene throughout the studies. In addition to the housekeeper control, non-template controls, in which cDNA was substituted with water, were also added to the plate. All samples were performed in triplicate. qPCR plates were centrifuged at 8,000g for 2 min, to ensure all samples and master mix were at the bottom of the wells. Samples were run on the Quantstudio 7 or Quantstudio 12 real time PCR system and were subject to 10 min at 95°C before undergoing 40 cycles of denaturing at 95°C for 15 s, followed by 60 s at 60°C for primer annealing and primer extension. Following the final reaction step, samples were subjected to melting curve analysis to assess whether the intercalating SYBR dye produced a single, specific product.

Table 2-2: SYBR green primer sequences.
Exon spanning lncRNA primers were designed to each lncRNA to ensure no genomic DNA was assessed during qRT-PCR.

Primer Name	Gene Name	Sequence 5' - 3'
SMILR_F	RP11-94a24.1_F	ACCTTGGAGGTCTTGGGAGT
SMILR_R	RP11-94a24.1_R	TTGCAGACACCTTCCAAACA
LncRNA_4_F	RP11-709B3.2_F	AAAAACTGCCACCTGTGACC
LncRNA_4_R	RP11-709B3.2_R	TTGGTGTAGGTCTGGGGAAG
LncRNA_5_F	RP11-761I4.4_F	AGGCCACCTATAAGCATTCAG
LncRNA_5_R	RP11-761I4.4_R	TTAGACGGCATCCATGTCAC
LncRNA_6_F	RP11-760H22.2(2)_F	CTGCATTGGAGAGACAGGAAT
LncRNA_6_R	RP11-760H22.2(2)_R	AAAGCTGAAACCCTAAAGTCATTG
LncRNA_7_F	RP11-91K9.1 (2) (720)_F	TGGCTAGGAGGGGGTCTATC
LncRNA_7_R	RP11-91K9.1 (2) (720)_R	CACGGTGGCTCACACTTTTA
LncRNA_8_F	AC018647.3-003 – 144 (1)_F	CCAAGGTGATGAGCACAAAA
LncRNA_8_R	AC018647.3-003 – 144 (1)_R	AAAGGTGGCAGAGTCCTTGA
UBC_F	UBC_F	TTGCCTTGACATTCTCGATG
UBC_R	UBC_R	ATCGCTGTGATCGTCACTTG
GAPDH_F	GAPDH_F	ACAGTCCATGCCATCACTGCC
GAPDH_R	GAPDH_R	GCCTGCTTCACCACCTTCTTG
MALAT1_F	MALAT1_F	GTGATGCGAGTTGTTCTCCG
MALAT1_R	MALAT1_R	CTGGCTGCCTCAATGCCTAC
C.elegans_AMA1_F	C.elegans_AMA1_F	CAGTGGCTCATGTCGAGTTTCCAGA
C.elegans_AMA1_R	C.elegans_AMA1_R	CGACCTTCTTTCCATCATTCATCGG

2.6.3 Taqman® qRT-PCR – Analysis of gene expression

TaqMan® qRT-PCR was performed using TaqMan® Gene Expression assays and TaqMan® Universal Master Mix II (both Thermo Fisher) in accordance with the manufacturer's instructions. A table of Taqman probes utilised is provided in Table 2-3. For both mRNA and microRNA analysis (microRNA described in section 2.6.5) fluorescently labelled probes were used. TaqMan® qRT-PCR assays are labelled with a 5' fluorescent reporter dye, such as VIC or FAM, and a quencher molecule at the 3' end. When the TaqMan® probe is intact, fluorescence released from the 5' dye is transferred to the 3' quencher molecule 88 by a phenomenon known as fluorescence resonance energy transfer (FRET). However, during the amplification process, if the target sequence is present in the sample, the probe anneals and the quencher is cleaved via the action of the Taq DNA polymerase – present in the reaction mixture. The Taq polymerase enzyme contains a 5' nuclease domain, which allows degradation of DNA bound to the target, downstream of DNA synthesis. This results in the degradation of the TaqMan® probe, and cleavage of the 3' quencher molecule, therefore preventing FRET and allowing for the detection of the reporter fluorophores. The strength of the fluorescence is increased with each amplification cycle, and is relative to the amount of a specific mRNA or miRNA within a sample.

Reactions were performed in 384-well plates, and contained 1 x Taqman® assay (5 µL), and 1 x TaqMan® master mix (0.5 µL), as well as 1.5 µL cDNA (Section 2.6.2) and 3 µL nuclease free H_2O – giving a total reaction volume of 10 µL. Samples were run in triplicate on the Quantstudio 7 or Quantstudio 12 real time PCR system and were subject to 10 min at 95°C before undergoing 40 cycles at 95°C for 15 s, followed by 60 s at 60°C.

Table 2-3: Taqman Gene Assays.

Gene name	Assay ID
HAS1	Hs00987418_m1
HAS2	Hs00193435_m1
HAS3	Hs00193436_m1
OAS1	Hs00973637_m1
IRF7	Hs01014809_g1
ZHX2	Hs00208916_m1

2.6.4 MicroRNA reverse transcription

For miRNA analysis, cDNA was generated using the TaqMan® miRNA Reverse Transcription kit (Thermo Fisher). Each reaction contained 5 ng total RNA. RNA was added to the following reagents: 1 x reverse transcription buffer, 0.25 U/µL RNase inhibitor, 3.33 U/µL Multiscribe™ Reverse Transcriptase, 1 mM of each dNTP (all provided with the kit), 1 x TaqMan® miRNA reverse transcription primers (purchased from Thermo Fisher and described in Table 2-4). H_2O was then added to make a final reaction volume of 7.5 µL. Synthesis was performed using the following thermal cycling conditions: 16°C for 30 min, 42°C for 30 min and 85°C for 5 min. Samples were then removed from the thermal cycler and stored at -20°C until required. Reverse transcription of an endogenous control miRNA (RNU48) was also performed, in order to allow for normalisation of changes in miRNA expression.

Table 2-4: MicroRNA probes.

microRNA	Assay ID
miR-146a-5p	478399_mir
RNU48	001006

2.6.5 MicroRNA qRT-PCR

miRNA expression qRT-PCR was performed using TaqMan® miRNA RT-PCR probes (provided in same assay as reverse transcription primers), and TaqMan® Universal Master Mix II in accordance with the manufacturer's instructions. Each reaction contained 5 µL TaqMan® mastermix, 0.5 µL miRNA probe, 3.83 µL nuclease-free H_2O and 0.67 µL cDNA from miRNA reverse transcription, and were performed in triplicate in 384-well plates. Samples were run on the Quantstudio 7 or Quantstudio 12 real time PCR system and were subject to 10 min at 95°C, 40 cycles at 95°C for 15 s and 60 s at 60°C. As before samples were stored at -20°C until required.

2.6.6 Analysis of qRT-PCR

For all qRT-PCR analysis (SYBR, mRNA and microRNA): as the cycle number increases, the detected fluorescence also increases due to exponential amplification of PCR products. Midway through the exponential phase of amplification, the Taqman machine records the number of cycles taken to reach this threshold, which is known as the Ct value. Data was then analysed using the comparative Ct method, also known as $2^{-\Delta\Delta Ct}$ method (Livak and Schmittgen, 2001). The ΔCt is the difference in the Ct between the gene of interest and the appropriate housekeeping gene. The mean ΔCt of all biological triplicates for the same gene of interest was calculated and used to calculate the ΔΔCt, which shows the difference in gene expression between a sample and control group. $2^{-\Delta\Delta Ct}$ is then used to calculate the fold increase or decrease in gene expression between a sample and the control group, whose value is equal to 1.

2.7 Assessment of HSVSMC proliferation

HSVSMC proliferation was quantified using a DNA bromodeoxyuride (BrdU) incorporation assay (Millipore, Watford, UK), or 5-ethynyl-2′-deoxyuridine (EdU) incorporation (ThermoFisher) according to the manufacturer's instructions. Both BrdU and EdU are nucleoside analogues of thymidine and are incorporated into DNA during active DNA synthesis. The amount of incorporated BrdU or EdU is a

measurement of DNA synthesis of the cells and thus an indirect measurement of proliferation.

For BrdU analysis, cells were seeded into 96 well plates at a density of $1x10^4$ cells per well and cells were allowed to settle overnight. Control reactions were also included that composed of 1. Blank: Tissue culture media only, no cells and 2. Background: cells were present in the wells but did not have any BrdU reagent added. Culture media was removed, cells washed in 1 x PBS and cells quiesced in 0.2 % FCS media for 48 h prior to stimulation. After this period the media was removed and cells washed in 1x PBS. Cells were stimulated with either 10 ng/ml IL1α, 20 ng/ml PDGF or a combination of both for 24, 48 or 72 h. 5 h after stimulation the BrdU substrate was prepared by diluting the 500X concentrated stock 1:500 in cell media. 20 µL of the diluted BrdU label was added to the appropriate wells. Following proliferation, the media was removed, 200 µL/well of the Fixing Solution was added and incubated at RT for 30 min. Fixing Solution was removed and plates washed 3 times with 1X Wash Buffer, provided in the kit. 100 µL/well of pre-diluted anti-BrdU antibody was added and incubated for 1 h at RT. Cells were washed 3 times in 1X Wash Buffer. The Goat anti-Mouse IgG, Peroxidase Conjugate antibody was prepared by diluting the Conjugate 1:2000 in the Conjugate Dilute provided and 0.22 µm syringe filtered to reduce background signal in the assay. 100 µL/well of the antibody was added and samples were incubated for 30 min at RT. Cells were washed as above and a final wash step was performed by flooding the 96 well plate with distilled water. 100 µL/well of TMB Peroxidase Substrate was added and incubated for 30 min at RT in the dark. Positive wells were visible by a blue colour, the intensity of which was proportional to the amount of BrdU incorporation in the proliferating cells. After adding the substrate solution, the immune complexes were detected using a plate reader set at dual wavelength of 450/550 nm, Victor (Perkin Elmer, Waltham, USA).

For EdU analysis HSVSMC were plated at $5x10^4$ cells/ well in 12 well plates and were subjected to the same quiescent and stimulatory conditions as above with the exception that EdU was added at a 1:1000 dilution to the stimulatory media. Cells were incubated with EdU for 48 h. Stock solutions of reagents were prepared accordingly: 10 mM solution of EdU, was prepared by adding 8 mL of

DMSO (Component C) to Component A and mixing well. EdU was aliquoted and stored at –20°C. 1X Click-iT® saponin-based permeabilisation and wash reagent was prepared by diluting a volume of Component E 1:10 with 1 % BSA in PBS and was stored at 2–8°C for a maximum of 6 months. 10X stock solution of the Click-iT® EdU buffer additive (Component G) was prepared by adding 2 mL of deionized water to the vial and mixing until the Click-iT® EdU buffer additive was fully dissolved. The reagent was aliquoted and subsequently stored at -20°C.

Following stimulation cells were washed once in PBS and 100 µl 1X trypsin solution added to each well to allow detachment of cells. Following detachment, trypsin was neutralised with the addition of 100 µl complete SMC media and cells transferred to a new 1.5 ml Eppendorf. Cells were centrifuged at 600 xg for 6 min, no brake, and the supernatant discarded. Cells were then fixed overnight at 4 °C. In order to fix cells, cells were resuspended in 100 µl PBS and fixed by adding 900 µl ice cold 70 % ethanol. Cells must be in suspension before the addition of ethanol or will fix as a clump. Thus, 70 % ethanol was added whilst vortexing. Following overnight incubation cells were centrifuged at 600 xg for 5 min, no brake. The supernatant was removed and 750 µl 0.2 % Triton X-100 was added, mixed well and incubated for 30 min at RT. 750 µl PBS +1 % BSA was added per tube and allowed to sit for 60 sec. Samples were centrifuged as above and supernatant removed. Click it Alexa reagent stock was prepared according to Table 2-5. 500 µl click it reagent was added per tube and incubated in the dark at RT for 60 min. Cells were washed in 1 mL PBS+1 % BSA, centrifuged as above and resuspended in 300 µL PBS. Samples were transferred to FACS tubes for analysis. Samples were analysed using the BD Biosciences FACSCanto II with FACSDiva software. Control samples, lacking EdU, were used as negative controls and used to set gates. 10,000 events were collected for each sample and analysis of flow cytometry data was performed using FlowJo analysis software (Tree Star, Ashland, USA).

Table 2-5: EdU 'Click it' preparation table.

Reaction component	Number of Reactions (500 µL volumes)						
	1	3	5	10	15	30	50
PBS	438 µL	1.31 mL	2.19 mL	4.38 mL	6.57 mL	13.2 mL	21.9 mL
$CuSO_4$	10 µL	30 µL	50 µL	100 µL	150 µL	300 µL	500 µL
Alex Fluoride	0.8 µL	2.4 µL	4 µL	12 µL	8 µL	24 µL	40 µL
1 x Reaction buffer additive	50 µL	150 µL	250 µL	500 µL	750 µL	1.5 mL	2.5 mL

2.8 MEKK1 and P38 inhibitor studies

For inhibitor studies, HSVSMC were plated in 6 well plates at a density of $2x10^5$ cells per well. As previously stated, cells were serum starved for 48 h prior to the experiment. 1 h before stimulation, cells were incubated with either 10, 15 or 20 μM AZD6244 (MEKK1 inhibitor, Selleckchem, Suffolk, UK) or 5, 10 or 20 μM P38 (SB 203580) which were diluted in serum free DMEM. Cells were then stimulated with either 0.2 % media as a control or a combination of 10 ng/ml IL1α and 20 ng/ml PDGF for 24 h for RNA quantification.

2.9 5' and 3' Rapid amplification of cDNA ends

5' 3' Rapid amplification of cDNA ends (RACE) was performed to determine the full length transcript of lncRNAs using the SMARTer RACE 5'/3' Kit (Clontech, Saint-Germain-en-Laye, France) according to manufacturer's instructions. SMARTer RACE 5'/3' utilises two steps as shown in Figure 2.1:

1. First-strand cDNA synthesis is primed using a modified oligo (dT) primer. After SMARTScribe Reverse Transcriptase (RT) reaches the end of the mRNA template, it adds several nontemplated residues. The SMARTer II A Oligonucleotide anneals to the tail of the cDNA and serves as an extended template for SMARTScribe RT.

2. RACE PCR that utilises gene specific primers (GSP) and the universal primer in order to identify additional sequences at the 5' and 3' end.

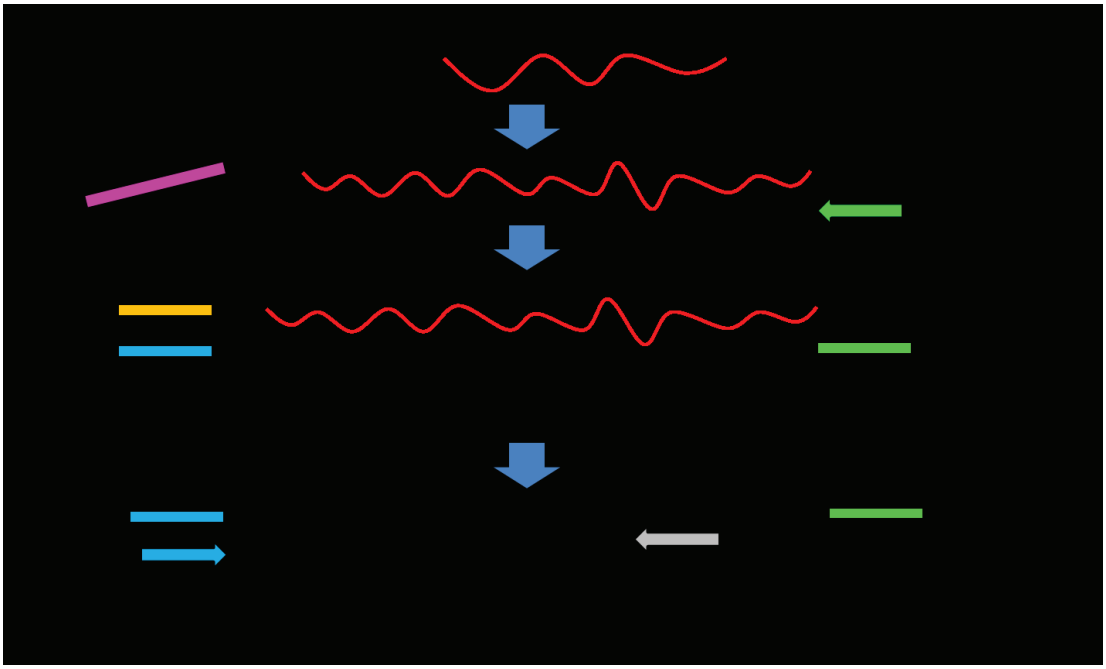

Figure 2-1: Overview of RT and RACE reaction.
General schema for 5' and 3' RACE experiments. Total RNA is reverse transcribed with a dTn primer. When the polymerase reaches the end of the sequence it adds an additional couple of bases. These bases act as a template for the Smarter II Oligonucleotide to generate complementary DNA strands. These strands are used as template to generate the first sets of RACE products using a universal primer and a gene specific primer to the gene of interest.

2.9.1 Primer design

Gene-Specific Primers (GSPs) were designed to be 23–28 nt, to ensure specific annealing, 50–70 % GC, had a Tm of >70°C, which enabled the use of touchdown PCR, not complementary to the 3'-end of the Universal Primer, specific to the gene of interest and had 15 bp sequence which overlapped with the vector at the 5' ends. This was required for subsequent cloning steps. RACE primer sequences are provided in Table 2-6.

Table 2-6: Race Primer Sequences.

Primer name	Gene name	Sequence
LncRNA_2_RACE_F	RP11-94A24.1_F	GATTACGCCAAGCTTTGCAAACATTG GGATCAGCCGTGA
LncRNA_2_RACE_R	RP11-94A24.1_R	GATTACGCCAAGCTTTCTCACAGCCA TGCTCTGGCCATT

2.9.2 First Strand cDNA synthesis

First strand cDNA synthesis was performed accordingly: Buffer Mix (BM) for all of the 5'- and 3'-RACE-Ready cDNA synthesis reactions was prepared. The reagents were added to a 1.5 ml Eppendorf, spun briefly and then set aside at RT until required: 4.0 µl 5X First-Strand Buffer 0.5 µl DTT (100 mM) 1.0 µl dNTPs (20 mM) per reaction. The second section of buffer was prepared separately for 5' and 3' reactions utilising as much RNA as possible (maximum 1 µg):

For preparation of 5'-RACE-Ready cDNA		For preparation of 3'-RACE-Ready cDNA	
1.0–10 µl	RNA*	1.0–11 µl	RNA*
1.0 µl	5'-CDS Primer A	1.0 µl	3'-CDS Primer A
0–9 µl	Sterile H_2O	0–10 µl	Sterile H_2O
11 µl	**Total Volume**	**12 µl**	**Total Volume**

*For the control reactions, use 1 µl of Control Mouse Heart Total RNA (1 µg/µl).

Control mouse heart total RNA was utilised as a +ve control as final 5' RACE results in the visualisation of mouse transferrin receptor at a size of 3.0 kb, while 3' RACE yields bands at 3.2 kb and 2.1 kb respectively, indicating that all RACE components function efficiently.

Samples were transferred into a 96 well PCR plate and incubated at 72°C for 3 min, then 42°C for 2 min in a thermal cycler. After cooling, plates were centrifuges briefly for 10 s at 14,000 x g to collect the contents at the bottom. Following centrifugation 1 µl of the SMARTer II A Oligonucleotide was added per reaction to the 5' RACE samples only. The final buffer mix was made accordingly:

5.5 µl	Buffer Mix from Step 1
0.5 µl	RNase Inhibitor (40 U/µl)
2.0 µl	SMARTScribe Reverse Transcriptase (100 U)
8.0 µl	**Total Volume**

8 µl of the Master Mix above was added to the denatured RNA for a total volume of 20 µl per cDNA synthesis reaction. Plates were incubated at 42°C for 90 min in a thermal cycler and then at 70°C for 10 min. The first-strand cDNA synthesis reaction product was diluted with the addition of 10 µl EDTA and stored at -20°C until required.

2.9.3 RACE PCR

RACE master mix was prepared as below:

15.5 µl	PCR-Grade H_2O
25.0 µl	2X SeqAmp Buffer
1.0 µl	SeqAmp DNA Polymerase
41.5 µl	**Total Volume**

Mastermix was combined in a 96 well PCR plate as shown below with the addition of appropriate controls:

Component	5' or 3' RACE	UPM (- control)
5' or 3' RACE ready cDNA	2.5 µL	2.5 µL
10X UPM	5 µL	5 µL
5' or 3' GSP (10 µM)	1 µL	-
H_2O	-	1 µL
Master Mix (Previous step)	41.5 µL	41.5 µL
Total	**50 µL**	**50 µL**

Samples were subjected to Touchdown PCR in a thermal cycler utilising the conditions shown:

*5 cycles:
94°C 30 sec
72°C 3 min

*5 cycles:
94°C 30 sec
70°C 30 sec
72°C 3 min

*25 cycles
94°C 30 sec
68°C 30 sec
72°C 3 min

Following PCR, samples were run on an agarose gel and single bands were gel extracted as detailed in sections 2.14.3 and 2.14.4.

2.9.4 In Fusion Cloning

1 µl of lineareised pRACE vector (provided with SMARTer RACE 5'/3' Kit Components) was added to 7 µl gel-purified RACE product and 2 µl In-Fusion HD Master Mix. Reagents were incubated at 50°C for 15 min then transferred to ice. Stellar Competent cells were transformed utilising 2.5 µl of master mix and the general heat shock protocol described in detail in section 2.14.7.1. Colonies were selected and subjected to small and large scale plasmid DNA extraction and sequencing described in sections 2.14.7.2, 2.14.7.3 and 2.14.7.4. Sequences were compared to the annotated sequence available from Ensembl and additional bases identified through alignment using the CLC genomics tool version 8.0.3.

2.10 RNA-Fluorescent In-Situ Hybridisation (FISH)

Custom RNA-FISH tiled probe sets were generated to all exons of *SMILR*. RNA FISH utilises "branch tree" technology. As shown in Figure 2.2, a target specific probe set, containing 40 oligo probes, hybridises to the target mRNA as 20 oligo pairs. Each oligo pair forms a required platform for assembly of the signal amplification structure through a series of sequential hybridisation steps. Each fully assembled structure covers a space of 40-50 nt of the target RNA, and has the capacity for 400-fold signal amplification. Therefore, a typical RNA probe set (containing 20 oligo pairs) has the capacity to generate 8,000-fold signal amplification. Due to this technology, each fluorescent signal constitutes one single RNA molecule.

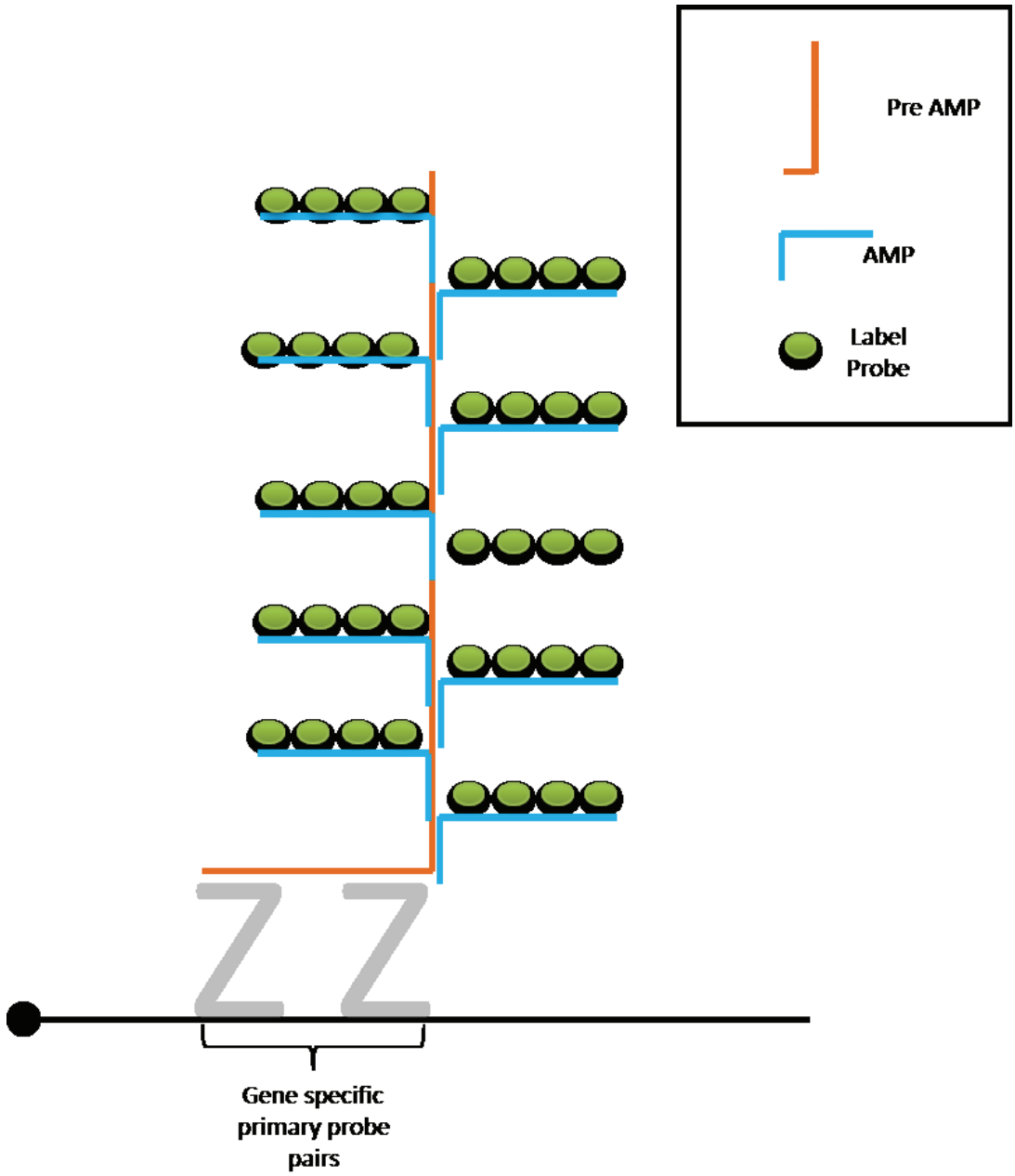

Figure 2-2: Overview of RNA-FISH branch tree technology.
Target RNA-specific oligonucleotide probes (Z) are hybridized in pairs (ZZ) to multiple RNA targets. Multiple signal pre-amplification (orange) and amplification (blue) molecules are hybridized, each recognising a specific target probe. This allows the visualisation of multiple targets within the one cell. Multiple label probes, each conjugated to a different fluorophore or enzyme, are bound to the amplification molecule. This creates a tree like appearance with the signal from a single molecule being amplified up to 8000 times.

2.10.1 RNA-FISH technique

All lncRNA probes were custom designed by Affymetrix (California, USA). All lncRNA probes were Type 1 and all control (SNORD3 and UBC) were Type 6 probes. Type 1 probes excite at 550 nm while Type 6 excite at 650 nm. SNORD3 and UBC were used as positive controls to determine spatial location of lncRNAs. RNA-FISH was performed according to manufacturer's instructions (ViewRNA™ cell FISH) with minor modifications. For cellular analysis, HSVSMC ± IL1α/PDGF (as above) were grown on 16 mm coverslips to 80 % confluency, washed in PBS and fixed in 400 µl of 4 % paraformaldehyde (PFA) supplemented with 1 % glacial acetic acid for 30 min at RT. PFA solution was removed and cover slips gently rinsed three times, in 2 mL/well 1X PBS. PBS was removed, 400 µL/well of Detergent Solution QC added to permeabilise the cells and incubated for 5 min at RT. Cells were washed twice in 2 mL/well as above. Working Protease Solution was prepared by diluting the Protease QS 1:4,000 in 1X PBS. PBS was replaced with 400 µL/well of Working Protease Solution and incubated for 10 min at RT. 3 further PBS washes were performed. Working Probe Set Solution was prepared by diluting each Probe Set 1:100 in pre-warmed Probe Set Diluent QF and adding 400 µL/well. For most instances one lncRNA and one control reaction were performed in one well, thus both probe sets were added to the QF diluent. No probe/DAPI only controls were also performed at this stage, in which the probe was omitted. Plates were covered and incubated at 40 ± 1 °C for 3 h. Probe was aspirated and cells washed three times, each with 2 mL/well of Wash Buffer. Cells were soaked for 2 min between aspirations. Working Pre Amplifier Mix Solution was prepared by diluting Pre Amplifier Mix 1:25 in pre-warmed Amplifier Diluent QF and vortexed briefly to mix. Wash buffer was removed and cells incubated with 400 µL/well Working Pre Amplifier Mix Solution for 1 h at 40 ± 1 °C. Cells were washed a further 3 times with 2 min soaking in wash buffer and the Working Amplifier Mix Solution prepared by diluting Amplifier Mix 1:25 in pre-warmed Amplifier Diluent QF. 400 µL/well of Working Amplifier Mix Solution was added and incubated for 30 min at 40 ± 1 °C. Cells were washed 3 times as before and Working Label Probe Mix Solution prepared by diluting Label Probe Mix 1:25 in pre-warmed Label Probe Diluent QF. 400 µL/well was added and incubated for 30 min at 40 ± 1 °C. Cells were washed three times for 2x 2 min and then 10 min respectively. Cover slips were mounted onto glass slides

utilising prolong gold mounting medium (Thermo Fisher) and cured with clear nail varnish.

2.10.2 Image Acquisition and quantification

Images were acquired on a Zeiss 510 confocal system. At least 5 images were taken per condition. Parameters for acquisition and post analysis were identical for all conditions. For quantification of lncRNA molecules/ cell, individual fluorescent spots were counted and considered as individual molecules. At least 5 cells were counted per image taken.

2.11 RNA Fractionation

RNA fractionation was performed according to the manufacturer's instructions provided in the PARIS™ Kit (Thermo Fisher). HSVSMC were plated at 1 x 10^5 cells per well in a 6 well culture dish and stimulated as described above for 72 h. Before utilisation of the kit 415 µL 2-mercaptoethanol was added to the 2X Lysis/Binding Solution and 64 mL 100 % ethanol to Wash Solution 2/3. Media was aspirated and discarded and cells washed once with PBS. Cells were trypsinised and trypsin inactivated with complete SMC media. Cells were pelleted by centrifugation at 1,500 rpm for 5 min, supernatant discarded and cells washed by gentle resuspension in 1 mL PBS. Cells were pelleted as before, supernatant removed and cells placed on ice. 500 µL of ice-cold Cell Fractionation Buffer was added to the cells, resuspended by gentle pipetting and incubated on ice for 10 min. Samples were centrifuged for 5 min at 4°C and 500 x g, supernatant removed and placed into an additional tube and placed on ice. This fraction contained the cytoplasmic RNA. The remaining nuclear pellet was washed in 500 µL of ice-cold Cell Fractionation Buffer and repelleted via centrifugation for 1 min at 4°C and 500 x g. The supernatant was aspirated and discarded. 500 µL of ice-cold Cell Disruption Buffer was added to the nuclear pellet and vigorously vortexed to lyse the nuclei. This sample contained the nuclear RNA. 500 µL 2X Lysis/Binding Solution at room temp was added to both the cytoplasmic and nuclear samples and mixed immediately by pipetting 3–4 times. 500 µL 100 % ethanol was added to both tubes and mixed thoroughly by pipetting 3–4 times. The sample was added to the Filter Cartridge (maximum 700 µL) and centrifuged at 12,000 rpm for 1 min. Flow through was discarded and the procedure

repeated until the complete sample had been passed. This procedure was repeated utilising 700 µL Wash Solution 1 followed by 500 µL Wash Solution 2/3. 20 µL Elution Solution preheated to 95°C was added and the column centrifuged as before. The elute was reapplied to the column and the procedure repeated. The eluted RNA was stored at -80°C until required.

2.12 LncRNA stability assays

HSVSMC were plated at 1 x 10^5 cells per well in a 6 well culture plate and stimulated for 72 h as described above. Following stimulation 5 µg/mL actinomycin D or DMSO control was added per well to inhibit transcription. Transcriptional inhibition of HSVSMC was conducted for 19 h, with cells harvested at time zero (0 h) and after 4, 8, and 19 h. Cells were collected trypsinisation and total RNA extracted using miRNeasy columns.

2.13 Dicer substrate siRNA (dsiRNA) mediated transfection

Double stranded dicer substrate siRNA targeting lncRNAs and Si-control were synthesised (Integrated DNA Technologies, Leuven, Belgium). The Si-control does not target any sequence in the human, mouse, or rat transcriptomes. Transient transfection was performed with Lipofectamine 2000 (Thermo Fisher). Cells were transfected with either 25 nM Si-lncRNA or Si-Control as detailed. All incubations for the dsiRNA were performed in a dark hood. Reactions were scaled up or down according. For 1 reaction 250 µL Opti-MEM (Gibco) was added to a 1.5 mL Eppendorf tube, with the addition of 3 µL Lipoefctamine 2000. In an adjacent 1.5 mL Eppendorf, 250 µL Opti-MEM was added 2.5 µL of either lncRNA dsiRNA or control dsiRNA. Mock tubes were also prepared which lacked the dsiRNA. After a10 minincubation at RT, the 2 Eppendorfs were combined to give a total volume of 500 µL. Transfection reagents were incubated for another 20 min at RT to allow the formation of cations required to penetrate cell membranes. During this incubation period cells were trypsinised, as described before, and a stock of 2x10^5 cells/mL, in smooth muscle cell transfection media, was prepared. SMC transfection media contained all supplements, as per the

SMC complete media, but lacked Penstrep, as antibiotics in the media can prove toxic for Lipofectamine transfections. Following the 20 min incubation, 500 µL of transfection reagent mix was added to the bottom of a 12 well plate and 500 µL of cells added on top to give a final density of $1x10^5$ cells/well. Six h post transfection, cells were quiesced in 0.2 % media for 48 h and stimulated for a further 48 h with 0.2 % media containing IL1α/PDGF.

2.14 General Cloning Techniques

LncRNA SMILR was cloned into the SFFV-LV plasmid in order to over express this lncRNA within SMC (described in detail in section 2.15). General cloning techniques were also employed when generating lncRNA probes for RNA: protein analysis (described in section 2.21).

2.14.1 Polymerase Chain Reaction (PCR)

Standard PCR conditions are described below. PCR trouble shooting was undertaken when standard PCR conditions failed. All PCR was performed using Platinum®Taq DNA Polmerase (Thermo Fisher). The following reagents were prepared in a 96 well PCR plate:

Per Reaction	
10x Reaction Buffer	2.5 µL
50 mM $MgCl_2$	0.75 µL
10 mM dNTP Mix	0.5 µL
10 µM Forward Primer	0.5 µL
10 µM Reverse Primer	0.5 µL
Template DNA	500 ng
Platinum®Taq DNA Polmerase	0.1 µL
H_2O	to 50 µL

Samples were subjected to the following PCR conditions in a thermal cycler:

***Initial denature**:
94°C 2 min

***35 cycles**:
94°C 30 sec
55°C 30 sec
72°C 1 min

***Hold**
10°C forever

All PCR reactions were stored at -20°C until required.

2.14.2 Restriction Digest

Restriction digests were not only utilised for inserting sections of DNA into plasmids but also utilised as diagnostic tools to ensure the insertion of the correct sized DNA fragment. All restriction enzymes utilised were purchased from New England Biolabs (Ipswich, UK). For small diagnostic purposes 100 ng of plasmid DNA was utilised. However, for larger reactions 1 µg of plasmid DNA was used. Small reactions were prepared accordingly: 1 µL appropriate NEB buffer, 0.5 µL of each restriction enzyme, 100 ng plasmid DNA and H_2O to 10 µL final volume. For large reactions: 5 µL appropriate NEB buffer, 1 µL of each restriction enzyme, 1 µg plasmid DNA and H_2O to 50 µL final volume. If multiple restriction enzymes were utilised it was ensured that the enzyme volume did not exceed 10 % of the total reaction volume to prevent star activity due to excess glycerol. Star activity is the ability of certain restriction enzymes to cleave sequences similar, but not identical, to their defined recognition sequence. This is caused by excess glycerol altering the standard reaction conditions.

All restriction digests were performed in a water bath set at 37°C and were incubated for 2 h. If required, gel purification was performed according to section 2.14.4.

2.14.3 Agarose gel electrophoresis

Agarose gel electrophoresis allows the separation of DNA molecules according to their molecular size, as compared to an appropriate DNA ladder. A suitable percentage agarose gel was utilised (0.8-2.5 % w/v) based on the DNA fragment

size, with lower percentage gels used to separate high molecular weight DNA and the reciprocal. Agarose was dissolved and electrophoresed in 1 x Tris-Borate EDTA (TBE) buffer (Gibco, Paisley, UK). Ethidium bromide (1 ng/100 mL) was added to molten agarose before the gels were poured. Ethidium bromide becomes intercalated into DNA and fluoresces under ultra violet light, allowing the easy detection of DNA. Samples were mixed with a 6X orange/blue dye and loaded onto gels along with a DNA marker (100 bp ladder for smaller fragments and 1 kb marker for larger fragments) (Promega, Southampton, UK). Gels were run in BIO-RAD electrophoresis tanks and using a BIO-RAD Power Pac 300, at a constant voltage of 50-120 V and bands visualised using trans UV illumination on a ChemiDoc XRS+ Imaging System.

2.14.4 Gel Extraction

Gel extraction was utilised to isolate desired fragments of intact DNA from an agarose gel following agarose gel electrophoresis. Following excision, and subsequent removal of excess gel, utilising a scalpel blade and UV light box, samples were subjected to extraction and subsequent cleaning utilising the Wizard® SV Gel and PCR Clean-Up System (Promega). Gel fragments were weighed and placed into 1.5 mL Eppendorf tubes. If large gel fragments were required then the gel was split between Eppendorfs. Membrane Binding Solution was added at a ratio of 10 µL of solution per 10 mg of agarose gel slice. The tube was vortexed and placed in a heat block at 65°C for 10 min or until the gel slice was completely dissolved. Gel slices were regularly vortexed during this incubation to aid in the melting of the gel slice. The dissolved gel was transferred into a SV Minicolumn inserted into a collection tube and incubated at RT for 1 min. Tubes were centrifuges at 16,000 × g for 1 min and waste discarded. Tubes were washed with 700 µL of Membrane Wash Solution and centrifuged as before. Waste was discarded and a second 500 µL wash was performed. Waste was discarded and empty tubes were centrifuged at 16,000 × g for 2 min to aid the ethanol evaporation. The SV Minicolumn was transferred to a clean 1.5 mL microcentrifuge tube and 50 µL of nuclease-free water added. Tubes were incubated for 1 min at RT and centrifuged as above. The eluate was placed back through the column a second time and the final step repeated. This second elute improves the recovery of DNA from the column.

2.14.5 Dephosphorylation and Ligation

Digested DNA typically possesses a 5’ phosphate group that is required for ligation. In order to prevent self-ligation, the 5' phosphate can be removed prior to ligation. This was performed using Antartic Alkaline Phosphatase (New England Biolab Ltd, Hertfordshire, UK), following the manufacturers’ protocol. 10 µL reactions were prepared accordingly: 2 µL Antartic Phosphatase enzyme, 1 µL 10 x Antartic Phosphatase buffer, 500 ng plasmid DNA and made up to 10 µL total using nuclease free H_2O. Reactions were incubated in a water bath set to 37°C for 30 min and were terminated by heat-inactivation at 80°C for 2 min. Ligation of inserts into dephosphorylated plasmid was performed using T4 DNA ligase (New England Biolabs Ltd) as per manufactures’ instructions. Several ratios of plasmid: insert were typically utilised. Ratios of 1:1 and 1:3 were used and 1:0 utilised as a negative control reaction. Molar ratios were calculated using the following equation:

(ng of vector x Kb of insert / Kb of vector) x molar ratio = ng of insert

Ligation reactions were prepared in PCR tubes as follows: 50 ng of dephosphorylated plasmid vector, specific amount of insert DNA (as calculated above), 1 µL T4 DNA ligase enzyme, 2 µL 10x T4 ligase buffer and reaction made up to 20 µL total using nuclease-free H_2O. Samples were incubated at 16°C overnight in a thermal cycler. Ligations were subjected to diagnostic digests and sequencing before being transformed into competent *E-coli*.

2.14.6 Sequencing

Sequencing was routinely used to ensure that the PCR of cloned DNA did not contain any mutations or incorrect sequences. Each sequencing reaction contained 200 ng of plasmid DNA, 2 nM of forward or reverse sequencing primers, 0.5 µL Ready Reaction Mix (Thermo Fisher) and 3.5 µL Big Dye Sequencing Buffer (Thermo Fisher). All reactions were assembled in a 96 well PCR plate. The reaction was then made up to a final volume of 20 µL using nuclease-free H2O. Individual forward and reverse reactions were always performed in duplicate and control sequencing reactions lacking the template

DNA were performed in order to ensure no reagents were contaminated with genomic DNA.

Samples were then subject to 25 PCR cycles at the following conditions:

* **30 cycles**:
96°C for 50 sec
50°C for 20 sec
60°C for 3 min

The PCR products were then cleaned using CleanSEQ (Agencourt Bioscience Corporation, MA, USA) following the manufacturers' protocol. This protocol utilises SPRI® paramagnetic bead technology to bind DNA allowing subsequent washes to be performed without the loss of DNA. Briefly, 10 µL CleanSeq was added per well. 62 µL of 85 % ethanol was added, the plate sealed, vortexed and centrifuged to return all material to the bottom of the plate. The reaction was then placed on a magnetic plate to remove the beads from the solution. The supernatant was removed and 100 µL of 85 % ethanol was added. The plate was sealed, vortexed and centrifuged as before and placed on the magnetic plate. The supernatant was removed and the beads allowed to air dry at RT. 40 µL H_2O was added per well and pipetted up and down to dislodge the beads from the sides of the plate. The plate was placed back on the magnet and 20 µL supernatant loaded into an optically clear barcoded 96-well PCR plate for capillary electrophoresis, which was performed on a 48-capillary Applied Biosystems 3730 Genetic Analyser with 36 cm capillaries. All sequencing and alignment were performed on CLC genomics.

2.14.7 Plasmid Purification

2.14.7.1 Transformation of Competent Bacteria

Bacterial transformation of competent *Escherichia coli* (*E coli*), was exploited as a means of replicating plasmid DNA. All transformations were performed through the standard 'heat shock' protocol utilising either commercially available JM109 (Thermo Fisher) or Stellar (Clontech) bacteria. 50 µL aliquots of competent

bacteria were thawed on ice. 1 ng of plasmid DNA was added to the cells and the tube gently flicked to mix. Samples were placed back on ice for 5 min before immersion in a water bath set to 42 ºC for exactly 45 seconds before being removed and immediately incubated on ice for a further 2 min. 450 µL SOC media at RT was added per tube and the tube was shaken, horizontally, for 1 h at 200 rpm and 37˚C in a shaking incubator. A tube containing bacteria, without DNA was included as a negative control, this ensured that the antibiotic was working efficiently. Varying amounts of *E coli*/SOC media mix were plated onto 100 µg/mL ampicillin Luria agar plates (Thermo Fisher). Plates were incubated at 37 ˚C to allow colony formation.

2.14.7.2 Picking of Colonies

The following day, individual bacterial colonies were selected and grown overnight in 10 mL Luria broth (LB) (Thermo Fisher), containing 100 µg/mL ampicillin, before being screened using diagnostic restriction digests, DNA electrophoresis and plasmid sequencing (described below).

2.14.7.3 Mini-Prep

Small scale DNA purification was performed using the PureLink® Quick Plasmid Miniprep Kit (Thermo Fisher). 3 mL of overnight culture was centrifuged at 6,000 xg for 5 min. Supernatant was removed and discarded. 250 µL of Resuspension Buffer (50 mM Tris-HCl, pH 8.0; 10 mM EDTA) with RNase A (100 µg/mL) was added to the cell pellet and resuspended until homogeneous. 250 µL Lysis Buffer (200 mM NaOH, 1 % w/v SDS) was added and mixed gently by inverting the capped tube until the mixture was homogeneous. The sample was then incubated for 5 min at RT to allow complete lysis of the bacteria. 350 µL Precipitation Buffer was added and mixed immediately by vigorously shaking the tube, until the mixture was homogeneous. Tubes were centrifuged at 12,000 × g for 10 min. The supernatant was transferred into a spin column and centrifuged for a further minat 12,000 × g. The flow through was discarded and columns were washed with 500 µL Wash Buffer (W10) for 1 min at 12,000 × g. A second 700 µL wash using Wash Buffer (W9) was performed and columns centrifuged as before. The wash through was discarded and columns centrifuged again to aid in the removal of ethanol. The spin column was transferred to a new 1.5 mL

Eppendorf and plasmid DNA was then eluted from the column using 50 µL nuclease-free H_2O. H_2O was allowed to bind to the column for 1 min at RT before centrifugation. DNA concentration was measured using the Nanodrop (Thermo Fisher) and stored at -20°C until required.

2.14.7.4 Maxi-Prep

The PureLink® HiPure Plasmid Maxiprep Kit was used to perform large scale DNA purification. The remaining 7 mL of the starter culture was placed into a conical flask containing 500 mL of LB broth and 100 µg/mL ampicillin. Cultures were incubated overnight in a shaking incubator at 37°C at 170 rpm. Following overnight culture bacteria were collected by centrifugation at 4,000 x g for 10 min at 4°C, in a Beckman Coulter Avanti J-26XP. During centrifugation columns were equilibrated with the addition of 30 mL Equilibration Buffer (EQ1) (0.1 M Sodium acetate pH 5.0, 0.6 M NaCl, 0.15 % (v/v) Triton® X-100). The columns were allowed to drain by gravity flow. 10 mL Resuspension Buffer (R3)(50 mM Tris-HCl pH 8.0, 10 mM EDTA) with RNase A (20 mg/mL) was added to the cell pellet and gently shaken until the cell suspension was homogenous. 10 mL Lysis Buffer (L7) (0.2 M NaOH, 1 % (w/v) SDS) was added and mixed gently by inverting the capped tube until the mixture was homogeneous. Samples were incubated at RT for 5 min to ensure complete lysis of bacteria. 10 mL of Precipitation Buffer (N3) (3.1 M Potassium acetate pH 5.5) was added and the contents mixed thoroughly. The precipitated lysate was then centrifuged at 20,000 x g for 20 min. The clarified supernatant was added to a HiPure Column and allowed to drain by gravity flow. Once all of the clarified supernatant had passed through the column, 60 mL wash buffer W8 was added (0.1 M Sodium acetate, pH 5.0; 825 mM NaCl). A sterile 15 mL centrifuge tube was placed under the column and 5 mL Elution Buffer (E4) added. The solution was allowed to pass by gravity flow. 10.5 mL isopropanol (2-propanol) was used to precipitate the DNA, before the mixture was centrifuged at 15,000 x g for 30 min at 4°C. The pelleted DNA was then washed in 4 mL 70 % ethanol, and 4 x 1 mL aliquoted into 4 x 1.5 mL Eppendorfs. Eppendorf's were centrifuged at 14,000 × g for 5 min at 4°C. The supernatant was removed and the pellets were allowed to air dry until all the ethanol had precipitated. DNA was resuspended in 200 µL of H_2O which was passed sequentially between each of the 4 tubes. DNA concentration was

determined on the nano drop and occasionally additional H_2O had to be added to dilute the DNA sample. DNA was stored at -20°C until required.

2.14.7.5 Glycerol Stocks

Plasmids were stored long-term storage as glycerol stocks. 500 µL of the overnight culture, before maxi-prep, was added to a 2 mL cyrovial with the addition of 500 µL of 50 % glycerol. Glycerol stocks were stored at -80°C. Recovery of bacteria from these stocks was performed by thawing, followed by streaking for single colonies on antibiotic containing agar plates.

2.15 Lentiviral Manipulation of lncRNA expression

2.15.1 Lentivirus primer design and cloning of LV plasmid

LncRNA2/SMILR was cloned into the SFFV:LV plasmid utilising the XhoI and MluI restriction sites. Lentivirus primers were designed that would generate a XhoI and MluI restriction site at the 5' and 3' end of the lncRNA. Lentivirus primer sequences are provided in Table 2-7. Cloning was performed according to section 2.14. The SFFV:SMILR/LncRNA2 plasmid map is shown in Figure 2.3.

Table 2-7: Lentivirus plasmid primers.

Primer Name	Gene Name	Sequence 5' - 3'
LncRNA_2_LV_F	RP11-94A24.1_F	GATACCTCGAGACTCTTGCTGCAAACATTGGGA
LncRNA_2_LV_R	RP11-94A24.1_R	GATACACGCGTTATGACAAGATTTTACTCAAGATT

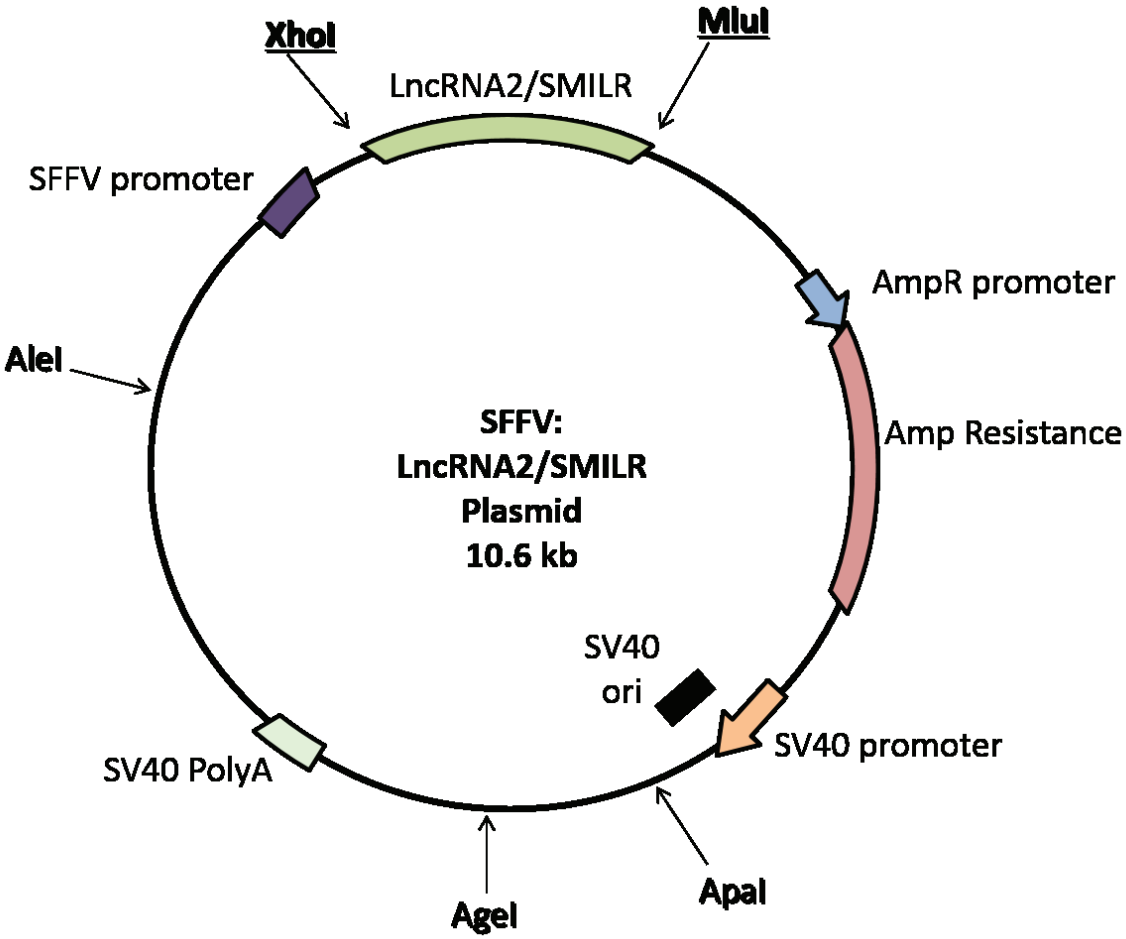

Figure 2-3: Plasmid map of SFFV plasmid with lncRNA2/SMILR sequence.
LncRNA2/SMILR sequence was cloned into the SFFV: LV plasmid between XhoI and MluI restriction sites. SFFV plasmid is under the control of the SFFV promoter and exhibits ampicillin resistance.

2.15.2 Production of Lentivirus via triple transfection method

Lentiviral vectors were produced using a transient triple transfection protocol, whereby HEK293Ts were transfected with 3 different plasmids, required for viral production; the expression plasmid (pHR'SIN-cPPT-SFFV-MCS-WPRE; pSFFV Lenti MCS) containing the desired gene under the control of the spleen focus-forming virus (SFFV) promoter (a kind gift of Prof. Adrian Thrasher, Institute of Child Health, University College London, London, UK), a packaging plasmid (pCMVΔ8.74) which contains Gag, Pol, Tat and Rev, and a plasmid endcoding the envelope of vesicular stomatitis virus (VSVg) (pMDG). Polyethylenimine (PEI) was used as the transfection reagent. Lentivirus preparations were performed in batches of 12 150 cm^2 flasks.

For each 150 cm^2 flask, 2 mixes were prepared; one containing the 3 plasmids for transfection, and one containing the PEI. Each DNA mix contained 50 µg expression plasmid, 17.5 µg PMDG and 32.5 µg pCMVΔ8.74, in 5 mL Opti-MEM reduced serum medium with GlutaMAX™ supplement (Gibco), and was filtered using a 0.22 µm sterile filter. 5 mL Opti-MEM containing 1 µL PEI was then sterile filtered and added directly to the DNA mixture. Tubes containing DNA and PEI were then incubated in a tissue culture cabinet, at RT, avoiding exposure to light, for 20 min. This allows for the formation of DNA:PEI complexes, which have endosomolytic activity, and are protected from lysosomal degradation. Culture medium was removed from HEK293Ts and cells were gently washed with 5 mL Opti-MEM medium. This was then removed and 10 mL of medium containing DNA:PEI complexes were added to the flask. Cells were incubated for 4 h at 37°C and 5 % CO_2. After 4 h Opti-MEM was removed, replaced with 20 mL fresh complete culture medium and cells were returned to the incubator. Lentiviral particles are produced and released into the medium by the cells after successful transfection of the 3 plasmids. Medium was collected after 48 h, replaced with 10 mL fresh complete culture medium and filtered using a 0.22 µm sterile filter unit. Cells were cultured for a further 24 h, when medium was collected, filtered and combined with the medium removed at 48 h.

2.15.3 Concentration of lentivirus

Concentration of lentivirus was performed using ultracentrifugation. Briefly, media collected from triple-transfected cells was aliquoted into Beckman 14 x 95 mm (14 mL) plastic tubes (Beckman Coulter, London, UK). Tubes had been previously rinsed with 70 % ethanol. Tubes were loaded into a SW-32.1 Ti rotor buckets and placed into the SW32 Ti rotor (Beckman Coulter). Samples were subjected to centrifugation at 23,000 rpm for 1 h at 4°C in an Optima L-80 XP Ultracentrifuge (Beckman Coulter). Supernatant was discarded and this process was repeated until all virus-containing medium had been used. The final supernatant was discarded and tubes placed up-side down to remove all traces of media. Tubes were placed on ice and 100 µL Opti-MEM® reduced serum medium with GlutaMAX™ supplement (Gibco) was added to each tube. Tubes were incubated on ice for 30 min. Lentivirus pellets were resuspended in the OptiMEM and the virus was aliquoted and stored at -80°C until required. Lentivirus does not withstand freeze thaw, thus aliquots were only used once.

2.15.4 Calculation of lentivirus titre

The concentration of produced lentivirus, in particle infectious units per mL (PIU/mL), was determined using a TaqMan® qRT-PCR based method. The sequence of the primers used was as follows; forward (F) - 5'-TGTGTGCCCGTCTGTTGTGT-3', reverse (R) – 5'- GAGTCCTGCGTCGAGAGAGC-3'. The probe used was FAM labelled with a TAMRA quencher, with the following sequence; 5'-(FAM)-CAGTGGCGCCCGAACAGGGA- (TAMRA)-3'. HEK293T cells were cultured and seeded into a 12-well plate, at a density of $5x10^4$ cells per well and left overnight. Decreasing concentrations of lentivirus were added to each well and left for 72 h. Cells were gently washed in 1X PBS and 200 µL PBS was added to each well. Plates, containing cells, were placed at -20°C and underwent one freeze thaw cycle prior to DNA extraction. DNA was extracted using the QIAamp Mini and Blood Mini kit. DNA concentration was determined using the Nanodrop and all samples were diluted to 250 ng/µL using nuclease-free H_2O. In order to titre the virus, serial dilutions of the expression plasmid, SFFV-LV plasmid, were utilised to generate a standard curve of $1x10^{13}$ to $1x10^4$ plasmid copies. The calculations required to determine the µL of virus needed to generate the top standard are shown below:

1. **Molecular weight of 1 copy of expression plasmid**

$$\frac{\text{Size of plasmid (bp) x size of 1 bp (660Da)}}{\text{Avogadro's Constant}} = \text{g per molecule}$$

Daltons = g/mole
Avogadro's Constant = 6.023×10^{23} molecules/mole

2. **Determine copy number of plasmids in 1 mL stock.**

$$\frac{\text{Concentration of stock plasmid (g/ mL)}}{\text{g per molecules}} = \text{no. of molecules per mL}$$

3. **Preparation of top standard ($1x10^{13}$ copies)**

$$\frac{\text{No. of molecules per 1 mL}}{1x\ 10^{13}} = \text{initial dilution factor}$$

$$\frac{1000}{\text{Initial dilution factor for top standard}} = \mu\text{L of plasmid needed to make } 1x\ 10^{13} \text{ standard}$$

A reaction master mix was prepared and 11.5 µL was added to each well of a 384-well PCR plate. Each reaction consisted of 2x TaqMan® Universal Master Mix, 2 µL Primer/Probe mix, 3.125 µL Nuclease-free H2O, 1 µL of DNA standard or DNA samples collected from lentiviral titre. All reactions were performed in triplicate and run Taqman qRT-PCR conditions described in section 2.6.3. The titre of each samples was calculated by plotting the cT values from the standard curve and solving the equation of the line for each sample. Utilising this method leads to the copies of plasmid DNA in each samples. The number of copies per cell was then identified by using the equation below (250 ng was the amount of DNA utilised in the PCR reaction):

Copies of plasmid in sample x no. of cells used in 250 ng = copies of plasmid per cell

This was subsequently utilised to generate both the PIU/ml and the MOI (multiplicity of infection) respectively (shown in 1. and 2. below).

1. $$\text{Copies of plasmid per cell} \times \left[\frac{\text{dilution factor of virus stock used} \times 1000}{\mu\text{L virus added to cells}}\right] = \text{PIU/mL}$$

2. $\frac{\text{Cell no. x MOI}}{\text{Viral titre}}$ = µL of virus / well

2.15.5 Lentivirus Transduction of HSVSMC

Lentivirus transduction was performed on a confluent monolayer of HSVSMC. Briefly, HSVSMC were plated at a density of $1x10^5$ cells/well of a 12 well plate. Cells were incubated overnight at 37°C and 5 % CO_2. Control (empty) or lncRNA lentivirus was added at an MOI of 25 or 50 in 0.2 % DMEM as described above. The MOI is the ratio of the number of virus particles to the number of target cells. Following 24 h incubation with the virus, the media was changed to 0.2 % DMEM and incubated for a further 24 h before stimulation with either IL1α and/or PDGF or control (0.2 %) media. Cells were them analysed either for proliferation or RNA analysis.

2.16 Protein Analysis

2.16.1 Protein Extraction

Protein lysis buffer was prepared on ice containing the following reagents: 20 mM Tris pH 7.5, 150 mM NaCl, 1 mM EDTA, 1 mM ethylene glycol tetra-acetic acid (EGTA), 2.5 mM Na pyrophosphate, 1 mM ß-glycerophosphate, 2.5 mM Na yrophosphate, 1 mM Na3VO4, 0.5 % (w/v) sodium deoxycholate and 1X Roche Complete Mini Protease Inhibitor cocktail tablets (made up in H_20) (Roche Diagnostics, Risch-Rotkreuz, Switzerland). Protein extraction was performed on HSVSMC. Briefly, media was removed and cells washed 1 x in ice cold PBS. PBS was removed and replaced with PBS at 5 ml/ $75cm^2$ flask. Flasks were scraped, on ice, with a rubber scraper to detach cells from the flask. Cells plus PBS were transferred into a 50 ml falcon and centrifuged at 4,000 x g for 15 min at 4°C. Supernatant was carefully removed from the cell pellet and 500 µL of protein lysis buffer was added. Cells were placed on ice and centrifuged every 5 min to aid in protein lysis. Finally, sampled were transferred to a new 1.5 mL Eppendorf and spun at 12,000 rpm, 4ºC for 15 min. The protein supernatant was removed and stored at -80ºC.

2.16.2 Determining protein content

Protein concentration was determined using the Pierce BCA Protein Assay Kit (Thermo Scientific) in accordance with the manufacturer's instructions and read at 570 nm using the Wallac VICTOR2 plate reader (Thermo Fisher). Protein concentrations were identified from the standard curve produced by the protein standards.

2.17 Assessment of lncRNA in conditioned media

RNA extraction on conditioned HSVSMC media was performed using a standard volume (2 mL). The conditioned media was first centrifuged (10 min; 2000 g; 4°C) to remove all cells and debris. After addition of 1.4 mL of QIAzol (Qiagen), 3 µL of c.elegans total RNA at 25 ng/µL was added to each sample. Following 5 min incubation at RT, 140 µL of chloroform was added and samples centrifuged (15 min; 15000 g; 4°C). The clear upper aqueous phase was used to isolate RNA using miRNEasy mini kit (Qiagen) as previously described with alteration of the final wash step (75 % ethanol in DEPC water). Different quantities of total RNA were spiked and a dose response effect was observed. The quality of the amplicon was assessed via analysis of melting curves and subsequent visualisation on agarose gel. This showed a unique amplification product corresponding to the cDNA fragment of *ama-1*. Due to the strong correlation observed between quantity of spike-in and *ama-1* expression, we utilised 75 ng in all subsequent extractions. This amount allowed reproducibility of our method, with the Ct values of *ama-1* being 29.4 ± 0.3 across 5 separate extractions in non-conditioned media.

2.18 Assessment of non-coding RNA in unstable atherosclerotic plaques

All imaging to determine the uptakof ^{18}F and ^{18}F-FDG was performed by Dr Alex Vesey.

Carotid cohort

Patients with symptomatic carotid artery stenosis (≥50 % by NASCET criteria (Hathout et al., 2005)) scheduled to undergo carotid endarterectomy were recruited from neurovascular clinics at the Royal Infirmary of Edinburgh between January 2013 and April 2014. Exclusion criteria included a modified Rankin score of 3, insulin-dependent diabetes mellitus, women of child-bearing age not receiving contraception, severe chronic kidney disease (eGFR <30 mL/min/1.73 m^2), known iodine-based contrast media allergy, prior ipsilateral carotid intervention, prior neck irradiation, and inability to provide informed consent. Patients underwent a standard baseline clinical assessment including blood sampling (for standard clinical haematological and biochemical indices, including C reactive protein, and plasma RNA analysis) before undergoing separate [^{18}F]-fluoride and [^{18}F]-fluorodeoxyglucose ([^{18}F]-FDG) positron emission tomography combined with computed tomography (CT) scans with the use of a hybrid scanner (Biograph mCT, Siemens Medical Systems, Erlangen, Germany). Both of these tracers have been used by our group and others for plaque imaging and highlight high-risk actively calcifying (Irkle et al., 2015) and inflamed or hypoxic atherosclerotic plaques.

For [^{18}F]-fluoride imaging, a target dose of 250 MBq was administered intravenously. Scanning took place after a 60 min delay. Following an attenuation-correction CT scan (non-enhanced, low dose 120 kV, 50 mAs) PET imaging was performed in static mode covering 2 bed positions (15 min each) with the superior bed centered over the carotid bifurcation. Following PET acquisition, a CT carotid angiogram was performed without moving the patient (Care Dose 4D, 120 kV, 145 mA, rotation time 0.5 s, pitch 0.8).

[^{18}F]-FDG PET/CT was performed on a separate day. A target dose of 125 MBq was administered intravenously and scanning commenced after a 90-min delay. PET/CT acquisition was identical to [^{18}F]-Fluoride save for a longer bed time of 20 min and a pre-scan fast of 6 h. Static images were reconstructed using the Siemens Ultra-HD algorithm (time of flight + True X) with corrections applied for attenuation, dead time, scatter, and random coincidences.

PET tracer uptake was quantified using an OsiriX workstation (OsiriX version 3.5.1 64-bit; OsiriX Imaging Software, Geneva, Switzerland). PET/CT image data were reviewed for evidence of tracer uptake, image quality and registration. The CT angiogram was examined to establish plaque presence, location and characteristics. Regions of interest were then drawn on three adjacent 3-mm PET slices to incorporate the internal carotid artery plaque. Three ROI were then drawn around adjacent healthy portions of carotid artery and the lumen of the SVC to derive control values for “normal” arterial uptake and the blood pool respectively. Arterial standardized uptake values (SUV) were recorded and also indexed to blood pool activity thus giving a target-to-background-ratio (TBR).

At the time of surgery, plaques were collected immediately following excision and photographed. Two-millimeter diameter core biopsy specimens for RNA analysis were taken from regions of focally high uptake on PET and from normal tissue at the periphery of the endarterectomy specimen. These, along with the main specimen, were immediately frozen and placed in an -80°C fridge for subsequent batch analysis.

2.19 Assessment of lncRNA in plasma

Human plasma samples were utilised from a previously published study: Carotid Ultrasound and Risk of Vascular disease in Europeans and South Asians (CURVES) (Ghouri et al., 2015). The study was approved by the West of Scotland Research Ethics Committee (09/S0703/118). All patients had metabolic syndrome and varying levels of C reactive Protein (CRP). Blinding of CRP levels was undertaken before RNA extraction and un-blinding was not performed until after qRT-PCR analysis for lncRNA and control gene expression analysis.

A standard volume of each plasma sample (300 µL) was used to extract RNA. Five volumes of QIAzol lysis reagent (Qiagen) was added per extraction and supplemented with spike-in RNA controls: 3.5 µL of miRNeasy Serum/Plasma Spike-In Control at 1.6 x 10^8 copies/µL (C. elegans miR-39 miRNA mimic; Qiagen) and 3 µL of c.elegans total RNA at 25 ng/µL. Following 5-min incubation at RT, chloroform was added at equal volumes to the starting sample. Following

centrifugation (15 min; 8000 g; 4°C) the clear upper aqueous phase was used to isolate RNA as described in section 2.4.

2.20 Detection of lncRNA in exosomes secreted from HSVSMC

SMILR expression in conditioned media was assessed utilising both ultracentrifugation and exosome isolation kits. RNA extraction of exosome free HSVSMC media was performed using a standard volume (15 mL). The conditioned media was centrifuged at 2000 g at 4°C for 10 min and then at 12000 g for 45 min to remove all cell debris. The supernatant was filtered (0.22 µm) followed by ultracentrifugation at 110 000 g, 4°C for 90 min (Optima L-80 XP ultracentrifuge Beckman coulter) to obtain microvesicles (Thakar et al.) and exosomes and exosome free media compartments. Additional experiments were performed utilising the Total exosome isolation kit (Thermo Fisher) following the manufacturer's instructions. The presence of microvesicles and exosomes was verified using the Nanosight technology

For exosomes and microvesicles, 700 µL of Qiazol (Qiagen) was added and 3 µL of c.elegans total RNA at 25 ng/µL and the RNA was extracted using miRNEasy mini kit (Qiagen) as previously described. For the exosome free media compartment, RNA was extracted from 2 mL and following the same protocol as describe in the manuscript. SMILR relative expression was determined in these 2 compartments by qRT-PCR.

2.21 RNA-protein Interactions

2.21.1 T7 primer design

T7 primers were designed to convert LncRNA2/SMILR DNA to RNA. Primers were designed to encompass several key traits as detailed below for the forward and reverse primers.

Forward Template: 5′- (N6–10)TAATACGACTCACTATAGGG(N3–6)CCACCATGG(N17–22)-3′

Green: 6-10 nucleotide (N) sequence upstream of T7 promoter – increases promoter activity.
Teal: T7 promoter sequence – essential for the conversion of DNA to RNA.
Red: 3-6 nucleotide spacer between promoter sequence and Kozak sequence. Ensures transcription starts a few bases upstream of the Kozak sequence and allows better ribosome binding to RNA.
Pink: Kozak consensus sequence.
Yellow: Gene-specific sequence of 17-22 nucleotides. Needed to allow priming of the target gene

Reverse Template: 5′-T30stop anticodon(N17–22)-3

Green: Addition of a 30 nucletotode poly (A) tail results in greater RNA stability and higher levels of translation.
Teal: Reverse complement of stop codon (TTA, CTA or TCA) if not present in the sequence being amplified. Terminates translation, allowing efficient release of ribosomes for further rounds of translation.
Pink: Gene-specific sequence. Needed to allow priming of the target gene

The T7 SMILR primers are shown below:

SMILR_T7_F
5'-GATACCTAATACGACTCACTATAGGGGATACCCACCATGGACTCTTGCTGCAAACAT-3'

SMILR_T7_R
5'-TTTTTTTTTTTTTTTTTTTTTTTTTTTTTTTTTAATGACAAGATTTTACTCAAGAT-3'

2.21.2 Generation of DNA

SMILR DNA was generated through Platinum Taq Polymerase PCR as described in section 2.14.1. PCR was performed utilising the SFFV:SMILR plasmid that encompasses the full length transcript of SMILR. PCR utilised the T7 primers as

described above to generate full length SMILR DNA with the addition of the T7 promoter to allow for RNA generation.

2.21.3 T7 generation of RNA

LncRNA2/SMILR RNA was generated utilising the RiboMAX™ Large Scale RNA Production System according to manufacturer instructions. RiboMAX™ utilises a T7 RNA polymerase. T7 is an RNA polymerase from the T7 bacteriophage that catalyses the formation of RNA in the 5'→ 3' direction. LncRNA and control reactions were prepared as below in PCR grade tubes:

Table 2-8: Reagents required for T7 polymerase generation of lncRNA probes.

T7 Reaction Components	Sample Reaction	Control Reaction
RiboMAX™ Express T7 2X Buffer	10µl	10µl
linear DNA template (1µg total)	1-8µl	-
pGEM® Express Positive Control Template (1µg)	-	1µl
Nuclease-Free Water	0-7µl	7µl
Enzyme Mix, T7 Express	2µl	2µl
Total Volume	**20**µl	**20**µl

Tubes were incubated in a thermal cycler at 37°C for 30 min. Following incubation RNase-Free DNase (Thermo Fisher) was added at a concentration of 1 unit per microgram of template DNA and incubated at 37°C for 15 min. RNA was then extracted using 20 µL of phenol: chloroform: isoamyl alcohol (125:24:1). Samples were vortexed for 1 min and spun at top speed in a microcentrifuge for 2 min at RT. The upper aqueous phase was transferred to a new tube. 2 µL of 3 M Sodium Acetate (pH 5.2) and 50 µL of 95 % ethanol was added, mixed and place on ice for 5 min. Samples were spun at top speed in a microcentrifuge for 10 min, the supernatant was removed and pellet washed with 1 ml of 70 % ethanol. The pellet was air dried, to remove any ethanol, and resuspended in 20 µL of nuclease free H_20. RNA was run on a 1 % agarose gel to confirm the

presence of bands at 1 kb and 2 kb for the control and 1 kb for lncRNA2/SMILR RNA. RNA was stored at -80°C until required.

2.21.4 Biotinylation of RNA

Biotinylation was performed utilising Thermo Scientific Pierce RNA 3´ Desthiobiotinylation Kit, according to manufacturer's instructions. The kit utilises T4 RNA ligase to attach a single biotinylated nucleotide to the 3´ terminus of a RNA strand. Briefly, all kit components were thawed on ice and prepared according to the table below. Samples containing the appropriate lncRNA or control RNA were added to microcentrifuge tubes.

Table 2-9: Components and preparation of the RNA ligation reaction.

Components	Volume
Nuclease-free H_2O	3 µL
10X RNA Ligase Buffer	3 µL
RNase Inhibitor	1 µL
Non-Labelled Control or Test RNA	5 µL (50 pmol)
Biotinylated Cytidine Bisphosphate	1 µL
T4 RNA Ligase	2 µL
PEG 30%	15 µL
Total	**30 µL**

Samples were incubated overnight in a thermal cycler at 16°C. Following overnight incubation, 70 µL of nuclease free H_2O plus 100 µL chloroform:isoamyl alcohol mix (24:1) was added to each reaction to extract the RNA ligase. The mixture was briefly vortexed, then centrifuge 2-3 min at 16,000 x g in a micro centrifuge to separate the phases. The top (aqueous) phase was removed and transferred to a nuclease-free tube. 10 µL of 5 M NaCl, 1 µL of glycogen and 300 µL of ice-cold 100 % ethanol was added and precipitated for 6 h at -20°C.

Samples were centrifuged at 16,000 × g for 15 min at 4˚C. The supernatant removed and pellet washed in ice cold ethanol. The pellet was air dried and re suspended in 20 µL of nuclease-free water.

2.21.5 Confirmation of RNA biotinylation

All solutions used in this process were made using H_20 which had been treated with 0.1 % diethylpyrocarbonate (DEPC), which inactivates RNase enzymes, for 24 h before autoclaving to remove traces of DEPC. All equipment and surfaces used were treated with RNAseZap® (Thermo Fisher) to inhibit RNase enzymes. Biotinylation was confirmed by spotting 2 µl of 10 nM biotinylated RNA or control RNA plus sequential dilutions onto Amersham Hybond-NX Membrane (GE Life sciences, Buckinghamshire, UK). Membranes were transferred to N-Ethyl-N′-(3-dimethylaminopropyl)carbodiimide hydrochloride (EDC) cross-linking solution (2 mM EDC, 1 % (v/v) 1- Methylimidazole) in order to crosslink RNA molecules to the nylon membrane. Cross-linking was carried out for 1 h at 60ºC before membranes were washed twice in DEPC H_20. Membranes were place in 1x blocking solution (Roche blocking reagent) plus 1:10,000 streptavidin licor antibody (IRDye® Streptavidin 800CW, Licor), in the dark for 1 h at RT, with shaking. Membranes were washed 2 x 15 min in wash buffer (0.1 M maleic acid, 0.15 M NaCl , 0.3 % Tween 20, pH 7.5), placed in PBS and imaged on the B446 - LI-COR Odyssey machine.

2.21.6 Protein extractions

Protein was extracted from HSVSMC stimulated with IL1α and PDGF for 72 h. Protein was extracted as described in section 2.16.1 and was subjected to BCA analysis to determine protein concentration, described in section 2.16.2.

2.21.7 Pull down protocol

An overview of the experimental technique is shown in Figure 2.4. Pull downs were performed utilising Thermo Scientific Pierce RNA Protein pulldown kit.

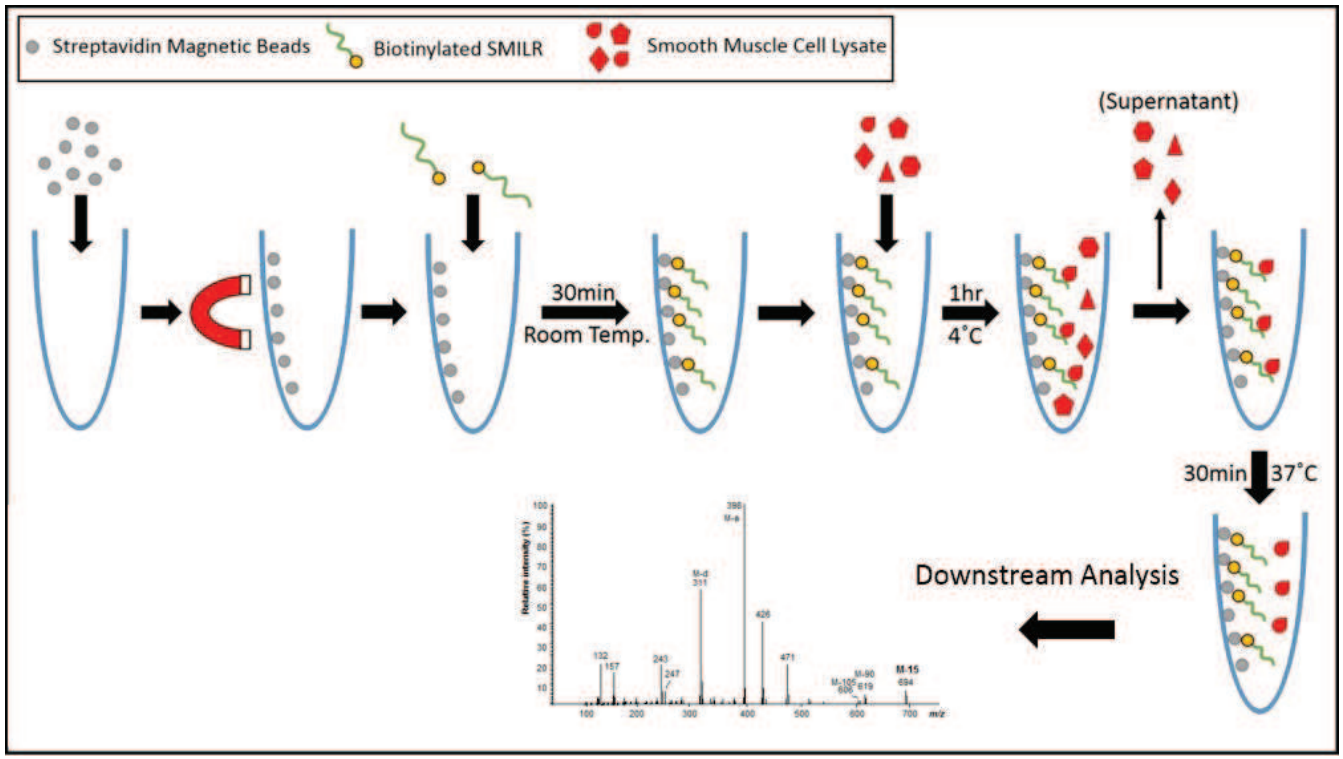

Figure 2-4: Schematic overview of the desthiobiotin protein pulldown.
Streptavidin magnetic beads are bound to biotinylated SMILR or control probes. SMC cell lysate is added and the samples incubated at 4°C for 30 min to allow the binding of SMC proteins to the lncRNA. Unbound proteins are removed and the beads washed multiple times. Bound proteins are eluted and subjected to downstream analysis such as mass spectrometry.

Briefly, 50 µL magnetic streptavidin beads were added to a 1.5 mL microcentrifuge tube and collected at the side of the tube utilising the DynaMag™- Spin Magnet (Thermo Fisher). Supernatant was removed and beads washed three times each with 50 µL 20 mM Tris (pH 7.5). The beads were collected at the side of the tube utilising the magnet and supernatant removed. 50 µL 1X RNA Capture Buffer was added and beads resuspended by pipetting. 50 pmol biotinylated SMILR or biotinylated poly A control was added to the beads and rotated at RT for 30 min to allow binding of biotin to the streptavidin beads. Tubes were placed into the magnetic stand to collect the beads against the side of the tube, the supernatant was removed and discarded and beads washed a further 3 times as before. Supernatants were removed and 10X Protein-RNA Binding Buffer was diluted to 1X in nuclease free H_2O. 100 µL of 1X Protein-RNA Binding Buffer was added to the beads and mixed well. The basic RNA-Protein Binding Reaction Mix was prepared as detailed below:

Table 2-10: Reaction components for the Master Mix of RNA-Protein Binding Reaction.

Reagent	Volume
10X Protein-RNA Binding Buffer	10 µL
50% Glycerol	30 µL
Lysate >2 mg/mL	30 µL
Nuclease Free H_2O	30 µL
Total	**100 µL**

Low stringency pulldowns contained no salt or Tween-20, as detailed in the table above. However, high stringency pulldowns contained the addition of 200 mM $NaCl_2$ and 0.01 % Tween-20. 100 µL lysate mix was added and the tubes place with end to end rotation at 4°C for 1 h. Un-bound supernatant was removed and samples washed 3X in 100 µL wash buffer (20 mM Tris (pH 7.5), 10 mM NaCl, 0.1 % Tween-20 Detergent). Wash supernatants were saved to confirm the complete removal of non-bound proteins. The elution step utilised the greater binding affinity of biotin to outcompete with the binding of desthiobiotin, thus dislodging both lncRNA2/SMILR and the protein from the beads. 50 µL of Elution Buffer was added to the beads and mixed well by vortexing. Beads were incubated for 30 min at 37°C with agitation. The supernatant, containing the

proteins of interest, was transferred to a new tube and samples heat for 10 min at 95°C. Samples were stored at -20°C until required.

2.21.8 Gel electrophoresis

Protein samples were mixed with NUPAGE® 4X LDS Sample Buffer (Thermo Fisher) and denatured by heating at 95ºC for 10 min. Samples were loaded onto NuPAGE™ Novex™ 4-12 % Bis-Tris Protein Gels (Thermo Fisher) along with the reference ladder Full-Range Rainbow Molecular Weight Ladder (GE Life sciences, Buckinghamshire, UK). Electrophoresis was performed at 80-120 V in running buffer (25 mM Tris, 0.2 M glycine, 1 % (w/v) SDS) until the dye front reached the bottom of the gel. Gels were removed from their casing and washed briefly in H_2O prior to silver stain analysis.

2.21.9 Silver stain analysis

Silver staining is a highly sensitive method for detecting proteins and nucleic acids located with gel slabs. Proteins bind silver ions, which can be reduced under appropriate conditions to build up a visible image made of finely divided silver metal (Wray et al., 1981). Silver staining was performed using Pierce® Silver Stain Kit (Thermo Fisher). Following gel electrophoresis, gels were incubated 2 x 15 min in distilled H_2O followed by immersion in 30 % ethanol: 10 % acetic acid solution for 2 x 15 min, allowing fixing of the gel. Gels were then subjected to 2 × 5 min washes in 10 % ethanol, and then 2 × 5 min washes in distilled water. Gels were sensitised for 1 min(50 µL Sensitizer with 25 mL water) and washed 2 x 1 min in H_2O. Gels were stained for 30 min at RT in working solution (0.5 mL Enhancer with 25 mL Stain) and washed twice briefly in H_2O. Gels were then developed (0.5 mL Enhancer with 25 mL Developer) for approximately 2-3 min or until the required bands were at sufficient intensity. Development was stopped with the addition of 5 % acetic acid for 10 min. Gels were imaged and stored at 4ºC if required.

2.21.10 Mass spectrometry analysis

Additional samples in PBS, were mixed with NUPAGE® 4X LDS Sample Buffer (Life Technologies) and denatured by heating at 95ºC for 10 min. Samples were

loaded onto a NuPAGE™ Novex™ 12 % Bis-Tris Protein Gels (Thermo Fisher) and run for 5 min to allow samples to run into the gel. The protein band was extracted using a scalpel blade and gel sections were digested with trypisin. Following gel digest 2 ug protein was injected utilising an EASY-Spray column, 50 cmx75 µm ID, PepMap RSLC C18, 2 µm. Mass spectrometry analysis was performed on a Q Exactive mass spectrometer coupled to a coupled on-line to Ultimate 3000 RSLCnano Systems (Dionex; Thermo Fisher). Between each sample an in-house blank sample was injected to avoid any carryover. A 60 min gradient (100 min total run) time was applied to each sample.
Data analysis was performed using the MaxQuant software platform (ver. 1.5.2.8) and searches were conducted against a Human Uniprot database. Carbamidomethylation of cysteine and oxidation of methionine were selected as fixed and variable modifications respectively. Trypsin was selected as the digestion enzyme allowing 2 missed cleavages. All analysis was performed by the Mass Spec core facility at the University of Edinburgh.

2.22 Statistical Analysis

Statistical analysis was performed according to Figure legends. Data in graphs are shown on relative expression scales as referenced by (Livak and Schmittgen, 2001). Data are given as mean ± standard error of the mean. Note that as the relative expression scale is inherently skewed, the bar indicate the geometric mean of the relative expression fold change with the SEM whiskers denoting the relative expression fold change equivalent to an increase of one SEM above the mean on the log transformed scale. All statistical analysis is performed on the dCt scale (a logarthmic transformation of the data shown on the RQ in the plots) (Livak and Schmittgen, 2001). No evidence of unequal variances across groups was found for any of analyses of the dCt scale data using Levene's test on minitab version 17 prior to statistical analysis. Comparisons between 2 groups were analysed using 2-tailed unpaired or paired Student's t test. One-way ANOVA with Tukey's post hoc or one way ANOVA multiple comparison test for pooled samples, via Graph Pad Prism version 5.0, was used for comparisons among 3 or more groups. Statistical significance is denoted by a P value of less than 0.05.

Chapter 3 Results – Identification and validation of lncRNA during SMC proliferation.

3.1 Introduction

Recently, next generation transcriptome sequencing (RNA-Seq) has provided a method to delineate the entire set of transcripts within a cell (Wang et al., 2009). Understanding the transcriptome is essential for determining key factors that may be involved in both cellular development and disease. The key aims of RNA-sequencing are therefore to catalogue all transcripts, including mRNA, lncRNA, processed transcripts and pseudogenes and to quantify the change in expression levels of each transcript between different experimental conditions. The popularity of the new sequencing methods is supported by the numerous papers recently published in high profile publications and by the increasing number of submissions to public data repositories (Smith, 2016).

After 1964, in which the first report of RNA sequencing was published, Northern Blots and RT-PCR were developed for RNA and transcriptome study (Alwine et al., 1977), (Bustin, 2000). Following this, the sequencing of RNA was transformed via the progression of several sequencing methods that have eventually led to the development of RNA-seq. (Table 3-1).

Table 3-1: The history of RNA.
History of progresses and developments of RNA and transcriptome studies culminating in RNA-seq. Adapted from (Morozova et al., 2009).

Year	Discovery
1964	First RNA molecule sequenced
1977	Development of Northern Blot technique
1988	The first experiment reports of RT-PCR for transcriptome analysis
1992	Introduction of Differential Displays (DD) technique for differentially expressed gene discovery
1995	Introduction of microarrays and SAGE
2003	CAGE development
2005	Introduction of first technology of next generation sequencing to the market
2008	The first reports of RNA-Sequencing

Profiling of gene expression via-high throughput methods was first achieved in 1992 with the development of the Differential Displays protocol (Liang and Pardee, 1992) and was closely followed in 1995 with the development of complementary DNA microarrays (Schena et al., 1995), (Spies and Ciaudo, 2015). Differential display was developed as a method to allow the systematic screening for molecular differences in mRNA expression between different cells or tissues. The technique relied on the amplification of messenger RNA at the 3' end, labelling of the amplified cDNA with radioisotopes followed by distribution on a denaturing polyacrylamide gel to allow visualisation via autoradiography. Side-by-side comparison of mRNA species from different samples allowed the identification of genes that were up or down-regulated between the different conditions (Liang and Pardee, 1997). Complementary DNA microarrays utilised a collection of microscopic DNA sequences attached to a solid support and were used to measure the expression levels of large numbers of genes simultaneously or to genotype multiple regions of a genome. Complete mRNA was fluorescently tagged with one round of reverse transcription to generate cDNA and incubated on top of the solid glass slide (Trevino et al., 2007). The core principle behind

microarrays is hybridisation between two DNA strands. Complementary nucleic acid sequences will specifically pair with each other by forming hydrogen bonds between complementary nucleotide base pairs. Several rounds of washes removed any non-specific binding and analysis of fluorescent spot intensity allowed the quantification of gene expression. Additionally, differential gene expression can be performed through the utilisation of two fluorescent tags. The tagged cDNA from individual conditions in then mixed and hybridised to one single glass slide. Spot intensity of the different tags allowed the quantification of mRNAs that are up or down-regulated between conditions. This method relies on the spotting of previously known DNA sequences onto the glass slide and as such, cannot be utilised for the detection of unknown genes or novel transcripts (Trevino et al., 2007). Subsequently, several other large scale techniques were developed like Serial Analysis of Gene Expression (SAGE), Massive Parallel Signature Sequencing (MPSS), Cap Analysis Gene Expression (CAGE) and tiling arrays. SAGE was developed by Dr. Victor Velculescu at the Oncology Center of Johns Hopkins University (Yamamoto et al., 2001). The method of SAGE relies primarily on the generation of short sequence tags, typically 10-14 base pairs in length (Yamamoto et al., 2001). These tags are generated via the conversion of total mRNA to cDNA from each sample utilised followed by cleavage at random sites via a restriction enzyme. These tags contain sufficient information to identify a transcript provided that the tag is obtained from a unique position within each transcript. Tags are then cloned and sequenced. Quantification of the number of times a particular tag is observed provides the expression level of the corresponding transcript (Yamamoto et al., 2001). This process is therefore based on sequencing mRNA and not hybridisation of mRNA onto probes, as is the case for microarrays. Thus, SAGE allowed the transcription levels of mRNA to be measured more quantitatively than microarray. Additionally, SAGE relies on sequencing, thus permitting the detection of both known and unknown transcripts and genes as well as the identification of abnormal gene changes, such as SNP's, to be determined between samples. Although an improvement over the current technique at that time, SAGE still required extensive sequencing techniques, deep bioinformatic knowledge and powerful computer software to assemble and analyse the SAGE results (Yamamoto et al., 2001). As such, this resulted in SAGE producing greater sensitivity to the microarray method but at a greater cost. MPSS utilises a similar technique to SAGE with the

exception of using longer tag sequences, typically 17-20 base pairs. These tag sequences are loaded onto microbeads that can be sequenced together. The longer tag sequences allowed for higher specificity however, several disadvantages still existed with this technique. These included the inability to define certain tags due to their capability to be mapped to several genomic locations. As such, SAGE was then developed into CAGE. The original CAGE method involved the introduction of a biotin group into the diol residue of the cap structure of eukaryotic mRNA (Seki et al., 1998). The biotin was bound to streptavidin magnetic beads to remove any incomplete mRNAs. The RNA was converted to cDNA and sequenced. Unlike the similar technique SAGE in which the tag is produced from other parts of the transcript, CAGE is primarily used to identify the exact transcription start sites of the genome (Kawaji et al., 2006). Finally, RNA-seq technology was developed in 2008 and offers several advantages over the conventional sequencing mechanisms.

RNA-Seq uses recently developed deep-sequencing technologies and an overview of the complete sequencing process is illustrated in Figure 3-1 below. In general, total RNA is extracted from the specific cell of choice and fractionated into either poly A or ribosomal depleted RNA. Regardless of the eventual goal, determination of mRNA or lncRNA, all data analysis will begin with quality control (QC) and pre-processing. Quality control checks, utilising Agilent™ technology are employed to determine the overall quality and degradation state of the RNA and as such, each sample is assigned an RNA integrity number (RIN). The RIN algorithm is applied to electrophoretic RNA measurements and is based on a combination of different features that contribute information about the RNA integrity to provide a universal measure. The higher the RIN value, the lower the degradation of the RNA (Schroeder et al., 2006). Following obtainment of an adequate RIN value, the RNA is converted to a library of cDNA fragments, containing adaptor sequences at each end. Subsequent construction libraries are hybridised to a flow cell which contains a layer of covalently bound oligonucleotides complementary to the sequencing adapters that were introduced during library preparation (Ozsolak and Milos, 2011). Once the primers are hybridised, DNA polymerase extension results in a covalently bound full-length complimentary copy of the cDNA fragment. This fragment is then subjected to several rounds of PCR to allow sufficient levels for detection. Each

fragment is then sequenced in a high throughput manner from either one (single end sequencing) or both (paired end sequencing) ends and each read is typically 300-400 bases long. Quality control of RNA-sequencing is of paramount importance to obtain good quality results (Conesa et al., 2016). QC assessments include agilent testing, read quality, GC content, mapping statistics and reproducibility between biological replicates. Each of these QC parameters will be described in detail in section 3.3.3. Following sequencing, two different assembly methods are used for producing a transcriptome from raw sequence reads: *de novo* (Li et al., 2014) and genome-guided (Florea and Salzberg, 2013). The first approach does not rely on a on a reference genome and instead relies on the overlap between each read to ensure the correct transcript is constructed. Although this approach is difficult, a few computer software packages, such as Oases and Trinity (Li et al., 2014), are capable of this type of approach. *De novo* assembly of read sequences harbours several key advantages over existing technologies. This method provides a powerful framework to uncover, new and previously un-annotated RNA species, thus is used frequently for the discovery of lncRNA. The easier and relatively computationally cheaper approach is to align all the reads to a reference genome and recently specialised algorithms for transcriptome alignment have been developed. The Tuxedo package is the most widely used software for transcript assembly following RNA-seq and consists of a number of different programs. These include Bowtie for RNA-seq short read alignment, TopHat for aligning reads to a reference genome to discover splice sites and Cufflinks to assemble the transcripts (Trapnell et al., 2012). The abundance of each transcript can then be determined by the Fragments Per Kilobase of transcript per Million mapped reads (FPKM) number. One of the most frequent applications of RNA-seq is to identify differentially expressed genes between two or more groups. The number of reads mapping to each RNA species is linearly related to its abundance within the cell and as such the greater the FPKM, the more abundant the transcript. Differential expression analysis can be performed through utilisation of programs such as EdgeR and utilises two steps. First, a table containing number of reads corresponding to each lncRNA of interest for every sample is prepared using a Python script called HTSeq-count. Next, edgeR uses the counts table with biological replicates to calculate variation and test for statistically significant differential expression (Robinson et al., 2010).

RNA-sequencing offers many advantages over the conventional microarray and tag based methods. It not only allows the accurate quantification of gene expression but allows, for the first time, the complete transcript including splice variants and genomic changes such as SNPs to be identified at the one point (Chen et al., 2014), (Piskol et al., 2013). Additionally, continual refinement has allowed the per base sequencing costs to decrease significantly with a parallel increase in sequencing output (Muir et al., 2016). Output increases are largely due to increased number of reads and longer read length and this trend continues rapidly. Furthermore, input requirements are currently at the stage where RNA of a single eukaryotic cell can be sequenced with existing technologies. This opens up new avenues of research and has the potential to change our understanding of whole organisms since cell lineages can be traced and heterogeneity inside an organ be described with high resolution (Saliba et al., 2014). For example, single cell RNA-seq was recently utilised to determine the differences between mesodermal cells and to establish how these cells are eventually primed for hematopoietic or cardiac development (Chan et al., 2016). Thus, RNA-seq, at the single cell level, allows the more accurate assessment of cardiovascular development. Finally, even organisms lacking a reference genome can be sequenced and *de novo* assembly performed in order to determine the expression levels of new transcripts and genes from previously unstudied organisms. As such, this method has now been utilised, for example, in several plant genomes as a method to better understand the control of traits relevant to crop productivity and quality (Sudheesh et al., 2015).

RNA Sequencing

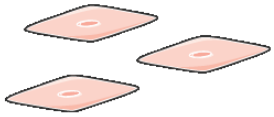

1. Select cell type and conditions

Quality Control

Ensure correct pathways activated by qRT-PCR

2. Extract total RNA

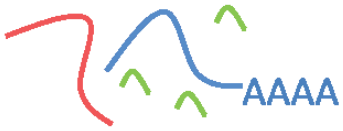

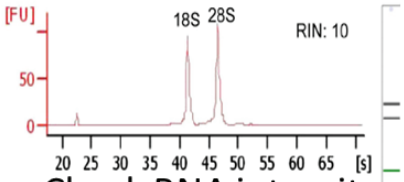

Check RNA integrity

3. Select RNA based on polyA tail or remove ribosomal RNA

4. Fragment RNA

5. Convert to cDNA Library

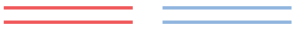

6. Construct Library

7. Sequence

Phred Sequencing control

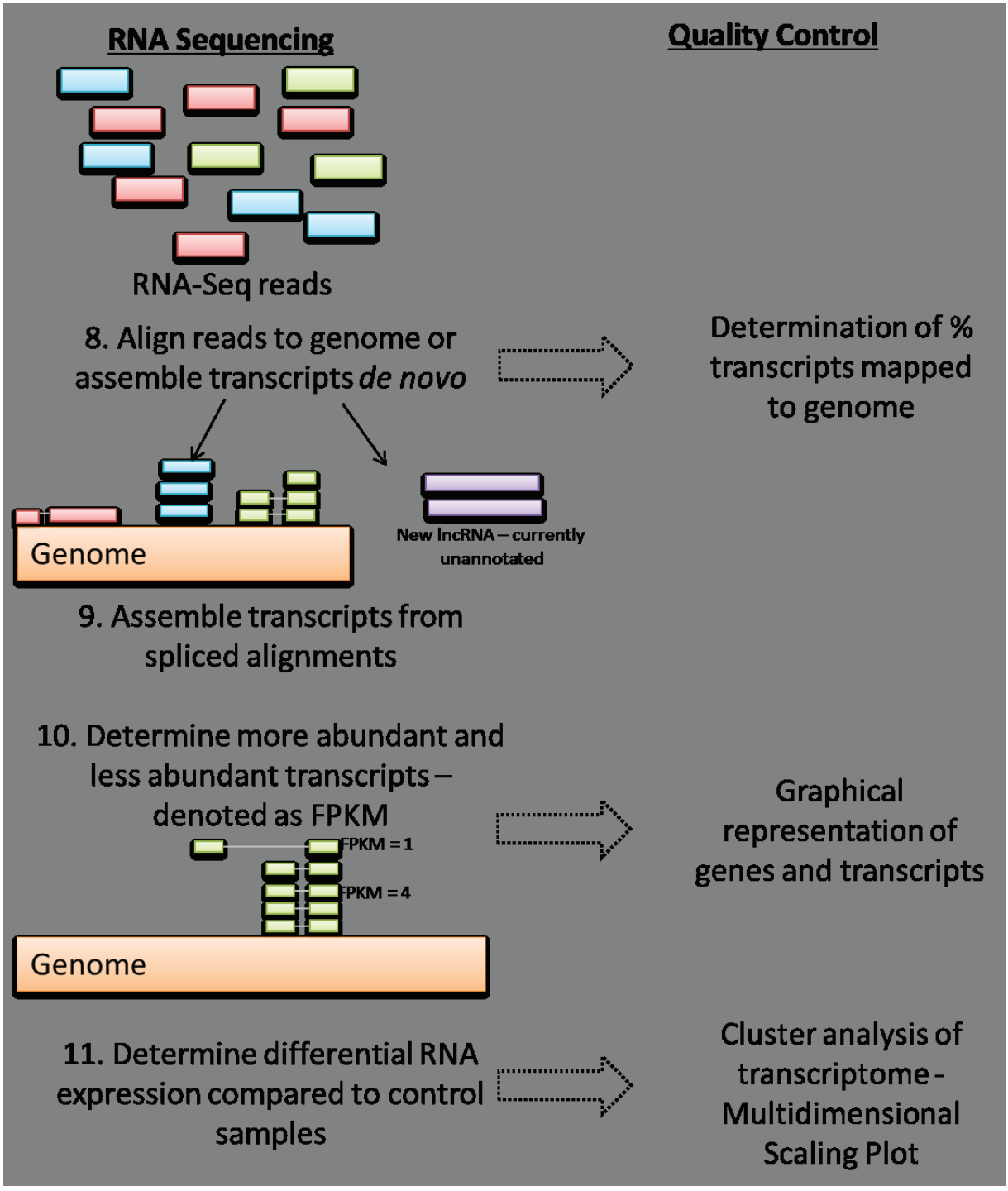

Figure 3-1: Schematic diagram of RNA-seq library construction.
Total RNA is extracted from the desired cell population following confirmation that key pathways are activated and a small aliquot is used to measure the integrity of the RNA. rRNA is then depleted through one of several methods and mRNA is fragmented into a uniform size distribution. The cDNA is then built into a library. cDNA libraries are sequenced and the sequence subjected to Phred scoring. Mapping programs align reads to the reference genome and map splice junctions. Gene expression can be quantified as absolute read counts or normalized values such as FPKM. If RNA-seq data sets are deep enough and the reads are long enough to map enough splice junctions, the mapped reads can be assembled into transcripts. The sequence transcripts can be compared to control samples to allow the quantification of differential RNA expression patterns.

The utilisation of RNA-sequencing has truly revolutionised the non-coding, and particularly the lncRNA field. Through the ENCODE (Encyclopedia of DNA Elements) project and other global sequencing initiatives, it became clear that up to 90 % of the human genome is transcribed and the majority of the transcripts do not code for proteins (Hangauer et al., 2013). Although the total number of lncRNA is currently unknown, RNA-sequencing has identified several key features of lncRNA. These include that lncRNA are ubiquitously expressed (Jiang et al., 2016), they are expressed at lower levels than protein coding genes but show greater cell and tissue restrictive expression patterns (Elder et al., 2015). Additionally, it is now known that lncRNA are not located uniformly with respect to protein coding genes and in fact can be found within introns, exons, overlapping or antisense to key protein coding genes (Atianand and Fitzgerald, 2014). The classification of lncRNAs as antisense transcripts is due to continual improvements and development of RNA-sequencing technology, allowing strand specific protocols to be utilised (Mills et al., 2013). Due to the easy application of RNA-seq, lncRNAs have now received immense interest in recent years and this can be evidenced by the vast increase in lncRNA publications (Figure 3-2).

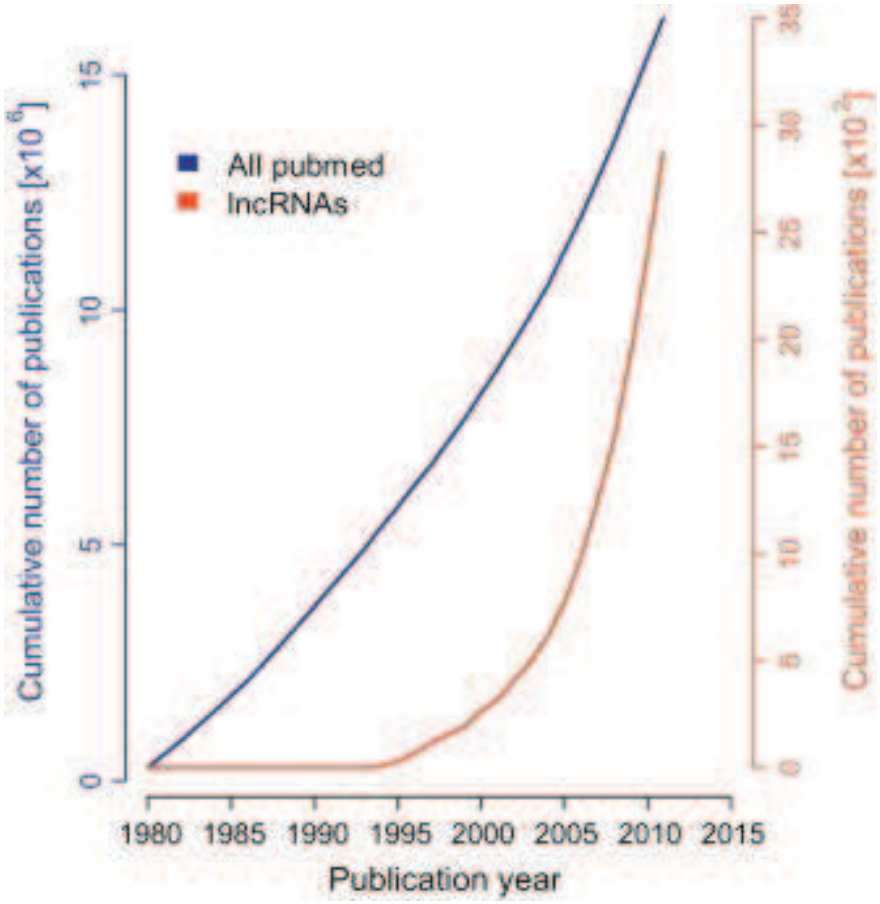

Figure 3-2: Research on long non-coding RNAs is rapidly increasing.
Cumulative plot of the total number of publication entries in PubMed (blue line and axis) and of entries related to long non-coding RNAs (red line and axis). Image taken from (Atkinson et al., 2012).

Apart from RNA-sequencing to identify transcriptomic differences between samples, more in-depth sequencing and epigenetic studies can provide other useful information that may significantly advance our understanding of biological processes.

RNA-sequencing has proved beneficial in the setting of cardiovascular disease as sequencing of the entire human genome has exponentially expanded the understanding of genetic contributions to cardiovascular disease. Multiple novel genetic loci have been identified in common cardiovascular conditions including myocardial infarction, hypertension, heart failure and stroke. At present 26 key risk loci have been identified, via RNA-seq that are associated with coronary artery disease (Manace et al., 2009), and, as such, research is now ongoing to better understand how these genetic areas influence vascular disease and to determine if therapies can be developed. Additionally, the genetic traits of several key hereditary cardiac traits have been established via RNA-seq. Hypertrophic cardiomyopathy and dilated cardiomyopathy are two major clinical forms of inherited cardiomyopathy. HCM, the major cause of sudden death in young people and is characterised by left ventricular hypertrophy. Conversely, DCM is characterised by dilated ventricular cavity with systolic dysfunction. The clinical symptom of DCM is heart failure, often associated with sudden death. More than half of HCM patients have a family history of the disease consistent with an autosomal dominant genetic trait. In the case of DCM, about 20 %-35 % of patients show a family history of the disease. RNA-seq offers a new approach in the diagnosis of cardiomyopathies and has identified that these conditions are caused by mutations in 30 genes (Vecoli, 2015). Research is ongoing to identify key therapies based on these genes, but, has allowed the screening of family members to identify their risk of cardiac conditions. Finally, small RNA-seq has identified key microRNAs that may prove beneficial for the discovery of new cardiovascular biomarkers. In 2008, the presence of miRNA was detected in human plasma and serum. This was the first results demonstrating the robust stability of circulating microRNAs (Mitchell et al., 2008). Since 2008, small RNA-seq has expanded exponentially in an attempt to discover new and novel biomarkers for disease states. Zampetaki et al identified three miRNAs (miR-126, miR-197, and miR-223) that could predict acute myocardial infarction in a

prospective study of cardiovascular disease with 10-year follow-up. The addition of these three miRNAs to the Framingham Risk Score improved classification to a greater degree than the currently utilised cardiac Troponin T biomarker (Mayr et al., 2012). While further validation is required, these results suggest a potential role for miRNAs in predicting risk of future AMI. Taken together, these results highlight the key advancements in cardiovascular research due to RNA-seq.

In addition to the improvements in RNA-seq technique, advances have also been made in the detection of cellular proliferation. The development of intimal hyperplasia following vein grafting or vessel stenting involves altered rates of SMC proliferation induced by cytokine and growth factor signalling (see Chapter1 – Section 1.3). Various techniques have been developed to evaluate and quantify proliferation rates in the laboratory. Mitotic count estimates are widely used as a simple measure of cellular proliferation. Cellular proliferation involves several difined stages (reviewed in Chapter 1- Section 1.4) and was first measured by counting mitotic bodies on paraffin embedded specimens stained using haematoxylin-eosin. The characteristic appearance of the chromosome during M phase allowed mitotic figures to be distinguished. Newer techniques have since been utilised and typically involve incorporation of radiolabelled thymidine or thymidine analogues, such as 5-bromodeoxyuridine (BrdU) and 5-ethynyl-2'-deoxyuridine (EdU), into the DNA of proliferating cells. Detection of these agents, therefore provides an indirect marker of cellular proliferation. In 1982 Gratzner described the use of monoclonal antibodies specific for BrdU in the detection of DNA replication (Gratzner, 1982). This allowed the detection of cellular proliferation without the use of radiolabelled thymidine. The success of BrdU incorporation as a marker of proliferation led to the production of EdU, another thymidine analogue. The detection of EdU relies on the subsequent reaction of EdU with a fluorescent azide in a copper–catalyse cycloaddition (“Click” reaction). The utilisation of both BrdU and EdU to measure SMC proliferation has been demonstrated effective by several laboratories (Thakar et al., 2009), (Tanaka et al., 1996).

3.2 Aims

Identification of lncRNA via RNA-sequencing, is thus, the first step to characterise lncRNA function and clinical applicability. Therefore, the aims of this chapter were as follows:

- To perform deep RNA-sequencing on HSVSMC under quiesced and cytokine and growth factor stimulated conditions.

- To identify lncRNA that were differentially regulated following cytokine and growth factor stimulation which may be functionally important in vascular SMC disease.

- To validate each lncRNA selected from the RNA-Seq to confirm the expression profile under basal and stimulated conditions.

3.3 Experimental Design and quality control

3.3.1 Experimental Design

IL1α and PDGF are two of the main cytokine and growth factors implicated in vascular disease, and are involved in the switching of SMC from a contractile to a pro proliferative and pro migratory state (Brody et al., 1992), (Zhan et al., 2003) (described in detail in Chapter 1- Section 1.5). It was hypothesised that IL1α and PDGF treatment solely and in combination would alter lncRNA expression profiles when compared to 0.2 % FBS-treated, quiescent human saphenous vein smooth muscle cells (HSVSMC). To pursue this hypothesis RNA-sequencing was performed on HSVSMC cultured from CABG patients, each of which had been exposed to 0.2 % FBS, 10 ng/ml IL1α, 20 ng/ml PDGF or a combination of 10 ng/ml IL1α and 20 ng/ml PDGF. These concentrations were previously shown to elicit synergistic effects on the NF-κB pathway in human smooth muscle cells (Bond et al., 2001). To control and add sufficient power, 4 sets of patient cells were utilised per condition. Prior to sequencing, and throughout the sequencing process, quality control checkpoints were undertaken to ensure high quality results would be obtained (See sections 3.3.2 and 3.3.3). According to Figure 3-1, all QC checks up to point 2 (extraction of total RNA), including confirmation of pathway activation and RNA integrity checks were performed in the lab. Points 3-11 and the corresponding QC was performed by Beckman Genomics. Following conversion to cDNA, fragmentation and sequencing, Bowtie and Tophat bioinformatic programs were utilised to align each fragment back to the human genome. Cufflinks program was utilised to identify transcripts and EdgeR allowed the assessment of differential expression between stimulated and quiescent conditions. All mRNA and lncRNA transcripts were identified and classified according to Ensembl classification (Figure 3-3).

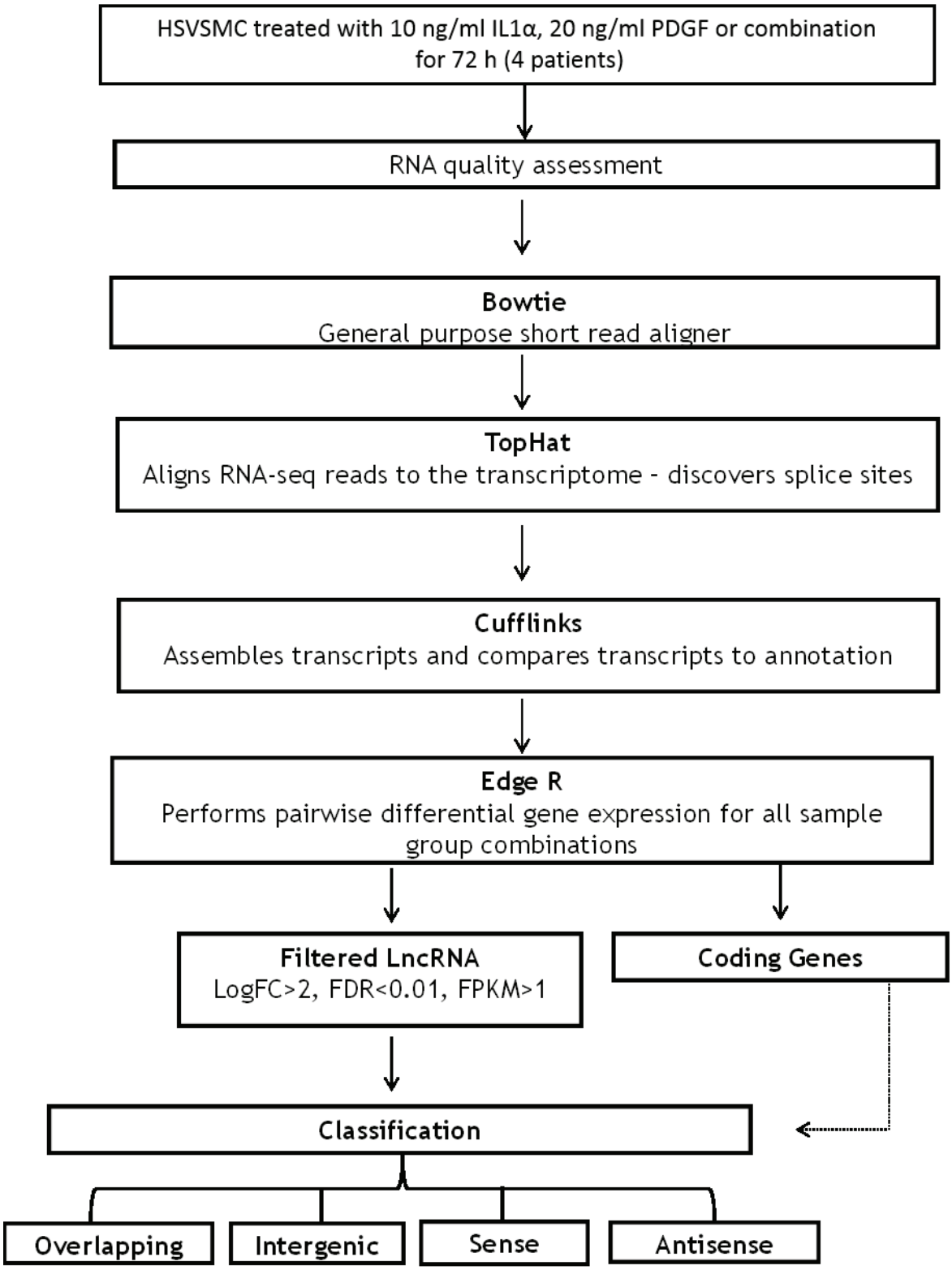

Figure 3-3: Study design for determination of the transcriptome in quiescent and stimulated. HSVSMC.

HSVSMC were quiesced for 48 h prior to stimulation with IL1α, PDGF or combination for 72 h. RNA quality was assessed via agilent and samples subjected to RNA-sequencing following the Tuxedo pipeline for analysis. LncRNAs were selected based on a Log fold change (FC) greater than 2 (Fold change greater than 4), False discovery Rate (FDR) <0.01 and fragments per kilobase of mapped reads greater than 1 in at least one condition. LncRNAs were classified based on Ensembl classification into overlapping, intergenic, sense or antisense lncRNA.

3.3.2 Quality control of HSVSMC prior to sequencing

In order to assure high quality RNA was obtained prior to the RNA sequencing screen, several quality control mechanisms were undertaken. PDGF is a potent proliferative agent for HSVSMC (Li et al., 2011b), thus, proliferation experiments were performed in order to confirm that PDGF had a proliferative role in the cells analysed. BrdU incorporation was utilised as an indirect marker of cellular proliferation due to its incorporation into the DNA of replicating cells only (Mandyam et al., 2007). PDGF and PDGF in combination with IL1α, but not IL1α alone induced a 7.3 ± 1.6 and 7.9 ± 0.4 fold change in proliferation respectively, indicating that the PDGF has a proliferative role within the HSVSMC analysed (Figure 3-4). Additionally, stimulation with IL1α has been shown to induce the expression of the inflammatory microRNA miR-146a (Iyer et al., 2012). Thus, the expression of this microRNA was assessed in all RNA samples prior to submission for RNA-sequencing, to ensure the function of the IL1α pathway. Figure 3-5 shows that miR146a was induced by both IL1α and PDGF in the following ranking PDGF<IL1α<IL1α + PDGF. IL1α alone induced a 78.5 ± 28.6 fold induction of miR146a. Interestingly, although PDGF had no significant effect on miR-146a expression alone, PDGF in combination with IL1α induced a 151.9 ± 48.5 fold expression in miR-146a expression indicating synergistic activation of the microRNA.

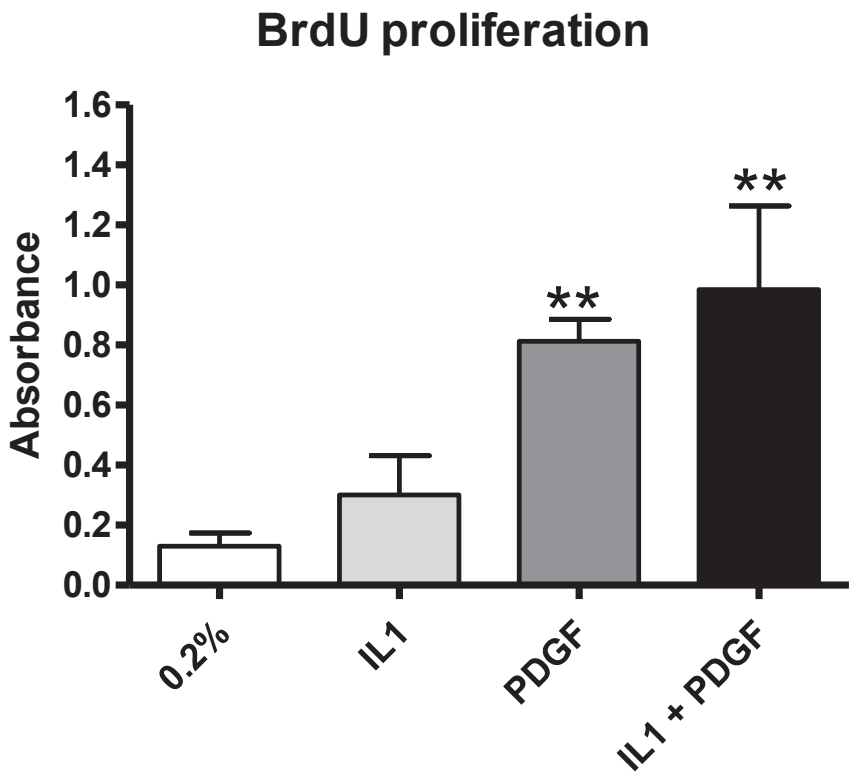

Figure 3-4: BrdU proliferation of HSVSMC.
HSVSMC were quiesced in 0.2 % media for 48 h prior to stimulation with 0.2 % (control) or media containing IL1α, PDGF or combination of IL1α and PDGF for 72 h with the addition of a BrdU constituent. BrdU incorporates into the DNA of replicating cells and as such acts as an indirect marker of cell proliferation. Cells were fixed and BrdU incorporation assessed in all patients via a BrdU kit (Millipore). Proliferation was performed in triplicate within each patient (n=4). Significance determined by multiple comparison one way ANOVA and significance denoted by **P<0.01 vs. 0.2 % condition.

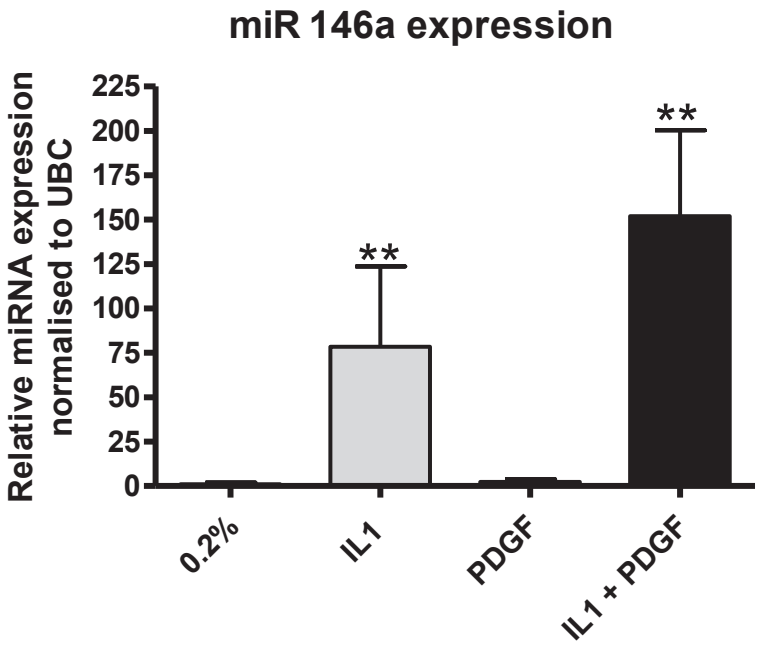

Figure 3-5: miR146a expression in basal and stimulated HSVSMC.
HSVSMC were quiesced in 0.2 % media for 48 h prior to stimulation with 0.2 % (control) or media containing IL1α, PDGF or combination of IL1α and PDGF for 72 h. Samples were subjected to RNA extraction and the expression of the inflammatory microRNA, miR-146a, was determined via qRT-PCR. miR-146a expression was performed in triplicate within each patient (n=4). Significance determined by multiple comparison one way ANOVA and significance denoted by **P<0.01 vs. 0.2 % condition.

The integrity of short and longer RNA molecules is of paramount importance for experiments that try to reflect the snapshot of gene expression at the moment of RNA extraction. Thus, all samples were subjected to AgilentTM testing and RNA Integrity Number (RIN) values were obtained. All RIN values were greater than 8, which ensured high quality RNA was submitted for analysis (Table 3-2). A greater Agilent test score indicates lower levels of RNA degradation thus producing greater success in RNA-sequencing experiments (Schroeder et al., 2006).

Table 3-2: RIN values of RNA-seq samples.
Prior to sequencing, RNA integrity was determined via Agilent™ testing. RIN – RNA Integrity Number. The greater the RIN value, the lower the level of RNA degradation.

Condition	Patient Number	RIN value
0.2% FBS	Patient 1	10
0.2% FBS	Patient 2	10
0.2% FBS	Patient 3	9.2
0.2% FBS	Patient 4	10
IL1α	Patient 1	9.6
IL1α	Patient 2	10
IL1α	Patient 3	8.5
IL1α	Patient 4	10
PDGF	Patient 1	10
PDGF	Patient 2	10
PDGF	Patient 3	10
PDGF	Patient 4	10
IL1α + PDGF	Patient 1	10
IL1α + PDGF	Patient 2	10
IL1α + PDGF	Patient 3	10
IL1α + PDGF	Patient 4	10

3.3.3 Quality control of RNA-Seq

The acquisition of RNA-seq data consists of several steps — obtaining raw reads, read alignment and quantification. At each of these steps, specific checks were applied to monitor the quality of the data.

3.3.3.1 Phred score – sequencing quality

Phred is a base calling program for DNA sequence traces and assesses sequencing quality. Phred reads DNA sequence chromatograms and assigns quality scores to each base call. Quality scores range from 0 to 40, with the higher values corresponding with higher sequencing quality. The quality scores are logarithmically linked to error probabilities, as shown in the table below (Ewing and Green, 1998):

Table 3-3: Phred score table.
The Phred score indicates the probability of the sequenced base being incorrect.

Phred Quality Score	Probability that the base is wrong	Accuracy of base call
10	1 in 10	90%
20	1 in 100	99%
30	1 in 1,000	99.9%
40	1 in 10,000	99.99%

Figure 3-6 displays the average Phred quality per sample over the forward (red) and reverse (blue) reads. Apart from the end of the reverse reads, all samples had a minimum Phred score of 30 denoting a 99.9 % chance that the DNA sequenced was correctly identified.

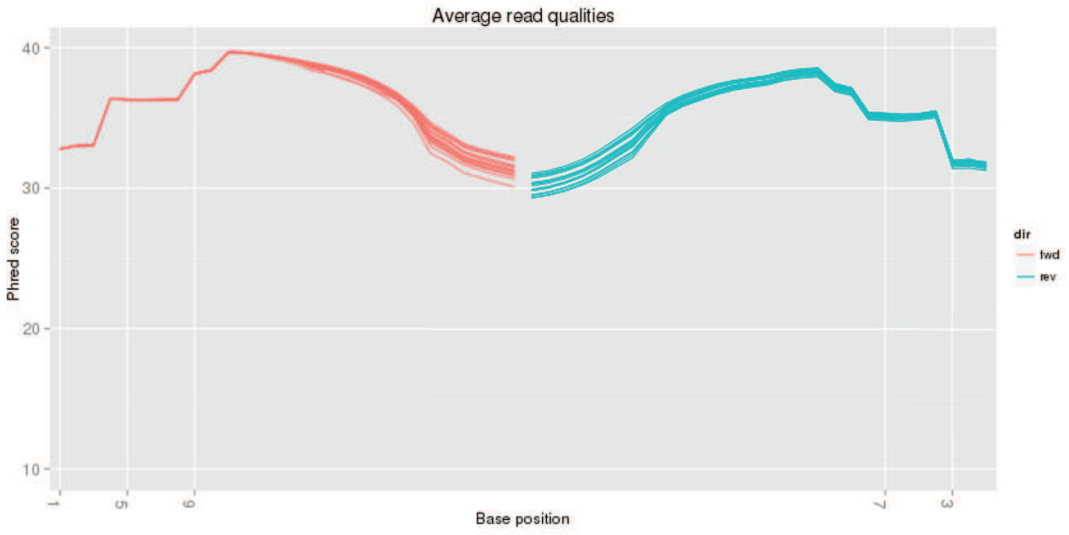

Figure 3-6: Per sample quality as a function of position in read.
Graph indicates the Phred quality of the forward (red) and reverse (blue) reads. The beginning and the end of a read has lower quality (X-axis). While the position (bases) is provided on the Y-axis.

.

3.3.3.2 Sequence mapping and expression analysis

Mapping was performed on the human genome reference sequence GRCh37, using Tophat in conjunction with Bowtie. Tophat was provided with a transcriptome reference generated from the Ensembl annotation of GRCh37. The number of reads mapped to the genome for all samples was 69 ± 3.5 $x10^6$. The individual mapped reads for each sample is shown in Table 3-4. Additionally, the abundance of each gene and isoform are measured and denoted by the fragments per kilobase of mapped reads (FPKM) number: the greater the FPKM, the greater the expression of the transcript in a given sample. The abundance of genes and isoforms vs. FPKM are shown in Figure 3-7.

Table 3-4: Number of reads per sample mapped to the genome per condition.

Group	QC passed reads	raw reads mapped
IL1 + PDGF 1	76,364,982	79,327,299
IL1 + PDGF 2	81,790,616	85,160,763
IL1 + PDGF 3	74,679,220	71,380,968
IL1 + PDGF 4	73,334,180	75,306,173
IL1 1	57,087,540	58,596,954
IL1 2	66,523,536	70,822,819
IL1 3	32,999,754	34,351,686
IL1 4	60,568,838	63,897,920
PDGF 1	70,765,332	70,826,368
PDGF 2	65,287,750	70,155,304
PDGF 3	65,267,300	69,248,255
PDGF 4	78,473,040	80,535,799
Control 1	71,174,440	71,823,885
Control 2	92,795,728	97,214,677
Control 3	53,179,712	56,016,312
Control 4	63,808,760	65,220,185

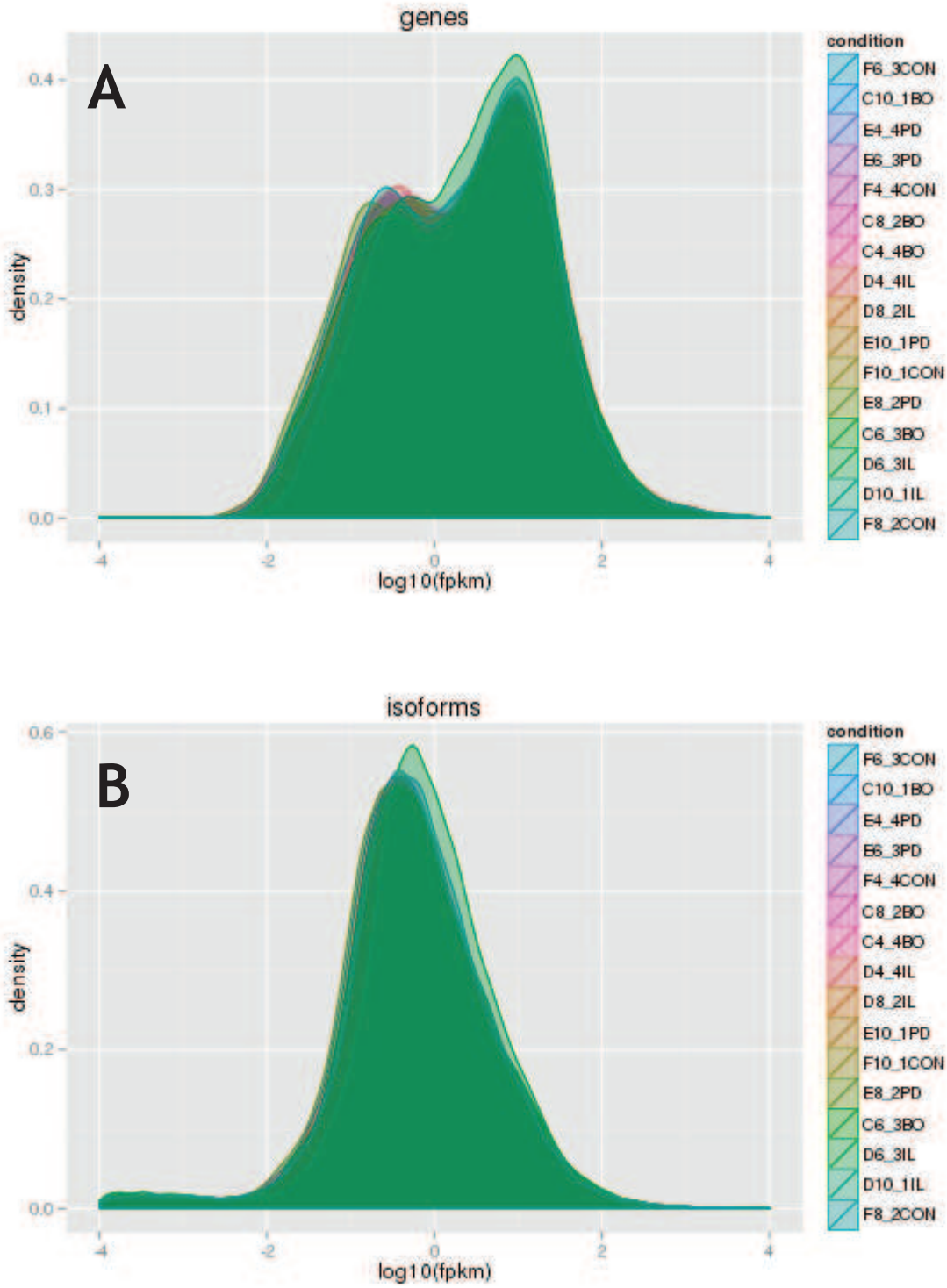

Figure 3-7: Gene and Isoform expression levels in 10log (FPKM).
A: Isoform and **B:** gene expression is determined from RNA-seq alignment to the human genome. Gene expression is the sum of all the isoforms, thus gene expression levels are higher than individual isoform levels. CON – 0.2 %, IL – IL1α treatment, PD – PDGF treatment, BO - IL1α and PDGF treatment.

3.3.3.3 Differential expression

A multidimensional scaling plot (MSD) was designed utilising EdgeR. A MSD plot provides a visual representation of the pattern of proximity amongst samples, the closer the samples to each other, the more similar the transcriptome. As shown in Figure 3-8 all control (CON-grey), PDGF (PD-yellow), IL1α (IL-blue) and IL1α + PDGF (BO-green) samples cluster together indicating similar transcription of RNA regardless of the patient. However, some patient specific differences were still observed as all samples from the same patient (patients numbered 1-4) lie along the same diagonal line as indicated by the dotted lines.

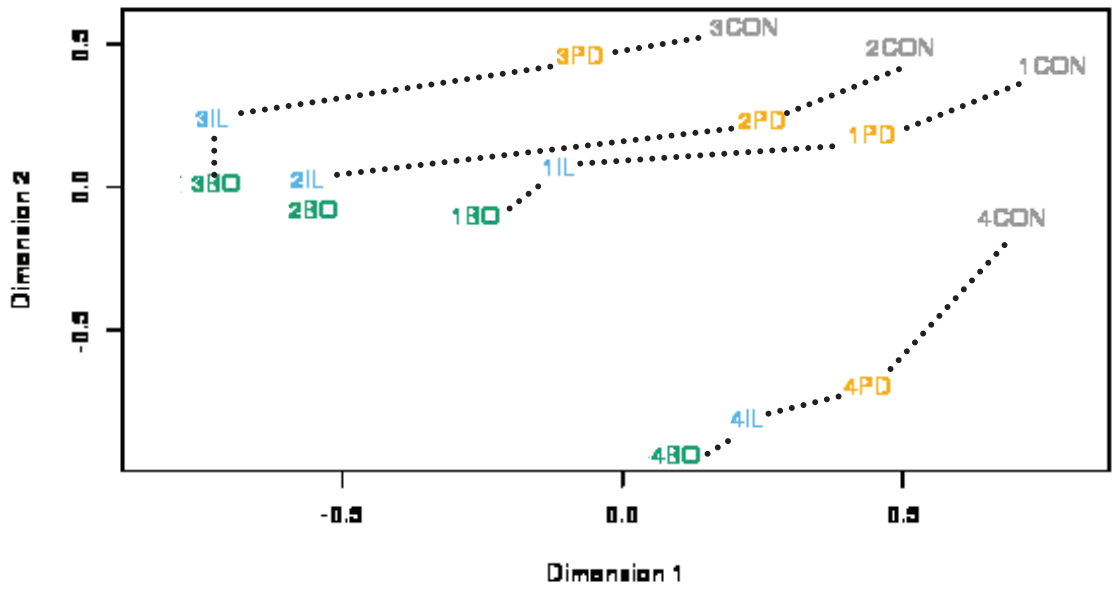

Figure 3-8: Multidimensional scaling plot (MSD) of all RNA-seq samples.
MSDs indicate the similarity of the transcriptome between all samples. CON = 0.2 % control, PD =PDGF treated cells, IL = IL1α treated cells and BO= IL1α and PDGF treated cells. Numbers 1-4 indicate each specific patient.

3.4 Results

Following EdgeR differential analysis, RNA was classified into protein coding, microRNA or lncRNAs according to Ensembl classification (Figure 3-3). To confirm that RNA-seq analysis demonstrated similar levels to that obtained by qRT-PCR, miR-146a expression was determined from the sequencing results, however it should be noted that the RNA-seq performed is not used specifically for the detection of microRNA. However, a 78 fold increase was obtained in SMC treated with IL1α alone and 194 fold increase in SMC treated with IL1α and PDGF (Figure 3-9). This is similar to the 78.5 ± 28.6 and 151.9 ± 48.5 fold induction obtained in by qRT-PCR prior to sequencing in section 3.3.2, and highlights similarities between RNA-seq and qRT-PCR analysis.

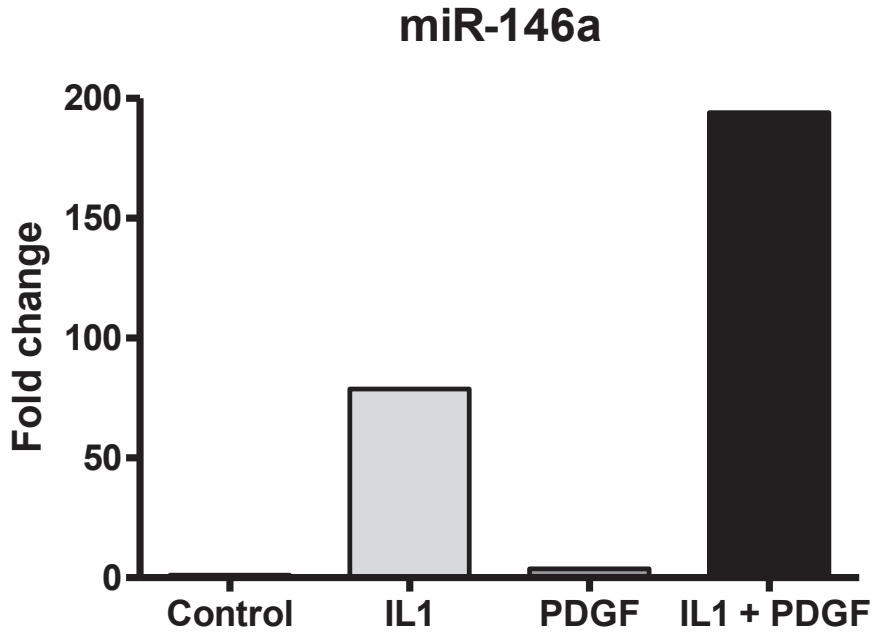

Figure 3-9: miR-146a expression from RNA-sequencing.
HSVSMC were quiesced in 0.2 % media for 48 h and then stimulated with 0.2 % (control), IL1α, PDGF or a combination of IL1α and PDGF for 72 h. RNA was extracted and subjected to RNA-seq analysis. Results indicate the expression of miR-146a from RNA-seq results. Expression is relative to 0.2 % condition (set to 1) (n=4).

3.4.1 Induction of inflammatory and cell cycle pathways by IL1α and PDGF – analysis of mRNA from RNA-Seq

The majority of reads obtained from the RNA-seq, under all conditions, corresponded to mRNA (49.6 ± 0.2 %, FPKM>0.1, Figure 3-10). Global characterisation of the divergence of mRNA expression between control and treatment groups was assessed using the strict criteria of a false discovery rate (FDR) < 0.01. To identify the biological function, networks, and canonical pathways that were affected by VSMC stimulation, Ingenuity Pathway Analysis (IPA) was performed. IPA is an application that enables analysis, integration and understanding of data from RNA-seq experiments and allows the biological context of the expression analysis to be determined. IPA confirmed the mRNAs with altered expression following IL1α treatment were significantly enriched in pathways related to cellular movement ($P=1.3 \times 10^{-36}$) and inflammatory disease ($P=4.3 \times 10^{-23}$) (Table 3-5), while PDGF stimulation led to the marked enrichment in cell cycle pathways ($P=2.5 \times 10^{-29}$) (Table 3-6). Interestingly, co-stimulation led to enrichment in cell cycle ($P=1.0 \times 10^{-45}$) and cardiovascular development pathways ($P=12.2 \times 10^{-29}$) (Table 3-7). Additionally, the P values obtained for the cell cycle pathway for dual stimulation of IL1α and PDGF were much lower than with single treatment, indicating additive effects of this cytokine and growth factor. Further analysis of differentially expressed mRNAs identified 518 protein coding genes altered following IL1α treatment and 540 following PDGF treatment. Notably, dual stimulation altered 1133 known protein-coding genes with 480 uniquely associated with dual stimulation and not affected by IL1α or PDGF treatment alone, further highlighting additive or synergistic effects of this cytokine and growth factor combination (Figure 3-11).

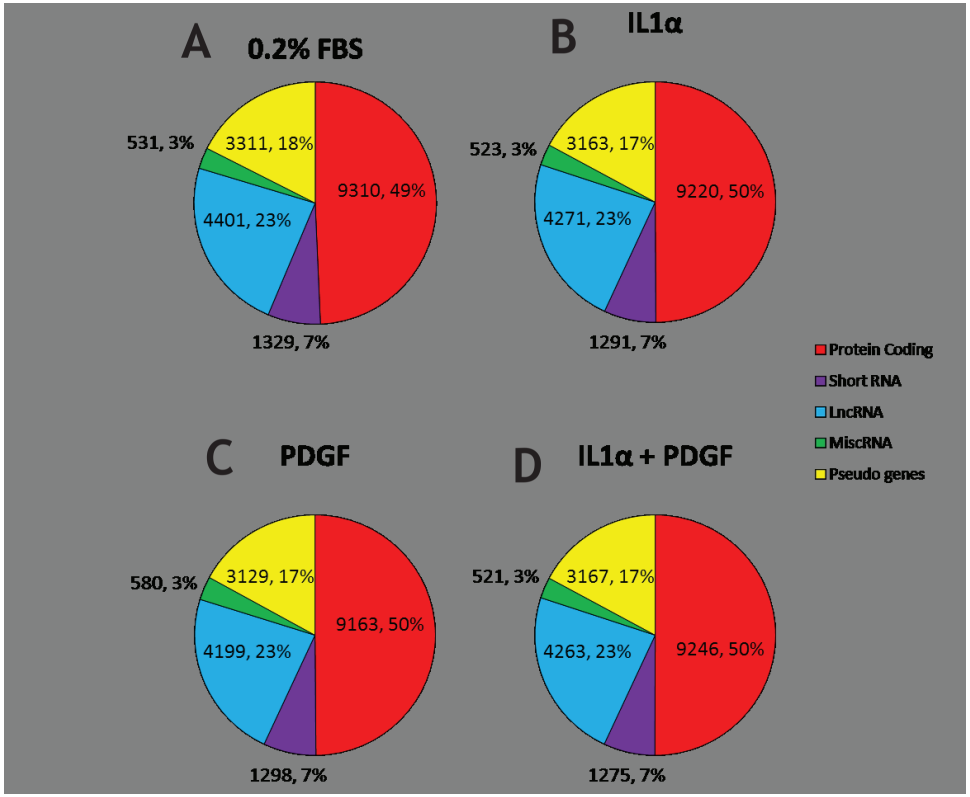

Figure 3-10: Pie chart of identified transcripts from RNA-Seq.

HSVSMC were quiesced in 0.2 % media for 48 h and then stimulated with **A**: 0.2 % (control), **B**: IL1α, **C**: PDGF or **D**: a combination of IL1α and PDGF for 72 h. RNA was extracted and subjected to RNA-seq analysis. Piecharts indicate the biotype distribution of all transcripts identified by RNA-seq analysis generated from HSVSM cells untreated or treated with IL1α and/or PDGF, cut off at FPKM>0.1. (n=4 patients per pie chart).

Table 3-5: IL1α stimulation Ingenuity Pathway Analysis.
Top 10 disease and functional pathways predicted to be altered by IPA in HSVSM cells stimulated with IL1α when compared to 0.2 % control cells (n=4 patients). P-values are used to score expression changes derived from 0.2% and Il1 + PDGF stimulated cells and indicates the likelihood that the pathway associated is significantly changed between the conditions.

0.2% VS IL1α

Categories	Disease or Function Annotation	p-value
Cellular Movement	cellular movement	$1.3x10^{-36}$
Cell Death and Survival	necrosis	$1.6x10^{-33}$
Cellular Growth and Proliferation	proliferation of cells	$2.4x10^{-28}$
Organismal Development	angiogenesis	$2.3x10^{-26}$
Cancer	growth of tumour	$6.7x10^{-25}$
Connective Tissue Disorder	arthropathy	$8.1x10^{-24}$
Inflammatory Disease	chronic inflammatory disorder	$1.4x10^{-22}$
Cellular Movement	leukocyte migration	$1.9x10^{-23}$
Inflammatory Response	Inflammatory response	$4.3x10^{-23}$
Gastrointestinal Response	Digestive system cancer	$6.9x10^{-23}$

Table 3-6: PDGF stimulation Ingenuity Pathway Analysis.
Top 10 disease and functional pathways predicted to be altered by IPA in HSVSM cells stimulated with PDGF when compared to 0.2 % control cells (n=4 patients). P-values are used to score expression changes derived from 0.2% and Il1 + PDGF stimulated cells and indicates the likelihood that the pathway associated is significantly changed between the conditions.

0.2% VS PDGF

Categories	Disease or Function Annotation	p-value
Cellular Growth and Proliferation	proliferation of cells	$2.5x10^{-29}$
Cell Death and Survival	apoptosis	$3.3x10^{-25}$
Cellular Movement	migration of cells	$5.3x10^{-23}$
Cardiovascular System Development	development of the cardiovascular system	$2.3x10^{-26}$
Organismal Development	angiogenesis	$7.1x10^{-21}$
Cellular Development	proliferation of tumour cell lines	$8.5x10^{-21}$
Cancer	cancer	$1.5x10^{-20}$
Cell Cycle	mitosis	$1.7x10^{-17}$
Cell Morphology	morphology of cells	$5.3x10^{-16}$
Tissue Development	growth of connective tissue	$6.7x10^{-16}$

.

Table 3-7: IL1α and PDGF stimulation Ingenuity Pathway analysis.
Top 10 disease and functional pathways predicted to be altered by IPA in HSVSM cells stimulated with IL1α and PDGF when compared to 0.2 % cells (n=4 patients). P-values are used to score expression changes derived from 0.2% and Il1 + PDGF stimulated cells and indicates the likelihood that the pathway associated is significantly changed between the conditions.

0.2% VS IL1α + PDGF

Categories	Disease or Function Annotation	p-value
Cellular Growth and Proliferation	proliferation of cells	$1.0x10^{-45}$
Cell Death and Survival	apoptosis	$7.2x10^{-44}$
Cancer	cancer	$1.2x10^{-37}$
Cellular Movement	migration of cells	$2.3x10^{-34}$
Gastrointestinal Response	digestive system cancer	$7.0x10^{-30}$
Cellular Development	proliferation of tumour cell lines	$8.5x10^{-28}$
Reproductive System Disease	tumour	$4.8x10^{-27}$
Cell Cycle	Cell cycle progression	$6.2x10^{-26}$
Cardiovascular System development	morphology of cells	$2.2x10^{-24}$
Cardiovascular System development	angiogenesis	$4.8x10^{-24}$

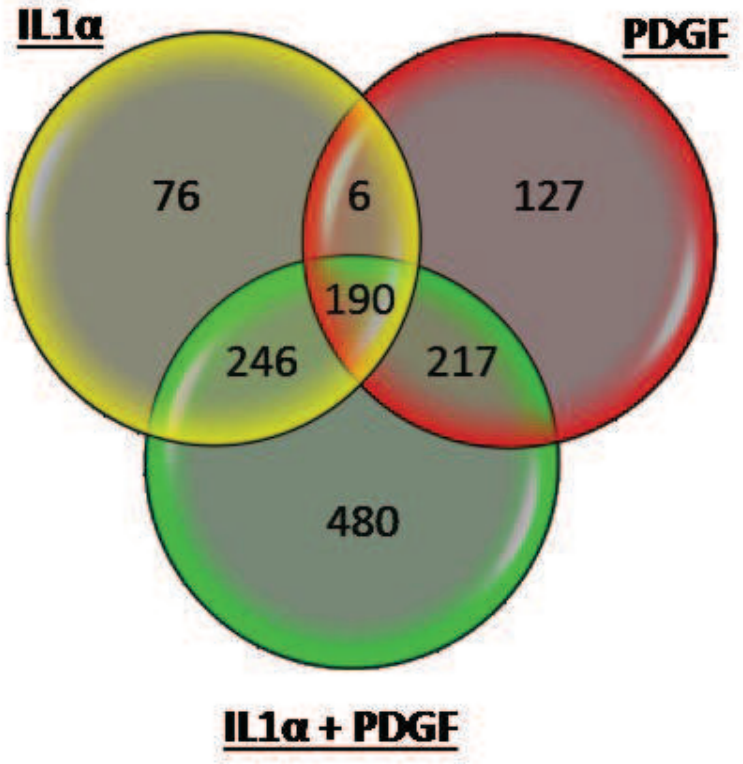

Figure 3-11: Venn diagram of differentially expressed mRNA with FPKM >0.1 identified from RNA-seq.
HSVSMC were quiesced in 0.2 % media for 48 h and then stimulated with 0.2 % (control), IL1α, PDGF or a combination of IL1α and PDGF for 72 h. RNA was extracted and subjected to RNA-seq analysis. Venn diagram indicate overlap of protein coding genes with altered expression (analysed using EdgeR, FDR<0.01) across each treatment (n=4 patients).

Further synergistic effects of dual IL1α and PDGF treatment were documented in the expression patterns of certain exemplar mRNA: MMP-3 and MMP-10. Single treatment with IL1α alone induced a 103 fold increase in MMP-3 ($P=8.6 \times 10^{-11}$) and 147 fold increase in MMP-10 ($P=6.6 \times 10^{-7}$). PDGF treatment alone induced a 3 and 0.2 fold increase respectively, however, dual stimulation of HSVSMC with both IL1α and PDGF resulted in a 724 ($P=1.1 \times 10^{-14}$) and 1357 ($P=1.8 \times 10^{-11}$) fold increase respectively, highlighting the ability of IL1α and PDGF to work in concert and exert synergistic effects on downstream mRNA (Figure 3-12).

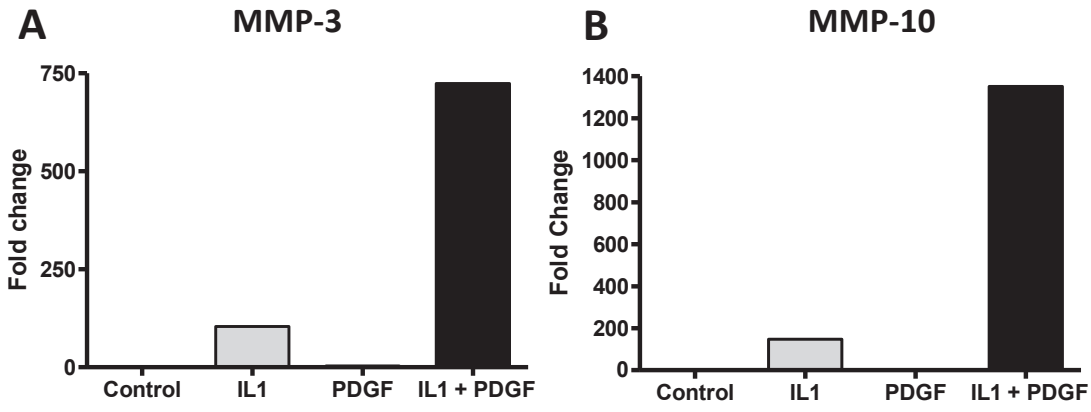

Figure 3-12: Synergistic effects of IL1α and PDGF on A: MMP-3 and B: MMP-10 expression. HSVSMC were quiesced in 0.2 % media for 48 h and then stimulated with 0.2 % (control), IL1α, PDGF or a combination of IL1α and PDGF for 72 h. RNA was extracted and subjected to RNA-seq analysis. MMP-3 and MMP-10 expression was determined from the RNA-seq analysis and results are relative to 0.2 % conditions (n=4 patients).

3.4.2 Identification of differentially expressed lncRNA in HSVSMC

Next it was assessed whether lncRNAs were dynamically regulated by growth factor and cytokine stimulation. Approximately 23 % of reads in each condition aligned to known or predicted lncRNAs (Figure 3-10 above). Differential expression analysis confirmed substantial differences in lncRNA expression between control and stimulated cells. Using the stringent criteria of a false discovery rate (FDR) ≤0.01 and log2 fold change (FC) ≥2 (Fold change >4), to declare significance, and fragments per kilobase of exon per million fragments mapped (FPKM) >1, to confirm quantifiable expression, 224, 215 and 369 differentially expressed lncRNAs were identified following IL1α, PDGF or dual stimulation respectively (Figure 3-13A, C and E). Since lncRNAs can typically

contain multiple splice variants, the numbers quoted refer to a single consensus gene model and therefore do not reflect the multiple transcripts of each lncRNA. To determine if specific biotypes of lncRNA were enriched following HSVSMC stimulation, those differentially expressed were further subdivided according to biotype in the Ensembl database. These are based upon their relative orientation to protein coding genes; intervening lncRNA (lincRNA), antisense, overlapping and processed transcripts. Utilising control and dual stimulation as an example, the distribution of different lncRNA biotypes was: intervening (45.5 %), antisense (45.3 %), overlapping (1.4 %) and processed transcripts (7.9 %). Similar proportions of lncRNA biotype were identified under all conditions (Figure 3-13B, D and F).

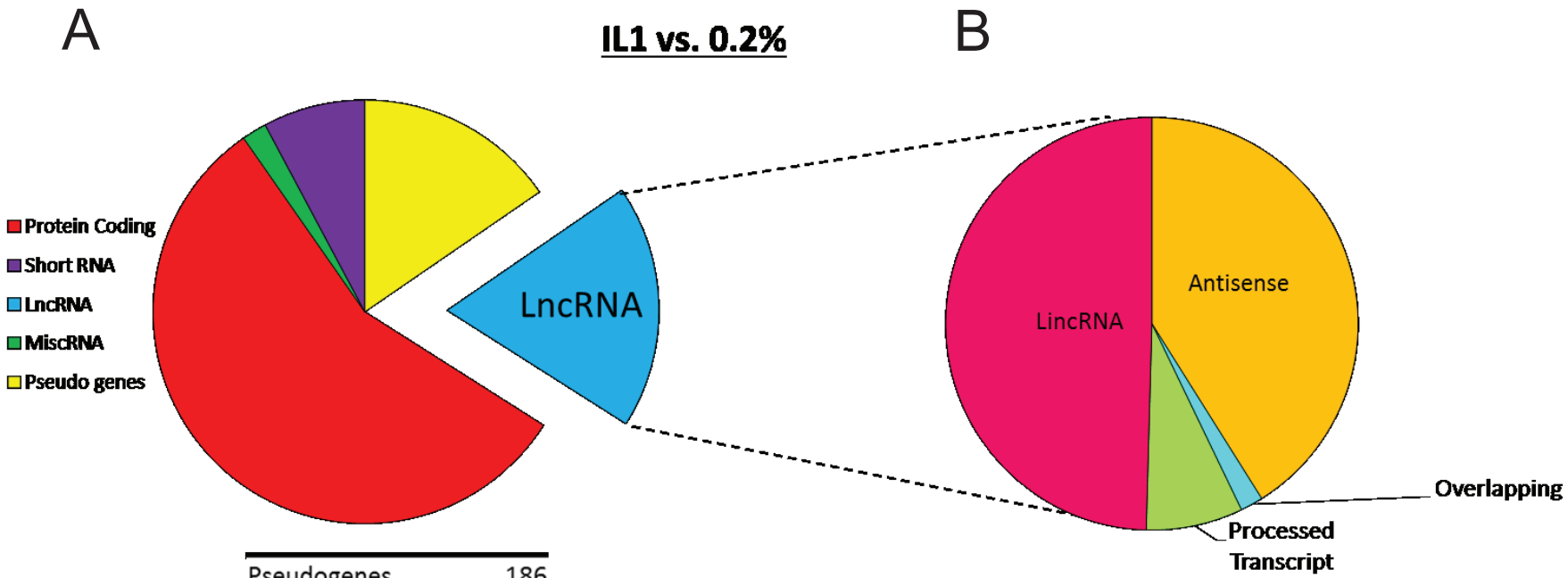

Pseudogenes	186
LncRNA	224
Protein Coding	679
misc-RNA	23
Short RNA	94

Antisense	92
Overlapping	4
Processed Transcript	17
LincRNA	111

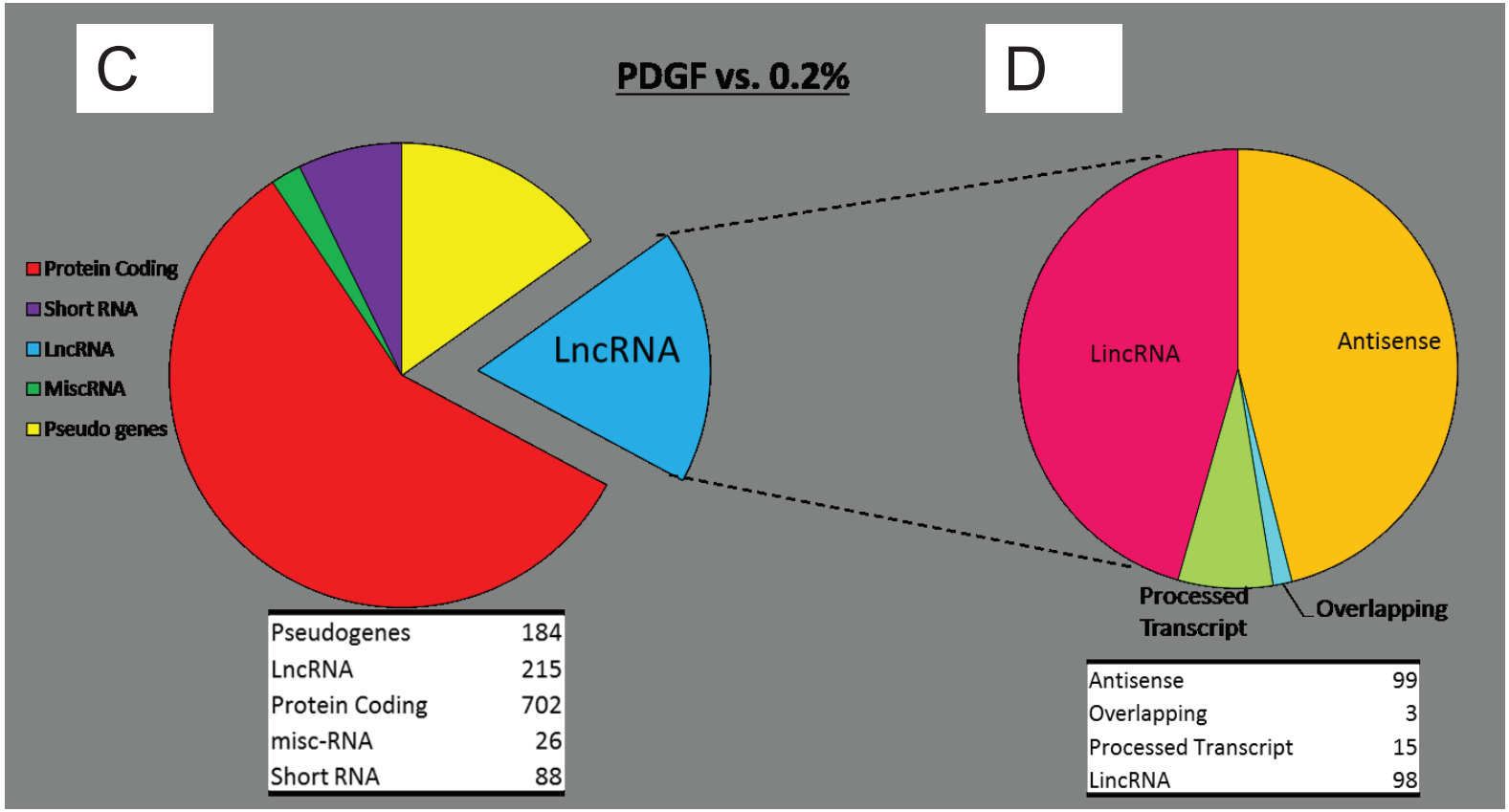
C
PDGF vs. 0.2%
D
Protein Coding
Short RNA
LncRNA
MiscRNA
Pseudo genes
LncRNA
LincRNA
Antisense
Processed Transcript
Overlapping
Pseudogenes 184
LncRNA 215
Protein Coding 702
misc-RNA 26
Short RNA 88
Antisense 99
Overlapping 3
Processed Transcript 15
LincRNA 98

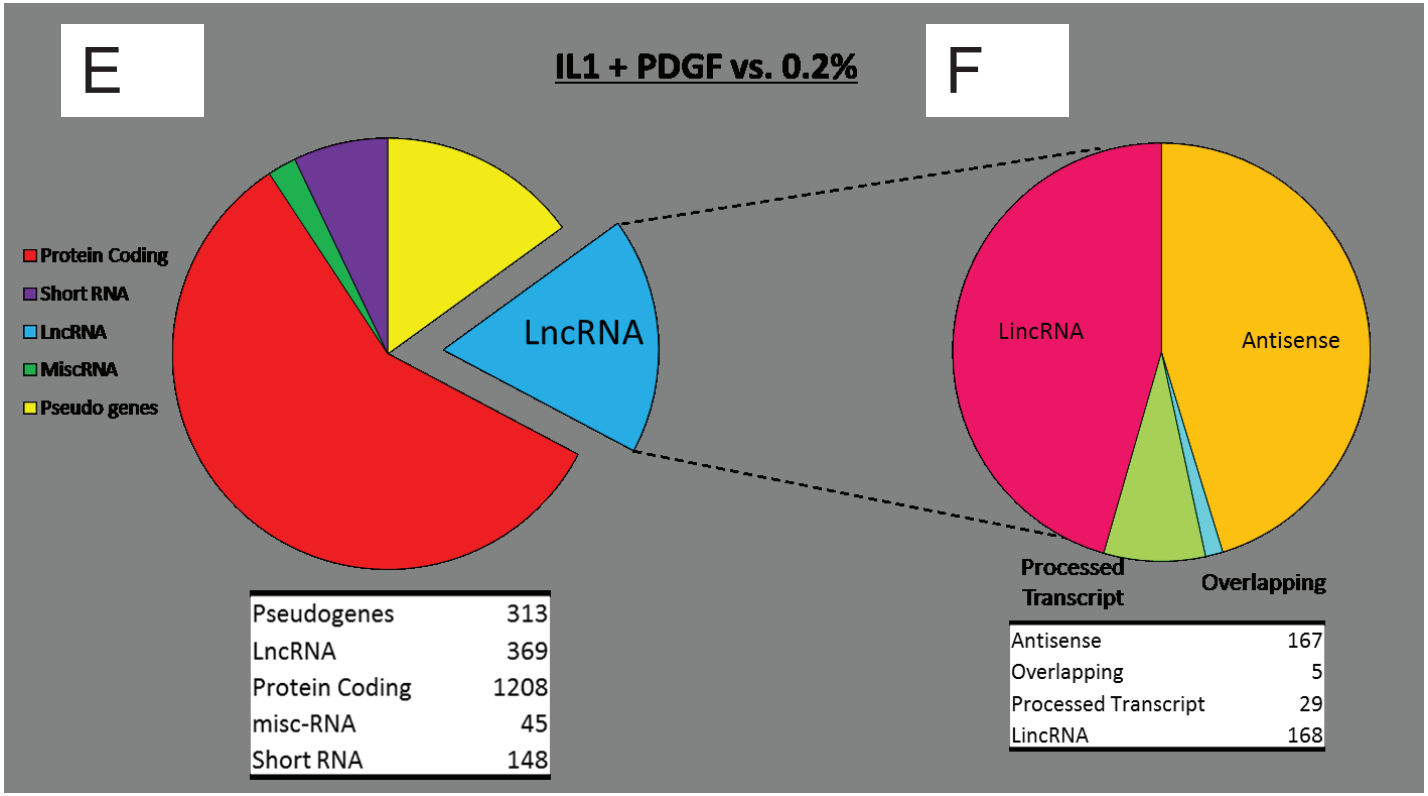

Figure 3-13: Identification of differentially expressed LncRNAs in HSVSMC treated with IL1α and PDGF.
HSVSMC were quiesced in 0.2 % media for 48 h and then stimulated with 0.2 % (control), IL1α, PDGF or a combination of IL1α and PDGF for 72 h. RNA was extracted and subjected to RNA-seq analysis. **(A):** Transcripts differentially expressed between 0.2 % and IL1 treatment ($p<0.01$), pie chart indicates the relative percentage, and tables present numbers, of each biotype differentially expressed. **(B):** LncRNAs differentially expressed between 0.2 % vs IL1α can be subdivided based on lncRNA biotype. Groups include intervening lncRNA (lincRNA), antisense, overlapping and processed transcripts. Graphs indicate absolute number identified (n=4 patients). **(C):** Transcripts differentiall expressed between 0.2% control and PDGF treatment ($P<0.01$). **(D):** LncRNA subtypes differentially regulated between 0.2% and PDGF treatment. **(E):** Transcripts differentially regulated between 0.2% control and IL1 and PDGF treatment ($P<0.01$). **(F):** LncRNA subtypes differentially regulated between 0.2% control and dual IL1 and PDGF treatment.

Due to being the two largest groups of lncRNA, intergenic and antisense lncRNAs were focussed on. To identify possible synergistic lncRNAs, the candidates (control vs IL1α and PDGF, FDR<0.01, LogFC<2, FPKM>1) were ranked according to their FPKM and level of up/down-regulation (Figure 3-14, See Appendix Figure 1 for heat map containing all conditions and Table 1, 2 and 3 for all RNA differentially expressed with a FDR<0.01 and LogFC >2 in IL1α, PDGF and IL1α + PDGF vs. 0.2 % conditions). A subset of the most differentially expressed transcripts included RP11-91k9.1, RP11-94a24.1, RP11-761I4.4, RP11-709B3.2, RP11-760H22.2 and AC018647.3 and are highlighted via a star (*) in the heat maps in Figure 3-14 (FPKM values of candidate lncRNA from RNA-seq are indicated in Appendix Table 4). The location of each lncRNA visualised on the UCSC genome browser is shown in Panel A of Figures 3-15 to 3-20. It has been shown that lncRNA are dysregulated in clusters around protein coding genes, possibly highlighting that these lncRNA/ mRNA pairs are under the same promoter control. As such, the expression of the most proximal protein coding genes to each lncRNA were determined from the RNA-seq results. The expression pattern, genomic loci and expression of proximal protein coding genes for lncRNAs RP11-91k9.1, RP11-94a24.1, RP11-761I4.4, RP11-709B3.2, RP11-760H22.2 and AC018647.3 are described in detail below.

RP11-94a24.1, illustrated in Figure 3-15, was up-regulated by both IL1α and PDGF alone and in combination with a 9, 21 and 42 fold change respectively. RP11-94a24.1 is located on chromosome 8 on the antisense strand, 775 kbp away from the HAS2 gene and 350 kbp away from ZHX2 located on the sense strand. Interestingly HAS2 mRNA was regulated in the same manner as RP11-94a24.1 and exhibited a 12, 42 and 84 fold change respectively following IL1α, PDGF or dual treatment. ZHX2, located on the opposite strand was not regulated in the same manner with cytokine and growth factor treatment.

LncRNA RP11-709B3.2, illustrated in Figure 3-16, was downregulated 2.8, 2.5 and 5 fold following IL1α, PDGF and dual treatment. RP11-709B3.2 is located on chromosome 15 on the antisense strand, 3 kbp away from Fem1b and 1 kbp away from ITGA11, both located on the sense strand. IL1α, PDGF or dual stimulation did not alter Fem1b expression, but resulted in a 2, 2 and 2.8 fold decrease in ITGA11 expression, a similar pattern to that observed with RP11-709B3.2.

RP11-761I4.4, illustrated in Figure 3-17, is located on chromosome 15 and is positioned antisense to IL-16, overlapping one exon of this gene. IL1α, PDGF and dual stimulation evoked identical changes in the expression of RP11-761I4.4 and IL-16 resulting in a 4, 5 and 5 fold decrease respectfully.

LncRNA RP11-760H22.2, illustrated in Figure 3-18, is found on the sense strand of chromosome 8. It lies in close proximity to the adjacent genes; deptor, located 1 kbp upstream and col14a1 which lies 3 kbp downstream of this lncRNA. An identical change in expression of deptor was observed following IL1α, PDGF and dual stimulation, while col14a1 was only responsive to IL1α treatment. IL1α, PDGF and dual stimulation evoked a 4.1, 4 and 11 fold decrease in deptor expression compared to a 3.6 and 4.2 fold decrease in col14a1 following IL1α and dual stimulation.

RP11-91K9.1, illustrated in Figure 3-19, was also up-regulated in the RNA-seq data set by both IL1α and IL1α in combination with PDGF. IL1α alone induced a 54 increase in this lncRNA and a significant, but lower level of expression was observed via dual stimulation (33 fold up-regulation). RP11-91K9.1 is located 50knp upstream if the lncRNA LINC00578 and 300kbp away from TBL1XR1 on the antisense strand. RP11-91K9.1pattern of expression was unique and not mimicked by the surrounding genes.

LncRNA AC018647.3, illustrated in Figure3-20, is found on chromosome 7, 200 kbp upstream of SEPT7 and 20 kbp away from HERPUD2 on the antisense strand. IL1α, PDGF and dual stimulation all led to greater than 100 fold decrease in the expression of this lncRNA, an effect that was not mimicked by the adjacent genes.

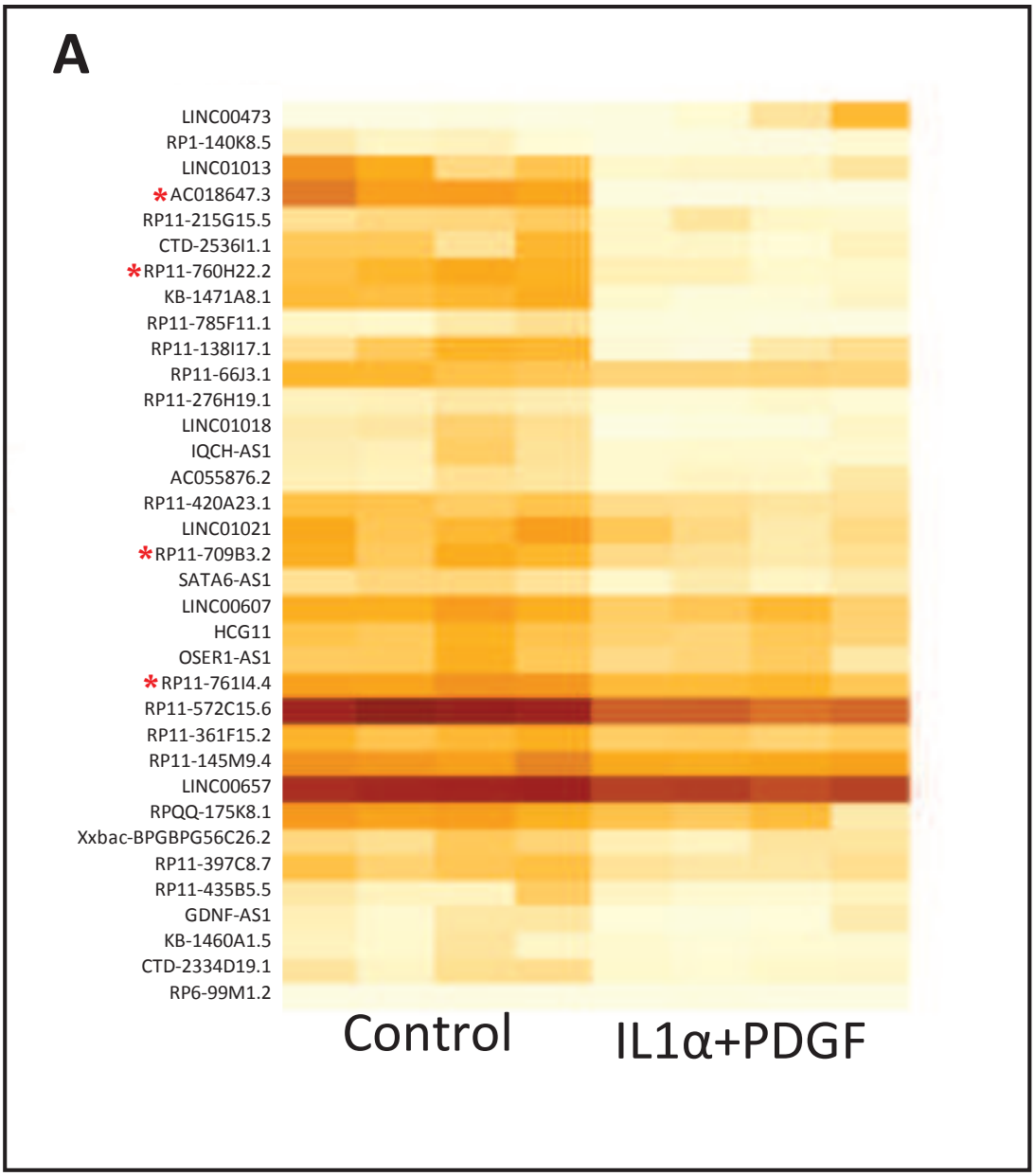
A
LINC00473
RP1-140K8.5
LINC01013
*AC018647.3
RP11-215G15.5
CTD-2536I1.1
*RP11-760H22.2
KB-1471A8.1
RP11-785F11.1
RP11-138I17.1
RP11-66J3.1
RP11-276H19.1
LINC01018
IQCH-AS1
AC055876.2
RP11-420A23.1
LINC01021
*RP11-709B3.2
SATA6-AS1
LINC00607
HCG11
OSER1-AS1
*RP11-761I4.4
RP11-572C15.6
RP11-361F15.2
RP11-145M9.4
LINC00657
RPQQ-175K8.1
Xxbac-BPGBPG56C26.2
RP11-397C8.7
RP11-435B5.5
GDNF-AS1
KB-1460A1.5
CTD-2334D19.1
RP6-99M1.2
Control
IL1α+PDGF

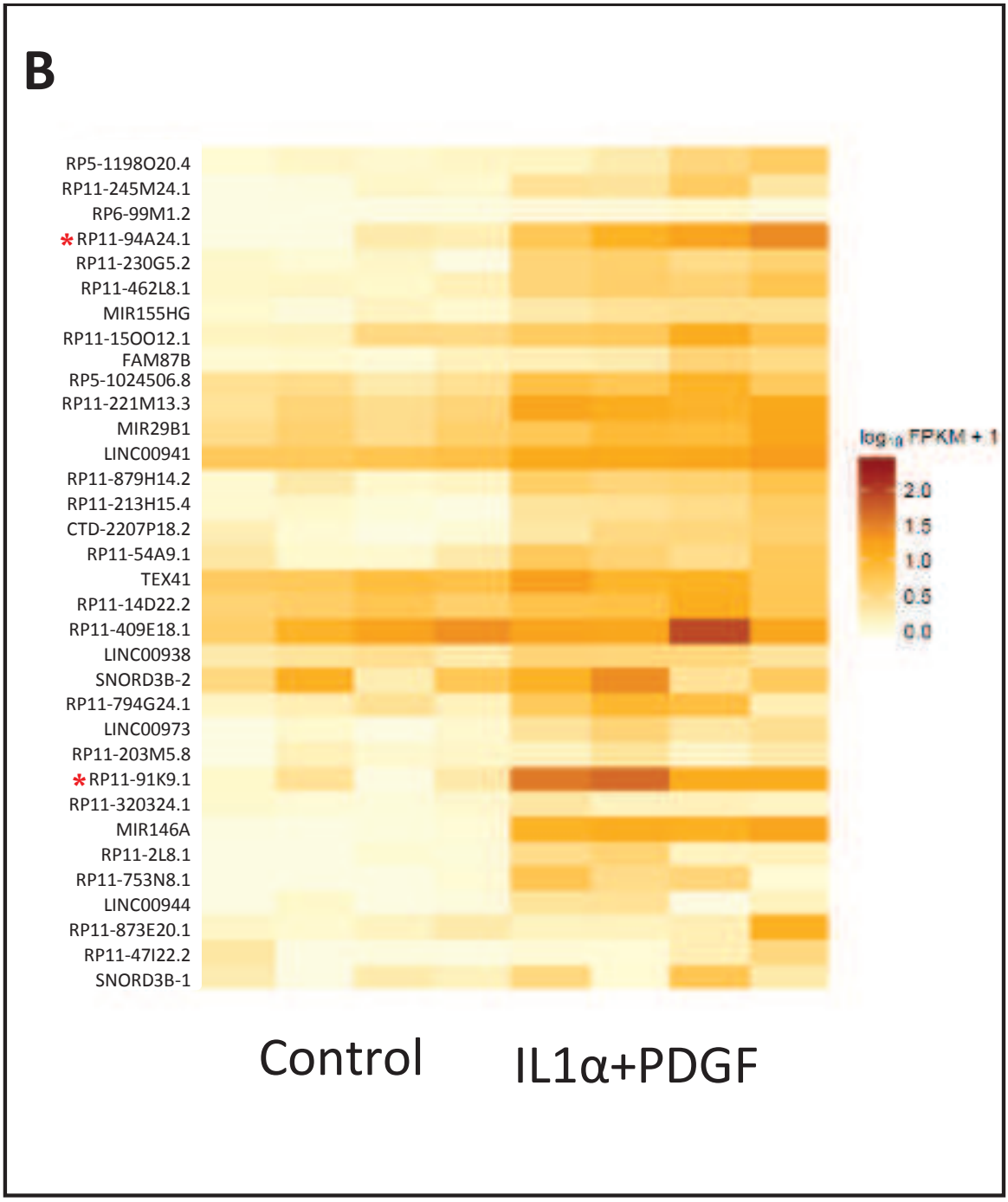

Figure 3-14: Heat map of differentially expressed lncRNA 0.2 % FCS vs IL1α and PDGF treatment.
HSVSMC were quiesced in 0.2 % media for 48 h and then stimulated with 0.2 % (control), IL1α, PDGF or a combination of IL1α and PDGF for 72 h. RNA was extracted and subjected to RNA-seq analysis. Heatmaps showing order of differentially expressed transcripts within the 4 patient samples before and after IL1α/PDGF treatment. **(A):** Downregulated lncRNAs **(B):** Upregulated lncRNAs (n=4 patients).

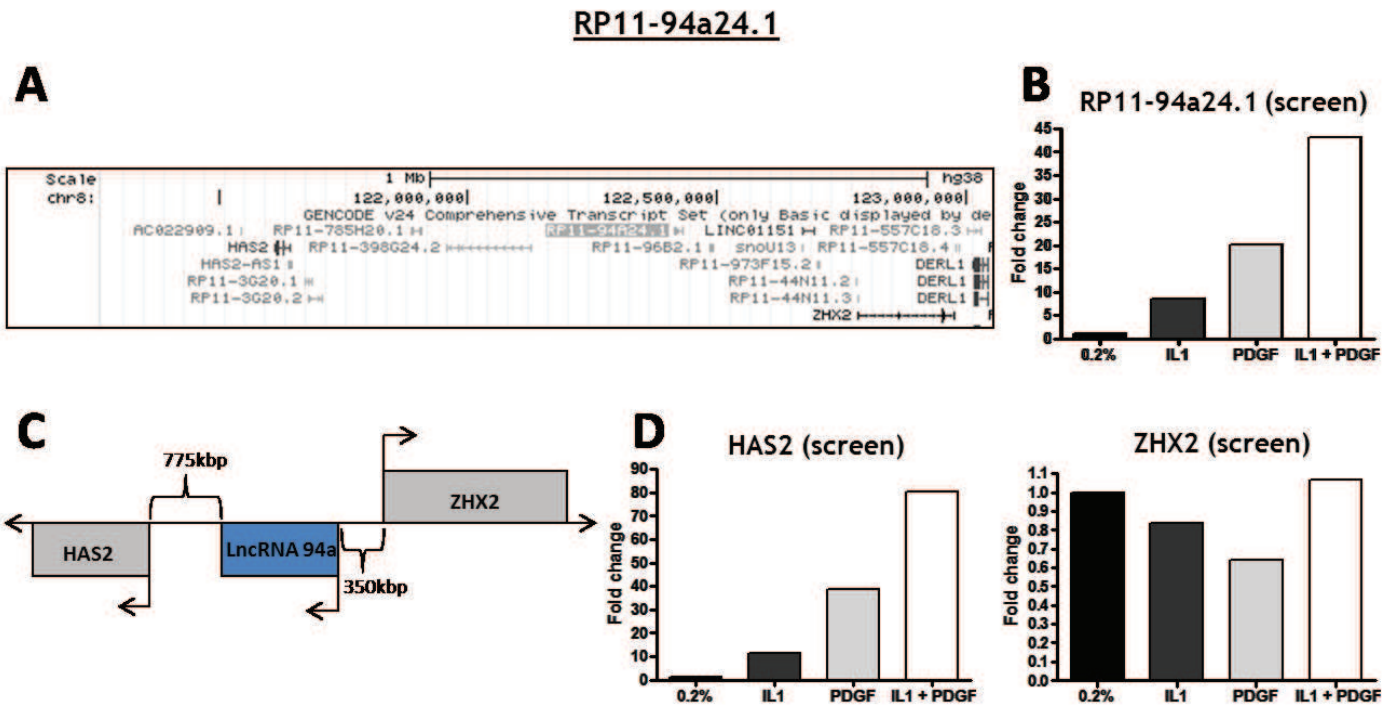

Figure 3-15: Treatment with IL1α and PDGF significantly altered LncRNA expression of RP11-94a24.1.
HSVSMC were quiesced for 48 h in 0.2 % media and then stimulated with 0.2 %, IL1α, PDGF or IL1α + PDGF for 72 h and subjected to RNA-sequencing. (A): Overview of genomic location of RP11-94a24.1 on UCSC genome browser. (B): Expression of lncRNA from screen. (C): Location of lncRNA relevant to known protein coding genes. (D): Expression of adjacent genes from screen.

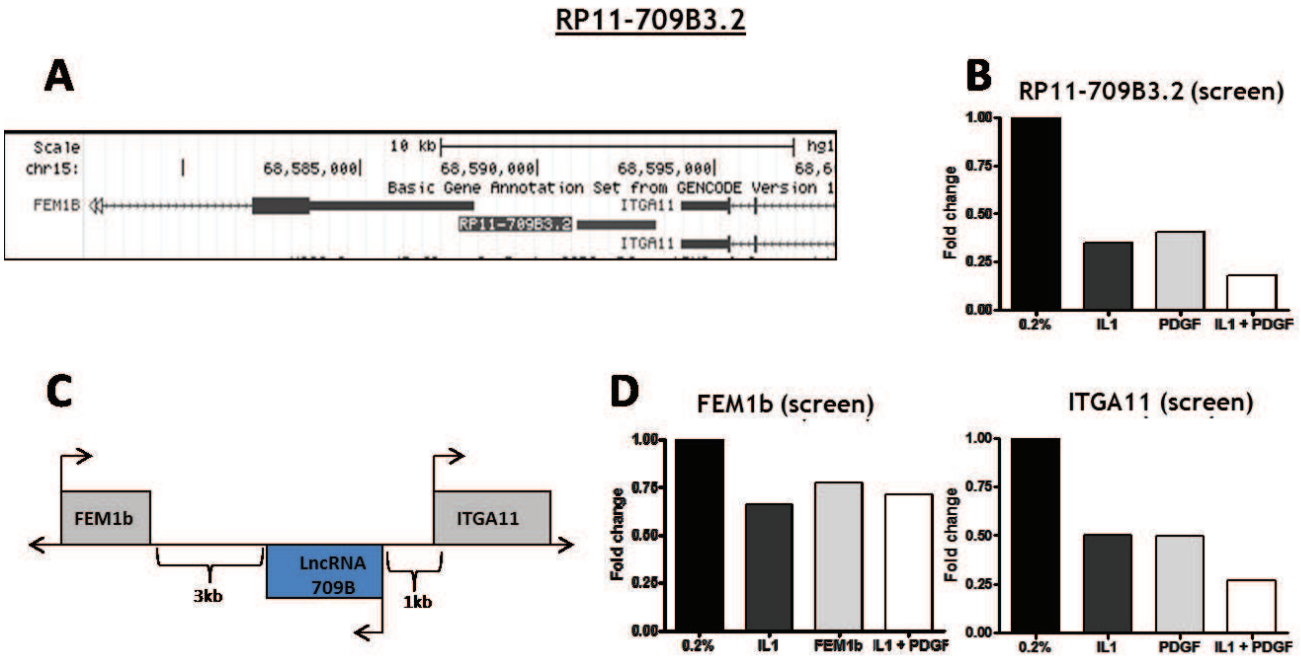

Figure 3-16: Treatment with IL1α and PDGF significantly altered LncRNA expression of RP11-709B3.2.

HSVSMC were quiesced for 48 h in 0.2 % media and then stimulated with 0.2 %, IL1α, PDGF or IL1α + PDGF for 72 h and subjected to RNA-sequencing. (A): Overview of genomic location of RP11-709B3.2 on UCSC genome browser. (B): Expression of lncRNA from screen. (C): Location of lncRNA relevant to known protein coding genes. (D): Expression of adjacent genes from screen.

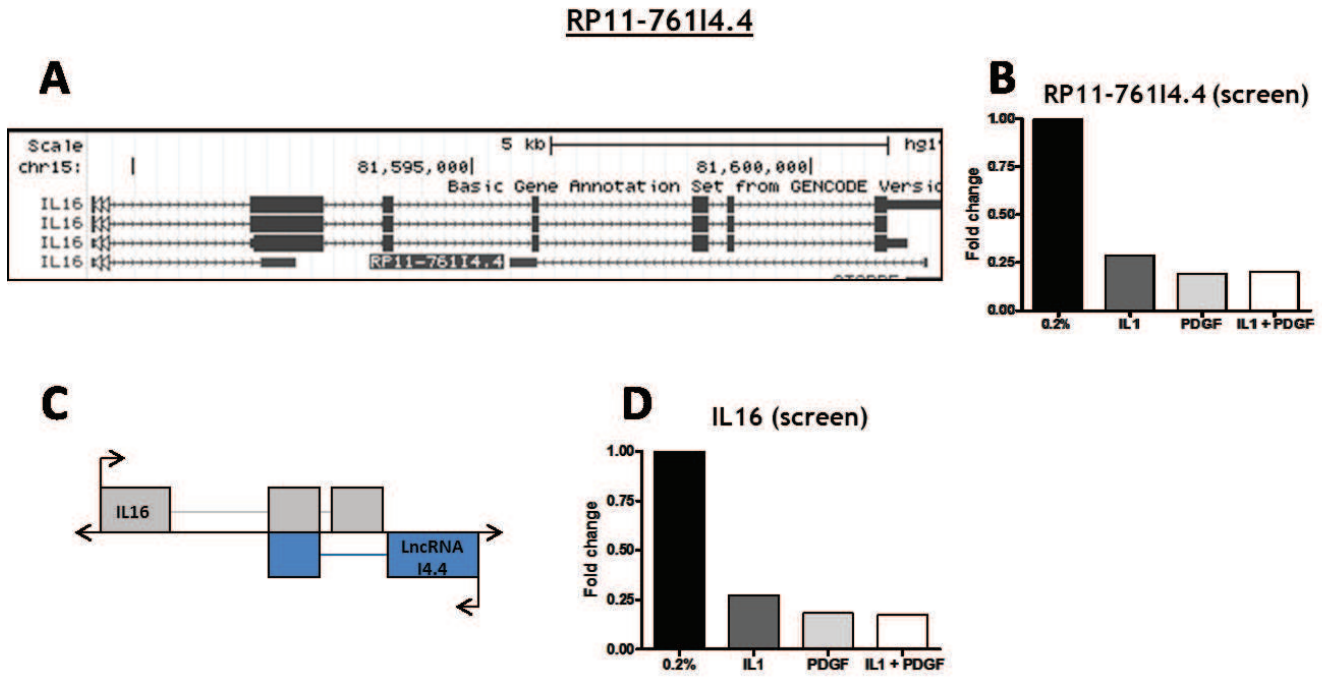

Figure 3-17: Treatment with IL1α and PDGF significantly altered LncRNA expression of RP11-761I4.4.

HSVSMC were quiesced for 48 h in 0.2 % media and then stimulated with 0.2 %, IL1α, PDGF or IL1α + PDGF for 72 h and subjected to RNA-sequencing. (A): Overview of genomic location of RP11-761I4.4 on UCSC genome browser. (B): Expression of lncRNA from screen. (C): Location of lncRNA relevant to known protein coding genes. (D): Expression of adjacent genes from screen.

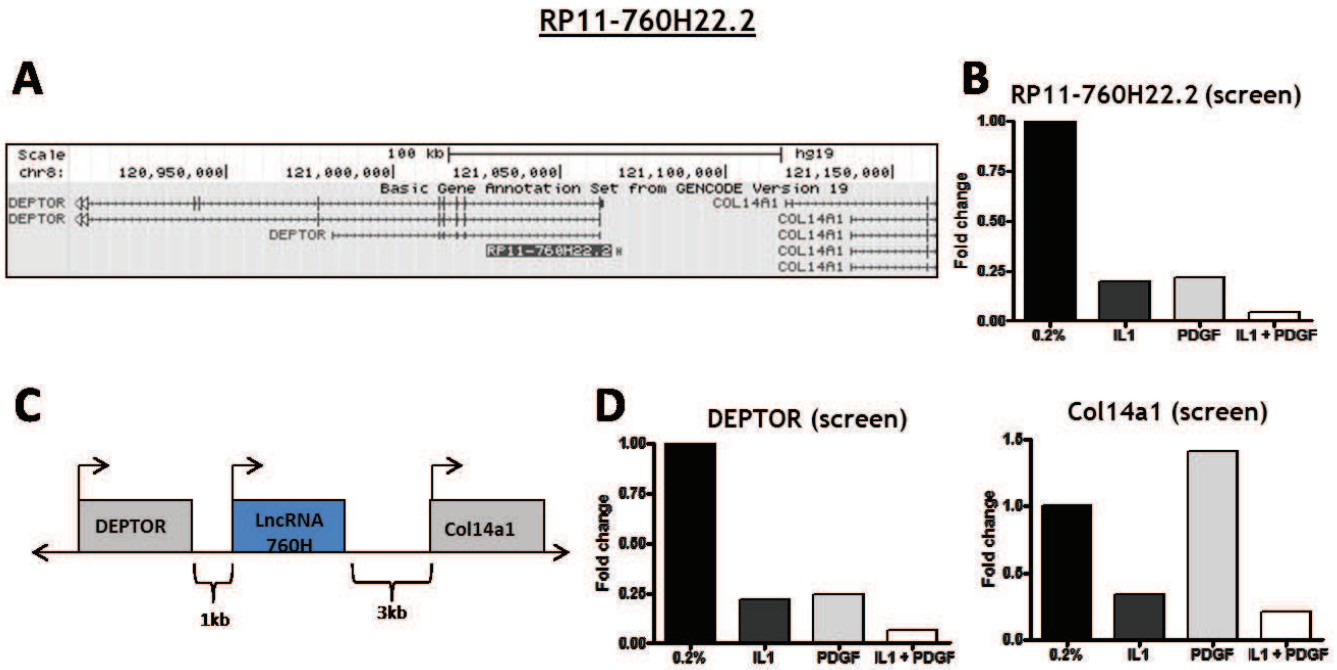

Figure 3-18: Treatment with IL1α and PDGF significantly altered LncRNA expression of RP11-760H22.2.

HSVSMC were quiesced for 48 h in 0.2 % media and then stimulated with 0.2 %, IL1α, PDGF or IL1α + PDGF for 72 h and subjected to RNA-sequencing. (A): Overview of genomic location of RP11-760H22.2 on UCSC genome browser. (B): Expression of lncRNA from screen. (C): Location of lncRNA relevant to known protein coding genes. (D): Expression of adjacent genes from screen.

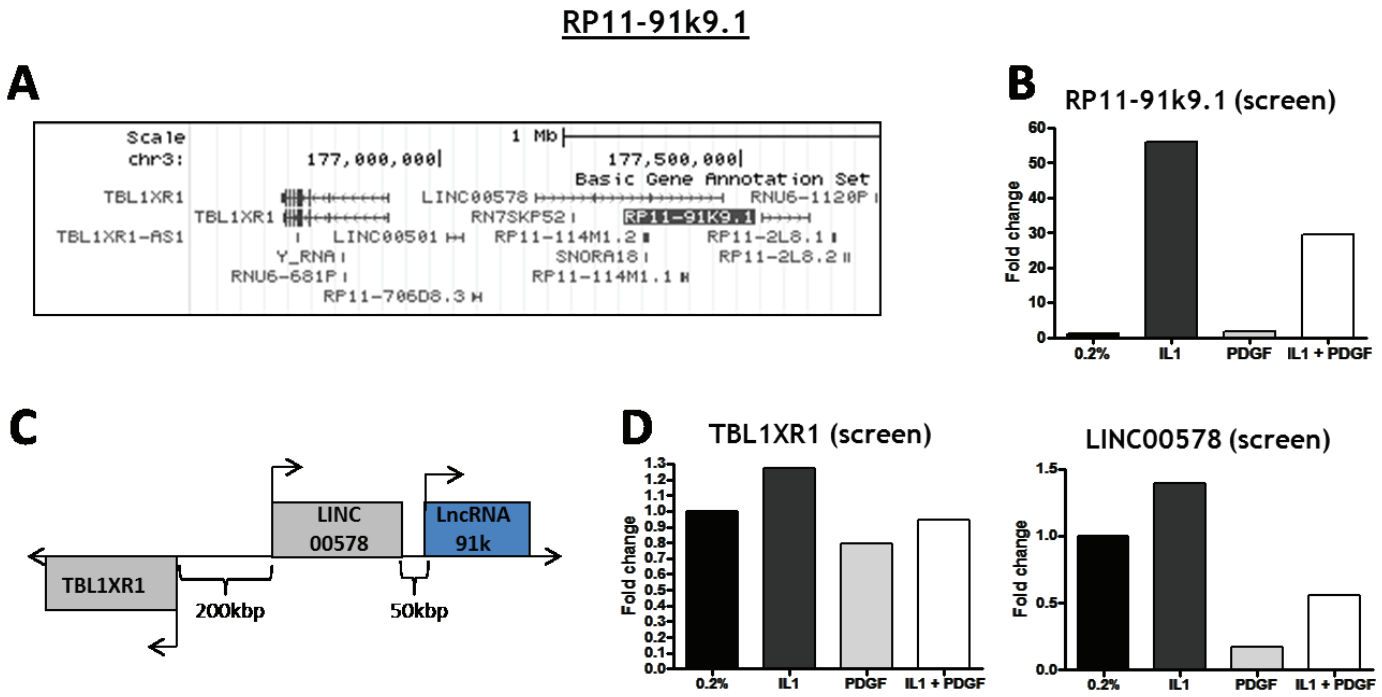

Figure 3-19: Treatment with IL1α and PDGF significantly altered LncRNA expression of RP11-91k9.1.

HSVSMC were quiesced for 48 h in 0.2 % media and then stimulated with 0.2 %, IL1α, PDGF or IL1α + PDGF for 72 h and subjected to RNA-sequencing. (A): Overview of genomic location of RP11-91k9.1 on UCSC genome browser. (B): Expression of lncRNA from screen. (C): Location of lncRNA relevant to known protein coding genes. (D): Expression of adjacent genes from screen.

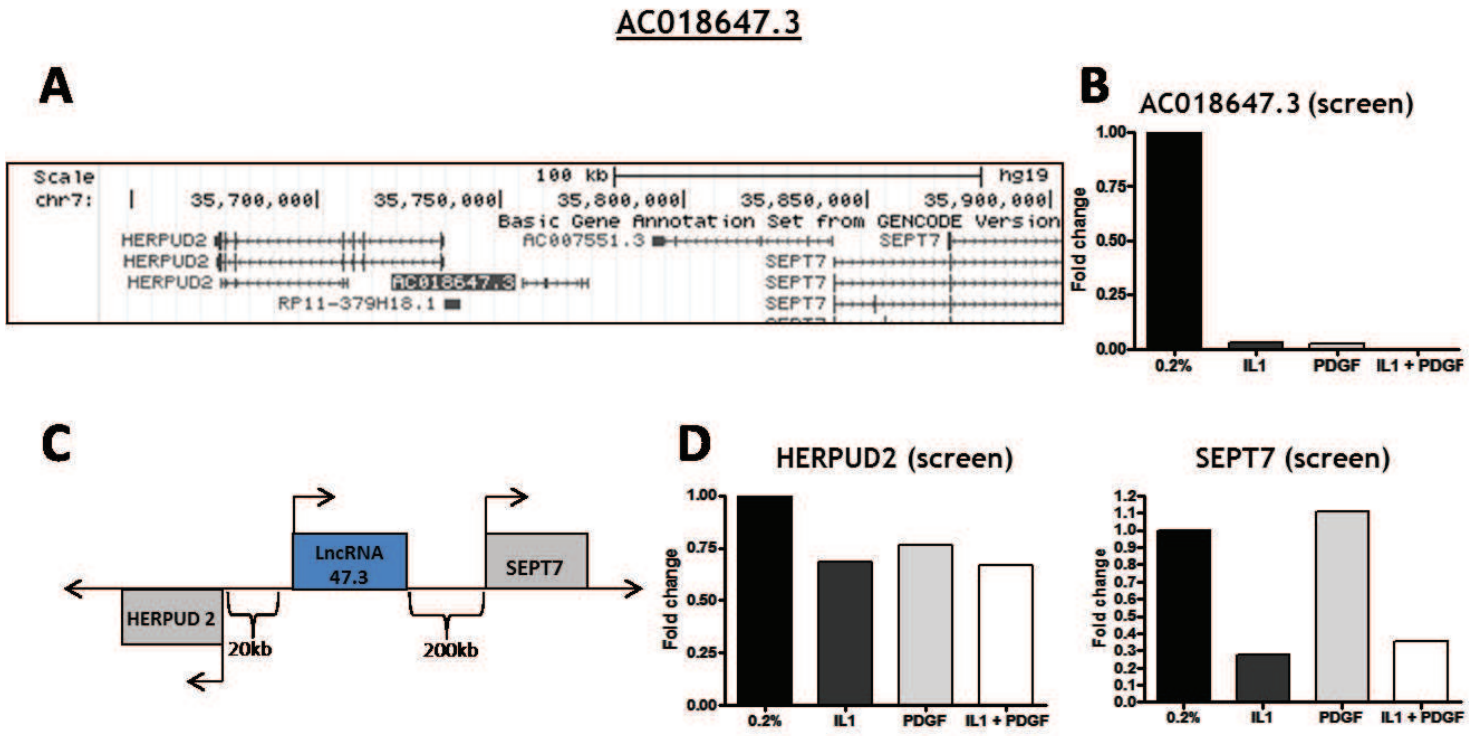

Figure 3-20: Treatment with IL1α and PDGF significantly altered LncRNA expression of AC018647.3.

HSVSMC were quiesced for 48 h in 0.2 % media and then stimulated with 0.2 %, IL1α, PDGF or IL1α + PDGF for 72 h and subjected to RNA-sequencing. (A): Overview of genomic location of AC018647.3 on UCSC genome browser. (B): Expression of lncRNA from screen. (C): Location of lncRNA relevant to known protein coding genes. (D): Expression of adjacent genes from screen.

3.4.3 Validation of lncRNA

Validation of the 6 key lncRNA was performed *in vitro* by reverse transcription PCR (RT-PCR) and quantitative real-time PCR (qPCR) (Figure 3-21), utilising custom designed primers. In accordance with the RNA-seq results RP11-94a24.1 and RP11-91k9.1 were upregulated 35 ± 7.7 and 38.3 ± 10.4 fold respectively following co-stimulation and lncRNAs RP11-709B3.2, RP11-761I4.4, RP11-760H22.2 and AC018647.3 were down regulated 7.03 ± 2.9, 16.6 ± 5.3, 24.8 ± 3.8 and 1130 ± 5 fold, respectively (Figure 3-21A-F respectively). Interestingly, the expression of all lncRNA, except RP11-91k9.1, were altered by both IL1α and PDGF stimulation.

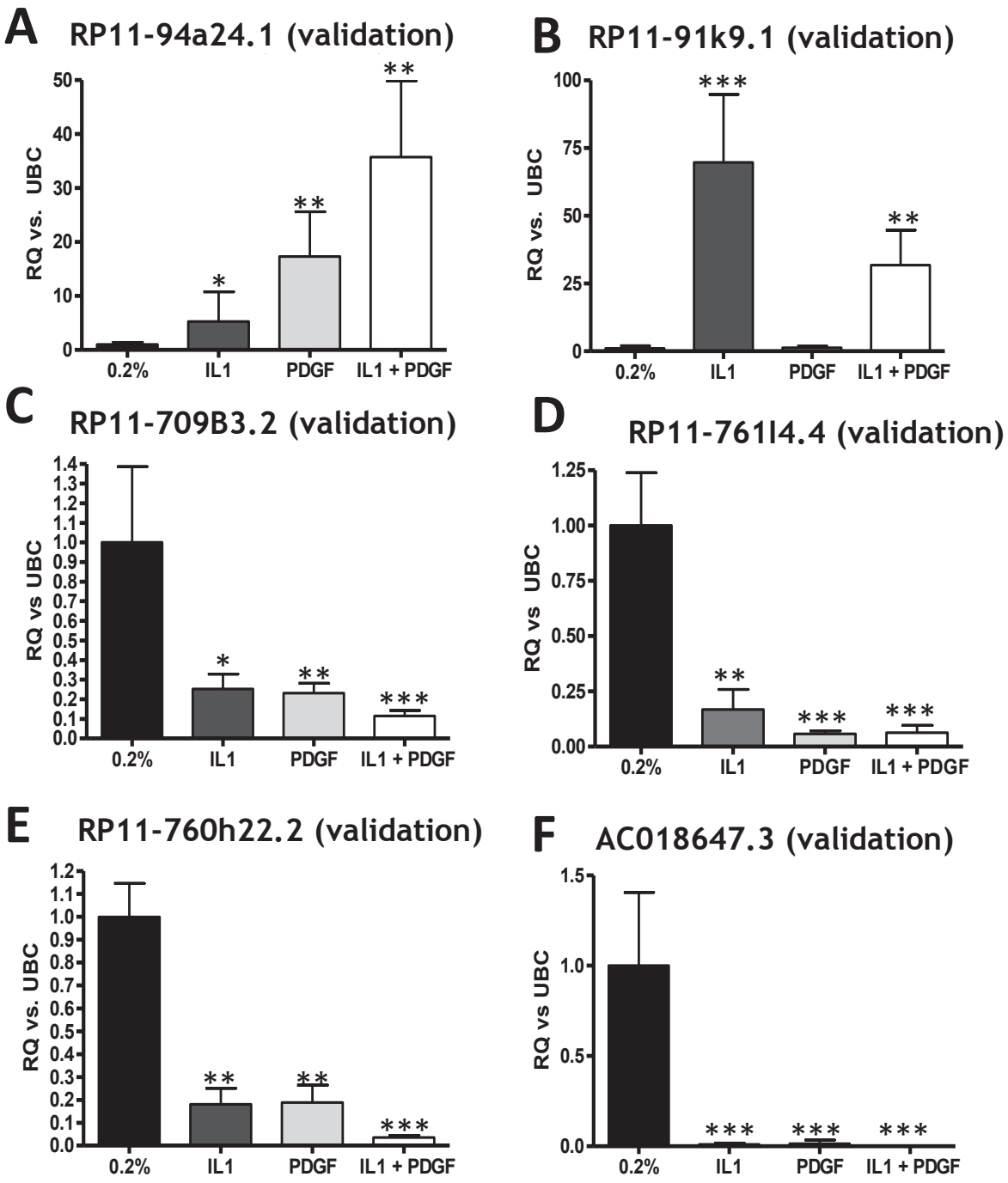

Figure 3-21: Validation of lncRNA from RNA-seq.
HSVSMC were quiesced in 0.2 % media for 48 h and then stimulated with 0.2 % (control), IL1α, PDGF or a combination of IL1α and PDGF for 72 h. RNA was extracted and subjected to RNA-seq analysis. Graphs indicate qRT-PCR analysis of lncRNA expression relative to control (0.2 %) conditions and normalised to UBC housekeeper (n=4 patients). * = P<0.05, ** =P< 0.01 and *** P<0.001 vs. 0.2 % multiple comparisons ANOVA. Graphs indicate lncRNA quantity relative to control samples (Relative Quantity, RQ).

3.4.4 Discussion

Recent advances in RNA-sequencing have demonstrated that previously thought "genome deserts" are in fact pervasively transcribed and are populated by lncRNAs (Marx, 2014). Here, the presented studies focus on the experimental design and QC of the RNA-sequencing experiment and the differential expression landscape of protein coding and non-coding transcripts in HSVSMC under a proliferative state The data demonstrated that dual IL1α and PDGF treatment of HSVSMC had synergistic effects on MMP-3 and MMP-10 expression and that lncRNA, in a similar manner to mRNA, can be dysregulated by the IL1α cytokine and PDGF growth factor. Six of the most differentially expressed lncRNA following IL1α and PDGF treatment were chosen for further analysis. Validation performed by qPCR analysis confirmed the accuracy of the RNA-seq study.

RNA-Seq is a powerful tool for whole-transcriptome analysis. The technology provides unbiased data across the entire transcriptome, enabling a broad range of transcript discovery applications not possible with microarray-based analysis (O'Brien et al., 2012). Utilising paired end-sequencing allowed accurate alignment of reads to the human genome (GRCh37), the 93 % alignment rate met quality standards for the RNA-seq technique (Mortazavi et al., 2008) and ensured that the RNA-seq provided a high quality profile of the HSVSMC transcriptome during quiescent and stimulated conditions. The RNA-seq depth of 70 million reads was sufficient to identify lncRNAs within HSVSMC, however, it should be noted that greater read depths and use of refined capture-seq technique would be beneficial in order to offer greater annotation of specific areas within the genome.

Remarkably, the large majority of the RNA expressed under all conditions resulted from the protein-coding fraction, despite the entire genome consisting of only 2 % protein coding genes. These findings are in agreement with recent attempts to characterise lncRNA expression in other cell types, where 50 % of the transcripts identified were from protein coding genes and 22 % from lncRNA genes (Voellenkle et al., 2016). This is possibly due to the higher levels of expression of protein coding genes and higher percentages of lncRNAs may be obtained with greater read depth and read counts. Additionally, lncRNA annotation of the human genome is not complete and new lncRNA are identified

daily. The lncRNAs identified in this RNA-seq were previously known lncRNA and higher percentages of lncRNA may be identified via further bioinformatic analysis of the data to discover non-annotated transcripts.

The biological relevance of the obtained gene expression profiles was determined via bioinformatic enrichment analysis of functional pathways. IPA pathway analysis positioned cellular movement, inflammatory response and necrosis amongst the most significant pathways differentially regulated between 0.2 % quiescent cells and cells stimulated with IL1α. This is in agreement with previous findings that have demonstrated a role of IL1α in mediating the inflammatory response and inducing cellular migration in cells from various lineages. Additionally IPA analysis revealed proliferation of cells, apoptosis and cellular morphology to be amongst the most enriched pathways following PDGF treatment, all of which are prominent features that have previously been associated with PDGF signalling, thus, this analysis further confirmed the induction of the IL1α and PDGF pathways. Finally, proliferation, migration, apoptosis and cell cycle progression were most highly enriched during co-stimulation with both IL1α and PDGF treatment. The P values for these pathways were lower than that observed with the individual treatments, further highlighting the ability of this cytokine and growth factor to activate common downstream pathways. The pathways identified via IPA are of key importance as they have been proposed to play a role in smooth muscle cell disease and are known to be important in atherosclerosis, neointimal formation and in-stent restenosis. As mentioned previously, both intimal formation, associated with in-stent restenosis and vein graft failure, and atherosclerosis are characterised by platelet aggregation, release of growth factors, inflammatory cell infiltration and smooth muscle cell proliferation and migration. Proliferation of SMCs is paramount in the occlusion of the blood vessel leading to intimal hyperplasmia. As such, this data confirms that pathways activated with dual IL1α and PDGF stimulation are involved in vascular disease progression.

It is worth mentioning that, for comparison between studies, it is crucial to consider the measurement technique and the annotation used for lncRNA identification. Indeed, criteria for naming, categorising and validating lncRNAs are not well defined yet. Several databases exist, containing very different

numbers of lncRNA genes. However, the identification that approximately 40-45 % of the lncRNA identified are intergenic and approximately 40 % are antisense is consistent with previous findings suggesting that intergenic and antisense lncRNA constitute the largest classes of lncRNAs identified during RNA-seq analysis (Gaiti et al., 2015), (Huang et al., 2016).

Although the pathways involved in VSMC proliferation are relatively well defined, very little is known as to the role of lncRNAs in vascular smooth muscle cells and particularly during proliferation and migration. What is known is that a few lncRNA can control key aspects of SMC physiology. For example, work performed by Leung et al., identified lncRNA via de novo assembly of transcripts from RNA-sequencing experiments in Ang II treated VSMCs. One lncRNA identified via this method, Lnc-Ang362, was shown to function as a host transcript for miR-221 and miR-222, two miRNAs that function in cell proliferation. Indeed, loss of Lnc-Ang362 resulted in a reduction in the expression of these two miRNAs and a decrease in proliferation of VSMCs, thus demonstrating a functional role for this lncRNAs in VSMC and Angiotensin II action (Leung et al., 2013). Additionally, lncRNA *SENCR* was identified via *de novo* assembly of transcripts following RNA-seq in human coronary artery smooth muscle cells (HCASMC). *SENCR* has been described to stabilise the differentiated state of human vascular smooth muscle cells and is transcribed antisense from the first intron of the Friend Leukemia Integration virus 1 (FLI1) gene (Bell et al., 2014). The exact mechanism by which *SENCR* promotes SMC contraction still remains unknown, however, new vascular lncRNAs are being revealed at a steady rate and new techniques are being developed to aid in the discovery of the molecular mechanisms governing lncRNA function.

Applying a stringent significance threshold, RNA-sequencing identified 309 known lncRNAs that were upregulated by co-stimulation with IL1α and PDGF. Bioinformatic analysis of the RNA-seq only utilised the genome alignment method to determine lncRNA of interest. Further bioinformatic analysis could be employed to identify *de novo* transcripts that have not yet been identified in the human genome. Bioinformatic analysis is improving daily and it is hoped that analysis of both lncRNA and mRNA partners may be utilised to identify lncRNA functional networks.

It has been previously determined that lncRNAs expression may be correlated with that of nearby mRNAs. Four of the six validated lncRNAs were associated with significantly differentially expressed mRNAs. These mRNAs were involved in SMC physiological processes. LncRNA RP11-94a24.1 was shown to be expressed in a similar manner to HAS2, hyaluronan synthase 2. HAS2 is an enzyme that synthesises hyaluronan (HA). HAS2 is the main isoform found within SMC and HA is constituent of ECM that has been shown to regulate SMC proliferation(van den Boom et al., 2006). ITGA11, integrin subunit alpha 11, is an alpha integrin protein. Although results from smooth muscle cells are lacking, it has been shown that ITGA11 is overexpressed by tumour stroma of head and neck squamous cell carcinoma and correlates positively with alpha smooth muscle actin expression. Increased alpha smooth muscle actin expression is associated with a reduction in vascular smooth muscle cell proliferation and as such, alterations in ITGA11 and the associated lncRNA RP11-709B3.2 may therefore control key aspects of SMC proliferation (Parajuli et al., 2016). DEPTOR, DEP Domain Containing MTOR-Interacting Protein, is a negative regulator of the mTORC1 and mTORC2 signalling pathways. DEPTOR has been shown to play a role in down regulation of the p53 pathway and promotion of PI3K/AKT signalling (Feng et al., 2005). Interestingly, it has been shown that p53 signalling is implicated in VSMC apoptosis and involved in abdominal aortic aneurysm formation (Leeper et al., 2013). Additionally, it is known that apoptosis of VSMCs occurs in human atherosclerotic plaques and that VSMC apoptosis may promote plaque rupture and subsequent myocardial infarction. Consistent with this, human plaque VSMCs exposure to p53 overexpression induced apoptosis. This effect was not observed with healthy aortic SMCs, suggesting that SMCs from human plaques have an increased sensitivity to p53-mediated apoptosis compared with normal VSMCs (Bennett et al., 1997). Consistently, up-regulation of the PI3K/AKT pathway in VSMCs is associated with proliferation and cellular survival, key events involved in vascular repair and vascular disease (Suwanabol et al., 2012, Liu et al., 2010a). Interleukin 16 (IL1α6), has been shown to play a role in SMC induced migration and proliferation through the p38 MAPK pathway (Park et al., 2015). Taken together these data indicate that cytokine stimulation of HSVSMC proliferation is associated with genome-wide changes in lncRNA expression. The 6 identified candidate lncRNA show significant dysregulation following cytokine stimulation of HSVSMC and the co-regulated protein coding

genes associated with the lncRNAs have previously been shown to modulate VSMC proliferation, VSMC survival, inflammatory response and extracellular matrix production, key events that control vascular disease. However, the mechanisms by which these mRNA are connected to the designated lncRNAs, or if this conveys any functional significance remains unknown. Nevertheless, it has been previously shown that lncRNA may regulate the function of the nearby genes (Vance and Ponting, 2014). In one study, multiple 17B-oestradiol (E2)-induced lncRNA transcripts were found to interact with cohesion, a protein complex that regulates the separation of sister chromatids during cell division. It was found that these lncRNAs could induce looping interactions between their enhancer elements and the promoters of nearby target genes (Li et al., 2013). Additional studies found that lncRNAs, ncRNA-a3 and ncRNA-a7, also promoted looping interactions with the promoters of proximal genes to regulate local gene expression (Lai et al., 2013). Finally, knockdown of a key lncRNA found within the MyoD1 core enhancer region, lead to both a reduction in MyoD1chromatin accessibility and RNA polymerase II (PolII) occupancy (Mousavi et al., 2013). It should be noted that several other lncRNA have been identified that modulate mRNA expression but the mechanism by which they exert this function still remains unknown and cannot yet be predicted from lncRNA sequence alone.

In conclusion, next-generation sequencing approach was used to identify protein-coding and long non-coding RNAs modulated in HSVSMCs during quiescent and stimulated conditions. Further descriptive characterisation and mechanistic studies are required to identify the impact of these lncRNAs on VSMC physiology and function.

Chapter 4 Identifying the function and mechanism of lncRNA *SMILR*

4.1 Introduction

It is apparent that many lncRNAs are becoming known to be key regulators of transcription and translation and therefore have a fundamental role in cell function (Mercer et al., 2009). Identification of lncRNA function has led to intense focus on elucidating the molecular mechanisms that underlie this function. Although the vast majority of lncRNAs described in the literature have not yet been studied in mechanistic detail, the few that have provide clues regarding how lncRNAs might carry out their biological roles. Interestingly lncRNAs, unlike mRNAs, are found in several sections of the cell and have been shown to have varying functions and mechanisms of action depending on the cellular compartment in which they are located.

4.1.1 Function of cytoplasmic lncRNAs

Substantial proportions of lncRNAs reside within, or are dynamically shuttled to, the cytoplasm (Rashid et al., 2016). The mechanism by which lncRNAs are transported out of the nucleus currently remains unknown; however, it has been shown that cytoplasmic lncRNAs regulate mRNA stability, protein translation, microRNA availability and protein modifications (Rashid et al., 2016). Examples of lncRNA harbouring these cytoplasmic functions are detailed below and illustrated in Figure 4-1.

Some of the best characterised cytoplasmic lncRNAs are associated with neurodegenerative diseases. The main pathological change associated with Alzheimer's disease is the aggregation of neuronal amyloid plaques that are derived from the proteolytic processing of the amyloid precursor protein (APP) by the ß-site amyloid precursor protein-cleaving enzyme (BACE1) (Faghihi et al., 2008). Recently Faghihi et al. discovered and characterised an antisense lncRNA, known as BACE1-AS (Modarresi et al., 2011) which was shown to increase BACE1 mRNA stability in cells exposed to cellular stress (Faghihi et al., 2008) (Figure 4-1A). BACE1-AS acts by masking the binding site for miR-485-5p on the 6th exon of BACE1, thereby perturbing the BACE1-miR-485-5p interaction and attenuating

miR-485-5p-mediated repression of BACE1 gene expression(Faghihi et al., 2010). I*n vivo* knockdown of BACE1-AS by the continuous infusion of siRNAs directly into the brain resulted in a significant decrease in BACE1 and a reduction in amyloid plaque formation, underlining the therapeutic potential of targeting BACE1-AS for the treatment of Alzheimer's disease(Faghihi et al., 2008).

LincRNA-p21 was originally discovered in mice, where it is expressed as a transcript of ~3 kb from a genomic locus located proximal to the gene encoding the cell-cycle regulator p21/Cdkn1a. It was demonstrated that under conditions of stress, p53 activates transcription of lincRNA-p21 which has been shown to accumulate in the nucleus and regulates the transcription of key genes through the association with the heterogeneous nuclear ribonucleoprotein K (hnRNP-K) (Huarte et al., 2010), (Dimitrova et al., 2014). This observation was assessed in two separate carcinoma cell lines: bone osteocarcinoma cells (U-2OS) and colon colorectal carcinoma cells (HCT-116). However, it has since been identified that linc-p21 is more abundant in the cytoplasm than the nucleus and is known to co-distribute with ribosomes, where it has been shown to negatively regulate the translation of JUNB transcripts by imperfect base pairing with the JUNB mRNA at 8 different sites (Figure 4-1, B) (Yoon et al., 2013). This interaction was quantified by affinity pull-down using biotin-labelled antisense lincRNA-p21 oligonucleotides. The formation of the linc-p21-JUNB complex enhances the interaction between JUNB mRNA and the translational repressor RCK, resulting in reduced JUNB translation (Chu and Rana, 2006). Since lincRNA-p21 is a p53-induced lncRNA, the reduced translation of JUNB via lincRNA-p21 is consistent with the tumour suppressive role of p53 (Tang et al., 2015).

Unlike miRNA, lncRNA are not confined to one single generic mechanism of action. One example of this is linc-MD1, a muscle and cytoplasmic specific lncRNA with two distinct mechanisms of action for controlling physiology (Figure 4-1, C). Linc-MD1 was the first lncRNA to be shown to play a relevant role in muscle differentiation by regulating specific myogenic factors required for the onset of late muscle gene transcription. Linc-MD1 is processed to produce two different microRNAs, miR-206, in one intron, and miR-133b, in one exon (Liu et al., 2012), and also contains binding sites for miR-135 and miR-133b (Figure 4-1D) (Ballantyne et al., 2016). Linc-MD1 is activated during the early phases of muscle

differentiation and functions as a trigger inducing the later stages of differentiation via its sponge activity for miR-133 and miR-135. By this mode of action linc-MD1 affects the distribution and availability of these microRNA thus altering the levels of the natural targets for these micoRNA, initiating an additional level of posttranscriptional control. Of the sponged microRNAs, miRNA-135 targets MEF2C and miR-133b targets MAML1, two known transcripts that regulate myoblast differentiation (Leung et al., 2016),(Neguembor et al., 2014). Consistent with this function, inhibition of linc-MD1 compromises muscle differentiation, as assayed by reduced expression of myogenic markers. Interestingly, reduced levels of linc-MD1 RNA have been found in patients with Duchenne Muscular Dystrophy and rescuing levels via ectopic expression partially restored normal myogenesis (Erriquez et al., 2013).

Finally, lncRNAs may alter protein modifications (Figure 4-1, E). Nuclear factor-κB (NF-κB) is a family of transcription factors that play critical roles in inflammation, immunity, cell proliferation, differentiation and survival (Gilmore, 2006). Over-activation of the NF-κB pathway has been linked to tumourigenesis and metastasis, by inhibiting apoptosis and increasing invasion (Yan et al., 2010), (Niesporek et al., 2007). Liu et al. recently identified a cytoplasmic lncRNA known as NF-κB interacting lncRNA (NKILA), which inhibits NF-κB by binding directly to the NF-κB inhibitor, IκB, and blocking IKK-induced IκB phosphorylation (Liu et al., 2015). Abrogation of IKK-mediated IκB phosphorylation leads to the sequestration of NF-κB in the cytoplasm, preventing it from acting as a nuclear transcription factor (Whiteside and Israel, 1997). Mutation of NKILA all failed o bind IKK (Liu et al., 2015). Consistent with its anti-NF-κB role, NKILA increased apoptosis and reduced invasion in a cancer cell line (Liu et al., 2015). Interestingly, the expression of NKILA is also upregulated by NF-κB and appears to act as a negative feedback loop to inhibit over-activation of the NF-κB pathway.

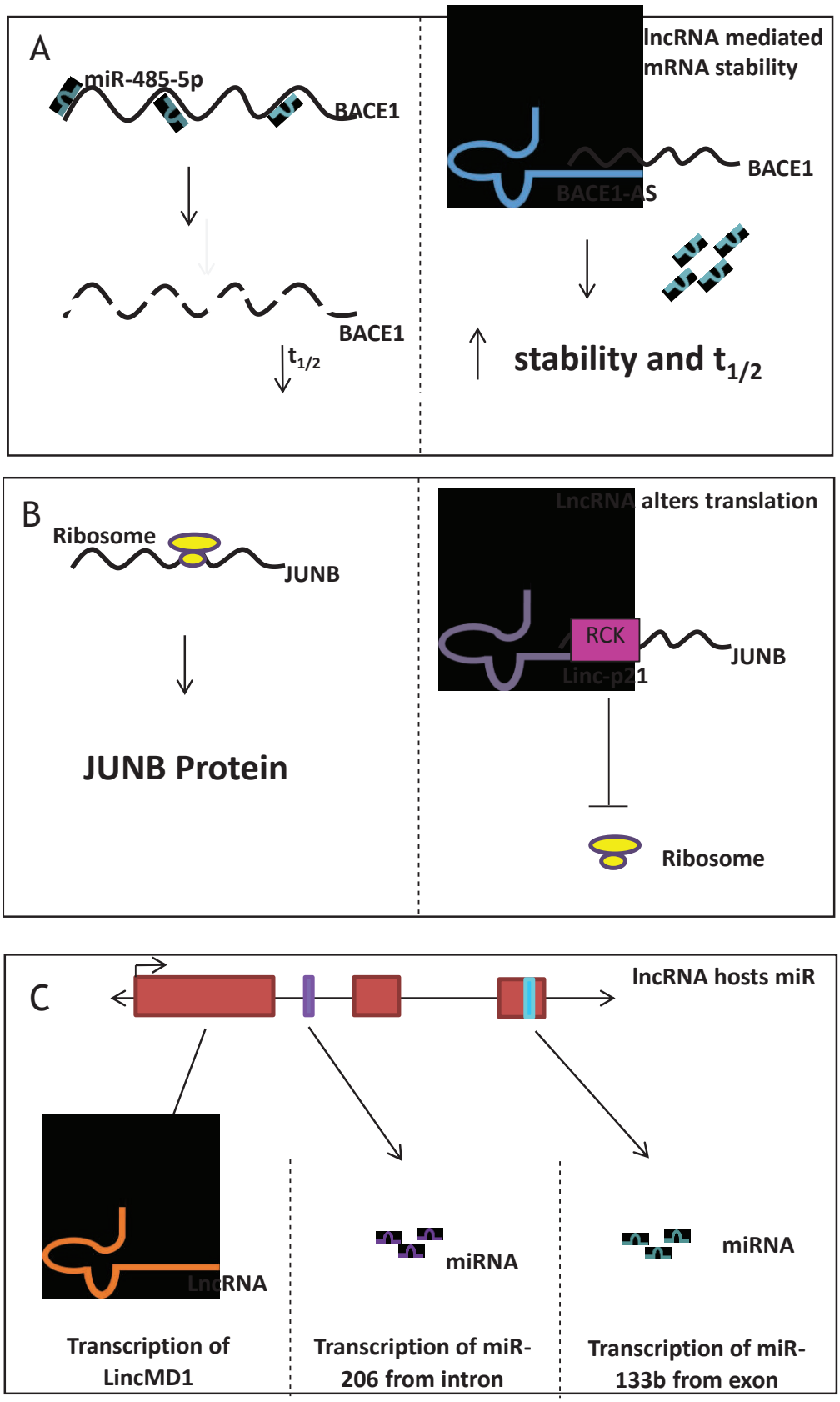
A
miR-485-5p
BACE1
BACE1
t1/2
lncRNA mediated mRNA stability
BACE1
BACE1-AS
stability and t1/2
B
Ribosome
JUNB
JUNB Protein
LncRNA alters translation
RCK
JUNB
Linc-p21
Ribosome
C
lncRNA hosts miR
LncRNA
miRNA
miRNA
Transcription of LincMD1
Transcription of miR-206 from intron
Transcription of miR-133b from exon

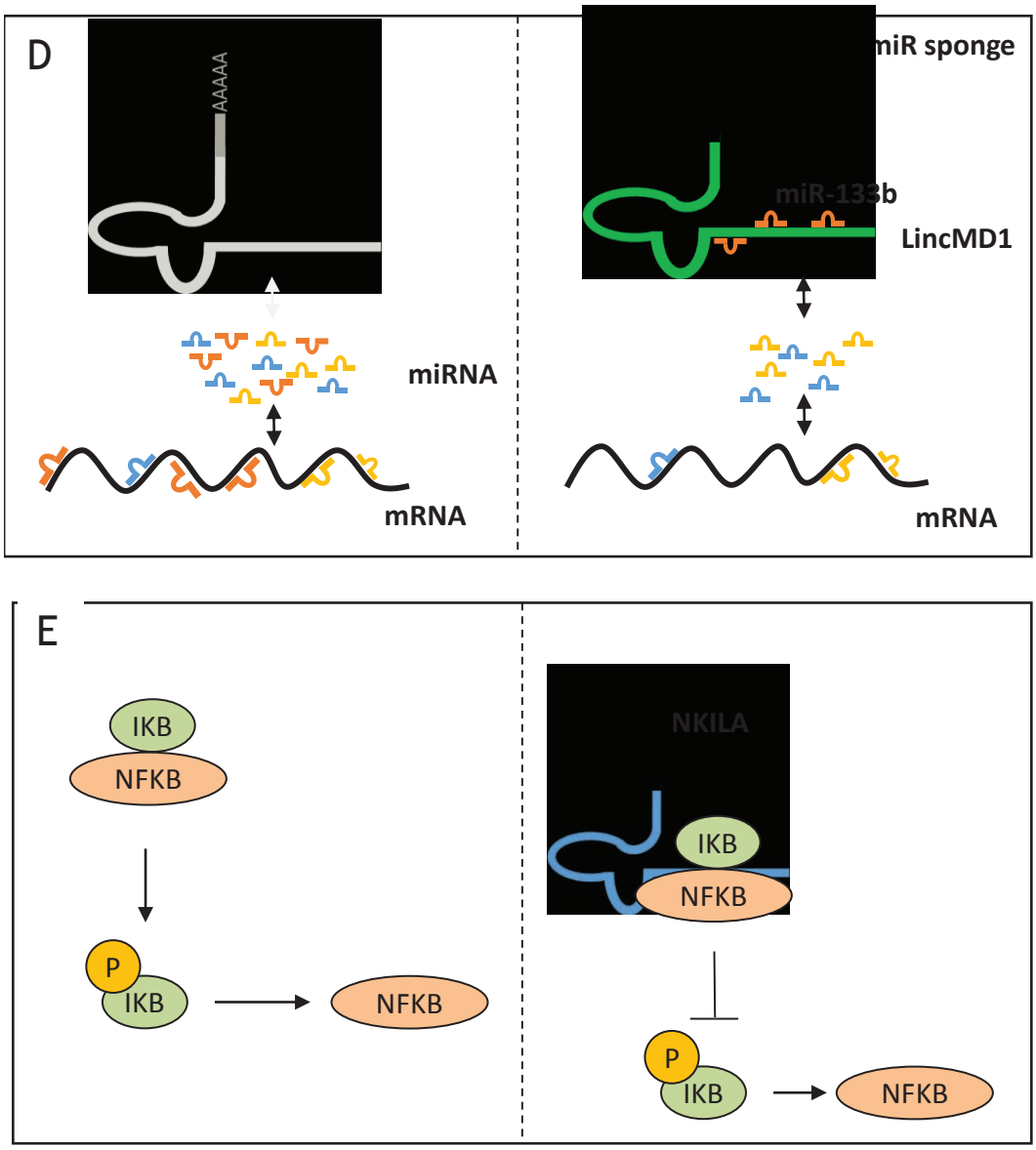

Figure 4-1: Known working models of cytoplasmic lncRNA function.
(A): lncRNAs modify mRNA stability, BACE1-AS lncRNA increases BACE1 stability. (B): LncRNAs regulate mRNA translation, with ***lincRNA-p21*** inhibiting the JUNB translation. (C): LncRNAs can give rise to microRNAs; LincMD1 produces miR-206 and miR-133b from one intron and one exon. (D): LncRNAs may act as microRNA sponges. LincMD1 has multiple functions and can bind miR-133b creating a negative feedback loop. (E): LncRNAs can affect modifications. Binding of lncRNA NKILA inhibits IKB phosphorylation thus inhibiting the activation of NFKB (Rashid et al., 2016).

4.1.2 Function of nuclear lncRNAs

Nuclear lncRNAs, unlike cytoplasmic lncRNAs, typically function as transcriptional regulators that can act locally, near their genomic loci, to regulate the expression of nearby genes, or distally to regulate gene expression across multiple chromosomes (Kornienko et al., 2013). More specifically lncRNAs may act as enhancers to affect the promoters of nearby genes (Derrien and Guigo, 2011), bind chromatin to either initiate or repress gene expression (D et al., 2016) or may directly affect transcription via binding and modulation of transcriptional machinery (Geisler and Coller, 2013).

As a class, lncRNAs are generally enriched in the nucleus and specifically within the chromatin-associated fraction. (Flynn and Chang, 2012) Consistent with their localisation, many lncRNAs have been implicated in the regulation of gene expression and in shaping three dimensional nuclear organisation (Quinodoz and Guttman, 2014). Genome-wide studies of histone modification and enhancer elements has provided an additional layer of complexity to the mammalian genome (Kimura, 2013). ChIP-seq analysis of H3K4me1, H3K27ac, and p300 marks associated with gene activating enhancers showed these regions also produce lncRNA transcripts (Rinn and Chang, 2012). Typically, lncRNA can interact with various chromatin regulatory proteins and recruit them to specific sites on DNA to regulate gene expression (Quinodoz and Guttman, 2014). Evidence for this comes from a recent study that identified that 7 out of the 12 studied lncRNA altered the expression of proximal protein coding genes and that it was the RNA itself, rather than the act of transcription, that produced this effect (Orom et al., 2010).

The mammalian HOXA locus consists of a cluster of 11 HOX genes with a graded expression pattern along body appendages from proximal (close to the main body) to distal (appendage tip) (Gaunt, 2001). Recently, Wang et al. investigated the functions of a lincRNA encoded at the 5′ end of the HOXA cluster, on the antisense strand to the HOXA genes (Wang et al., 2011). This lncRNA, consistent with its genomic position within the HOXA cluster, was expressed in distal fibroblasts such as from the hands and feet and its expression pattern was confirmed in mouse embryos. Owing to these properties, the lncRNA was termed HOXA transcript at the distal tip' (HOTTIP). HOTTIP knock down

experiments in human fibroblasts identified that HOTTIP exhibited enhancer activity on the proximal HOXA genes however, knockdown did not affect expression from the highly homologous HOXD locus, indicating that HOTTIP acts in *cis*, close to its site of transcription. Interestingly, *in vivo* knockdown of HOTTIP in chickens depleted the expression of distal HOXA genes but also resulted in shortened distal forelimb bones (Wang et al., 2011). In an attempt to determine HOTTIP mechanism the authors used chromosome conformation capture carbon copy (5C) in human fibroblasts. This is a high-throughput method that can identify physical chromatin interactions based on the analysis of DNA ligation products (Dostie et al., 2006). This method revealed that actively expressed HOXA regions are characterised by compact chromosome loops. Chromosomal looping of DNA, in an enhancer like manner, brings HOTTIP into spatial proximity with multiple HOXA genes. Additionally, via cellular pulldown methods, it was identified that HOTTIP directly interacts with a key protein, WDR5, involved in catalysing the activation of H3K4me3 (Wang et al., 2011). Increased activity of H3K4me3 promotes transcriptional elongation and enhanced transcription (Chen et al., 2015) and, as such, WDR5 introduces H3K4m3 marks into the HOXA cluster to keep it transcriptionally active (Chen et al., 2015).

The involvement of RNAs in epigenetic silencing was proposed by various investigators based on the observation that while many enzymatic members of the chromatin remodelling complexes did not have DNA binding domains, they possessed RNA binding domains (Bernstein and Allis, 2005), (Sun and Zhang, 2005, Saxena and Carninci, 2011). Molecular investigations have revealed that several lncRNAs such as Kcnq1ot1, Airn, Xist, HOX transcript antisense RNA (HOTAIR) all associate with key chromatin remodelling complexes (Saxena and Carninci, 2011). X chromosome inactivation is the mechanism that has evolved in mammals to ensure dosage compensation between XX females and XY males and depends on the effective silencing of genes of one of the two X chromosomes in females (Avner and Heard, 2001). This mechanism is depended on a specific portion of the X chromosome that contains the gene for the lncRNA xist. Xist encodes a 17-kb lncRNA that is retained in the nucleus. Initiation of X chromosome inactivation results in the upregulation of the xist lncRNA and coating of the X chromosome to be inactivated (Sarkar et al., 2015). This triggers a cascade of events, including the acquisition of repressive chromatin

modifications, removal of active histone marks and DNA methylation (Sarkar et al., 2015). The combination of all these actions ensures the stable repression of the entire X chromosome and maintenance of the silent state. The complete molecular function of xist is currently unknown; however, key interactions between Ezh2 and Suz12, 2 components of the Polycomb repressive complex 2 (PRC2) complex, have been identified (Sarma et al., 2014).PCR2 catalyses methylation of histone H3 at K27 on chromatin, ultimately shutting down transcription. In agreement with this mechanism, Engreitz et al. (Engreitz et al., 2013) and Simon et al. (Simon et al., 2013) found linear correlations between Xist and PRC2 localisation. However, it should be noted that most of the studies supporting a direct interaction between xist and PCR2 complex (Zhao et al., 2008), (Kaneko et al., 2010), (Maenner et al., 2010), do not utilise any pulldown techniques to confirm the direct association.

Besides modulation of chromatin, lncRNAs have also been shown to regulate transcription through alternative mechanisms. One example of this is during heat shock, in which basal transcription is halted and HSF1 (Heat shock factor 1) is activated to drive transcription of heat shock-specific genes (Richter et al., 2010). One mechanism by which heat shock suppresses gene expression is through the upregulation of inhibitory lncRNA that function in *trans* to block general RNA polymerase II (Pol II) activity. Two lncRNA species, B2 RNA in mice and Alu RNA in humans, are upregulated greater than 40 fold following heat shock and can directly bind to the active site within Pol II, disrupting its interaction with promoter DNA (Place and Noonan, 2014).

The continued discovery of new lncRNAs and more thorough characterisation of those already known will surely reveal additional themes and functions. This will, ultimately, occur through detailed, mechanistic dissection of the genetic pathways and cellular activities for each individual lncRNA.

4.2 Aims

The aims of this chapter were as follows:

- To better characterise 4 of the 6 validated lncRNA (2 upregulated and 2 downregulated lncRNAs) identified in Chapter 3.
- To define one lncRNA to take further for detailed analysis (*SMILR*).
- To determine the cellular characteristics and localisation of *SMILR*.
- To identify the function of *SMILR* in stimulated HSVSMCs.
- To identify the molecular mechanisms governing *SMILR* function.

4.3 Results

Despite 6 lncRNAs being validated from the RNA-seq (Chapter 3- Section 3.4.3), only 4 lncRNAs (2 up-regulated and 2-downregulated) were taken forward for further functional analysis. These lncRNA were pursued as they exhibited the greatest fold changes between basal and stimulated cells.

4.3.1 Expression in tissue and cell panels

LncRNAs show more pronounced tissue and cell specific patterns of expression that protein coding genes, offering a variety of benefits in clinical applications for both early identification and control of disease progression (Jiang et al., 2016), (Kornienko et al., 2016). In order to gain insight into the expression of these lncRNA from a whole organ perspective, the expression of each lncRNA was quantified in a range of 10 normal human tissues including specimens derived from brain, gastrointestinal, reproductive, and endocrine systems. In general, the 4 lncRNA examined were expressed at relatively low levels across the tissue panel, when compared to protein coding genes. However, it was observed that RP11-94a24.1 (Figure 4-2A) was expressed highest in the heart, while AC018647.3 and RP11-91K9.1 showed preferential expression within the liver and brain respectively (Figure 4-2B and C). RP11-761I4.4 also displayed highest expression in the brain (Figure 4-2D).

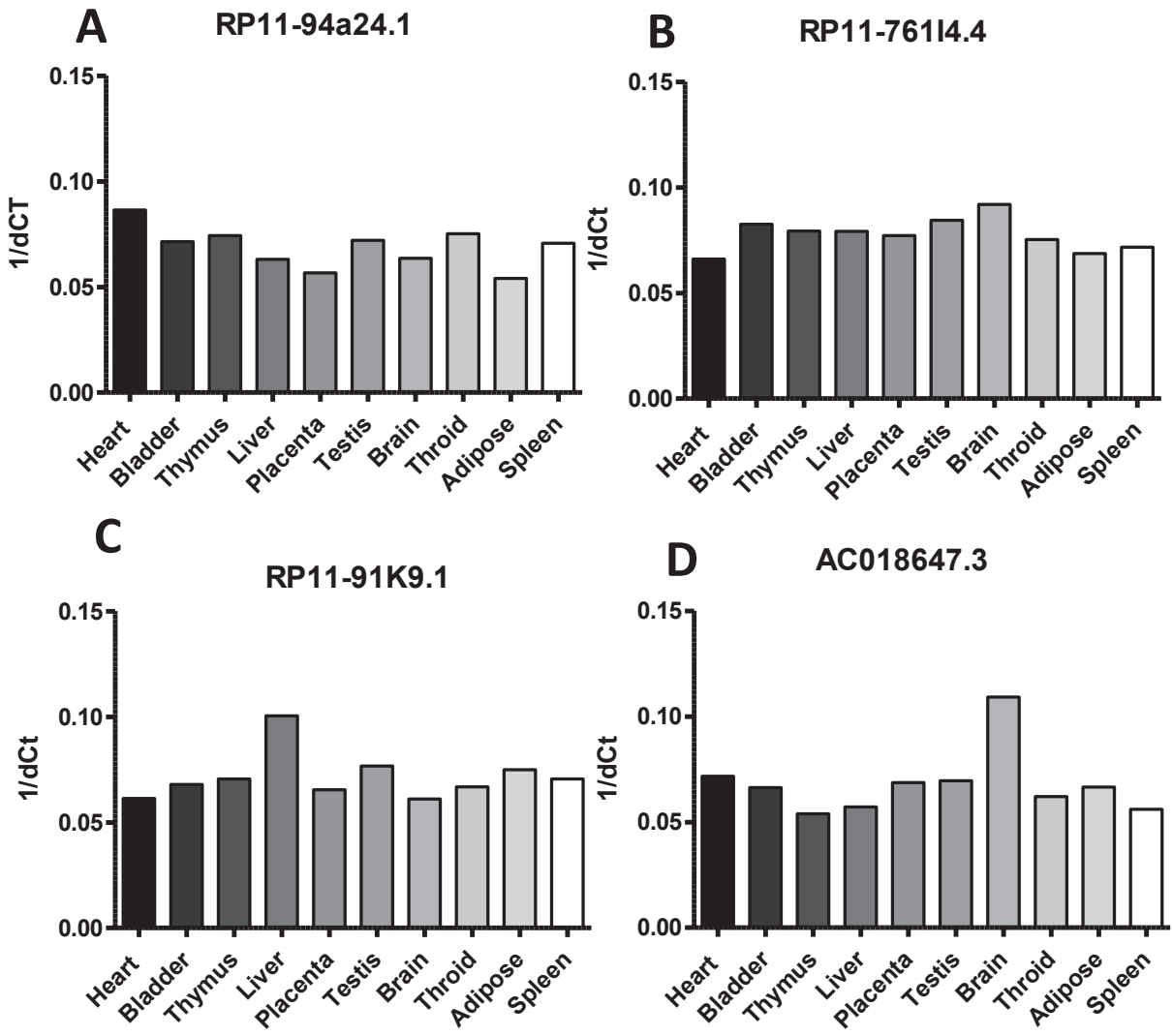

Figure 4-2: LncRNA tissue specific analysis.
Expression of lncRNAs A; RP11-94a24.1,B: RP11-761I4.4,CL RP11-91k9.1 and D: AC018647.3 was examined by qRT-PCR in a panel of RNAs derived from various normal tissues consisting of heart, bladder, thymus, liver, placenta, testis, brain, thyroid, adipose and spleen. The results are displayed as 1/ΔCT, normalised to UBC housekeeper (n=1).

Due to the specific interest in identifying lncRNA that modulate VSMC proliferation and inflammation and thus vascular disease, lncRNA expression was assessed by qRT-PCR analysis in different vascular cells. LncRNA expression was determined in saphenous vein endothelial cells (HSVEC), HSVSMC and human coronary artery SMC (HCASMC) was assessed. This was performed in order to ascertain if each lncRNA would show differential expression from a cellular specific rather than whole tissue perspective. All lncRNAs had higher expression in basal VSMCs of either venous or arterial lineage compared to endothelial cells, suggesting VSMC enrichment (Figure 4-3A-D). Due to the specific modulation of these lncRNAs by IL1α and PDGF treatment in HSVSMC and the specific role of IL1α and PDGF in vascular disease, the expression of these lncRNA, following stimulation, was determined in additional cell types, HSVEC and HCASMC.

For ease of interpretation, HSVSMC stimulation with IL1α and PDGF is provided in the left hand panel of Figure 4-4 and HCASMC stimulation in the right hand panel. Stimulation of HCASMCs induced a significant reduction in RP11-761I4.4 ($P<0.001$) (Figure 4-4A) and AC018647.3 ($P<0.001$) (Figure 4-4B) consistent with HSVSMC stimulation, while RP11-91k9.1 was significantly up-regulated ($P<0.01$) but to a lesser extent than in HSVSMC (Figure 4-4C). Notably, RP11-94a24.1 was significantly downregulated ($P<0.05$) with dual stimulation in HCASMC despite a ~30 fold induction in HSVSMCs (Figure 4-4D).

Due to the already low expression of certain lncRNA in unstimulated HSVEC (Figure 4-3), subsequent downregulation of RP11-761I4.4 and AC018647.3 was not observed, as was the case in HSVSMC. However, stimulation of HSVECs produced a significant 3.8 ± 0.7 and 8.7 ± 2.1 fold up regulation of RP11-91K9.1 following IL1α and IL1α/PDGF treatment respectively (Figure 4-5A). Stimulation had no effect on RP11-94a24.1 expression (Figure 4-5B), indicating selective regulation in HSVSMC.

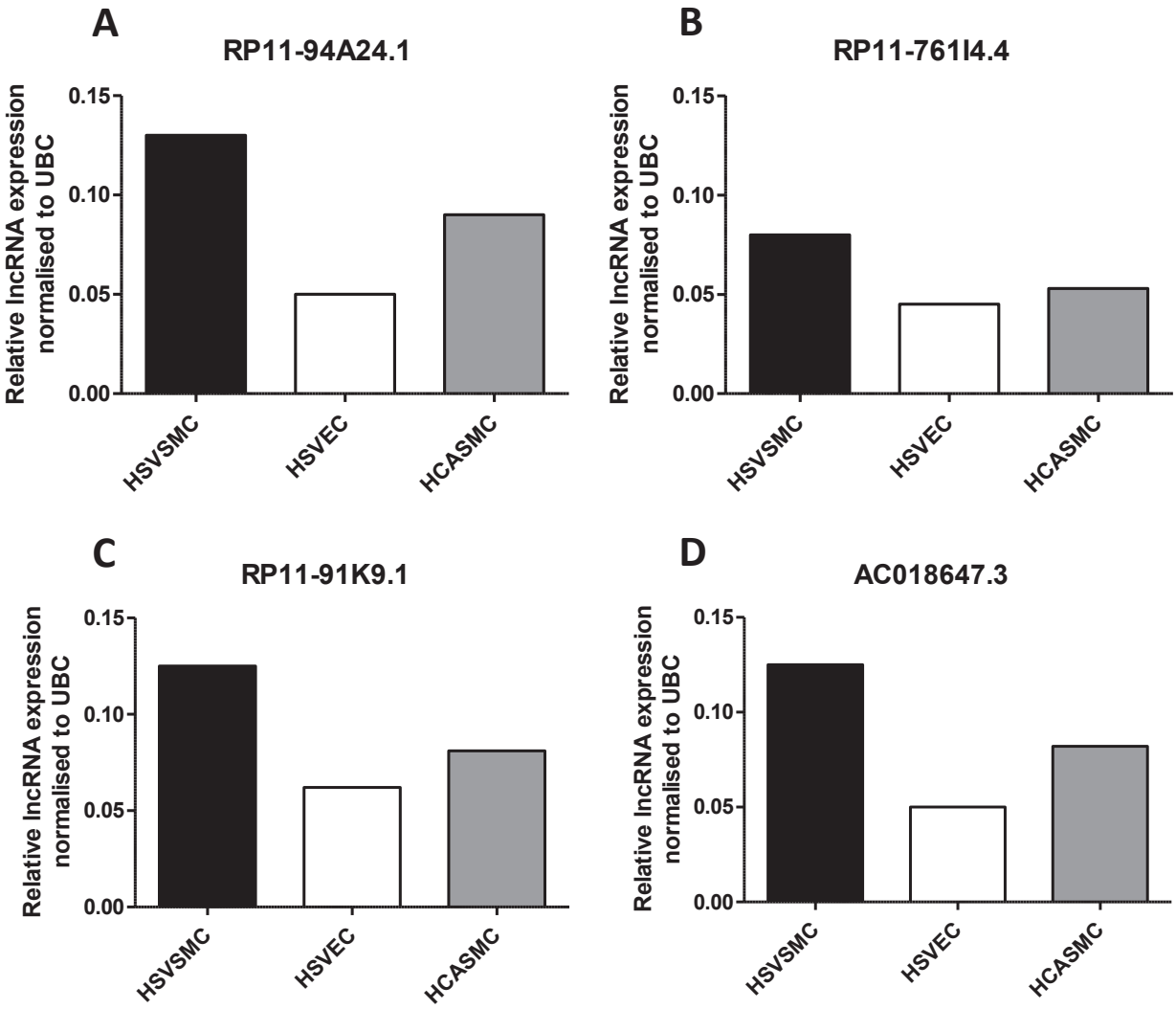

Figure 4-3: Cell specificity analysis.
The expression of lncRNAs A: RP11-94a24.1, B: RP11-761I4.4, C: RP11-91k9.1 and D: AC018647.3 was examined in basal human saphenous vein smooth muscle cells (HSVSMC), human saphenous vein endothelial cells (HSVEC) and human coronary artery smooth muscle cells (HCASMCs) by qRT-PCR analysis (n=2 patients). Data is expressed as 1/ΔCT normalised to UBC house keeper.

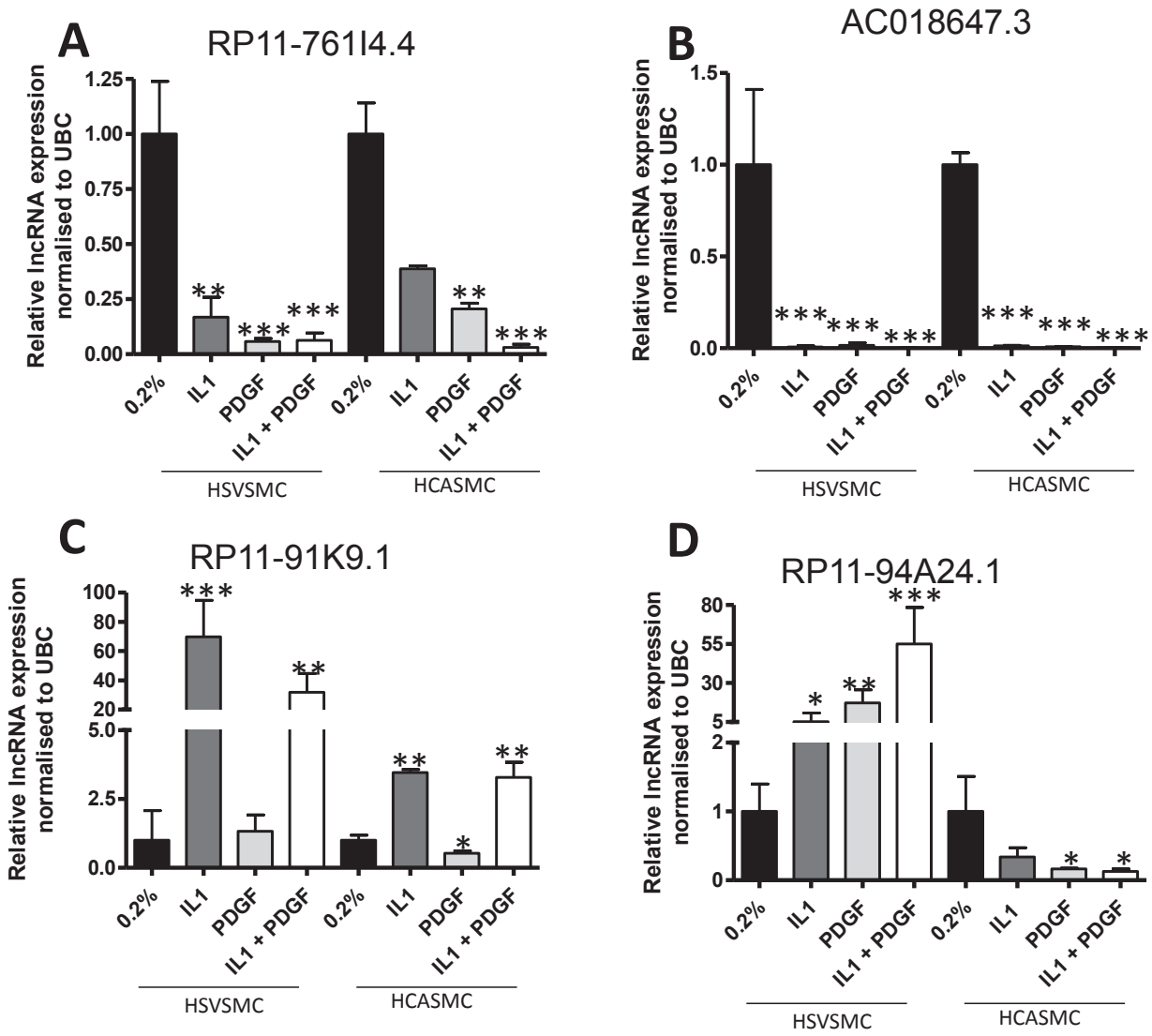

Figure 4-4: Expression of lncRNA in stimulated HCASMC.
A: RP11-761I4.4, B: AC018647.3, C: RP11-91k9.1 and D: RP11-94a24.1. HSVSMC (left panel) and HCASMC (right panel) were quiesced in media containing 0.2 % FBC for 48 h followed by stimulation with IL1α, PDGF or a combination of both for 72 h. LncRNA expression was assessed by qRT-PCR (n=2, graph indicates representative graph with stats performed on technical replicates for HCASMCs and n=4 patients for HSVSMC). *P<0.05, **P<0.01 and ***=P<0.001 vs. 0.2 % control sample, one-way ANOVA.

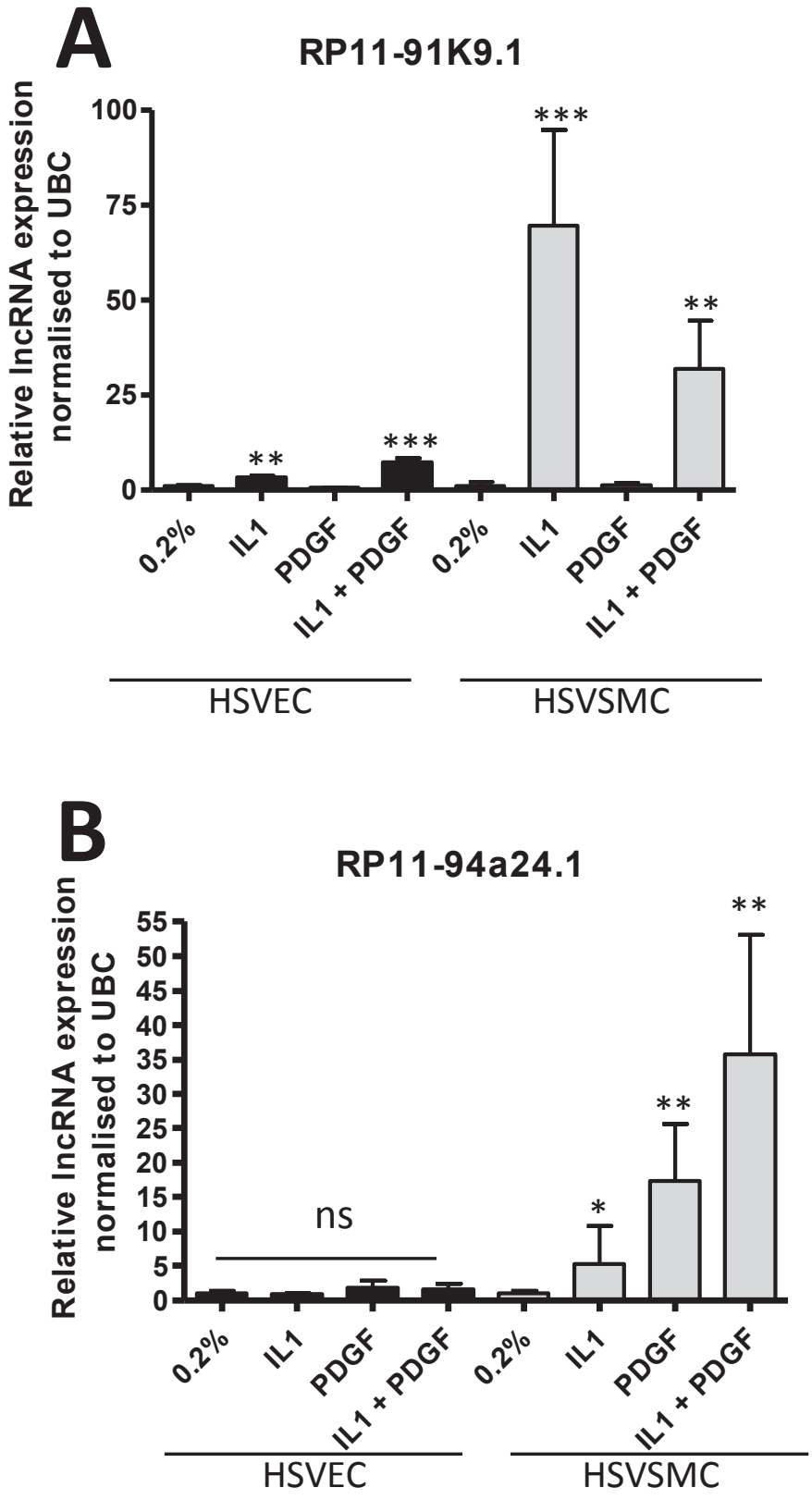

Figure 4-5: LncRNA show cell specific expression.
Human saphenous vein endothelial cells (HSVEC) and human saphenous vein smooth muscle cells (HSVSMC) were quiesced in 0.2 % media for 48 h then stimulated with 0.2 % media as a control, IL1α, PDGF or a combination of IL1α and PDGF for 72 h. Expression of **(A):** RP11-91k9.1 and **(B):** RP11-94a24 was assessed via qRT-PCR (n=4, * P<0.05, ** P<0.01, *** P<0.001 vs 0.2 % in each specific cell type, one way ANOVA) (n=3 for HSVEC and n=4 for HSVSMC).

4.3.2 Time course of expression

Due to the highest level of expression and greatest fold change of the lncRNA in HSVSMC, this cell type was continually used for all subsequent experiments. The expression of each lncRNA was assessed 72 h after stimulation during RNA-seq analysis. To investigate the longitudinal regulation of these lncRNA, HSVSMCs were stimulated with IL1α and PDGF for 1.5, 4, 24, 48 and 72 h. For RP11-94a24.1 a significant up regulation in response to PDGF was observed as early as 4 h post stimulation ($p<0.001$) (Figure 4-6A). By 24 h RP11-94a24.1 expression was increased by treatment with PDGF or IL1α as well as in combination. This expression of this lncRNA was further increased at 48 and 72 h post stimulation ($P<0.001$). RP11-761I4.4 was significantly down-regulated by PDGF and IL1α treatment 1.5 h post stimulation ($P<0.01$) (Figure 4-6B). The levels of RP11-761I4.4 decreased until the 24 h time point in which the levels remained similar out to 72 h ($P<0.001$). RP11-91k9.1 and AC018647.3 showed no change in expression until the 24 h time point (Figure 4-6) ($P<0.001$ for both) (Figure 4-6C and D).

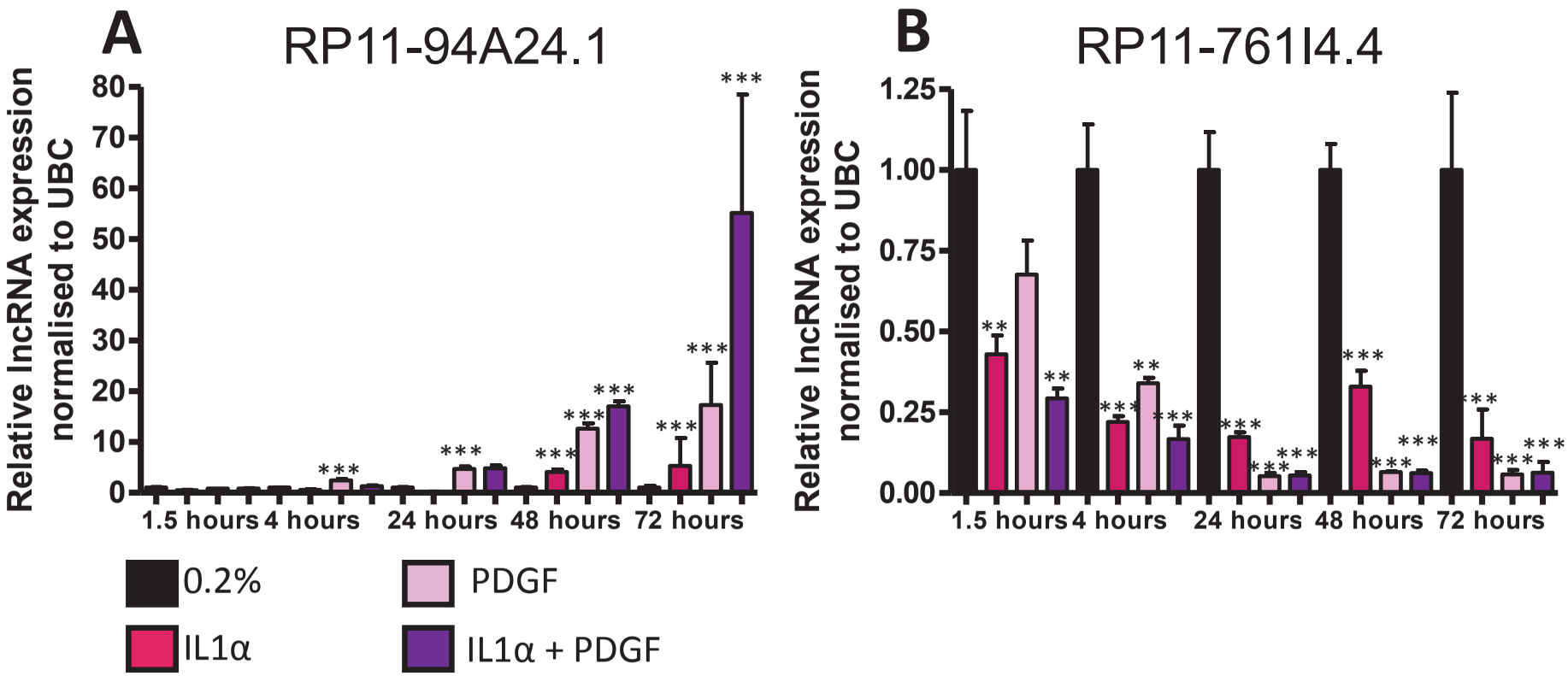
A
RP11-94A24.1
Relative lncRNA expression normalised to UBC
80
70
60
50
40
30
20
10
0
1.5 hours
4 hours
24 hours
48 hours
72 hours
0.2%
PDGF
IL1α
IL1α + PDGF
B
RP11-761I4.4
Relative lncRNA expression normalised to UBC
1.25
1.00
0.75
0.50
0.25
0.00
1.5 hours
4 hours
24 hours
48 hours
72 hours

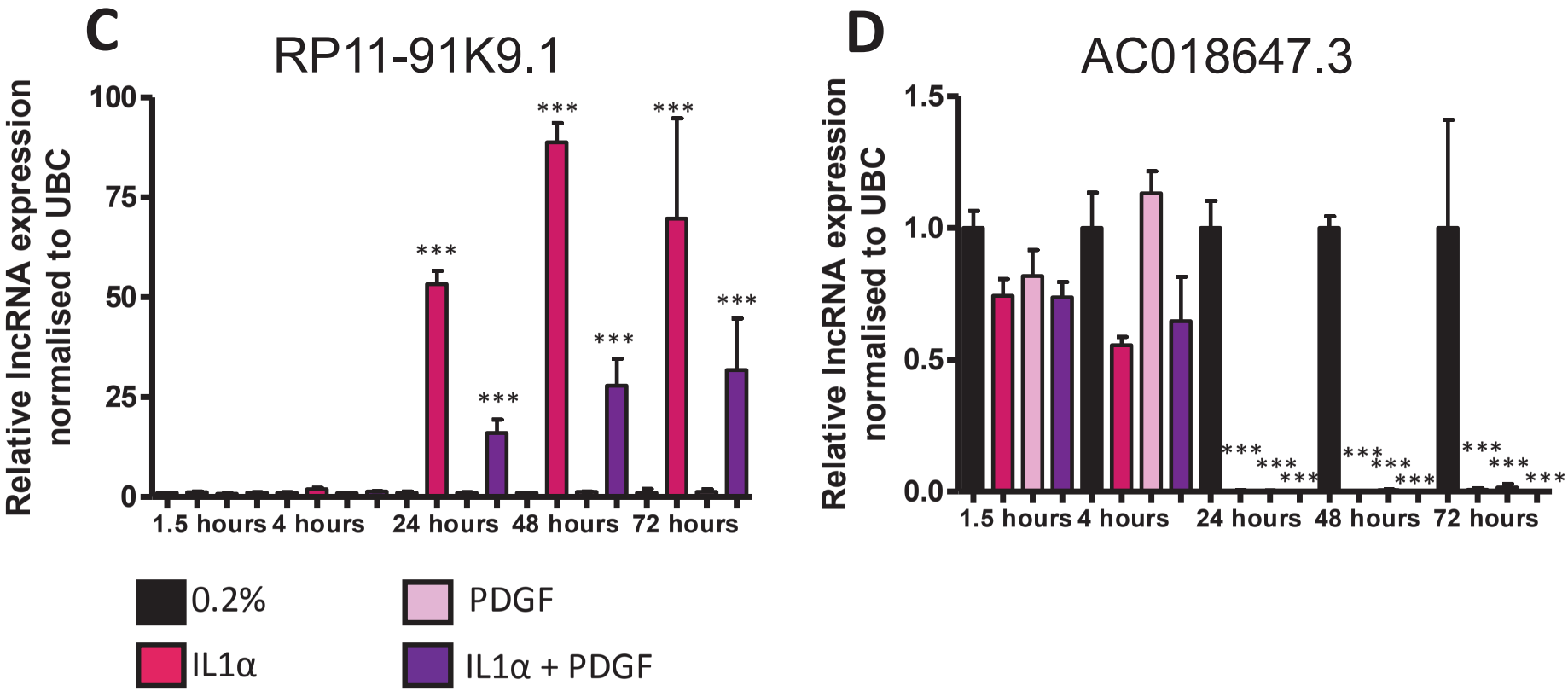
C
RP11-91K9.1
Relative lncRNA expression normalised to UBC
100
75
50
25
0
***
1.5 hours
4 hours
24 hours
48 hours
72 hours
0.2%
PDGF
IL1α
IL1α + PDGF
D
AC018647.3
1.5
1.0
0.5
0.0

Figure 4-6: Temporal regulation of lncRNAs assessed by qRT-PCR.

A: RP11-94a24.1, B: Rp11-761I4.4, C: RP11-91k9.1 and D: AC018647.3. HSVSMC were quiesced for 48 h in 0.2 % media and then stimulated with 0.2 % media (control, black bars) or IL1α (dark pink bars), PDGF (light pink bars) or a combination of IL1α and PDGF (purple bars) for 1.5, 4, 24, 48 or 72 h and the RNA extracted. LncRNA expression of RP11-94a24.1, RP11-761I4.4, RP11-91k9.1 and AC018647.3 was assessed by qRT-PCR analysis (n=3, pooled data).* P<0.05, ** P<0.01 and *** P<0.001 vs 0.2 % control at each respective time point, significance measured by one way ANOVA.

4.3.3 LncRNA stability

To date, tens of thousands of lncRNA have been identified. Despite progress in their functional characterisation, little is known about the post-transcriptional regulation of lncRNAs and their half-lives. Although many are easily detectable by a variety of techniques, such as qRT-PCR, it has been assumed that most lncRNAs are generally unstable due to large scale genome wide analysis of lncRNA stability (Clark et al., 2012). However, several stable lncRNA have now been proposed as potential biomarkers. To examine the stability of lncRNAs, HSVSMC transcription was halted with Actinomycin D (ActD) and RNA levels measured over a 19 h time course. In the absence of transcription, the levels of expression of any RNA are thus determined by its rate of decay. The prolonged time course allowed for improved half-life measurements for transcripts with slow decay rates, compared to previous transcriptional experiments in mammalian cells which typically extended to a maximum of 8 h (Raghavan et al., 2002),(Sharova et al., 2009). In order to identify an appropriate housekeeper, the expression of the GAPDH housekeeping gene was measured across conditions. Under quiesced and stimulated conditions (Figure 4-7 Ai and Bi respectively), GAPDH mRNA levels remained stable regardless of the addition of ActD. To confirm transcriptional blockage, the expression of the ubiquitin C mRNA, UBC, was determined by qRT-PCR. UBC has been previously shown to exhibit a short half-life of approximately 2.9 h (Padovan-Merhar et al., 2015). Consistent with previous observations UBC exhibited a short half-life of 4.2 and 3.2 h under quiesced and stimulated conditions respectively, indicating that ActD was indeed inhibiting transcription (Figure 7-Aii and Bii).

Stability was determined in conditions which induce the greatest lncRNA expression, thus, RP11-761I4.4 and AC018647.3 (Figure 7-Aiii and iv), which were down regulated by IL1α and PDGF treatment, were examined under 0.2 % conditions and RP11-94a24.1 and RP11-91k9.1 (Figure 7-Biii and iv), which are up regulated by IL1α and PDGF, were examined under stimulated conditions. In order to induce the greatest expression quiesced HSVSMCs were stimulated with IL1α /PDGF or 0.2 % media for 72 h prior to the addition of ActD for a further 19 h.

RP11-761I4.4 exhibited a short half-life of 6.4 h, this is consistent with the time course data which indicated that this lncRNA was down regulated as early as 4 h post stimulation and we hypothesised that this rapid down regulation was due to lncRNA degradation (Section 4.2.2). AC018647.3 exhibited a greater stability with a half-life greater than 19 h. RP11-91k9.1 exhibited a similar stability with a half-life of 19 h, while RP11-94a24.1 expression in both Act-D and control cells showed marked degradation after 8 h. This was initially proposed to be due to the exhaustion of PDGF in the culture medium. However similar experiments where PDGF was replenished after 48 h, exhibited a similar effect.

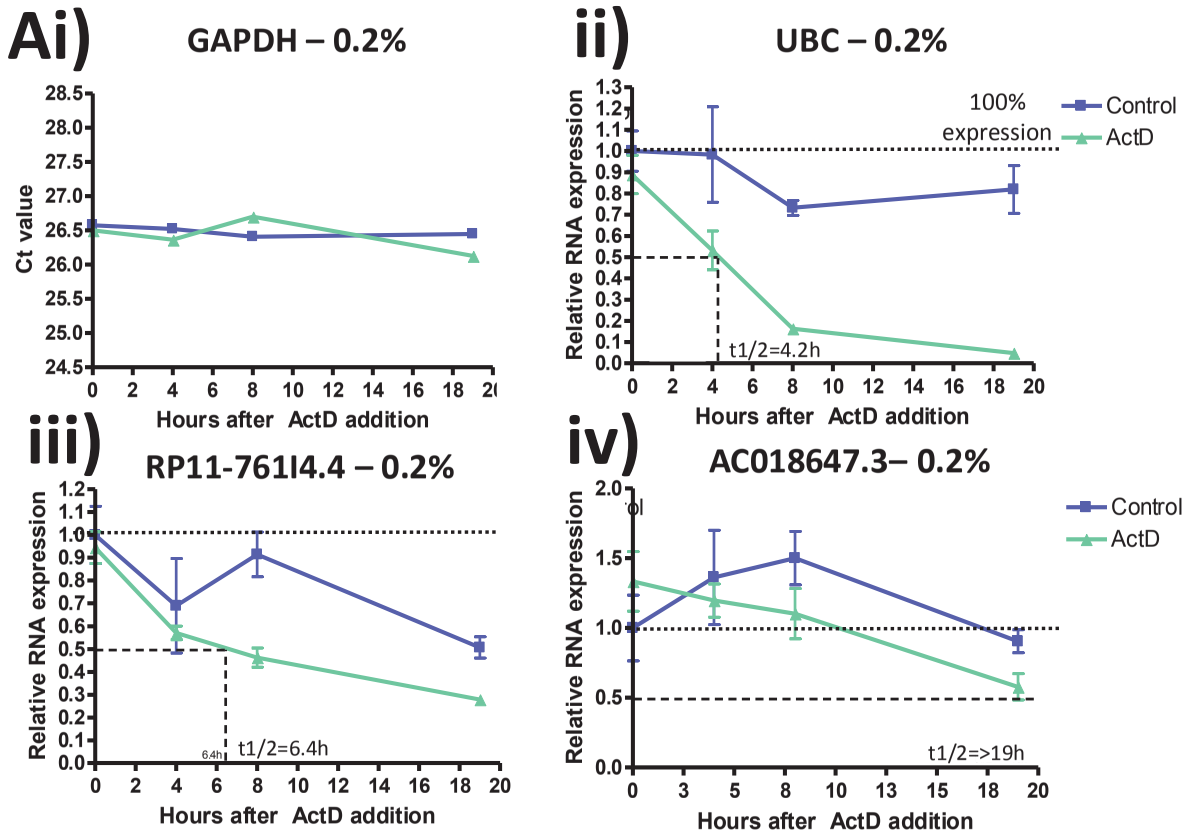
Ai)
GAPDH – 0.2%
Ct value
Hours after ActD addition
ii)
UBC – 0.2%
100% expression
Control
ActD
Relative RNA expression
t1/2=4.2h
Hours after ActD addition
iii)
RP11-761I4.4 – 0.2%
Relative RNA expression
t1/2=6.4h
Hours after ActD addition
iv)
AC018647.3– 0.2%
Control
ActD
Relative RNA expression
t1/2=>19h
Hours after ActD addition

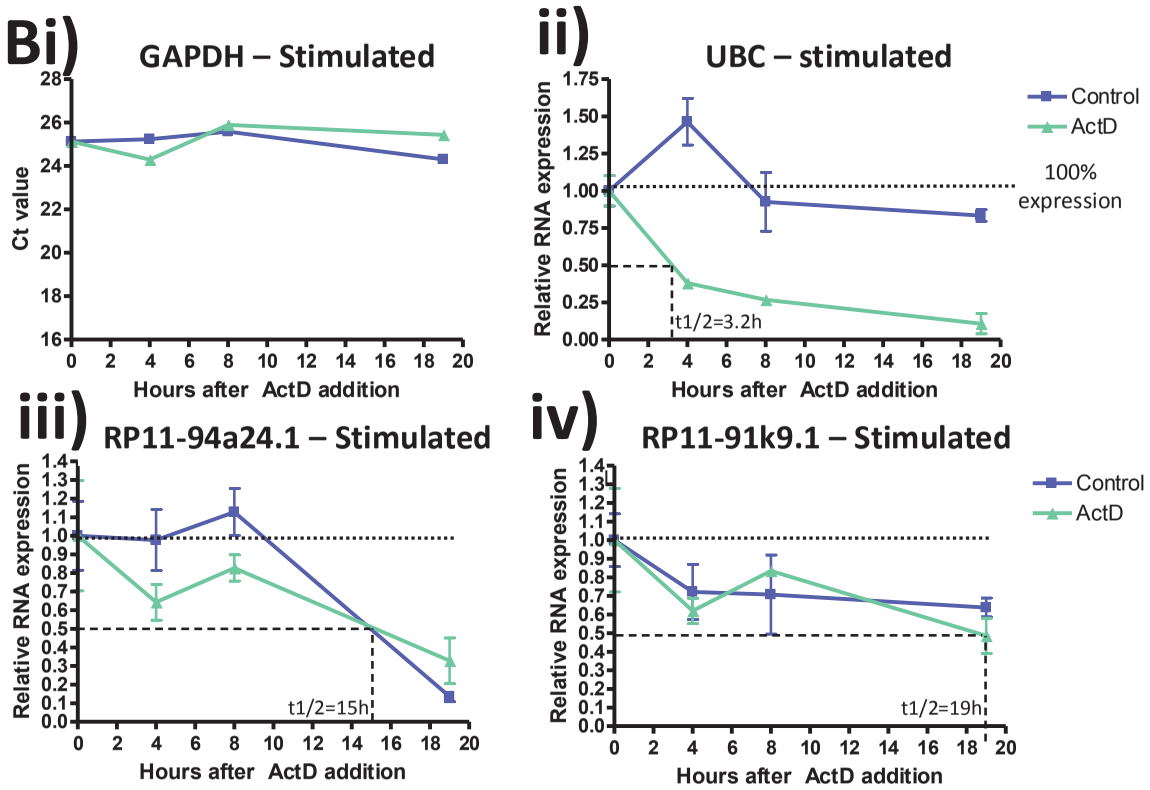

Figure 4-7: LncRNA stability in 0.2 % and stimulated conditions.

HSVSMC were quiesced in 0.2 % media for 48 h and then stimulated in either 0.2 % media or media containing IL1α + PDGF for 72 h. Following stimulation Actinomycin D (green line) or DMSO (blue line) was added per well and cells incubated for a further 0, 4, 8 or 19 h to allow inhibition of transcription. Samples were RNA extracted and lncRNA half-life ($t_{1/2}$) assessed by qRT-PCR. LncRNA stability was assessed under the conditions allowing the maximum expression of the lncRNA All RNA are normalised to GAPDH housekeeper levels (A and B - Panel i). GAPDH was shown to be an appropriate house keeper due to its stability under all conditions. (n=2 biological replicates). UBC positive control (A and B – panel ii) **(A):** Stability of each lncRNA under 0.2 % conditions (iii- RP11-761I4.4 and iv – AC018647.3) and **(B):** Stability under IL1α and PDGF stimulated conditions (iii – RP11-94a24.1 and iv – PR11-91k9.1). Dotted line indicates 100 % expression and dashed line indicates 50 % expression. Error bars indicate technical triplicates from one single biological replicate.

4.3.4 Pathway analysis

It is well established that IL1α and PDGF can have synergistic effects on vascular cell activation (Weber et al., 2010), (Andrae et al., 2008). To assess the roles of these pathways in the regulation of lncRNA expression in HSVSMC, selective pharmacological inhibitors AZD6244 (MEKK1) and SB 203580 (p38 MAPK) were utilised (Figures 4-8A and C). Following 60 min pre-treatment with inhibitors, HSVSMC were stimulated with IL1α/PDGF and the expression of each lncRNA was determined at 24 h. Pre-treatment with the p38 MAPK inhibitor (5, 10 and 20 μM) significantly inhibited the upregulation of RP11-94a24.1 at all concentrations ($P<0.001$) and inhibited RP11-91k9.1 up-regulation in response to IL1α and PDGF at the maximum concentration only ($P<0.05$). P38 inhibition dose dependently reversed IL1α and PDGF down-regulation of RP11-761I4.4 with only the top concentration being significant ($P<0.01$); however, inhibition of p38 did not affect the downregulation of AC018647.3 in response to IL1α and PDGF treatment indicating that this particular lncRNA is not induced through the p38 arm of the signalling pathway (Figure 4-8B).

Pre-treatment with the MEKK1 inhibitor significantly reduced RP11-94a24.1 expression at all 3 concentrations ($P<0.01$) and increased AC018647.3 expression at all 3 doses ($P<0.01$). MEKK1 inhibition did not affect RP11-761I4.4 nor RP11-91k9.1 at any dose, indicating that these lncRNA are not regulated through this part of the IL1α or PDGF pathway.

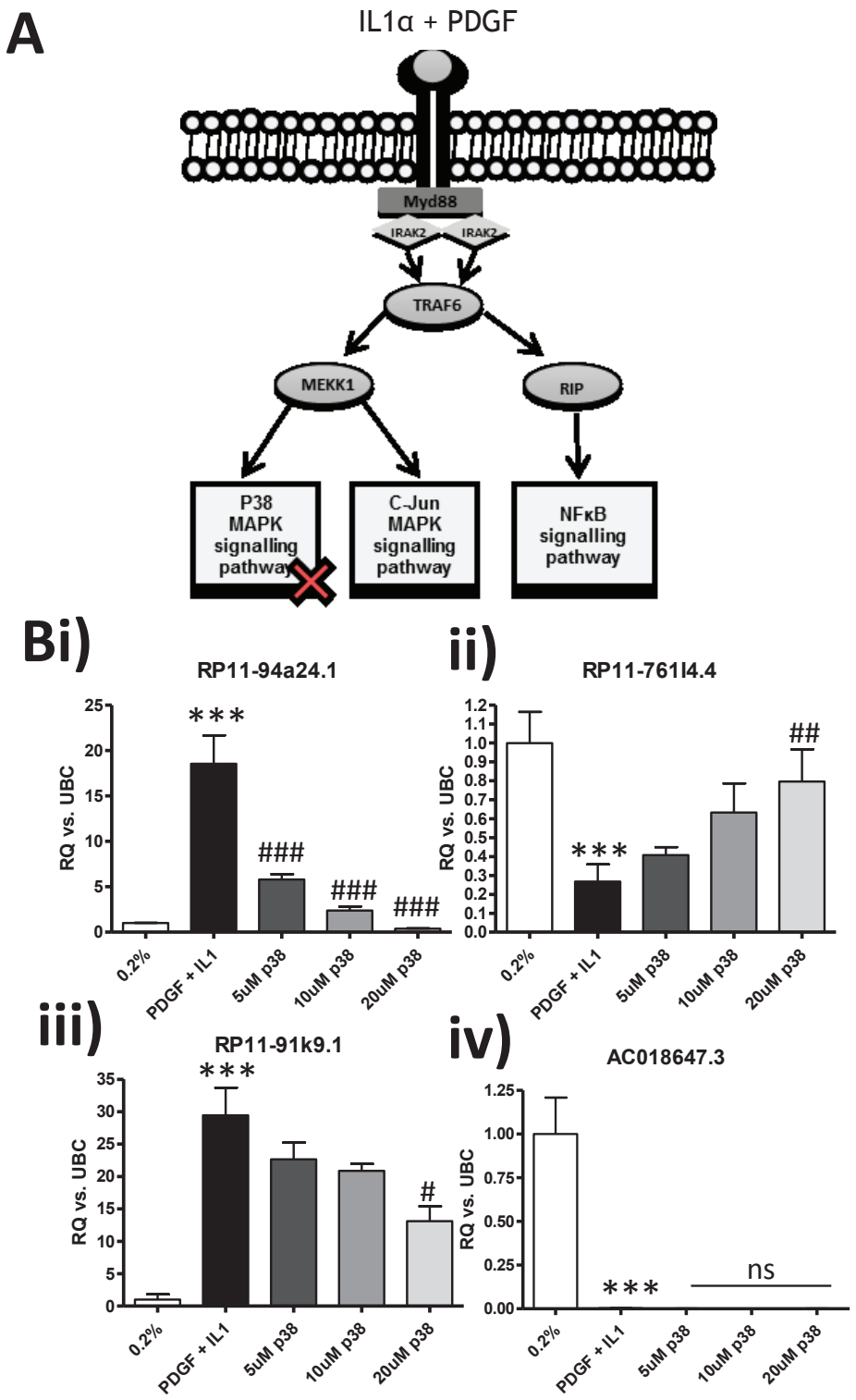
A
IL1α + PDGF
Myd88
IRAK2
IRAK2
TRAF6
MEKK1
RIP
P38 MAPK signalling pathway
C-Jun MAPK signalling pathway
NFκB signalling pathway
Bi)
RP11-94a24.1
RQ vs. UBC
***
###
###
###
0.2%
PDGF + IL1
5uM p38
10uM p38
20uM p38
ii)
RP11-761I4.4
RQ vs. UBC
***
##
0.2%
PDGF + IL1
5uM p38
10uM p38
20uM p38
iii)
RP11-91k9.1
RQ vs. UBC
***
#
0.2%
PDGF + IL1
5uM p38
10uM p38
20uM p38
iv)
AC018647.3
RQ vs. UBC
***
ns
0.2%
PDGF + IL1
5uM p38
10uM p38
20uM p38

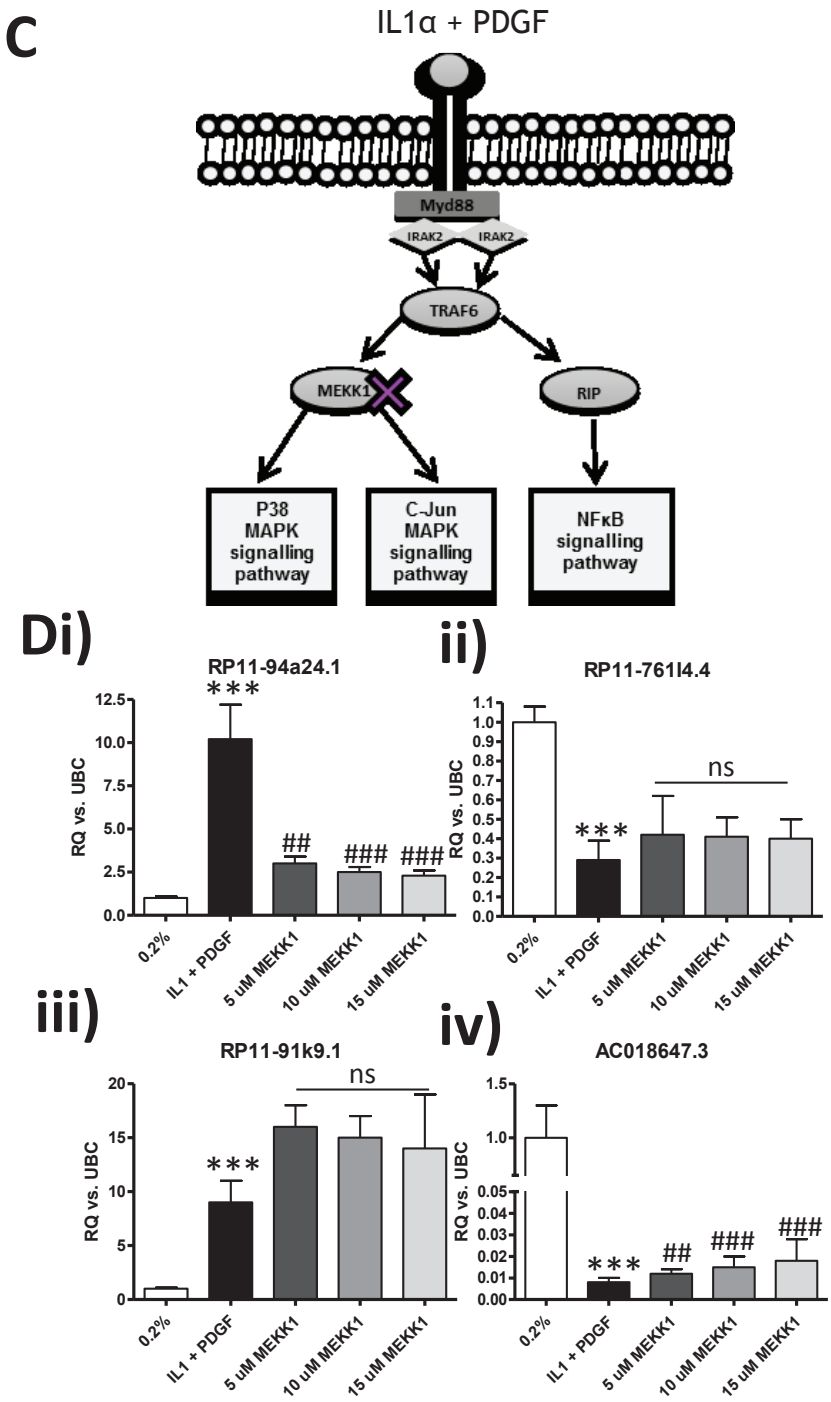

Figure 4-8: Upstream pathways regulating lncRNA expression.
(A): Schematic diagram showing specific site of p38 inhibition using SB 203580. HSVSMC were pre-treated for 60 min with the indicated concentration of the inhibitor. Following exposure to control (0.2 % media) or IL1α and PDGF for 24 h expression of lncRNAs RP11-94a24.1 (Panel i), RP11-761I4.4 (Panel ii), RP11-91k9.1 (Panel iii) and AC018647.3 (Panel iv) was determined by qRT-PCR. **(B):** LncRNA expression following p38 inhibition. ***P<0.001 vs 0.2 % media, # P< 0.05, ## P<0.01 and ### P<0.001 vs IL1α/PDGF treatment. Repeated measures ANOVA. n=3. **(C):** Schematic diagram showing specific site of MEKK1 inhibition using AZD6244. HSVSMC were pre-treated for 60 min with the indicated concentration of the inhibitor. Following exposure to control (0.2 % media) or IL1α and PDGF for 24 h expression of lncRNAs RP11-94a24.1, RP11-761I4.4, RP11-91k9.1 and AC018647.3 was determined by qRT-PCR **(D):** LncRNA expression following MEKK1 inhibition. Repeated measures ANOVA. ***P<0.01 vs 0.2 % media, # P<0.05, ## P< 0.01 and ### P<0.001 vs IL1α/PDGF treatment alone n=3 patients. All graphs indicate lncRNA expression relative to 0.2 % controls (Relative Quantity, RQ).

4.3.5 Cellular Localisation

Knowledge of lncRNA subcellular localisation patterns can provide fundamental insights into their biology and fosters hypotheses for potential molecular roles. As mentioned in the introduction, lncRNA in the cytoplasm typically act as microRNA sponges or block binding sites for protein activation. Nuclear lncRNA, on the other hand, act as DNA enhancers or repressors to modulate gene expression. Cellular compartmentalisation of lncRNAs and controls in quiesced and stimulated HSVSMC (Figure 4-9 top and bottom graphs respectively) was determined via cellular fractionation. To evaluate the separation quality of the isolated fractions, MALAT1 and NEAT1, two known nuclear lncRNA (Tripathi et al., 2010), (Clemson et al., 2009), were assessed by qRT-PCR. Under both control (0.2 %) (Figure 4-9A)and stimulated (IL1α + PDGF)(Figure 4-9B) conditions NEAT1 and MALAT1 showed greater than 90 % expression in the nuclear fraction, suggesting sufficient separation between the two fractions. Additionally, the expression of the housekeepers UBC and GAPDH were assessed. GAPDH and UBC have been previously shown to be expressed both in the nuclear and cytoplasmic fraction of cells. Under 0.2 % conditions 17 % of GAPDH was located within the cytoplasm and 28 % following stimulation. A greater percentage of UBC was found to be cytoplasmic with 48 % and 89 % corresponding to the cytoplasm during quiesced and stimulated conditions. RP11-94a24.1, RP11-761I4.4 and RP11-91k9.1 all exhibit both nuclear and cytoplasmic expression under quiesced and stimulated conditions. AC018647.3 exhibited greater nuclear expression under both conditions.

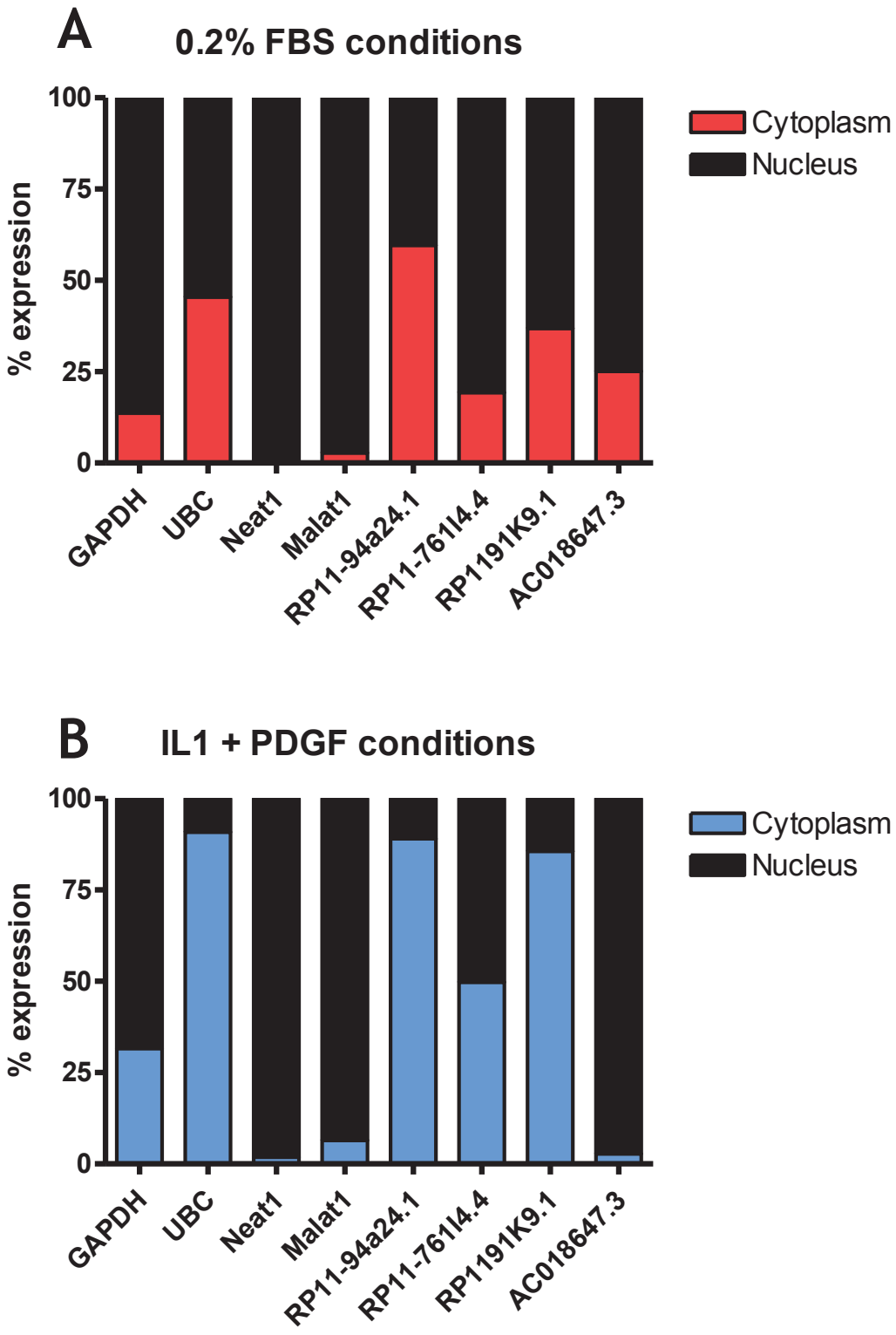

Figure 4-9: Expression of lncRNA in nuclear and cytoplasmic fractions.
A: 0.2 % conditions and **B:** IL1 and PDGF treatment. HSVSMC were quiesced in 0.2 % media for 48 h then stimulated with either 0.2 % media (red bars) or IL1α and PDGF (blue bars) for 72 h. Cells were fractionated into cytoplasmic and nuclear fractions utilising the PARIS fractionation kit and lncRNA expression of RP11-94a24.1, RP11-761I4.4, RP11-91k9.1 and AC018647.3 was determined by qRT-PCR (n=2). Nuclear lncRNAs Neat1 and MALAT1 served as nuclear controls. Graph indicated % expression of each RNA in the nucleus (black bars) or cytoplasm (coloured bars).

4.3.6 Selection of single lncRNA for further analysis – *SMILR* lncRNA

Due to the high expression of RP11-94a24.1 in HSVSMC and its cell specific induction in response to pathological mediators of vascular injury, further studies focussed on RP11-94a24.1. This lncRNA was termed, smooth muscle induced lncRNA enhances replication (*SMILR*). *SMILR* expression was assessed through the utilisation of 3 independent primer sets targeting different exons of the lncRNA. qRT-PCR analyses revealed similar Ct values and fold changes amongst the 3 sets, further confirming the previous data (Figure 4-10A-C). The longest putative open reading frame within *SMILR* is 57 amino acids. Analysis of this open reading frame using the Coding Potential Calculator (http://cpc.cbi.pku.edu.cn) did not reveal any similarity to known protein coding sequences suggesting that this RNA has no protein coding potential.

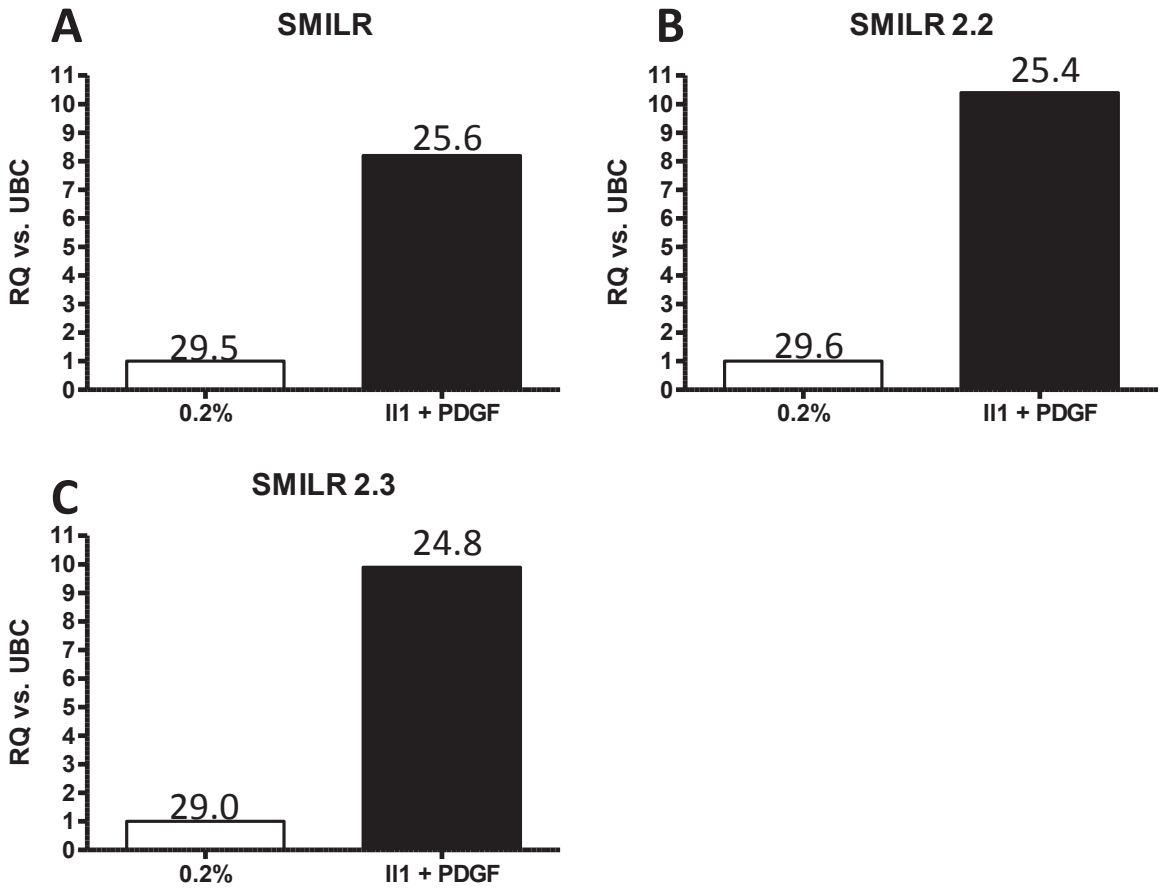

Figure 4-10: Validation of additional SMILR primers.
To confirm the expression of lncRNA *SMILR* three additional primer sets were designed targeting different sequences of the *SMILR* transcript. HSVSMC were quiesced in 0.2 % media for 48 h then stimulated with either 0.2 % media or IL1α and PDGF for 72 h. **(Tabas et al.):** Assessment of *SMILR* via qRT-PCR expression via 3 independent primer sets. The number on top of graphs represent Ct values obtained under 0.2 % and dual stimulated conditions.

4.3.7 *SMILR* 5' 3' RACE and RNA FISH

Rapid amplification of cDNA ends (Billings et al.) (RACE), was utilised to design specific RNA FISH probes and to identify if splice variants or additional isoforms were expressed in HSVSMC. RACE identified a single *SMILR* isoform, consisting of an additional 6 bp at the 5' end and 316 bp at the 3' end (Figure 4-11A). The full sequence of *SMILR* is provided in Figure 4-11B and the RACE data is supported by the raw RNA-seq files (Figure 4-12).

RNA-FISH was then performed to provide visuospatial information as to the location of *SMILR* within HSVMSC, and to confirm fractionation results. Negative control samples showed no fluorescent signal (Figure 4-13A) while fluorescent activity of the nuclear lncRNA SNORD3 (positive control) confirmed the nuclear permeabilisation of cells (Figure 4-13B). Ideally a scrambled probe should be utilised as a negative control, however these were not available from the company at the time of experimentation. In the absence of growth factor and cytokine stimulation, HSVSMC typically exhibited between 0 and 3 positive fluorescent signals corresponding to *SMILR* localisation (Figure 4-13C). IL1α/PDGF treatment induced a marked increase in fluorescent signal within the nucleus and cytoplasm of HSVSMC (Figure 4-13D). Quantification of FISH samples is provided in Figure 4-13E. In the absence of stimulation 2 ± 3.6 *SMILR* molecules were observed. Following stimulation, 25 ± 5 individual *SMILR* molecules were observed within the nucleus and cytoplasm.

A

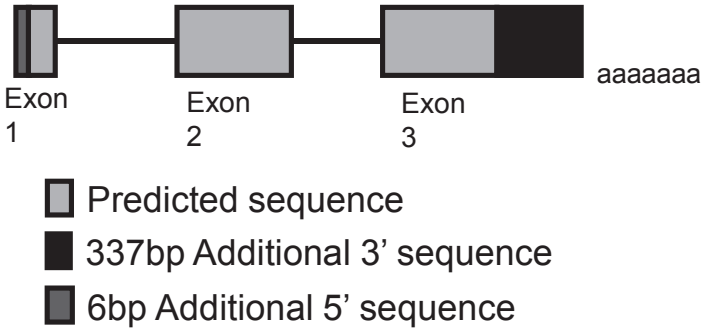

B

RP1194A24.1 SMILR sequence

ACTCTTGCTGCAAACATTGGGATCAGCCGTGACTATCCCATAACATAATATTTCTG
ATTTCATTCTTTTCCTTTCTCCTACCAATTTAATCTGCAATCACTTCAAGAGAAGT
CTGTTTAAAGGATATTCACATTCTG (intron1-11,398 bp)

TTCACAGAGTTTGAGAGAAACTGTATTCAAGTTGCTGAAACCAAGAAGCTACAC
TCACGAGTCTCACCTAAACTCGAATCTGATTTAGATGACATCATCCTGGACTTTG
AGTTGATGAAACCTTGGAGGTCTTGGGAGTAAAGCAAGTGTGATTTGCATATGA
TGGATATGAATTGTAATGGCCAGAGCATGGCTGTG (intron 2- 2,269 bp)

AGATGAAAACTCCCATTTTAGGGAACCAAGACTGAATTCCATAATTTACATGGATG
TTTGGAAGGTGTCTGCAACTTAATCTGTGTTCGTTTCTGAGATGTTGGGCAACT
CCTTCTTGGAAGATGTGGTAATGGTCTCTTCGAAAAGAAAATAATCATCTGAGTT
TTGGCCAAAATAGTTGATCGGATTACCTATGAAAATGACTCTCACCCAACTACAAG
AATGTTATGATGTAGAAACTCTAAATATATGAGTAATTAACTATACAACACTCCATC
CCCATGTGAAAATCTTTAATCTTTTAAGATACTGAAATTTTGTGTATGTCTCATAAT
TTTCTGTATATGGTCAATGAGTTTTGCCTTAGCCATAAGTGGTCTGTCTGAAATC
TTCTCTATTATTTGTGCATTTTCTTCCTGATGTACCAAGCCTAGTCTGTTTGTTTT
TTCCTAAGAGAAAAGCAGATGATTCAACTGTGTATTTCTCAGTGTTGATATTGTG
GTTTGAGGTATTTCATAATCTTGAGTAAAATCTTGTCATAAAAAAAAAAAAAAAA
AAAA

Ensembl Sequence
New Sequence from RACE

Figure 4-11: Visual representation of full SMILR transcript.
5'3' RACE was performed on HSVSMC stimulated with IL1α and PDGF for 72 h. RACE was performed through the utilisation of the SMARTER 5' 3' RACE kit **(A):** Grey boxes indicate the predicted *SMILR* sequence obtained from UCSC genome browser (RP11-94A24.1). Black boxes represent additional 337 base pair sequence obtained via 3' RACE of *SMILR* transcript and 6 base pair sequence obtained by 3' RACE. **(B):** Full length sequence of *SMILR*. Black letters are the sequence obtained from Ensembl and green letters are the additional sequence of *SMILR* obtained via RACE analysis.

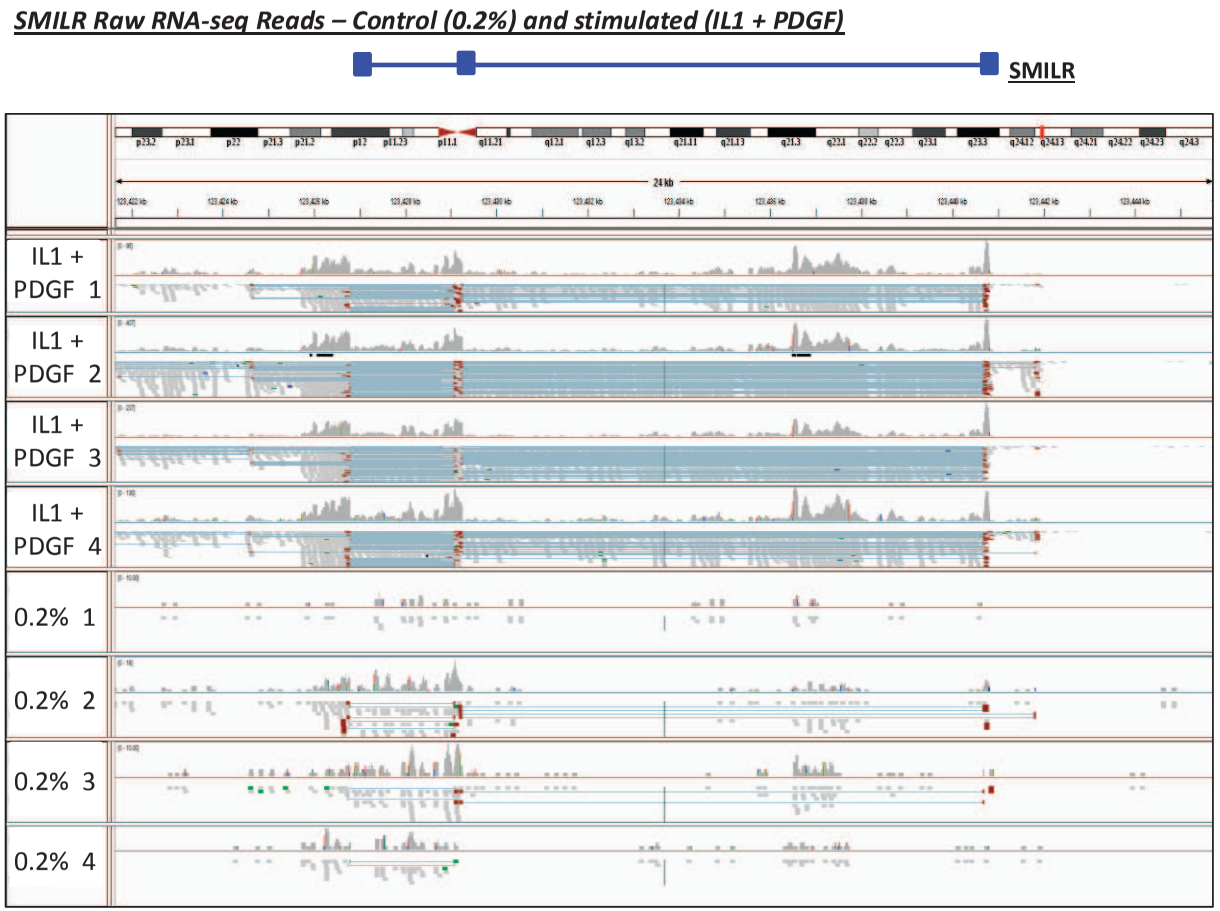

Figure 4-12: Raw sequencing profiles generated utilising tophat files from the RNA-sequencing pipeline and constructed on integrative genome viewer (IGV).
Raw sequencing reads of *SMILR* under both basal and dual stimulated (IL1α + PDGF) conditions n=4 patients.

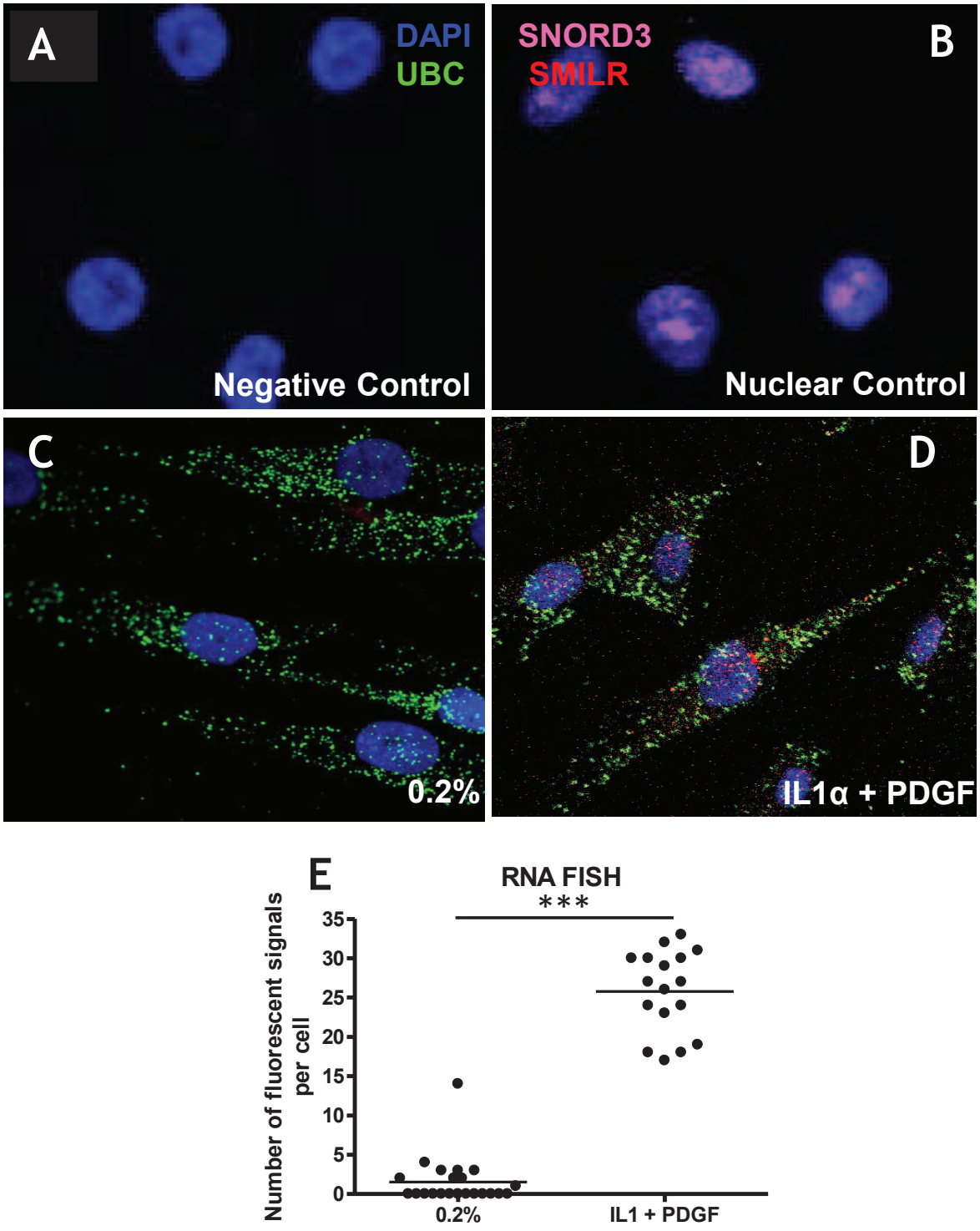

Figure 4-13: Localisation of SMILR.
HSVSMC were quiesced in 0.2 % media for 48 h then stimulated for 72 h in either 0.2 % media or media containing IL1α and PDGF. RNA FISH analysis of *SMILR*, UBC mRNA and nuclear SNORD3 RNA was perfoemed in HSVSMC, Magnification x630 for all panels. **(A):** Negative DAPI control. **(B):** SNORD3 was utilised as a marker of nuclear permeabilisation. **(C):** 0.2 % control conditions. UBC was utilised as a marker of cell border. **(D):** IL1 and PDGF conditions. Blue – DAPI, Pink – SNORD3, Green – UBC and Red- *SMILR*. RNA fish utilises branch tree technology, therefore, one single dot represents one RNA molecule. **(E):** Quantification of *SMILR* molecules per cell in indicated conditions n=22 for 0.2 % and n=17 for IL1α and PDGF treatment. ***P<0.001 vs. 0.2 % control, paired students t test.

4.3.8 Modulation of *SMILR* expression via siRNA and lentivirus

4.3.8.1 Effect of *SMILR* modulation on HSVSMC proliferation

Due to the significant upregulation by PDGF and the close proximity of *SMILR* and *HAS2*, a known SMC proliferative gene, modulation of *SMILR* expression was performed via dicer substrate siRNA (dsiRNA)-mediated knockdown and lentivirus mediated overexpression followed by assessment of HSVSMC proliferation. Initially, expression of the interferon response genes OAS1 and IRF7 were assessed in dsiRNA treated cells, as activation of the interferon pathway has previously been linked to dsiRNA off target effects (Karpala et al., 2005). No effect of dsiRNA transfection on the interferon pathway was observed upon assessment of the response genes OAS1 and IRF7 (Figure 4-14A and B respectively).

25.6

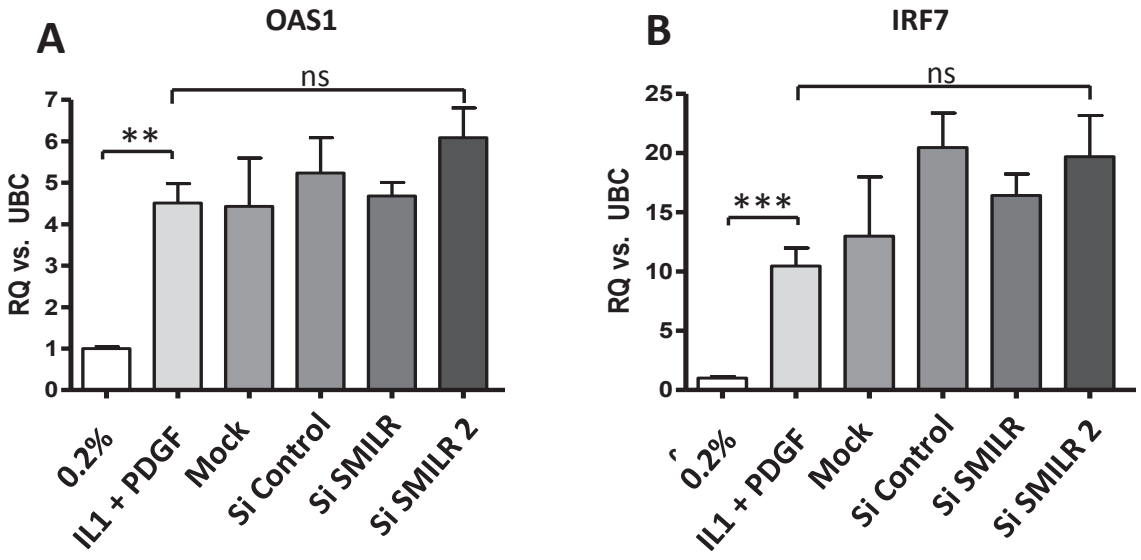

Figure 4-14: DsiRNA effects on interferon pathway.
HSVSMC were transfected with either Lipofectamine alone (mock), control siRNA (SiControl) or siRNA targeting two regions of *SMILR* (SiSMILR and SiSMILR2). Cells were then quiesced in 0.2 % media for 48 h and then stimulated for 48 h in 0.2 % media or media containing IL1α and PDGF. RNA was extracted and qRT-PCR analysis of interferon gamma associated mRNA OAS1 (Panel A) and IRF7 (Panel B) was performed. ** P<0.01 and *** P<0.001 vs 0.2 % controls, one way ANOVA. SiSMILR and SiSMILR2 were not significant when compared to SiControl. One way ANOVA (n=3 patients). RQ= relative quantity.

DsiRNA *SMILR* caused a 51 ± 2 % decrease in *SMILR* expression when compared to dsiControl (P<0.01)(Figure 4-15A). 48 h post stimulation, IL1α and PDGF treatment induced a 34 ± 15 % increase in HSVSMC proliferation compared to control (Figure 4-15B)(P<0.05) and subsequent *SMILR* knock down with dsiRNA, reduced HSVSMC proliferation by 56 ± 15 % (Figure 4-15C) (P<0.01). Results were confirmed through the use of a second dsiRNA targeting an alternative region of *SMILR* (P<0.01) (Figures 4-15D and E).

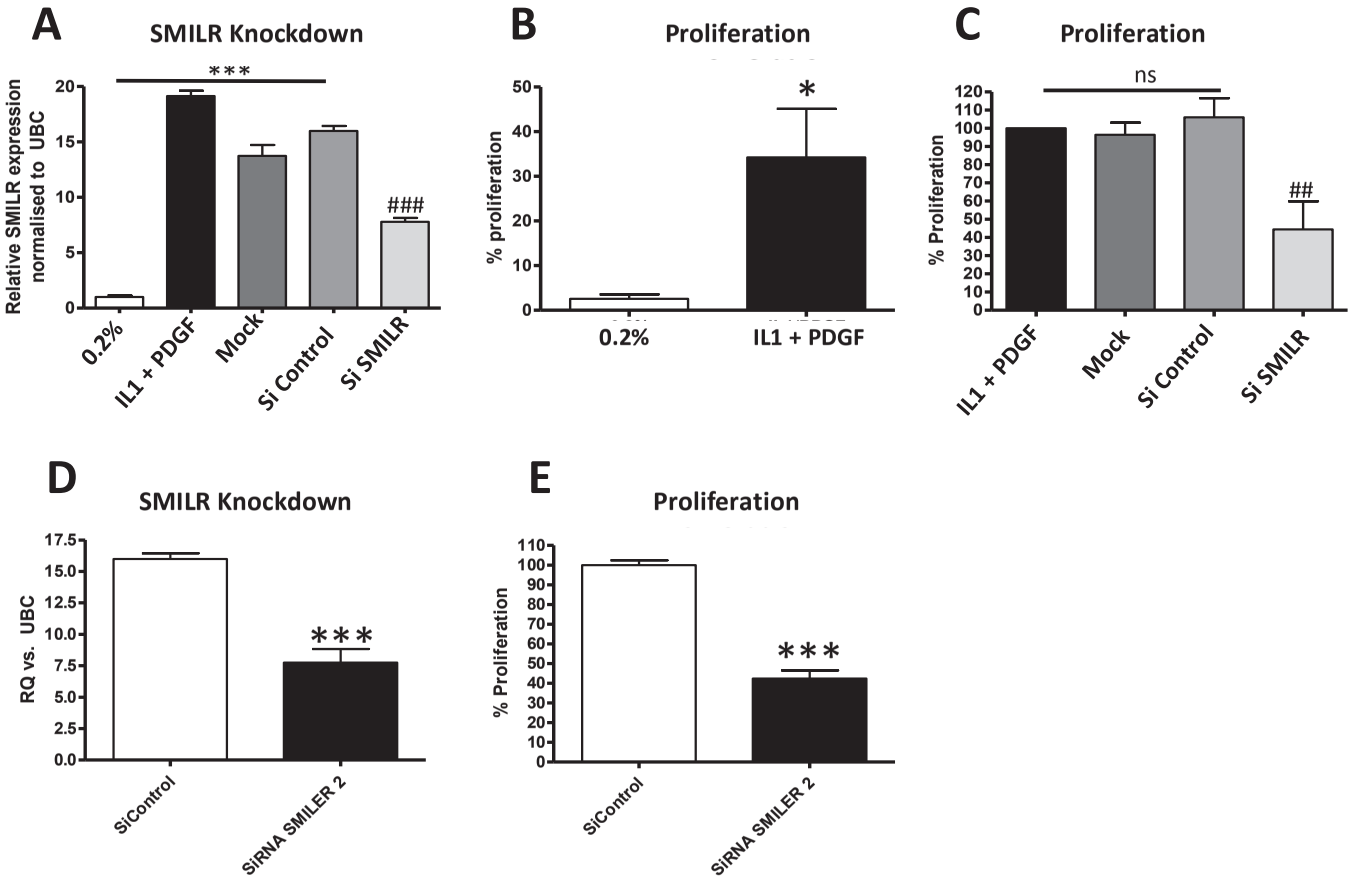

Figure 4-15: Functional Regulation of SMILR via dsiRNA.
For all experiments HSVSMC were quiesced in 0.2 % media for 48 hand then stimulated with IL1α and PDGF for 48 h**. (A):** Proliferation of HSVSMC 0.2 % vs IL1α + PDGF treatment. P<0.05 students t test (n=3). **(B):** Confirmation of the effect of siRNA targeting *SMILR* in HSVSMC using qRT-PCR, representative image of technical

triplicates (n=5 patients) **(C):** IL1α /PDGF induced proliferation classed as 100 % for analysis across patient samples, knockdown of *SMILR* inhibits EdU incorporation in HSVSMC (n=4 patients) 1 way ANOVA vs Si Control. **(D):** Confirmation of siRNA mediated down regulation of *SMILR* using second siRNA targeting a separate sequence of *SMILR*. **(E):** Confirmation of knockdown of *SMILR* using second siRNA. Analysed by students t-test ***P<0.001 vs SiControl.

Additionally the effect of *SMILR* overexpression on SMC proliferation was investigated. HSVSMC were infected with *SMILR* lentivirus or empty control for 24 h prior to stimulation. Infection at a multiplicity of infection of 25 and 50 was utilised as had been previously reported by the lab and had no toxicity effects on HSVSMC. Lentivirus at an MOI of 25 and 50 produced a 5.5 ± 3.5 and 11.4 ± 4.7 fold increase in *SMILR* expression, respectively, when compared to the empty control, (Figure 4-16A). Overexpression produced a dose dependent increase of 1.3 ± 0.3 fold and 1.66 ± 0.5 fold in HSVSMC proliferation respectively (Figure 4-16B), confirming the knock down data.

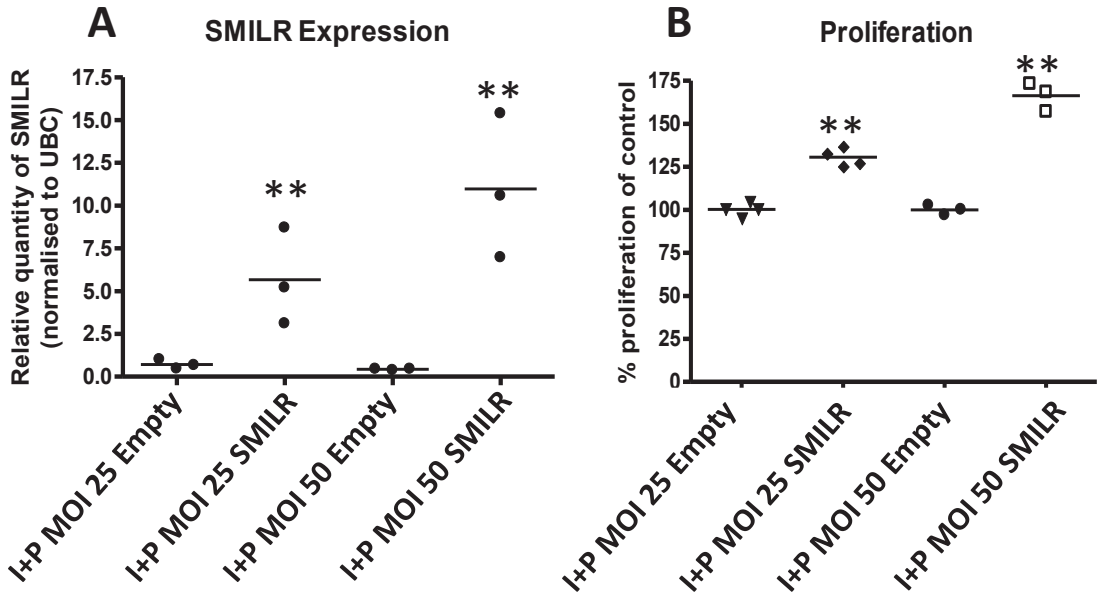

Figure 4-16: Functional Regulation of SMILR by lentivirus.
HSVSMC were infected with lentivirus for 24 h, quiesced for 48 h and stimulated with IL1α and PDGF for 48 h. A: qRT-PCR analysis of *SMILR* expression following infection with either an empty lentivirus or lentivirus containing *SMILR* sequence (at an MOI of 25 (n=4) and MOI 50 (n=3) ***P<0.001 vs. relevant empty control assessed via multiple comparison ANOVA. B: Proliferation of HSVSMC following infection of Lentivirus at an MOI of 25 (n=4) and MOI 50 (n=3) ***P<0.001 vs. relevant empty control assessed via multiple comparison ANOVA.

4.3.8.2 IL1α and PDGF induces transcriptional changes around *SMILR*

The expression of lncRNAs can correlate with the expression of adjacent genes and other RNAs within the genomic locale. The expression of genes and non-coding RNAs within 5 million base pairs of *SMILR*, from *COL14A1* on the forward strand to *FERIL6-AS1* on the reverse strand (Figure 4-17A), were assessed using the RNA-seq data set (Figure 4-17B). Up-regulation of *SMILR* was not associated with a widespread increase in transcriptional activity within the region (Figure 4-17B). However, similar changes in expression in response to HSVSMC stimulation were observed in two proximal transcripts (*HAS2* and *HAS2-AS1*). *SMILR* is located ~750 kbp upstream of *HAS2* on the same (reverse) strand and ~350 kbp from *ZHX2* and ~ 750 kbp from *HAS2-AS1* on the opposite strand of chromosome 8 (Figure 4-17C). The upregulation of *HAS2* was accompanied by an increase in *HAS1* but not *HAS3* following dual stimulation (Figure 4-18A-C). Interestingly, IL1α and PDGF in combination had no effect on *HAS3* expression as IL1α and PDGF have opposing effects on HAS3 expression. In addition to *SMILR*, up-regulation of *HAS2-AS1* was evident following IL1α and PDGF treatment, but not *ZHX1* in the RNA-seq data (Figure 4-18D-F*)*

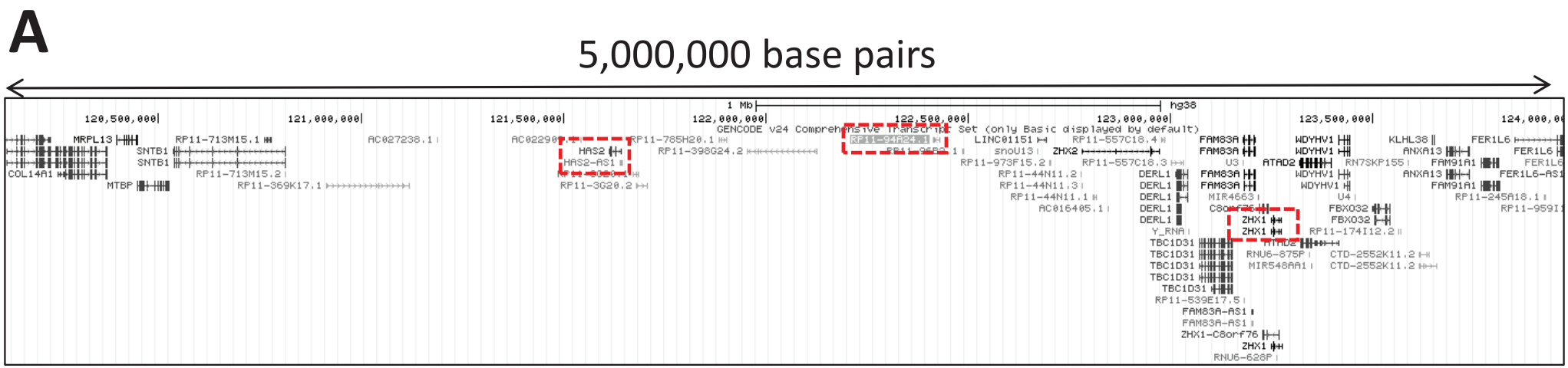
A
5,000,000 base pairs
1 Mb
hg38
120,500,000
121,000,000
121,500,000
122,000,000
122,500,000
123,000,000
123,500,000
124,000,00
GENCODE v24 Comprehensive Transcript Set (only Basic displayed by default)
MRPL13
RP11-713M15.1
AC027238.1
SNTB1
SNTB1
COL14A1
RP11-713M15.2
MTBP
RP11-369K17.1
AC022907.1
RP11-785H20.1
HAS2
HAS2-AS1
RP11-398G24.2
RP11-3G20.2
RP11-94A24.1
LINC01151
RP11-557C18.4
snoU13
ZHX2
RP11-973F15.2
RP11-557C18.3
RP11-44N11.2
RP11-44N11.3
RP11-44N11.1
AC016405.1
DERL1
DERL1
DERL1
DERL1
DERL1
Y_RNA
TBC1D31
TBC1D31
TBC1D31
TBC1D31
TBC1D31
RP11-539E17.5
FAM83A-AS1
FAM83A-AS1
ZHX1-C8orf76
ZHX1
RNU6-628P
FAM83A
FAM83A
FAM83A
FAM83A
MIR4663
C8orf76
ZHX1
ZHX1
RNU6-875P
MIR548AA1
U3
U4
ATAD2
ATAD2
WDYHV1
WDYHV1
WDYHV1
WDYHV1
RN7SKP155
FBXO32
FBXO32
RP11-174I12.2
CTD-2552K11.2
CTD-2552K11.2
KLHL38
ANXA13
ANXA13
FAM91A1
FAM91A1
FER1L6
FER1L6
FER1L6
FER1L6-AS1
RP11-245A18.1
RP11-959I1

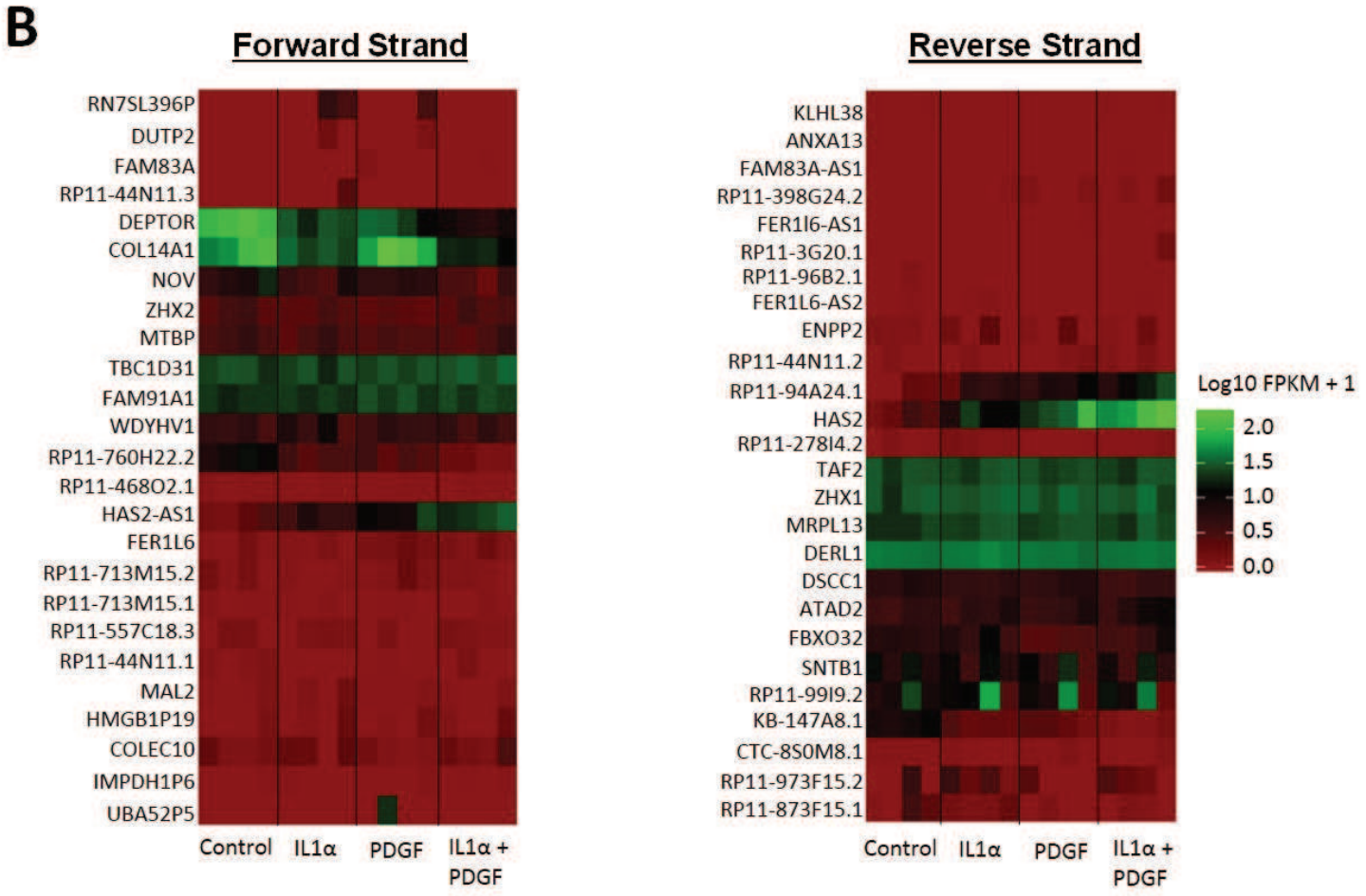
B
Forward Strand
RN7SL396P
DUTP2
FAM83A
RP11-44N11.3
DEPTOR
COL14A1
NOV
ZHX2
MTBP
TBC1D31
FAM91A1
WDYHV1
RP11-760H22.2
RP11-468O2.1
HAS2-AS1
FER1L6
RP11-713M15.2
RP11-713M15.1
RP11-557C18.3
RP11-44N11.1
MAL2
HMGB1P19
COLEC10
IMPDH1P6
UBA52P5
Control
IL1α
PDGF
IL1α + PDGF
Reverse Strand
KLHL38
ANXA13
FAM83A-AS1
RP11-398G24.2
FER1I6-AS1
RP11-3G20.1
RP11-96B2.1
FER1L6-AS2
ENPP2
RP11-44N11.2
RP11-94A24.1
HAS2
RP11-278I4.2
TAF2
ZHX1
MRPL13
DERL1
DSCC1
ATAD2
FBXO32
SNTB1
RP11-99I9.2
KB-147A8.1
CTC-8S0M8.1
RP11-973F15.2
RP11-873F15.1
Control
IL1α
PDGF
IL1α + PDGF
Log10 FPKM + 1
2.0
1.5
1.0
0.5
0.0

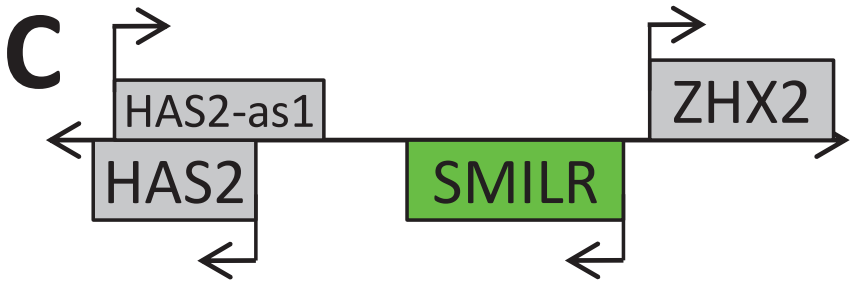

Figure 4-17: Regulation of 5 million base pair region around SMILR.
(A): Schematic view of the 8q24.1 region showing lncRNAs and protein coding genes over the 5,000,000 bp region from Ensemble. SMILI (RP11-94a24.1), HAS2, HAS2-AS1 and ZHX2 are highlighted with red boxes. **(B):** Regulation of protein coding and non-coding genes within the selected region following IL1α and PDGF treatment, heatmap depicts expression of genes found with RNA-seq in 4 patient samples. **(C):** Region containing *SMILR* lncRNA and closest protein coding genes *HAS2* and *ZHX2*.

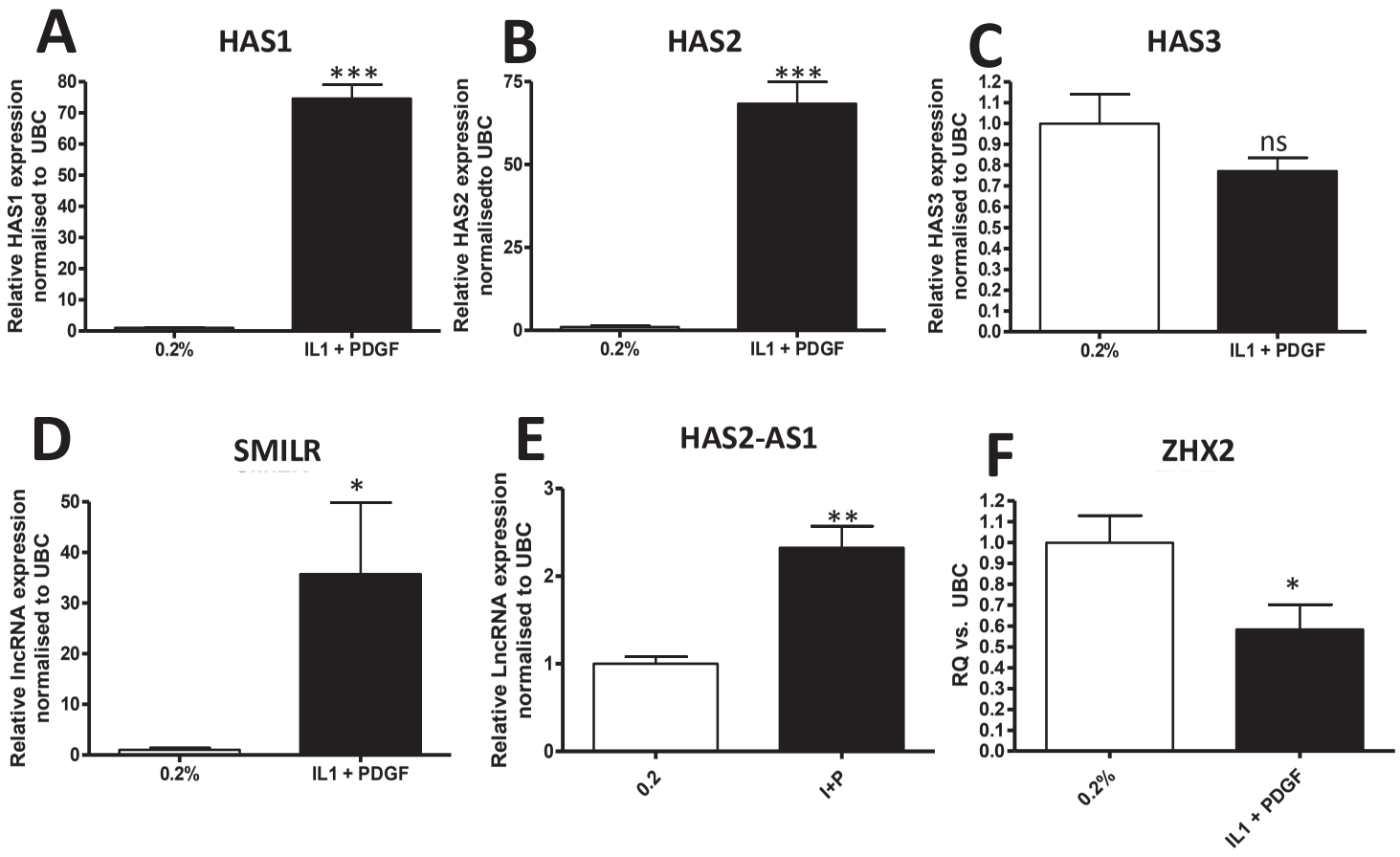

Figure 4-18: qRT-PCR analysis of the transcripts surrounding SMILR.

(Tabas et al.): Expression of proximal gene *HAS2* - modulated in the same manner as *SMILR* with IL1α and PDGF treatment and additional HAS isoforms are differentially modulated by IL1α and PDGF. **(D-F):** Validation of RNA seq data for lncRNAs *SMILR*, HAS2-AS1 and ZHX2 mRNA by qRT-PCR (n=3), * P<0.05, **P<0.01 and ***P<0.001 vs. 0.2 % control, students t-test. All graphs show lncRNA or mRNA levels relative to 0.2 % conditions (Relative Quantity, RQ).

4.3.8.3 Effect of siRNA treatment on neighbouring gene expression

As stated previously, lncRNAs can modulate the expression of nearby protein coding genes. Thus, the expression of proximal genes *HAS2*, *ZHX2* and *HAS2-AS1* were determined following *SMILR* knockdown. RNAi-mediated knockdown of *SMILR* significantly altered levels of *HAS2* mRNA. However, no change in the *HAS2-AS1* lncRNA or the *ZHX2* gene was observed via qRT-PCR (Figure 4-19A-C). Additionally, no effect on *HAS1* or *HAS3* expression was observed while utilising *SMILR* siRNA, indicating that the effect of *SMILR* knockdown is specific to *HAS2* and not all isoforms of HAS (Figure 4-19D and E). Results were confirmed using a second siRNA targeting an alternative region of the *SMILR* transcript(Figure 4-19F-H).

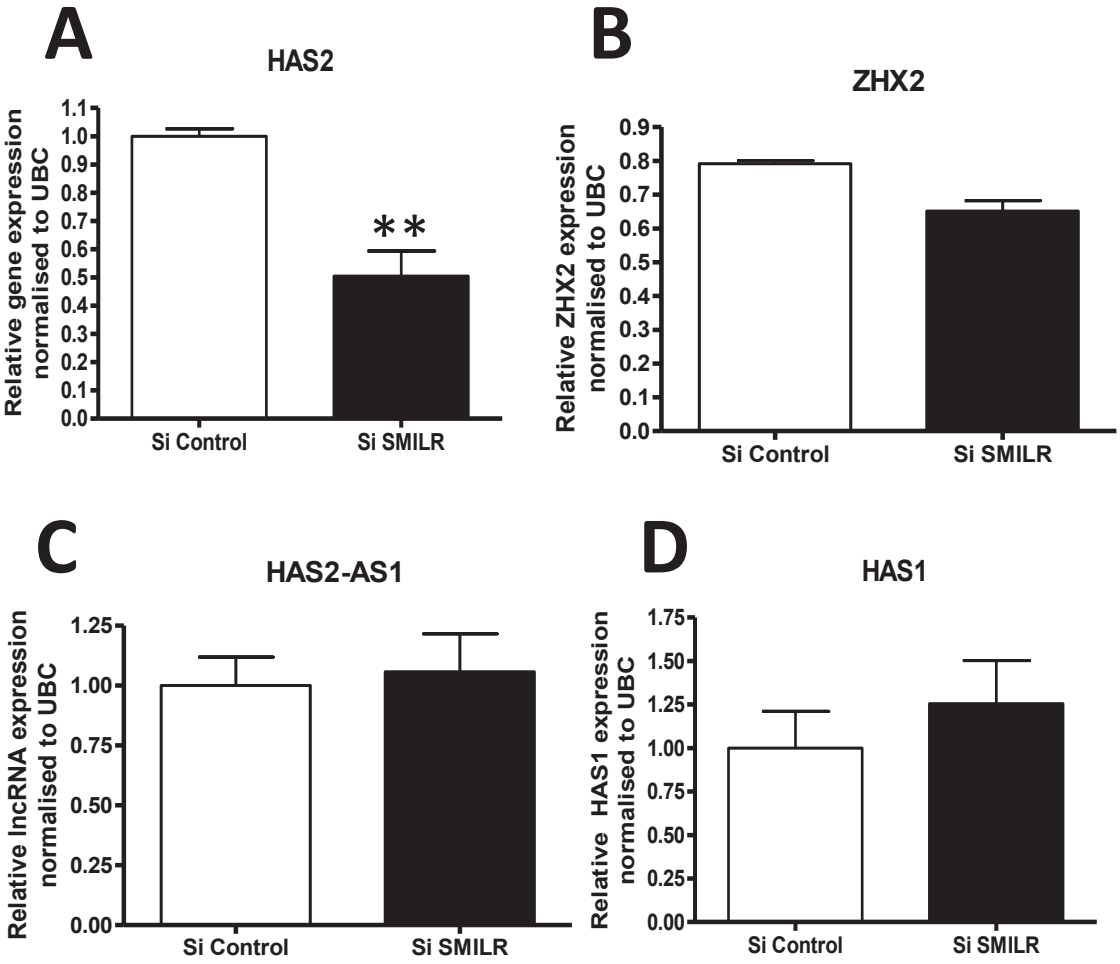
A
HAS2
Relative gene expression normalised to UBC
1.1
1.0
0.9
0.8
0.7
0.6
0.5
0.4
0.3
0.2
0.1
0.0
**
Si Control
Si SMILR
B
ZHX2
Relative ZHX2 expression normalised to UBC
0.9
0.8
0.7
0.6
0.5
0.4
0.3
0.2
0.1
0.0
Si Control
Si SMILR
C
HAS2-AS1
Relative lncRNA expression normalised to UBC
1.25
1.00
0.75
0.50
0.25
0.00
Si Control
Si SMILR
D
HAS1
Relative HAS1 expression normalised to UBC
1.75
1.50
1.25
1.00
0.75
0.50
0.25
0.00
Si Control
Si SMILR

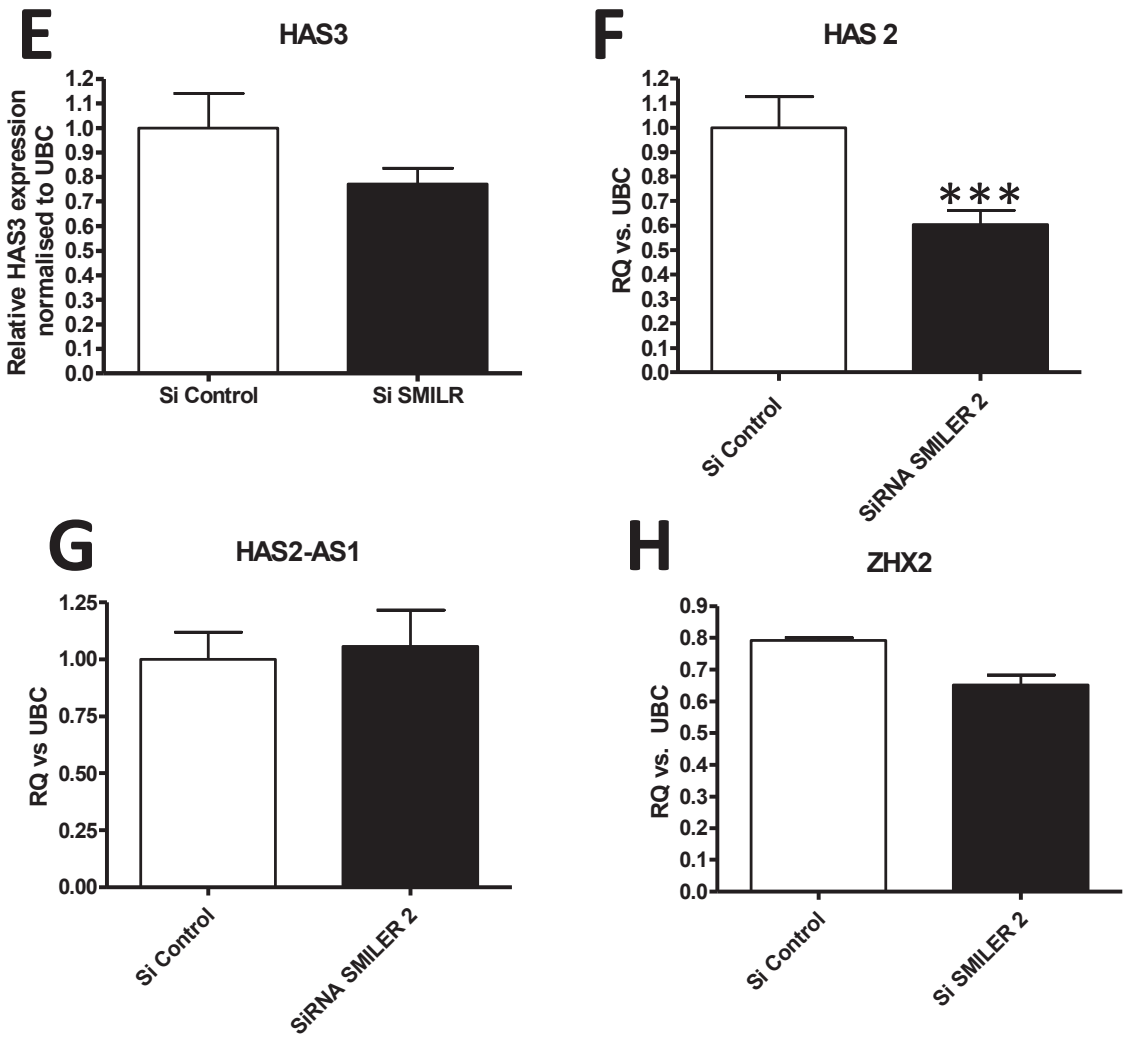

Figure 4-19: SMILR regulates proximal gene HAS2 on chromosome 8.
(A): Inhibition of *SMILR* expression via dsiRNA treatment significantly inhibits HAS2 expression determined by qRT-PCR **P<0.005 vs. Si Control. One way-ANOVA. **(B-E):** *SMILR* inhibition had no effect on proximal genes ZHX2 or HAS2-AS1 nor additional HAS isoforms, HAS1 or HAS3 (n=3). One way ANOVA. **(F-H):** all results confirmed utilising a second siRNA targeting an additional region of *SMILR*.

4.3.8.4 Effect of Lentivirus on neighbouring gene expression

Due to the significant effect of dsiRNA on *HAS2*, it was investigated whether overexpression of *SMILR* could produce the inverse effect. Lentiviral mediated overexpression produced a 6.1 ± 2.3 and a 11.3 ± 2.0 fold increase in *SMILR* expression at an MOI of 25 and 50 respectively (Figure 4-20A). However lentiviral up regulation of *SMILR* had no effect on *HAS1* (Figure 4-20B) , *HAS2* (Figure 4-20C) , *HAS3* (Figure 4-20D) or *HAS2-AS1* expression (Figure 4-21E).

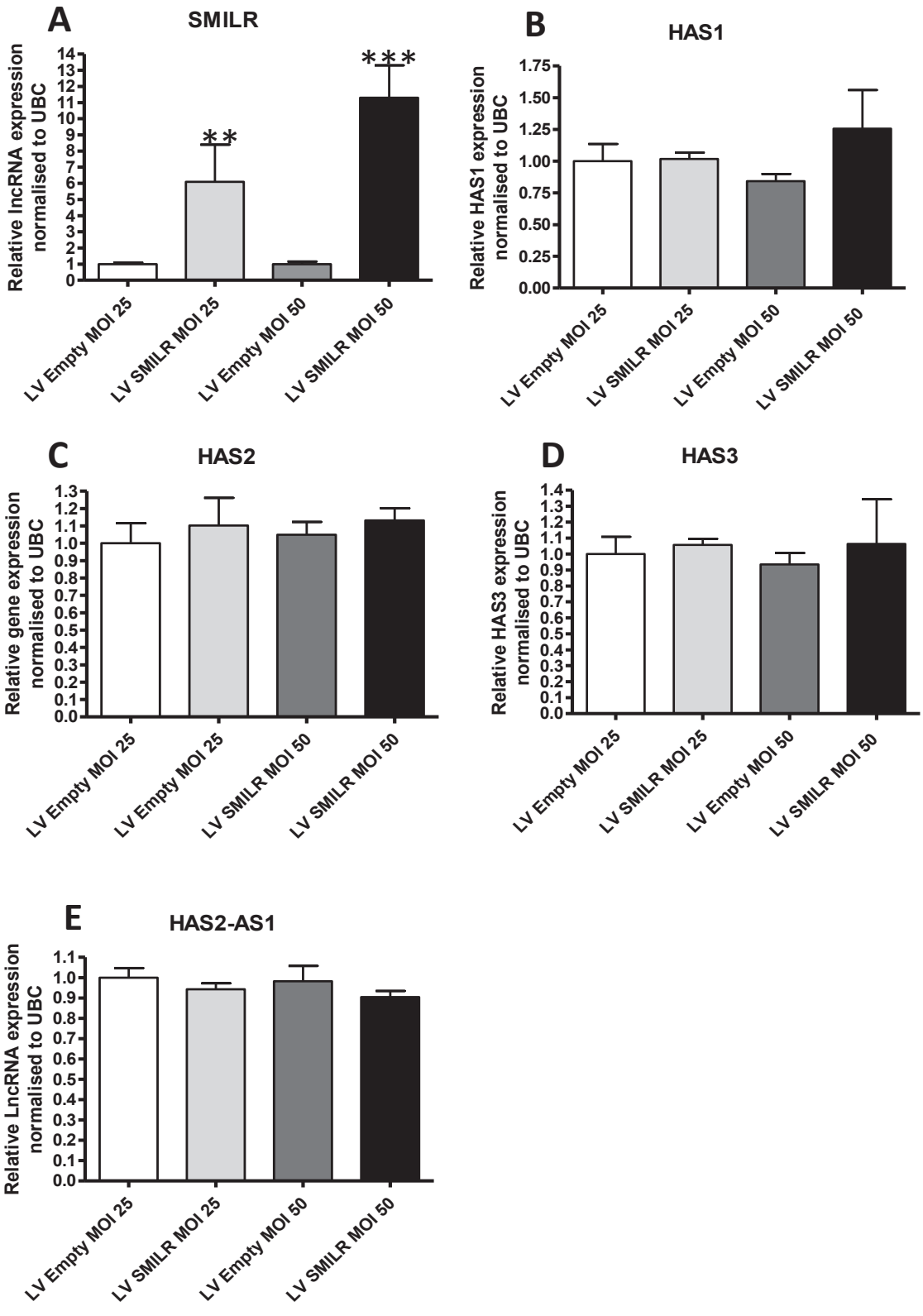

Figure 4-20: Effect of SMILR overexpression on proximal genes.
HSVSMC were infected with lentivirus for 24 h, quiesced for 48 h in 0.2 % media and stimulated with IL1α and PDGF for 48 h. qRT-PCR analysis of *SMILR*, HAS1-3 and HAS1-AS1expression was performed following infection with either an empty lentivirus or lentivirus containing *SMILR* sequence (at an MOI of 25 (n=4 patients) and MOI 50 (n=3 patients). All graphs show mRNA or lncRNA levels relative to appropriate Empty LV control and normalised to UBC. .

4.3.8.5 HAS2 and HAS2-AS1 specific knockdown

Due to the effect of *SMILR* knockdown on *HAS2* expression, it was determined if *HAS2-AS1* or *HAS2* knockdown regulated genes located within the region. Similar to the effect observed with *SMILR*, knockdown of *HAS2-AS1* greatly reduced *HAS2* expression (Figure 4-21 A and 4-21B). However, the reverse experiment utilising *HAS2* knockdown, did not affect the expression of *HAS2-AS1*. Neither *HAS2* nor *HAS2-AS1* silencing modulated *SMILR* expression levels (Figure 4-21C).

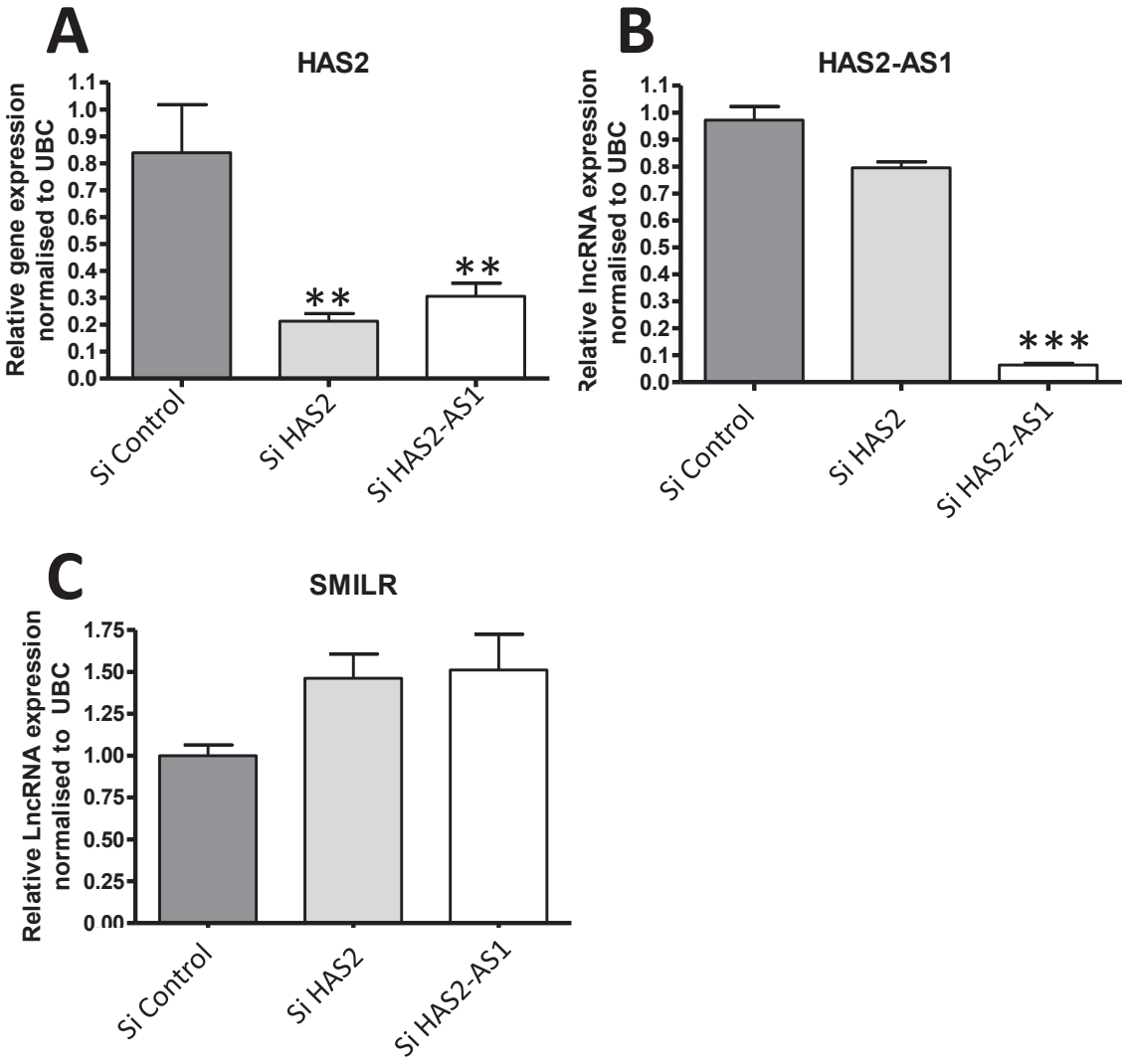

Figure 4-21: Effect of HAS2 and HAS2-AS1 knockdown on SMILR expression.
HSVSMC were transfected with siRNA control (dark grey bars) or siRNA to HAS2 (light grey bars) or HAS2-AS1 (white bars) and cells quiesced for 48 h and stimulated with IL1α and PDGF for 48 h**(A):** qRT-PCR expression of HAS2. **(B):** qRT-PCR analysis of HAS2-AS1. **(C):**qRT-PCR analysis of SMILR. (n=2), graphs indicate representative graph showing technical triplicates. All samples are normalised to UBC housekeeper and are relative to SiControl. ** P<0.01 and ***P<0.001 vs. Si Control assessed via one way ANOVA.

4.3.9 Release of lncRNA into the media – validation of c.elegans probe, RNA extraction technique and RNA release.

MicroRNAs have been reported to be secreted from cells as a means of cell to cell communication (Glynn et al., 2013). To investigate whether HSVSMCs release *SMILR*, a method commonly utilised to evaluate the expression of secreted miRNAs was modified (Morley-Smith et al., 2014). As no endogenous housekeeping/control gene was stably expressed across all conditions in this study, an exogenous control was added in order to monitor extraction efficiency and to normalise data. Total RNA from *C.elegans* was used as a spike-in RNA and the *C.elegans* gene *ama-1* (encoding polymerase II) was chosen as a control for its high constitutive expression (see Chapter 2- Sections 2.17). In order to optimise the protocol different quantities of *C.elegans* RNA were spiked in and a dose response effect was observed (Figure 4-22A). The quality of the amplicon was assessed via analysis of melting curves (Figure 4-22B) and subsequent visualisation on agarose gel (Figure 4-22C). This showed a single amplification product corresponding to the cDNA fragment of *ama-1*. Based on the correlation observed between quantity of spike-in and *ama-1* expression (Figure 4-22D), we utilised 75 ng in all subsequent extractions. This amount allowed reproducibility of our method, with the Ct values of *ama-1* being 29.4 ± 0.3 across 5 separate extractions in non-conditioned media (Figure 4-22E).

Interestingly, *SMILR* was detected at low levels in media from quiesced HSVSMCs and those stimulated by either PDGF or IL1α alone, while conditioned media obtained from HSVSMC stimulated by PDGF and IL1α in combination contained significantly higher levels of *SMILR* (4.8 ± 4.5 fold) (Figure 4-23), consistent with the increased intracellular expression of *SMILR* following co-stimulation of HSVSMC. Thus, treatment with PDGF and IL1α increased intracellular and released levels of *SMILR*.

Additionally, experiments were performed to identify if *SMILR* was encapsulated within exosomes or microvesicles. Two different isolation techniques were employed: ultracentrifugation, to remove cell debris, and an exosome isolation kit. Figure 4-24 A and B confirms the presence of microvesicles and exosomes using Nanosight technology and the expression of the previously described miR-143 within the exosomes/MV (Deng et al., 2015). The data highlights the

expression of *SMILR* restricted to exosome free media (Figure 4-24C) and inability to detect *SMILR* expression in the exosomes/MV compartment using both techniques of isolation. This observation was been confirmed by agarose gel electrophoresis (Figure 4-24D). Primer melting curves are also shown in Figure 4-24E. The data confirms that *SMILR* is secreted into the media and located in a non-exosome/MV fraction. This could possibly be through interaction with specific membrane channels but requires additional experimentation.

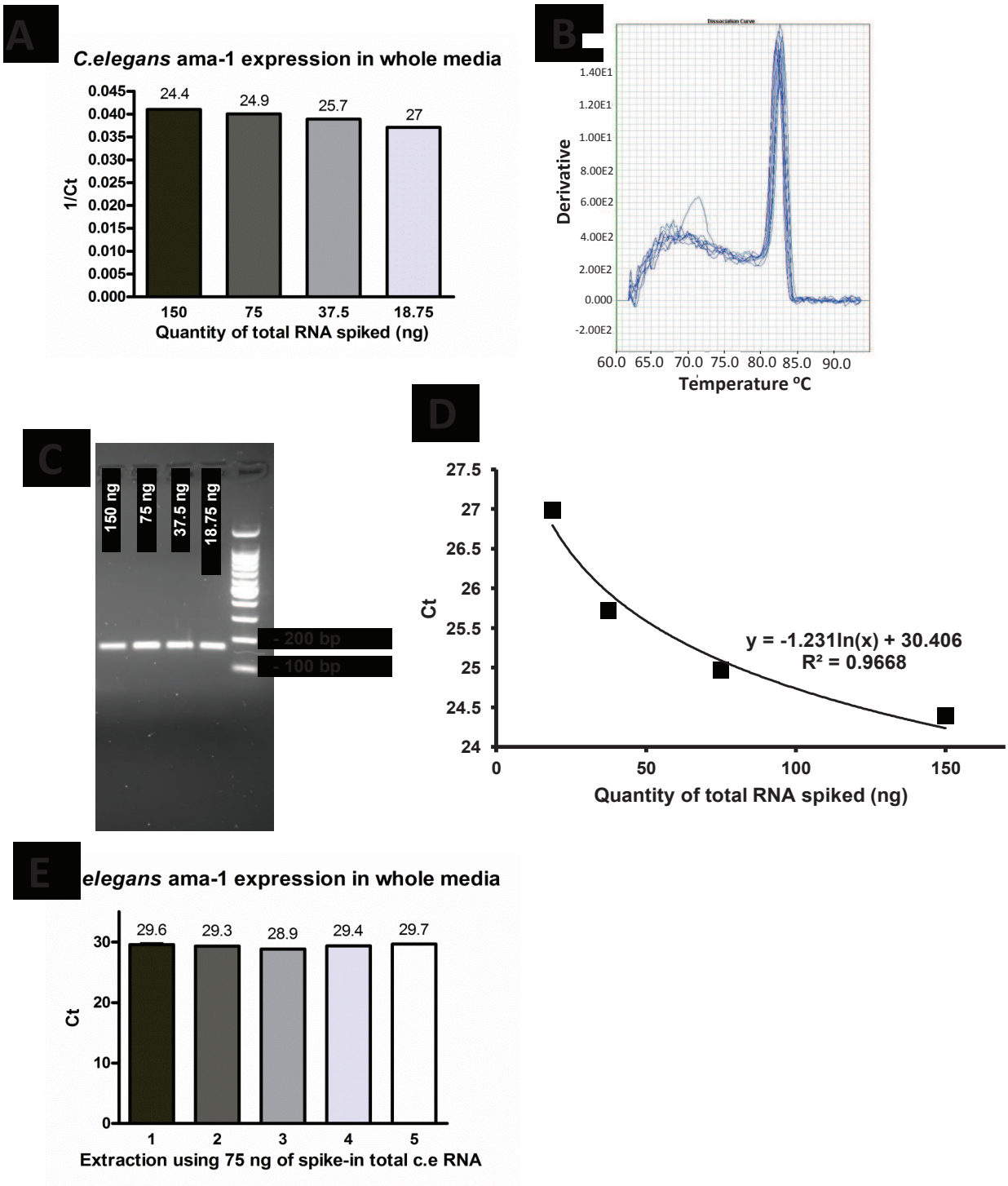

Figure 4-22: Spike-in method of C.elegans total RNA in whole HSVSMC media.
(A): Dose response effect of *C.elegans ama-1* expression. Expression determined by qRT-PCR and results displayed as 1/Ct. Number at the top of each histogram corresponds to Ct values. **(B):** Specificity of products analysis by melting curve. **(C):** Specificity of products analysed using agarose gel. The cDNA amplicon size has been resolved by migration on a 2 % agarose gel using 100 bp ladder. **(D):** Correlation between quantity spike-in and *ama-1* expression. *C.elegans ama-1* expression follow a logarithmic function: y=-1.231ln(x)+30.406 with a coefficient of correlation r^2=0.9668. **(E):** Reproducibility of the technique. Following RNA extraction after 75 ng of spike-in total *C.elegans* RNA, *ama-1* expression was determined by qRT-PCR and the results have been displayed as Ct.

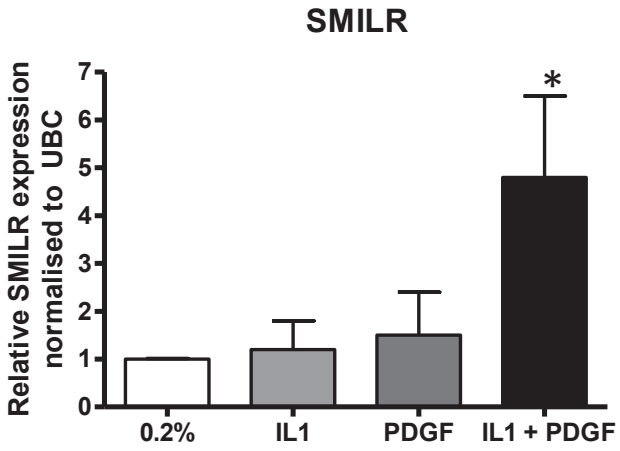

Figure 4-23: Release of SMILR detected in conditioned media.
HSVSMC were quiesced in 0.2 % media for 48 h and stimulated with 0.2 %, IL1α, PDGF or a combination of both of 72 h. Conditioned media was collected and *SMILR* expression assessed via qRT-PCR analysis. 1 way ANOVA * $P<0.05$ vs. 0.2 % (n=5 patients).

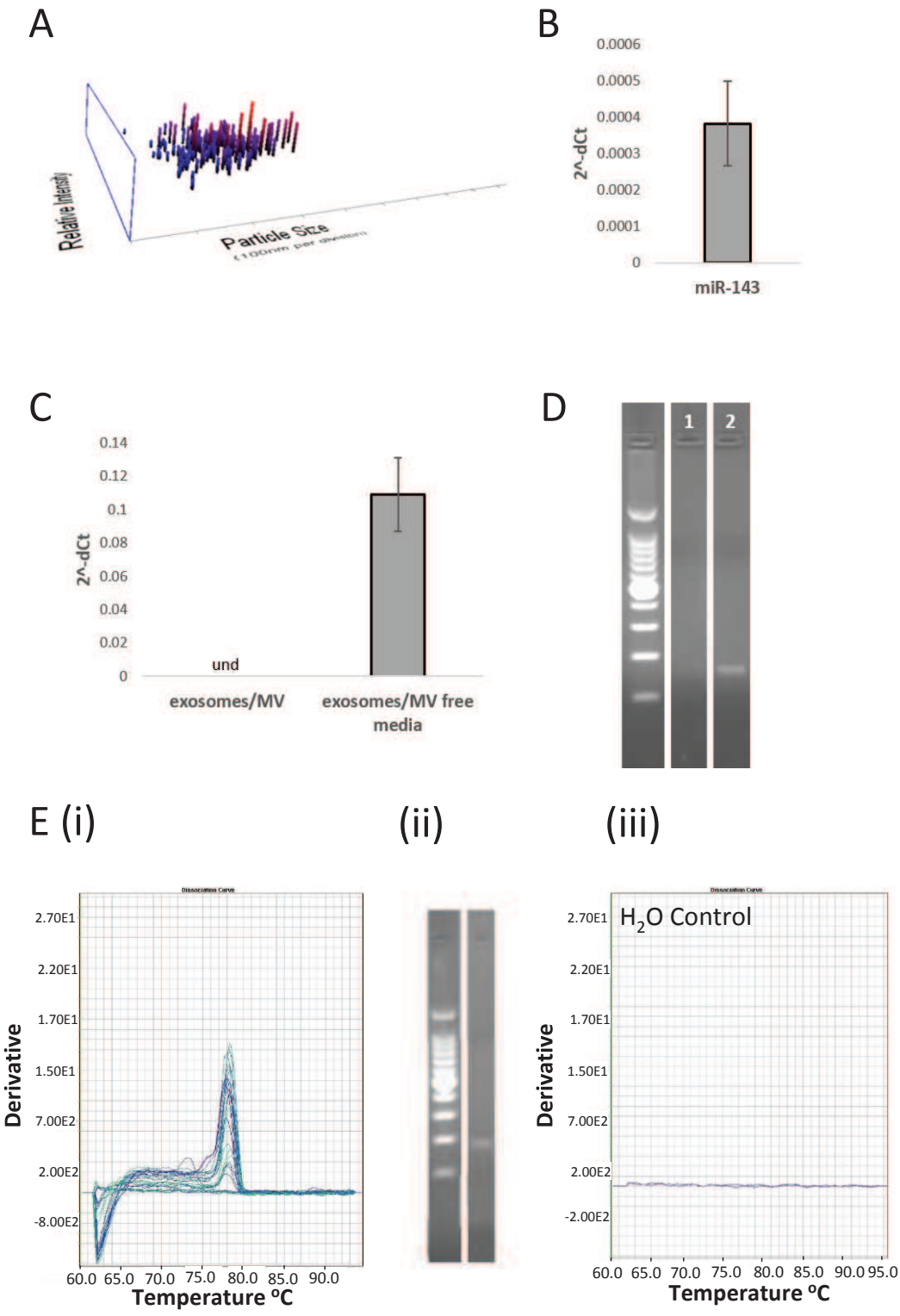

Figure 4-24: Exosome isolation from HSVSMC conditioned media.
(A): Size evaluation using the Nanosight of exosomes and MV isolated using the Total exosome isolation kit from 0.2 % conditioned media. Sizes obtained between 70 and 600 nm. **(B):** Quantification of miR-143 in exosomes/MV isolated using the Total exosome isolation kit from 0.2 % conditioned media. **(C):** *SMILR* expression analysed by qRT-PCR in exosomes/MV and exosomes/MV free media compartment from IL-1α + PDGF conditioned media. **(D):** Agarose gel of qRT-PCR products obtained in C; 1: exosomes/MV compartment, 2: exosomes/MV free media. **(Ei):** melting curves obtained from SMILR primer set in conditioned media. **ii)** Gel electrophoresis image of *SMILR* primer set in conditioned media and **iii)** Melt curves of the negative control water samples obtained by qRT-PCR using the SMILR primer set.

Additionally, *SMILR* release following lentiviral overexpression in IL1α and PDGF treated cells was assessed. Lentiviral overexpression resulted in a 11.3 ± 2.0 fold increase in intracellular *SMILR* RNA. However, only a marginal (not significant) increase was observed within conditioned media analysed from infected cells (Figure 4-25A). When this media was transferred onto additional quiesced cells, no change in proliferation was detected (Figure 4-25B). This may suggest that the release of *SMILR* is under stringent control mechanisms and simply increasing *SMILR* expression via a lentiviral approach is not sufficient to induce the additional release of this lncRNA from the cells. In addition, these cells were stimulated with IL1α and PDGF, which strongly enhances *SMILR* expression in HSVSMC. The secretory machinery may have been saturated with the high levels of lncRNA within the cytoplasm. This has previously been demonstrated with microRNA where high levels of miR, via overexpression with microRNA mimics, saturated the exportin-5 pathway of endogenous miRNAs (Soifer et al., 2007, Grimm et al., 2006).

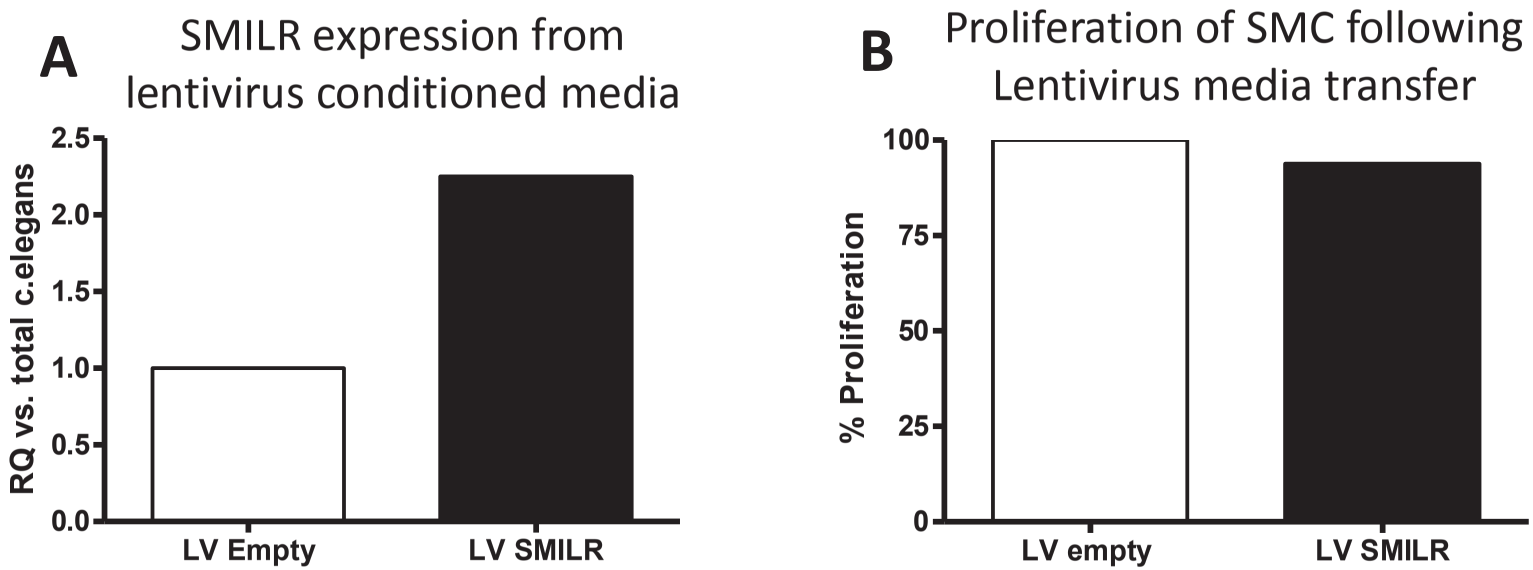

Figure 4-25: SMILR expression from lentivirus conditioned media and transfer of media onto quiescent cells.

HSVSMC were infected with lentivirus for 24 h, quiesced for 48 h and stimulated with IL1α and PDGF for 72 h. Media was collected and qRT-PCR analysis of *SMILR* performed from RNA collected from conditioned media (Panel A) (n=2). Additionally this media was transferred onto HSVSMC that had been quiesced in 0.2 % media for 48 h and proliferation of these cells was assessed following 48 h incubation with media (Panel B).

4.3.10 *SMILR*-protein pulldown to determine protein interacting partners

New lncRNAs are rapidly being uncovered, however, their mechanism of action remains to be elucidated. As mentioned in section 4.3.5, lncRNA *SMILR* is localised to both the nucleus and cytoplasm of HSVSMCs. Due to the significant reduction in HAS2 mRNA expression following treatment with dsiRNA targeting *SMILR*, but lack of effect utilising *SMILR* lentivirus, it is proposed that, in the nucleus, *SMILR* acts in *cis* to modulate HAS2 expression. The mechanism of action of *SMILR* in the cytoplasm remained unknown. RNA pull-down assays are preliminary RNA-centric *in vitro* methods that enable the identification and characterisation of various proteins which interact with a given lncRNA of interest. We therefore performed optimisation and refinement of known RNA pulldown protocols to identify *SMILR* interaction protein partners.

4.3.10.1 Confirmation of *SMILR* RNA following T7

Initially lncRNA probes were synthesised and labelled with the high affinity tag, desthio-biotin. As described in the materials and methods section- Chapter 2 – Section 2.21.1 a T7 promoter sequence was added to the 5' end of *SMILR* DNA through the utilisation of specific T7 primers and DNA polymerase. *SMILR* RNA probes were generated via T7 conversion of plasmid DNA, containing the full length transcript of *SMILR*, into RNA. The T7 RiboMAX™ Express Large Scale RNA Production System is an *in vitro* transcription system designed for consistent production of milligram amounts of RNA in a short amount of time. Provided with the kit is a T7 positive control: pGEM® Express Positive Control Template DNA. This positive control produces transcripts that are 1.1kb and 2.3kb in length. In order to ensure that the correct transcript was being generated, gel analysis was performed after T7 conversion of plasmid DNA to RNA. As shown in Figure 4-26, biotinylated *SMILR* was identified at ~1kb whilst the biotinylation control was evident as 2 bands: one at 2.3kb and one at 1.1kb. This confirmed that the T7 kit was working efficiently.

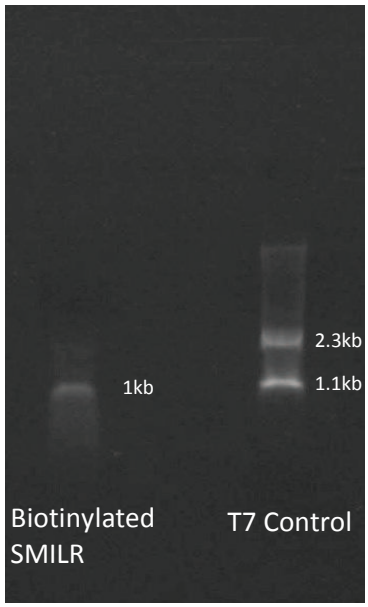

Figure 4-26: Gel product after T7 transcription.
A T7 promoter sequence was added to the 5' end of SMILR DNA via utilisation of specific T7 primers and DNA polymerase. SMILR DNA was converted to RNA through the utilisation of the T7 RiboMAX™ Express Large Scale RNA Production System. The generated RNA for SMILR was observed at 1kb and the positive pGEM was correctly identified at 2.3 kb and 1.1 kb.

4.3.10.2 Confirmation that *SMILR* was biotinylated

The resultant RNA, generated from T7 transcription, was then 3'-biotinylated with the Pierce Desthiobiotinylation kit (ThermoScientific). This kit utilises the T4 restriction enzyme to add a destiobiotin molecule onto the 3' end of RNA transcripts. The kit also provides a negative unlabelled RNA with the sequence 5´-CCUGGUUUUUAAGGAGUGUCGCCAGAGUGCCGCGAAUGAAAAA-3´ and a positive pre-biotinylated control with the sequence 5´ UCCUGCUUCAACAGUGCUUGG ACGGAAC-3´-Biotin. Following utilisation of the kit for biotinylation of *SMILR*, biotinylation had to be confirmed. Biotinylation products were spotted onto neutral membrane along with the negative and positive control sample provided with the kit. The negative control lacked the 3' end biotinylation signal, while the positive control was pre biotinylated. Membranes were cross linked to bind the RNA to the membrane and final incubated with a fluorescently tagged streptavidin-GFP licor antibody and imaged on the licor imaging system. As shown in Figure 4-27, *SMILR* produces a fluorescent signal indicating that biotin is present. Serial dilutions of the biotinylated product produce a lower fluorescent signal, while negative control samples lack any specific signal. This highlights that *SMILR* is indeed biotinylated.

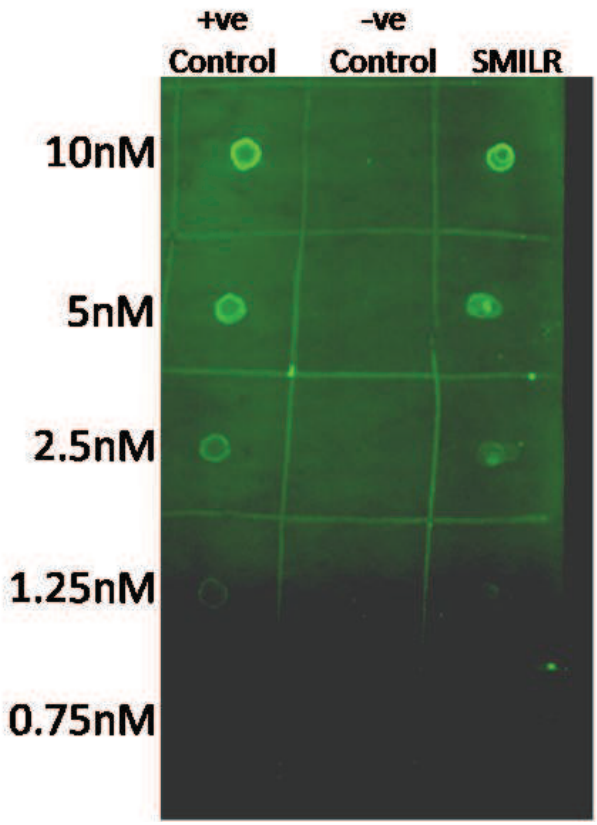

Figure 4-27: Confirmation of SMILR biotinylation.
RNA generated from T7 transcription was biotinylated utilising the 3'-biotinylated with the Pierce Desthiobiotinylation kit (ThermoScientific). Biotinylation was performed according to manufacturer's instructions and the biotinylated RNA was spotted onto neutral membrane at the concentrations indicated in order to confirm biotinylation. Negative and positive controls, provided in the kit, were also spotted. Negative control is an RNA molecule that lacks the 3' biotin and the positive control is a pre-biotinylated RNA. Membranes were cross linked to bind the RNA to the membrane and incubated with a streptavidin conjugated licor antibody (1:10,000). Green spots indicate biotinylation.

4.3.10.3 Differential proteins Identified during mass spec analysis

Desthiobiotinylated RNAs were incubated with streptavidin-bound magnetic beads from Pierce Magnetic RNA-Protein Pull-Down Kit (Thermo Scientific) as per the manufacturer's protocol. Bead only controls served as a negative control to identify any 'sticky proteins' that bound non-specifically. Beads only and beads containing bound *SMILR* were incubated with protein lysates extracted from IL1α and PDGF treated HSVSMC. Two RNA-pulldowns were performed utilising a low and high stringent wash as detailed in the materials and methods- Chapter 2 – Section 2.21.7. Following pulldown experiments utilising biotinylated *SMILR* as bait, mass spectrometry analysis, performed on a Q Exactive mass spectrometer, was utilised to analyse any potential *SMILR* binding partners. Mass spectrometry 'hits' were analysed for the number of unique peptides identified and only those with two or more unique peptides were considered to be true hits. Data analysis was performed using the MaxQuant software platform (ver. 1.5.2.8) and searches were conducted against a Human Uniprot database. Analysis was performed in order to identify proteins that were identified in both the low and high stringency pulldown (Table 4-1), those identified in only the low stringency pulldown (Table 4-2) and those only identified in the high stringency pulldown (Table 4-3). As described above the low and high stringency related to the salt levels present during the pulldown as described Chapter 2 – Section 2.21.7. The low stringency lacked salt and as such would allow a greater number of proteins to bind, whereas, the high salt and high stringent buffer would be more selective, thus removing the possibility of binding of non-specific proteins.

Mass spectrometry analysis following *SMILR* pulldown identified 17 proteins only identified in the less stringent and 13 proteins from only the more stringent pulldown. However, only 8 proteins were identified that was present in the *SMILR* pulldown from both the low and high stringent conditions and absent in the all control sample. Notably, 7 out of the 8 proteins, TPM2, RBMS1, IA36, IB50, HNRH2, PABP2 and STRBP exhibited additional isoforms that were identified in both the control and *SMILR* pulldowns. Thus the only unique protein to be identified under both stringency conditions was Staufen1 (STAU1). Interestingly 6 unique peptides relating to STAU1 were identified in the low stringent *SMILR* pulldown and 0 unique peptides in the control pulldown (Figure

4-28) and mass spectrometry analysis of the more stringent pulldown identified 11 unique peptides in the *SMILR* pulldown and 0 in the control pulldown. This increase in unique peptides in the stringent pulldown is often seen as there are fewer peptides bound therefore less peptides to mask the STAU1 signal. Interestingly STAU1 has previously been shown to bind a small group of lncRNAs and has been recently shown to induce mRNA decay. Further reverse pulldowns utilising tagged staufen1 as bait and the assessment of *SMILR* enrichment will be required to validate these results.

.

Table 4-1: Proteins identified from both low and high stringency pulldown conditions.
Destiobiotinylated *SMILR* was bound to streptavidin magnetic beads and incubated with protein lysates obtained from IL1α and PDGF stimulated HSVSMC. Beads only served as the negative control in order to identify any non-specific binding of proteins. Mass spec 'hits' were analysed for the number of unique peptides identified and only those with two or greater were considered to be true hits. The coloured bars indicate the number of unique peptides identified per protein (provided in the 1st column) for the low and high stringent pulldowns. The low stringent pulldowns had no salt added and as such, would allow a greater number of proteins to bind. The high stringent pulldown contained higher levels of salt allowing only more specific binding to occur. The control (bead only) columns indicate how many unique peptides were identified in the control samples. The full protein name is provided in the very right hand column. This table represents proteins identified that had at least 2 unique peptides in both the low and high stringent pulldowns and 0 peptides identified in either of the control, bead only pulldowns.

	Low Stringent SMILR	Low Stringent Control	High Stringent SMILR	High Stringent Control	Total peptides Identified	Full Protein Name
STAU1_HUMAN	6	0	11	0	17	Staufen homolog 1
TPM2_HUMAN	4	0	3	0	7	Isoform 3 of Tropomyosin beta chain
RBMS1_HUMAN	2	0	2	0	4	Isoform 2 of RNA-binding motif, single-stranded-interacting protein 1
1A36_HUMAN	3	0	3	0	6	HLA class I histocompatibility antigen, A-36 alpha chain
1B50_HUMAN	5	0	3	0	8	HLA class I histocompatibility antigen, B-50 alpha chain
HNRH2_HUMAN	4	0	3	0	7	Heterogeneous nuclear ribonucleoprotein H2
PABP2_HUMAN	5	0	2	0	7	Isoform 2 of Polyadenylate-binding protein 2
STRBP_HUMAN	3	0	5	0	8	Isoform 2 of Spermatid perinuclear RNA-binding protein

Table 4-2: Protein identified in low stringency pulldown alone.
Destiobiotinylated *SMILR* was bound to streptavidin magnetic beads and incubated with protein lysates obtained from IL1α and PDGF stimulated HSVSMC. Beads only served as the negative control in order to identify any non-specific binding of proteins. Mass spec 'hits' were analysed for the number of unique peptides identified and only those with two or greater were considered to be true hits. The coloured bars indicate the number of unique peptides identified per protein (provided in the 1st column) for the low and high stringent pulldowns. The low stringent pulldowns had no salt added and as such, would allow a greater number of proteins to bind. The high stringent pulldown contained higher levels of salt allowing only more specific binding to occur. The control (bead only) columns indicate how many unique peptides were identified in the control samples. The full protein name is provided in the very right hand column. This table represents proteins identified that had at least 2 unique peptides in the low stringent pulldown only and 0 peptides identified in either of the control, bead only pulldowns.

	Low Stringent SMILR	Low Stringent Control	High Stringent SMILR	High Stringent Control	Total peptides Identified	Full Protein Name
FADS1_HUMAN	2	0	0	0	2	Fatty acid desaturase 1
ANR17_HUMAN	2	0	0	0	2	Isoform 6 of Ankyrin repeat domain-containing protein
TOP1_HUMAN	3	0	0	0	3	DNA topoisomerase 1
MYH7_HUMAN	2	0	0	0	2	Myosin-7
CLH2_HUMAN	11	0	0	0	11	Isoform 2 of Clathrin heavy chain 2
RL19_HUMAN	2	0	0	0	2	60S ribosomal protein L19
RAB32_HUMAN	2	0	0	0	2	Ras-related protein Rab-32
RB11B_HUMAN	8	0	0	0	8	Ras-related protein Rab-11B
CDC37_HUMAN	2	0	0	0	2	Hsp90 co-chaperone Cdc37
IF2GL_HUMAN	4	0	0	0	4	Putative eukaryotic translation initiation factor 2 subunit 3-like proteinfactor 2 subunit 3
RHG17_HUMAN	2	0	0	0	2	Isoform 4 of Rho GTPase-activating protein 17
SEPT8_HUMAN	3	0	0	0	3	Isoform 2 of Septin-8
PTCD3_HUMAN	2	0	0	0	2	Pentatricopeptide repeat domain-containing protein 3, mitochondrial
H2A1J_HUMAN	3	0	0	0	3	Histone H2A type 1-J
MYH2_HUMAN	3	0	0	0	3	Myosin-2
TLN2_HUMAN	8	0	0	0	8	Talin-2
MYH4_HUMAN	2	0	0	0	2	Myosin-4

Table 4-3: Proteins identified in high stringency pulldown alone.
Destiobiotinylated *SMILR* was bound to streptavidin magnetic beads and incubated with protein lysates obtained from IL1α and PDGF stimulated HSVSMC. Beads only served as the negative control in order to identify any non-specific binding of proteins. Mass spec 'hits' were analysed for the number of unique peptides identified and only those with two or greater were considered to be true hits. The coloured bars indicate the number of unique peptides identified per protein (provided in the 1st column) for the low and high stringent pulldowns. The low stringent pulldowns had no salt added and as such, would allow a greater number of proteins to bind. The high stringent pulldown contained higher levels of salt allowing only more specific binding to occur. The control (bead only) columns indicate how many unique peptides were identified in the control samples. The full protein name is provided in the very right hand column. This table represents proteins identified that had at least 2 unique peptides in the high stringent pulldown only and 0 peptides identified in either of the control, bead only pulldowns.

	Low Stringent SMILR	Low Stringent Control	High Stringent SMILR	High Stringent Control	Total peptides Identified	Full Protein Name
K2C6B_HUMAN	0	0	25	0	25	Keratin, type II cytoskeletal 6B
RFA2_HUMAN	0	0	2	0	2	Replication protein A 32 kDa subunit
RFA1_HUMAN	0	0	3	0	3	Replication protein A 70 kDa DNA-binding subunit
SPB4_HUMAN	0	0	9	0	9	Serpin B4
KLK7_HUMAN	0	0	3	0	3	Kallikrein-7
YBOX1_HUMAN	0	0	4	0	4	Nuclease-sensitive element-binding protein 1
ACTS_HUMAN	0	0	12	0	12	Actin, alpha skeletal muscle
RED1_HUMAN	0	0	2	0	2	Isoform 3 of Double-stranded RNA-specific editase
POTEE_HUMAN	0	0	6	0	6	POTE ankyrin domain family member E
RBMS3_HUMAN	0	0	2	0	2	Isoform 3 of RNA-binding motif, single-stranded-interacting protein 3
S1A7A_HUMAN	0	0	4	0	4	Protein S100-A7A
RAB6B_HUMAN	0	0	3	0	3	Ras-related protein Rab-6B
STAU2_HUMAN	0	0	2	0	2	Double-stranded RNA-binding protein Staufen homolog 2

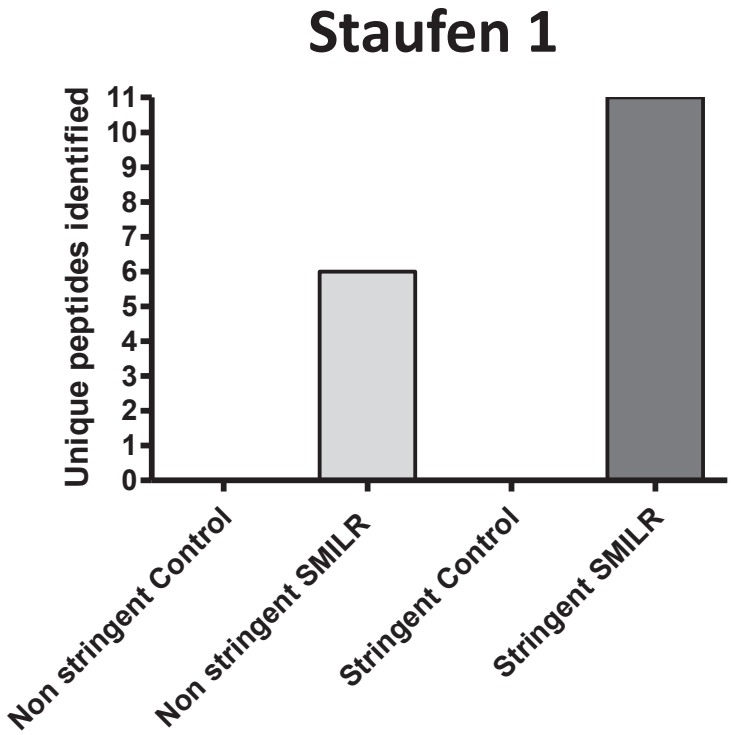

Figure 4-28: SMILR binds Staufen1 in both low and high stringent conditions. Biotinylated *SMILR* was incubated with cell lysates from IL1α and PDGF treated HSVSMC. Pulldown utilising magnetic beads followed by mass spec analysis revealed the interaction of Staufen1. Staufen1 was identified in both non stringent and stringent experiments.

4.4 Discussion

Mechanistically, HSVSMC proliferation involves complex networks of genes, transcription factors, signalling networks and non-coding RNAs, all of which work together to tightly regulate this process. Here, the presented studies focus on the initial characterisation of the novel lncRNAs identified via RNA-sequencing in Chapter 3 and the functional and mechanistic role of one such identified lncRNA, SMILR, in HSVSMC. The data demonstrated the cell and tissue specific expression of four candidate lncRNAs, the ability of lncRNA *SMILR* to regulate proliferation and HAS2 expression in HSVSMC and the identification of protein binding partners that will undoubtedly aid in the identification of *SMILR* function in the cytoplasm and nucleus.

SMILR was pinpointed as an IL1α/PDGF responsive intergenic lncRNA located on chromosome 8, 750 kbp from the closest protein-coding gene, on the same strand. This gene, *HAS2*, encodes a hyaluronic acid (HA) synthase, a critical component of the extracellular matrix that accumulates in human restenotic and atherosclerotic lesions (Papakonstantinou et al., 1998, Riessen et al., 1996). The results show that knockdown of *SMILR* reduces *HAS2* expression and HSVSMC proliferation. This mechanism of action is supported by a number of studies demonstrating HA can enhance VSMC proliferation and migration (Papakonstantinou et al., 1995). Recent studies using transgenic mice with VSMC specific over-expression of HA have found increased susceptibility to atherosclerosis (Chai et al., 2005) and enhanced neointima formation in response to cuff injury (Kashima et al., 2013). The ability of *SMILR* to specifically target *HAS2* with no effect on *HAS1* or *HAS3* allows a means of specifically altering *HAS2* expression, the main HAS isoform expressed and functioning in SMC pathology (Van den Boom et al., 2005). Interestingly, overexpression of *SMILR* did not alter *HAS2* expression, an effect commonly seen with lncRNA lentiviral vectors and caused by the inability of lentiviruses to insert *SMILR* into the correct orientation within the cells. This possibly suggests that *SMILR* regulates *HAS2* expression via a *cis* acting mechanism in the nucleus and may even require tethering to its site of transcription in order to function. Additionally, lncRNAs can regulate other RNAs via a number of mechanisms (Geisler and Coller, 2013), including changes in chromatin signatures within their locus. For example, the *HOTAIR* lncRNA is capable of repressing transcription across 40 kbp of the HOXD

locus (Rinn et al., 2007). Thus *SMILR* may also act as an enhancer or scaffold via interaction with the promoter region, and potentially other transcription factors of *HAS2*, to regulate expression following inflammatory cytokine stimulation. However, further detailed co-immunoprecipitation or site directed mutagenesis studies would be required to demonstrate whether *SMILR* participates in transcription factor complexes with NF-κβ or other transcription factors.

Previous work has found that *HAS2* is regulated by an additional lncRNA, *HAS2-AS1* (Vigetti et al., 2014). Interestingly, the RNA-seq data shows that HAS2-AS1 expression was also upregulated by PDGF treatment alone and in combination with IL1α. However, knockdown of *SMILR* did not alter *HAS2-AS1* expression. LncRNA *HAS2-AS1* modulates chromatin structures around the gene in order to allow more efficient binding of the RNA polymerase 2 and enhanced HAS2 gene expression(Vigetti et al., 2014). This suggests both *SMILR* and *HAS2-AS1* can regulate *HAS2* by independent mechanisms. Interestingly, knockdown of *HAS2* did not affect either *SMILR* or *HAS2-AS1* expression indicating that the expression of these lncRNA is not directly linked to *HAS2* expression. This suggests that *SMILR* may act in *cis* as an enhancer to promote the expression of HAS2 in the nucleus.

Through analysis of tissue and cellular panels, it was identified that the four candidate lncRNA exhibit restricted expression in tissues and cells and show marked differences in their subcellular localisation. It has been proposed that their tissue and cellular specific expression makes them attractive as therapeutic targets and as such may lead to fewer off target effects (Fatima et al., 2015). Our results demonstrate *SMILR* is up-regulated by a combination of PDGF and IL1α in HSVSMCs but not ECs, suggesting modulation of *SMILR* could specifically alter HSVSMC proliferation without detrimental effects on vessel re-endothelialisation. If this is the case, it would provide a suitable candidate to improve current anti-proliferative therapies since current pharmacological agents target cell proliferation in a non-cell specific manner, events which can lead to late stent thrombosis (Lemesle et al., 2010).

The release of *SMILR* could affect function in neighbouring cells, particularly in a vascular injury setting where phenotypic switching of VSMCs occurs in distinct

areas of the vessel wall. In support of this theory, it has been shown that miR 143/145 can be transferred from VSMC into EC (Climent et al., 2015). This transfer produced physiological effects within EC including modulation of migration and tube formation.

Despite the multitude of non-coding transcripts discovered by second-generation deep sequencing, lncRNAs mechanisms of action remains largely unknown. Understanding the molecular mechanisms governing lncRNA function is of paramount importance. (Ellis et al., 2007). LncRNAs may act as guides, decoys or scaffolds and in several cases lncRNA have been shown to act via multiple mechanisms (Wang and Chang, 2011). For example, HOTAIR is a scaffold for PCR2 and LSD1 as well as a guide to recruit PCR2 to its target loci (Rinn et al., 2007). As such, the molecular mechanisms behind lncRNA–protein interactions are complicated and rarely described. *SMILR* pulldown utilising protein lysates from HSVSMC stimulated with IL1α and PDGF identified Staufen1 (STAU1) as a binding partner. Interestingly the number of unique peptides identified in the mass spec analysis was greater under higher stringency pulldown conditions providing evidence that this interaction is real. Staufen 1 is an RNA binding protein noted to play a role in messenger RNA decay. This involves the degradation of translationally active mRNAs whose 3'-untranslated regions (3' UTRs) bind to STAU1. STAU1 will only bind to double-stranded RNA, thus *SMILR* must bind an additional RNA within the cytoplasm in order to elicit the recruitment of STAU1. Interestingly, recent studies indicate that STAU1-bound mRNAs mainly code for proteins involved in transcription and cell cycle control (Furic et al., 2008), (Laver et al., 2013). Consistently, it has been shown that STAU1 abundance fluctuates through cell cycle: it is high from the S phase to the onset of mitosis and rapidly decreases as cells transit through mitosis (Boulay et al., 2014). One such cell cycle protein that was identified via STAU1 pulldown followed by RNA-seq was cyclin F (Boulay et al., 2014). Although no follow up was reported, cyclin F is known to inhibit cell proliferation by initiating an additional checkpoint and halting cells in the G2 phase and thus inhibiting cell division (Klein et al., 2015).

LncRNA binding of STAU1 has been previously identified in additional cell types. One example of this is the lncRNA TINCR. Through high throughput protein-RNA analysis, a direct interaction between TINCR and STAU1 was identified (Kretz,

2013). Both knockdown of TINCR and STAU1 resulted in impaired differentiation of epidermal tissue. The exact site at which STAU1 binds nor the associated mRNA interacting partner is currently known. The role of lncRNA mediated STAU1 mRNA decay is a relatively new mechanism of action and will ultimately require further in depth analyses to determine the full role of STAU1 and lncRNAs. Despite a clear role of STAU1 in mRNA mediated decay, no role of STAU1 has ever been associated with cardiovascular disease. Further analyses via STUA1 pulldowns followed by RNA-sequencing in HSVSMCs will be required to identify other SMC specific lncRNAs that bind STAU1 and thus identify the global role of STAU1 and bound lncRNAs in vascular disease. This will ultimately open up new avenues for lncRNA research. The proposed mechanism of action of STAU1/*SMILR* is highlighted in Figure 4-29 and described in detail in section 4.4.1. Additional experiments are still required to confirm this observation and to identify any *SMILR*:RNA binding partners that may be present. As technologies improve, we may one day better understand evolution and functional mechanisms of lncRNAs.

4.4.1 Proposed nuclear and cytoplasmic mechanism of action for *SMILR* lncRNA

As mentioned, overexpression of *SMILR* did not alter *HAS2* expression, however, *SMILR* knockdown reduced *HAS2* levels. This effect is commonly due to the inability of the lentivirus to overexpress the lncRNA in the correct orientation. As such it is proposed that *SMILR* acts via a currently unknown *cis* mechanism, meaning that it may be tethered to its site of transcription and requires complex looping of the DNA in order to target *HAS2* (Figure 4-27). Further in depth chromatin and epigenetic studies would be required to validate this hypothesis.

In our proposed model, *SMILR* is transcribed in the nucleus and is also transported to the cytoplasm. In the cytoplasm, *SMILR* potentially binds a mRNA that plays a role in inhibiting SMC proliferation, although it is currently unknown if SMILR may also mediate proliferation on its own. The binding of *SMILR* to the yet unknown mRNA leads to generation of a double stranded RNA. Formation of the double stand promotes the binding of STAU1 to an ALU element located within the 3’ UTR of the mRNA, targeting it for degradation and thus promoting

SMC proliferation. It is proposed that this mRNA inhibits HSVSMC proliferation and that *SMILR* binding and targeting this mRNA for STAU1-mediate decay allows the proliferation of HSVSMC.

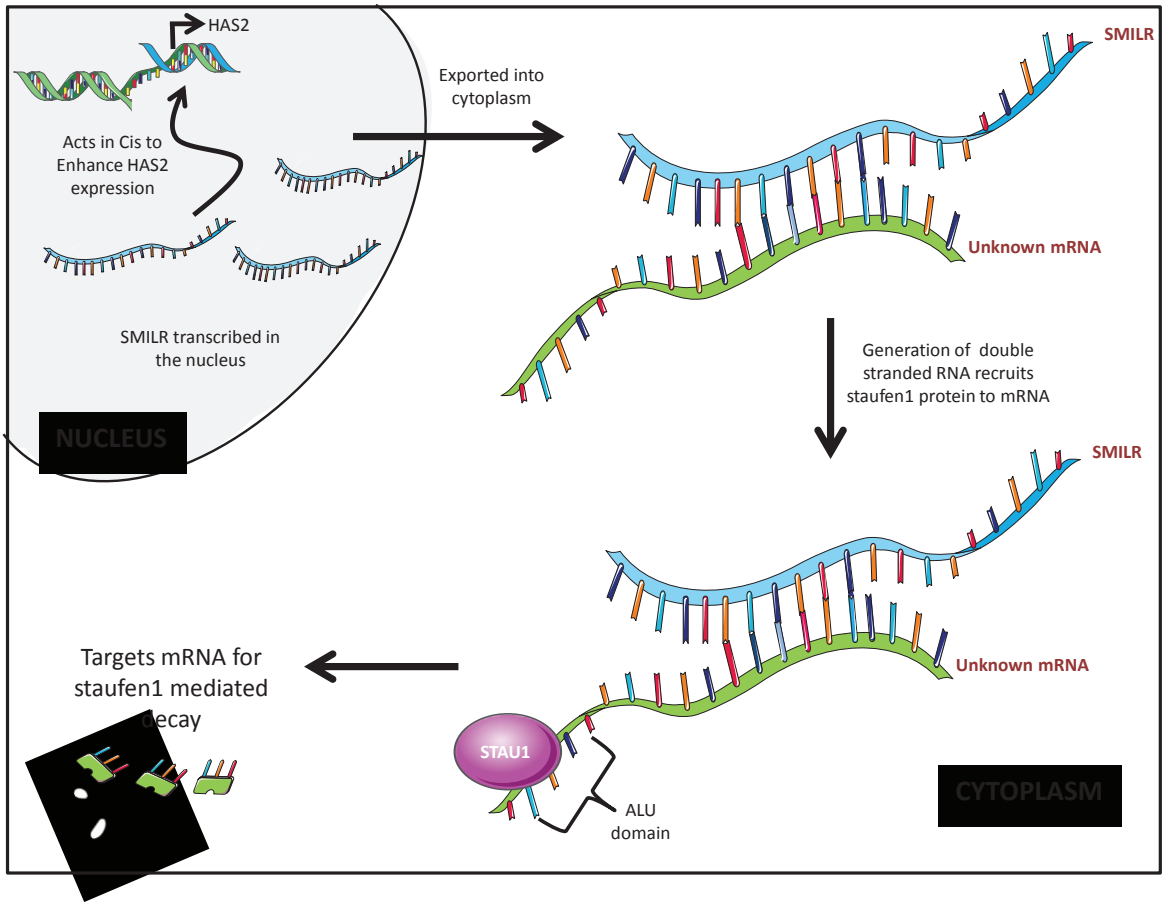

Figure 4-29: Schematic overview of proposed mechanism of action of SMILR.
It is proposed that *SMILR* acts via 2 distinct mechanisms. In the nucleus *SMILR* may act via an unknown cis mechanism to promote the production of HAS2. In the cytoplasm, it is proposed that *SMILR* binds a currently unknown mRNA. The formation of a double stranded RNA bond promotes the recruitment of staufen1 (STAU1) to an ALU element located on the mRNA, targeting it for STAU1 mediated decay.

Taking everything together, these observations broaden our awareness of the complex interplay between lncRNA and protein coding genes. The emergence of lncRNAs as regulators of gene expression will undoubtedly alter our understanding of the complex regulation network of pathological VSMC proliferation in vascular disease and may provide a means to specifically target VSMC or identify patients at risk of major adverse vascular outcomes.

Chapter 5 Clinical expression of lncRNA in vascular pathology

5.1 Introduction

The discovery of dysregulated lncRNA expression in several human pathologies has not only added an additional layer of complexity within the molecular architecture of disease, but has also opened up new avenues for their potential use as biomarkers and therapeutic targets. It has already been shown that lncRNA can be readily detected in bodily fluids (Sanchez and Huarte, 2013) and lncRNAs offer advantages as biomarkers as they exhibit tissue and context restricted patterns of expression (Quinn and Chang, 2016), suggesting that their expression signatures could successfully be used for accurate disease diagnostics and classification. Although research in this area in still in the early stages, a few key lncRNAs have been demonstrated to be effective biomarkers. One prominent example is PCA3, a prostate specific lncRNA that is significantly over expressed in prostate cancer. PCA3 was identified in collaborative research efforts between Johns Hopkins Hospital, Baltimore and Radboud University, Nijmegen, Netherlands (Shaw et al., 2007) whilst examining the expression patterns of RNA in normal and cancerous prostatic tissue. PCA3 is overexpressed in 95 % of all prostate cancer samples (Hessels and Schalken, 2009) and its expression patterns can allow the differentiation between benign and cancerous samples with almost 100 % accuracy (Marks and Bostwick, 2008). Furthermore, PCA3 has not been detected in any additional tissues except cancerous prostate samples, is not affected by age, prostate volume or other prostatic diseases, making it the most specific lncRNA biomarker to date (Marks and Bostwick, 2008). PCA3 can be detected in urine samples using a magnetic bead recovery system and due to its profound sensitivity, a commercially available kit is now available (ProgensaTM PCA3 assay (Gen-Probe, San Diego, CA, USA))(Vlaeminck-Guillem et al., 2010). PCA3 outperforms the previously utilised prostate-specific biomarker, prostate-specific antigen (Psaltis and Simari) and highlights the ability of lncRNAs to function as disease and tissue specific markers.

A study of plasma levels of the lncRNA LIPCAR was the first proof of principle experiment to highlighting the possible role of plasma lncRNA as prognostic biomarkers in cardiovascular diseases. The initial lncRNA screening was

performed according to the level of left ventricular (LV) remodelling in a echocardiographic study of patients after myocardial infarction (MI). One-year echocardiographic follow-up was completed on the patients and LV remodelling was assessed. From this population, 15 male patients with high LV remodelling and 15 male patients without LV remodelling were used in the initial cohort. Utilising these 30 patients, lncRNA microarray was performed on RNA isolated from plasma samples. Hierarchical clustering analysis clearly distinguished the 2 groups of patients based on a specific signature of detectable and significantly regulated circulating lncRNAs. One lncRNA called LIPCAR showed greatest correlation and greatest change in expression between the two patient populations(Kumarswamy et al., 2014). Longitudinal studies in larger cohorts and at 1, 3 and 12 months post myocardial infarction, LIPCAR showed a time dependent increase and significantly higher levels in patients developing LV remodelling. Additional experiments in a cohort of 344 heart failure (HF) patients identified that LIPCAR levels were even higher in chronic HF than in patients with ongoing LV remodelling 1 year after myocardial infarction(Kumarswamy et al., 2014).

Another example is CoroMarker (AC100865.1), a lncRNA that is markedly overexpressed in coronary artery disease (CAD). Patients with CAD have benefited from improvements in surgical revascularisation techniques (e.g coronary artery bypass grafting (CABG)); however, the rate of mortality from CAD remains high. This is due to the inability of CAD to be detected in its early stages by routine examinations such as electrocardiography and cardiac ultrasound (Glagov et al., 1987), (Hoffmann and Butler, 2005). As such, there is great interest in identifying novel biomarkers associated with early stage CAD , which could be assessed using non-invasive methods. Yang et al. hypothesised that circulating lncRNAs could serve as specific CAD biomarkers. The initial cohort encompassed 15 male patients with and 15 male patients without CAD. Plasma lncRNA expression was profiled using a lncRNA microarray and 265 lncRNAs were found to be significantly altered between the control and disease groups with a fold change greater than 2 and $P<0.01$. Due to the large quantity of lncRNAs identified, the top 5 most highly up-regulated (>8 fold) were selected for further validation. The relationship between each lncRNA and CAD was performed via ROC analysis and only CoroMarker (AC100865.1) was shown to be a

good candidate biomarker to predict CAD. The predictive value of CoroMarker was assessed in a larger cohort with 221 CAD patients and 187 control individuals and was able to successfully identify 78.05 % of CAD patients (Yang et al., 2015a). Stability across different sample storage conditions (e.g temperature) is an essential prerequisite to ensure biomarker reliability. Exposure of plasma to various periods at RT had very little effect on CoroMarker expression and even after 48 h, CoroMarker levels were still at 80 % of the unexposed levels (Yang et al., 2015a). Additionally, samples must be able to withstand freeze-thaw cycles. As such, three freeze–thaw cycles had no effect on CoroMarker levels, although seven freeze–thaw cycles did reduce CoroMarker to half its original levels (Yang et al., 2015a). CoroMarker is thus a stably expressed lncRNA within the plasma and further test to confirm and evaluate its ability to detect CAD are currently underway.

Laboratory and experimental evidence indicate that atherosclerosis and subsequent intimal hyperplasia are initiated by inflammatory pathways following endothelial injury. This inflammation also regulates the production of acute phase proteins such as C-reactive protein (CRP). Thus, it was hypothesised that inflammatory markers such as high-sensitivity CRP may provide an adjunctive method for global assessment of cardiovascular risk. As such, it has now been shown that the serum concentration of CRP can increase >1000 fold upon inflammation and with a half-life of 19 h, CRP is currently utilised as a predictive measure of atherosclerotic progression (Libby and Ridker, 2004) and risk of myocardial infarction (Osman et al., 2006), (Libby and Ridker, 2004). However, it should be noted that the utilisation of CRP as a biomarker has its own limitations. Inflammatory markers, such as CRP, may be nonspecific and can increase with acute infection or trauma, an effect that may result in misclassification. As such caution must be taken when performing diagnostic tests and CRP testing will not be performed during times of infection or if the patient has a known systemic inflammatory condition.

CRP is one of the substances found within atherosclerotic plaques, most specifically within the intima where it has been shown to co-localise with monocytes, macrophages and lipoproteins (Torzewski et al., 1998). CRP has also been identified to be produced by both SMC and monocytes within atherosclerotic plaques (Calabro et al., 2003), (Yasojima et al., 2001). Whether

CRP has any functional effect on atherosclerotic plaque progression has been extensively studied. In vitro exposure of vascular endothelial cells to CRP inhibits nitric oxide synthase expression and upregulates expression of interleukin-8, intercellular adhesion molecule-1, and vascular cell adhesion molecule-1, consistent with a role of CRP in endothelial dysfunction (Venugopal et al., 2002). CRP can also bind to an activate innate immunity, a process that has already been linked to cardiovascular disease. In situ hybridisation has shown intense mRNA signals for CRP and complement compound C4 in SMCs present in the thickened intima of lesions (Jiang et al., 1992).

Attempts to define new lncRNA biomarkers will also require a better characterisation of non-coding RNA molecules within atherosclerotic plaques. Thus key clinical samples are of paramount importance in the discovery and characterisation of non-coding molecules that regulate vascular disease.

5.2 Aims

The aims of the current chapter were as follows:

- To profile ncRNA expression in atherosclerotic plaque and adjacent control tissue.

- To assess if lncRNA expression is altered in atherosclerotic versus control tissue.

- To assess if *SMILR* is secreted and could be detected in plasma from CAD patients with varying levels of C reactive protein (CRP).

5.3 Results

5.3.1 Correlation of non-coding RNA with atherosclerotic plaques

To investigate the importance of lncRNA in human vascular pathologies, the levels of the 4 characterised lncRNAs *SMILR*, RP11-761I4.4, RP11-9ak9.1 and AC018647.3 (from chapters 3 and 4) were assessed in unstable atherosclerotic plaques using qRT-PCR.

5.3.1.1 Study Design and Analysis

12 patients (seven evaluable) undergoing carotid endartectomy for symptomatic carotid artery disease were recruited from the Royal Infirmary of Edinburgh. Patient characteristics are shown in Table 5-1.Two established inflammatory PET radiotracers ([^{18}F]-fluorodeoxyglucose (FDG) and calcification ([^{18}F]-Sodium fluoride (NaF)) were used to prospectively define portions of high-risk plaque (Rudd et al., 2002), (Joshi et al., 2014), (Vesey et al., 2015) for RNA extraction. All FDG and NAF imaging was performed by Dr Alex Vessey. FDG is a radiopharmaceutical used in medical imaging. Chemically it is a glucose analogue with the positron-emitting radionuclide fluorine-18 substituted for the normal hydroxyl group at the C-2 position in the glucose molecule (Miele et al., 2008). FDG preferentially accumulates in macrophages and is thus an effective marker of atherosclerotic plaques (Ogawa et al., 2004). ^{18}F-NaF, an additional radiotracer has been shown to bind to areas of microcalcification and as such is capable of defining stable atherosclerotic plaques (Irkle et al., 2015).

Table 5-1: Baseline patient characteristics for carotid cohort.

	Carotid (n=7)
Age in years, mean (SD)	63 (13.8)
Men, n (%)	4 (57)
BMI (kg/m^2), mean (SD)	26.3 (5.8)
Systolic blood pressure (mmHg), mean (SD)	141.1 (22.5)
Diastolic blood pressure (mmHg), mean (SD)	88.4 (16.6)
Presenting syndrome, n (%)	
Stroke	2 (29)
TIA/Amaurosis fugax	5 (71)
Cardiovascular history, n (%)	
Ischemic heart disease	3 (43)
Myocardial infarction	1 (14)
Risk Factors, n (%)	
Hypertension	5 (71)
Diabetes	1 (14)
Hypercholesterolemia	7 (100)
Current smoker	3 (43)
Medication, n (%)	
Aspirin	2 (29)
Clopidogrel	5 (71)
Anti-coagulant	1 (14)
Statin	7 (100)
ACEI/ARB	3 (43)
B-blocker	2 (29)
Hematology, mean (SD)	
Hemoglobin	137.0 (23.1)
White cell count	8.1 (1.8)
Platelet count	284 (66)
Serum biochemistry, mean (SD)	
Creatinine (mmol/L)	90 (21.1)
Total cholesterol (mmol/L)	4.7 (1.3)

Exclusion criteria were age younger than 50 years, insulin-dependent diabetes mellitus, women of childbearing age not receiving contraception, severe renal failure (serum creatinine >250 μmol/L), known contrast allergy and inability to provide informed consent. Only patients older than 50 years were recruited in the study to reduce any long-term risks associated with radiation exposure. Uncontrolled diabetes and high blood glucose concentrations (>11 mmol/L) interfere with the quality of ^{18}F-FDG PET imaging because of the competition between glucose and ^{18}F-FDG for cellular entry. The convention is therefore to exclude such patients from vascular ^{18}F-FDG PET studies (Joshi et al., 2014).

Patients underwent ^{18}F-NaF and ^{18}F-FDG PET-CT (Joshi et al., 2014). The maximum standard uptake value (the decay corrected tissue concentration of the tracer divided by the injected dose per bodyweight) was measured and corrected for blood pool activity in the superior vena cava to provide tissue-to-background ratio (TBRs) measurements. Coronary plaques were defined as ^{18}F-NaF or ^{18}F-FDG positive if the plaque had a focal uptake with a TBR more than 25 % higher than a proximal reference section.

Intact atherosclerotic plaques were retrieved at the time of carotid endarterectomy and scanned using *ex vivo* PET-CT to allow precise anatomical co localisation of ^{18}F-NaF activity with pathological evidence of plaque rupture. Plaques were divided into ^{18}F F-NaF and ^{18}F-FDG positive and negative areas and are defined below as 'plaque' and 'healthy artery'. These samples are a unique samples set as the 'plaque' and 'healthy artery' were defined from within the one patient. This is of key importance as it permits the assessment of non-coding RNA expression from within each microenvironment (plaque vs. non plaque) from within the one vessel.

Compared to quiescent adjacent tissue, portions of high-risk plaque showed higher uptake of both [^{18}F]-FDG (maximum tissue-to-background ratio (TBR_{max}) 1.81 ± 0.21 *versus* 1.31 ± 1.6) and [^{18}F]-fluoride (TBR_{max} 2.32 ± 0.52 *versus* 1.31 ± 0.43) indicating that plaques subjected to RNA analysis had enhanced rates of inflammation and calcification (Figure 5-1A-G for image examples and Figure 5-2 A-D for graphs of tracer uptake).

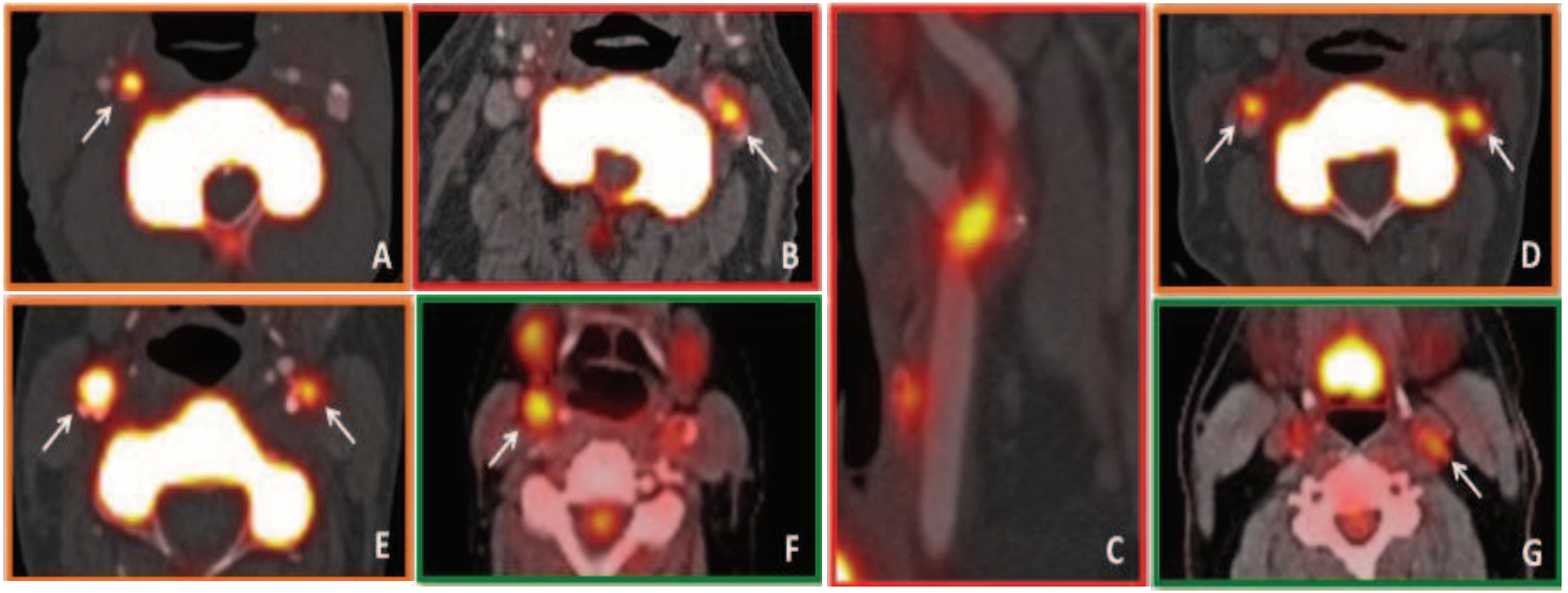

Figure 5-1: Uptake of [^{18}F]-Fluoride and [^{18}F]-FDG within plaque and normal artery.
All patients undergoing endarterectomy following an acute and symptomatic neurovascular event were subjected to separate [^{18}F]-fluoride and [18F]-fluorodeoxyglucose ([^{18}F]-FDG) positron emission tomography combined with computed tomography (CT) scanning. Both ^{18}F-FDG and 18F are reported to be up taken by areas of high risk plaque. Scans are representative images of patients and show axial images demonstrating unilateral **(A, B)** or bilateral [18F]-Fluoride carotid uptake **(D, E).** Image **C** is a multi-planar reformat of **B**. Axial images demonstrating [^{18}F]-FDG carotid uptake **(F, G).** White arrows indicate carotid radio-ligand uptake.

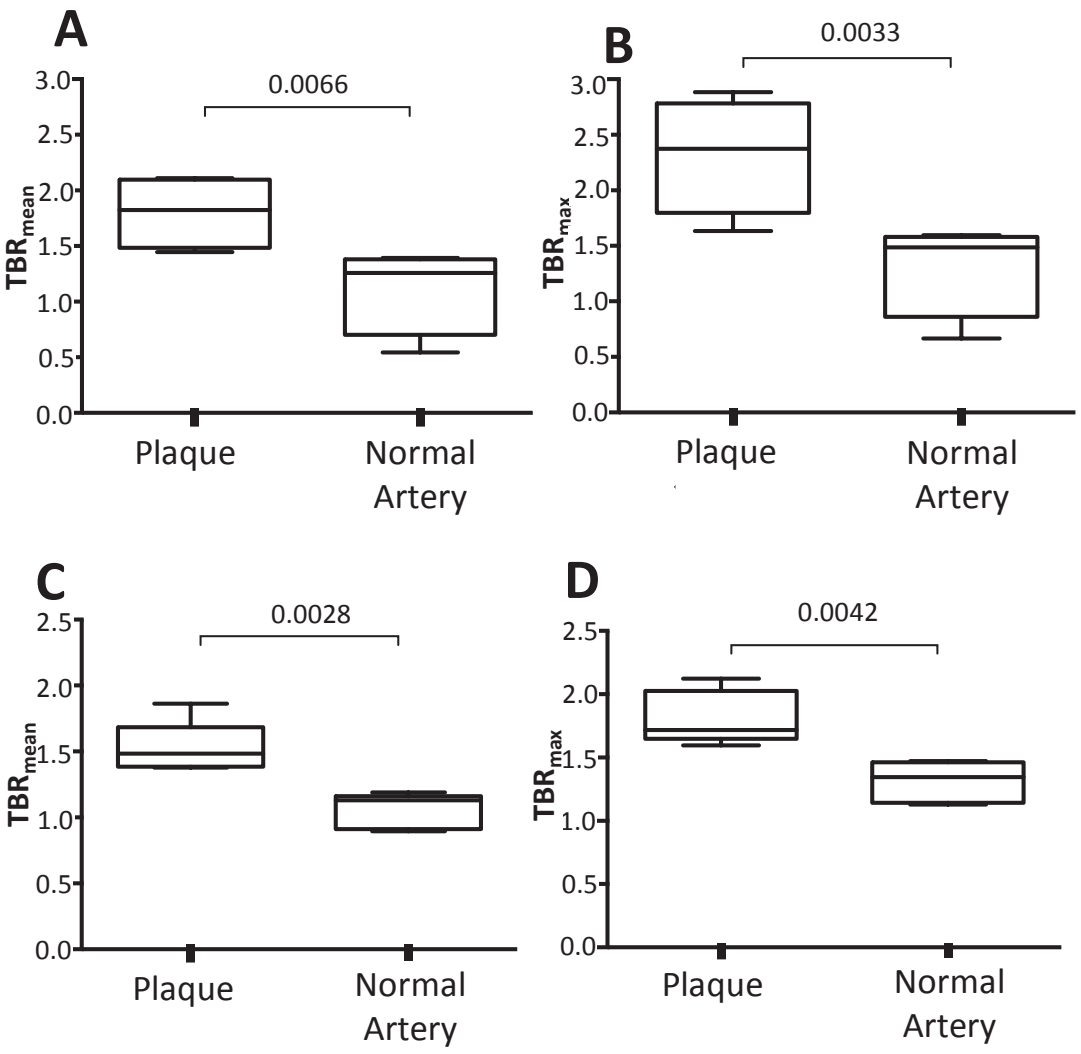

Figure 5-2: Quantification of uptake of image tracer in plaque and adjacent normal artery. All patients undergoing endarterectomy following an acute and symptomatic neurovascular event were subjected to separate [^{18}F]-fluoride and [^{18}F]-fluorodeoxyglucose ([^{18}F]-FDG) positron emission tomography combined with computed tomography (CT) scanning. Both ^{18}F-FDG and 18F are reported to be up taken by areas of high risk plaque. ^{18}F and ^{18}F-FDG was quantified from all patients that underwent tracer uptake (n=6 patients)**: (A and B):** indicate the mean and maximum signal to background uptake of [^{18}]-FDG **(C and D):** indicate the mean and maximum signal to background uptake of [^{18}]-Fluoride.

5.3.1.2 Expression of non-coding RNA within plaque and control tissue samples

Since non-coding RNAs have not been assessed in a similar sample set before, the expression of a panel of miRNAs, known to be associated with atherosclerosis processes, were evaluated in atherosclerotic plaque samples and adjacent healthy vascular tissue ('control samples') by qRT-PCR (Raitoharju et al., 2011). An overview of the method of extraction is shown in Figure 5-3A. Figure 5-3Ai depicts an illustrative image indicating the area of plaque (P) and adjacent control tissue (C) obtained via carotid endarterectomy. Example images of the sections removed as plaque (P) and control (C) are provided in Figure 5-3A subsection ii and iii. As expected, inflammation-associated miRNAs-146a and -146b were significantly upregulated in unstable plaques compared to adjacent quiescent tissue, while miR-29, which is inversely associated with osteoblastogenesis and arterial calcification, was down regulated in mineralised regions of the atherosclerotic plaque (Du et al., 2012, Cui et al., 2012). In addition, downregulation of the miR-143/145 cluster was observed, which is associated with SMC differentiation and aortic aneurysm formation (Ella et al., 2009), an event which has previously been linked to osteogenic differentiation of SMC (Figure 5-3B). Thus, expression of small non-coding RNAs was associated with PET/CT defined high-risk plaques.

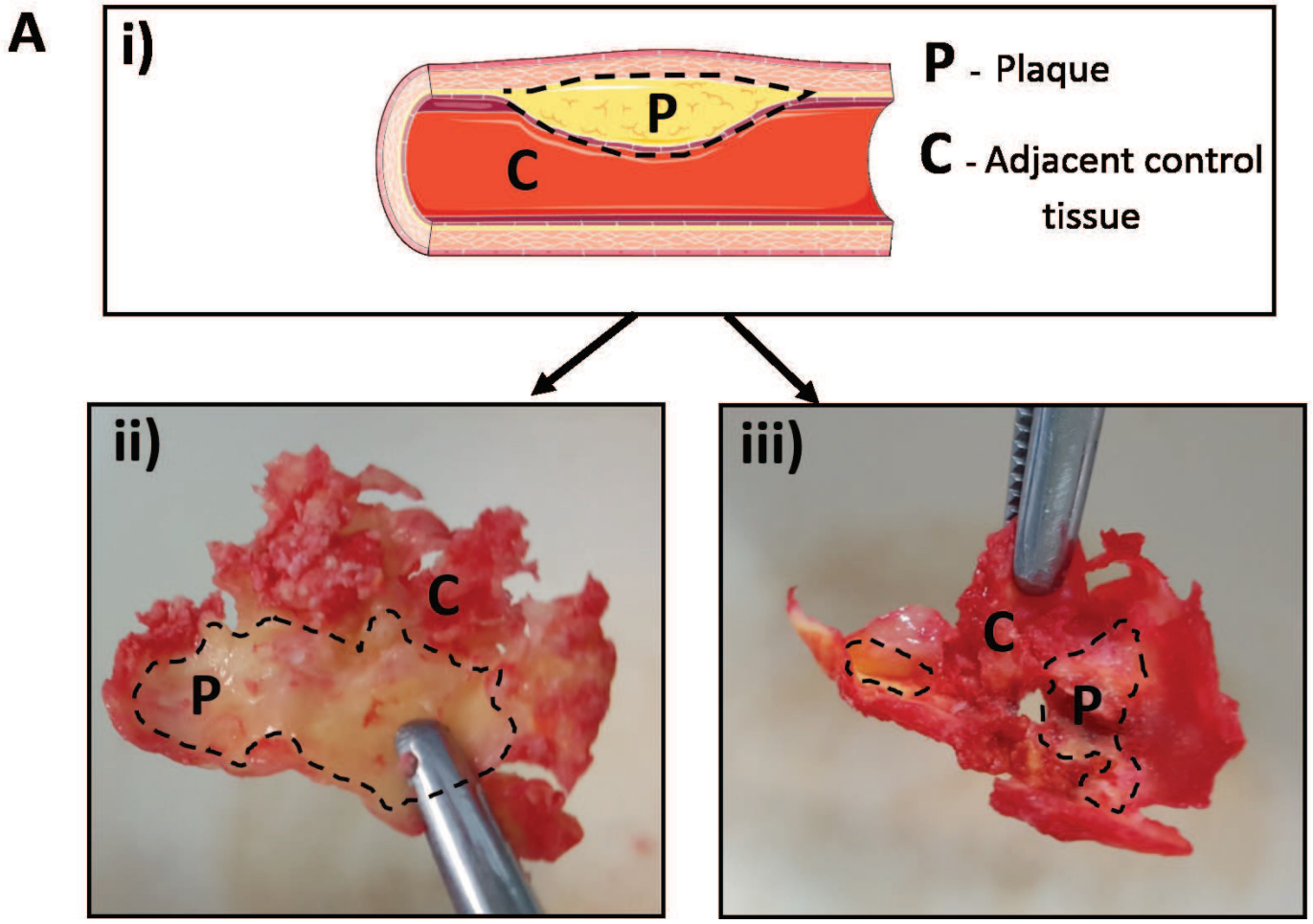
A
i)
P
C
P - Plaque
C - Adjacent control tissue
ii)
C
P
iii)
C
P

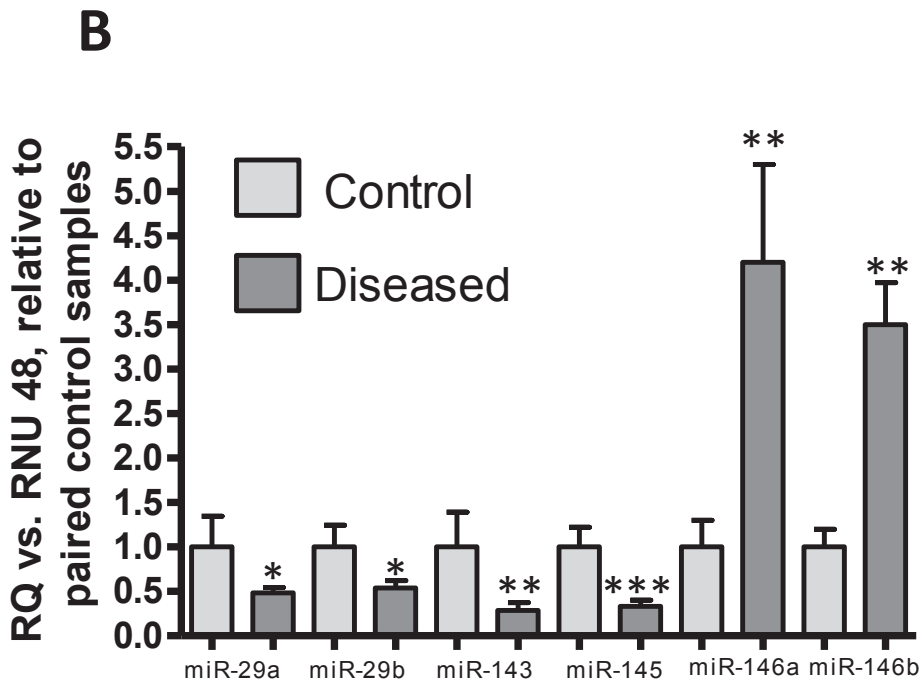

Figure 5-3: Plaue sectioning and microRNA panel in atherosclerotic plaque samples. A: Overview of the dissection of plaques into control and diseased samples. B: Expression levels of 6 atherosclerosis associated microRNAs (miR-29a, -29b, -143, -145, 146a, -146b) were analysed in atherosclerotic plaque and paired healthy carotid controls samples (*n=6 patients*) assessed by qRT-PCR. All data are presented as microRNA levels relative to the respective control samples and normalised to RNU48. Grouped analysis was performed between sample pairs as control and adjacent diseased samples were acquired from the one patient. Light grey bars indicate adjacent 'healthy' tissue while dark grey bars indicate calcified disease plaque. *P<0.05, **P<0.01 and ***P<0.001 vs. control, (paired students t test).

Having confirmed the dysregulated expression of key microRNAs known to drive atherogenesis, the same cohort of samples was utilised to assess *SMILR*, RP11-761I4.4, RP11-91k9.1 and AC018647.3 expression levels by qRT-PCR (Figure 5-4A-D respectivelt. A significant upregulation of 3.9 ± 1.9 and 12.3 ± 8.9 fold was observed in *SMILR* and RP11-91k9.1 expression, respectively, in high-risk plaques compared to adjacent stable regions of the carotid artery. A significant down regulation of 2.5 ± 0.2 fold expression was noted for RP11-761I4.4 in plaque regions. No significant difference in the level of AC018647.3 was observed (Figure 5-4). Interestingly, exposure of HSVSMC to IL1α and PDGF resulted in up/downregulation of these key lncRNA in a similar manner, although smaller fold change, to that observed between control and atherosclerotic samples (Chapter 3 – Section 3.4.3).

Due to the up-regulation of *SMILR*, and previous knowledge that in HSVSMC *SMILR*, HAS2 and HAS2-AS1 were all upregulated in a similar manner, *HAS2* and *HAS2-AS1* levels were also assessed in the atherosclerotic cohort. Intriguingly, a 4.4 fold increase in HAS2 but no change in *HAS2-AS1* was observed (Figure 5-5A and B).

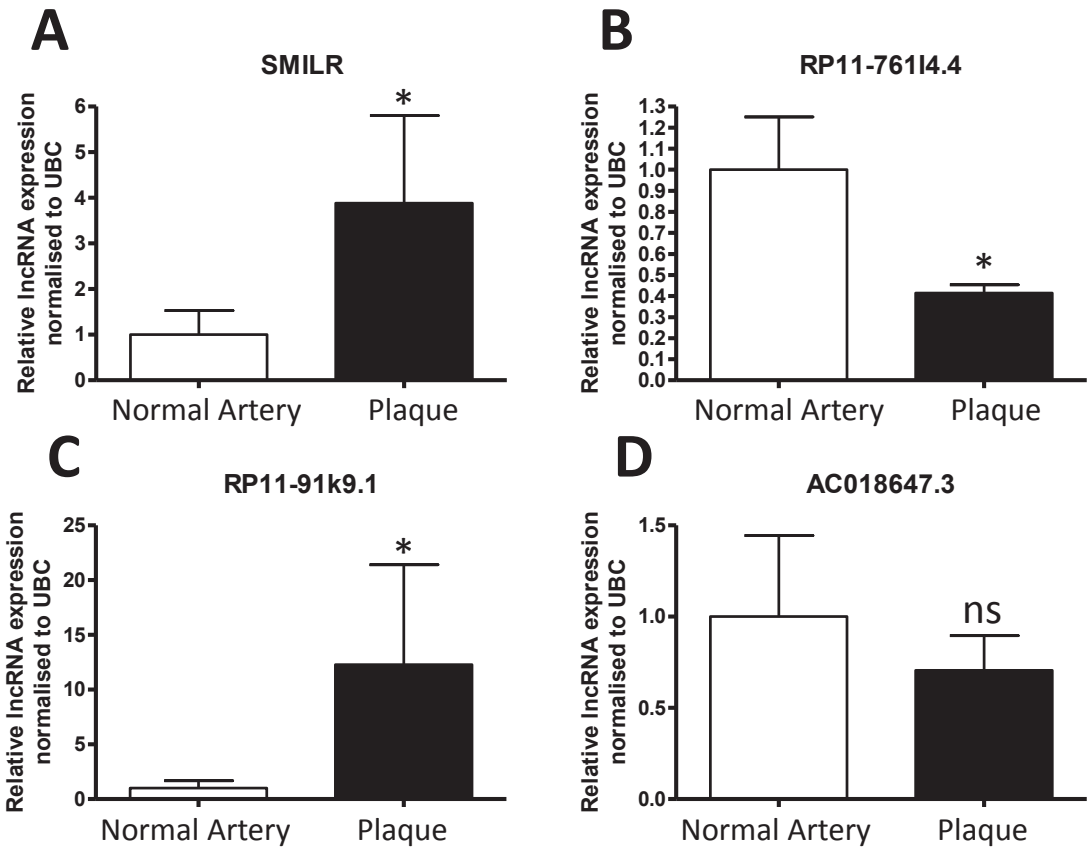

Figure 5-4: LncRNA expression in atherosclerotic plaque samples.
Expression levels of the 4 previously characterised lncRNAs (A: *SMILR*, B: RP11-761I4.4, C: RP11-91k9.1 and D: AC018647.3) were analysed in atherosclerotic plaque and paired healthy carotid controls samples (*n=5 patients*) assessed by qRT-PCR. All data are presented as lncRNA levels relative to the respective control samples and normalised to UBC. Grouped analysis was performed between sample pairs as control and adjacent diseased samples were acquired from the one patient. *P<0.05 vs. control, (paired students t test).

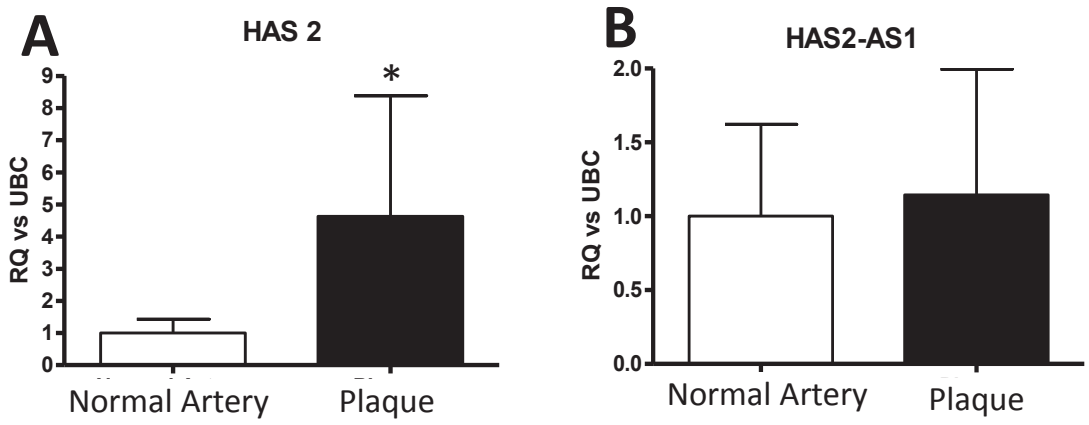

Figure 5-5: HAS2 and HAS2-AS1 expression in atherosclerotic plaques.
Expression levels of A: HAS2 and B: HAS2-AS1 were analysed in atherosclerotic plaque and paired healthy carotid controls samples (*n=5 patients*) assessed by qRT-PCR. All data are presented as mRNA or lncRNA levels relative to the respective control samples and normalised to UBC (RQ= relative quantity). Grouped analysis was performed between sample pairs as control and adjacent diseased samples were acquired from the one patient. *P<0.05 vs. control, (paired students t test).

In summary, miRNA and lncRNA expression profiling shows significant differences in atherosclerotic plaques vs. 'healthy' control samples.

5.3.2 Expression of lncRNA *SMILR* within plasma

The data presented above indicate that *SMILR* is upregulated during the development of cardiovascular disease. Since it was also shown that *SMILR* was secreted from stimulated cells (Chapter 4 - Section 4.3.9), *SMILR* expression was assessed in plasma samples from a cohort of patients with cardiovascular disease.

5.3.2.1 Study design and patient demographics

One hundred South Asian (defined as having both parents of Indian, Pakistani, Bangladeshi or Sri Lankan origin) and 100 European (both parents of white European origin) men living in the UK, aged 40–70 were recruited into the cross-sectional Carotid Ultrasound and Risk of Vascular disease in Europeans and South Asians (CURVES) study. The CURVES study had the primary aim of comparing prevalence of, and risk factors for, carotid atherosclerotic plaques between middle-aged South Asian and European men (Ghouri et al., 2013).

Venous blood samples were obtained after an overnight fast of 10–12 h and C-reactive protein levels (CRP) were analysed on the day of collection in the National Health Service Biochemistry Laboratory in Glasgow, using the standard automated immunoturbidimetric method (Ghouri et al., 2013).A subset of these patients was utilised to assess lncRNA expression in plasma. Patient characteristics for the samples utilised in the study of lncRNA expression are documented in Table 5-2.

As mentioned in Chapter 1 – Section 1-3 and in the above introduction, atherosclerosis is considered to be a multifactorial disease driven by inflammatory reactions. C reactive protein is an acute phase protein and its concentration in serum reflects the inflammatory condition in the patient. Levels of CRP are therefore capable of predicting both myocardial infarction and stroke (Paffen and Demaat, 2006). Therefore, all plasma samples were ranked in order of the serologic parameter CRP levels into 3 groups: CRP <2, CRP 2-5 and CRP >5 mg/L representing broad tertiles of CRP. All samples were blinded to the CRP levels until lncRNA analysis had been performed.

Table 5-2: Baseline CRP Patient Characteristics.
CRP matched plasma samples. Values are represented in mean ± SEM with *p* values calculated by one-way ANOVA or by Fisher's exact test for categorical variables.

	group 1: crp<2 (n=13)	group 2: 2<crp<5 (n=13)	group 3: crp>5 (n=15)	*p* values
Age (years)	48.5 ± 1.8	48.5 ± 1.9	50.7 ± 2.1	0.66
CRP (mg/L)	1.24 ± 0.15	3.56 ± 0.28	7.09 ± 0.48	**p<0.0001**
Systolic BP (mmHg)	123 ± 2.9	131.2 ± 6.5	137.5 ± 4.6	0.12
Diastolic BP (mmHg)	77.5 ± 1.9	76.2 ± 2.0	79.0 ± 2.7	0.68
BMI (kg/m^2)	26.0 ± 0.5	28.7 ± 1.3	29.6 ± 1.7	0.14
WHR	0.96 ± 0.02	1.00 ± 0.02	0.99 ± 0.02	0.23
cIMT (mm)	0.64 ± 0.03	0.59 ± 0.03	0.64 ± 0.04	0.47
Smoking status, n (%)				0.015
Never smoker	61.5	61.5	60.0	
Ex-smoker	15.4	38.5	0.0	
Current	23.1	0.0	40.0	
SIMD quintile, n (%)				0.111
1	30.8	0.0	0.0	
2	23.1	7.7	6.7	
3	7.7	23.1	40	
4	7.7	15.4	13.3	
5	30.8	53.8	40	

5.3.2.2 LncRNA correlation in plasma

Due to differences in plasma lncRNA expression in different disease states, a stable plasma lncRNA housekeeper has not been identified. For microRNA, the current approach is to normalise sample input by using a synthetic spike-in microRNA. Thus samples were spiked with 75 ng c.elegans total RNA as was optimised in the extraction of RNA from conditioned media samples (Chapter 4 - Section 4.3.9). Quality control checks were pursued in order to confirm successful amplification of one single product following qRT-PCR analysis. Melting curves and gel products of *SMILR* primers in plasma are shown in Figure 5-6 and highlight one single peak in the melting curve, that is absent in the water control and one single band visualised by gel electrophoresis.

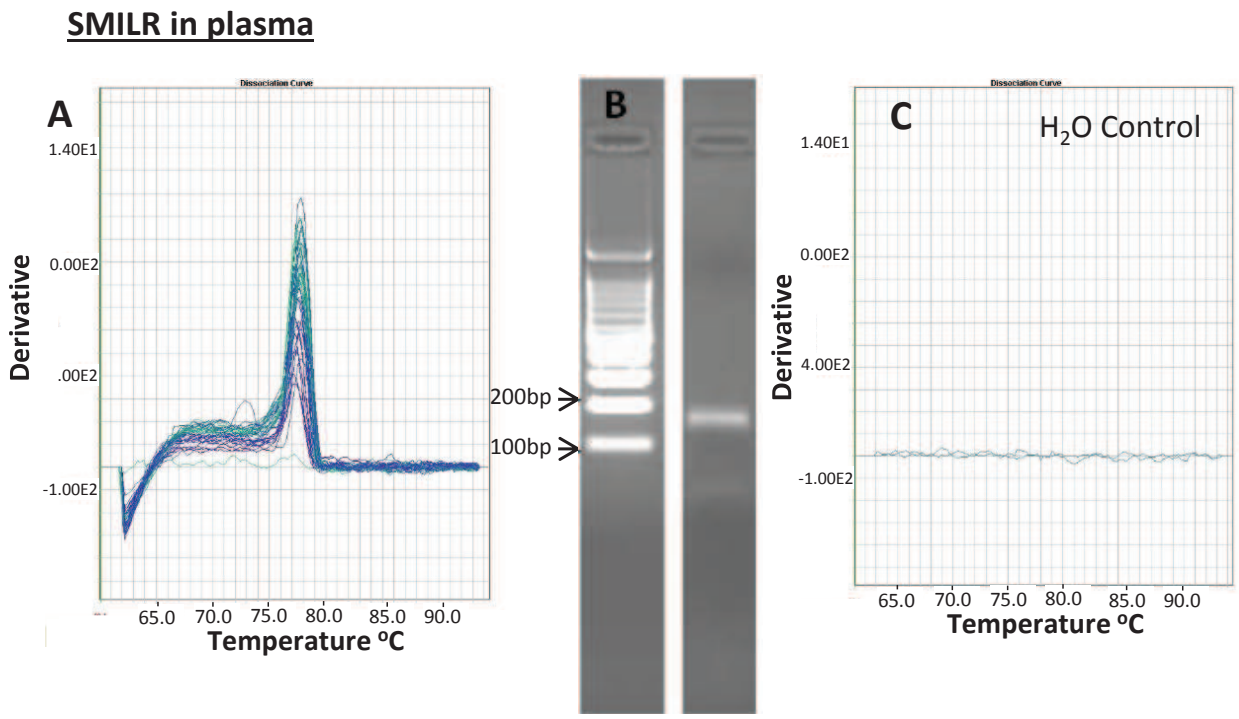

Figure 5-6: Primer validation and quality control in plasma samples.
Quality control checks were performed following qRT-PCR analysis to ensure only one product was being detected by qRT-PCR. **(A):** Melting curve for *SMILR* in plasma indicating one single peak. **(B):** Agarose gel of the qPCR product, indicating a single band. **(C):** Water melting curve. Indicating that no amplification occurred in the water control samples.

qRT-PCR analysis of *SMILR* showed no difference in patients with CRP levels below 2 mg versus 2-5 mg/L. However, a 3.4 ± 1.2 fold increase in *SMILR* was observed when CRP concentrations were greater than 5 mg/L (Figure 5-7A).

Furthermore, a significant positive correlation was observed between *SMILR* and CRP (R^2=0.33, P<0.0001) (Figure 5-7B). However, there was no correlation between *SMILR* and additional risk factors including age (P=0.66), blood pressure (P=0.12), BMI (P=0.14) or social deprivation status (P=0.11) (Table 5-2).

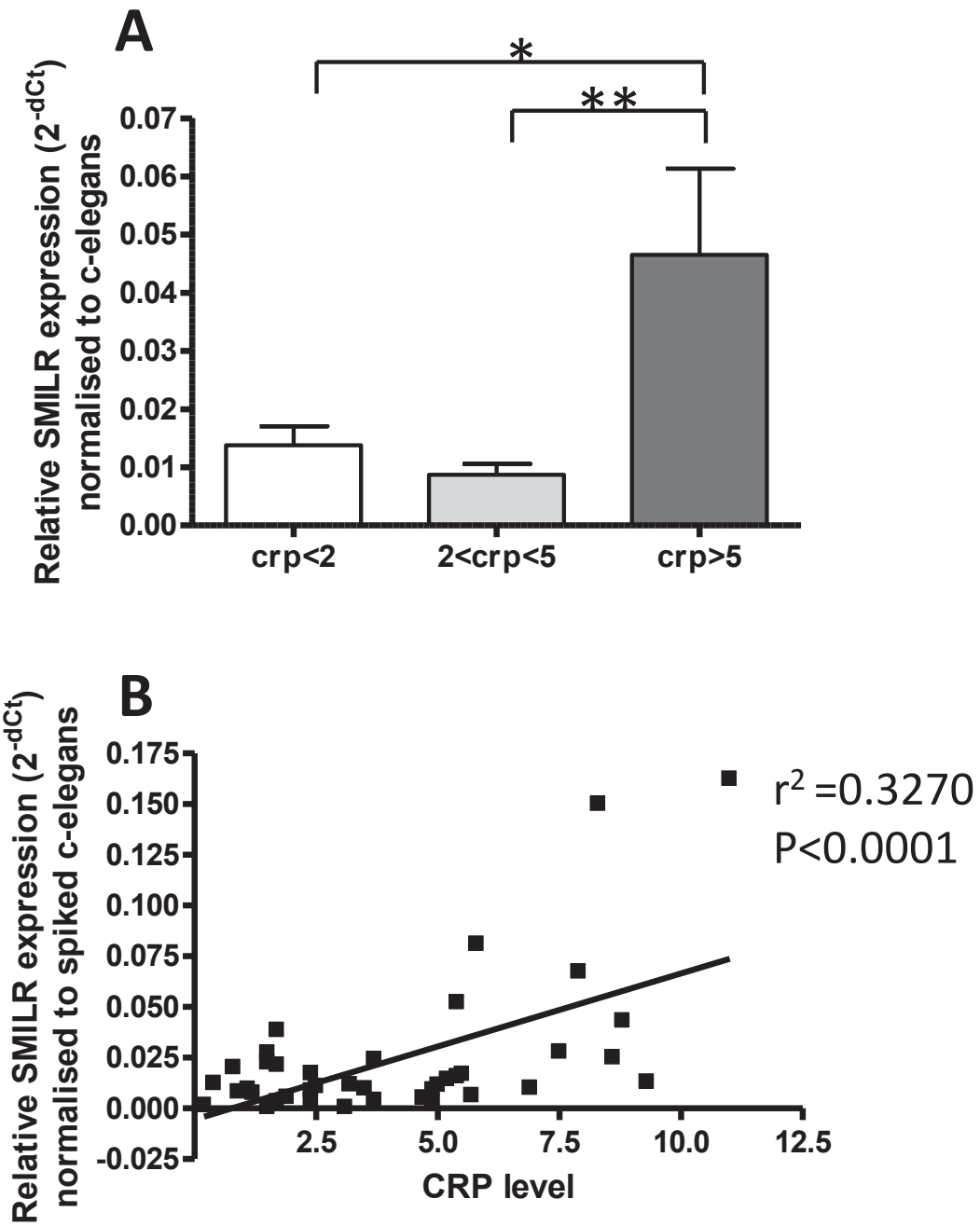

Figure 5-7: SMILR is detectable within plasma samples and correlates with patient CRP levels.
SMILR expression was assessed in plasma samples with varying degrees of CRP expression. All samples were blinded until analysis had been performed. **(A):** *SMILR* expression is increased in patients with higher CRP levels, analysed by qRT-PCR (n=13 CRP<2, n=13 CRP2-5 and n=15 CRP>5, *P<0.05, **P<0.01 via One-way ANOVA). Samples indicate *SMILR* levels normalised to spiked in c. elegans ama-1 and presented as 1/deltaCt. **(B):** Correlation between *SMILR* expression and CRP levels (linear regression P<0.0001).

In summary, this highlights *SMILR* as an inflammatory associated lncRNA that can be released and detected in the plasma from patients with cardiovascular disease.

5.4 Discussion

LncRNAs not only provide us with a new perspective to our understanding of disease mechanisms but also provide fresh therapeutic opportunities (Wapinski and Chang, 2011). In fact, lncRNAs have an advantage over protein coding genes in that their expression is more tissue specific, thus making them attractive as biomarkers and therapeutic targets. Additionally, a requirement of biomarkers is stability and lncRNAs are remarkably stable in body fluids and tissues, leading to the avoidance of invasive procedures (Qi and Du, 2013), (Tong and Lo, 2006). The experiments in this chapter aimed at identifying whether lncRNA expression was dysregulated in atherosclerotic plaque samples and if lncRNAs (*SMILR*), which was shown to be secreted in Chapter 4 – Section 4.3.9, could be sequentially detected in plasma from patients with inflammatory disease. The data presented here confirms that previously characterised atherosclerotic microRNAs are dysregulated in the atherosclerotic plaque endarterectomy samples from CAD patients. Utilising this model, lncRNAs and, in the case of *SMILR*, their associated mRNA, were shown to be dysregulated in a manner similar to that observed in VSMCs stimulated with inflammatory and proliferative stimuli. Finally, *SMILR* was identified in plasma samples and correlated with plasma CRP levels, highlighting the possibility that this lncRNA may be utilised as a biomarker.

The composition of ECM, the phenotype of cells within it and the volume of neointima, assists in the determination of the stability of atherosclerotic plaques (Finn et al., 2010). During the progression of atherosclerosis, VSMC are exposed to a plethora of signalling molecules, including inflammatory cytokines. Using the clinical gold-standard methods of ^{18}F-FDG and ^{18}F-fluoride PET/CT imaging to identify inflamed, necrotic and calcified atherosclerotic plaque (Rudd et al., 2002), (Joshi et al., 2014) it was identified that microRNAs -29, -143, -145 and 146 were differentially expressed in unstable regions when compared to controls. These microRNAs have been previously associated with key phenotypes

of atherosclerotic plaques including VSMC differentiation, inflammatory cell signalling (Taganov et al., 2006) and VSMC calcification (Du et al., 2012). For example, it is also known that the wingless-type MMTV integration site family member (Wnt) is required for osteoblast function and is involved in SMC transdifferentiation (Bostrom et al., 2011). MiR-29 regulates Wnt inhibitors, thus a downregulation of miR-29 potentiates the osteogenic phenotype (Kapinas et al., 2010). These effects have been confirmed via cellular transfection with miR-29 mimics which inhibited and miR-29 antagomiRs which enhanced SMC calcification under osteogenic conditions (Du et al., 2012). In concert with SMC transdifferentiation and acquisition of an osteoblast like phenotype, calcifying SMC also lose the expression of the contractile gene network. This phenotypic switch involves the miR-143/-145 cluster that regulates the SMC differentiated phenotype, in part by targeting the transcription factor, myocardin (Li et al., 2008). SMC transdifferentiation leads to a downregulation of this cluster and this is in agreement with studies indicating that circulating miR-145 levels are reduced in patients with atherosclerotic coronary artery disease, a disease that is often associated with vascular calcification (Rangrez et al., 2011). MiR-146, on the other hand, is the only microRNA from the panel that was upregulated in atherosclerotic plaques. MiR-146a has been shown to be induced by inflammatory stimuli but is proposed to exhibit a protective role in the setting of atherosclerosis via repression of nuclear factor-κB (NF-κB) signalling (Cheng et al., 2014). This is induced through miR-146 binding to multiple components of proinflammatory signalling pathways, including TRAF6, IRAK1, IRAK2, MyD88, RelB, STAT1, CARD10, and TLR4 and inducing their degradation (Cheng et al., 2014). Delivery of miR-146a mimetics has been shown to inhibit atherogenesis in a mouse model (Ma et al., 2015) and these findings establish that enhancing miR-146a expression can antagonise atherogenesis.

The association and co-localisation of *SMILR* with this classical miRNA profile and focal ^{18}F-FDG and ^{18}F-fluoride uptake within unstable atherosclerotic plaques suggested that *SMILR* may play a role in atherosclerosis through inflammatory and proliferative pathways. In keeping with the results that showed *HAS2* regulation by *SMILR* (Chapter 4), *HAS2* was also upregulated in the atherosclerotic plaque samples examined. This expression profile has been previously documented for *HAS2* and has been confirmed *in vitro* through the

utilisation of Thrombospondin-1 (TSP-1) treatment. TSP-1 is known to regulate genes involved in atherosclerosis and treatment of HSVSMC induced an increase in HAS2 expression (Maier et al., 2010). However, despite a significant up-regulation of HAS2, it is proposed that the hyaluron (HA), the protein produced by HAS2, is the main instigator in the control of atherosclerotic progression and vessel wall thickening and has been shown to be upregulated in atherosclerosis (Johnson, 2007), (Jain et al., 1996), (Riessen et al., 1996). Indeed, HA has been implicated in the recruitment of inflammatory cells (Jameson et al., 2005), known to play a prominent role in the initiation and progression of atherosclerotic lesion to an unstable plaque phenotype (Cuff et al., 2001) and is believed to function via CD44, for which HA is the principle ligand (Cuff et al., 2001). CD44 is an adhesion protein expressed on inflammatory and vascular cells and supports the adhesion of leukocytes to EC and SMCs (Ponta et al., 2003). Cuff et al. set out to evaluate the potential contribution of CD44 to atherosclerosis via assessment of atherosclerotic progression in CD-44 null mice on the $ApoE^{-/-}$ background. The authors noted a 50-70 % reduction in aortic lesions when compared to CD44 heterozygote littermates (Cuff et al., 2001). Additionally, it was shown that CD44 was required for phenotypic switching of SMC to a synthetic phenotype, a key trait of HA. The authors showed that HA was increased in their lesions and suggest that CD44 is the main mechanism of action of HA (Cuff et al., 2001). This further highlights the importance of the *SMILR*/HAS2/HA pathway in both phenotypic switching and in the progression of atherosclerosis. One limitation of this study is the inability to determine what exact cell type is producing the microRNAs, *SMILR* or *HAS2*. It is known that monocytes are an important group of cells in the innate immune system and in inflamed tissue, monocytes transform into macrophages that clear pathogens and modulate tissue repair and healing. Previous studies have shown a pivotal role for these cells in the pathogenesis of atherosclerotic plaque progression (Dickhout et al., 2008) and as such, further experiments to examine *SMILR* expression in inflammatory macrophages and monocytes and additional cell types will be required to confirm or deny if this is expression is solely from calcified SMC. Additionally, RNA FISH in tissue samples would provide further information as to the cellular localisation of *SMILR* within the plaque samples.

The ability to identify confidently a plaque, or patient, at particular risk of a major adverse cardiovascular event (i.e plaque rupture) remains an important goal of cardiovascular research. Long RNA transcripts, both mRNA and non-coding RNA, have previously been shown to be stable *in vivo* for up to 3 weeks (Pinel et al., 2014). As such the search for prognostic RNA biomarkers has greatly increased in recent years. qPCR analysis of plasma samples was performed to identify *SMILR* expression levels. qPCR is considered to be a reliable method for quantitative gene expression due to its accuracy, sensitivity and reproducibility (Lardizabal et al., 2012). However, to produce accurate results in qPCR assays, the use of robust normalisation strategy is important (Sauer et al., 2014). Generally, the use of a reference gene as an endogenous controls is the most commonly method for normalising qPCR gene expression data. However, no one gene has emerged as a universal reference gene and much debate surrounds some of the more commonly used reference genes, such as glyceraldehyde-3-phosphate dehydrogenase (GAPDH), which has shown variable expression under hypoxic conditions and in certain cancers (Rubie et al., 2005). Additionally, no gene encoding for a plasma membrane protein serves as a reference gene in plasma. This is because plasma membrane proteins are typically soluble proteins and their expression can vary greatly (Calcagno et al., 2006). As such, spiked in c.elegans RNA was utilised to account for variability between samples during RNA extraction and RT-PCR. This is an adaptation of the method commonly utilised for microRNA (Li and Kowdley, 2012). Utilising this method, it was found that *SMILR* could be detected in the plasma of patients with higher CRP levels indicative of chronic low grade inflammation. In light of these studies, it is proposed that this release could be due to the increased levels of *SMILR* in the diseased vasculature, although delineating whether plasma *SMILR* is simply a by-product of increased intracellular levels or is functionally active in disease pathology is difficult to definitively demonstrate. However, circulating levels of other non-coding RNA such as miR 143 and 145 have been associated with in-stent restenosis and as such have been proposed as biomarkers (He et al., 2014). The correlation of *SMILR* and high CRP further supports its expression in low grade chronic inflammatory settings as well as proliferative settings. Further large clinical cohorts will be required to ascertain if *SMILR* has prognostic potential in inflammatory vascular disease, and if so, whether it provides enhanced prognostic value over current biomarkers. For example, the lncRNA

LIPCAR was evaluated in 788 patients in order to ascertain its ability to survival in patients with heart failure (Kumarswamy et al., 2014). Similar patient numbers were observed in the validation of potential cancer biomarkers, where 559 patients were assessed (Zhou et al., 2015). Therefore, *SMILR* analysis would need to be performed in a similar sized cohort of patients to confirm the results.

Stability is a basic requirement for any biomarker. Previous studies have shown that the stability of miRNAs in plasma is due to their ability to be packaged into microvesicles or formation of protein complexes with miRNA-binding proteins and lipoproteins (Vickers et al., 2015, Zernecke et al., 2009). Whether lncRNAs have properties similar to these described for miRNAs is not known. However, what is known is that *SMILR* is not secreted from HSVSMC within microvesicles (Chapter 4). Further experiments are warranted to identify if *SMILR* is release attached to a protein in order to remain stable within the plasma. This would require lncRNA-protein pull down assays to be performed in plasma samples, however, to date, no lncRNA-protein interactions in the plasma have ever been examined.

Taken everything together, the results have demonstrated that lncRNAs, in a manner similar to microRNA, show differential expression patterns in diseased and healthy vessels and demonstrated that plasma levels of *SMILR* may potentially be useful as a biomarker of vascular disease. Nevertheless, many issues must be addressed before these findings can be translated into a clinically useful therapeutic or biomarker. The confirmation of the usefulness of plasma *SMILR* would need to be ascertained in a larger number of patients and from patients with different vascular pathologies. Furthermore, determination of *SMILR* plasma binding partners and how it is secreted would also need addressing. Nonetheless, these experiments highlight a potential role of ncRNAs as biomarkers and therapeutic targets in the setting of vascular disease.

Chapter 6 General Discussion

6.1 Discussion

This thesis contains work concerned with identifying and characterising novel lncRNA associated with VSMC proliferation, inflammation and vascular disease. Modulation of VSMC proliferation has translational potential in the treatment of several disease states, including vein graft failure, in-stent restenosis and atherosclerosis. Although surgical procedures have improved vastly over the years, there is still a lack of effective anti-proliferative therapeutics and successful biomarkers for these disease states. LncRNAs have been demonstrated to play roles in a variety of biological processes and cellular functions, however, very little is known as to the role of lncRNA in vascular pathology. As such, it was hypothesised that lncRNA would exhibit differential regulation in quiescent and proliferative SMCs and that functional characterisation of these lncRNA may enable the identification of targets for lncRNA therapeutics.

Initially, RNA-sequencing was performed on VSMCs treated with IL1α and PDGF in order to induce a pro-proliferative, pro-migratory phenotype and to identify novel lncRNA regulated by this cytokine and growth factor pair. The dual stimulation with IL1α and PDGF has been previously shown to induce synergistic effects on mRNA expression levels via joint activation of the NF-κB pathway (Fabunmi et al., 1996). In order to ensure high quality data was obtained, several quality control checks were utilised. Prior to sequencing RIN values and assessment of known IL1α responsive microRNA, miR146a, were determined to ensure quality RNA was sent for sequencing and assessment of read counts, mapping statistics and cluster analysis performed by Beckman Genomics ensured that the RNA-seq met quality standards. Following RNA sequencing, miR146a levels were further confirmed in the RNA-seq data set along with the synergistic up-regulation of MMP-3 and MMP-10.

The majority of reads obtained from the RNA-seq, under all conditions, corresponded to mRNA. Interestingly, IPA pathway analysis of canonical pathways confirmed the mRNAs with altered expression following IL1α treatment were significantly enriched in pathways related to cellular movement and inflammatory disease, while PDGF stimulation led to the marked enrichment in

cell cycle pathways. Furthermore, co-stimulation led to enrichment in cell cycle and cardiovascular development pathways, further confirming the activation of the IL1α and PDGF pathway. Of particular interest was the vast increase in protein coding gene expression when both IL1α and PDGF were present together. 1133 genes were significantly altered in dual stimulation compared to 518 protein coding genes altered following IL1α treatment and 540 following PDGF treatment, further highlighting the synergistic actions of this cytokine and growth factor. In accordance with this, lncRNA also showed differential expression patterns following IL1α, PDGF or dual stimulation utilising strict cut-off criteria (FDR<0.01, FPKM>1 and Fold change >4). Under all conditions the majority of lncRNA dysregulated following treatment corresponded to either antisense of intronic lncRNA as assigned by the Ensembl database. Due to being the two largest groups of lncRNA, intergenic and antisense lncRNAs were focussed on. To identify possible synergistic lncRNAs, the candidates (control vs IL1α and PDGF, FDR<0.01, LogFC<2, FPKM>1) were ranked according to their FPKM and level of up/down-regulation. 6 lncRNA, RP11-91k9.1, RP11-94a24.1 (*SMILR*), RP11-761I4.4, RP11-709B3.2, RP11-760H22.2 and AC018647.3, with the greatest fold change were selected as candidate lncRNA. LncRNA RP11-91k9.1 and RP11-94a24.1 both exhibited significant up-regulation following IL1α and PDGF treatment, however RP11-91k9.1 was only responsive to IL1α while RP11-94a24.1 (*SMILR*) exhibited an increase following both IL1α and PDGF treatment. All other lncRNAs, RP11-761I4.4, RP11-709B3.2, RP11-760H22.2 and AC018647.3, exhibited significant downregulation to both IL1α and PDGF treatment but to varying degrees. It has been shown that lncRNA are dysregulated in clusters around protein coding genes, possibly highlighting that these lncRNA/ mRNA pairs are under the same promoter control. As such, the expression of the most proximal protein coding genes to each lncRNA were determined from the RNA-seq results. Interestingly, 4 out of 6 of the lncRNA exhibited a similar change in expression to the most proximal protein coding gene and all 4 genes HAS2, ITGA11, DEPTOR and IL1α6, have all been associated with SMC function or vascular disease. Finally, each lncRNA was validated using qRT-PCR and the results exhibited almost identical expression patterns to those achieved in the RNA-sequencing.

Chapter 4 examined the descriptive characteristics of 4 validated lncRNAs (RP11-94a24.1(*SMILR*), RP11-761I4.4, RP11-91k9.1 and AC018647.3). Despite 6 lncRNAs being validated from the RNA-seq (Chapter 3- Section 3.4.3), only 4 lncRNAs (2 up-regulated and 2-downregulated) were taken forward for further functional analysis. These lncRNA were pursued as they exhibited the greatest fold changes between basal and stimulated cells and the functional characterisation of 6 lncRNAs was not possible to achieve within one single PhD project. All of these lncRNA were expressed in a tissue specific manner, consistent with previous reports (Tsoi et al., 2015), (Jiang et al., 2016) and all exhibited greater expression patterns in basal vascular smooth muscle cells, of either arterial or venous lineage, when compared to endothelial cells. This distinct patterns of expression is of key importance and it is believed that lncRNAs may prove beneficial biomarkers due to their distinct cellular and tissue patterns (Shi et al., 2016). Interestingly, all lncRNA, with the exception of RP11-94a24.1 (*SMILR*) showed similar patterns of expression in IL1α and PDGF stimulated venous SMC as arterial SMCs. RP11-94a24.1 (*SMILR*), on the other hand, exhibited significant upregulation to IL1α and PDGF in venous cells and significant down regulation in arterial cells, highlighting the stark differences between venous and arterial SMCs. . Interestingly, reports by Deng et al. revealed significant differences in the function and global transcriptome between coronary artery and saphenous vein SMC subtypes in response to oxidised low density lipoprotein (OxLDL), a key protein known to promote an inflammatory phenotype in vascular smooth muscle cells. Ttreatment induced opposite proliferative responses between HCASMCs and HSVSMCs, moderately inhibiting both proliferation and migration in HCASMCs but significantly promoting proliferation in HSVSMCs (Deng et al., 2006). OxLDL also elicited strong and dramatic differences in global gene expression responses and activated distinct signalling pathways between HCASMCs and HSVSMCs. For example, 2262 genes (13.8 %) were significantly altered by OxLDL in HCASMCs compared to only 835 genes (5.1 %) in HSVSMCs. These genes were enriched in distinct pathways and of particular interest were the stark differences in genes associated with extracellular matrix production, cell proliferation, calcium ion binding and cell growth (Deng et al., 2006). Arterial and venous SMC are derived from different embryological origins and are exposed to different signalling agents. Additional studies have also reported that venous SMCs under stress, such as exposure to the arterial hemodynamic environment in bypass surgery,

are prone to develop accelerated atherosclerosis, an important pathological process in vein graft disease (Motwani and Topol, 1998) and may explain, in part, the up-regulation of *SMILR* in stimulated venous and not arterial SMCs. It was also observed that stimulation of HSVEC led to a significant upregulation of RP11-91k9.1 but to a lower level than that observed in VSMC. Despite stimulated SMCs exhibiting a significant increase in *SMILR* expression, no increase was observed in EC treated with the same conditions. This is of clinical significance as several potential antiproliferative agents not only prevented smooth muscle cell proliferation but also delayed reendothelialisation in the stented segment(Joner et al., 2006), (Nakazawa et al., 2008). This is of importance as incomplete endothelialisation leads to delayed vessel healing and the induction of tissue factor expression which results in a prothrombogenic environment. This promotes thrombotic occlusion of the vessel and has been linked with higher rates of mortality in stent patients(Farooq et al., 2013). Therapeutic knockdown of *SMILR* could potentially lead to the inhibition of SMC proliferation and lack of effect on endothelial growth, as EC do not express *SMILR*.

Contrary to some expectations, examination of lncRNA stability revealed that lncRNAs are not generally unstable but rather show a wide variation in their stability profiles. LncRNA half-life values ranged from 4 h to greater than 19 h after cell transcription was blocked. The large variation in lncRNA stability is consistent with their functional diversity and is likely a reflection of their complex post-transcriptional regulation. Additionally, it has previously been demonstrated that a number of lncRNA characteristics correlate with stability, including genomic location, subcellular localisation, splicing and GC content (Clark et al., 2012). As such, the cellular location was determined via RNA fractionation. Neat1 and MALAT1, two known nuclear lncRNA exhibited almost 100 % nuclear expression under both quiesced and stimulated conditions. Interestingly both IL1α and PDGF up-regulated lncRNA, RP11-94a24.1 (*SMILR*) and RP11-91k9.1, exhibited a greater expression in the cytoplasm when at their highest levels of expression. AC018647.3 and RP11-761I4.4, lncRNAs down-regulated by IL1α and PDGF, both exhibited greater nuclear expression in quiescent cells. Interestingly, large studies have revealed that lncRNA typically favour nuclear lncRNA and a recent study suggests that as many as 95 % exhibit preferential nuclear localisation (Cabili et al., 2015).

Due to the high expression of RP11-94a24.1 in HSVSMC and its cell specific induction in response to pathological mediators of vascular injury, further studies focussed on RP11-94a24.1. This lncRNA was termed, smooth muscle induced lncRNA enhances replication (*SMILR*). Further QC of the *SMILR* transcript was performed in order to confirm its expression and to identify the full length sequence. An additional 2 primer sets targeting different exons of *SMILR* exhibited almost identical fold change results as the original primer set. Additionally, 5' and 3' RACE identified 6 additional base pairs at the 5' end and 316 base pairs at the 3' end of *SMILR*. This was fundamental for the generation of lncRNA FISH probes and was fundamental for the cloning of the full length sequence of *SMILR* required for LV production. RNA FISH confirmed the qRT-PCR results for the *SMILR* transcript, indicating a 30 fold increase following stimulation and also confirmed that *SMILR* was expressed both in nuclear and cytoplasmic compartments.

Functional analysis of *SMILR* was performed both through the utilisation of dicer substrate siRNA and a lentiviral vector. Firstly, dsiRNA are known for their off target effects on the interferon pathway. Probes to 2 known interferon genes revealed that administration of neither the dsiRNA to *SMILR* nor the negative control altered these interferon genes. Secondly, administration of the *SMILR* dsiRNA not only significantly altered *SMILR* expression but also significantly reduced proliferation and lowered the expression of the most proximal gene, HAS2 a known SMC proliferative gene. This is consistent with the literature where it has been previously shown that many lncRNA regulate the expression of adjacent genes. In order to confirm these results, all experiments were repeated with a second dsiRNA targeting and additional exon of *SMILR*. All experiments utilising the second dsiRNA directly mirrored the previous results. Additionally, *SMILR* overexpression was performed via the utilisation of a lentivirus at an MOI of 25 and an MOI of 50. Both concentrations elicited a dose dependent increase in *SMILR* expression that translated into a significant increase in SMC proliferation, consistent with the *SMILR* knock down data. However, overexpression of *SMILR* did not upregulate HAS2 expression. This is consistent with a *cis* acting lncRNA and several other studies have demonstrated that if the lncRNA is not inserted into the genome in the correct orientation or correct place then it cannot alter the expression of nearby genes. *SMILR*

upregulation following IL1α and PDGF treatment was not a unique event and two other genes were also activated around the *SMILR* locus, HAS2 and HAS2-AS1. Although the effect on HAS2 has been discussed already, it is also known that HAS2-AS1 regulates HAS2 expression via an alternative mechanism (Vigetti et al., 2014). Interestingly knock down of HAS2 did not affect either SMILR or HAS2-AS1 expression and knockdown of either lncRNA did not affect the expression of the other lncRNA, highlighting that these 2 mechanisms act independently to control HAS2 expression.

MicroRNAs have been reported to be secreted from cells as a means of cell to cell communication (Glynn et al., 2013). The ability of *SMILR* to be secreted from HSVSMC was determined from conditioned media. It was identified that *SMILR* is secreted from SMC following dual IL1α and PDGF treatment. However, *SMILR* was not detected in microvesicles (Thakar et al.) and it is proposed that *SMILR* is secreted via a non-exosome, non-MV method.

New lncRNAs are rapidly being uncovered, however, their mechanism of action remains to be elucidated. RNA pull-down assays are preliminary RNA-centric *in vitro* methods that enable the identification and characterisation of various proteins which interact with a given lncRNA of interest. *SMILR* pulldown assays were therefore optimised and refined to identify *SMILR* interaction protein partners. Mass spectrometry analysis of the lysates recovered from the *SMILR* pulldown experiments identified one protein, Staufen1 (STAU1), which was shown to be bound to *SMILR* and absent in all the control samples. Interestingly STAU1 has previously been shown to bind a small group of lncRNAs with various functions and has been recently shown to induce mRNA decay. During staufen mediated mRNA decay (SMD), STAU1, a double-stranded RNA-binding protein, recognises dsRNA structures formed by base pairing of 3'-UTR sequences with a lncRNA. STAU1 then recruits UPF1 to mRNA 3'UTRs thus triggering mRNA decay (Park and Maquat, 2013). This mechanism only exists in the cytoplasm and is required for the dynamic regulation of gene expression (Park and Maquat, 2013).

The final chapter of this thesis (Chapter 5) is concerned with the clinical aspects of lncRNA and their possible clinical utility. As such, the expression of all 4 previously studied lncRNA (*SMILR*, RP11-91k9.1, RP11-761I4.4 and AC018647.3) were all assessed in RNA obtained from carotid endarterectomy samples. These

samples were split into areas of plaque and adjacent ‘healthy’ tissue. Initially a panel of known inflammatory, SMC phenotypic switching and calcification microRNA were assessed to confirm adequate separation of plaque and ‘healthy’ tissue and to confirm that non-coding RNA molecules could be differentially expressed between samples. As expected, inflammation-associated miRNAs-146a and -146b were significantly upregulated in unstable plaques compared to adjacent quiescent tissue, while miR-29, which is inversely associated with osteoblastogenesis and arterial calcification, was down regulated in mineralised regions of the atherosclerotic plaque (Du et al., 2012, Cui et al., 2012). In addition, downregulation of the miR-143/145 cluster was observed, which is associated with SMC differentiation and aortic aneurysm formation (Ella et al., 2009), an event which has previously been linked to osteogenic differentiation of SMC, confirming that the expression of small non-coding RNAs was associated with PET/CT defined high-risk plaques. Assessment of lncRNA expression in the same sample set revealed that 3 out of 4, lncRNAs (*SMILR*, RP11-91k9.1 and RP11-761I4.4) exhibited similar patterns of expression in plaque samples and proliferative SMCs when compared to control vessels or quiescent cells. In alignment with the upregulation of HAS2 in stimulated SMC, HAS2 was also up-regulated in the atherosclerotic plaque when compared to control vessel. Interestingly, HAS2-AS1 was not significantly altered between the plaque and control samples. It has been previously documented that SMCs undergo phenotypic switching during atherosclerosis progression; however, one limitation of this study is the inability to determine which exact cell is responsible for the production of these lncRNAs, as experiments were performed on whole-plaque homogenates. As such, more detailed analysis in isolated inflammatory cells, such as monocytes and macrophages and fibroblasts will be required before it can be definitively determined that the expression changes are due solely to SMCs. To date, RNA-sequencing has been performed on 15 sets of human monocyte cells. Analysis of all 15 data sets did not identify the expression of any of the 4 lncRNAs (SMILR, RP11-91k9.1, RP11-761I4.4 or AC018674.3), possibly highlighting the potential that these lncRNA are smooth muscle specific (Mirsafian et al., 2016). However, these studies looked at peripheral blood mononuclear cell and not tissue macrophages.

The data presented thus far indicated that *SMILR* was upregulated during the development of cardiovascular disease and since it was also shown that *SMILR* was secreted from stimulated cells (Chapter 4 - Section 4.3.9), *SMILR* expression was assessed in plasma samples from a cohort of patients with atherosclerotic plaques and at risk of cardiovascular events and in a cohort of patients. As mentioned in Chapter 1 – Section 1-3, atherosclerosis is considered to be a multifactorial disease driven by inflammatory reactions. C reactive protein is an acute phase protein and its concentration in serum reflects the inflammatory condition in the patient. Levels of CRP are therefore capable of predicting both myocardial infarction and stroke (Paffen and Demaat, 2006). Therefore, all plasma samples were ranked in order of the serologic parameter CRP levels into 3 groups: CRP <2, CRP 2-5 and CRP >5 mg/L representing broad tertiles of CRP. *SMILR* could be detected in plasma samples from patients and correlated with plasma CRP levels. This highlights *SMILR* as an inflammatory associated lncRNA that can be released and detected in the plasma from patients with cardiovascular disease. A number of limitations must be addressed before these findings can be translated into a clinically useful, non-invasive screening strategy for vascular disease patients. These will be discussed in the future perspectives section below (Section 6.2).

6.2 Future Perspectives

As stated previously, large quantities of data have been generated via RNA-sequencing, documented in Chapter 3. Bioinformatic analysis of the RNA-seq only utilised the genome alignment method to determine lncRNA of interest. Further bioinformatic analysis could be employed to identify *de novo* transcripts that have not yet been identified in the human genome. Bioinformatic analysis is improving daily and it is hoped that analysis of both lncRNA and mRNA partners may be utilised to identify lncRNA functional networks that may be useful for implying lncRNA function. Additionally, RNA-sequencing techniques are also improving. Further refined sequencing utilising capture-seq or single cell methodologies may provide further analysis of lncRNA in vascular disease.

Although identification of lncRNAs is relatively straightforward, investigating how these lncRNAs function, is a much greater challenge. At present lncRNAs do not harbour any known consensus sequences to detail how they function nor do they exhibit predictable or well defined mechanisms of action. Knockdown and overexpression experiments currently remain the best method to delineate function, while RNA: RNA and RNA: protein pulldowns remain the best methods to identify specific binding partners and thus begin to infer mechanism of action. As such, further experiments examining the whole transcriptome following *SMILR* knockdown and subsequent overexpression are still required to examine the global effects of *SMILR* on SMC function. This data has been sent for RNA-sequencing and will undoubtedly provide further information as to what genes and pathways *SMILR* may be affecting. Additionally, PDGF is known for its effect on SMC proliferation, however further cell cycle analysis to identify if cell cycle arrest is occurring and to determine is *SMILR* may affect SMC migration in response to IL1α alone still remains to be elucidated.

As efforts to identify new and novel lncRNA progress, so too does our ability to modulate their expression. The emergence of precision-guided genome editing will be of great value in this context. Many lncRNA are localised solely to the nucleus, which can make robust knockdown utilising RNAi difficult to achieve. Thus genetic editing at a genome level would prove advantageous. Several tools have previously been utilised for this purpose, for example zinc finger nuclease (ZFN) (Urnov et al., 2010) and transcription activation-like element nuclease (TALEN) (Gaj et al., 2013). Recently a new mechanism has been employed called clustered regularly interspaced short palindromic repeats (CRISPR)/CRISPR-associated (Cas) genes. Originally identified in select bacteria as a mechanism of adaptive immunity to protect the organism from invading genetic material (Barrangou et al., 2007), CRISPR is now commonly utilised as a tools to edit genetic material. Different types of CRISPR mechanisms have been discovered, of which the type II mechanism is the most studied and employed. In this case invading DNA, in the form of virus or plasmid, is fragmented and incorporated into the CRISPR locus. The locus is transcribed and the transcripts are processed to generate small RNAs (CRISPR-RNA). These small RNAs guide effector endonucleases that target invading DNA based on sequence complementarity. One Cas protein, Cas9, has been shown to be required for type

II CRISPR function. Cas9 participates in the processing of CRISPR-RNA and the destruction of target DNA. The function of Cas9 in these steps relies on the presence of two key nuclease domains, a RuvC-like nuclease domain located at the amino terminus and a HNH-like nuclease domain that resides in the mid-region of the protein. During DNA destruction the HNH and RuvC-like nuclease domains cut both DNA strands, generating double-stranded breaks at sites defined by a 20-nucleotide target sequence within an associated CRISPR-RNA transcript (Rath et al., 2015). The simplicity of the type II CRISPR nuclease makes this system amenable to adaptation for genomic editing. Generation of a synthetic CRISPR-RNA, now known as a guide RNA, targets endonuclease activity to any genetic site required (Sander and Joung, 2014). CRISPR/Cas9 was initially utilised in protein coding genes, however, one of the challenges for knockout of non-coding genes is that a small deletion or insertion generated by the standard CRISPR/Cas9 system may not necessarily lead to functional loss of a given non-coding gene because of the lack of an open reading frame. As such, the CRISPR/Cas9 system has been edited to allow the utilisation of a dual guide RNA vector that can make two cuts simultaneously at designated sites so that a large fragment can be deleted (Ho et al., 2015). This approach has now been utilised for the successful deletion of miR-21, miR-29a, lncRNA-21a and AK023948 in various human cell lines (Ho et al., 2015). However, utilisation of CRISPR/Cas9 in primary human VSMCs is currently problematic. Following CRISPR transfection, cells need to be single cell seeded to obtain a clonal population. Due to their propensity to terminally differentiate, as well as issues with contaminating adventitial fibroblasts, utilisation of primary HSVSMC cultures is frequently restricted to passages 3-5. This renders the application of CRISPR/Cas9 methodologies infeasible for HSVSMCs, due to the inability to maintain and bulk up cultures beyond passage 5. One way to overcome these inherent limitations when aiming to modulate lncRNA expression may be the utilisation of CRISPR methodologies in stem cells and subsequent differentiation to functional SMCs.

Unlike microRNAs, which almost universally function through a predictable and well-defined process (Wahid et al., 2010), lncRNAs function and mechanisms of action are as diverse as protein coding genes. LncRNAs may act as decoys, sponges, activators or repressors or scaffolds and many have been shown to harbour multiple mechanisms and functions depending on their cellular

localisation (Wang and Chang, 2011). This creates several difficulties when attempting to derive the mechanism of action. Additionally, lncRNAs do not always undergo canonical base-pairing (Baker, 2011), so the sequence of the transcript yields very few clues about how lncRNAs interact with the genome and other protein/RNA partners. One such mechanism that has been employed to bypass this problem is the utilisation of a technique for identifying lncRNAs bound to particular proteins. RNA immunoprecipitation followed by sequencing (RIP-seq) uses antibodies to pull ribonucleoproteins from cell lysates and determines which RNA molecules are associated with them. This has been utilised to identify which lncRNAs are attached to the polycomb complex in embryonic stem cells. Lee et al. identified more than 9000 lncRNAs that interact with the complex allowing the mechanism of vast quantities of lncRNAs to be deduced from one single experiment (Zhao et al., 2010). However, identifying precisely what lncRNAs are doing requires more than identification of the lncRNAs protein binding partner.

Although work has begun investigating the RNA: protein interactions of *SMILR* and has revealed a possible mechanism through STAU1 mediated mRNA decay, further experiments are still warranted to confirm this interaction. This will include transfection of HA tagged staufen or a control plasmid and *SMILR* into cells followed by pulldown using an HA antibody to identify *SMILR* enrichment in the pulldown samples using the staufen plasmid. Additionally, pulldown experiments should be performed to pulldown endogenous staufen using a staufen anti-body to determine the enrichment of *SMILR* in smooth muscle cells. Finally, RNA-seq analysis of both *SMILR* pulldowns and staufen pulldowns in smooth muscle cells will be required to identify which mRNA *SMILR* may be guiding to staufen for degradation. Additionally, this will identify if other SMC specific lncRNAs may bind staufen and will allow a more global effect of staufen to be assessed in VSMCs. At present no data exists as to the role of staufen in VSMCs. The ultimate drawback of this will undoubtedly be the extraction of sufficient quantities of RNA from SMCs in order to perform RNA-seq. Additionally, STAU1 mediate *SMILR* function is proposed to be the cytoplasmic function of *SMILR* and additional nuclear experiments will be required to determine by which mechanism *SMILR* alters HAS2 expression.

The results from the atherosclerotic sections from Chapter 5 identified that both small and long non-coding RNA were differentially regulated in carotid endarterectomy plaque sections and adjacent 'healthy' control tissue. Further RNA-sequencing experiments have recently been performed within the lab from additional samples. This newly collected data will allow the complete transcriptome to be discovered in these unique samples and will open up new avenues for research on both mRNA and lncRNA in CVD. The one limitation of this study is that RNA-sequencing will be performed on whole tissue homogenates. Further tissue and cell panel analysis will be require to identify which cell or cell types are owing to the changes in lncRNA expression between plaque and control sections.

Work described in this thesis has only focussed on vascular pathologies including intimal formation and atherosclerosis. If possible it would be interesting to assess the levels of *SMILR* in sections of failed vein grafts. This would also require the optimisation of RNA in-situ in human sections in order to identify what cells are expressing *SMIRL*. Additionally, other smooth muscle cell proliferative diseases exist, including pulmonary artery hypertension. Therefore, similar profiling and siRNA mediated experiments could also be performed in this setting of vascular pathology in order to determine the role of *SMILR* in this disease state. Moreover, *SMILR* showed greatest levels of expression in the heart in the tissue panel analysis. Therefore, it may be of interest to identify if *SMILR* expression is altered in areas of the heart following myocardial infarction. Additionally, it is already known that *SMILR* can be detected in plasma samples. It would be interesting to assess if secreted levels of *SMILR* are altered in patients before and after myocardial infarction and if *SMILR* may be used as a biomarker in the setting of MI.

LncRNAs such as *SMILR* are poorly conserved and the apparent lack of orthologous mouse lncRNA gene constrains the extent to which experimental analyses can be performed to rigorously determine function. On the other hand, mouse only specific lncRNAs have limited translational relevance to study human development and disease. It is hoped that with a better understanding of lncRNA function, greater lncRNA orthologues may be discovered that may not contain complete conservation but sufficient conservation or synteny to conserve their

function. Additionally structural similarity between lncRNAs, with little sequence homology, may nevertheless exhibit comparable function across species. Further identification of the structure of *SMILR* may lead to the identification of a similar lncRNA in mouse models. Nevertheless, the third exon of *SMILR* is conserved in the pig genome. Further analysis to identify if IL1α and PDGF treatment induces both the pig HAS2 and pig *SMILR* will be of great importance. Additional RNA samples are available from pig stent studies previously performed in the lab. If the pig version of *SMILR* is expressed in pig, then this opens up new means to employ experimental models of *SMILR* knockdown to assess the effects on neointimal formation.

Chapter 4 demonstrated that *SMILR* could be released from SMC following dual stimulation with IL1α and PDGF. *SMILR* was not detected within microvesicles released from these SMCs and it was hypothesised that *SMILR* was released via a non microvesicle method. Further confirmation could be performed through the transfection of a tagged *SMILR* into SMCs. The expression of this tagged version could be determined in cell media. One of the recent and emerging areas of interest in regard to lncRNA biology is the role of lncRNAs in cell-cell communication locally and at a distance. LncRNA cell: cell communication is a relatively new area of research, as such, no data is available on lncRNA cell: cell communication in vascular cells. From cancer studies it appears that lncRNA that are enriched with microRNA binding sites appear to be enriched in cancer exosomes, along with the subsequent microRNA, however, results from this study did not identify the function of these lncRNAs in cancer biology (Ahadi et al., 2016). One additional study highlighted that cancer exosomes could be uptaken into mesenchymal stem cells that are recruited to the area in an attempt to provide them with genetic material. Mesenchymal stem cells can be attracted to tumour sites contributing to tumour development. The authors found that lung tumour cell derived exosomes could be up taken by the mesenchymal stem cells leading to a change lncRNA expression within the stem cells, this altered the differention of the stem cell (Wang et al., 2016a). Again with this study it was identified that the lncRNA could be up taken by the receipt cell, however, the function of the lncRNAs was not addressed. Vast amounts of research are still required to identify the function and mechanisms by which lncRNA cell: cell interaction occurs. Although nothing is known as to

the cell: cell communication of lncRNA in vascular cells, data exists about microRNA. Previously, it has been documented that microRNA are packaged into microvesicles for communication between vascular EC and SMCs, highlighting their ability to function at distant sites (Deng et al., 2015). One prominent example of this is the enrichment of the miR cluster miR143/145 in HUVEC exosomes following shear stress or transduction by Krüppel-like factor 2 (KLF2), a critical regulator of endothelial gene expression patterns. Co-culture experiments between KLF2 transduced HUVECs and aortic SMCs demonstrated that both miR143 and miR145 could be transferred to SMCs via exosomes thus allowing cell: cell communication (Hergenreider et al., 2012). As documented *SMILR* is not expressed in exosomes, however conditioned media could be removed from SMCs and added to EC, which do not express *SMILR,* to determine if *SMILR* may be taken up by endothelial cells. Additionally, if any of the other validated lncRNA are expressed in exosomes then the co-culture method could prove beneficial in the assessment of lncRNA cell: cell communication.

Due to their ability to be secreted from cells microRNA research then moved to focus on microRNA biomarkers. As such, many microRNAs have been found to be dysregulated in cardiovascular diseases such as acute myocardial infarction and coronary artery disease. MiR-208a is a heart muscle specific microRNA, which is involved in the regulation of myosin heavy chain production during cardiac development (Cordes and Srivastava, 2009). In a study of 33 acute myocardial infarction and 30 non-acute myocardial infarction patients that presented with chest pain, miR-208a was not detected in the plasma of any of the non-myocardial infarction patients and was detected in 90.9 % of myocardial patients within 4 h of the onset of chest pain, even in patients where cardiac troponin I (cTnI) levels, the main marker of myocardial infarction, were not yet affected (Wang et al., 2010). Accordingly, lncRNA research has followed a similar manner and the release of lncRNAs from cells and potential use as biomarkers has now been investigated. LncRNAs such as LIPCAR and CoroMarker have been shown to be expressed in plasma and correlate with disease states (Kumarswamy et al., 2014). Chapter 5 assessed the levels of *SMILR* in plasma from patients with CVD, however, there were some limitations to this study. Firstly, *SMILR* expression was only assessed in a relatively small cohort of patients (n=13 or n=15 per tertile group). Further analysis of a larger cohort will be required to validate

these observations, and to verify if the expression of *SMILR* is correlated with CRP levels. Secondly, it is proposed that plasma lncRNAs must be protected as RNase activity in plasma is high. Thus further experiments will be required not only to detect how stable *SMILR* is in relation to RNAse A treatment but also if it can withstand periods of incubation at RT and subsequent freeze thaw cycles, key traits required as a biomarker. Finally, it must be addressed how this lncRNA is secreted out of the cell and if it remains bound to a carrier within the plasma. This will require the utilisation of RNA: protein pulldown experiments from plasma samples, something that has never been performed before and will undoubtedly require optimisation to achieve. Further detailed analysis of lncRNAs in larger cohorts is still required, but they hold promise that one day lncRNA biomarkers may be clinically utilised.

The transition from lncRNA biomarkers to lncRNA therapeutics is also showing promising advances and may hold promise that some of these techniques may be employed in a therapeutic setting for *SMILR*. Companies and organisations such as MiRagen Therapeutics and Regulus are developing ncRNA-based strategies (microRNA) against cancer, cardiovascular and neurological diseases. In March 2016, MiRagen Therapeutics announced the initiation of a Phase I clinical trial of its anti-cancer product MRG-106, a microRNA antagonist of miR-155. miR-155 is pathologically increased in many forms of lymphoma including cutaneous T-cell lymphoma (Kopp et al., 2013), the main target of the clinical trial. It has been shown that MRG-106 enters lymphoma cells and initiates programmed cell death via inhibition of miR-155 (Seto et al., 2015). MiR-155 has previously been shown to control differentiation and proliferation of blood and lymph cells (Seddiki et al., 2014) and as such inhibition of miR-155 in lymphoma cells prevents the aberrant proliferation associated with cancer cells (Seto et al., 2015). This is the first clinical trial in lymphoma patients of an antimiR that targets a well-known oncogenic microRNA and holds promise that one-day lncRNAs may also be utilised therapeutically. Additionally, Regulus Therapeutics, a joint venture of Alnylam Pharmaceuticals and Isis Pharmaceuticals based in La Jolla, California, is also developing several microRNA therapeutics including oligonucleotide inhibitors of miR-21 for the treatment of fibrotic diseases and cancer. RG-012 is a single stranded oligonucleotide that binds to and inhibits the function of miR-21 and is being designed for the treatment of Alport syndrome, a genetic

condition where the main symptom is kidney disease and fibrosis (Thorner, 2007). Alport syndrome is caused by mutations in the type IV collagen genes (Col4A3, Col4A4 and Col4A5) (Thorner, 2007) and type IV collagen is important for maintaining the integrity of the glomerular basement membrane, a vital component in the kidney structure and filtration process (Scott and Quaggin, 2015). The genetic mutation in the collagen gene results in thickening in the glomerular basement membrane and impairment of glomerulus filtration, thus Alport syndrome patients experience a progressive loss of kidney function, which ultimately leads to end stage renal disease requiring dialysis or kidney transplantation (Kruegel et al., 2013). With no approved therapies, Alport syndrome is a disease with an urgent unmet medical need. miR-21 is up-regulated in Col4A3 deficient mouse models of Alport syndrome and in human kidney disease patients (Gomez et al., 2015), (Chau et al., 2012). Pre-clinical data demonstrated that RG-012 induced potent inhibition of miR-21 *in vitro* and *in vivo* and demonstrated a decreased renal fibrosis and increased life span in pre-clinical mouse models (2015). In December 2015 Regulus initiated the Phase 1 first in man, randomised, double blinded, placebo-controlled study to evaluate safety and tolerability of subcutaneous RG-012 in healthy volunteers. RG-012 was well tolerated and did not show any adverse effects in the 40 participants (2015) and will therefore be progressing to Phase II clinical trials in the near future. This highlights the current advances in RNA therapeutics and their translational importance. If required, these technique could potentially be employed for the translational evaluation of SMILR as a lncRNA therapeutic.

Although lncRNA clinical trials are still several years away and the full mechanism of lncRNAs has still to be elucidated, several types of approaches can be considered to target lncRNA and to modulate their expression for therapeutic purposes. An overview of the proposed mechanisms is shown in Figure 6-1. Similar to other genes, lncRNAs can be targeted for degradation through the utilisation of siRNA mediated degradation via the RISC associated complex or through the use of single stranded GapmeRs. GapmeRs consist of a DNA stretch flanked by locked nucleic acid nucleotides that complementary bind to lncRNA, inducing their degradation via an RnaseH-dependent mechanism (Castanotto et al., 2015). The final mechanism for degradation is via catalytic degradation. Hammerhead ribozymes have ~20 nt long arms flanked by a central loop. These

arms facilitate the binding to lncRNA leading to degradation via a protein-independent mechanism (Fukuda et al., 2012). It is also well known that lncRNAs exhibit dynamic binding affinities for other DNA, RNA and proteins. Small molecule inhibitors could mask the binding site for lncRNAs and interrupt the association with its binding partners. Some lncRNA have been shown to exhibit multiple binding partners (Yang et al., 2015b) and as such, specific binding site inhibitors could be designed to disrupt one single binding partner, allowing its other functions to remain intact. Small molecules could also be utilised to interfere with the formation of RNA secondary structure and disrupt folding patterns required for the lncRNA to function, a key trait previously demonstrated between small molecules and DNA structure (Waller et al., 2009). Finally, aptamers, single stranded oligonucleotides or peptide aptamers, have shown great promise therapeutically (Ni et al., 2011). Aptamers are short synthetic single-stranded oligonucleotides that specifically bind to various molecular targets such as small molecules, proteins and nucleic acids. The term “Aptamer” is from the Latin word aptus, meaning “to fit”, which was chosen to describe the lock and key relationship between aptamers and their binding targets (Ni et al., 2011). They are currently undergoing clinical trials for many different diseases such as non-small-cell lung cancer, breast cancer and acute myeloid leukemia (Soundararajan et al., 2008),(Bates et al., 2009). In 2004, an anti-VEGF aptamer (Eyetech Pharmaceutics/Pfizer) was approved by the FDA for macular degeneration (Trujillo et al., 2007). Aptamers can be designed to inhibit binding sites in a similar manner to small molecule inhibitors, or can be utilised to stabilise lncRNAs thus increasing their half-life and functional availability. All of these techniques could be adapted and employed therapeutically to reduce *SMILR* expression in both the setting of atherosclerosis and intimal hyperplasia.

Despite the proposed mechanisms to target lncRNA, a major challenge of all of these approaches is to accomplish target-specific delivery (Tiwari et al., 2012). The use of synthetic nanoparticles for delivery of biologically active constructs has been extensively investigated with promising results (Deshayes and Gref, 2014). An alternative approach involves the use of extracellular vesicles, biologically derived particles that are involved in intercellular communication and could be packaged with RNA targets for successful targeted therapy (Chen et al., 2016). It has also been shown that lncRNAs within extracellular vesicles

retain their functional activity after being taken up by recipient cells (Parasramka et al., 2016). Further experiments are required to ascertain if these mechanisms will work with lncRNAs *in vivo*. However, the setting of coronary artery bypass grafting (CABG) provides an effective method for the delivery of therapeutic lncRNA without the need for systemic delivery. CABG offers the advantage of tissue accessibility *ex vivo* as there is a period, typically of up to 30 min, where the extracted saphenous vein segment is awaiting engraftment. This provides a window of opportunity for the transfection or incubation of lncRNA therapeutics under controlled conditions, reducing risks associated with inflammatory responses to therapeutics following systemic delivery. Furthermore, it has been demonstrated in a large animal model of vein graft failure that ex vivo adenoviral delivery of a therapeutic transgene (TIMP-3) is feasible and effectively attenuates neointima formation following surgical vein graft implantation (George et al., 2011). Delivery of lncRNA therapeutics in an *ex vivo* setting could potentially reduce any off target effects, by achieving specific delivery to the vascular bed of interest. Interestingly, therapeutic utilisation of a *SMILR* siRNA may be beneficial in this setting. *SMILR* is not expressed in endothelial cells, thus administration of an siRNA or other method targeting *SMILR* should result in a reduction of SMC proliferation with no effect of endothelial proliferation.

.

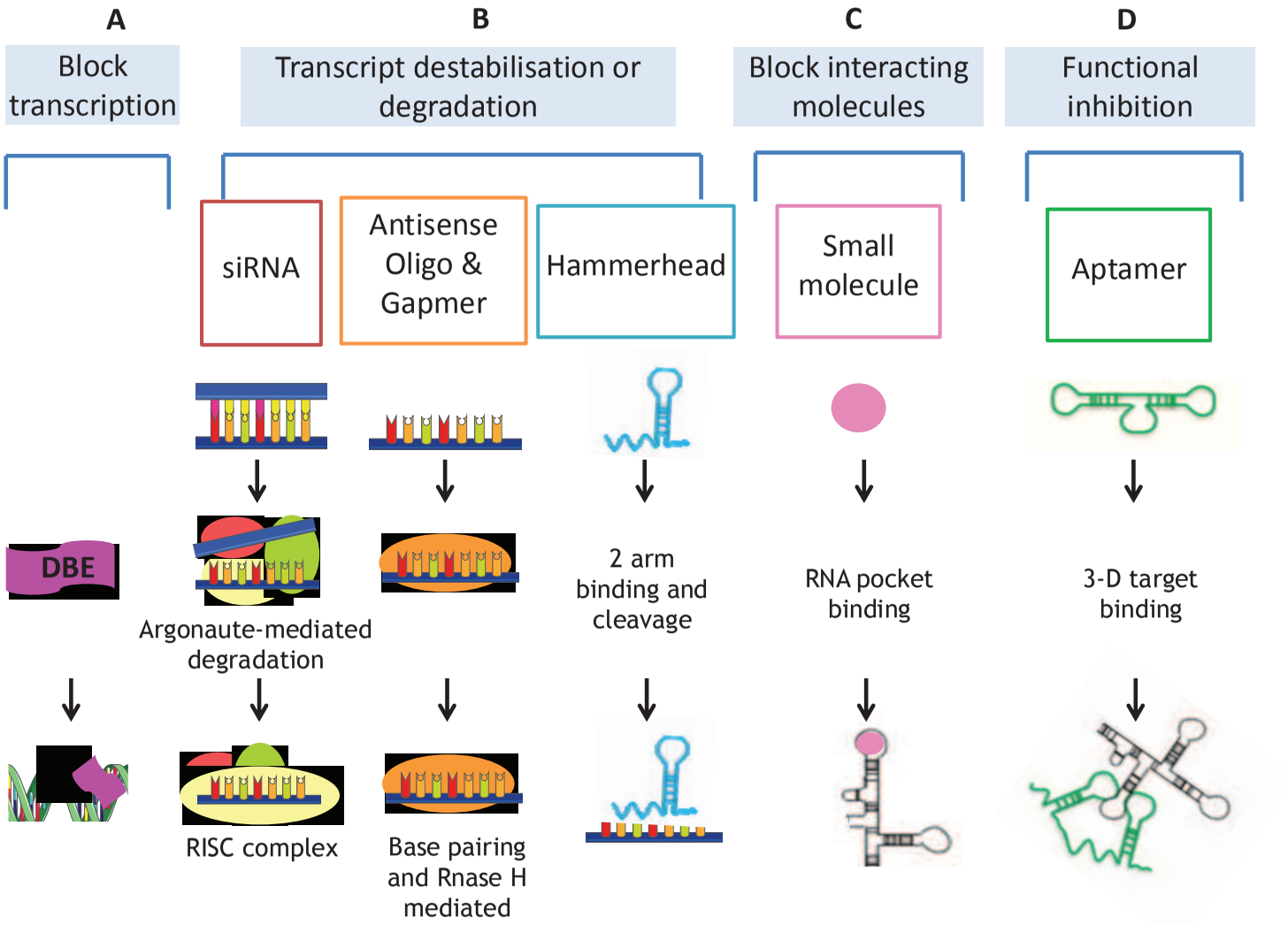
A
B
C
D
Block transcription
Transcript destabilisation or degradation
Block interacting molecules
Functional inhibition
siRNA
Antisense Oligo & Gapmer
Hammerhead
Small molecule
Aptamer
DBE
Argonaute-mediated degradation
2 arm binding and cleavage
RNA pocket binding
3-D target binding
RISC complex
Base pairing and Rnase H mediated

Figure 6-1: Strategies to target lncRNA.
(A): DNA-binding elements (DBE) can target the genomic locus to alter lncRNA transcription. **(B):** siRNAs can bind to complementary lncRNA sequences through RISC (RNA-induced silencing complex). Gapmers (8–50 nt long single-stranded DNAs or RNAs can carry out sequence specific and RNase H-mediated lncRNA degradation. Ribozymes (single-stranded RNA) can undergo cellular processing to expose the hammerhead structure of the binding arms that bind with target sites and result in cleavage of the target lncRNA. **(C):** Small synthetic molecules can block binding of lncRNAs with protein, DNA, RNA or other interacting complexes by associating with specific binding pockets. **(D):** Aptamers (3- dimensional short RNA or DNA oligonucleotides) can bind at specific structural regions to target lncRNA and antagonise their association with their binding partners. Figure adapted from (Parasramka et al., 2016).

6.3 Concluding remarks

In summary, the findings presented in this thesis confirm vast changes in global lncRNA expression profiles in quiescent and stimulated SMCs and uncover many previously un-studied lncRNA, including the human vascular SMC enriched lncRNA *SMILR*, that was shown to be dysregulated in the setting of atherosclerosis and cardiovascular disease. Functional characterisation of *SMILR* revealed that this novel lincRNA increases cell proliferation which may be linked to its ability to regulate the proximal gene HAS2. In the clinical setting, it was discovered that *SMILR* can be released from cells and is detectable in plasma from CVD patients with enhanced inflammation and thus susceptibility to atherosclerosis. These findings support the growing body of evidence that non-coding RNAs can act as mediators to modulate disease pathways. From a mechanistic point of view, it is proposed that *SMILR* regulates a cytoplasmic mRNA via the staufen1-decay pathway and regulates HAS2 via a currently unknown *cis* mechanism. Additional studies will need to be performed to identify other lncRNAs, using the RNA-seq data set to pinpoint their exact mechanisms and functions. Taken together, these observations broaden our awareness of the complex interplay between lncRNA and protein coding genes. The emergence of lncRNAs as regulators of gene expression will undoubtedly alter our understanding of the complex regulation network of pathological VSMC proliferation in vascular disease and may provide a means to specifically target VSMC or identify patients at risk of major adverse vascular outcomes.

Appendix

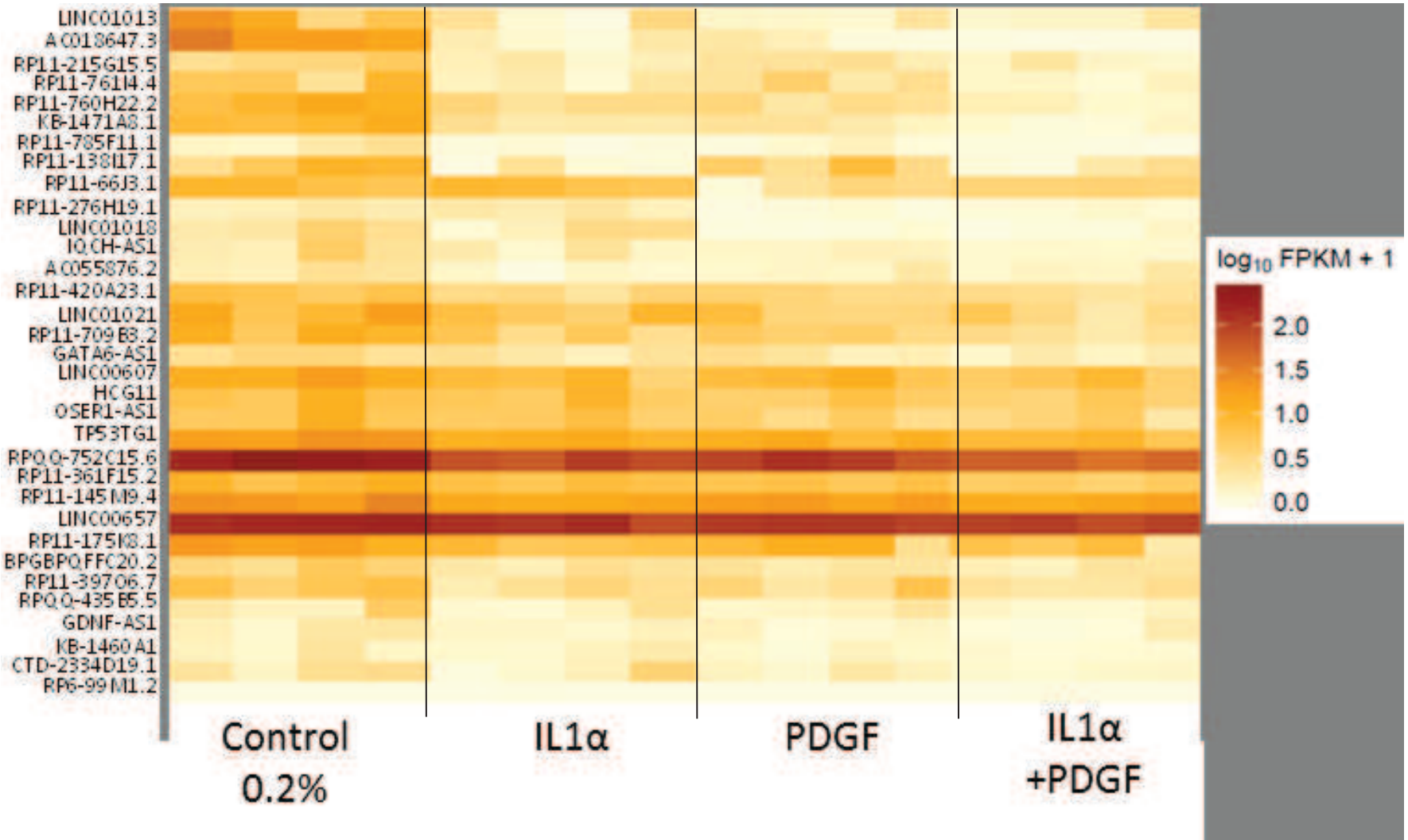
LINC01013
AC013647.3
RP11-215G15.5
RP11-761I4.4
RP11-760H22.2
KB-1471A8.1
RP11-785F11.1
RP11-138I17.1
RP11-66J3.1
RP11-276H19.1
LINC01018
IQCH-AS1
AC055876.2
RP11-420A23.1
LINC01021
RP11-709B3.2
GATA6-AS1
LINC00607
HCG11
OSER1-AS1
TP53TG1
RPQQ-752C15.6
RP11-361F15.2
RP11-145M9.4
LINC00657
RP11-175K8.1
BPGBPQFFC20.2
RP11-397O6.7
RPQQ-435B5.5
GDNF-AS1
KB-1460A1
CTD-2334D19.1
RP6-99M1.2
Control
0.2%
IL1α
PDGF
IL1α
+PDGF
log10 FPKM + 1
2.0
1.5
1.0
0.5
0.0

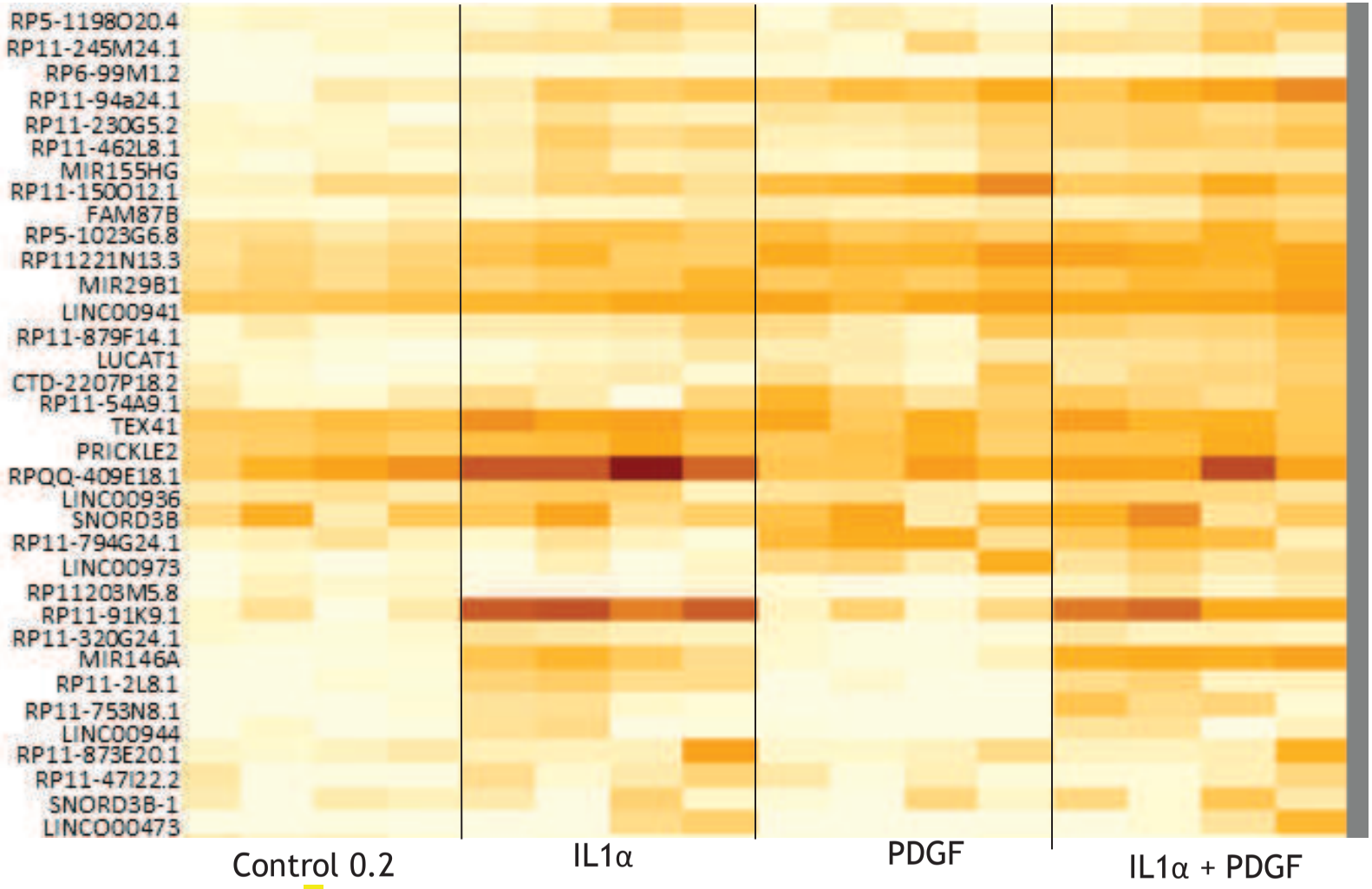
RP5-1198O20.4
RP11-245M24.1
RP6-99M1.2
RP11-94a24.1
RP11-230G5.2
RP11-462L8.1
MIR155HG
RP11-150O12.1
FAM87B
RP5-1023G6.8
RP11221N13.3
MIR29B1
LINC00941
RP11-879F14.1
LUCAT1
CTD-2207P18.2
RP11-54A9.1
TEX41
PRICKLE2
RPQQ-409E18.1
LINC00936
SNORD3B
RP11-794G24.1
LINC00973
RP11203M5.8
RP11-91K9.1
RP11-320G24.1
MIR146A
RP11-2L8.1
RP11-753N8.1
LINC00944
RP11-873E20.1
RP11-47I22.2
SNORD3B-1
LINC00473
Control 0.2
%
IL1α
PDGF
IL1α + PDGF

Appendix Figure 1: Heat Map. Expanded heat map of LncRNA differentially regulated between 0.2 % control and IL1α and PDGF conditions.

Appendix Table 1: Differential RNA expression in IL1α stimulated HSVSMC compared to 0.2 % control from RNA-seq. Results for RNA-seq were filtered on a log fold change (FC) greater than 2 or less than -2 (4 fold change up or down regulated) and a false discover rate (FDR) less than 0.1.

Gene	LogFC	FDR			
CXCL6	9.117569	1.72E-24	C2	4.063534	1.05E-10
CXCL3	6.813209	1.72E-24	C2	4.058054	1.08E-10
TNFAIP3	4.361765	3.76E-23	C2	4.06449	1.08E-10
CXCL2	5.461195	1.51E-21	C2	4.057413	1.08E-10
CXCL1	8.004426	1.95E-20	AC005549.3	3.864378	1.08E-10
CCL2	4.294493	3.50E-19	C2	4.044865	1.08E-10
CXCL5	7.833873	1.91E-18	IL1α7RD	-3.11226	1.34E-10
IL7R	5.466802	7.39E-18	C2	4.038458	1.75E-10
NAMPT	3.351557	1.89E-17	MT2A	3.504686	2.13E-10
NAMPTL	3.315296	2.31E-17	CA12	2.428266	4.35E-10
CDCP1	3.705249	2.65E-16	IRAK3	2.306713	4.46E-10
AMPD3	3.689674	1.92E-15	HSD11B1	4.300382	8.74E-10
IL6	4.081932	1.92E-15	AKR1B1	3.57613	8.74E-10
WWC1	5.909523	3.60E-15	BDKRB2	3.926338	1.17E-09
C1QTNF1	3.644883	5.18E-15	MFAP4	-3.17345	1.17E-09
IL8	7.501118	7.33E-15	OGN	-3.85253	1.22E-09
SOD2	3.549848	1.27E-14	TRAF3IP2	2.100023	2.64E-09
MIR146A	6.340469	3.17E-14	C3	4.642853	2.67E-09
EHF	6.949591	1.38E-13	CLDN1	5.458483	3.13E-09
CMKLR1	-4.37882	3.26E-13	KYNU	10.44975	3.49E-09
CSF2	7.642751	3.26E-13	TRPA1	3.741428	3.57E-09
STC1	6.457953	5.49E-13	DEPTOR	-2.20395	3.68E-09
CSF3	7.152789	5.97E-13	GPRC5B	3.638645	3.82E-09
ABI3BP	3.434324	6.49E-13	CD82	2.741757	3.82E-09
SLC39A14	2.530822	1.61E-12	WTAP	2.36673	3.88E-09
NFKBIA	2.183376	2.39E-12	IKBKE	2.358376	4.51E-09
RDH10	-2.77877	2.49E-12	CCL8	8.094048	6.81E-09
AC073072.5	3.803747	2.79E-12	IKBKE	2.349318	8.11E-09
ZC3H12A	2.861669	2.91E-12	PPP4R4	3.405332	8.23E-09
BIRC3	4.63469	4.60E-12	INMT	-3.08954	8.76E-09
RP11-91K9.1	5.808561	4.70E-12	TMEM171	3.350221	1.03E-08
TNFAIP6	3.798322	4.74E-12	HAS2	3.484411	1.22E-08
SAA1	7.841417	1.40E-11	PDLIM4	2.581537	1.31E-08
FNIP2	-2.48715	1.78E-11	SERPINE1	2.402141	1.64E-08
ELF3	6.785036	1.79E-11	MMP-3	6.772939	1.76E-08
PRG2	3.252568	1.81E-11	MMP-3	6.737373	1.77E-08
C2	4.067221	8.71E-11	CTSS	3.919927	2.85E-08

TMC3	-4.84079	4.21E-08
LPAR4	4.90506	4.38E-08
STEAP1	2.539334	5.49E-08
3-Mar	2.324811	5.73E-08
CGNL1	3.603506	7.03E-08
IL36RN	10.07754	1.00E-07
LIF	3.575373	1.02E-07
ZNF704	-4.12506	1.10E-07
POU2F2	4.000179	1.29E-07
CCL7	6.67148	1.29E-07
RASSF2	-3.41332	1.29E-07
RCAN1	3.578355	1.31E-07
SERPINB2	4.006923	1.36E-07
RP11-434I12.2	-3.45332	1.37E-07
RP11-2L8.1	5.844197	1.95E-07
CTC-378H22.1	6.205687	2.37E-07
RELB	2.855338	2.61E-07
AC018647.3	-4.99987	2.61E-07
AC002480.4	3.370958	2.87E-07
ICAM1	2.195521	3.77E-07
BEX1	5.558859	4.98E-07
DTNA	2.960481	5.50E-07
SEMA3B	-2.34515	5.74E-07
HSD17B6	-3.31606	6.22E-07
RP11-356I2.4	2.811137	7.84E-07
RP1-102K2.8	3.59885	8.20E-07
CCL5	2.945614	8.34E-07
CCL5	2.938031	8.90E-07
COL13A1	2.107731	9.24E-07
SEMA3B	-2.35697	9.80E-07
CD36	-2.52052	9.99E-07
RP11-1E6.1	9.221021	1.06E-06
TNFSF14	5.667041	1.71E-06
OAS2	2.747007	1.82E-06
MMP-12	8.637793	1.91E-06
MX1	3.246106	2.23E-06
MEX3B	-2.7611	2.32E-06
CCL20	5.760401	2.36E-06
IQCK	2.030246	2.71E-06
IRAK2	2.294509	2.83E-06
SLC19A3	3.911071	2.83E-06
SYTL5	-6.07082	3.50E-06
GFPT2	2.360847	3.78E-06
GCH1	3.092435	4.23E-06
SLC39A8	3.079642	4.28E-06
ASPN	-4.50885	4.29E-06
OMG	-2.50892	4.58E-06
STEAP2	2.502049	4.73E-06
SDPR	-2.60268	5.13E-06
BCL2A1	4.191714	5.60E-06
SLC22A4	2.508351	7.27E-06
CHI3L2	3.690094	7.83E-06
RP11-656G20.1	4.281334	9.63E-06
MMP-12	7.940146	1.09E-05
CTD-2369P2.8	2.16703	1.10E-05
RARRES1	2.744808	1.29E-05
DIO2	2.927348	1.34E-05
DACT1	-2.1126	1.48E-05
TNFRSF1B	2.332681	1.55E-05
ESM1	4.494391	1.71E-05
SCN1B	2.843557	1.86E-05
VCAM1	4.62042	1.97E-05
TMEM132A	2.253231	2.17E-05
FCRLA	3.014246	2.17E-05
OASL	5.365512	2.45E-05
AC007362.1	2.112907	2.46E-05
IGSF10	-2.31254	2.66E-05
BMF	-3.34037	2.69E-05
RRM2	3.811394	2.69E-05
DIRC1	5.083898	2.83E-05
RP11-753N8.1	5.715123	2.83E-05
DNER	6.807586	3.19E-05
IL32	3.039259	3.19E-05
RP11-138I17.1	-4.29233	3.36E-05
G0S2	3.018926	3.37E-05
LDLRAD4	-3.60911	3.77E-05
CCL26	2.437312	3.88E-05
CCL26	2.433034	4.28E-05
RP11-22N19.2	2.205652	4.60E-05
KB-1471A8.1	-2.09915	4.94E-05
CLSPN	2.861972	4.95E-05
RP11-760H22.2	-2.35588	5.38E-05
DCLK3	5.417343	5.51E-05
MMP-10	7.216971	5.74E-05
IDO1	7.137771	6.06E-05
TNFAIP2	2.479369	6.10E-05
LBH	-2.25179	6.10E-05
CALCRL	-2.59711	6.15E-05
PTPRO	-2.71303	6.53E-05
SPOCD1	2.437801	7.19E-05
CCL13	4.830949	7.26E-05
XXbac-BPG252P9.10	2.056233	8.48E-05
STYK1	5.000193	8.55E-05
MAN1A1	2.487595	8.78E-05
DSCR8	2.946002	9.05E-05
TMEM158	2.26902	9.20E-05
TNXB	-2.10506	9.25E-05

CYP7B1	6.063399	9.54E-05	LINC00968	2.235515	0.000781
RP11-58K22.5	3.006929	9.85E-05	TNIP3	5.25131	0.000828
RP11-301G23.1	2.566484	9.93E-05	IQGAP3	3.223914	0.000846
IER3	2.014142	0.000119	GPR126	-3.05072	0.000856
CH25H	4.27129	0.000127	TMEM132B	3.212379	0.000866
IER3	2.002274	0.000127	CCL11	5.004701	0.000884
DOCK2	3.599243	0.00014	TNFRSF11B	2.217865	0.000931
IER3	2.013049	0.000143	HIST1H3B	3.033744	0.000937
LINC01013	-3.77663	0.000147	EPHB3	-2.93838	0.000938
LIPM	6.604624	0.000147	KDR	-3.21535	0.000958
MFSD2A	2.638764	0.00016	PTGES	2.981645	0.000997
RSAD2	5.633157	0.000165	PTTG1	2.149111	0.001005
RP11-335I12.2	2.417313	0.000165	AC098617.1	-2.39418	0.001009
MMP-1	4.242418	0.000168	MAMDC2	-3.59842	0.001038
IL36B	5.382621	0.000179	AP001610.5	3.310047	0.001038
HES1	-2.54385	0.000179	DLGAP5	3.644977	0.001038
MAMDC2	-3.7054	0.000196	HMMR	3.301991	0.001038
NPR3	-2.05152	0.0002	SIPA1L2	-2.44019	0.001074
SLC40A1	-2.47329	0.000202	WTAPP1	3.725765	0.001217
C1orf147	2.555274	0.000231	RP11-839G9.1	3.194592	0.001228
C1orf147	2.550368	0.000246	TFPI2	5.506276	0.001228
TNXB	-2.18296	0.000257	AFF3	-3.61318	0.001244
MYPN	4.60792	0.000264	C7	-2.81545	0.001337
NEFM	4.347375	0.000265	COL8A2	-2.01493	0.001339
C7orf69	3.656035	0.000288	OAS3	2.985682	0.00134
IER3	2.101055	0.000296	RP11-245M24.1	2.988372	0.001393
OSR2	-3.21163	0.000315	RP11-435D7.3	2.899039	0.001488
DEPDC1	3.973426	0.000315	CDCA2	2.493607	0.001499
OAS1	3.982709	0.000345	RSPO3	2.624938	0.001508
AC005013.1	-3.15671	0.000351	LINC00473	6.746721	0.001512
IFI44L	2.466198	0.000386	MED12L	-2.07027	0.001547
RP11-94A24.1	3.10027	0.000389	IL1α5RA	2.03229	0.001562
ITGB2-AS1	3.931756	0.000424	MX2	2.427438	0.001607
CKAP2L	3.324946	0.00054	DIRAS2	-4.64987	0.001684
TNXA	-2.12546	0.00054	TOP2A	2.468433	0.001728
NOX4	-4.03417	0.000561	SMC5-AS1	-2.09984	0.001782
GREM2	-2.94863	0.000583	GBP5	4.31636	0.001788
TNXA	-2.11883	0.000622	RP3-437C15.1	2.002103	0.001854
RP11-785F11.1	-3.2354	0.00063	GALNT6	2.630361	0.001868
NCEH1	2.145637	0.000649	TNXB	-2.75868	0.002026
MT1L	4.418878	0.000653	PRELP	-2.23994	0.002123
RAB27B	2.954927	0.000675	SHCBP1	3.035018	0.002146
LAMB3	2.196411	0.000677	COL21A1	-3.88788	0.002146
IL1αRAPL1	-2.38671	0.000684	CTD-2536I1.1	-2.5474	0.002151
RN7SL124P	3.275351	0.000692	TP63	3.752236	0.002155
PDPN	2.865779	0.00071	SYBU	-2.30752	0.002155
PBK	3.476825	0.00072	IGFN1	-2.67144	0.002157
RP11-138H11.1	2.87796	0.00072	GFRA1	3.912055	0.002239
HBEGF	2.056653	0.000756	ACSL5	2.333903	0.002261

CYP21A2	-2.14704	0.002267	RASD1	4.77066	0.005063
KIRREL3	2.054932	0.002335	CMPK2	3.84955	0.005309
FAM64A	3.810149	0.00245	TTK	2.608326	0.005529
DTL	2.600753	0.002456	RIMS3	-3.53676	0.005891
RP11-320G24.1	2.402092	0.002505	RRAD	2.305114	0.005892
MKI67	3.056889	0.00256	KIFC1	2.654254	0.006414
SLC28A3	2.659878	0.002655	KIF20A	2.961916	0.006581
OMD	-4.59564	0.00267	THEMIS2	2.031208	0.006677
RP5-1198O20.4	2.452044	0.002708	RPSAP52	2.358832	0.00675
AC087645.1	3.628362	0.003029	SEPP1	-3.35199	0.006808
HIST1H3G	3.549788	0.003069	BUB1B	2.617981	0.006834
ZCCHC5	3.340318	0.003261	PTGS2	2.266999	0.00695
CEP55	2.568869	0.003303	NEK2	3.374144	0.007098
CYS1	-2.11732	0.003407	NUF2	2.959702	0.007146
CTB-174D11.1	-2.35454	0.003437	FAM111B	3.29565	0.007569
MCM10	3.490513	0.003714	ELOVL2	4.20172	0.007635
ITLN2	-3.93053	0.003727	CASC5	2.290888	0.007993
MPP7	2.294248	0.003798	ANLN	2.287278	0.008078
CHI3L1	4.204978	0.003938	KIF14	2.305907	0.008249
RP11-462L8.1	2.256903	0.003961	ITIH5	-3.10404	0.008261
KCNS2	-2.11962	0.004037	COL15A1	-2.332	0.008477
ADH1B	-3.68938	0.004314	BIRC5	2.841298	0.008939
KIAA1324L	-2.54197	0.004462	NEBL	-2.70633	0.008939
NUSAP1	2.405617	0.004559	KIFC1	2.52144	0.008961
KIFC1	2.818852	0.004756	HJURP	2.291114	0.009037
FAM13C	-2.08714	0.004813	IL1αB	4.290801	0.009346
MAMDC2-AS1	-2.5694	0.004823	PDE4B	2.702511	0.009743

Appendix Table 2: Differential RNA expression in PDGF stimulated HSVSMC compared to 0.2 % control from RNA-seq. Results for RNA-seq were filtered on a log fold change (FC) greater than 2 or less than -2 (4 fold change up or down regulated) and a false discover rate (FDR) less than 0.1.

Gene	LogFC	FDR
KYNU	7.899377	0.000213
RP11-1E6.1	6.731117	0.005133
MYB	6.252374	0.000662
MMP-1	5.923852	4.79E-06
WTAPP1	5.390493	5.35E-05
HAS2	5.26765	5.69E-17
LINC00973	5.053072	3.05E-05
TFPI2	4.929824	0.002331
ESM1	4.844523	1.64E-06
IL1αB	4.792647	0.001912
HIST1H3G	4.706529	2.00E-05
STYK1	4.502405	0.00037
NDP	4.41174	1.86E-05
DLGAP5	4.367995	3.79E-05
SLC14A1	4.35911	1.88E-06
RP11-94A24.1	4.324549	3.49E-07
CH25H	4.31952	0.000336
NEFM	4.286134	0.000177
DEPDC1	4.276894	5.22E-05
CADPS	4.275944	0.001426
FAM64A	4.242764	0.000399
MALL	4.203403	6.19E-07
MYPN	4.189592	0.000422
AURKB	4.126784	0.00436
AC087645.1	4.069259	0.000395
CDCP1	4.055431	6.86E-19
ANXA10	4.016228	0.007055
CKAP2L	4.015948	8.63E-06
MYEOV	3.986936	5.37E-07
RPLP0P2	3.946392	1.97E-05
SHCBP1	3.93043	1.02E-05
BCL2A1	3.869929	4.40E-05
GALNT6	3.823166	1.83E-06
KCNN4	3.820604	0.000889
MCM10	3.797098	0.001159
NCAPH	3.763217	0.004677
IL1α3RA2	3.750364	1.99E-05
IL1α3RA2	3.721051	1.57E-05
NEK2	3.709363	0.001849
RP11-150O12.1	3.634959	5.98E-07
STC1	3.626162	1.97E-05
DGKB	3.615159	0.004503
CDC20	3.595106	0.004512
PBK	3.574584	0.000294
RP11-54A9.1	3.559929	9.41E-05
IQGAP3	3.535663	0.000158
HIST1H3B	3.525733	5.75E-05
SYT7	3.518523	0.000175
MKI67	3.508925	0.000186
KIF20A	3.506064	0.000481
COL13A1	3.495972	1.40E-16
HMMR	3.438136	0.000361
RP11-80G7.1	3.425611	0.004163
GAP43	3.358645	8.38E-06
NUF2	3.353997	0.000823
LZTS1	3.341672	0.000771
RFX8	3.337038	0.00105
CTD-2587H24.5	3.331207	1.03E-05
APOBEC3B	3.310106	0.00288
RRM2	3.283304	0.000202
TMEM132B	3.261237	0.000568
BIRC5	3.242976	0.001031
ADTRP	3.218245	3.10E-08
HAS2-AS1	3.218127	1.30E-05
CLSPN	3.186215	3.83E-06
DUSP6	3.176597	2.42E-10
PLAT	3.175429	0.003296
LINC00704	3.156472	2.29E-05
SPOCD1	3.143154	8.51E-08
CEP55	3.120243	8.59E-05
TMEM100	3.107545	0.000401
LOXL4	3.107383	4.33E-07
TDO2	3.091517	0.003259
TDO2	3.080681	0.004945
E2F7	2.978651	1.20E-09
NES	2.963353	1.20E-15
CTD-2207P18.2	2.959277	0.004325
CSMD2	2.954446	0.001491
RNF128	2.924474	0.000194
RP11-34A14.3	2.902957	9.45E-08
DDIT4L	2.891992	0.000393

KIFC1	2.891867	0.001701
DTL	2.876089	0.000335
KIAA1755	2.870342	0.000437
KIF4A	2.846128	0.00026
AIM1	2.813368	0.002475
RGS2	2.794519	0.003303
AKR1B10	2.788643	0.006558
CASC5	2.772368	0.000359
KIF14	2.759372	0.000393
ITGA10	2.756616	0.007251
RP11-588H23.3	2.732653	0.000623
BUB1B	2.728926	0.001895
COL15A1	2.719718	0.001999
CCND1	2.719409	1.85E-11
ITGA10	2.714582	0.008846
HIST1H1B	2.698071	0.002867
BUB1	2.695707	0.006213
KIFC1	2.681544	0.002771
RP11-435D7.3	2.671735	0.003891
CNIH3	2.663966	2.54E-07
FRMD3	2.633946	0.002849
TTK	2.610676	0.002575
APCDD1L-AS1	2.609463	0.001141
PCOLCE2	2.603681	2.56E-07
RPSAP52	2.575246	0.0015
SLC4A8	2.573616	0.001589
MILR1	2.57079	1.04E-06
UNC13A	2.564783	1.10E-05
RGMB-AS1	2.564499	4.87E-05
IGFBP3	2.555969	2.41E-05
CDCA2	2.53827	0.000852
KIFC1	2.529841	0.004073
MT2A	2.513974	1.07E-05
PTPRB	2.502757	6.27E-06
SEMA3A	2.500465	6.61E-07
LTBP1	2.498628	0.004889
FCRLA	2.473635	0.000469
ANPEP	2.471408	2.99E-05
TOP2A	2.458669	0.000959
CXCL6	2.420435	0.003174
MILR1	2.413475	5.40E-10
ORAOV1	2.390048	1.27E-11
APCDD1L	2.382267	0.000731
DCBLD2	2.380425	1.69E-09
ANLN	2.377815	0.002439
NUSAP1	2.366859	0.00288
CENPF	2.361887	0.003061
PTTG1	2.352587	8.49E-05
UHRF1	2.3406	9.93E-05
KIF2C	2.339929	0.006445
TNFAIP3	2.338276	1.14E-07
RP11-1223D19.1	2.331651	0.004675
LRRC8B	2.322662	0.00306
ARHGAP22	2.306683	2.70E-10
TMEM158	2.282639	0.000189
TSLP	2.272652	0.001491
SH3BGRL3	2.271779	1.26E-10
PHLDA1	2.270164	2.53E-10
PLAUR	2.266036	4.11E-07
HMGA1	2.252216	1.64E-06
AC002480.4	2.240462	0.001446
RP11-221N13.3	2.229884	2.70E-05
RP11-3L21.2	2.226916	0.008748
IL7R	2.212244	0.001393
NTM	2.211386	0.00062
TNFAIP8L3	2.193182	0.002961
RNU6-26P	2.182213	0.004325
LMO2	2.181245	0.000437
LPXN	2.177686	3.80E-07
GNG11	2.171064	0.006723
SLC20A1	2.156468	3.18E-09
RGMB	2.151065	1.29E-06
RP6-99M1.3	2.146074	0.000393
RP6-99M1.3	2.146074	0.000393
RP11-290L1.3	2.136816	1.18E-06
SMIM3	2.108873	2.85E-07
PROCR	2.101845	5.26E-05
TRIP13	2.098842	0.009173
TENM4	2.080486	0.001213
TMEM171	2.073132	0.001393
THBD	2.047192	0.000911
F2RL1	2.04253	0.003397
DUSP5	2.030296	0.007281
YPEL3	-2.00057	0.000364
LINC00312	-2.00243	0.007794
MED12L	-2.01735	0.00306
C10orf54	-2.02873	6.78E-07
PODN	-2.02991	0.005876
RNF144B	-2.03665	0.000141
SFRP4	-2.0385	2.54E-07
DEPTOR	-2.04359	6.74E-08
PIM1	-2.05253	0.002888
FSTL3	-2.05767	0.00306
PTPRQ	-2.0693	0.005303
ANKRD37	-2.08718	0.000359

KB-1471A8.1	-2.09143	3.70E-05
KMO	-2.1007	6.76E-05
IRS2	-2.10796	0.002974
PTK2B	-2.12575	3.83E-06
TP53I11	-2.15142	0.002605
OPN3	-2.15422	1.45E-05
RTKN2	-2.15824	3.83E-06
CCDC81	-2.1592	0.00584
TUFT1	-2.17131	1.14E-07
SLC25A27	-2.18116	3.83E-06
RP11-760H22.2	-2.21251	0.000168
RP11-49C9.2	-2.21492	0.009737
RP11-49C9.2	-2.21492	0.009747
ATP8B4	-2.24108	0.000911
CTD-2653D5.1	-2.2434	0.002888
DACT1	-2.35448	5.43E-07
RP11-65J3.1	-2.35785	0.001798
PIEZO2	-2.36788	0.002145
RP11-761I4.4	-2.3718	6.45E-07
CCDC148	-2.40807	0.000472
PSG5	-2.42432	0.000926
SYNPO2	-2.42923	1.17E-07
LMOD1	-2.4429	1.33E-06
RP11-307B6.3	-2.44665	0.000607
IL1α6	-2.45047	3.70E-05
BMF	-2.45569	0.003227
C3	-2.45946	0.009489
RP11-434I12.2	-2.46982	0.000159
RP11-761I4.3	-2.54714	0.000434
PLCE1-AS1	-2.58035	0.00306
CTD-2319I12.1	-2.59148	0.001599
SORBS2	-2.59651	2.49E-06
C1QTNF7	-2.60506	0.002315
CTD-2319I12.2	-2.61767	0.002074
ISYNA1	-2.63111	0.001027
LYPD6	-2.6484	0.006184
PPARGC1A	-2.66488	0.000437
ANXA3	-2.69956	0.000437
OMG	-2.71787	8.69E-07
CCDC173	-2.72948	0.000852
RDH10	-2.73391	9.93E-13
FAM25G	-2.75632	0.000435
RP11-276H19.1	-2.77642	9.56E-05
FAM25HP	-2.79808	0.000434
AL591684.2	-2.81659	0.000437
KCND3	-2.8516	0.001706
MAMDC2-AS1	-2.8765	0.003231
INMT	-2.9017	3.80E-07
MFAP4	-2.91522	4.23E-09
MEX3B	-2.91674	1.93E-06
ELN	-2.93255	0.00014
ELN	-2.94451	0.000128
ID4	-2.94806	6.07E-08
IGFN1	-2.97206	0.000533
KCNE3	-2.98619	0.001282
DCHS2	-2.9925	0.00019
ADAMTS5	-2.99673	0.000489
RP1-140K8.5	-2.99985	0.009148
JAM2	-3.04739	0.000839
LINC00842	-3.04833	5.86E-07
SEMA3B	-3.21513	1.80E-11
IGSF10	-3.2252	4.91E-09
SEMA3B	-3.23637	3.53E-11
CNN1	-3.31828	3.80E-07
GSG1	-3.37148	1.00E-05
SEBOX	-3.37331	1.14E-07
BMP6	-3.40106	0.001586
DIRAS2	-3.43607	0.006357
ZNF704	-3.49988	3.59E-06
SLC40A1	-3.50708	5.37E-07
VTN	-3.52226	9.47E-08
SBSPON	-3.52405	4.94E-05
KRT18	-3.72224	0.001995
TDRD6	-3.74038	2.21E-06
ART4	-3.78616	0.000879
AC107016.1	-3.83041	0.00486
ITIH5	-3.93066	0.000235
LDLRAD4	-3.94179	1.03E-05
RERG	-3.98906	0.003936
TMEM130	-4.06314	0.000278
TNNC1	-4.12136	0.000311
THSD7B	-4.21077	0.000594
TMEM130	-4.28104	0.000149
MAMDC2	-4.38212	2.41E-05
NOX4	-4.41943	0.000346
SEL1L2	-4.42415	0.004348
MAMDC2	-4.43438	9.84E-05
LINC01018	-4.50019	3.89E-05
FGF9	-4.54141	1.57E-10
IGF1	-4.64892	9.84E-05
LINC01013	-4.86455	4.32E-06
HSD17B6	-4.87256	9.03E-12
KRT7	-5.01852	2.41E-05
AC018647.3	-5.23644	3.80E-07
AC244230.2	-5.29998	4.40E-05

RARRES2	-5.62307	1.32E-08	TGM1	-6.2788	9.58E-08
NPY4R	-5.72924	2.41E-05	TMC3	-6.5779	1.18E-11
NPY4R	-5.84563	2.41E-05	LEP	-7.18742	3.24E-06
ITLN2	-6.06369	2.41E-05	AC244230.1	-11.2264	8.47E-07

Appendix Table 3: Differential RNA expression in IL1α and PDGF stimulated HSVSMC compared to 0.2 % control from RNA-seq. Results for RNA-seq were filtered on a log fold change (FC) greater than 2 or less than -2 (4 fold change up or down regulated) and a false discover rate (FDR) less than 0.1.

gene	logFC	FDR
KYNU	12.28895	2.92E-12
IL36RN	12.23314	3.97E-12
RP11-1E6.1	11.90896	1.48E-12
MMP-10	10.39235	2.57E-09
CXCL5	9.766849	1.04E-24
MMP-3	9.546768	3.01E-12
MMP-3	9.521337	2.92E-12
CSF2	9.488442	9.12E-20
CXCL6	9.1874	2.00E-25
CSF3	9.070587	3.95E-19
CXCL1	8.652238	5.14E-23
IL8	8.583378	4.07E-18
CXCL3	8.389216	1.15E-32
IL1αB	8.017521	1.46E-07
MMP-12	7.994867	2.59E-06
NEFM	7.882253	4.55E-14
LINC00473	7.731944	0.000158
CCL20	7.718259	2.28E-10
MIR146A	7.638436	4.56E-19
IL36B	7.430524	1.62E-07
MMP-12	7.299507	1.26E-05
EHF	7.299202	4.06E-15
OASL	7.263964	8.45E-10
RP11-753N8.1	7.245167	4.12E-08
STC1	7.135825	7.94E-16
RSAD2	7.021871	1.51E-06
DNER	6.990562	3.42E-06
MYB	6.538619	0.000149
BCL2A1	6.513526	1.07E-13
TFPI2	6.508859	2.91E-05
STYK1	6.48947	4.70E-08
CTC-378H22.1	6.430849	2.94E-08
HAS2	6.330048	1.65E-23
ESM1	6.282971	3.88E-10
MMP-1	6.279031	2.95E-07
CCL7	6.247353	2.32E-07
CCL8	6.200573	2.98E-06
LIPM	6.183449	0.000213
PTPRN	6.158363	3.15E-05
GBP5	6.119091	4.68E-06
CXCL2	6.043869	1.51E-24
CDCP1	6.040634	1.17E-37
TNIP3	5.97484	7.96E-05
MYPN	5.862899	4.12E-07
BEX1	5.801582	8.79E-08
IDO1	5.7898	0.000998
WTAPP1	5.760893	3.85E-06
IL7R	5.655992	1.74E-18
POU2F2	5.595679	9.23E-13
RP11-94A24.1	5.433629	4.91E-11
GNGT1	5.405652	0.00153
WWC1	5.39562	2.78E-13
TNFSF14	5.381022	7.86E-06
LIF	5.338383	1.97E-15
DCLK3	5.323989	6.79E-05
TMEM132B	5.31291	1.02E-09
RP1-102K2.8	5.196617	4.19E-13
RASD1	5.191783	0.000908
DEPDC1	5.181667	3.87E-07
CYP7B1	5.179997	0.000337
CH25H	5.17799	3.49E-06
MT1L	5.171371	1.10E-05
HIST1H3G	5.121625	1.30E-06
OAS1	4.982337	2.26E-06
FAM64A	4.981983	7.82E-06
RP11-2L8.1	4.974023	4.75E-06
AURKB	4.973843	0.000178
SERPINB2	4.967247	1.52E-11
IL1α1	4.956034	4.12E-08
SPC25	4.93342	0.001616
CMPK2	4.87835	0.000142
RP11-91K9.1	4.87606	1.10E-09
MT2A	4.875838	1.39E-17
DLGAP5	4.850384	1.85E-06
IL6	4.802506	9.12E-20
ELF3	4.793214	1.49E-06
FCRLA	4.792894	1.37E-12
TNFAIP3	4.771571	1.25E-26
ANXA10	4.76061	0.000574
LPAR4	4.751724	6.14E-08
CKAP2L	4.721695	6.06E-08
MX1	4.696151	1.56E-12
AP001610.5	4.652843	5.45E-07
MKI67	4.588233	2.56E-07

RRM2	4.579905	6.06E-08
RPLP0P2	4.538508	2.90E-07
BIRC3	4.53783	1.95E-11
MCM10	4.524614	2.84E-05
NCAPH	4.478981	0.000229
AC073072.5	4.474189	9.39E-16
OAS3	4.473117	7.14E-08
DIRC1	4.462216	0.000213
NEK2	4.440063	5.42E-05
KCNA3	4.418027	0.009645
HMMR	4.417401	1.15E-06
LINC00944	4.391701	0.009068
NEFL	4.386784	0.003892
AC087645.1	4.361379	4.83E-05
RP11-80G7.1	4.327099	6.27E-05
CDC20	4.294444	0.000219
CLSPN	4.26494	8.79E-11
RP11-839G9.1	4.26133	8.69E-06
SHCBP1	4.258569	5.48E-07
IFI44L	4.258462	8.79E-11
PTGS2	4.20858	3.58E-09
RP11-435D7.3	4.192785	3.54E-07
APOBEC3B	4.18857	2.59E-05
VCAM1	4.171716	5.09E-05
OAS2	4.160101	1.79E-13
AMPD3	4.123688	1.59E-18
CTSS	4.11916	1.02E-08
BDKRB2	4.116075	1.28E-10
HIST1H3B	4.108629	5.91E-07
HAS2-AS1	4.102591	7.00E-09
CLDN1	4.046464	8.02E-06
IQGAP3	4.036269	4.56E-06
AC002480.4	4.027379	1.75E-10
RAB27B	3.995636	2.28E-06
NUF2	3.978259	1.99E-05
COL7A1	3.958516	4.20E-06
PBK	3.944656	1.95E-05
GTSE1	3.916144	0.006
FAM111B	3.908716	0.000208
LINC00973	3.892489	0.000645
C3	3.881236	4.45E-07
LUCAT1	3.880284	6.38E-06
FAM167A	3.852722	0.000574
RPSAP52	3.822872	1.58E-07
KIF20A	3.774113	6.36E-05
DOCK2	3.759115	3.48E-05
RP11-245M24.1	3.758624	1.22E-05
TMEM158	3.738659	1.75E-11
RP11-138H11.1	3.71581	2.92E-06
TP63	3.68642	0.001014
HIST1H2AJ	3.674909	4.36E-05
BIRC5	3.65389	6.98E-05
UBE2C	3.646006	0.005416
CEP55	3.625427	1.51E-06
CCL2	3.624678	7.00E-15
TMEM171	3.616843	1.10E-09
HBEGF	3.602917	4.27E-11
SPOCD1	3.600794	1.84E-10
TK1	3.576814	0.001003
RSPO3	3.549379	7.52E-07
KIFC1	3.545633	2.60E-05
DTNA	3.532815	1.34E-09
MYEOV	3.528161	3.79E-06
BUB1B	3.51511	1.22E-05
TOP2A	3.50817	2.74E-07
CDC45	3.506273	0.000863
RFX8	3.49612	0.000224
TTK	3.49367	8.54E-06
BUB1	3.484147	8.17E-05
BST2	3.482757	4.01E-06
CTD-2207P18.2	3.470085	0.000255
ABI3BP	3.465786	8.21E-13
C1QTNF1	3.463352	1.08E-14
MFSD2A	3.450061	2.30E-07
GALNT6	3.417821	6.82E-06
HIST1H1B	3.393747	3.81E-05
CDCA2	3.386725	1.37E-06
DTL	3.385887	3.79E-06
EPSTI1	3.380132	0.00021
KIF14	3.371483	2.98E-06
DUSP6	3.370322	1.76E-12
PTPN22	3.35632	0.001394
KIFC1	3.348933	3.78E-05
RELB	3.347919	1.11E-09
HIST1H2AL	3.344276	0.000365
RN7SL124P	3.334361	0.001002
IL1αA	3.322352	0.000902
HIST1H3C	3.317171	0.001003
TNFAIP6	3.307652	6.59E-09
CCL13	3.305739	0.005605
LRRC15	3.304712	0.000935
HIST1H2BO	3.303672	0.002455
CASC5	3.303301	5.21E-06

RP11-301G23.1	3.29114	8.33E-07
KIF4A	3.278625	5.72E-06
CDCA8	3.263876	0.006701
CENPF	3.258644	6.82E-06
RP11-54A9.1	3.245242	0.000176
GFPT2	3.243668	1.75E-10
KIF2C	3.241338	1.70E-05
CTD-2587H24.5	3.238092	7.18E-06
LPXN	3.22154	1.27E-15
THEMIS2	3.213298	8.85E-06
NUSAP1	3.209291	6.85E-06
KIFC1	3.199745	5.51E-05
HERC6	3.168679	8.67E-11
HSD11B1	3.16774	8.09E-06
MX2	3.147432	9.46E-06
PPP4R4	3.122044	1.01E-07
IFI44	3.115004	1.21E-07
ZCCHC5	3.096831	0.003286
RP11-58K22.5	3.073146	3.92E-05
TNC	3.069427	3.87E-07
CD82	3.059382	1.40E-10
NAMPT	3.057084	3.23E-14
ADAMTS14	3.056456	0.002035
CSMD2	3.054085	0.000306
PREX1	3.050593	0.000127
HIST1H1A	3.046848	0.00051
RP11-462L8.1	3.042898	9.46E-06
COL13A1	3.034088	1.39E-13
EXO1	3.033091	0.00037
PRG2	3.02909	1.10E-09
ANLN	3.01954	2.62E-05
SGOL1	3.003616	0.001208
AC005549.3	2.99369	2.50E-07
HIST1H3F	2.990084	0.00446
PSD4	2.97448	0.000101
TSLP	2.963132	4.77E-06
NAMPTL	2.93376	2.13E-13
NDP	2.930736	0.00279
CDK1	2.926625	0.000515
IL21R	2.925406	0.000144
RP11-356I2.4	2.923506	7.80E-08
IL33	2.919852	0.001887
TNFRSF1B	2.911811	3.84E-08
CDKN3	2.896706	0.000278
C14orf182	2.886716	6.27E-05
GRAMD1B	2.874466	0.005482
RN7SL257P	2.852398	0.008118
SERPINE1	2.851107	1.75E-11
SYT7	2.848517	0.001433
Metazoa_SRP	2.8484	0.004028
Metazoa_SRP	2.8481	0.008227
HJURP	2.839147	0.000186
Metazoa_SRP	2.836993	0.008503
Metazoa_SRP	2.834891	0.008557
RN7SL471P	2.831505	0.008126
SOD2	2.829604	3.80E-10
GCH1	2.826202	2.34E-05
FCRLB	2.817923	6.49E-05
IFI6	2.817742	3.61E-09
ANPEP	2.813159	4.35E-07
PLAUR	2.795184	2.20E-11
TMEM132A	2.795036	1.71E-08
PLK4	2.772998	0.000189
SLC28A3	2.769092	0.001724
IL32	2.76732	7.42E-05
IL21R-AS1	2.765281	0.002535
ISG15	2.745797	1.97E-11
ZC3H12A	2.740219	2.62E-11
PTTG1	2.734159	1.21E-06
DSCR8	2.731427	0.000457
RGMB-AS1	2.726967	6.00E-06
APCDD1L	2.718106	2.52E-05
DAW1	2.706497	0.004784
ZSWIM5	2.705189	0.001066
RP11-150O12.1	2.701134	0.000117
RCAN1	2.694967	1.50E-05
PDPN	2.690741	0.002583
SMOX	2.686477	0.000842
RP11-588H23.3	2.661917	0.000393
CDC25C	2.660107	0.001432
HMGA2	2.648506	1.44E-08
E2F1	2.646832	0.002961
PDE4B	2.646317	0.003477
GPR68	2.643242	0.000636
HIST2H3C	2.64121	0.000207
LRIG1	2.640339	1.37E-12
HIST2H3A	2.638955	0.000207
PTGES	2.628947	0.007182
STEAP1	2.602946	6.62E-08
MT1E	2.601622	2.43E-08
RP11-879F14.2	2.598974	0.000873
HIST2H3A	2.596925	0.000273
HIST2H3C	2.596925	0.00028

SEMA7A	2.587842	0.000255
PRC1	2.578958	0.000108
LOXL3	2.567595	6.82E-05
BLM	2.561953	0.00194
CA12	2.559608	2.20E-10
RGMB	2.558947	1.48E-09
SMIM3	2.555295	4.84E-11
RAC2	2.549835	7.96E-05
POLQ	2.535345	0.001078
SLC22A4	2.528099	9.96E-07
FOXM1	2.520536	0.000882
RP11-230G5.2	2.519161	7.67E-05
MIR155HG	2.518736	0.0032
NR4A3	2.499725	0.00093
DGAT2	2.497284	0.005092
LOXL4	2.488832	2.04E-05
MAN1A1	2.485316	6.94E-05
CCNB2	2.485259	0.002344
PLOD2	2.473141	2.95E-05
SLC39A14	2.460535	5.76E-12
PID1	2.453571	4.01E-06
TMEM100	2.445689	0.005589
PFKFB4	2.444505	6.58E-07
SLC19A3	2.438751	0.005617
FOSL1	2.434388	2.50E-07
SKA3	2.433849	0.001124
PTPRB	2.426096	4.55E-06
SLC4A8	2.42312	0.001708
DIO2	2.410131	0.00014
RP11-221N13.3	2.408208	2.28E-06
KIF15	2.404572	0.001029
PDCD1LG2	2.402511	1.62E-09
TRIP13	2.400912	0.000911
UHRF1	2.380698	2.40E-05
LRP8	2.380265	2.16E-10
PDLIM4	2.370393	6.06E-08
CCL26	2.367088	1.78E-05
CCL26	2.365391	1.74E-05
LMNB1	2.364554	0.000333
MILR1	2.358869	3.36E-06
NCEH1	2.357554	1.57E-05
RP11-335I12.2	2.356874	0.000157
IRAK2	2.349034	7.56E-07
HIST1H2AI	2.34187	0.005266
SRPX2	2.33856	1.01E-07
STEAP2	2.335587	1.53E-05
NT5E	2.334921	1.99E-12
RP11-331K21.1	2.334176	0.000768
CIT	2.332019	0.001483
C1orf147	2.328056	0.000564
C1orf147	2.325885	0.000585
CENPE	2.317095	0.000171
CDCA5	2.311508	0.007761
SPAG4	2.302234	0.001884
AKR1B1	2.302201	3.25E-05
MILR1	2.296912	9.45E-10
ASPHD1	2.286395	0.000709
SCN1B	2.272659	0.001948
RP11-34A14.3	2.270935	1.23E-05
SLC16A3	2.269914	2.63E-06
BRIP1	2.239453	0.000882
PRDM1	2.217748	0.006125
ULBP2	2.21628	0.000234
MOXD1	2.208759	1.33E-05
IRAK3	2.204946	3.65E-09
RP6-99M1.3	2.19782	8.75E-05
RP6-99M1.3	2.19782	8.75E-05
DNAH5	2.197559	0.003239
NCAPG	2.182993	0.000141
RRAD	2.173786	0.003829
IKBKE	2.165885	6.06E-08
IKBKE	2.154385	1.03E-07
LRRC8B	2.14859	0.003867
ABLIM3	2.141098	2.30E-07
ADAMTS4	2.136056	7.50E-05
GNG11	2.128976	0.004667
CENPI	2.11807	0.000101
ST3GAL1	2.117651	1.37E-12
C10orf90	2.099553	0.001127
RP11-90K6.1	2.090608	1.84E-05
RP11-290L1.3	2.086965	6.21E-07
MIR29A	2.0862	2.06E-05
HIST1H2BI	2.084754	0.003833
ELTD1	2.082647	1.38E-09
WTAP	2.077644	1.83E-07
PHLDA1	2.055187	2.88E-09
SH3RF2	2.054664	0.001106
AURKA	2.052884	0.001113
RP13-143G15.4	2.049842	0.008882
CCNB1	2.040095	0.002121
LIPG	2.039576	0.007615
NFKBIE	2.037169	0.000512

B3GNT5	2.032629	0.004727
3-Mar	2.030572	1.97E-06
MT1X	2.030467	0.000867
DCBLD2	2.027948	8.79E-08
IER3	2.024614	6.36E-05
RP6-99M1.2	2.023133	1.10E-09
RP6-99M1.2	2.0218	1.28E-09
SLC2A6	2.018264	0.000123
USP18	2.016524	0.000267
ULBP3	2.008981	0.006494
VEGFC	2.007687	4.76E-08
SMTN	2.007441	5.39E-07
OSBPL10	-2.00141	0.000629
LIMS2	-2.00467	1.88E-05
IQCH-AS1	-2.01295	0.000752
DOCK11	-2.03185	1.20E-08
KCND2	-2.04012	9.46E-06
SHROOM3	-2.05463	0.000697
RP11-736K20.5	-2.0573	0.001398
RP11-175K6.1	-2.06385	0.000716
PIM1	-2.08231	0.001127
5-Sep	-2.08298	0.00216
CCDC148	-2.08346	0.001494
SYPL2	-2.08422	0.007031
BAMBI	-2.08998	0.000499
KCTD16	-2.09041	0.002464
FBLN5	-2.09524	7.98E-07
KMO	-2.09736	2.23E-05
ABCA8	-2.10181	2.10E-06
NOV	-2.11317	0.000753
TNXB	-2.12229	0.008956
LINC01021	-2.12499	0.00037
MYH10	-2.12573	2.40E-06
RP11-215G15.5	-2.12574	0.00341
OPN3	-2.13158	5.36E-06
ANGPT2	-2.14122	0.003999
CCDC173	-2.14477	0.006207
MYOM1	-2.14751	0.000766
CPA4	-2.15018	0.000623
RP11-263K19.4	-2.15601	1.09E-05
TUFT1	-2.16106	3.90E-08
ZNF860	-2.1698	0.005234
ADAMTS15	-2.17505	0.003779
CSRP2	-2.17722	2.07E-08
PCSK5	-2.185	5.81E-06
SERPINA4	-2.18709	3.62E-05
PDE5A	-2.19968	7.30E-09
CRISPLD1	-2.23816	0.000441
THBS3	-2.25575	1.20E-08
A2M-AS1	-2.28059	0.005861
SMC5-AS1	-2.28315	0.00028
RIMS1	-2.2851	0.001443
COL14A1	-2.29286	6.97E-09
SEBOX	-2.31094	0.000138
RP11-761I4.4	-2.3193	3.74E-07
GCNT4	-2.32127	0.000646
ANKRD37	-2.32246	1.38E-05
FAT3	-2.32836	7.45E-05
F2R	-2.32881	3.38E-05
C12orf60	-2.33598	0.000524
PLXDC2	-2.33787	3.25E-07
NYNRIN	-2.34806	0.001643
ANXA3	-2.34897	0.00107
SESN3	-2.35539	1.34E-05
RP11-761I4.3	-2.36164	0.000535
VTN	-2.3635	0.000168
TGFB3	-2.36668	1.97E-07
CNN1	-2.3669	0.000176
BMP4	-2.36806	0.000988
RAPGEF4	-2.37234	0.001615
hsa-mir-335	-2.38975	1.35E-09
hsa-mir-335	-2.39057	1.34E-09
ARHGAP20	-2.39423	2.77E-06
PTPRQ	-2.39457	0.000383
TNFRSF21	-2.39581	0.009437
FBLN1	-2.40307	1.66E-08
ZNF483	-2.40809	3.92E-05
TNXB	-2.42306	8.07E-06
NLGN1	-2.42486	0.00406
PPL	-2.43457	0.003762
MRVI1	-2.44552	3.92E-05
MEST	-2.44959	2.22E-09
MEST	-2.44991	2.22E-09
TNXB	-2.45232	5.01E-05
PSG5	-2.45675	0.000339
PDE1A	-2.45692	4.70E-08
TSPAN12	-2.46394	0.006
RP11-709B3.2	-2.46838	1.97E-06
TP53I11	-2.46891	0.00013
FNIP2	-2.47143	1.23E-11
MKX	-2.47367	0.003171
SETBP1	-2.48113	1.55E-06
LBH	-2.48793	1.40E-05
SIPA1L2	-2.51009	9.74E-05

IL1α6	-2.51942	6.66E-06
KCNE3	-2.51995	0.004054
TNXA	-2.53855	3.41E-06
VIT	-2.55615	0.004892
PRR15	-2.57634	0.009136
TNXB	-2.59475	1.06E-07
DAAM2	-2.62465	2.42E-06
HES1	-2.62784	8.37E-05
MMP-11	-2.65052	0.000296
SORBS2	-2.66072	2.86E-07
TNXA	-2.66275	1.30E-06
PLEKHG3	-2.67437	9.46E-06
KCND3	-2.69061	0.001603
GDPD5	-2.69177	1.17E-05
ROR1	-2.7016	8.24E-12
CYP21A2	-2.70719	0.000941
HTR2B	-2.71971	2.41E-05
CYS1	-2.72642	0.00013
HAPLN3	-2.7276	0.000812
FXYD1	-2.73109	0.000358
FOXO1	-2.74476	1.44E-10
ECM2	-2.74604	2.81E-07
CYP21A2	-2.75181	0.002413
RCAN2	-2.77531	3.72E-05
CYP21A2	-2.78031	0.001053
GSG1	-2.78736	0.000108
ITGA8	-2.8004	4.03E-06
AGT	-2.81236	0.008587
KIAA1324L	-2.81323	0.000228
CYP21A2	-2.81903	0.000768
RTKN2	-2.82671	9.26E-11
FHL1	-2.83321	9.54E-13
TNXA	-2.84003	2.27E-07
CYP21A2	-2.84999	9.80E-07
SYBU	-2.86404	1.52E-05
SULF2	-2.86441	8.20E-14
RP11-334A14.5	-2.86868	0.003797
TPD52L1	-2.8894	7.12E-11
CNKSR2	-2.902	9.93E-08
CD36	-2.92523	1.56E-08
PODN	-2.92788	1.32E-05
TNXA	-2.93289	6.06E-08
RP1-140K8.5	-2.93632	0.005685
MGP	-2.95507	0.000135
MED12L	-2.95657	1.91E-06
CTB-174D11.1	-2.95739	0.000192
PRELP	-2.96578	2.08E-05
COL8A2	-2.98031	1.72E-07
KRT8	-2.98362	0.001074
RP11-434I12.2	-2.98773	1.80E-06
JAM2	-2.99039	0.000461
KCNS2	-2.9919	4.51E-06
NXPH3	-3.02352	0.000939
APOD	-3.07414	9.96E-05
ISYNA1	-3.11642	2.09E-05
LSP1	-3.12365	0.001566
COMP	-3.14059	0.003421
PKIB	-3.14069	0.003239
FAM13C	-3.15705	1.00E-05
ACADL	-3.17419	0.005416
CTD-2536I1.1	-3.19774	8.28E-05
PALM	-3.20144	0.002781
TDRD6	-3.20579	2.32E-05
MBP	-3.25446	1.32E-14
TMEFF2	-3.26764	0.002236
CALCRL	-3.28918	1.83E-07
RDH10	-3.319	2.05E-18
PTPRO	-3.32337	6.03E-07
RP11-195E11.3	-3.3489	0.000374
SEMA3B	-3.34917	6.36E-13
KCNK15	-3.35191	0.000157
PLCE1-AS1	-3.36593	2.98E-05
COPG2IT1	-3.36659	2.19E-07
SEMA3B	-3.37111	1.37E-12
IQGAP2	-3.41365	0.001313
CYP21A2	-3.42894	2.22E-08
OLFM2	-3.43686	0.0049
OMG	-3.49109	5.39E-11
IL1α7RD	-3.49501	3.46E-13
IL1αRAPL1	-3.50573	2.85E-07
TGM1	-3.50957	0.000303
OMD	-3.51633	0.00941
KDR	-3.52145	0.000139
LEP	-3.54118	0.008202
FGF9	-3.55584	1.15E-07
CTD-2653D5.1	-3.56617	4.35E-07
AC098617.1	-3.57082	4.84E-07
NOX4	-3.57908	0.002175
GPR126	-3.57913	1.88E-05
RIMS3	-3.59215	0.001526
KRT7	-3.59571	0.00093
RP11-138I17.1	-3.59736	0.000278
RP11-	-3.59947	2.55E-05

785F11.1		
CCDC3	-3.60566	0.001124
LINC01018	-3.63431	0.000405
SBSPON	-3.65031	8.37E-06
MEX3B	-3.66282	6.66E-10
MAMDC2-AS1	-3.67935	3.45E-05
ID4	-3.68606	1.34E-12
SDPR	-3.69507	1.06E-10
OSR2	-3.7031	4.53E-06
RARRES2	-3.72148	4.79E-05
ITLN1	-3.77696	0.004088
OGN	-3.79451	2.92E-10
C1QTNF7	-3.82698	1.94E-06
SLC38A4	-3.83211	0.001053
KB-1471A8.1	-3.93322	2.00E-15
THSD7B	-3.95069	0.00059
DEPTOR	-3.96896	3.46E-26
MFAP4	-3.97013	5.83E-16
IGSF10	-3.98489	2.30E-13
INMT	-4.01648	2.66E-13
TMEM130	-4.12633	0.000113
CTD-2325A15.5	-4.14319	0.001614
RASSF2	-4.22001	1.35E-10
TMEM130	-4.2216	0.000103
AC005013.1	-4.29424	4.35E-07
NEBL	-4.29708	1.10E-05
TNNC1	-4.33472	6.48E-05
HSD17B6	-4.38376	5.74E-11
BMF	-4.43263	4.39E-08
RP11-760H22.2	-4.47658	1.27E-14
SEPP1	-4.58622	4.80E-05
A2M	-4.69522	1.76E-05
NTRK2	-4.69576	3.59E-05
C7	-4.8284	5.43E-08
KRT18	-4.89729	1.26E-05
PKP2	-4.9128	0.002236
LDLRAD4	-4.95202	2.54E-08
SYTL5	-4.97352	4.31E-05
SLC40A1	-4.99137	6.36E-13
ASPN	-5.07332	1.07E-07
ITIH5	-5.09779	1.16E-06
AC107016.1	-5.18083	4.42E-05
LINC01013	-5.29024	2.69E-07
MAMDC2	-5.37302	7.98E-07
MAMDC2	-5.50364	4.18E-08
DIRAS2	-5.70164	3.24E-06
PTPRZ1	-5.88562	0.000123
ZNF704	-5.88613	1.39E-13
AC244230.1	-5.92197	0.000122
ITLN2	-6.28314	6.62E-06
TMC3	-6.33294	5.64E-12
ADH1B	-7.70804	9.35E-10
H19	-7.74992	0.000189
AC018647.3	-10.36	1.66E-16

AppendixTable 04: FPKM values for candidate lncRNA. Table indicates the individual FPKM values per patient condition for the lncRNA selected for validation.

LncRNA	0.2%	0.2%	0.2%	0.2%	IL1	IL1	IL1	IL1	PDGF	PDGF	PDGF	PDGF	IL1 +PDGF	IL1 +PDGF	IL1 +PDGF	IL1 +PDGF
RP11-94a24.1	0.74443	0.69018	0	0	4.50913	4.24539	2.88769	0.76333	10.0978	4.8975	3.71676	6.60028	4.65113	9.30047	23.5488	13.6635
RP11-761I4.4	1.876	2.54188	4.12102	0.494879	0.23948	0.951455	0.47380	2.01405	0	0.232726	0.223197	0	0.955003	0	0.425045	0.42713
RP11-91k9.1	0	0.69538	0.254313	0.913137	49.0672	57.6444	23.1136	49.3061	1.70268	0.151931	0.399878	2.33808	29.5996	35.0636	8.24117	9.51922
RP11-709B3.2	9.52826	7.67842	10.2505	4.27384	1.52624	1.99675	3.60384	4.6578	1.89635	3.24096	4.42151	3.35442	1.94357	1.52642	1.36044	0.743632
RP11-760H22.2	8.47033	4.90263	3.31437	2.99269	1.8845	1.29165	1.62117	2.19987	0.734647	0.876054	1.83707	0.903207	0	0	0.298449	0
AC018647.3	6.19224	3.83598	12.8385	6.71143	0.13503	0.079134	0	0.07043	0	0	0.213804	0.252813	0	0	0	0

List of References

1983. Classics in arteriosclerosis research: On experimental cholesterin steatosis and its significance in the origin of some pathological processes by N. Anitschkow and S. Chalatow, translated by Mary Z. Pelias, 1913. *Arteriosclerosis,* 3**,** 178-82.

2015. *RG-012 Shown to Directly Inhibit microRNA-21, Demonstrates Favorable Preclinical Profile Supporting Proof of Mechanism and Clinical Development* [Online]. Available: http://ir.regulusrx.com/releasedetail.cfm?releaseid=935181.

2016. *Long non-coding RNAs in human disease,* New York, NY, Springer Berlin Heidelberg.

AHADI, A., BRENNAN, S., KENNEDY, P. J., HUTVAGNER, G. & TRAN, N. 2016. Long non-coding RNAs harboring miRNA seed regions are enriched in prostate cancer exosomes. *Scientific Reports,* 6.

AIKAWA, M., RABKIN, E., VOGLIC, S. J., SHING, H., NAGAI, R., SCHOEN, F. J. & LIBBY, P. 1998. Lipid lowering promotes accumulation of mature smooth muscle cells expressing smooth muscle myosin heavy chain isoforms in rabbit atheroma. *Circulation Research,* 83**,** 1015-1026.

AIKAWA, M., SAKOMURA, Y., UEDA, M., KIMURA, K., MANABE, I., ISHIWATA, S., KOMIYAMA, N., YAMAGUCHI, H., YAZAKI, Y. & NAGAI, R. 1997. Redifferentiation of smooth muscle cells after coronary angioplasty determined via myosin heavy chain expression. *Circulation,* 96**,** 82-90.

AIRD, W. C. 2004. Endothelium as an organ system. *Critical Care Medicine,* 32**,** S271-S279.

ALWINE, J. C., KEMP, D. J. & STARK, G. R. 1977. Method for detection of specific RNAs in agarose gels by transfer to diazobenzyloxymethyl-paper and hybridization with DNA probes. *Proc Natl Acad Sci U S A,* 74**,** 5350-4.

ANDRAE, J., GALLINI, R. & BETSHOLTZ, C. 2008. Role of platelet-derived growth factors in physiology and medicine. *Genes Dev,* 22**,** 1276-312.

APRELIKOVA, O., XIONG, Y. & LIU, E. T. 1995. Both P16 and P21 Families of Cyclin-Dependent Kinase (Cdk) Inhibitors Block the Phosphorylation of Cyclin-Dependent Kinases by the Cdk-Activating Kinase. *Journal of Biological Chemistry,* 270**,** 18195-18197.

ATIANAND, M. K. & FITZGERALD, K. A. 2014. Long non-coding RNAs and control of gene expression in the immune system. *Trends Mol Med,* 20**,** 623-31.

ATKINSON, S. R., MARGUERAT, S. & BAHLER, J. 2012. Exploring long non-coding RNAs through sequencing. *Seminars in Cell & Developmental Biology,* 23**,** 200-205.

AVNER, P. & HEARD, E. 2001. X-chromosome inactivation: counting, choice and initiation. *Nat Rev Genet,* 2**,** 59-67.

BAI, J., MEI, P. J., LIU, H., LI, C., LI, W., WU, Y. P., YU, Z. Q. & ZHENG, J. N. 2012. BRG1 expression is increased in human glioma and controls glioma cell proliferation, migration and invasion in vitro. *J Cancer Res Clin Oncol,* 138**,** 991-8.

BAIRD, P. 2001. The Human Genome Project, genetics and health. *Community Genet,* 4**,** 77-80.

BAKER, M. 2011. Long noncoding RNAs: the search for function. *Nature Methods,* 8**,** 379-383.

BALLANTYNE, M. D., MCDONALD, R. A. & BAKER, A. H. 2016. lncRNA/MicroRNA Interactions in the Vasculature. *Clinical Pharmacology & Therapeutics,* 99**,** 494-501.

BARBIERI, S. S., ZACCHI, E., AMADIO, P., GIANELLINI, S., MUSSONI, L., WEKSLER, B. B. & TREMOLI, E. 2011. Cytokines present in smokers' serum interact with smoke components to enhance endothelial dysfunction. *Cardiovasc Res,* 90**,** 475-83.

BARRANGOU, R., FREMAUX, C., DEVEAU, H., RICHARDS, M., BOYAVAL, P., MOINEAU, S., ROMERO, D. A. & HORVATH, P. 2007. CRISPR provides acquired resistance against viruses in prokaryotes. *Science,* 315**,** 1709-1712.

BARRY-LANE, P. A., PATTERSON, C., VAN DER MERWE, M., HU, Z. Y., HOLLAND, S. M., YEH, E. T. H. & RUNGE, M. S. 2001. p47phox is required for atherosclerotic lesion progression in ApoE(-/-) mice. *Journal of Clinical Investigation,* 108**,** 1513-1522.

BARTEL, D. P. 2004. MicroRNAs: genomics, biogenesis, mechanism, and function. *Cell,* 116**,** 281-97.

BARTON, M. & MEYER, M. R. 2009. Postmenopausal Hypertension Mechanisms and Therapy. *Hypertension,* 54**,** 11-18.

BATES, P. J., LABER, D. A., MILLER, D. M., THOMAS, S. D. & TRENT, J. O. 2009. Discovery and development of the G-rich oligonucleotide AS1411 as a novel treatment for cancer. *Experimental and Molecular Pathology,* 86**,** 151-164.

BAZZONI, G. & DEJANA, E. 2004. Endothelial cell-to-cell junctions: Molecular organization and role in vascular homeostasis. *Physiological Reviews,* 84**,** 869-901.

BEAMISH, J. A., HE, P., KOTTKE-MARCHANT, K. & MARCHANT, R. E. 2010. Molecular regulation of contractile smooth muscle cell phenotype: implications for vascular tissue engineering. *Tissue Eng Part B Rev,* 16**,** 467-91.

BELL, R. D., LONG, X., LIN, M., BERGMANN, J. H., NANDA, V., COWAN, S. L., ZHOU, Q., HAN, Y., SPECTOR, D. L., ZHENG, D. & MIANO, J. M. 2014. Identification and initial functional characterization of a human vascular cell-enriched long noncoding RNA. *Arterioscler Thromb Vasc Biol,* 34**,** 1249-59.

BENNETT, M. R., LITTLEWOOD, T. D., SCHWARTZ, S. M. & WEISSBERG, P. L. 1997. Increased sensitivity of human vascular smooth muscle cells from atherosclerotic plaques to p53-mediated apoptosis. *Circ Res,* 81**,** 591-9.

BENNETT, M. R., SINHA, S. & OWENS, G. K. 2016. Vascular Smooth Muscle Cells in Atherosclerosis. *Circ Res,* 118**,** 692-702.

BENTZON, J. F., OTSUKA, F., VIRMANI, R. & FALK, E. 2014. Mechanisms of plaque formation and rupture. *Circ Res,* 114**,** 1852-66.

BERENSON, G. S., WATTIGNEY, W. A., TRACY, R. E., NEWMAN, W. P., SRINIVASAN, S. R., WEBBER, L. S., DALFERES, E. R. & STRONG, J. P. 1992. Atherosclerosis of the Aorta and Coronary-Arteries and Cardiovascular Risk-Factors in Persons Aged 6 to 30 Years and Studied at Necropsy (the Bogalusa Heart-Study). *American Journal of Cardiology,* 70**,** 851-858.

BERNSTEIN, E. & ALLIS, C. D. 2005. RNA meets chromatin. *Genes & Development,* 19**,** 1635-1655.

BERTERO, T., LU, Y., ANNIS, S., HALE, A., BHAT, B., SAGGAR, R., SAGGAR, R., WALLACE, W. D., ROSS, D. J., VARGAS, S. O., GRAHAM, B. B., KUMAR, R., BLACK, S. M., FRATZ, S., FINEMAN, J. R., WEST, J. D., HALEY, K. J., WAXMAN, A. B., CHAU, B. N., COTTRILL, K. A. & CHAN, S. Y. 2014. Systems-level regulation of microRNA networks by miR-130/301 promotes pulmonary hypertension. *J Clin Invest,* 124**,** 3514-28.

BERTOLI, C., SKOTHEIM, J. M. & DE BRUIN, R. A. 2013. Control of cell cycle transcription during G1 and S phases. *Nat Rev Mol Cell Biol,* 14**,** 518-28.

BHATNAGAR, P., WICKRAMASINGHE, K., WILLIAMS, J., RAYNER, M. & TOWNSEND, N. 2015. The epidemiology of cardiovascular disease in the UK 2014. *Heart,* 101**,** 1182-9.

BICKNELL, K. A., SURRY, E. L. & BROOKS, G. 2003. Targeting the cell cycle machinery for the treatment of cardiovascular disease. *Journal of Pharmacy and Pharmacology,* 55**,** 571-591.

BILLINGS, F. T. T., BALAGUER, J. M., C, Y., WRIGHT, P., PETRACEK, M. R., BYRNE, J. G., BROWN, N. J. & PRETORIUS, M. 2012. Comparative effects of angiotensin receptor blockade and ACE inhibition on the fibrinolytic and inflammatory responses to cardiopulmonary bypass. *Clin Pharmacol Ther,* 91**,** 1065-73.

BJARTVEIT, K. & TVERDAL, A. 2005. Health consequences of smoking 1-4 cigarettes per day. *Tob Control,* 14**,** 315-20.

BOETTGER, T., BEETZ, N., KOSTIN, S., SCHNEIDER, J., KRUGER, M., HEIN, L. & BRAUN, T. 2009. Acquisition of the contractile phenotype by murine arterial smooth muscle cells depends on the Mir143/145 gene cluster. *Journal of Clinical Investigation,* 119**,** 2634-2647.

BOND, M., CHASE, A. J., BAKER, A. H. & NEWBY, A. C. 2001. Inhibition of transcription factor NF-kappaB reduces matrix metalloproteinase-1, -3 and -9 production by vascular smooth muscle cells. *Cardiovasc Res,* 50**,** 556-65.

BOND, M., FABUNMI, R. P., BAKER, A. H. & NEWBY, A. C. 1998. Synergistic upregulation of metalloproteinase-9 by growth factors and inflammatory cytokines: an absolute requirement for transcription factor NF-kappa B. *Febs Letters,* 435**,** 29-34.

BOSTROM, K. I., RAJAMANNAN, N. M. & TOWLER, D. A. 2011. The regulation of valvular and vascular sclerosis by osteogenic morphogens. *Circ Res,* 109**,** 564-77.

BOULAY, K., GHRAM, M., VIRANAICKEN, W., TREPANIER, V., MOLLET, S., FRECHINA, C. & DESGROSEILLERS, L. 2014. Cell cycle-dependent regulation of the RNA-binding protein Staufen1. *Nucleic Acids Research,* 42**,** 7867-7883.

BRIKOS, C., WAIT, R., BEGUM, S., O'NEILL, L. A. J. & SAKLATVALA, J. 2007. Mass spectrometric analysis of the endogenous type I interleukin-1 (IL-1) receptor signaling complex formed after IL-1 binding identifies IL-1RAcP, MyD88, and IRAK-4 as the stable components, Interleukin-1 (IL-1) Pathway. *The American Society for Biochemistry and Molecular Biology*.

BRODIE, B., POKHAREL, Y., FLEISHMAN, N., BENSIMHON, A., KISSLING, G., HANSEN, C., MILKS, S., COOPER, M., MCALHANY, C. & STUCKEY, T. 2011. Very Late Stent Thrombosis After Primary Percutaneous Coronary Intervention With Bare-Metal and Drug-Eluting Stents for ST-Segment Elevation Myocardial Infarction A 15-Year Single-Center Experience. *Jacc-Cardiovascular Interventions,* 4**,** 30-38.

BRODY, J. I., PICKERING, N. J., CAPUZZI, D. M., FINK, G. B., CAN, C. A. & GOMEZ, F. 1992. Interleukin-1-Alpha as a Factor in Occlusive Vascular-Disease. *American Journal of Clinical Pathology,* 97**,** 8-13.

BROWN, K. W., VILLAR, A. J., BICKMORE, W., CLAYTON-SMITH, J., CATCHPOOLE, D., MAHER, E. R. & REIK, W. 1996. Imprinting mutation in the Beckwith-Wiedemann syndrome leads to biallelic IGF2 expression through an H19-independent pathway. *Hum Mol Genet,* 5**,** 2027-32.

BUSTIN, S. A. 2000. Absolute quantification of mRNA using real-time reverse transcription polymerase chain reaction assays. *Journal of Molecular Endocrinology,* 25**,** 169-193.

BUTTERY, L. D., CHESTER, A. H., SPRINGALL, D. R., BORLAND, J. A., MICHEL, T., YACOUB, M. H. & POLAK, J. M. 1996. Explanted vein grafts with an intact endothelium demonstrate reduced focal expression of endothelial nitric oxide synthase specific to atherosclerotic sites. *J Pathol,* 179**,** 197-203.

CABILI, M. N., DUNAGIN, M. C., MCCLANAHAN, P. D., BIAESCH, A., PADOVAN-MERHAR, O., REGEV, A., RINN, J. L. & RAJ, A. 2015. Localization and abundance analysis of human lncRNAs at single-cell and single-molecule resolution. *Genome Biology,* 16.

CALABRO, P., WILLERSON, J. T. & YEH, E. T. 2003. Inflammatory cytokines stimulated C-reactive protein production by human coronary artery smooth muscle cells. *Circulation,* 108**,** 1930-2.

CALCAGNO, A. M., CHEWNING, K. J., WU, C. P. & AMBUDKAR, S. V. 2006. Plasma membrane calcium ATPase (PMCA4): A housekeeper for RT-PCR relative quantification of polytopic membrane proteins. *Bmc Molecular Biology,* 7.

CAMICI, G. G., STEFFEL, J., AMANOVIC, I., BREITENSTEIN, A., BALDINGER, J., KELLER, S., LUSCHER, T. F. & TANNER, F. C. 2010. Rapamycin promotes arterial thrombosis in vivo: implications for everolimus and zotarolimus eluting stents. *European Heart Journal,* 31**,** 236-242.

CASTANOTTO, D., LIN, M., KOWOLIK, C., WANG, L. A., REN, X. Q., SOIFER, H. S., KOCH, T., HANSEN, B. R., OERUM, H., ARMSTRONG, B., WANG, Z. G., BAUER, P., ROSSI, J. & STEIN, C. A. 2015. A cytoplasmic pathway for gapmer antisense oligonucleotide-mediated gene silencing in mammalian cells. *Nucleic Acids Research,* 43**,** 9350-9361.

CASTELLOT, J. J., JR., WONG, K., HERMAN, B., HOOVER, R. L., ALBERTINI, D. F., WRIGHT, T. C., CALEB, B. L. & KARNOVSKY, M. J. 1985. Binding and internalization of heparin by vascular smooth muscle cells. *J Cell Physiol,* 124**,** 13-20.

CAVUSOGLU, Y., TIMURALP, B., US, T., AKGUN, Y., KUDAIBERDIEVA, G., GORENEK, B., UNALIR, A., GOKTEKIN, O. & ATA, N. 2004. Cigarette smoking increases plasma concentrations of vascular cell adhesion molecule-1 in patients with coronary artery disease. *Angiology,* 55**,** 397-402.

CEMAN, S. & SAUGSTAD, J. 2011. MicroRNAs: Meta-controllers of gene expression in synaptic activity emerge as genetic and diagnostic markers of human disease. *Pharmacology & Therapeutics,* 130**,** 26-37.

CHAI, S., CHAI, Q., DANIELSEN, C. C., HJORTH, P., NYENGAARD, J. R., LEDET, T., YAMAGUCHI, Y., RASMUSSEN, L. M. & WOGENSEN, L. 2005. Overexpression of hyaluronan in the tunica media promotes the development of atherosclerosis. *Circulation Research,* 96**,** 583-591.

CHAN, S. S., CHAN, H. H. & KYBA, M. 2016. Heterogeneity of Mesp1+ mesoderm revealed by single-cell RNA-seq. *Biochem Biophys Res Commun,* 474**,** 469-75.

CHANG, M. W., BARR, E., LU, M. M., BARTON, K. & LEIDEN, J. M. 1995. Adenovirus-mediated over-expression of the cyclin/cyclin-dependent kinase inhibitor, p21 inhibits vascular smooth muscle cell proliferation and neointima formation in the rat carotid artery model of balloon angioplasty. *J Clin Invest,* 96**,** 2260-8.

CHAU, B. N., XIN, C. Y., HARTNER, J., REN, S. Y., CASTANO, A. P., LINN, G., LI, J., TRAN, P. T., KAIMAL, V., HUANG, X. Q., CHANG, A. N., LI, S. Y., KALRA, A., GRAFALS, M., PORTILLA, D., MACKENNA, D. A., ORKIN, S. H. & DUFFIELD, J. S. 2012. MicroRNA-21 Promotes Fibrosis of the Kidney by Silencing Metabolic Pathways. *Science Translational Medicine,* 4.

CHEN, J., GUO, Z., TIAN, H. & CHEN, X. 2016. Production and clinical development of nanoparticles for gene delivery. *Mol Ther Methods Clin Dev,* 3**,** 16023.

CHEN, J. W., HOU, K., QIN, P., LIU, H. C., YI, B., YANG, W. T. & WU, W. 2014. RNA-Seq for gene identification and transcript profiling of three Stevia rebaudiana genotypes. *Bmc Genomics,* 15.

CHEN, K. F., CHEN, Z., WU, D. Y., ZHANG, L. L., LIN, X. Q., SU, J. Z., RODRIGUEZ, B., XI, Y. X., XIA, Z., CHEN, X., SHI, X. B., WANG, Q. B. & LI, W. 2015. Broad H3K4me3 is associated with increased transcription elongation and enhancer activity at tumor-suppressor genes. *Nature Genetics,* 47**,** 1149-+.

CHENG, C., VAN HAPEREN, R., DE WAARD, M., VAN DAMME, L. C., TEMPEL, D., HANEMAAIJER, L., VAN CAPPELLEN, G. W., BOS, J., SLAGER, C. J., DUNCKER, D. J., VAN DER STEEN, A. F., DE CROM, R. & KRAMS, R. 2005. Shear stress affects the intracellular distribution of eNOS: direct demonstration by a novel in vivo technique. *Blood,* 106**,** 3691-8.

CHENG, H. S., NJOCK, M. S., KHYZHA, N., DANG, L. T. & FISH, J. E. 2014. Noncoding RNAs regulate NF-kappaB signaling to modulate blood vessel inflammation. *Front Genet,* 5**,** 422.

CHENG, Y. H., LIU, X. J., YANG, J., LIN, Y., XU, D. Z., LU, Q., DEITCH, E. A., HUO, Y. Q., DELPHIN, E. S. & ZHANG, C. X. 2009. MicroRNA-145, a Novel Smooth Muscle Cell Phenotypic Marker and Modulator, Controls Vascular Neointimal Lesion Formation. *Circulation Research,* 105**,** 158-U113.

CHEREPANOVA, O. A., PIDKOVKA, N. A., SARMENTO, O. F., YOSHIDA, T., GAN, Q., ADIGUZEL, E., BENDECK, M. P., BERLINER, J., LEITINGER, N. & OWENS, G. K. 2009. Oxidized Phospholipids Induce Type VIII Collagen Expression and Vascular Smooth Muscle Cell Migration. *Circulation Research,* 104**,** 609-U112.

CHIANG, H. Y., KORSHUNOV, V. A., SEROUR, A., SHI, F. & SOTTILE, J. 2009. Fibronectin Is an Important Regulator of Flow-Induced Vascular Remodeling. *Arteriosclerosis Thrombosis and Vascular Biology,* 29**,** 1074-U157.

CHIU, J. J. & CHIEN, S. 2011. Effects of disturbed flow on vascular endothelium: pathophysiological basis and clinical perspectives. *Physiol Rev,* 91**,** 327-87.

CHONG, J. L., TSAI, S. Y., SHARMA, N., OPAVSKY, R., PRICE, R., WU, L., FERNANDEZ, S. A. & LEONE, G. 2009. E2f3a and E2f3b contribute to the control of cell proliferation and mouse development. *Mol Cell Biol,* 29**,** 414-24.

CHRISTEN, T., BOCHATON-PIALLAT, M. L., NEUVILLE, P., RENSEN, S., REDARD, M., VAN EYS, G. & GABBIANI, G. 1999. Cultured porcine coronary artery smooth muscle cells - A new model with advanced differentiation. *Circulation Research,* 85**,** 99-107.

CHU, C. Y. & RANA, T. M. 2006. Translation repression in human cells by microRNA-induced gene silencing requires RCK/p54. *Plos Biology,* 4**,** 1122-1136.

CINES, D. B., POLLAK, E. S., BUCK, C. A., LOSCALZO, J., ZIMMERMAN, G. A., MCEVER, R. P., POBER, J. S., WICK, T. M., KONKLE, B. A., SCHWARTZ, B. S., BARNATHAN, E. S., MCCRAE, K. R.,

HUG, B. A., SCHMIDT, A. M. & STERN, D. M. 1998. Endothelial cells in physiology and in the pathophysiology of vascular disorders. *Blood,* 91**,** 3527-61.

CLARK, M. B., JOHNSTON, R. L., INOSTROZA-PONTA, M., FOX, A. H., FORTINI, E., MOSCATO, P., DINGER, M. E. & MATTICK, J. S. 2012. Genome-wide analysis of long noncoding RNA stability. *Genome Res,* 22**,** 885-98.

CLARK, M. B., MERCER, T. R., BUSSOTTI, G., LEONARDI, T., HAYNES, K. R., CRAWFORD, J., BRUNCK, M. E., CAO, K. A., THOMAS, G. P., CHEN, W. Y., TAFT, R. J., NIELSEN, L. K., ENRIGHT, A. J., MATTICK, J. S. & DINGER, M. E. 2015. Quantitative gene profiling of long noncoding RNAs with targeted RNA sequencing. *Nat Methods,* 12**,** 339-42.

CLEMSON, C. M., HUTCHINSON, J. N., SARA, S. A., ENSMINGER, A. W., FOX, A. H., CHESS, A. & LAWRENCE, J. B. 2009. An Architectural Role for a Nuclear Noncoding RNA: NEAT1 RNA Is Essential for the Structure of Paraspeckles. *Molecular Cell,* 33**,** 717-726.

CLIMENT, M., QUINTAVALLE, M., MIRAGOLI, M., CHEN, J., CONDORELLI, G. & ELIA, L. 2015. TGFbeta Triggers miR-143/145 Transfer From Smooth Muscle Cells to Endothelial Cells, Thereby Modulating Vessel Stabilization. *Circ Res,* 116**,** 1753-64.

CONESA, A., MADRIGAL, P., TARAZONA, S., GOMEZ-CABRERO, D., CERVERA, A., MCPHERSON, A., SZCZESNIAK, M. W., GAFFNEY, D. J., ELO, L. L., ZHANG, X. & MORTAZAVI, A. 2016. A survey of best practices for RNA-seq data analysis. *Genome Biol,* 17**,** 13.

CORDES, K. R., SHEEHY, N. T., WHITE, M. P., BERRY, E. C., MORTON, S. U., MUTH, A. N., LEE, T. H., MIANO, J. M., IVEY, K. N. & SRIVASTAVA, D. 2009. miR-145 and miR-143 regulate smooth muscle cell fate and plasticity. *Nature,* 460**,** 705-U80.

CORDES, K. R. & SRIVASTAVA, D. 2009. MicroRNA Regulation of Cardiovascular Development. *Circulation Research,* 104**,** 724-732.

CUFF, C. A., KOTHAPALLI, D., AZONOBI, I., CHUN, S., ZHANG, Y., BELKIN, R., YEH, C., SECRETO, A., ASSOIAN, R. K., RADER, D. J. & PURE, E. 2001. The adhesion receptor CD44 promotes atherosclerosis by mediating inflammatory cell recruitment and vascular cell activation. *J Clin Invest,* 108**,** 1031-40.

CUI, R. R., LI, S. J., LIU, L. J., YI, L., LIANG, Q. H., ZHU, X., LIU, G. Y., LIU, Y., WU, S. S., LIAO, X. B., YUAN, L. Q., MAO, D. A. & LIAO, E. Y. 2012. MicroRNA-204 regulates vascular smooth muscle cell calcification in vitro and in vivo. *Cardiovasc Res,* 96**,** 320-9.

CURZEN, N. P. & FOX, K. M. 1997. Do ACE inhibitors modulate atherosclerosis? *European Heart Journal,* 18**,** 1530-1535.

D, G. H., KELLEY, D. R., TENEN, D., BERNSTEIN, B. & RINN, J. L. 2016. Widespread RNA binding by chromatin-associated proteins. *Genome Biol,* 17**,** 28.

DAEMEN, J., WENAWESER, P., TSUCHIDA, K., ABRECHT, L., SOPHIA, V., MORGER, C., KUKREJA, N., JUNI, P., SIANOS, G., HELLIGE, G., DOMBURG, R. T., HESS, O. M., BOERSMA, E., MEIER, B., WINDECKER, S. & SERRUYS, P. W. 2007. Early and late coronary stent thrombosis of sirolimus-eluting and paclitaxel-eluting stents in routine clinical practice: data from a large two-institutional cohort study. *Lancet,* 369**,** 667-678.

DAHM, R. 2005. Friedrich Miescher and the discovery of DNA. *Developmental Biology,* 278**,** 274-288.

DANESH, J., WHEELER, J. G., HIRSCHFIELD, G. M., EDA, S., EIRIKSDOTTIR, G., RUMLEY, A., LOWE, G. D. O., PEPYS, M. B. & GUDNASON, V. 2004. C-reactive protein and other circulating markers of inflammation in the prediction of coronary heart disease. *New England Journal of Medicine,* 350**,** 1387-1397.

DAVID, A. R., KERSHAW, A. & HEAGERTY, A. 2010. Atherosclerosis and diet in ancient Egypt. *Lancet,* 375**,** 718-9.

DAVIDGE, S. T., BAKER, P. N., LAUGHLIN, M. K. & ROBERTS, J. M. 1995. Nitric oxide produced by endothelial cells increases production of eicosanoids through activation of prostaglandin H synthase. *Circ Res,* 77**,** 274-83.

DAVIES, M. G., OWENS, E. L., MASON, D. P., LEA, H., TRAN, P. K., VERGEL, S., HAWKINS, S. A., HART, C. E. & CLOWES, A. W. 2000. Effect of platelet-derived growth factor receptor-alpha and -beta blockade on flow-induced neointimal formation in endothelialized baboon vascular grafts. *Circ Res,* 86**,** 779-86.

DAVIS, B. N., HILYARD, A. C., NGUYEN, P. H., LAGNA, G. & HATA, A. 2009. Induction of microRNA-221 by platelet-derived growth factor signaling is critical for modulation of vascular smooth muscle phenotype. *J Biol Chem,* 284**,** 3728-38.

DE VRIES, M. R., SIMONS, K. H., JUKEMA, J. W., BRAUN, J. & QUAX, P. H. 2016. Vein graft failure: from pathophysiology to clinical outcomes. *Nat Rev Cardiol,* 13**,** 451-70.

DEATON, R. A., GAN, Q. & OWENS, G. K. 2009. Sp1-dependent activation of KLF4 is required for PDGF-BB-induced phenotypic modulation of smooth muscle. *American Journal of Physiology-Heart and Circulatory Physiology,* 296**,** H1027-H1037.

DELA PAZ, N. G. & D'AMORE, P. A. 2009. Arterial versus venous endothelial cells. *Cell and Tissue Research,* 335**,** 5-16.

DENG, D. X., SPIN, J. M., TSALENKO, A., VAILAYA, A., BEN-DOR, A., YAKHINI, Z., TSAO, P., BRUHN, L. & QUERTERMOUS, T. 2006. Molecular signatures determining coronary artery and saphenous vein smooth muscle cell phenotypes: Distinct responses to stimuli. *Atherosclerosis Supplements,* 7**,** 230-230.

DENG, L., BLANCO, F. J., STEVENS, H., LU, R. F., CAUDRILLIER, A., MCBRIDE, M., MCCLURE, J. D., GRANT, J., THOMAS, M., FRID, M., STENMARK, K., WHITE, K., SETO, A. G., MORRELL, N. W., BRADSHAW, A. C., MACLEAN, M. R. & BAKER, A. H. 2015. MicroRNA-143 Activation Regulates Smooth Muscle and Endothelial Cell Crosstalk in Pulmonary Arterial Hypertension. *Circulation Research,* 117**,** 870-883.

DERRIEN, T. & GUIGO, R. 2011. [Long non-coding RNAs with enhancer-like function in human cells]. *Med Sci (Paris),* 27**,** 359-61.

DESFAITS, A. C., RAYMOND, J. & MUIZELAAR, J. P. 2000. Growth factors stimulate neointimal cells in vitro and increase the thickness of the neointima formed at the neck of porcine aneurysms treated by embolization. *Stroke,* 31**,** 498-507.

DESHAYES, S. & GREF, R. 2014. Synthetic and bioinspired cage nanoparticles for drug delivery. *Nanomedicine (Lond),* 9**,** 1545-64.

DICKHOUT, J. G., BASSERI, S. & AUSTIN, R. C. 2008. Macrophage function and its impact on atherosclerotic lesion composition, progression, and stability: the good, the bad, and the ugly. *Arterioscler Thromb Vasc Biol,* 28**,** 1413-5.

DIMITROVA, N., ZAMUDIO, J. R., JONG, R. M., SOUKUP, D., RESNICK, R., SARMA, K., WARD, A. J., RAJ, A., LEE, J. T., SHARP, P. A. & JACKS, T. 2014. LincRNA-p21 Activates p21 In cis to Promote Polycomb Target Gene Expression and to Enforce the G1/S Checkpoint. *Molecular Cell,* 54**,** 777-790.

DIODATO, M. & CHEDRAWY, E. G. 2014. Coronary artery bypass graft surgery: the past, present, and future of myocardial revascularisation. *Surg Res Pract,* 2014**,** 726158.

DODT, M., ROEHR, J. T., AHMED, R. & DIETERICH, C. 2012. FLEXBAR-Flexible Barcode and Adapter Processing for Next-Generation Sequencing Platforms. *Biology (Basel),* 1**,** 895-905.

DOLL, R. & PETO, R. 1976. Mortality in relation to smoking: 20 years' observations on male British doctors. *Br Med J,* 2**,** 1525-36.

DOSTIE, J., RICHMOND, T. A., ARNAOUT, R. A., SELZER, R. R., LEE, W. L., HONAN, T. A., RUBIO, E. D., KRUMM, A., LAMB, J., NUSBAUM, C., GREEN, R. D. & DEKKER, J. 2006. Chromosome Conformation Capture Carbon Copy (5C): A massively parallel solution for mapping interactions between genomic elements. *Genome Research,* 16**,** 1299-1309.

DRACHMAN, D. E., EDELMAN, E. R., SEIFERT, P., GROOTHUIS, A. R., BORNSTEIN, D. A., KAMATH, K. R., PALASIS, M., YANG, D., NOTT, S. H. & ROGERS, C. 2000. Neointimal thickening after stent delivery of paclitaxel: change in composition and arrest of growth over six months. *J Am Coll Cardiol,* 36**,** 2325-32.

DU, Y., GAO, C., LIU, Z., WANG, L., LIU, B., HE, F., ZHANG, T., WANG, Y., WANG, X., XU, M., LUO, G. Z., ZHU, Y., XU, Q., WANG, X. & KONG, W. 2012. Upregulation of a disintegrin and metalloproteinase with thrombospondin motifs-7 by miR-29 repression mediates vascular smooth muscle calcification. *Arterioscler Thromb Vasc Biol,* 32**,** 2580-8.

DYNLACHT, B. D. 1997. Regulation of transcription by proteins that control the cell cycle. *Nature,* 389**,** 149-152.

DYSON, N. 1998. The regulation of E2F by pRB-family proteins. *Genes Dev,* 12**,** 2245-62.

EDDY, S. R. 2001. Non-coding RNA genes and the modern RNA world. *Nature Reviews Genetics,* 2**,** 919-929.

ELDER, J. T., TSOI, L. C., IYER, M. K., STUART, P. E., SWINDELL, W. R., GUDJONSSON, J. E., TEJASVI, T., SARKAR, M. K., LI, B., DING, J., VOORHEES, J. J., KANG, H. M., NAIR, R. P., CHINNAIYAN, A. M. & ABECASIS, G. 2015. Analysis of long non-coding RNAs highlights tissue-specific expression patterns and epigenetic profiles in normal and psoriatic skin. *Journal of Investigative Dermatology,* 135**,** S75-S75.

ELLA, L., QUINTAVALLE, M., ZHANG, J., CONTU, R., COSSU, L., LATRONICO, M. V. G., PETERSON, K. L., INDOLFI, C., CATALUCCI, D., CHEN, J., COURTNEIDGE, S. A. & CONDORELLI, G. 2009. The knockout of miR-143 and-145 alters smooth muscle cell maintenance and vascular homeostasis in mice: correlates with human disease. *Cell Death and Differentiation,* 16**,** 1590-1598.

ELLIS, J. J., BROOM, M. & JONES, S. 2007. Protein-RNA interactions: structural analysis and functional classes. *Proteins,* 66**,** 903-11.

ENGREITZ, J. M., PANDYA-JONES, A., MCDONEL, P., SHISHKIN, A., SIROKMAN, K., SURKA, C., KADRI, S., XING, J., GOREN, A., LANDER, E. S., PLATH, K. & GUTTMAN, M. 2013. The Xist lncRNA exploits three-dimensional genome architecture to spread across the X chromosome. *Science,* 341**,** 1237973.

ERRIQUEZ, D., PERINI, G. & FERLINI, A. 2013. Non-Coding RNAs in Muscle Dystrophies. *International Journal of Molecular Sciences,* 14**,** 19681-19704.

EWING, B. & GREEN, P. 1998. Base-calling of automated sequencer traces using phred. II. Error probabilities. *Genome Research,* 8**,** 186-194.

FABUNMI, R. P., BAKER, A. H., MURRAY, E. J., BOOTH, R. F. & NEWBY, A. C. 1996. Divergent regulation by growth factors and cytokines of 95 kDa and 72 kDa gelatinases and tissue inhibitors or metalloproteinases-1, -2, and -3 in rabbit aortic smooth muscle cells. *Biochem J,* 315 (Pt 1)**,** 335-42.

FAGHIHI, M. A., MODARRESI, F., KHALIL, A. M., WOOD, D. E., SAHAGAN, B. G., MORGAN, T. E., FINCH, C. E., LAURENT, G. S., KENNY, P. J. & WAHLESTEDT, C. 2008. Expression of a noncoding RNA is elevated in Alzheimer's disease and drives rapid feed-forward regulation of beta-secretase. *Nature Medicine,* 14**,** 723-730.

FAGHIHI, M. A., ZHANG, M., HUANG, J., MODARRESI, F., VAN DER BRUG, M. P., NALLS, M. A., COOKSON, M. R., ST-LAURENT, G. & WAHLESTEDT, C. 2010. Evidence for natural antisense transcript-mediated inhibition of microRNA function. *Genome Biology,* 11.

FAROOQ, V., SERRUYS, P. W., ZHANG, Y. J., MACK, M., STAHLE, E., HOLMES, D. R., FELDMAN, T., MORICE, M. C., COLOMBO, A., BOURANTAS, C. V., DE VRIES, T., MOREL, M. A., DAWKINS, K. D., KAPPETEIN, A. P. & MOHR, F. W. 2013. Short-Term and Long-Term Clinical Impact of Stent Thrombosis and Graft Occlusion in the SYNTAX Trial at 5 Years Synergy Between Percutaneous Coronary Intervention With Taxus and Cardiac Surgery Trial. *Journal of the American College of Cardiology,* 62**,** 2360-2369.

FATEMI, R. P., SALAH-UDDIN, S., MODARRESI, F., KHOURY, N., WAHLESTEDT, C. & FAGHIHI, M. A. 2015. Screening for Small-Molecule Modulators of Long Noncoding RNA-Protein Interactions Using AlphaScreen. *Journal of Biomolecular Screening,* 20**,** 1132-1141.

FATIMA, R., AKHADE, V. S., PAL, D. & RAO, S. M. 2015. Long noncoding RNAs in development and cancer: potential biomarkers and therapeutic targets. *Mol Cell Ther,* 3**,** 5.

FAXON, D. P., CREAGER, M. A., SMITH, S. C., PASTERNAK, R. C., OLIN, J. W., BETTMANN, M. A., CRIQUI, M. H., MILANI, R. V., LOSCALZO, J., KAUFMAN, J. A., JONES, D. W. & PEARCE, W. H. 2004. Atherosclerotic vascular disease conference - Executive summary - Atherosclerotic vascular disease conference proceeding for healthcare professionals from a special writing group of the American Heart Association. *Circulation,* 109**,** 2595-2604.

FENG, Z., ZHANG, H., LEVINE, A. J. & JIN, S. 2005. The coordinate regulation of the p53 and mTOR pathways in cells. *Proc Natl Acad Sci U S A,* 102**,** 8204-9.

FERREIRA, P., HEMERLY, A., DE ALMEIDA ENGLER, J., BERGOUNIOUX, C., BURSSENS, S., VAN MONTAGU, M., ENGLER, G. & INZE, D. 1994. Three discrete classes of Arabidopsis cyclins

are expressed during different intervals of the cell cycle. *Proc Natl Acad Sci U S A,* 91**,** 11313-7.

FIGUEROA, X. F. & DULING, B. R. 2009. Gap Junctions in the Control of Vascular Function. *Antioxidants & Redox Signaling,* 11**,** 251-266.

FINN, A. V., NAKANO, M., NARULA, J., KOLODGIE, F. D. & VIRMANI, R. 2010. Concept of Vulnerable/Unstable Plaque. *Arteriosclerosis Thrombosis and Vascular Biology,* 30**,** 1282-1292.

FISCHMAN, D. L., LEON, M. B., BAIM, D. S., SCHATZ, R. A., SAVAGE, M. P., PENN, I., DETRE, K., VELTRI, L., RICCI, D., NOBUYOSHI, M., CLEMAN, M., HEUSER, R., ALMOND, D., TEIRSTEIN, P. S., FISH, R. D., COLOMBO, A., BRINKER, J., MOSES, J., SHAKNOVICH, A., HIRSHFELD, J., BAILEY, S., ELLIS, S., RAKE, R. & GOLDBERG, S. 1994. A Randomized Comparison of Coronary-Stent Placement and Balloon Angioplasty in the Treatment of Coronary-Artery Disease. *New England Journal of Medicine,* 331**,** 496-501.

FITZGIBBON, G. M., KAFKA, H. P., LEACH, A. J., KEON, W. J., HOOPER, G. D. & BURTON, J. R. 1996. Coronary bypass graft fate and patient outcome: angiographic follow-up of 5,065 grafts related to survival and reoperation in 1,388 patients during 25 years. *J Am Coll Cardiol,* 28**,** 616-26.

FLOREA, L. D. & SALZBERG, S. L. 2013. Genome-guided transcriptome assembly in the age of next-generation sequencing. *IEEE/ACM Trans Comput Biol Bioinform,* 10**,** 1234-40.

FLYNN, R. A. & CHANG, H. Y. 2012. Active chromatin and noncoding RNAs: an intimate relationship. *Curr Opin Genet Dev,* 22**,** 172-8.

FOLEY, E., O'FARRELL, P. H. & SPRENGER, F. 1999. Rux is a cyclin-dependent kinase inhibitor (CKI) specific for mitotic cyclin-Cdk complexes. *Curr Biol,* 9**,** 1392-402.

FUKUDA, M., KURIHARA, K., TANAKA, Y. & DESHIMARU, M. 2012. A strategy for developing a hammerhead ribozyme for selective RNA cleavage depending on substitutional RNA editing. *Rna-a Publication of the Rna Society,* 18**,** 1735-1744.

FURCHGOTT, R. F. & ZAWADZKI, J. V. 1980. The Obligatory Role of Endothelial-Cells in the Relaxation of Arterial Smooth-Muscle by Acetylcholine. *Nature,* 288**,** 373-376.

FURIC, L., MAHER-LAPORTE, M. & DESGROSEILLERS, L. 2008. A genome-wide approach identifies distinct but overlapping subsets of cellular mRNAs associated with Staufen1- and Staufen2-containing ribonucleoprotein complexes. *RNA,* 14**,** 324-35.

GAITI, F., FERNANDEZ-VALVERDE, S. L., NAKANISHI, N., CALCINO, A. D., YANAI, I., TANURDZIC, M. & DEGNAN, B. M. 2015. Dynamic and Widespread lncRNA Expression in a Sponge and the Origin of Animal Complexity. *Molecular Biology and Evolution,* 32**,** 2367-2382.

GAJ, T., GERSBACH, C. A. & BARBAS, C. F. 2013. ZFN, TALEN, and CRISPR/Cas-based methods for genome engineering. *Trends in Biotechnology,* 31**,** 397-405.

GARVEY, S. M., SINDEN, D. S., SCHOPPEE BORTZ, P. D. & WAMHOFF, B. R. 2010. Cyclosporine up-regulates Kruppel-like factor-4 (KLF4) in vascular smooth muscle cells and drives phenotypic modulation in vivo. *J Pharmacol Exp Ther,* 333**,** 34-42.

GAUNT, S. J. 2001. Gradients and forward spreading of vertebrate Hox gene expression detected by using a Hox/lacZ transgene. *Developmental Dynamics,* 221**,** 26-36.

GEISLER, S. & COLLER, J. 2013. RNA in unexpected places: long non-coding RNA functions in diverse cellular contexts. *Nature Reviews Molecular Cell Biology,* 14**,** 699-712.

GEORGE, S. J., WAN, S., HU, J., MACDONALD, R., JOHNSON, J. L. & BAKER, A. H. 2011. Sustained Reduction of Vein Graft Neointima Formation by Ex Vivo TIMP-3 Gene Therapy. *Circulation,* 124**,** S135-S142.

GERMING, A. 2005. Angiotensin-converting enzyme inhibition in stable coronary artery disease. *Medizinische Klinik,* 100**,** 123-123.

GHOURI, N., PURVES, D., DEANS, K. A., LOGAN, G., MCCONNACHIE, A., WILSON, J., GILL, J. M. & SATTAR, N. 2015. An investigation of two-dimensional ultrasound carotid plaque presence and intima media thickness in middle-aged South Asian and European men living in the United kingdom. *PLoS One,* 10**,** e0123317.

GHOURI, N., PURVES, D., MCCONNACHIE, A., WILSON, J., GILL, J. M. R. & SATTAR, N. 2013. Lower cardiorespiratory fitness contributes to increased insulin resistance and fasting glycaemia

in middle-aged South Asian compared with European men living in the UK. *Diabetologia,* 56**,** 2238-2249.

GILMORE, T. D. 2006. Introduction to NF-kappaB: players, pathways, perspectives. *Oncogene,* 25**,** 6680-4.

GINN, S. L., ALEXANDER, I. E., EDELSTEIN, M. L., ABEDI, M. R. & WIXON, J. 2013. Gene therapy clinical trials worldwide to 2012 an update. *Journal of Gene Medicine,* 15**,** 65-77.

GLAGOV, S., WEISENBERG, E., ZARINS, C. K., STANKUNAVICIUS, R. & KOLETTIS, G. J. 1987. Compensatory enlargement of human atherosclerotic coronary arteries. *N Engl J Med,* 316**,** 1371-5.

GLYNN, C. L., KHAN, S., KERIN, M. J. & DWYER, R. M. 2013. Isolation of secreted microRNAs (miRNAs) from cell-conditioned media. *Microrna,* 2**,** 14-9.

GOLDIE, L. C., NIX, M. K. & HIRSCHI, K. K. 2008. Embryonic vasculogenesis and hematopoietic specification. *Organogenesis,* 4**,** 257-63.

GOMEZ, D. & OWENS, G. K. 2012. Smooth muscle cell phenotypic switching in atherosclerosis. *Cardiovasc Res,* 95**,** 156-64.

GOMEZ, D., SHANKMAN, L. S., NGUYEN, A. T. & OWENS, G. K. 2013. Detection of histone modifications at specific gene loci in single cells in histological sections. *Nat Methods,* 10**,** 171-7.

GOMEZ, I. G., MACKENNA, D. A., JOHNSON, B. G., KAIMAL, V., ROACH, A. M., REN, S. Y., NAKAGAWA, N., XIN, C. Y., NEWITT, R., PANDYA, S., XIA, T. H., LIU, X. Q., BORZA, D. B., GRAFALS, M., SHANKLAND, S. J., HIMMELFARB, J., PORTILLA, D., LIU, S. G., CHAU, B. N. & DUFFIELD, J. S. 2015. Anti-microRNA-21 oligonucleotides prevent Alport nephropathy progression by stimulating metabolic pathways. *Journal of Clinical Investigation,* 125**,** 141-156.

GORBULEV, V. G., AXEL'ROD, V. D. & BAYEV, A. A. 1977. Primary structure of baker's yeast tRNAVal 2b. *Nucleic Acids Res,* 4**,** 3239-58.

GOUKASSIAN, D., DIEZ-JUAN, A., ASAHARA, T., SCHRATZBERGER, P., SILVER, M., MURAYAMA, T., ISNER, J. M. & ANDRES, V. 2001. Overexpression of p27(Kip1) by doxycycline-regulated adenoviral vectors inhibits endothelial cell proliferation and migration and impairs angiogenesis. *FASEB J,* 15**,** 1877-85.

GOWANS, J. L. 1959. The Recirculation of Lymphocytes from Blood to Lymph in the Rat. *Journal of Physiology-London,* 146**,** 54-&.

GRATZNER, H. G. 1982. Monoclonal antibody to 5-bromo- and 5-iododeoxyuridine: A new reagent for detection of DNA replication. *Science,* 218**,** 474-5.

GRIMM, D., STREETZ, K. L., JOPLING, C. L., STORM, T. A., PANDEY, K., DAVIS, C. R., MARION, P., SALAZAR, F. & KAY, M. A. 2006. Fatality in mice due to oversaturation of cellular microRNA/short hairpin RNA pathways. *Nature,* 441**,** 537-41.

GROTE, P., WITTLER, L., HENDRIX, D., KOCH, F., WAHRISCH, S., BEISAW, A., MACURA, K., BLASS, G., KELLIS, M., WERBER, M. & HERRMANN, B. G. 2013. The tissue-specific lncRNA Fendrr is an essential regulator of heart and body wall development in the mouse. *Dev Cell,* 24**,** 206-14.

GRUBE, E., SONODA, S., IKENO, F., HONDA, Y., KAR, S., CHAN, C., GERCKENS, U., LANSKY, A. J. & FITZGERALD, P. J. 2004. Six- and twelve-month results from first human experience using everolimus-eluting stents with bioabsorbable polymer. *Circulation,* 109**,** 2168-2171.

HALVORSEN, B., OTTERDAL, K., DAHL, T. B., SKJELLAND, M., GULLESTAD, L., OIE, E. & AUKRUST, P. 2008. Atherosclerotic plaque stability--what determines the fate of a plaque? *Prog Cardiovasc Dis,* 51**,** 183-94.

HANGAUER, M. J., VAUGHN, I. W. & MCMANUS, M. T. 2013. Pervasive Transcription of the Human Genome Produces Thousands of Previously Unidentified Long Intergenic Noncoding RNAs. *Plos Genetics,* 9.

HAO, H., ROPRAZ, P., VERIN, V., CAMENZIND, E., GEINOZ, A., PEPPER, M. S., GABBIANI, G. & BOCHATON-PIALLAT, M. L. 2002. Heterogeneity of smooth muscle cell populations cultured from pig coronary artery. *Arterioscler Thromb Vasc Biol,* 22**,** 1093-9.

HATHOUT, G. M., FINK, J. R., EL-SADEN, S. M. & GRANT, E. G. 2005. Sonographic NASCET index: a new doppler parameter for assessment of internal carotid artery stenosis. *AJNR Am J Neuroradiol,* 26**,** 68-75.

HATTORI, M. 2005. [Finishing the euchromatic sequence of the human genome]. *Tanpakushitsu Kakusan Koso,* 50**,** 162-8.

HAUTMANN, M. B., MADSEN, C. S. & OWENS, G. K. 1997. A transforming growth factor beta (TGFbeta) control element drives TGFbeta-induced stimulation of smooth muscle alpha-actin gene expression in concert with two CArG elements. *J Biol Chem,* 272**,** 10948-56.

HAYASHI, S., YAMAMOTO, A., YOU, F., YAMASHITA, K., IKEGAME, Y., TAWADA, M., YOSHIMORI, T., SHIMIZU, S. & NAKASHIMA, S. 2009. The Stent-Eluting Drugs Sirolimus and Paclitaxel Suppress Healing of the Endothelium by Induction of Autophagy. *American Journal of Pathology,* 175**,** 2226-2234.

HE, M. J., GONG, Y. T., SHI, J., PAN, Z. W., ZOU, H., SUN, D. H., TU, X., TAN, X. Y., LI, J. Q., LI, W. M., LIU, B., XUE, J. Y., SHENG, L., XIU, C. H., YANG, N., XUE, H. J., DING, X., YU, C. Y. & LI, Y. 2014. Plasma MicroRNAs as Potential Noninvasive Biomarkers for In-Stent Restenosis. *Plos One,* 9.

HEDIN, U., BOTTGER, B. A., FORSBERG, E., JOHANSSON, S. & THYBERG, J. 1988. Diverse effects of fibronectin and laminin on phenotypic properties of cultured arterial smooth muscle cells. *J Cell Biol,* 107**,** 307-19.

HELDMAN, A. W., CHENG, L., JENKINS, G. M., HELLER, P. F., KIM, D. W., WARE, M., NATER, C., HRUBAN, R. H., REZAI, B., ABELLA, B. S., BUNGE, K. E., KINSELLA, J. L., SOLLOTT, S. J., LAKATTA, E. G., BRINKER, J. A., HUNTER, W. L. & FROEHLICH, J. P. 2001. Paclitaxel stent coating inhibits neointimal hyperplasia at 4 weeks in a porcine model of coronary restenosis. *Circulation,* 103**,** 2289-2295.

HENDRIX, J. A., WAMHOFF, B. R., MCDONALD, O. G., SINHA, S., YOSHIDA, T. & OWENS, G. K. 2005. 5 ' CArG degeneracy in smooth muscle alpha-actin is required for injury-induced gene suppression in vivo. *Journal of Clinical Investigation,* 115**,** 418-427.

HERDEG, C., OBERHOFF, M., BAUMBACH, A., BLATTNER, A., AXEL, D. I., SCHRODER, S., HEINLE, H. & KARSCH, K. R. 2000. Local paclitaxel delivery for the prevention of restenosis: biological effects and efficacy in vivo. *J Am Coll Cardiol,* 35**,** 1969-76.

HERGENREIDER, E., HEYDT, S., TREGUER, K., BOETTGER, T., HORREVOETS, A. J. G., ZEIHER, A. M., SCHEFFER, M. P., FRANGAKIS, A. S., YIN, X. K., MAYR, M., BRAUN, T., URBICH, C., BOON, R. A. & DIMMELER, S. 2012. Atheroprotective communication between endothelial cells and smooth muscle cells through miRNAs. *Nature Cell Biology,* 14**,** 249-+.

HESSELS, D. & SCHALKEN, J. A. 2009. The use of PCA3 in the diagnosis of prostate cancer. *Nature Reviews Urology,* 6**,** 255-261.

HO, T. T., ZHOU, N. J., HUANG, J. G., KOIRALA, P., XU, M., FUNG, R., WU, F. T. & MO, Y. Y. 2015. Targeting non-coding RNAs with the CRISPR/Cas9 system in human cell lines. *Cancer Research,* 75.

HOFFMANN, U. & BUTLER, J. 2005. Noninvasive detection of coronary atherosclerotic plaque by multidetector row computed tomography. *Int J Obes (Lond),* 29 Suppl 2**,** S46-53.

HOR, G., KANEMOTO, N., STANDKE, R., MAUL, F. D., KLEPZIG, H., KOBER, G. & KALTENBACH, M. 1980. Trans-Luminal Angioplasty - Control of Efficiency by Nuclear Medical Methods after Non-Operative Dilatation of Critical Coronary-Artery Stenoses. *Herz,* 5**,** 168-176.

HU, H. Y., HE, L. & KHAITOVICH, P. 2014. Deep sequencing reveals a novel class of bidirectional promoters associated with neuronal genes. *BMC Genomics,* 15**,** 457.

HU, Y. & XU, Q. 2011. Adventitial biology: differentiation and function. *Arterioscler Thromb Vasc Biol,* 31**,** 1523-9.

HUANG, Z. K., LUO, Q., YAO, F. Y., QING, C., YE, J. Q., DENG, Y. T. & LI, J. M. 2016. Identification of Differentially Expressed Long Non-coding RNAs in Polarized Macrophages. *Scientific Reports,* 6.

HUARTE, M., GUTTMAN, M., FELDSER, D., GARBER, M., KOZIOL, M. J., KENZELMANN-BROZ, D., KHALIL, A. M., ZUK, O., AMIT, I., RABANI, M., ATTARDI, L. D., REGEV, A., LANDER, E. S.,

JACKS, T. & RINN, J. L. 2010. A Large Intergenic Noncoding RNA Induced by p53 Mediates Global Gene Repression in the p53 Response. *Cell,* 142**,** 409-419.

HUNG, T., WANG, Y. L., LIN, M. F., KOEGEL, A. K., KOTAKE, Y., GRANT, G. D., HORLINGS, H. M., SHAH, N., UMBRICHT, C., WANG, P., WANG, Y., KONG, B., LANGEROD, A., BORRESEN-DALE, A. L., KIM, S. K., VAN DE VIJVER, M., SUKUMAR, S., WHITFIELD, M. L., KELLIS, M., XIONG, Y., WONG, D. J. & CHANG, H. Y. 2011. Extensive and coordinated transcription of noncoding RNAs within cell-cycle promoters. *Nature Genetics,* 43**,** 621-U196.

IKEDA, U., IKEDA, M., OOHARA, T., OGUCHI, A., KAMITANI, T., TSURUYA, Y. & KANO, S. 1991. Interleukin 6 stimulates growth of vascular smooth muscle cells in a PDGF-dependent manner. *Am J Physiol,* 260**,** H1713-7.

IMANISHI, M., TOMITA, S., ISHIZAWA, K., KIHIRA, Y., UENO, M., IZAWA-ISHIZAWA, Y., IKEDA, Y., YAMANO, N., TSUCHIYA, K. & TAMAKI, T. 2014. Smooth muscle cell-specific Hif-1alpha deficiency suppresses angiotensin II-induced vascular remodelling in mice. *Cardiovasc Res,* 102**,** 460-8.

IRKLE, A., VESEY, A. T., LEWIS, D. Y., SKEPPER, J. N., BIRD, J. L., DWECK, M. R., JOSHI, F. R., GALLAGHER, F. A., WARBURTON, E. A., BENNETT, M. R., BRINDLE, K. M., NEWBY, D. E., RUDD, J. H. & DAVENPORT, A. P. 2015. Identifying active vascular microcalcification by (18)F-sodium fluoride positron emission tomography. *Nat Commun,* 6**,** 7495.

ISHIZAKA, N., ISHIZAKA, Y., TODA, E., HASHIMOTO, H., NAGAI, R. & YAMAKADO, M. 2004. Association between white blood cell count and carotid arteriosclerosis in Japanese smokers. *Atherosclerosis,* 175**,** 95-100.

IYER, A., ZUROLO, E., PRABOWO, A., FLUITER, K., SPLIET, W. G., VAN RIJEN, P. C., GORTER, J. A. & ARONICA, E. 2012. MicroRNA-146a: a key regulator of astrocyte-mediated inflammatory response. *PLoS One,* 7**,** e44789.

JAFFE, E. A., NACHMAN, R. L., BECKER, C. G. & MINICK, C. R. 1973. Culture of human endothelial cells derived from umbilical veins. Identification by morphologic and immunologic criteria. *J Clin Invest,* 52**,** 2745-56.

JAIN, M., HE, Q., LEE, W. S., KASHIKI, S., FOSTER, L. C., TSAI, J. C., LEE, M. E. & HABER, E. 1996. Role of CD44 in the reaction of vascular smooth muscle cells to arterial wall injury. *J Clin Invest,* 98**,** 877.

JAIN, M., SINGH, A., SINGH, V. & BARTHWAL, M. K. 2015. Involvement of interleukin-1 receptor-associated kinase-1 in vascular smooth muscle cell proliferation and neointimal formation after rat carotid injury. *Arterioscler Thromb Vasc Biol,* 35**,** 1445-55.

JAMESON, J. M., CAUVI, G., SHARP, L. L., WITHERDEN, D. A. & HAVRAN, W. L. 2005. Gammadelta T cell-induced hyaluronan production by epithelial cells regulates inflammation. *J Exp Med,* 201**,** 1269-79.

JIANG, C., LI, Y., ZHAO, Z., LU, J., CHEN, H., DING, N., WANG, G., XU, J. & LI, X. 2016. Identifying and functionally characterizing tissue-specific and ubiquitously expressed human lncRNAs. *Oncotarget,* 7**,** 7120-33.

JIANG, H., ROBEY, F. A. & GEWURZ, H. 1992. Localization of Sites through Which C-Reactive Protein Binds and Activates Complement to Residues 14-26 and 76-92 of the Human C1q-a Chain. *Journal of Experimental Medicine,* 175**,** 1373-1379.

JIANG, X. & NING, Q. 2015. The emerging roles of long noncoding RNAs in common cardiovascular diseases. *Hypertens Res,* 38**,** 375-9.

JOHNSON, J. L. 2007. Matrix metalloproteinases: influence on smooth muscle cells and atherosclerotic plaque stability. *Expert Rev Cardiovasc Ther,* 5**,** 265-82.

JOHNSSON, P., LIPOVICH, L., GRANDER, D. & MORRIS, K. V. 2014. Evolutionary conservation of long non-coding RNAs; sequence, structure, function. *Biochim Biophys Acta,* 1840**,** 1063-71.

JONER, M., FINN, A. V., FARB, A., MONT, E. K., KOLODGIE, F. D., LADICH, E., KUTYS, R., SKORIJA, K., GOLD, H. K. & VIRMANI, R. 2006. Pathology of drug-eluting stents in humans - Delayed healing and late thrombotic risk. *Journal of the American College of Cardiology,* 48**,** 193-202.

JOSHI, N. V., VESEY, A. T., WILLIAMS, M. C., SHAH, A. S. V., CALVERT, P. A., CRAIGHEAD, F. H. M., YEOH, S. E., WALLACE, W., SALTER, D., FLETCHER, A. M., VAN BEEK, E. J. R., FLAPAN, A. D., UREN, N. G., BEHAN, M. W. H., CRUDEN, N. L. M., MILLS, N. L., FOX, K. A. A., RUDD, J. H. F., DWECK, M. R. & NEWBY, D. E. 2014. F-18-fluoride positron emission tomography for identification of ruptured and high-risk coronary atherosclerotic plaques: a prospective clinical trial. *Lancet,* 383**,** 705-713.

KALLEN, A. N., ZHOU, X. B., XU, J., QIAO, C., MA, J., YAN, L., LU, L., LIU, C., YI, J. S., ZHANG, H., MIN, W., BENNETT, A. M., GREGORY, R. I., DING, Y. & HUANG, Y. 2013. The imprinted H19 lncRNA antagonizes let-7 microRNAs. *Mol Cell,* 52**,** 101-12.

KANEKO, S., LI, G., SON, J., XU, C. F., MARGUERON, R., NEUBERT, T. A. & REINBERG, D. 2010. Phosphorylation of the PRC2 component Ezh2 is cell cycle-regulated and up-regulates its binding to ncRNA. *Genes & Development,* 24**,** 2615-2620.

KANNEL, W. B., DAWBER, T. R., KAGAN, A., REVOTSKIE, N. & STOKES, J., 3RD 1961. Factors of risk in the development of coronary heart disease--six year follow-up experience. The Framingham Study. *Ann Intern Med,* 55**,** 33-50.

KAPINAS, K., KESSLER, C., RICKS, T., GRONOWICZ, G. & DELANY, A. M. 2010. miR-29 Modulates Wnt Signaling in Human Osteoblasts through a Positive Feedback Loop. *Journal of Biological Chemistry,* 285**,** 25221-25231.

KARPALA, A. J., DORAN, T. J. & BEAN, A. G. 2005. Immune responses to dsRNA: implications for gene silencing technologies. *Immunol Cell Biol,* 83**,** 211-6.

KASHIMA, Y., TAKAHASHI, M., SHIBA, Y., ITANO, N., IZAWA, A., KOYAMA, J., NAKAYAMA, J., TANIGUCHI, S., KIMATA, K. & IKEDA, U. 2013. Crucial Role of Hyaluronan in Neointimal Formation after Vascular Injury. *Plos One,* 8.

KASTAN, M. B. & BARTEK, J. 2004. Cell-cycle checkpoints and cancer. *Nature,* 432**,** 316-23.

KATAYAMA, S., TOMARU, Y., KASUKAWA, T., WAKI, K., NAKANISHI, M., NAKAMURA, M., NISHIDA, H., YAP, C. C., SUZUKI, M., KAWAI, J., SUZUKI, H., CARNINCI, P., HAYASHIZAKI, Y., WELLS, C., FRITH, M., RAVASI, T., PANG, K. C., HALLINAN, J., MATTICK, J., HUME, D. A., LIPOVICH, L., BATALOV, S., ENGSTROM, P. G., MIZUNO, Y., FAGHIHI, M. A., SANDELIN, A., CHALK, A. M., MOTTAGUI-TABAR, S., LIANG, Z., LENHARD, B., WAHLESTEDT, C., CORE, R. G. N. P., GRP, G. S. & CONSORTIUM, F. 2005. Antisense transcription in the mammalian transcriptome. *Science,* 309**,** 1564-1566.

KAWAJI, H., FRITH, M. C., KATAYAMA, S., SANDELIN, A., KAI, C., KAWAI, J., CARNINCI, P. & HAYASHIZAKI, Y. 2006. Dynamic usage of transcription start sites within core promoters. *Genome Biology,* 7.

KHALIL, A. M., GUTTMAN, M., HUARTE, M., GARBER, M., RAJ, A., MORALES, D. R., THOMAS, K., PRESSER, A., BERNSTEIN, B. E., VAN OUDENAARDEN, A., REGEV, A., LANDER, E. S. & RINN, J. L. 2009. Many human large intergenic noncoding RNAs associate with chromatin-modifying complexes and affect gene expression. *Proceedings of the National Academy of Sciences of the United States of America,* 106**,** 11667-11672.

KHANDELWAL, A., BACOLLA, A., VASQUEZ, K. M. & JAIN, A. 2015. Long non-coding RNA: A new paradigm for lung cancer. *Mol Carcinog,* 54**,** 1235-51.

KIM, D., PERTEA, G., TRAPNELL, C., PIMENTEL, H., KELLEY, R. & SALZBERG, S. L. 2013. TopHat2: accurate alignment of transcriptomes in the presence of insertions, deletions and gene fusions. *Genome Biol,* 14**,** R36.

KIM, H. S., AIKAWA, M., KIMURA, K., KURO-O, M., NAKAHARA, K., SUZUKI, T., KATOH, H., OKAMOTO, E., YAZAKI, Y. & NAGAI, R. 1993. Ductus arteriosus. Advanced differentiation of smooth muscle cells demonstrated by myosin heavy chain isoform expression in rabbits. *Circulation,* 88**,** 1804-10.

KIMURA, H. 2013. Histone modifications for human epigenome analysis. *J Hum Genet,* 58**,** 439-45.

KLEIN, D. K., HOFFMANN, S., AHLSKOG, J. K., O'HANLON, K., QUAAS, M., LARSEN, B. D., ROLLAND, B., ROSNER, H. I., WALTER, D., KOUSHOLT, A. N., MENZEL, T., LEES, M., JOHANSEN, J. V., RAPPSILBER, J., ENGELAND, K. & SORENSEN, C. S. 2015. Cyclin F suppresses B-Myb activity to promote cell cycle checkpoint control. *Nature Communications,* 6.

KOBAYASHI, R., KUBOTA, T. & HIDAKA, H. 1994. Purification, characterization, and partial sequence analysis of a new 25-kDa actin-binding protein from bovine aorta: a SM22 homolog. *Biochem Biophys Res Commun,* 198**,** 1275-80.

KONSTANTINOV, I. E. & JANKOVIC, G. M. 2013. Alexander I. Ignatowski: a pioneer in the study of atherosclerosis. *Tex Heart Inst J,* 40**,** 246-9.

KONSTANTINOV, I. E., MEJEVOI, N. & ANICHKOV, N. M. 2006. Nikolai N. Anichkov and his theory of atherosclerosis. *Tex Heart Inst J,* 33**,** 417-23.

KOPP, K. L., RALFKIAER, U., GJERDRUM, L. M., HELVAD, R., PEDERSEN, I. H., LITMAN, T., JONSON, L., HAGEDORN, P. H., KREJSGAARD, T., GNIADECKI, R., BONEFELD, C. M., SKOV, L., GEISLER, C., WASIK, M. A., RALFKIAER, E., ODUM, N. & WOETMANN, A. 2013. STAT5-mediated expression of oncogenic miR-155 in cutaneous T-cell lymphoma. *Cell Cycle,* 12**,** 1939-47.

KORNIENKO, A. E., DOTTER, C. P., GUENZL, P. M., GISSLINGER, H., GISSLINGER, B., CLEARY, C., KRALOVICS, R., PAULER, F. M. & BARLOW, D. P. 2016. Long non-coding RNAs display higher natural expression variation than protein-coding genes in healthy humans. *Genome Biology,* 17.

KORNIENKO, A. E., GUENZL, P. M., BARLOW, D. P. & PAULER, F. M. 2013. Gene regulation by the act of long non-coding RNA transcription. *BMC Biol,* 11**,** 59.

KOZAKI, K., KAMINSKI, W. E., TANG, J. J., HOLLENBACH, S., LINDAHL, P., SULLIVAN, C., YU, J. C., ABE, K., MARTIN, P. J., ROSS, R., BETSHOLTZ, C., GIESE, N. A. & RAINES, E. W. 2002. Blockade of platelet-derived growth factor or its receptors transiently delays but does not prevent fibrous cap formation in ApoE null mice. *American Journal of Pathology,* 161**,** 1395-1407.

KRETZ, M. 2013. TINCR, staufen1, and cellular differentiation. *Rna Biology,* 10**,** 1597-1601.

KRUEGEL, J., RUBEL, D. & GROSS, O. 2013. Alport syndrome-insights from basic and clinical research. *Nature Reviews Nephrology,* 9**,** 170-178.

KUMARSWAMY, R., BAUTERS, C., VOLKMANN, I., MAURY, F., FETISCH, J., HOLZMANN, A., LEMESLE, G., DE GROOTE, P., PINET, F. & THUM, T. 2014. Circulating long noncoding RNA, LIPCAR, predicts survival in patients with heart failure. *Circ Res,* 114**,** 1569-75.

KURO-O, M., NAGAI, R., TSUCHIMOCHI, H., KATOH, H., YAZAKI, Y., OHKUBO, A. & TAKAKU, F. 1989. Developmentally regulated expression of vascular smooth muscle myosin heavy chain isoforms. *J Biol Chem,* 264**,** 18272-5.

LAI, F., OROM, U. A., CESARONI, M., BERINGER, M., TAATJES, D. J., BLOBEL, G. A. & SHIEKHATTAR, R. 2013. Activating RNAs associate with Mediator to enhance chromatin architecture and transcription. *Nature,* 494**,** 497-501.

LANDER, E. S. 2011. Initial impact of the sequencing of the human genome. *Nature,* 470**,** 187-197.

LANDMESSER, U., DIKALOV, S., PRICE, S. R., MCCANN, L., FUKAI, T., HOLLAND, S. M., MITCH, W. E. & HARRISON, D. G. 2003. Oxidation of tetrahydrobiopterin leads to uncoupling of endothelial cell nitric oxide synthase in hypertension. *J Clin Invest,* 111**,** 1201-9.

LARDIZABAL, M. N., NOCITO, A. L., DANIELE, S. M., ORNELLA, L. A., PALATNIK, J. F. & VEGGI, L. M. 2012. Reference Genes for Real-Time PCR Quantification of MicroRNAs and Messenger RNAs in Rat Models of Hepatotoxicity. *Plos One,* 7.

LAVER, J. D., LI, X., ANCEVICIUS, K., WESTWOOD, J. T., SMIBERT, C. A., MORRIS, Q. D. & LIPSHITZ, H. D. 2013. Genome-wide analysis of Staufen-associated mRNAs identifies secondary structures that confer target specificity. *Nucleic Acids Research,* 41**,** 9438-9460.

LAWRENCE, T. 2009. The nuclear factor NF-kappaB pathway in inflammation. *Cold Spring Harb Perspect Biol,* 1**,** a001651.

LEE, R. C., FEINBAUM, R. L. & AMBROS, V. 1993. The C. elegans heterochronic gene lin-4 encodes small RNAs with antisense complementarity to lin-14. *Cell,* 75**,** 843-54.

LEEPER, N. J., RAIESDANA, A., KOJIMA, Y., CHUN, H. J., AZUMA, J., MAEGDEFESSEL, L., KUNDU, R. K., QUERTERMOUS, T., TSAO, P. S. & SPIN, J. M. 2011. MicroRNA-26a Is a Novel Regulator of Vascular Smooth Muscle Cell Function. *Journal of Cellular Physiology,* 226**,** 1035-1043.

LEEPER, N. J., RAIESDANA, A., KOJIMA, Y., KUNDU, R. K., CHENG, H., MAEGDEFESSEL, L., TOH, R., AHN, G. O., ALI, Z. A., ANDERSON, D. R., MILLER, C. L., ROBERTS, S. C., SPIN, J. M., DE

ALMEIDA, P. E., WU, J. C., XU, B., CHENG, K., QUERTERMOUS, M., KUNDU, S., KORTEKAAS, K. E., BERZIN, E., DOWNING, K. P., DALMAN, R. L., TSAO, P. S., SCHADT, E. E., OWENS, G. K. & QUERTERMOUS, T. 2013. Loss of CDKN2B promotes p53-dependent smooth muscle cell apoptosis and aneurysm formation. *Arterioscler Thromb Vasc Biol,* 33**,** e1-e10.

LEMESLE, G., MALUENDA, G., COLLINS, S. D. & WAKSMAN, R. 2010. Drug-eluting stents: issues of late stent thrombosis. *Cardiol Clin,* 28**,** 97-105.

LEMSON, M. S., TORDOIR, J. H. M., DAEMEN, M. J. A. P. & KITSLAAR, P. J. E. H. M. 2000. Intimal hyperplasia in vascular grafts. *European Journal of Vascular and Endovascular Surgery,* 19**,** 336-350.

LEUNG, A., STAPLETON, K. & NATARAJAN, R. 2016. Functional Long Non-coding RNAs in Vascular Smooth Muscle Cells. *Curr Top Microbiol Immunol,* 394**,** 127-41.

LEUNG, A., TRAC, C., JIN, W., LANTING, L., AKBANY, A., SAETROM, P., SCHONES, D. E. & NATARAJAN, R. 2013. Novel long noncoding RNAs are regulated by angiotensin II in vascular smooth muscle cells. *Circ Res,* 113**,** 266-78.

LI, B., FILLMORE, N., BAI, Y., COLLINS, M., THOMSON, J. A., STEWART, R. & DEWEY, C. N. 2014. Evaluation of de novo transcriptome assemblies from RNA-Seq data. *Genome Biol,* 15**,** 553.

LI, L., BLUMENTHAL, D. K., TERRY, C. M., HE, Y., CARLSON, M. L. & CHEUNG, A. K. 2011a. PDGF-induced proliferation in human arterial and venous smooth muscle cells: molecular basis for differential effects of PDGF isoforms. *J Cell Biochem,* 112**,** 289-98.

LI, L., BLUMENTHAL, D. K., TERRY, C. M., HE, Y. X., CARLSON, M. L. & CHEUNG, A. K. 2011b. PDGF-Induced Proliferation in Human Arterial and Venous Smooth Muscle Cells: Molecular Basis for Differential Effects of PDGF Isoforms. *Journal of Cellular Biochemistry,* 112**,** 289-298.

LI, L., MIANO, J. M., CSERJESI, P. & OLSEN, E. N. 1996. SM22 alpha, a marker of adult smooth muscle, is expressed in multiple myogenic lineages during embryogenesis. *Circulation Research,* 78**,** 188-195.

LI, S. J., WANG, D. Z., WANG, Z. G., RICHARDSON, J. A. & OLSON, E. N. 2003. The serum response factor coactivator myocardin is required for vascular smooth muscle development. *Proceedings of the National Academy of Sciences of the United States of America,* 100**,** 9366-9370.

LI, W. B., NOTANI, D., MA, Q., TANASA, B., NUNEZ, E., CHEN, A. Y., MERKURJEV, D., ZHANG, J., OHGI, K., SONG, X. Y., OH, S., KIM, H. S., GLASS, C. K. & ROSENFELD, M. G. 2013. Functional roles of enhancer RNAs for oestrogen-dependent transcriptional activation. *Nature,* 498**,** 516-+.

LI, Y. & KOWDLEY, K. V. 2012. Method for microRNA isolation from clinical serum samples. *Analytical Biochemistry,* 431**,** 69-75.

LI, Z., HASSAN, M. Q., VOLINIA, S., VAN WIJNEN, A. J., STEIN, J. L., CROCE, C. M., LIAN, J. B. & STEIN, G. S. 2008. A microRNA signature for a BMP2-induced osteoblast lineage commitment program. *Proceedings of the National Academy of Sciences of the United States of America,* 105**,** 13906-13911.

LIANG, P. & PARDEE, A. B. 1992. Differential display of eukaryotic messenger RNA by means of the polymerase chain reaction. *Science,* 257**,** 967-71.

LIANG, P. & PARDEE, A. B. 1997. Differential display. A general protocol. *Methods Mol Biol,* 85**,** 3-11.

LIBBY, P. & RIDKER, P. M. 2004. Inflammation and atherosclerosis: role of C-reactive protein in risk assessment. *Am J Med,* 116 Suppl 6A**,** 9S-16S.

LIBBY, P., RIDKER, P. M. & HANSSON, G. K. 2011. Progress and challenges in translating the biology of atherosclerosis. *Nature,* 473**,** 317-325.

LIBBY, P., WARNER, S. J. & FRIEDMAN, G. B. 1988. Interleukin 1: a mitogen for human vascular smooth muscle cells that induces the release of growth-inhibitory prostanoids. *J Clin Invest,* 81**,** 487-98.

LIMA, J. A. C., DESAI, M. Y., STEEN, H., WARREN, W. P., GAUTAM, S. & LAI, S. H. 2004. Statin-induced cholesterol lowering and plaque regression after 6 months of magnetic resonance imaging-monitored therapy. *Circulation,* 110**,** 2336-2341.

LINDNER, V., OLSON, N. E., CLOWES, A. W. & REIDY, M. A. 1992. Inhibition of smooth muscle cell proliferation in injured rat arteries. Interaction of heparin with basic fibroblast growth factor. *J Clin Invest,* 90**,** 2044-9.

LIU, B., SUN, L., LIU, Q., GONG, C., YAO, Y., LV, X., LIN, L., YAO, H., SU, F., LI, D., ZENG, M. & SONG, E. 2015. A cytoplasmic NF-kappaB interacting long noncoding RNA blocks IkappaB phosphorylation and suppresses breast cancer metastasis. *Cancer Cell,* 27**,** 370-81.

LIU, C. H., SU, T., LI, F., LI, L. F., QIN, X. P., PAN, W. N., FENG, F., CHEN, F., LIAO, D. F. & CHEN, L. X. 2010a. PI3K/Akt signaling transduction pathway is involved in rat vascular smooth muscle cell proliferation induced by apelin-13. *Acta Biochimica Et Biophysica Sinica,* 42**,** 396-402.

LIU, H. T., LI, F., WANG, W. Y., LI, X. J., LIU, Y. M., WANG, R. A., GUO, W. Y. & WANG, H. C. 2010b. Rapamycin Inhibits Re-Endothelialization after Percutaneous Coronary Intervention by Impeding the Proliferation and Migration of Endothelial Cells and Inducing Apoptosis of Endothelial Progenitor Cells. *Texas Heart Institute Journal,* 37**,** 194-201.

LIU, N., WILLIAMS, A. H., MAXEINER, J. M., BEZPROZVANNAYA, S., SHELTON, J. M., RICHARDSON, J. A., BASSEL-DUBY, R. & OLSON, E. N. 2012. microRNA-206 promotes skeletal muscle regeneration and delays progression of Duchenne muscular dystrophy in mice. *J Clin Invest,* 122**,** 2054-65.

LIU, X., CHENG, Y., ZHANG, S., LIN, Y., YANG, J. & ZHANG, C. 2009. A necessary role of miR-221 and miR-222 in vascular smooth muscle cell proliferation and neointimal hyperplasia. *Circ Res,* 104**,** 476-87.

LIU, Y., SINHA, S., MCDONALD, O. G., SHANG, Y. T., HOOFNAGLE, M. H. & OWENS, G. K. 2005. Kruppel-like factor 4 abrogates myocardin-induced activation of smooth muscle gene expression. *Journal of Biological Chemistry,* 280**,** 9719-9727.

LIVAK, K. J. & SCHMITTGEN, T. D. 2001. Analysis of relative gene expression data using real-time quantitative PCR and the 2(-Delta Delta C(T)) Method. *Methods,* 25**,** 402-8.

LORENTZEN, K. A., CHAI, S., CHEN, H., DANIELSEN, C. C., SIMONSEN, U. & WOGENSEN, L. 2016. Mechanisms involved in extracellular matrix remodeling and arterial stiffness induced by hyaluronan accumulation. *Atherosclerosis,* 244**,** 195-203.

LOSCALZO, J. 1998. The antithrombotic effects of nitric oxide. *Vascular Endothelium,* 294**,** 99-102.

LUHESHI, N. M., ROTHWELL, N. J. & BROUGH, D. 2009. Dual functionality of interleukin-1 family cytokines: implications for anti-interleukin-1 therapy. *Br J Pharmacol,* 157**,** 1318-29.

MA, S. T., TIAN, X. Y., MU, C. F., SHEN, H. F., BISMUTH, J. & WONG, W. T. 2015. Targeted delivery of microRNAs by microparticles to inflamed endothelium ameliorates endothelial inflammation and atherosclerosis. *Faseb Journal,* 29.

MAAS, A. H. E. M. & APPELMAN, Y. E. A. 2010. Gender differences in coronary heart disease. *Netherlands Heart Journal,* 18**,** 598-602.

MACK, C. P. 2011. Signaling Mechanisms That Regulate Smooth Muscle Cell Differentiation. *Arteriosclerosis Thrombosis and Vascular Biology,* 31**,** 1495-1505.

MACK, C. P. & OWENS, G. K. 1999. Regulation of smooth muscle alpha-actin expression in vivo is dependent on CArG elements within the 5 ' and first intron promoter regions. *Circulation Research,* 84**,** 852-861.

MAENNER, S., BLAUD, M., FOUILLEN, L., SAVOYE, A., MARCHAND, V., DUBOIS, A., SANGLIER-CIANFERANI, S., VAN DORSSELAER, A., CLERC, P., AVNER, P., VISVIKIS, A. & BRANLANT, C. 2010. 2-D Structure of the A Region of Xist RNA and Its Implication for PRC2 Association. *Plos Biology,* 8.

MAIER, K. G., HAN, X., SADOWITZ, B., GENTILE, K. L., MIDDLETON, F. A. & GAHTAN, V. 2010. Thrombospondin-1: a proatherosclerotic protein augmented by hyperglycemia. *J Vasc Surg,* 51**,** 1238-47.

MAJED, B. H. & KHALIL, R. A. 2012. Molecular Mechanisms Regulating the Vascular Prostacyclin Pathways and Their Adaptation during Pregnancy and in the Newborn. *Pharmacological Reviews,* 64**,** 540-582.

MANABE, I. & OWENS, G. K. 2001. CArG elements control smooth muscle subtype-specific expression of smooth muscle myosin in vivo. *J Clin Invest,* 107**,** 823-34.

MANACE, L. C., GODIWALA, T. N. & BABYATSKY, M. W. 2009. Genomics of Cardiovascular Disease. *Mount Sinai Journal of Medicine,* 76**,** 613-U4.

MANDYAM, C. D., HARBURG, G. C. & EISCH, A. J. 2007. Determination of key aspects of precursor cell proliferation, cell cycle length and kinetics in the adult mouse subgranular zone. *Neuroscience,* 146**,** 108-22.

MANKA, D. R., WIEGMAN, P., DIN, S., SANDERS, J. M., GREEN, S. A., GIMPLE, L. W., RAGOSTA, M., POWERS, E. R., LEY, K. & SAREMBOCK, I. J. 1999. Arterial injury increases expression of inflammatory adhesion molecules in the carotid arteries of apolipoprotein-E-deficient mice. *J Vasc Res,* 36**,** 372-8.

MARCHAND, A., ABI-GERGES, A., SALIBA, Y., MERLET, E. & LOMPRE, A. M. 2012. Calcium signaling in vascular smooth muscle cells: from physiology to pathology. *Adv Exp Med Biol,* 740**,** 795-810.

MARKS, L. S. & BOSTWICK, D. G. 2008. Prostate Cancer Specificity of PCA3 Gene Testing: Examples from Clinical Practice. *Rev Urol,* 10**,** 175-81.

MARX, S. O., TOTARY-JAIN, H. & MARKS, A. R. 2011. Vascular smooth muscle cell proliferation in restenosis. *Circ Cardiovasc Interv,* 4**,** 104-11.

MARX, V. 2014. A blooming genomic desert. *Nat Methods,* 11**,** 135-8.

MATHELIER, A. & CARBONE, A. 2013. Large scale chromosomal mapping of human microRNA structural clusters. *Nucleic Acids Res,* 41**,** 4392-408.

MATOUK, I. J., HALLE, D., GILON, M. & HOCHBERG, A. 2015. The non-coding RNAs of the H19-IGF2 imprinted loci: A focus on biological roles and therapeutic potential in Lung Cancer. *Journal of Translational Medicine,* 13.

MATSUSHITA, H., MORISHITA, R., AOKI, M., TOMITA, N., TANIYAMA, Y., NAKAGAMI, H., SHIMOZATO, T., HIGAKI, J., KANEDA, Y. & OGIHARA, T. 2000. Transfection of antisense p53 tumor suppressor gene oligodeoxynucleotides into rat carotid artery results in abnormal growth of vascular smooth muscle cells. *Circulation,* 101**,** 1447-1452.

MATTICK, J. S. 2001. Non-coding RNAs: the architects of eukaryotic complexity. *EMBO Rep,* 2**,** 986-91.

MAYR, M., ZAMPETAKI, A., WILLEIT, P., TILLING, L., DROZDOV, I., SHAH, A., BOULANGER, C., WILLEIT, J., CHOWIENCYK, P. & KIECHL, S. 2012. Prospective study on circulating microRNAs and risk of myocardial infarction. *European Heart Journal,* 33**,** 490-491.

MCLAREN, J. E., MICHAEL, D. R., ASHLIN, T. G. & RAMJI, D. P. 2011. Cytokines, macrophage lipid metabolism and foam cells: Implications for cardiovascular disease therapy. *Progress in Lipid Research,* 50**,** 331-347.

MEHTA, N. J. & KHAN, I. A. 2002. Cardiology's 10 greatest discoveries of the 20th century. *Tex Heart Inst J,* 29**,** 164-71.

MERCER, T. R., DINGER, M. E. & MATTICK, J. S. 2009. Long non-coding RNAs: insights into functions. *Nature Reviews Genetics,* 10**,** 155-159.

MICHIELS, C. 2003. Endothelial cell functions. *Journal of Cellular Physiology,* 196**,** 430-443.

MIELE, E., SPINELLI, G. P., TOMAO, F., ZULLO, A., DE MARINIS, F., PASCIUTI, G., ROSSI, L., ZORATTO, F. & TOMAO, S. 2008. Positron Emission Tomography (PET) radiotracers in oncology--utility of 18F-Fluoro-deoxy-glucose (FDG)-PET in the management of patients with non-small-cell lung cancer (NSCLC). *J Exp Clin Cancer Res,* 27**,** 52.

MILLS, J. D., KAWAHARA, Y. & JANITZ, M. 2013. Strand-Specific RNA-Seq Provides Greater Resolution of Transcriptome Profiling. *Curr Genomics,* 14**,** 173-81.

MIRSAFIAN, H., MANDA, S. S., MITCHELL, C. J., SREENIVASAMURTHY, S., RIPEN, A. M., BIN MOHAMAD, S., MERICAN, A. F. & PANDEY, A. 2016. Long non-coding RNA expression in primary human monocytes. *Genomics,* 108**,** 37-45.

MITCHELL, P. S., PARKIN, R. K., KROH, E. M., FRITZ, B. R., WYMAN, S. K., POGOSOVA-AGADJANYAN, E. L., PETERSON, A., NOTEBOOM, J., O'BRIANT, K. C., ALLEN, A., LIN, D. W., URBAN, N., DRESCHER, C. W., KNUDSEN, B. S., STIREWALT, D. L., GENTLEMAN, R., VESSELLA, R. L., NELSON, P. S., MARTIN, D. B. & TEWARI, M. 2008. Circulating microRNAs as stable blood-based markers for cancer detection. *Proceedings of the National Academy of Sciences of the United States of America,* 105**,** 10513-10518.

MITRA, S., DESHMUKH, A., SACHDEVA, R., LU, J. J. & MEHTA, J. L. 2011. Oxidized Low-Density Lipoprotein and Atherosclerosis Implications in Antioxidant Therapy. *American Journal of the Medical Sciences,* 342**,** 135-142.

MIZRAHI, A., CZERNIAK, A., LEVY, T., AMIUR, S., GALLULA, J., MATOUK, I., ABU-LAIL, R., SORIN, V., BIRMAN, T., DE GROOT, N., HOCHBERG, A. & OHANA, P. 2009. Development of targeted therapy for ovarian cancer mediated by a plasmid expressing diphtheria toxin under the control of H19 regulatory sequences. *Journal of Translational Medicine,* 7.

MODARRESI, F., FAGHIHI, M. A., PATEL, N. S., SAHAGAN, B. G., WAHLESTEDT, C. & LOPEZ-TOLEDANO, M. A. 2011. Knockdown of BACE1-AS Nonprotein-Coding Transcript Modulates Beta-Amyloid-Related Hippocampal Neurogenesis. *Int J Alzheimers Dis,* 2011**,** 929042.

MONAHAN-EARLEY, R., DVORAK, A. M. & AIRD, W. C. 2013. Evolutionary origins of the blood vascular system and endothelium. *Journal of Thrombosis and Haemostasis,* 11**,** 46-66.

MONNIER, P., MARTINET, C., PONTIS, J., STANCHEVA, I., AIT-SI-ALI, S. & DANDOLO, L. 2013. H19 lncRNA controls gene expression of the Imprinted Gene Network by recruiting MBD1. *Proceedings of the National Academy of Sciences of the United States of America,* 110**,** 20693-20698.

MONS, U., MUEZZINLER, A., GELLERT, C., SCHOTTKER, B., ABNET, C. C., BOBAK, M., DE GROOT, L., FREEDMAN, N. D., JANSEN, E., KEE, F., KROMHOUT, D., KUULASMAA, K., LAATIKAINEN, T., O'DOHERTY, M. G., BUENO-DE-MESQUITA, B., ORFANOS, P., PETERS, A., VAN DER SCHOUW, Y. T., WILSGAARD, T., WOLK, A., TRICHOPOULOU, A., BOFFETTA, P., BRENNER, H. & CONSORTIUM, C. 2015. Impact of smoking and smoking cessation on cardiovascular events and mortality among older adults: meta-analysis of individual participant data from prospective cohort studies of the CHANCES consortium. *Bmj-British Medical Journal,* 350.

MOORE, S. 1981. Responses of the Arterial-Wall to Injury. *Diabetes,* 30**,** 8-13.

MORLEY-SMITH, A. C., MILLS, A., JACOBS, S., MEYNS, B., REGA, F., SIMON, A. R., PEPPER, J. R., LYON, A. R. & THUM, T. 2014. Circulating microRNAs for predicting and monitoring response to mechanical circulatory support from a left ventricular assist device. *European Journal of Heart Failure,* 16**,** 871-879.

MOROZOVA, O., HIRST, M. & MARRA, M. A. 2009. Applications of New Sequencing Technologies for Transcriptome Analysis. *Annual Review of Genomics and Human Genetics,* 10**,** 135-151.

MORTAZAVI, A., WILLIAMS, B. A., MCCUE, K., SCHAEFFER, L. & WOLD, B. 2008. Mapping and quantifying mammalian transcriptomes by RNA-Seq. *Nat Methods,* 5**,** 621-8.

MOTWANI, J. G. & TOPOL, E. J. 1998. Aortocoronary saphenous vein graft disease - Pathogenesis, predisposition, and prevention. *Circulation,* 97**,** 916-931.

MOUSAVI, K., ZARE, H., DELL'ORSO, S., GRONTVED, L., GUTIERREZ-CRUZ, G., DERFOUL, A., HAGER, G. L. & SARTORELLI, V. 2013. eRNAs Promote Transcription by Establishing Chromatin Accessibility at Defined Genomic Loci. *Molecular Cell,* 51**,** 606-617.

MUIR, P., LI, S. T., LOU, S. K., WANG, D. F., SPAKOWICZ, D. J., SALICHOS, L., ZHANG, J., WEINSTOCK, G. M., ISAACS, F., ROZOWSKY, J. & GERSTEIN, M. 2016. The real cost of sequencing: scaling computation to keep pace with data generation. *Genome Biology,* 17.

MURPHY, G. & DOCHERTY, A. J. P. 1992. The Matrix Metalloproteinases and Their Inhibitors. *American Journal of Respiratory Cell and Molecular Biology,* 7**,** 120-125.

NADAL, M., GIRAUDEAU, B., TAVERNIER, E., JONVILLE-BERA, A. P., LORETTE, G. & MARUANI, A. 2016. Efficacy and Safety of Mammalian Target of Rapamycin Inhibitors in Vascular Anomalies: A Systematic Review. *Acta Derm Venereol,* 96**,** 448-52.

NAGAI, R., KURO-O, M., BABIJ, P. & PERIASAMY, M. 1989. Identification of two types of smooth muscle myosin heavy chain isoforms by cDNA cloning and immunoblot analysis. *J Biol Chem,* 264**,** 9734-7.

NAKAYA, H. I., AMARAL, P. P., LOURO, R., LOPES, A., FACHEL, A. A., MOREIRA, Y. B., EL-JUNDI, T. A., DA SILVA, A. M., REIS, E. M. & VERJOVSKI-ALMEIDA, S. 2007. Genome mapping and

expression analyses of human intronic noncoding RNAs reveal tissue-specific patterns and enrichment in genes related to regulation of transcription. *Genome Biology,* 8.

NAKAZAWA, G., FINN, A. V., JONER, M., LADICH, E., KUTYS, R., MONT, E. K., GOLD, H. K., BURKE, A. P., KOLODGIE, F. D. & VIRMANI, R. 2008. Delayed arterial healing and increased late stent thrombosis at culprit sites after drug-eluting stent placement for acute myocardial infarction patients - An autopsy study. *Circulation,* 118**,** 1138-1145.

NEGUEMBOR, M. V., JOTHI, M. & GABELLINI, D. 2014. Long noncoding RNAs, emerging players in muscle differentiation and disease. *Skelet Muscle,* 4**,** 8.

NI, X., CASTANARES, M., MUKHERJEE, A. & LUPOLD, S. E. 2011. Nucleic Acid Aptamers: Clinical Applications and Promising New Horizons. *Current Medicinal Chemistry,* 18**,** 4206-4214.

NIESPOREK, S., WEICHERT, W., SINN, B., ROSKE, A., NOSKE, A., BUCKENDAHL, A. C., WIRTZ, R., SEHOULI, J., KOENSGEN, D., DIETEL, M. & DENKERT, C. 2007. [NF-kappaB subunit p65/RelA expression in ovarian carcinoma: prognostic impact and link to COX-2 overexpression]. *Verh Dtsch Ges Pathol,* 91**,** 243-9.

NISHIMURA, G., MANABE, I., TSUSHIMA, K., FUJIU, K., OISHI, Y., IMAI, Y., MAEMURA, K., MIYAGISHI, M., HIGASHI, Y., KONDOH, H. & NAGAI, R. 2006. DeltaEF1 mediates TGF-beta signaling in vascular smooth muscle cell differentiation. *Dev Cell,* 11**,** 93-104.

NISSEN, S. E., NICHOLLS, S. J., SIPAHI, I., LIBBY, P., RAICHLEN, J. S., BALLANTYNE, C. M., DAVIGNON, J., ERBEL, R., FRUCHART, J. C., TARDIF, J. C., SCHOENHAGEN, P., CROWE, T., CAIN, V., WOLSKI, K., GOORMASTIC, M., TUZCU, E. M. & INVESTIGATORS, A. 2006. Effect of very high-intensity statin therapy on regression of coronary atherosclerosis - The ASTEROID trial. *Jama-Journal of the American Medical Association,* 295**,** 1556-1565.

O'BRIEN, M. A., COSTIN, B. N. & MILES, M. F. 2012. Using Genome-Wide Expression Profiling to Define Gene Networks Relevant to the Study of Complex Traits: From RNA Integrity to Network Topology. *Bioinformatics of Behavior: Pt 2,* 104**,** 91-133.

OGAWA, M., ISHINO, S., MUKAI, T., ASANO, D., TERAMOTO, N., WATABE, H., KUDOMI, N., SHIOMI, M., MAGATA, Y., IIDA, H. & SAJI, H. 2004. (18)F-FDG accumulation in atherosclerotic plaques: immunohistochemical and PET imaging study. *J Nucl Med,* 45**,** 1245-50.

OKADA, N., TODA, T., YAMAMOTO, M. & SATO, M. 2014. CDK-dependent phosphorylation of Alp7-Alp14 (TACC-TOG) promotes its nuclear accumulation and spindle microtubule assembly. *Mol Biol Cell,* 25**,** 1969-82.

OROM, U. A., DERRIEN, T., BERINGER, M., GUMIREDDY, K., GARDINI, A., BUSSOTTI, G., LAI, F., ZYTNICKI, M., NOTREDAME, C., HUANG, Q., GUIGO, R. & SHIEKHATTAR, R. 2010. Long noncoding RNAs with enhancer-like function in human cells. *Cell,* 143**,** 46-58.

OSMAN, R., L'ALLIER, P. L., ELGHARIB, N. & TARDIF, J. C. 2006. Critical appraisal of C-reactive protein throughout the spectrum of cardiovascular disease. *Vasc Health Risk Manag,* 2**,** 221-37.

OTTAVIANO, Y. & GERACE, L. 1985. Phosphorylation of the nuclear lamins during interphase and mitosis. *J Biol Chem,* 260**,** 624-32.

OWENS, G. K., KUMAR, M. S. & WAMHOFF, B. R. 2004. Molecular regulation of vascular smooth muscle cell differentiation in development and disease. *Physiological Reviews,* 84**,** 767-801.

OZSOLAK, F. & MILOS, P. M. 2011. RNA sequencing: advances, challenges and opportunities. *Nature Reviews Genetics,* 12**,** 87-98.

PADOVAN-MERHAR, O., NAIR, G. P., BIAESCH, A. G., MAYER, A., SCARFONE, S., FOLEY, S. W., WU, A. R., CHURCHMAN, L. S., SINGH, A. & RAJ, A. 2015. Single Mammalian Cells Compensate for Differences in Cellular Volume and DNA Copy Number through Independent Global Transcriptional Mechanisms. *Molecular Cell,* 58**,** 339-352.

PAFFEN, E. & DEMAAT, M. P. M. 2006. C-reactive protein in atherosclerosis: A causal factor? *Cardiovascular Research,* 71**,** 30-39.

PALADE, G. E. 1953. Fine Structure of Blood Capillaries. *Journal of Applied Physics,* 24**,** 1424-1424.

PANTH, N., PAUDEL, K. R. & PARAJULI, K. 2016. Reactive Oxygen Species: A Key Hallmark of Cardiovascular Disease. *Adv Med,* 2016**,** 9152732.

PAPAKONSTANTINOU, E., KARAKIULAKIS, G., ROTH, M. & BLOCK, L. H. 1995. Platelet-Derived Growth-Factor Stimulates the Secretion of Hyaluronic-Acid by Proliferating Human Vascular Smooth-Muscle Cells. *Proceedings of the National Academy of Sciences of the United States of America,* 92**,** 9881-9885.

PAPAKONSTANTINOU, E., ROTH, M., BLOCK, L. H., MIRTSOU-FIDANI, V., ARGIRIADIS, P. & KARAKIULAKIS, G. 1998. The differential distribution of hyaluronic acid in the layers of human atheromatic aortas is associated with vascular smooth muscle cell proliferation and migration. *Atherosclerosis,* 138**,** 79-89.

PARAJULI, H., TEH, M. T., ABRAHAMSEN, S., CHRISTOFFERSEN, I., NEPPELBERG, E., LYBAK, S., OSMAN, T., JOHANNESSEN, A. C., GULLBERG, D., SKARSTEIN, K. & COSTEA, D. E. 2016. Integrin alpha11 is overexpressed by tumour stroma of head and neck squamous cell carcinoma and correlates positively with alpha smooth muscle actin expression. *J Oral Pathol Med*.

PARASRAMKA, M. A., MAJI, S., MATSUDA, A., YAN, I. K. & PATEL, T. 2016. Long non-coding RNAs as novel targets for therapy in hepatocellular carcinoma. *Pharmacology & Therapeutics,* 161**,** 67-78.

PARK, E. & MAQUAT, L. E. 2013. Staufen-mediated mRNA decay. *Wiley Interdisciplinary Reviews-Rna,* 4**,** 423-435.

PARK, S. L., HWANG, B., LEE, S. Y., KIM, W. T., CHOI, Y. H., CHANG, Y. C., KIM, W. J. & MOON, S. K. 2015. p21WAF1 Is Required for Interleukin-16-Induced Migration and Invasion of Vascular Smooth Muscle Cells via the p38MAPK/Sp-1/MMP-9 Pathway. *Plos One,* 10.

PEARSON, J. D. 1999. Endothelial cell function and thrombosis. *Best Practice & Research Clinical Haematology,* 12**,** 329-341.

PEDERSEN, T. R., KJEKSHUS, J., BERG, K., HAGHFELT, T., FAERGEMAN, O., THORGEIRSSON, G., PYORALA, K., MIETTINEN, T., WILHELMSEN, L., OLSSON, A. G., WEDEL, H., KRISTIANSON, K., THOMSEN, H., NORDERO, E., THOMSEN, B., LYNGBORG, K., ANDERSEN, G. S., NIELSEN, F., TALLERUPHUUS, U., MCNAIR, A., EGSTRUP, K., SIMONSEN, E. H., SIMONSEN, I., VEJBYCHRISTENSEN, H., SOMMER, L., EIDNER, P. O., KLARHOLT, E., HENRIKSEN, A., MELLEMGAARD, K., LAUNBJERG, J., FREUERGAARD, P., NIELSEN, L., MADSEN, E. B., IBSEN, H., ANDERSEN, U., ENEMARK, H., HAARBO, J., MARTINSEN, B., DAHLSTROM, C. G., THYRRING, L., THOMASSEN, K., JENSEN, G., RASMUSSEN, S. L., SKOV, N., HANSEN, K. N., LARSEN, M. L., HAASTRUP, B., HJAERE, I., THUROE, A., LETH, A., MUNCH, M., WORCK, R., NIELSEN, B., THORN, A. G., PEDERSENBJERGAARD, O., FOURNAISE, B., SIGURD, B., ENK, B., NIELSEN, H., JACOBSEN, L., SVENDSEN, T. L., HOEGHOLM, A., MUNTER, H., KAUFMANN, P., HAUNSO, S., GRANDE, P., ERIKSEN, C., NIELSEN, H. H., JURLANDER, B., PINBORG, T., PINDBORG, J., TOST, H., CHRISTIANSEN, B. D., OPPENHAGEN, M., EGEDE, F., HVIDT, S., KJAERBY, T., LEMMING, L., KLAUSEN, I., MIETTINEN, T. A., VANHANEN, H., STRANDBERG, T. E., HOLTTA, K., LUOMANMAKI, H., PEKURI, T., VUORINEN, A., PASTERNACK, A., OKSA, H., SIITONEN, L., RIMPI, R., KESANIEMI, Y. A., LILJA, M., KORHONEN, T., RANTALA, A., RANTALA, M., SAVOLAINEN, M., UKKOLA, O., LAINE, L., VIRKKALA, L., LEHTO, S., et al. 1994. Randomized Trial of Cholesterol-Lowering in 4444 Patients with Coronary-Heart-Disease - the Scandinavian Simvastatin Survival Study (4s). *Lancet,* 344**,** 1383-1389.

PEDRAM FATEMI, R., SALAH-UDDIN, S., MODARRESI, F., KHOURY, N., WAHLESTEDT, C. & FAGHIHI, M. A. 2015. Screening for Small-Molecule Modulators of Long Noncoding RNA-Protein Interactions Using AlphaScreen. *J Biomol Screen,* 20**,** 1132-41.

PINEL, K., LACOSTE, J., PLANE, G., VENTURA, M. & COUILLAUD, F. 2014. Long-term in vivo imaging of translated RNAs for gene therapy. *Gene Ther,* 21**,** 434-9.

PISKOL, R., RAMASWAMI, G. & LI, J. B. 2013. Reliable Identification of Genomic Variants from RNA-Seq Data. *American Journal of Human Genetics,* 93**,** 641-651.

PLACE, R. F. & NOONAN, E. J. 2014. Non-coding RNAs turn up the heat: An emerging layer of novel regulators in the mammalian heat shock response. *Cell Stress & Chaperones,* 19**,** 159-172.

PONTA, H., SHERMAN, L. & HERRLICH, P. A. 2003. CD44: From adhesion molecules to signalling regulators. *Nature Reviews Molecular Cell Biology,* 4**,** 33-45.

PROBSTFIELD, J. L. & RIFKIND, B. M. 1991. The Lipid-Research-Clinics Coronary Primary Prevention Trial - Design, Results, and Implications. *European Journal of Clinical Pharmacology,* 40**,** S69-S75.

PSALTIS, P. J. & SIMARI, R. D. 2015. Vascular wall progenitor cells in health and disease. *Circ Res,* 116**,** 1392-412.

QI, P. & DU, X. 2013. The long non-coding RNAs, a new cancer diagnostic and therapeutic gold mine. *Modern Pathology,* 26**,** 155-165.

QIU, P., FENG, X. H. & LI, L. 2003. Interaction of Smad3 and SRF-associated complex mediates TGF-beta1 signals to regulate SM22 transcription during myofibroblast differentiation. *J Mol Cell Cardiol,* 35**,** 1407-20.

QIU, P., RITCHIE, R. P., FU, Z., CAO, D., CUMMING, J., MIANO, J. M., WANG, D. Z., LI, H. J. & LI, L. 2005. Myocardin enhances Smad3-mediated transforming growth factor-beta1 signaling in a CArG box-independent manner: Smad-binding element is an important cis element for SM22alpha transcription in vivo. *Circ Res,* 97**,** 983-91.

QU, H. & FANG, X. 2013. A brief review on the Human Encyclopedia of DNA Elements (ENCODE) project. *Genomics Proteomics Bioinformatics,* 11**,** 135-41.

QUINN, J. J. & CHANG, H. Y. 2016. Unique features of long non-coding RNA biogenesis and function. *Nature Reviews Genetics,* 17**,** 47-62.

QUINODOZ, S. & GUTTMAN, M. 2014. Long noncoding RNAs: an emerging link between gene regulation and nuclear organization. *Trends in Cell Biology,* 24**,** 651-663.

RAGHAVAN, A., OGILVIE, R. L., REILLY, C., ABELSON, M. L., RAGHAVAN, S., VASDEWANI, J., KRATHWOHL, M. & BOHJANEN, P. R. 2002. Genome-wide analysis of mRNA decay in resting and activated primary human T lymphocytes. *Nucleic Acids Res,* 30**,** 5529-38.

RAITOHARJU, E., LYYTIKAINEN, L. P., LEVULA, M., OKSALA, N., MENNANDER, A., TARKKA, M., KLOPP, N., ILLIG, T., KAHONEN, M., KARHUNEN, P. J., LAAKSONEN, R. & LEHTIMAKI, T. 2011. miR-21, miR-210, miR-34a, and miR-146a/b are up-regulated in human atherosclerotic plaques in the Tampere Vascular Study. *Atherosclerosis,* 219**,** 211-217.

RAJENDRAN, P., RENGARAJAN, T., THANGAVEL, J., NISHIGAKI, Y., SAKTHISEKARAN, D., SETHI, G. & NISHIGAKI, I. 2013. The vascular endothelium and human diseases. *Int J Biol Sci,* 9**,** 1057-69.

RANGREZ, A. Y., MASSY, Z. A., METZINGER-LE MEUTH, V. & METZINGER, L. 2011. miR-143 and miR-145 Molecular Keys to Switch the Phenotype of Vascular Smooth Muscle Cells. *Circulation-Cardiovascular Genetics,* 4**,** 197-205.

RASHID, F., SHAH, A. & SHAN, G. 2016. Long Non-coding RNAs in the Cytoplasm. *Genomics Proteomics Bioinformatics,* 14**,** 73-80.

RATH, D., AMLINGER, L., RATH, A. & LUNDGREN, M. 2015. The CRISPR-Cas immune system: Biology, mechanisms and applications. *Biochimie,* 117**,** 119-128.

RECTENWALD, J. E., MOLDAWER, L. L., HUBER, T. S., SEEGER, J. M. & OZAKI, C. K. 2000. Direct evidence for cytokine involvement in neointimal hyperplasia. *Circulation,* 102**,** 1697-702.

REGAN, C. P., ADAM, P. J., MADSEN, C. S. & OWENS, G. K. 2000. Molecular mechanisms of decreased smooth muscle differentiation marker expression after vascular injury. *Journal of Clinical Investigation,* 106**,** 1139-1147.

RENSEN, S. S. M., DOEVENDANS, P. A. F. M. & VAN EYS, G. J. J. M. 2007. Regulation and characteristics of vascular smooth muscle cell phenotypic diversity. *Netherlands Heart Journal,* 15**,** 100-108.

REUSCH, P., WAGDY, H., REUSCH, R., WILSON, E. & IVES, H. E. 1996. Mechanical strain increases smooth muscle and decreases nonmuscle myosin expression in rat vascular smooth muscle cells. *Circ Res,* 79**,** 1046-53.

RHEE, A. Y. & BROZOVICH, F. V. 2000. The smooth muscle cross-bridge cycle studied using sinusoidal length perturbations. *Biophysical Journal,* 79**,** 1511-1523.

RIBATTI, D., NICO, B. & CRIVELLATO, E. 2015. The development of the vascular system: a historical overview. *Methods Mol Biol,* 1214**,** 1-14.

RICHTER, K., HASLBECK, M. & BUCHNER, J. 2010. The Heat Shock Response: Life on the Verge of Death. *Molecular Cell,* 40**,** 253-266.

RIESSEN, R., WIGHT, T. N., PASTORE, C., HENLEY, C. & ISNER, J. M. 1996. Distribution of hyaluronan during extracellular matrix remodeling in human restenotic arteries and balloon-injured rat carotid arteries. *Circulation,* 93**,** 1141-7.

RINN, J. L. & CHANG, H. Y. 2012. Genome regulation by long noncoding RNAs. *Annu Rev Biochem,* 81**,** 145-66.

RINN, J. L., KERTESZ, M., WANG, J. K., SQUAZZO, S. L., XU, X., BRUGMANN, S. A., GOODNOUGH, L. H., HELMS, J. A., FARNHAM, P. J., SEGAL, E. & CHANG, H. Y. 2007. Functional demarcation of active and silent chromatin domains in human HOX loci by Noncoding RNAs. *Cell,* 129**,** 1311-1323.

RIPOCHE, M. A., KRESS, C., POIRIER, F. & DANDOLO, L. 1997. Deletion of the H19 transcription unit reveals the existence of a putative imprinting control element. *Genes & Development,* 11**,** 1596-1604.

ROBINSON, M. D., MCCARTHY, D. J. & SMYTH, G. K. 2010. edgeR: a Bioconductor package for differential expression analysis of digital gene expression data. *Bioinformatics,* 26**,** 139-40.

ROGERS, S., WELLS, R. & RECHSTEINER, M. 1986. Amino acid sequences common to rapidly degraded proteins: the PEST hypothesis. *Science,* 234**,** 364-8.

RONG, J. X., SHAPIRO, M., TROGAN, E. & FISHER, E. A. 2003. Transdifferentiation of mouse aortic smooth muscle cells to a macrophage-like state after cholesterol loading. *Proc Natl Acad Sci U S A,* 100**,** 13531-6.

ROSENGREN, A., WILHELMSEN, L. & WEDEL, H. 1992. Coronary heart disease, cancer and mortality in male middle-aged light smokers. *J Intern Med,* 231**,** 357-62.

RUBANYI, G. M. 1993. The role of endothelium in cardiovascular homeostasis and diseases. *J Cardiovasc Pharmacol,* 22 Suppl 4**,** S1-14.

RUBIE, C., KEMPF, K., HANS, J., SU, T. F., TILTON, B., GEORG, T., BRITTNER, B., LUDWIG, B. & SCHILLING, M. 2005. Housekeeping gene variability in normal and cancerous colorectal, pancreatic, esophageal, gastric and hepatic tissues. *Molecular and Cellular Probes,* 19**,** 101-109.

RUDD, J. H., WARBURTON, E. A., FRYER, T. D., JONES, H. A., CLARK, J. C., ANTOUN, N., JOHNSTROM, P., DAVENPORT, A. P., KIRKPATRICK, P. J., ARCH, B. N., PICKARD, J. D. & WEISSBERG, P. L. 2002. Imaging atherosclerotic plaque inflammation with [18F]-fluorodeoxyglucose positron emission tomography. *Circulation,* 105**,** 2708-11.

RUDIJANTO, A. 2007. The role of vascular smooth muscle cells on the pathogenesis of atherosclerosis. *Acta Med Indones,* 39**,** 86-93.

RUECKSCHLOSS, U., GALLE, J., HOLTZ, J., ZERKOWSKI, H. R. & MORAWIETZ, H. 2001. Induction of NAD(P)H oxidase by oxidized low-density lipoprotein in human endothelial cells: antioxidative potential of hydroxymethylglutaryl coenzyme A reductase inhibitor therapy. *Circulation,* 104**,** 1767-72.

RZUCIDLO, E. M., MARTIN, K. A. & POWELL, R. J. 2007. Regulation of vascular smooth muscle cell differentiation. *J Vasc Surg,* 45 Suppl A**,** A25-32.

SABATINI, D. M., ERDJUMENT-BROMAGE, H., LUI, M., TEMPST, P. & SNYDER, S. H. 1994. RAFT1: a mammalian protein that binds to FKBP12 in a rapamycin-dependent fashion and is homologous to yeast TORs. *Cell,* 78**,** 35-43.

SALIBA, A. E., WESTERMANN, A. J., GORSKI, S. A. & VOGEL, J. 2014. Single-cell RNA-seq: advances and future challenges. *Nucleic Acids Res,* 42**,** 8845-60.

SANCHEZ, Y. & HUARTE, M. 2013. Long non-coding RNAs: challenges for diagnosis and therapies. *Nucleic Acid Ther,* 23**,** 15-20.

SANDER, J. D. & JOUNG, J. K. 2014. CRISPR-Cas systems for editing, regulating and targeting genomes. *Nature Biotechnology,* 32**,** 347-355.

SANDOO, A., VAN ZANTEN, J. J., METSIOS, G. S., CARROLL, D. & KITAS, G. D. 2010. The endothelium and its role in regulating vascular tone. *Open Cardiovasc Med J,* 4**,** 302-12.

SARKAR, M. K., GAYEN, S., KUMAR, S., MACLARY, E., BUTTIGIEG, E., HINTEN, M., KUMARI, A., HARRIS, C., SADO, T. & KALANTRY, S. 2015. An Xist-activating antisense RNA required for X-chromosome inactivation. *Nat Commun,* 6**,** 8564.

SARMA, K., CIFUENTES-ROJAS, C., ERGUN, A., DEL ROSARIO, A., JEON, Y., WHITE, F., SADREYEV, R. & LEE, J. T. 2014. ATRX directs binding of PRC2 to Xist RNA and Polycomb targets. *Cell,* 159**,** 869-83.

SAUER, E., BABION, I., MADEA, B. & COURTS, C. 2014. An evidence based strategy for normalization of quantitative PCR data from miRNA expression analysis in forensic organ tissue identification. *Forensic Science International-Genetics,* 13**,** 217-223.

SAXENA, A. & CARNINCI, P. 2011. Long non-coding RNA modifies chromatin: epigenetic silencing by long non-coding RNAs. *Bioessays,* 33**,** 830-9.

SCHAFER, K. A. 1998. The cell cycle: a review. *Vet Pathol,* 35**,** 461-78.

SCHENA, M., SHALON, D., DAVIS, R. W. & BROWN, P. O. 1995. Quantitative monitoring of gene expression patterns with a complementary DNA microarray. *Science,* 270**,** 467-70.

SCHERMULY, R. T., DONY, E., GHOFRANI, H. A., PULLAMSETTI, S., SAVAI, R., ROTH, M., SYDYKOV, A., LAI, Y. J., WEISSMANN, N., SEEGER, W. & GRIMMINGER, F. 2005. Reversal of experimental pulmonary hypertension by PDGF inhibition. *J Clin Invest,* 115**,** 2811-21.

SCHROEDER, A., MUELLER, O., STOCKER, S., SALOWSKY, R., LEIBER, M., GASSMANN, M., LIGHTFOOT, S., MENZEL, W., GRANZOW, M. & RAGG, T. 2006. The RIN: an RNA integrity number for assigning integrity values to RNA measurements. *Bmc Molecular Biology,* 7.

SCHWARTZ, S. M., VIRMANI, R. & ROSENFELD, M. E. 2000. The good smooth muscle cells in atherosclerosis. *Curr Atheroscler Rep,* 2**,** 422-9.

SCOTT, R. P. & QUAGGIN, S. E. 2015. The cell biology of renal filtration. *Journal of Cell Biology,* 209**,** 199-210.

SECHLER, J. L. & SCHWARZBAUER, J. E. 1998. Regulation of G1 cell cycle progression by assembly of a fibronectin matrix. *Matrix Biology,* 17**,** 160-161.

SEDDIKI, N., BREZAR, V., RUFFIN, N., LEVY, Y. & SWAMINATHAN, S. 2014. Role of miR-155 in the regulation of lymphocyte immune function and disease. *Immunology,* 142**,** 32-38.

SEIMON, T. & TABAS, I. 2009. Mechanisms and consequences of macrophage apoptosis in atherosclerosis. *J Lipid Res,* 50 Suppl**,** S382-7.

SEKI, M., CARNINCI, P., NISHIYAMA, Y., HAYASHIZAKI, Y. & SHINOZAKI, K. 1998. High-efficiency cloning of Arabidopsis full-length cDNA by biotinylated CAP trapper. *Plant J,* 15**,** 707-20.

SETO, A. G., BEATTY, X. T., PESTANO, L. A., DICKINSON, B. A., WARREN, M. S., RODMAN, D. M. & JACKSON, A. L. 2015. Preclinical Results Supporting Therapeutic Development of Mrg-106, an Oligonucleotide Inhibitor of Mir-155, in CTCL. *Blood,* 126.

SHARMA, N., LU, Y., ZHOU, G., LIAO, X., KAPIL, P., ANAND, P., MAHABELESHWAR, G. H., STAMLER, J. S. & JAIN, M. K. 2012. Myeloid Kruppel-like factor 4 deficiency augments atherogenesis in ApoE-/- mice--brief report. *Arterioscler Thromb Vasc Biol,* 32**,** 2836-8.

SHAROVA, L. V., SHAROV, A. A., NEDOREZOV, T., PIAO, Y., SHAIK, N. & KO, M. S. H. 2009. Database for mRNA Half-Life of 19 977 Genes Obtained by DNA Microarray Analysis of Pluripotent and Differentiating Mouse Embryonic Stem Cells. *DNA Research,* 16**,** 45-58.

SHAW, G., PURKISS, T. & OLIVER, R. T. D. 2007. Re: Christine McKillop. Interview with Jack Schalken: PCA3 and its use as a diagnostic test in prostate cancer. eur Urol 2006;50 : 153-154. *European Urology,* 51**,** 860-862.

SHERRATT, M. J. 2009. Tissue elasticity and the ageing elastic fibre. *Age,* 31**,** 305-325.

SHI, T., GAO, G. & CAO, Y. L. 2016. Long Noncoding RNAs as Novel Biomarkers Have a Promising Future in Cancer Diagnostics. *Disease Markers*.

SHRAGER, J. B. 1994. The Vineberg Procedure - the Immediate Forerunner of Coronary-Artery Bypass-Grafting. *Annals of Thoracic Surgery,* 57**,** 1354-1364.

SIMON, M. D., PINTER, S. F., FANG, R., SARMA, K., RUTENBERG-SCHOENBERG, M., BOWMAN, S. K., KESNER, B. A., MAIER, V. K., KINGSTON, R. E. & LEE, J. T. 2013. High-resolution Xist binding maps reveal two-step spreading during X-chromosome inactivation. *Nature,* 504**,** 465-9.

SINGH, R. B., MENGI, S. A., XU, Y. J., ARNEJA, A. S. & DHALLA, N. S. 2002. Pathogenesis of atherosclerosis: A multifactorial process. *Exp Clin Cardiol,* 7**,** 40-53.

SKALLI, O., ROPRAZ, P., TRZECIAK, A., BENZONANA, G., GILLESSEN, D. & GABBIANI, G. 1986. A monoclonal antibody against alpha-smooth muscle actin: a new probe for smooth muscle differentiation. *J Cell Biol,* 103**,** 2787-96.

SMITH, D. R. 2016. Goodbye genome paper, hello genome report: the increasing popularity of 'genome announcements' and their impact on science. *Brief Funct Genomics*.

SMITH, J. B., ARAKI, H. & LEFER, A. M. 1980. Thromboxane A2, Prostacyclin and Aspirin - Effects on Vascular Tone and Platelet-Aggregation. *Circulation,* 62**,** 19-25.

SMITH, R. J., JUSTEN, J. M., SAM, L. M., ROHLOFF, N. A., RUPPEL, P. L., BRUNDEN, M. N. & CHIN, J. E. 1991. Platelet-derived growth factor potentiates cellular responses of articular chondrocytes to interleukin-1. *Arthritis Rheum,* 34**,** 697-706.

SOIFER, H. S., ROSSI, J. J. & SAETROM, P. 2007. MicroRNAs in disease and potential therapeutic applications. *Mol Ther,* 15**,** 2070-9.

SOLLOTT, S. J., CHENG, L., PAULY, R. R., JENKINS, G. M., MONTICONE, R. E., KUZUYA, M., FROEHLICH, J. P., CROW, M. T., LAKATTA, E. G., ROWINSKY, E. K. & ET AL. 1995. Taxol inhibits neointimal smooth muscle cell accumulation after angioplasty in the rat. *J Clin Invest,* 95**,** 1869-76.

SOUNDARARAJAN, S., CHEN, W. W., SPICER, E. K., COURTENAY-LUCK, N. & FERNANDES, D. J. 2008. The nucleolin targeting aptamer AS1411 destabilizes bcl-2 messenger RNA in human breast cancer cells. *Cancer Research,* 68**,** 2358-2365.

SOUTHGATE, K. & NEWBY, A. C. 1990. Serum-Induced Proliferation of Rabbit Aortic Smooth-Muscle Cells from the Contractile State Is Inhibited by 8-Br-Camp but Not 8-Br-Cgmp. *Atherosclerosis,* 82**,** 113-123.

SPIES, D. & CIAUDO, C. 2015. Dynamics in Transcriptomics: Advancements in RNA-seq Time Course and Downstream Analysis. *Computational and Structural Biotechnology Journal,* 13**,** 469-477.

STARY, H. C. 1992. Composition and classification of human atherosclerotic lesions. *Virchows Arch A Pathol Anat Histopathol,* 421**,** 277-90.

STARY, H. C., CHANDLER, A. B., DINSMORE, R. E., FUSTER, V., GLAGOV, S., INSULL, W., ROSENFELD, M. E., SCHWARTZ, C. J., WAGNER, W. D. & WISSLER, R. W. 1995. A Definition of Advanced Types of Atherosclerotic Lesions and a Histological Classification of Atherosclerosis - a Report from the Committee on Vascular-Lesions of the Council on Arteriosclerosis, American-Heart-Association. *Circulation,* 92**,** 1355-1374.

STELZER, A. C., FRANK, A. T., KRATZ, J. D., SWANSON, M. D., GONZALEZ-HERNANDEZ, M. J., LEE, J., ANDRICIOAEI, I., MARKOVITZ, D. M. & AL-HASHIMI, H. M. 2011. Discovery of selective bioactive small molecules by targeting an RNA dynamic ensemble. *Nat Chem Biol,* 7**,** 553-9.

STENMARK, K. R., YEAGER, M. E., EL KASMI, K. C., NOZIK-GRAYCK, E., GERASIMOVSKAYA, E. V., LI, M., RIDDLE, S. R. & FRID, M. G. 2013. The Adventitia: Essential Regulator of Vascular Wall Structure and Function. *Annual Review of Physiology, Vol 75,* 75**,** 23-47.

STONE, G. W., MOSES, J. W., ELLIS, S. G., SCHOFER, J., DAWKINS, K. D., MORICE, M., COLOMBO, A., SCHAMPAERT, E., GRUBE, E., KIRTANE, A. J., CUTLIP, D. E., FAHY, M., POCOCK, S. J., MEHRAN, R. & LEON, M. B. 2007. Safety and efficacy of sirolimus- and paclitaxel-eluting coronary stents. *New England Journal of Medicine,* 356**,** 998-1008.

SUDHEESH, S., SAWBRIDGE, T. I., COGAN, N. O. I., KENNEDY, P., FORSTER, J. W. & KAUR, S. 2015. De novo assembly and characterisation of the field pea transcriptome using RNA-Seq. *Bmc Genomics,* 16.

SUKHOVERSHIN, R. A., TOLEDANO FURMAN, N. E., TASCIOTTI, E. & TRACHTENBERG, B. H. 2016. Local Inhibition of Macrophage and Smooth Muscle Cell Proliferation to Suppress Plaque Progression. *Methodist Debakey Cardiovasc J,* 12**,** 141-145.

SUN, Y. & ZHANG, H. 2005. A unified mode of epigenetic gene silencing: RNA meets polycomb group proteins. *RNA Biol,* 2**,** 8-10.

SURYADINATA, R., SADOWSKI, M. & SARCEVIC, B. 2010. Control of cell cycle progression by phosphorylation of cyclin-dependent kinase (CDK) substrates. *Biosci Rep,* 30**,** 243-55.

SUWANABOL, P. A., SEEDIAL, S. M., ZHANG, F., SHI, X., SI, Y., LIU, B. & KENT, K. C. 2012. TGF-beta and Smad3 modulate PI3K/Akt signaling pathway in vascular smooth muscle cells. *Am J Physiol Heart Circ Physiol,* 302**,** H2211-9.

TABAS, I., GARCIA-CARDENA, G. & OWENS, G. K. 2015. Recent insights into the cellular biology of atherosclerosis. *J Cell Biol,* 209**,** 13-22.

TABERNERO, J., SHAPIRO, G. I., LORUSSO, P. M., CERVANTES, A., SCHWARTZ, G. K., WEISS, G. J., PAZ-ARES, L., CHO, D. C., INFANTE, J. R., ALSINA, M., GOUNDER, M. M., FALZONE, R., HARROP, J., WHITE, A. C., TOUDJARSKA, I., BUMCROT, D., MEYERS, R. E., HINKLE, G., SVRZIKAPA, N., HUTABARAT, R. M., CLAUSEN, V. A., CEHELSKY, J., NOCHUR, S. V., GAMBA-VITALO, C., VAISHNAW, A. K., SAH, D. W., GOLLOB, J. A. & BURRIS, H. A., 3RD 2013. First-in-humans trial of an RNA interference therapeutic targeting VEGF and KSP in cancer patients with liver involvement. *Cancer Discov,* 3**,** 406-17.

TAGANOV, K. D., BOLDIN, M. P., CHANG, K. J. & BALTIMORE, D. 2006. NF-kappaB-dependent induction of microRNA miR-146, an inhibitor targeted to signaling proteins of innate immune responses. *Proc Natl Acad Sci U S A,* 103**,** 12481-6.

TANAKA, H., SUKHOVA, G., SCHWARTZ, D. & LIBBY, P. 1996. Proliferating arterial smooth muscle cells after balloon injury express TNF-alpha but not interleukin-1 or basic fibroblast growth factor. *Arterioscler Thromb Vasc Biol,* 16**,** 12-8.

TANG, S. S., ZHENG, B. Y. & XIONG, X. D. 2015. LincRNA-p21: Implications in Human Diseases. *International Journal of Molecular Sciences,* 16**,** 18732-18740.

TEN DIJKE, P. & ARTHUR, H. M. 2007. Extracellular control of TGF beta signalling in vascular development and disease. *Nature Reviews Molecular Cell Biology,* 8**,** 857-869.

TEPE, G., MUSCHICK, P., LAULE, M., REDDIG, F., CLAUSSEN, C. D., DINKELBORG, L. M., TIELEMANS, H., WEHRMANN, M. & DUDA, S. H. 2006. Prevention of carotid artery restenosis after sirolimus-coated stent implantation in pigs. *Stroke,* 37**,** 492-4.

THAKAR, R. G., CHENG, Q., PATEL, S., CHU, J., NASIR, M., LIEPMANN, D., KOMVOPOULOS, K. & LI, S. 2009. Cell-shape regulation of smooth muscle cell proliferation. *Biophys J,* 96**,** 3423-32.

THOMAS, W. A., FLORENTIN, R. A., REINER, J. M., LEE, W. M. & LEE, K. T. 1976. Alterations in population dynamics of arterial smooth muscle cells during atherogenesis. IV. Evidence for a polyclonal origin of hypercholesterolemic diet-induced atherosclerotic lesions in young swine. *Exp Mol Pathol,* 24**,** 244-60.

THORNER, P. S. 2007. Alport syndrome and thin basement membrane nephropathy. *Nephron Clin Pract,* 106**,** c82-8.

TIWARI, G., TIWARI, R., SRIWASTAWA, B., BHATI, L., PANDEY, S., PANDEY, P. & BANNERJEE, S. K. 2012. Drug delivery systems: An updated review. *Int J Pharm Investig,* 2**,** 2-11.

TONG, Y. K. & LO, Y. M. D. 2006. Diagnostic developments involving cell-free (circulating) nucleic acids. *Clinica Chimica Acta,* 363**,** 187-196.

TORZEWSKI, J., TORZEWSKI, M., BOWYER, D. E., FROHLICH, M., KOENIG, W., WALTENBERGER, J., FITZSIMMONS, C. & HOMBACH, V. 1998. C-reactive protein frequently colocalizes with the terminal complement complex in the intima of early atherosclerotic lesions of human coronary arteries. *Arterioscler Thromb Vasc Biol,* 18**,** 1386-92.

TRAPNELL, C., HENDRICKSON, D. G., SAUVAGEAU, M., GOFF, L., RINN, J. L. & PACHTER, L. 2013. Differential analysis of gene regulation at transcript resolution with RNA-seq. *Nature Biotechnology,* 31**,** 46-+.

TRAPNELL, C., ROBERTS, A., GOFF, L., PERTEA, G., KIM, D., KELLEY, D. R., PIMENTEL, H., SALZBERG, S. L., RINN, J. L. & PACHTER, L. 2012. Differential gene and transcript expression analysis of RNA-seq experiments with TopHat and Cufflinks. *Nat Protoc,* 7**,** 562-78.

TRAPNELL, C., WILLIAMS, B. A., PERTEA, G., MORTAZAVI, A., KWAN, G., VAN BAREN, M. J., SALZBERG, S. L., WOLD, B. J. & PACHTER, L. 2010. Transcript assembly and quantification by RNA-Seq reveals unannotated transcripts and isoform switching during cell differentiation. *Nat Biotechnol,* 28**,** 511-5.

TREVINO, V., FALCIANI, F. & BARRERA-SALDANA, H. A. 2007. DNA microarrays: a powerful genomic tool for biomedical and clinical research. *Mol Med,* 13**,** 527-41.

TRIPATHI, V., ELLIS, J. D., SHEN, Z., SONG, D. Y., PAN, Q., WATT, A. T., FREIER, S. M., BENNETT, C. F., SHARMA, A., BUBULYA, P. A., BLENCOWE, B. J., PRASANTH, S. G. & PRASANTH, K. V. 2010. The Nuclear-Retained Noncoding RNA MALAT1 Regulates Alternative Splicing by Modulating SR Splicing Factor Phosphorylation. *Molecular Cell,* 39**,** 925-938.

TRUJILLO, C. A., NERY, A. A., ALVES, J. M., MARTINS, A. H. & ULRICH, H. 2007. Development of the anti-VEGF aptamer to a therapeutic agent for clinical ophthalmology. *Clin Ophthalmol,* 1**,** 393-402.

TSOI, L. C., IYER, M. K., STUART, P. E., SWINDELL, W. R., GUDJONSSON, J. E., TEJASVI, T., SARKAR, M. K., LI, B., DING, J., VOORHEES, J. J., KANG, H. M., NAIR, R. P., CHINNAIYAN, A. M., ABECASIS, G. R. & ELDER, J. T. 2015. Analysis of long non-coding RNAs highlights tissue-specific expression patterns and epigenetic profiles in normal and psoriatic skin. *Genome Biol,* 16**,** 24.

URNOV, F. D., REBAR, E. J., HOLMES, M. C., ZHANG, H. S. & GREGORY, P. D. 2010. Genome editing with engineered zinc finger nucleases. *Nature Reviews Genetics,* 11**,** 636-646.

VAN DEN BOOM, M., SARBIA, M., LIPINSKI, K. V., MANN, P., MEYER-KIRCHRATH, J., RAUCH, B. H., GRABITZ, K., LEVKAU, B., SCHROR, K. & FISCHER, J. W. 2006. Differential regulation of hyaluronic acid synthase isoforms in human saphenous vein smooth muscle cells - Possible implications for vein graft stenosis. *Circulation Research,* 98**,** 36-44.

VAN DEN BOOM, M., SARBIA, M., RAUCH, B. H., MEYER-KIRCHRATH, J., GRABITZ, K., SCHROR, K. & FISCHER, J. W. 2005. Differential regulation of hyaluronic acid synthase-isoforms in human saphenous vein smooth muscle cells: Possible implications for vein graft stenosis. *Circulation,* 112**,** U257-U257.

VAN DEN BOS, H., SPIERINGS, D. C. J., TAUDT, A., BAKKER, B., PORUBSKY, D., FALCONER, E., NOVOA, C., HALSEMA, N., KAZEMIER, H. G., HOEKSTRA-WAKKER, K., GURYEV, V., DEN DUNNEN, W. F. A., FOIJER, F., COLOME-TATCHE, M., BODDEKE, H. W. G. M. & LANDSDORP, P. M. 2016. Single-cell whole genome sequencing reveals no evidence for common aneuploidy in normal and Alzheimer's disease neurons (vol 17, 116, 2016). *Genome Biology,* 17.

VANCE, K. W. & PONTING, C. P. 2014. Transcriptional regulatory functions of nuclear long noncoding RNAs. *Trends in Genetics,* 30**,** 348-355.

VECCHIONE, C., CARNEVALE, D., DI PARDO, A., GENTILE, M. T., DAMATO, A., COCOZZA, G., ANTENUCCI, G., MASCIO, G., BETTARINI, U., LANDOLFI, A., IORIO, L., MAFFEI, A. & LEMBO, G. 2009. Pressure-induced vascular oxidative stress is mediated through activation of integrin-linked kinase 1/betaPIX/Rac-1 pathway. *Hypertension,* 54**,** 1028-34.

VECOLI, C. 2015. Next-Generation Sequencing Technology in the Genetics of Cardiovascular Disease. *Cardiomyocytes: Methods and Protocols,* 1299**,** 51-64.

VENUGOPAL, S. K., DEVARAJ, S., YUHANNA, I., SHAUL, P. & JIALAL, I. 2002. Demonstration that C-reactive protein decreases eNOS expression and bioactivity in human aortic endothelial cells. *Circulation,* 106**,** 1439-1441.

VESEY, A. T., IRKLE, A., LEWIS, D. Y., SKEPPER, J. N., BIRD, J. L., DWECK, M. R., JOSHI, F. R., GALLAGHER, F. A., WARBURTON, E. A., BENNETT, M., BRINDLE, K., NEWBY, D. E., RUDD, J. H. & DAVENPORT, A. P. 2015. Identifying Active Vascular Microcalcification by F-18-Sodium Fluoride Positron Emission Tomography. *Atherosclerosis,* 241**,** E14-E14.

VICKERS, K. C., PALMISANO, B. T., SHOUCRI, B. M., SHAMBUREK, R. D. & REMALEY, A. T. 2015. MicroRNAs are transported in plasma and delivered to recipient cells by high-density lipoproteins (vol 13, pg 423, 2011). *Nature Cell Biology,* 17**,** 104-104.

VIGETTI, D., DELEONIBUS, S., MORETTO, P., BOWEN, T., FISCHER, J. W., GRANDOCH, M., OBERHUBER, A., LOVE, D. C., HANOVER, J. A., CINQUETTI, R., KAROUSOU, E., VIOLA, M., D'ANGELO, M. L., HASCALL, V. C., DE LUCA, G. & PASSI, A. 2014. Natural Antisense Transcript for Hyaluronan Synthase 2 (HAS2-AS1) Induces Transcription of HAS2 via Protein O-GlcNAcylation. *Journal of Biological Chemistry,* 289**,** 28816-28826.

VLAEMINCK-GUILLEM, V., RUFFION, A., ANDRE, J., DEVONEC, M. & PAPAREL, P. 2010. Urinary prostate cancer 3 test: toward the age of reason? *Urology,* 75**,** 447-53.

VOELLENKLE, C., GARCIA-MANTEIGA, J. M., PEDROTTI, S., PERFETTI, A., DE TOMA, I., DA SILVA, D., MAIMONE, B., GRECO, S., FASANARO, P., CREO, P., ZACCAGNINI, G., GAETANO, C. & MARTELLI, F. 2016. Implication of Long noncoding RNAs in the endothelial cell response to hypoxia revealed by RNA-sequencing. *Sci Rep,* 6**,** 24141.

WAHID, F., SHEHZAD, A., KHAN, T. & KIM, Y. Y. 2010. MicroRNAs: Synthesis, mechanism, function, and recent clinical trials. *Biochimica Et Biophysica Acta-Molecular Cell Research,* 1803**,** 1231-1243.

WALLER, Z. A. E., SEWITZ, S. A., HSU, S. T. D. & BALASUBRAMANIAN, S. 2009. A Small Molecule That Disrupts G-Quadruplex DNA Structure and Enhances Gene Expression. *Journal of the American Chemical Society,* 131**,** 12628-12633.

WALLEZ, Y. & HUBER, P. 2008. Endothelial adherens and tight junctions in vascular homeostasis, inflammation and angiogenesis. *Biochimica Et Biophysica Acta-Biomembranes,* 1778**,** 794-809.

WAMHOFF, B. R., HOOFNAGLE, M. H., BURNS, A., SINHA, S., MCDONALD, O. G. & OWENS, G. K. 2004. A G/C element mediates repression of the SM22 alpha promoter within phenotypically modulated smooth muscle cells in experimental atherosclerosis. *Circulation Research,* 95**,** 981-988.

WANG, G. K., ZHU, J. Q., ZHANG, J. T., LI, Q., LI, Y., HE, J., QIN, Y. W. & JING, Q. 2010. Circulating microRNA: a novel potential biomarker for early diagnosis of acute myocardial infarction in humans. *European Heart Journal,* 31**,** 659-666.

WANG, K. C. & CHANG, H. Y. 2011. Molecular mechanisms of long noncoding RNAs. *Mol Cell,* 43**,** 904-14.

WANG, K. C., YANG, Y. W., LIU, B., SANYAL, A., CORCES-ZIMMERMAN, R., CHEN, Y., LAJOIE, B. R., PROTACIO, A., FLYNN, R. A., GUPTA, R. A., WYSOCKA, J., LEI, M., DEKKER, J., HELMS, J. A. & CHANG, H. Y. 2011. A long noncoding RNA maintains active chromatin to coordinate homeotic gene expression. *Nature,* 472**,** 120-U158.

WANG, S. H., LI, X. X., ZHU, R. J., HAN, Q. & ZHAO, R. C. 2016a. Lung cancer exosomes initiate global long non-coding RNA changes in mesenchymal stem cells. *International Journal of Oncology,* 48**,** 681-689.

WANG, Y., QIU, J., LUO, S., XIE, X., ZHENG, Y., ZHANG, K., YE, Z., LIU, W., GREGERSEN, H. & WANG, G. 2016b. High shear stress induces atherosclerotic vulnerable plaque formation through angiogenesis. *Regen Biomater,* 3**,** 257-67.

WANG, Z., GERSTEIN, M. & SNYDER, M. 2009. RNA-Seq: a revolutionary tool for transcriptomics. *Nature Reviews Genetics,* 10**,** 57-63.

WANG, Z. B. & NEWMAN, W. H. 2003. Smooth muscle cell migration stimulated by interleukin 6 is associated with cytoskeletal reorganization. *Journal of Surgical Research,* 111**,** 261-266.

WANG, Z. G., WANG, D. Z., PIPES, G. C. T. & OLSON, E. N. 2003. Myocardin is a master regulator of smooth muscle gene expression. *Proceedings of the National Academy of Sciences of the United States of America,* 100**,** 7129-7134.

WANNAMETHEE, S. G., LOWE, G. D. O., SHAPER, A. G., RUMLEY, A., LENNON, L. & WHINCUP, P. H. 2005. Associations between cigarette smoking, pipe/cigar smoking, and smoking cessation, and haemostatic and inflammatory markers for cardiovascular disease. *European Heart Journal,* 26**,** 1765-1773.

WAPINSKI, O. & CHANG, H. Y. 2011. Long noncoding RNAs and human disease. *Trends in Cell Biology,* 21**,** 354-361.

WAUGH, J. & WAGSTAFF, A. J. 2004. The paclitaxel (TAXUS)-eluting stent: a review of its use in the management of de novo coronary artery lesions. *Am J Cardiovasc Drugs,* 4**,** 257-68.

WEBER, A., WASILIEW, P. & KRACHT, M. 2010. Interleukin-1 (IL-1) pathway. *Sci Signal,* 3**,** cm1.

WEINBERG, R. A. 1995. The retinoblastoma protein and cell cycle control. *Cell,* 81**,** 323-30.

WEINSTEIN, B. M. 1999. What guides early embryonic blood vessel formation? *Developmental Dynamics,* 215**,** 2-11.

WEISS, D., SORESCU, D. & TAYLOR, W. R. 2001. Angiotensin II and atherosclerosis. *Am J Cardiol,* 87**,** 25C-32C.

WENAWESER, P., DAEMEN, J., ZWAHLEN, M., VAN DOMBURG, R., JUNI, P., VAINA, S., HELLIGE, G., TSUCHIDA, K., MORGER, C., BOERSMA, E., KUKREJA, N., MEIER, B., SERRUYS, P. W. & WINDECKER, S. 2008. Incidence and correlates of drug-eluting stent thrombosis in routine clinical practice - 4-year results from a large 2-institutional cohort study. *Journal of the American College of Cardiology,* 52**,** 1134-1140.

WEST, N. E., QIAN, H., GUZIK, T. J., BLACK, E., CAI, S., GEORGE, S. E. & CHANNON, K. M. 2001. Nitric oxide synthase (nNOS) gene transfer modifies venous bypass graft remodeling: effects on vascular smooth muscle cell differentiation and superoxide production. *Circulation,* 104**,** 1526-32.

WHINCUP, P. H., GILG, J. A., EMBERSON, J. R., JARVIS, M. J., FEYERABEND, C., BRYANT, A., WALKER, M. & COOK, D. G. 2004. Passive smoking and risk of coronary heart disease and stroke: prospective study with cotinine measurement. *BMJ,* 329**,** 200-5.

WHITESIDE, S. T. & ISRAEL, A. 1997. I kappa B proteins: structure, function and regulation. *Seminars in Cancer Biology,* 8**,** 75-82.

WIDLANSKY, M. E., GOKCE, N., KEANEY, J. F. & VITA, J. A. 2003. The clinical implications of endothelial dysfunction. *Journal of the American College of Cardiology,* 42**,** 1149-1160.

WOLFRAM, J. A. & DONAHUE, J. K. 2013. Gene therapy to treat cardiovascular disease. *J Am Heart Assoc,* 2**,** e000119.

WRAY, W., BOULIKAS, T., WRAY, V. P. & HANCOCK, R. 1981. Silver staining of proteins in polyacrylamide gels. *Anal Biochem,* 118**,** 197-203.

WU, G., CAI, J., HAN, Y., CHEN, J., HUANG, Z. P., CHEN, C., CAI, Y., HUANG, H., YANG, Y., LIU, Y., XU, Z., HE, D., ZHANG, X., HU, X., PINELLO, L., ZHONG, D., HE, F., YUAN, G. C., WANG, D. Z. & ZENG, C. 2014. LincRNA-p21 regulates neointima formation, vascular smooth muscle cell proliferation, apoptosis, and atherosclerosis by enhancing p53 activity. *Circulation,* 130**,** 1452-65.

XIN, M., SMALL, E. M., SUTHERLAND, L. B., QI, X. X., MCANALLY, J., PLATO, C. F., RICHARDSON, J. A., BASSEL-DUBY, R. & OLSON, E. N. 2009. MicroRNAs miR-143 and miR-145 modulate cytoskeletal dynamics and responsiveness of smooth muscle cells to injury. *Genes & Development,* 23**,** 2166-2178.

YAMAMOTO, M., WAKATSUKI, T., HADA, A. & RYO, A. 2001. Use of serial analysis of gene expression (SAGE) technology. *Journal of Immunological Methods,* 250**,** 45-66.

YAN, M., XU, Q., ZHANG, P., ZHOU, X. J., ZHANG, Z. Y. & CHEN, W. T. 2010. Correlation of NF-kappaB signal pathway with tumor metastasis of human head and neck squamous cell carcinoma. *BMC Cancer,* 10**,** 437.

YANG, L. Q., LIN, C. R., LIU, W., ZHANG, J., OHGI, K. A., GRINSTEIN, J. D., DORRESTEIN, P. C. & ROSENFELD, M. G. 2013. ncRNA- and Pc2 Methylation-Dependent Gene Relocation between Nuclear Structures Mediates Gene Activation Programs (vol 147, pg 773, 2011). *Cell,* 155**,** 478-478.

YANG, Y., CAI, Y., WU, G., CHEN, X., LIU, Y., WANG, X., YU, J., LI, C., CHEN, X., JOSE, P. A., ZHOU, L. & ZENG, C. 2015a. Plasma long non-coding RNA, CoroMarker, a novel biomarker for diagnosis of coronary artery disease. *Clin Sci (Lond),* 129**,** 675-85.

YANG, Y. F., WEN, L. W. & ZHU, H. L. 2015b. Unveiling the hidden function of long non-coding RNA by identifying its major partner-protein. *Cell and Bioscience,* 5.

YASOJIMA, K., SCHWAB, C., MCGEER, E. G. & MCGEER, P. L. 2001. Generation of C-reactive protein and complement components in atherosclerotic plaques. *Am J Pathol,* 158**,** 1039-51.

YOO, Y. D., CHOI, J. Y., LEE, S. J., KIM, J. S., MIN, B. R., LEE, Y. I. & KANG, Y. K. 1999. TGF-beta-induced cell-cycle arrest through the p21(WAF1)/(CIP1)-G1 cyclin/Cdks-p130 pathway in gastric-carcinoma cells. *International Journal of Cancer,* 83**,** 512-517.

YOON, J. H., ABDELMOHSEN, K., SRIKANTAN, S., YANG, X. L., MARTINDALE, J. L., DE, S., HUARTE, M., ZHAN, M., BECKER, K. G. & GOROSPE, M. 2013. LincRNA-p21 Suppresses Target mRNA Translation (vol 47, pg 648, 2012). *Molecular Cell,* 50**,** 303-303.

YOSHIDA, T., HOOFNAGLE, M. H. & OWENS, G. K. 2004. Myocardin and Prx1 contribute to angiotensin II-induced expression of smooth muscle alpha-actin. *Circulation Research,* 94**,** 1075-1082.

YOSHIDA, T., KAESTNER, K. H. & OWENS, G. K. 2008. Conditional deletion of Kruppel-like factor 4 delays downregulation of smooth muscle cell differentiation markers but accelerates neointimal formation following vascular injury. *Circ Res,* 102**,** 1548-57.

YU, X. & LI, Z. 2014. MicroRNAs regulate vascular smooth muscle cell functions in atherosclerosis (Review). *International Journal of Molecular Medicine,* 34**,** 923-933.

YU, X. H., FU, Y. C., ZHANG, D. W., YIN, K. & TANG, C. K. 2013. Foam cells in atherosclerosis. *Clin Chim Acta,* 424**,** 245-52.

ZARIFIS, J. H. 2005. Atherosclerosis, thrombosis, and inflammatory risk factors, from history and the laboratory to real life. *Eur Heart J,* 26**,** 317-8.

ZEIHER, A. M., SCHACHINGER, V. & MINNERS, J. 1995. Long-term cigarette smoking impairs endothelium-dependent coronary arterial vasodilator function. *Circulation,* 92**,** 1094-100.

ZERNECKE, A., BIDZHEKOV, K., NOELS, H., SHAGDARSUREN, E., GAN, L., DENECKE, B., HRISTOV, M., KOPPEL, T., JAHANTIGH, M. N., LUTGENS, E., WANG, S. S., OLSON, E. N., SCHOBER, A. & WEBER, C. 2009. Delivery of MicroRNA-126 by Apoptotic Bodies Induces CXCL12-Dependent Vascular Protection. *Science Signaling,* 2.

ZHAN, Y., KIM, S., IZUMI, Y., IZUMIYA, Y., NAKAO, T., MIYAZAKI, H. & IWAO, H. 2003. Role of JNK, p38, and ERK in platelet-derived growth factor-induced vascular proliferation, migration, and gene expression. *Arterioscler Thromb Vasc Biol,* 23**,** 795-801.

ZHAO, J., OHSUMI, T. K., KUNG, J. T., OGAWA, Y., GRAU, D. J., SARMA, K., SONG, J. J., KINGSTON, R. E., BOROWSKY, M. & LEE, J. T. 2010. Genome-wide Identification of Polycomb-Associated RNAs by RIP-seq. *Molecular Cell,* 40**,** 939-953.

ZHAO, J., SUN, B. K., ERWIN, J. A., SONG, J. J. & LEE, J. T. 2008. Polycomb proteins targeted by a short repeat RNA to the mouse X chromosome. *Science,* 322**,** 750-6.

ZHAO, Y., FENG, G., WANG, Y., YUE, Y. & ZHAO, W. 2014. Regulation of apoptosis by long non-coding RNA HIF1A-AS1 in VSMCs: implications for TAA pathogenesis. *Int J Clin Exp Pathol,* 7**,** 7643-52.

ZHOU, M., ZHAO, H., WANG, Z., CHENG, L., YANG, L., SHI, H., YANG, H. & SUN, J. 2015. Identification and validation of potential prognostic lncRNA biomarkers for predicting survival in patients with multiple myeloma. *J Exp Clin Cancer Res,* 34**,** 102.

ZIMMERMANN, T. S., LEE, A. C., AKINC, A., BRAMLAGE, B., BUMCROT, D., FEDORUK, M. N., HARBORTH, J., HEYES, J. A., JEFFS, L. B., JOHN, M., JUDGE, A. D., LAM, K., MCCLINTOCK, K., NECHEV, L. V., PALMER, L. R., RACIE, T., ROHL, I., SEIFFERT, S., SHANMUGAM, S., SOOD, V., SOUTSCHEK, J., TOUDJARSKA, I., WHEAT, A. J., YAWORSKI, E., ZEDALIS, W., KOTELIANSKY, V., MANOHARAN, M., VORNLOCHER, H. P. & MACLACHLAN, I. 2006. RNAi-mediated gene silencing in non-human primates. *Nature,* 441**,** 111-4.